A FRACTURE MECHANICS APPROACH TO ENVIRONMENTAL AND ELASTIC-PLASTIC FATIGUE CRACK PROPAGATION

by

C.A.G. de MOURA BRANCO (Dipl.Eng., M.Sc., D.I.C.)

A thesis submitted for the award of the degree of Doctor of Philosophy of the Faculty of Engineering of the University of London

Department of Mechanical Engineering

Imperial College of Science and Technology

University of London

June 1976

ABSTRACT

A linear elastic fracture mechanics approach has been applied to an investigation of the fatigue crack propagation process in three different metals (high strength aluminium alloy RR58, cast aluminium alloy LM30 and mild steel BS15). The effects on the rate of crack growth of such parameters as the amplitude and mean level of the stress intensity factor, environment and loading frequency have been investigated. The experimental study has been performed using contoured double cantilever beam specimens (a constant stress intensity factor test piece) and covered the full sub-critical range from threshold to fast fracture. Based on the experimental data collected a semi-empirical model for the determination of the crack growth rate is proposed. The specific form of this model enables its representation in terms of such parameters as crack opening displacement, crack extension force and their respective threshold and critical values. The present model has been successfully applied to fatigue crack propagation data for steels taken from the literature.

Stress corrosion cracking has been investigated in aluminium alloys RR58 and LM30. The effects on the crack growth rate of the wetting method and loading history have been assessed, and an equation developed to predict the loading history effect under a decreasing stress intensity factor pattern.

An elastic-plastic study of fatigue crack growth under load cycling has been carried out. The crack growth rate in BS15 mild steel was found to be controlled by the range of the J contour integral in the loading cycle which was calculated both experimentally and theoretically for the contoured double cantilever beam geometry. The influence of unloading on J is discussed. The J integral has also been calculated for monotonic loading, and a critical J_{1c} value for crack propagation obtained in two different specimen geometries.

ACKNOWLEDGEMENTS

The author wishes to acknowledge the financial support provided by the Instituto de Alta Cultura, Ministry of Education and Scientific Research, Lisbon, Portugal during the period of engagement in this work. The leave of absence from the Lisbon Institute of Technology is gratefully acknowledged, and also the contribution of Prof. Luciano de Faria, in the Department of Mechanical Engineering.

In particular he wishes to extend his gratitude to his supervisors Drs. L.E. Culver and J.C. Radon whose advice, help and encouragement he has found extremely valuable.

The co-operation of the members of the technical staff in the laboratories, and in the departmental workshop in overcoming the problems associated with the preparation of the experiments is gratefully acknowledged.

Special thanks are due to Mrs. Maria Teresa Almeida for the preparation of the figures and to Miss M.K. Maxwell for typing the thesis. Co-operation of Mr. T. Etela, Mr. H. Hockenhull and Mr. M. Stephens who performed part of the corrosion fatigue tests on BS15, and stress corrosion on RR58 and LM30 as their final year projects are acknowledged.

The co-operation of the Ford Motor Co. in supplying the cast aluminium alloy LM30 and providing financial support for the experimental programme on that material is very much appreciated.

Finally the author wants to express his gratitude to his wife for her understanding and support during the course of this work.

CONTENTS

	Page
ABSTRACT	i
ACKNOWLEDGEMENTS	ii
CONTENTS	iii
NOMENCLATURE	xi
LIST OF TABLES	xix
LIST OF FIGURES	xx
CHAPTER 1 THE FATIGUE FAILURE PHENOMENON IN METALS AND THE ROLE OF FRACTURE MECHANICS	1
1.1 Definition	1
1.2 Introduction	1
1.3 Crack Initiation	2
1.4 Empirical Laws of Fatigue Behaviour	5
1.4.1 The S-N Curve	5
1.4.2 The Effect of Mean Stress	7
1.4.3 Fatigue Limit Under Varying Stress Amplitude; Cumulative Damage	8
1.4.4 Influence of Stress Concentrations	9
1.4.5 Influence of Complex Stress Systems	11
1.4.6 Low-cycle Fatigue	12
(A) Strain Cycling	12
(B) Load Cycling	15
(C) The Effect of Notches	16
1.5 The Effect of Environment on Fatigue Strength	17
1.5.1 Phenomenological Trends	17
1.5.2 The Mechanism of Corrosion Fatigue	19
1.6 The Crack Propagation Process in Metals	20
1.6.1 Introduction	20
1.6.2 Mechanisms of Crack Propagation	22

Page

1.7 Fracture Mechanics Approach to Fatigue Crack Propagation 25

1.7.1 Introduction 25

1.7.2 Fatigue Crack Growth Theories 26

1.7.3 Phenomenological Analysis of the Fatigue Crack Propagation Curve 29

1.7.4 The Effect of Mean Stress on Fatigue Crack Propagation - Crack Growth Laws 30

(A) Semi-empirical Relationships 30

(B) Theoretical Analyses 33

1.7.5 The Effect of Environment on Fatigue Crack Propagation 36

1.7.6 Superposition Models for Environmental Fatigue Crack Propagation 39

1.7.7 The Threshold for Fatigue Crack Propagation 42

1.7.8 The Effect of Several Other Parameters on Fatigue Crack Propagation 44

(A) The Load Frequency 44

(B) The Specimen Thickness 44

(C) Compressive Loading 45

(D) The Loading History 46

1.7.9 Fatigue Crack Growth at Large Plastic Stains 48

1.8 Fracture Mechanics Approach to Fatigue Crack Propagation in Components or Structures 51

1.8.1 Calculation of the Number of cycles to Failure 51

1.8.2 Analysis in Components or Structures 52

CHAPTER 2 ENVIRONMENTAL FATIGUE CRACK PROPAGATION IN THE AL-ALLOYS RR58 AND LM30 AND MILD STEEL BS15 54

2.1 Experimental Procedure 54

2.1.1 Material, Heat Treatment and Environment Selection 54

2.1.2 Design and Selection of the Specimens 55

2.1.3 Specimen Dimensions and Preparation 56

Page

2.1.4 Compliance Calibration and Calculation of K_c 58

2.1.5 Testing Programme 59

2.1.6 Testing Apparatus 60

2.1.7 Testing Procedure 60

2.2 Experimental Results 61

2.2.1 Fatigue Crack Propagation in RR58 in Air (21°C and 50% R.H.) and in 3.5% NaCl 61

(A) The da/dN-ΔK Relation and the Effects of K_m and ΔK in Air at 0.15 Hz 62

(B) The da/dN-ΔK Relation and the Effects of K_m and ΔK in Air at 35 Hz 64

(C) The da/dN-ΔK Relation and the Effect of K_m and ΔK in 3.5% NaCl 65

2.2.2 Fatigue Crack Propagation in BS15 Mild Steel in Air (21°C and 50% R.H.) and in 3.5% NaCl 67

(A) The da/dN-ΔK Relation and the Effects of K_m and ΔK in Air 67

(B) The da/dN-ΔK Relation and the Effects of K_m and ΔK in 3.5% NaCl 68

2.2.3 Fatigue Crack Propagation in LM30 in Air and in 3.5% NaCl 70

(A) The da/dN-ΔK Relation and the Effect of K_m and ΔK in Air 71

(B) The da/dN-ΔK Relation and the Effect of K_m and ΔK in 3.5% NaCl 71

2.3 Discussion of Results 72

2.3.1 The Threshold Results 72

(A) Threshold Results in RR58 and LM30 72

(B) Threshold Results in Mild Steel BS15 74

Page

2.3.2 The Effect of Environment and Loading Frequency 76

(A) Environmental and Loading Frequency Effects in RR58 and LM30 76

(B) Environmental and Loading Frequency Effects on BS15 78

2.3.3 A Semi-Empirical Fatigue Crack Propagation Model 80

(A) Proposed Model 80

(B) The Use of the Proposed Model for Representing Experimental Data 83

(C) Trends of Variation in α and A_c Coefficients 85

2.3.4 An Example of the Application of the Proposed Model to Calculate the Number of Cycles to Failure 86

CHAPTER 3 A SHORT REVIEW ON STRESS CORROSION CRACKING IN ALUMINIUM ALLOYS - A FRACTURE MECHANICS APPROACH 88

3.1 Introduction 88

3.2 The SCC Process in Aluminium Alloys and Parameters which Influence it 89

3.2.1 The Specimen Orientation in the Plate Material 89

3.2.2 The Effect of Stress 89

(A) The Stress Intensity Factor and Testing Techniques 89

(B) The da/dt-K Diagram 91

3.2.3 The Effect of Environment 92

3.2.4 Metallurgical Factors 94

3.3 Stress Corrosion Cracking Theories 95

3.3.1 Activation Energy Theories 95

3.3.2 Strain-Enhanced Theories 96

3.3.3 Hydrogen Embrittlement Theories 97

3.3.4 Other Stress Corrosion Theories 98

Page

CHAPTER 4 STRESS CORROSION CRACKING IN THE ALUMINIUM ALLOYS RR58 AND LM30 100

4.1 Experimental Procedure 100

4.1.1 Test Rigs 100

4.1.2 Material and Environmental Selection 101

4.1.3 Specimens 101

4.1.4 Compliance Calibration and Calculation of K_c 101

4.1.5 Testing Procedure 101

4.2 Experimental Results 102

4.2.1 Stress Corrosion Cracking in RR58 in 3.5% NaCl 102

4.2.2 Stress Corrosion Cracking in LM30 in 3.5% NaCl 105

4.3 Discussion of Results 105

4.3.1 The Influence of Load History 105

(A) Prediction of the Incubation Time Under Decreasing K 105

(B) The Incubation Time Under Increasing K 108

4.3.2 The da/dt-K Curves 108

(A) The Influence of Specimen Orientation 108

(B) Comparison Between Materials and Wetting Techniques 109

4.3.3 Comparison Between Static and Dynamic Crack Propagation 111

CHAPTER 5 THE J INTEGRAL APPROACH TO SLOW CRACK GROWTH UNDER MONOTONIC LOADING 112

5.1 Theoretical Analysis 112

5.1.1 The Energy Definition of the J Contour Integral for Monotonic Loading 112

5.1.2 Application to the Contoured DCB Geometry 114

(A) The Effect of Bending Moment on Deflections 114

(B) The Effect of Shear Force and Rotation at the Crack Tip on the Deflection Values 117

Page

(C) Theoretical Results for Deflections, Potential Energy and J Contour Integral 118

5.2 Experimental Procedure 119

5.2.1 Material and Specimens 119

5.2.2 Testing Procedure 120

(A) Tests for the Determination of A and n 120

(B) Precracking Tests 120

(C) Tests for the Determination of J_c 121

5.3 Experimental Results 122

5.3.1 Contoured DCB Results on BS15 122

5.3.2 Results from Compact Tension Specimens 123

5.4 Discussion of Results 123

5.4.1 Results for the DCB Specimen

5.4.2 The J_c Determination in DCB and Compact Tension Specimens 124

CHAPTER 6 A STUDY OF ELASTIC-PLASTIC FATIGUE CRACK GROWTH UNDER LOAD-CYCLING 126

6.1 Theoretical Analysis 126

6.1.1 Operational Definition of ΔJ for Elastic-Plastic Load Cycling 126

6.1.2 Application of ΔJ for the Contoured DCB Specimen 129

(A) Analysis for Small Deflections 129

(B) Analysis for Large Deflections 131

(C) The ΔJ Results 132

6.2 Experimental 133

6.2.1 Material 133

6.2.2 Specimens 133

6.2.3 Cyclic Creep Tests 133

Page

6.2.4 Fatigue Crack Growth Tests 134

6.3 Experimental Results 134

6.3.1 Cyclic Creep Results 134

6.3.2 Fatigue Crack Propagation Results 135

6.4 Discussion of Results 136

CONCLUSIONS AND PROPOSALS FOR FUTURE WORK 138

REFERENCES 143

APPENDIX A A BRIEF REVIEW ON FRACTURE MECHANICS

A.1 Elastic Stress Distribution at the tip of a Crack - the Elastic Stress Intensity Factor K 163

A.2 Methods of Determining Stress Intensity Factors 165

A.3 Fracture Analysis Using K-Linear Elastic Fracture Mechanics 168

A.4 Test Techniques to Evaluate K_c 168

A.5 Energy Balance Criteria 169

A.6 Elastic-Plastic Stress Analysis of Cracks. Non-Linear Fracture Mechanics 171

A.6.1 The Dugdale Model and the Crack Opening Displacement 171

A.6.2 The J Contour Integral 172

References 175

Figs. A1 and A2 178

APPENDIX B NON-LINEAR BEAM THEORY USED IN THE PRESENT ANALYSIS 179

B.1 The General Curvature Equations 179

B.2 The Curvature Due to Cyclic Creep in Load Cycling 180

B.3 Determination of the Error Factor for Large Deflections 181

B.4 Shear Stress Distribution in Variable Height Beams for Linear and Non-Linear Elastic Materials 182

B.5 The Deflection Caused by Rotation at the Crack Tip 186

Listing of Computer Programs 187

Page

TABLES 192

FIGURES 219

LIST OF PUBLICATIONS 296

NOMENCLATURE

Symbol	Meaning
A	Strain hardening constant
A_c	Constant in crack growth rate equation
A_L	Area under the load-deflection curve
a	Crack length
a_c	Critical value of crack length for unstable crack propagation
a_D	Crack length corresponding to the delay period
a_i	Crack length in the incubation period
a_o	Initial crack length
B	Beam thickness
B_1, B_2, B_3	Constants in crack growth rate equations
B_n	Crack width
b	Uncracked ligament length
b'	Ellipse minor axis length
b_1, b_1'	Constants in crack growth rate equations
C	Compliance (extension/unit load)
C_1	Constant in the cyclic creep equation
$C_2, C_3, C_4,$ etc. C_{20}	Constants in crack growth rate equations
C'	Constant
C_o'	Solute concentration at the crack tip
C_i	Constant in the incubation time equation
C_o	Constant
C_{pl}	Constant in crack growth rate equation
c	Fatigue ducitility exponent
D	Constant
D_1	Constant in crack growth rate equation
d_τ	Ligament size at the crack tip

E, E'	Young's modulus
f	Loading frequency
G	Strain energy release rate or crack extension force
G_c	Critical value of G for unstable crack propagation
G_{max}, G_{min}	Maximum and minimum values of G in the loading cycle
$\Delta G = G_{max} - G_{min}$	Range of G in the loading cycle
ΔG_{th}	Value of ΔG associated with crack growth rates below 10^{-7} mm/cycle
G_{fc}	Non linear fracture toughness value
G'	Shear modulus
h	Specimen height
h_o	Height of the first beam element
h_1	Geometrical constant in the DCB specimen
h_u	Uncracked ligament height
J	J contour integral
J_c, J_{1c}	Critical value of J for crack propagation
ΔJ	Cyclic value of the J contour integral
K	Stress intensity factor
K_I, K_{II}, K_{III}	Stress intensity factor for modes I, II and III
K_c	Critical value of K for unstable crack propagation
K_t	Theoretical elastic stress concentration factor
K_f	Fatigue strength reduction factor
K_{ISCC}	Threshold value of the stress intensity factor in stress corrosion
K_{1b}	Level of K required for crack branching
K_{1c}	Minimum value of K_c
K_{cl}	Level of K required to open the crack
K_Q	Apparent value of K_c

K_r, K_s	Two consecutive K values with $K_r > K_s$
K_{max}, K_{min}, K_m	Maximum, minimum and mean values of the stress intensity factor in the loading cycle
$\Delta K = K_{max} - K_{min}$	Range of the stress intensity factor in the loading cycle
ΔK_o	Range of the stress intensity factor above K_{cl} necessary for crack growth
ΔK_{ef}	Effective range of the stress intensity factor
$(K_{max})_{th}$, $(K_{min})_{th}$	Maximum and minimum values of the threshold value of the stress intensity factor in the loading cycle
$\Delta K_{th} = (K_{max})_{th} - (K_{min})_{th}$	Range of the the threshold value of the stress intensity factor in the loading cycle
k	Beam curvature
k_{el}	Elastic bending moment beam curvature
k_{cc}	Curvature caused by cyclic creep
k_o	Total curvature at the maximum load point in the first cycle
k_c	Boltzman's constant
K'	Cyclic strength coefficient
L	Beam length measured from the crack tip
M	Safe range of mean stress
m	Exponent in the cyclic creep equation
m_1	Constant
m_2, m_3	Constants in crack growth rate equation
m_o	Geometrical constant
N	Number of cycles
N_f	Number of cycles to failure
N_D	Number of cycles for delayed crack propagation
n	Strain hardening exponent
n_1	Exponent in Arad's law
n_i	Exponent in the incubation time equation
n'	Cyclic strain hardening exponent

P	Applied load
P_c	Critical load for unstable crack propagation
P_{max}, P_{min}	Maximum and minimum load values in the loading cycle
$\Delta P = P_{max} - P_{min}$	Range of applied load in the loading cycle
P_{cc}	Cyclic creep load
P_{ef}	Effective load
P_{SCC}	Applied load in the stress corrosion tests
P_{ys}	Yield load
$P_{pl} = P - P_{ys}$	Load required for plastic deformation
$p_1, p_2, p_3,$ etc., p_8	Constants in crack growth rate equations
Q	Activation energy
Q_o	Stress-free activation energy
q	Notch sensitivity factor
$q_o, q_1, q_2,$ etc., q_{12}	Constants in crack growth rate equations
R	Stress ratio
R_g	Gas constant
R_{cl}	Stress ratio value corresponding to crack closure
R_{cut}	Value of stress ratio for no dependence on crack growth rate
r	Radial coordinate at the crack tip
r_r, r_s	Crack tip plastic zone sizes corresponding to K_r and K_s
r_y	Plastic zone size at the crack tip
S	Range of applied stress
s	Arc length
T	Temperature
t	Time
t_i	Incubation time

U	Potential energy
U_o	Constant in the crack closure equation
U_1	Linear elastic potential energy
U_2	Plastic (non-linear elastic) potential energy
ΔU_1	Potential energy in the first cycle
ΔU_N	Potential energy after N cycles
$\Delta U = \Delta U_N - \Delta U_1$	Variation in potential energy
u	Displacement
V_o	Constant
V_m	Molar volume
V_u	Activation volume
v	Crack opening displacement (COD)
v_{max}, v_{min}	Maximum and minimum values of COD in the loading cycle
$\Delta v = v_{max} - v_{min}$	Range of COD in the loading cycle
Δv_{th}	Threshold value of v
W	Strain energy density
w	Specimen width measured from the loading points
w_o	Plastic zone size
x	Coordinate along the beam length
Y	Geometrical factor in the stress intensity factor equation
y	Coordinate along the beam height
Z_1, Z_2	Derivatives of deflection in order to x

Greek Symbols

α	Exponent in the proposed crack propagation model
α_1, α_2	Constants in crack growth rate equations
α'	Constant

β	Constant in Arad's law
β_1	Constant in crack growth rate equation
γ	Constant in the S-N curve equation
γ_s	Fracture surface energy
γ_p	Plastic fracture surface energy
γ'	Constant
δ	Deflection at the loading points
$\delta_{max}, \delta_{min}$	Maximum and minimum values of the deflection at the loading points
$\Delta\delta=\delta_{max}-\delta_{min}$	Range of the deflection at the loading points in the loading cycle
δ_{el}^{M}	Linear elastic bending moment deflection at the loading points
δ_{pl}^{M}	Plastic bending moment deflection at the loading points
δ_{el}^{s}	Linear elastic shear stress deflection at the loading points
δ_{pl}^{s}	Plastic shear stress deflection at the loading points
$\delta^{M}=\delta_{el}^{M}+\delta_{pl}^{M}$	Total bending moment deflection at the loading points
$\delta^{s}=\delta_{el}^{s}+\delta_{pl}^{s}$	Total shear stress deflection at the loading points
δ^{R}	Deflection at the loading points caused by crack tip rotation
$\delta_{el}=\delta_{el}^{M}+\delta_{el}^{s}$	Total linear elastic deflection at the loading points
$\delta_{pl}=\delta_{pl}^{M}+\delta_{pl}^{s}$	Total plastic (non-linear elastic) deflection at the loading points
δ_t	Total theoretical deflection at the loading points
δ_{exp}	Total experimental deflection at the loading points
$\Delta\delta_{el}$	Range of linear elastic deflection at the loading points in the loading cycle

$\Delta\delta_1$	Range of deflection at the loading points in the first loading cycle
$\Delta\delta_{cc}$	Range of deflection at the loading points accumulated by cyclic creep
$\Delta\delta_N=\Delta\delta_1+\Delta\delta_{cc}$	Range of deflection at the loading points accumulated after N loading cycles
ε_{cc}	Accumulated secondary cyclic creep strain
ε_o	Initial strain after the first cycle
$\varepsilon_{cct}=\varepsilon_o+\varepsilon_{cc}$	Total accumulated cyclic creep strain
ε_c	Critical strain
ε_f	Monotonic fracture ductility
ε_f'	Fatigue ductility coefficient
ε_{pl}	Plastic strain
$\Delta\varepsilon_e$	Elastic strain range
$\Delta\varepsilon_p$	Plastic strain range
$\Delta\varepsilon_t=\Delta\varepsilon_e+\Delta\varepsilon_p$	Total strain range
θ	Angular coordinate at the crack tip
θ'	Angle between the tangents at the deformed and undeformed beam
λ	Arad's parameter = $K_{max}^2-K_{min}^2$
λ_{th}	Threshold value of λ for crack propagation
ν	Poisson's ratio
σ	Applied stress level
σ_a	Range of applied stress
σ_c	Critical stress for fracture
σ_f	Gross fracture strength
σ_{eq}	Equivalent plastic stress
σ_o	Local stress
σ_{net}	Net stress

σ_b, σ_t	Stress ranges due to bending and torsion respectively
σ_{fb}, σ_{ft}	Fatigue limits in bending and torsion respectively
$\sigma_{max}, \sigma_m, \sigma_{min}$	Maximum, mean and minimum values of the applied stress in the loading cycle
σ_{ys}	Yield stress
σ_{UTS}	Ultimate tensile stress
$\sigma_{flow} = (\sigma_{ys}+\sigma_{UTS})/2$	Mean flow stress
$\sigma_{pl}=\sigma-\sigma_{ys}$	Plastic (non-linear elastic) stress
σ_{xx}, σ_{yy}	Normal stresses in the x and y directions
τ_{xy}	Shear stress in the x-y plane
τ_{xy}^{el}	Linear elastic shear stress
τ_{xy}^{pl}	Plastic (non-linear elastic) shear stress
ψ	Incubation time parameter
Φ	Proposed crack growth rate parameter $= \frac{\lambda - \lambda_{th}}{K_c^2 - K_{max}^2}$

Abbreviations

ASME	American Society of Mechanical Engineers
ASTM	American Society for Testing and Materials
BSC	British Steel Corporation
BISRA	British Iron and Steel Research Association
COD	Crack opening displacement
LEFM	Linear elastic fracture mechanics
NACE	National Association of Corrosion Engineers
NASA	National Aeronautics and Space Administration
NEL	National Engineering Laboratory
NRL	Naval Research Laboratory

PSB	Persistent slip bands
SCC	Stress corrosion cracking
STP	Special technical publications
TTF	Time to failure

LIST OF TABLES

		Page
TABLE 1	Composition and Mechanical Properties of the Materials	192
TABLE 2	Fracture Toughness Data for RR58 and LM30 (DCB Specimen - 9.5 mm thickness)	193
TABLE 3	Cyclic Crack Growth Data for RR58 in Laboratory Air and 3.5% NaCl at a Frequency of 0.15 Hz	194
TABLE 4	Cyclic Crack Growth Data for RR58 at a Frequency of 35Hz	198
TABLE 5	Cyclic Crack Growth Data for BS15 at a Frequency of 35Hz	201
TABLE 6	Cyclic Crack Growth Data for BS15 at a Frequency of 0.25Hz	204
TABLE 7	Cyclic Crack Growth Data for LM30 at a Frequency of 0.25Hz	207
TABLE 8	Fatigue Crack Growth Threshold Data	209
TABLE 9	Values of the Constants α and A_c in the Equation $\frac{da}{dN} = A_c \phi^{\alpha}$	210
TABLE 10	Stress Corrosion Data for RR58 (Horizontal Specimen Orientation)	211
TABLE 11	Stress Corrosion Data for RR58 (Vertical Specimen Orientation)	213
TABLE 12	Stress Corrosion Data for LM30	214
TABLE 13	Theoretical and Experimental Deflection Values (DCB Specimen - BS15) Monotonic Loading, P = 5.5kN	214
TABLE 14	Theoretical and Experimental Data for Load Cycling - DCB Specimen. BS15	215
TABLE 15	Theoretical and Experimental Data for Load Cycling - DCB Specimen.BS15	217

LIST OF FIGURES

		Page
FIG. 1	Sketch Showing the Formation of a Fatigue Striation	219
FIG. 2	A Typical Fatigue Crack Propagation Curve Showing the Environmental Effect	220
FIG. 3	The Alternating and Pulsating Plastic Zones Considered by Raju (105)	220
FIG. 4	The Directions in a Plate Material of a High Strength Aluminium Alloy	221
FIG. 5	The Delay and Transient Acceleration Phenomena	221
FIG. 6	The Contoured DCB Specimen Used in the Experimental Programme	222
FIG. 7	Typical Load vs. Deflection at the Loading Points Record, RR58 and LM30, Laboratory air	223
FIG. 8	Typical Compliance vs. Crack Growth Curve. RR58. Laboratory air.	224
FIG. 9	Typical Compliance vs. Crack Growth Curve. LM30. Laboratory air	225
FIG. 10	Loading and Drip Feed Arrangement	226
FIG. 11	Typical Compliance vs. Crack Growth Curve. BS15, Laboratory air	227
FIG. 12	Crack Growth Pattern at Different Values of ΔK for R = 0. RR58. Laboratory air. 0.15 Hz	228
FIG. 13	Crack Growth Pattern at Different low ΔK. RR58. Laboratory air. 0.15Hz	229
FIG. 14	Crack Growth Rate vs. ΔK. RR58. Laboratory air. 0.15 Hz	230
FIG. 15	Crack Growth Pattern at a Constant Value of K_m = 12.1 $MN/m^{3/2}$. RR58. Laboratory air. 0.15 Hz	231
FIG. 16	Crack Growth Pattern at a Constant Value of ΔK = 8$MN/m^{3/2}$. RR58. Laboratory air. 0.15 Hz.	231
FIG. 17	Crack Growth Pattern at a Constant Value of K_m = 12.1 $MN/m^{3/2}$, RR58. Laboratory air. 35 Hz.	232
FIG. 18	Crack Growth Pattern at a Constant Value of ΔK=5.5$MN/m^{3/2}$. RR58. Laboratory air and 3.5% NaCl. 35 Hz	233

Page

FIG. 19 Crack Growth Rate vs. ΔK, RR58. Laboratory air and 3.5% NaCl, 35 Hz 234

FIG. 20 Macroscopic Fracture Surface Appearance of the DCB Specimens 235

FIG. 21 Crack Growth Pattern at Different Values of ΔK for R = 0. RR58. Laboratory air and 3.5% NaCl. 0.15 Hz 236

FIG. 22 Crack Growth Pattern at a Constant Value of $K_m = 8.25 MN/m^{3/2}$. RR58. Laboratory air and 3.5% NaCl. 0.15 Hz 237

FIG. 23 Crack Growth Pattern at a Constant Value of $\Delta K = 5.5 MN/m^{3/2}$. RR58. Laboratory air and 3.5% NaCl. 0.15 Hz 237

FIG. 24 Crack Growth Rate vs. ΔK. RR58. 3.5% NaCl. 0.15 Hz 238

FIG. 25 Crack Growth Pattern at a Constant Value of $K_m = 31.6\ MN/m^{3/2}$. BS15. Laboratory air. 0.25 and 35 Hz 239

FIG. 26 Crack Growth Rate vs. ΔK. BS15. Laboratory air. 0.25 and 35 Hz 240

FIG. 27 Crack Growth Rate vs. ΔK. BS15. 3.5% NaCl. 35 Hz 241

FIG. 28 Crack Growth Curves Showing Crack Arrest. R = 0. BS15. 3.5% NaCl. 0.25 Hz 242

FIG. 29 Time for Crack Arrest vs. ΔK. BS15. 3.5% NaCl. 0.25 Hz 243

FIG. 30 Time for Crack Arrest vs. Crack Growth Rate for an Initially Sharp Crack. BS15. 3.5% NaCl. 0.25 Hz 244

FIG. 31 Crack Growth Curves Showing Crack Arrest and Continous Propagation, BS15. 3.5% NaCl. 0.25 Hz 245

FIG. 32 Crack Growth Rate vs. ΔK. BS15. Laboratory air and 3.5% NaCl. 0.25 Hz 246

FIG. 33 Crack Growth Rate vs. ΔK. LM30. Laboratory air and 3.5% NaCl. 0.25 Hz 247

FIG. 34 Threshold Value of ΔK vs. K_m. RR58 and LM30. Laboratory air and 3.5% NaCl. 0.15, 0.25 and 35 Hz 247

FIG. 35 $\Delta K_{th}/E$ vs. R. RR58 and LM30. Laboratory air and 3.5% NaCl. 0.15, 0.25 and 35 Hz 249

Page

FIG. 36 Threshold Value of ΔK vs. K_m, BS15 and Other Steels, Laboratory air 249

FIG. 37 $\Delta K_{th}/E$ vs. R, BS15 and Other Steels, Laboratory air 249

FIG. 38 Crack Growth Rate vs. ΔK Curves, RR58, Laboratory air and 3.5% NaCl, 0.25 Hz 250

FIG. 39 Crack Growth Rate vs. ΔK Curves. RR58 Laboratory air. 0.25 and 35 Hz 251

FIG. 40 Theoretical Lines of $(da/dN)/\beta'$ vs. ΔK for a Value of $n_i=1$ 252

FIG. 41 Crack Growth Rate vs. $\lambda = 2\Delta K K_m$. RR58. Laboratory air. 0.15 Hz 253

FIG. 42 Crack Growth Rate vs. $\lambda = 2\Delta K K_m$. BS15. Laboratory air. 0.25 and 35 Hz 254

FIG. 43 Crack Growth Rate vs. $\lambda = 2\Delta K K_m$. LM30. Laboratory air. 0.25 Hz 255

FIG. 44 Crack Growth Rate vs. $\Phi = \frac{\lambda - \lambda_{th}}{K_c^2 - K_{max}^2}$ 256

RR58, Laboratory air and 3.5% NaCl. 0.15 Hz

FIG. 45 Crack Growth Rate vs. $\Phi = \frac{\lambda - \lambda_{th}}{K_c^2 - K_{max}^2}$ 257

RR58, Laboratory air and 3.5% NaCl. 35 Hz

FIG. 46 Crack Growth Rate vs. $\Phi = \frac{\lambda - \lambda_{th}}{K_c^2 - K_{max}^2}$ 258

LM30, Laboratory air. 0.25 Hz

FIG. 47 Crack Growth Rate vs. $\Phi = \frac{\lambda - \lambda_{th}}{K_c^2 - K_{max}^2}$ 259

LM30. 3.5% NaCl. 0.25Hz.

FIG. 48 Crack Growth Rate vs. $\Phi = \frac{\lambda - \lambda_{th}}{K_c^2 - K_{max}^2}$ 260

BS15. Laboratory air. 0.25 and 35 Hz

FIG. 49 Crack Growth Rate vs. $\Phi = \frac{\lambda - \lambda_{th}}{K_c^2 - K_{max}^2}$ 261

BS15, 3.5% NaCl. 0.25 and 35 Hz

FIG. 50 Crack Growth Rate vs. $\Phi = \frac{\lambda - \lambda_{th}}{K_c^2 - K_{max}^2}$ 262

Mild Steel (94). Laboratory air

FIG. 51 Crack Growth Rate vs. $\Phi = \frac{\lambda - \lambda_{th}}{K_c^2 - K_{max}^2}$ 263

		Page
	Cold Rolled Mild Steel (95). Laboratory air	
FIG. 52	Crack Growth Rate vs. $\Phi = \frac{\lambda-\lambda_{th}}{K_c^2-K_{max}^2}$	264
	ASTM A533 B-1 Steel (96). Laboratory air	
FIG. 53	Crack Growth Rate vs. $\Phi = \frac{\lambda-\lambda_{th}}{K_c^2-K_{max}^2}$	265
	EN3A Mild Steel (97). Laboratory air	
FIG. 54	Number of Cycles to Failure vs. Initial Crack Length. R=O. BS15. Laboratory air. 0.25 and 35 Hz	266
FIG. 55	Two of the Stress Corrosion Rigs Used in the Experimental Programme	267
FIG. 56	A Typical Deflection at the Loading Points vs. Time Curve. RR58. 3.5% NaCl	268
FIG. 57	Deflection at the Loading Points vs. Time Curves Showing the Effect of Loading History. RR58. 3.5% NaCl	269
FIG. 58	Deflection at the Loading Points vs. Time Curves for Increasing Values of K. RR58. 3.5% NaCl	269
FIG. 59	Crack Growth Rate vs. K. for the Horizontal and Vertical Specimen Orientation. RR58. 3.5% NaCl	270
FIG. 60	Deflection at the Loading Points vs. Time Curves for Increasing K Values. LM30. 3.5% NaCl	271
FIG. 61	Crack Growth Rate vs. K. LM30. 3.5% NaCl.	272
FIG. 62	Incubation Time vs. ψ. RR58 and LM30. 3.5% NaCl	273
FIG. 63	Ratio K_s/K_c vs. the Incubation Time. RR58 and LM30. 3.5% NaCl	274
FIG. 64	Crack Growth Rate vs. K. RR58, LM30 and other 2000Series Aluminium Alloys. 3.5% NaCl	275
FIG. 65	The Energy Definition of the J Contour Integral for Monotonic Loading	276
FIG. 66	Specimen Geometry Used in the Theoretical Analysis	276
FIG. 67	Variation of the Yield Load with Crack Length. BS15. DCB Specimen.	277
FIG. 68	Variation of the Maximum Bending Stress with Crack Length for	277

Page

Different Load Values, BS15, DCB Specimen

FIG. 69 Theoretical Load-Total Deflection Curves, for Monotonic Loading at P=6kN. BS15, DCB Specimen. 278

FIG. 70 Theoretical Load-Total Deflection Curves for Monotonic Loading at P=7.0kN and Experimental Load Deflection Loops at ΔP = 5.5 kN, BS15. DCB Specimen 278

FIG. 71a Potential Energy vs. Crack Length P= 4.5, 5.0 and 5.5 kN. BS15, DCB Specimen 279

FIG. 71b Potential Energy vs. Crack Length. P=6.0 and 7.0 kN. BS15. DCB Specimen 280

FIG. 72 J vs. Crack Length. BS15. DCB Specimen 281

FIG. 73 The Compact Tension Specimen Used in the Experimental Programme. BS15 282

FIG. 74 J. vs. Crack Extension Curve (R-Curve). BS15 283

FIG. 75 Operational Definitions of Cyclic ΔG and ΔJ after N loading Cycles 284

FIG. 76 Total Deflection vs. Crack Length. ΔP = 4.5 and 5.0 kN. BS15, DCB Specimen 285

FIG. 77 Total Deflection vs. Crack Length. ΔP= 5.5, 6.0 and 6.5 kN. BS15, DCB Specimen 286

FIG. 78 ΔJ vs. Crack Length. ΔP=5.0 kN. BS15. DCB Specimen 287

FIG. 79 ΔJ vs. Crack Length. ΔP= 5.5, 6.0 and 6.5 kN. BS15. DCB Specimen 287

FIG. 80 View of one of the Specimens in a Load Cycling Test 288

FIG. 81 Total Cyclic Creep Strain vs. Number of Cycles. BS15 289

FIG. 82 Experimental Load - Deflection Loops. ΔP = 5.0 kN. BS15. DCB Specimen 290

FIG. 83 Crack Growth Pattern for Load Cycling, BS15 291

FIG. 84 Crack Growth Pattern for Load Cycling, BS15 291

FIG. 85 Crack Growth Pattern for Load Cycling, BS15 292

Page

FIG. 86 Total Potential Energy vs. Crack Length, ΔP = 5,0 kN. BS15 293

FIG. 87. Total Potential Energy vs. Crack Length, BS15 294

FIG. 88 CrackGrowth Rate vs. ΔJ, K^2/E, BS15 295

CHAPTER ONE

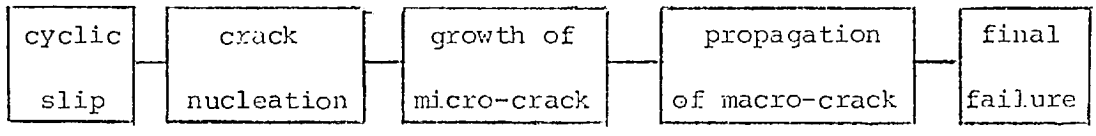
THE FATIGUE FAILURE PHENOMENON IN METALS AND THE ROLE OF FRACTURE MECHANICS

1.1 Definition

Metal fatigue is a failure phenomenon which has been recognised since the middle of the nineteenth century. The first such failures had been reported by that time and the word "fatigue" was then introduced to describe the progressive weakening of a test piece or component subjected to cyclic loading.

1.2 Introduction

With the increasing demand for more efficient and economic components and structures, the number of failures by fatigue has increased considerably and is now by far the most common cause of failure of load-carrying metallic parts operating at or close to room temperature. The fatigue phenomenon arises from the initiation and steady propagation of very small cracks under conditions of fluctuating stress. The fatigue process is now generally considered to be divided into a number of phases.



The first three phases belong to the pre-crack life or crack initiation period. The propagation of the macro-crack belongs to the crack propagation period. In unnotched specimens or components at low applied stress levels, the crack initiation period may cover 80 to 90% of the fatigue life. On the other hand in notched components, and at high applied stress levels, a macro-crack may be visible for say 50% of the fatigue life.

In the next paragraphs a brief review of literature on the mechanisms of crack initiation and the empirical laws of fatigue behaviour will be presented. The application of fracture mechanics to the fatigue crack propagation stage will then be reviewed in more detail.

1.3 Crack Initiation

The onset of damage in a cyclically stressed metal occurs either at the free surface or from an internal defect or flaw. The first condition occurs in polycrystalline ductile metals since a grain having a free surface will be able to deform plastically more easily than one which is surrounded by other grains. If the specimen surfaces are prepared for metallografic observation during a fatigue test it can be seen that early in the specimen life slip lines are formed, forming bands of parallel lines of various heights.

Ewing and Humphrey (1) recognized slip-line development on the surface of a fatigue specimen as early as 1903. Fifty years later Thompson, et al (2) observed what they called persistent slip bands (PSB) from which fatigue cracks grew. The intensive slip process occuring in the persistent slip bands gives rise to the formation of intrusions and extrusions on the specimen surfaces of various ductile metals, as recognised by Stubbington and Forsyth (3) on copper and nickel and Klesnil and Lukas (4) on steels. Crack initiation may also occur in other regions of strain localisation and is accompanied by changes in mechanical properties, lattice-defect concentration and distribution, and may lead to other structural changes such as polygonisation, recrystallisation etc.

Plumbridge and Ryder (5) and Grosskreutz (6) published to date the two more elaborate reviews in fatigue crack initiation. They conclude that crack initiation process in pure, single phase materials differs fromthat in polyphase materials. Hence in the first case slip band

initiation is very common, especially on the slip planes with the highest resolved shear stress (6). The slip band has at its surface a notch-peak geometry giving the characteristic intrusion and extrusion aspect. The slip bands are soft compared with the matrix and have a dislocation cell structure (4). Cottrell (7) has shown that slip band extrusions are produced when the soft material in the slip bands is "squeezed out" at the surface by the harder regions which surround it. In Lynch's work (8) a complete diagrammatic summary of the most important features of slip band extrusion and intrusion can be seen. The details of slip band formation depend on the material, stress, environment, etc. but some of the most important factors will be mentioned next.

The soft layers are usually regions of microstructural change induced by local cyclic shear. The cyclic stressing may remove strenghtening components within the persistent slip bands and make them softer than the surrounding matrix. In low-amplitude fatigue stressing (number of cycles to failure, N_f greater than 10^6) the cracks often initiate from intrusions and propagate through the slip bands. According to Wood (9) the process starts with subsurface pores which are surface-connected. Dover and Jones (10) have observed that the crack-tip regions are very irregular, consisting of a series of tubular holes extending to different depths into the PSB. Cross-slip is required for the formation of the slip bands, but it seems that it is also important that two slip systems should operate in the primary slip plane (6). The dislocation mechanisms of slip band crack initiation are not clear, despite the large amount of research on the subject. A short review is presented in (6). The effect of the environment in slip band formation and the initiation of fatigue cracks can be appreciable, and will be referred to in paragraph 1.5.2.

At high strain amplitudes corresponding to the early part of the S-N curve ($N_f < 10^5$ cycles) the initiation of fatigue cracks often occurs at grain boundaries. In this regime the intrusion mechanism described in (8)

may be opperative. Wood (9) proposed a mechanism to describe high strain fatigue crack initiation consisting of the formation of "micro-cracks". These are created by the multiplication of cavities formed by the coalescence of pores which appear early in the fatigue life (1/200th of the specimen life) at grain subboundaries. It should be pointed out that this mechanism is similar to the one described for low-amplitude fatigue, with the difference that in low-amplitude fatigue,the pores are formed in the slip bands which are concentrated in the grains. Under large strain amplitude the slip bands fill the entire surface of a grain giving a uniform deformation.

The crack initiation sites in single-phase materials have been briefly mentioned. They are slip band and grain boundary initiation. In polyphase materials such as aluminium alloy, titanium alloys and alloy steels, which are commercially important materials, the crack initiation mechanisms may also be derived from slip band and twin boundary initiation. However two important mechanisms are unique to polyphase alloys and occur in a large number of engineering materials. The first occurs mainly in high purity Al-Cu and Al-Cu-Mg alloys. Forsyth (11) has observed that in these materials the PSB are thin layers in which re-solution of precipitaties has occurred. Lynch (12) noted that the repeated to-and-fro motion of dislocations in fatigue will probably reduce the average precipitate size so that the second phase reverts into solid solution in the PSB, which contains a high dislocation density and a slightly lower than normal density of precipitaties already present before fatigue. The reversion of the precipitate softens the material by creating a fine sub-grain structure. The fatigue cracks are then initiated by a mechanism of intrusion when the thin layers are sucked in during tensile deformation and are not subsequently squeezed out again during unloading and reversal of stress (8).

The second mechanism is the most common for crack initiation in

engineering alloys. The crack initiates in the occasional particle which intersects the surface. These particles may be undissolved second phases (inclusions) and impurities. The cracks may initiate at the matrix-inclusion interface or from a crack within an inclusion. Inclusion cracking was observed by Pearson (13) in the aluminium alloys BS L65 and DTD 5050. Grosskreutz and Shaw (14) reported that cracks initiated at inclusion "clusters", zones of several undissolved second-phase particles in which phase boundaries can be distinguished. Hence inclusion cracking may occur in the weak boundaries between these second-phase particles. The cracking at the matrix-inclusion interface might be due to interface debounding (14). Crack initiation at inclusions has also been observed in mild steel by Yokobori et al (15) and in steel 35CD and Al-alloy 26ST by Delange (16), the latter using the plastic replica method.

As a final comment to the crack initiation problem it should be pointed out that the detailed mechanisms for crack initiation are not completely understood. However, the sites at which fatigue cracks initiate are identifiable and favourable conditions for these sites are well defined. It is clear that one single mechanism cannot explain the crack initiation phenomenon. A promising approach has been followed in (9) in relating the microstructural study of crack initiation to the different zones in the S-N curve. The effect of inclusion size in the crack initiation period in engineeering alloys is not yet completely understood. Quantitative theories for predicting the crack initiation time for each major initiation mechanism have not yet been put forward. Such a theory should take into account both microscopic and macroscopic aspects of the fatigue crack initiation.

1.4 Empirical Laws of Fatigue Behaviour

1.4.1 The S-N Curve

Over a hundred years ago Wohler (17) published the results of his

classical experiments on fatigue. He carried out the first fatigue tests on metallic specimens in which the magnitude of the applied loads could actually be measured. He concluded that the range of applied stress determined the life or fatigue strength of the specimen, and his results were plotted as range of applied stress, S against number of cycles to failure, N_f. This well known S-N curve is still one of the basic tools for fatigue design and interpretation of data. Since the Wohler days comprehensive collections of data on fatigue strengths of many metals and alloys have been assembled (e.g. by Cazaud (18) and Forrest (19)).

There are two basic types of S-N curves. All materials show failure at a larger number of applied load cycles as stress amplitude is reduced, but for materials such as mild steel there is a stress below which fatigue failure never occurs. This stress is called the fatigue limit. The S-N curves for other materials continue to fall indefinitely and so an arbitrary life of 10^8 cycles is chosen for their comparison. Wilson (20) has proposed that the presence of a fatigue limit may be due to the capability of the material to strain-age. Hence this behaviour is expected to occur in low carbon, low alloy steels and in a few aluminium alloys.

The ratio between the fatigue limits and the ultimate tensile stress, σ_{UTS} was the first empirical measure of fatigue behaviour. It gives only a rough correlation and it is called the fatigue ratio. The fatigue ratio for steels lies in the range of 0.4 to 0.6 and for aluminium alloys 0.25 to 0.5. Since the amount of scatter is usually large the lower, conservative figures should be taken.

Many attempts have been made to express the shape of the S-N curve in a mathematical form. One of the earliest equations is the Basquin relation (21).

$$\sigma_a^{\gamma} N_f = \text{const.} \qquad (1.1)$$

where $\pm\sigma_a$ is the stress range (zero mean load) and γ is a constant. The

above equation is applicable only to elastic macroscopic behaviour and within the steeply falling initial region of the S-N curve. Frost (22) compiled other more recent and elaborate equations for elastic loading conditions, capable of predicting the entire S-N curve.

1.4.2 The Effect of Mean Stress

If the mean stress σ_m applied to a specimen in addition to a given alternating stress varies from zero, the stress amplitude σ_a to cause failure in N_f cycles varies with it. Goodman (23) derived one of the earliest equations to predict the mean stress effect.

$$\sigma_a = \sigma_f\left(1 - \frac{\sigma_m}{\sigma_{UTS}}\right) \qquad (1.2)$$

where σ_f is the fatigue limit or the fatigue strength at 10^8 cycles. The above equation gives a linear relationship between σ_a and σ_m. The Gerber parabola (24) is another well known relation

$$\sigma_a = \sigma_f\left(1 - \left(\frac{\sigma_m}{\sigma_{UTS}}\right)^2\right) \qquad (1.3)$$

A more conservative design approach has been suggested by Soderberg. The maximum possible value of mean stress was taken as the yield stress, σ_{ys}, of the material. The Soderberg equation substitutes σ_{ys} for σ_{UTS} in equation (1.2). All the above relations can be written in a dimensionless form as

$$\frac{\sigma_a}{\sigma_f} = 1 - \left(\frac{\sigma_m}{\sigma_t}\right) \qquad (1.4)$$

with n=1 for the Goodman equation, n = 2 for the Gerber equation and $\sigma_t = \sigma_{ys}$ in the Soderberg modification. The above relation is often referred to as the R-M relation since it shows the relationship between the safe range of stress R and the mean stress M. More recent relationships predicting the mean stress effect may be found in the Heywood (25) work on fatigue design.

Data obtained on wrought ductile metallic alloys (steels, aluminium alloys, brass etc.) subjected to tensile mean stresses fall between the Goodman and Gerber lines (19). The relative merits of the above equations in predicting the trends in the experimental data are extensively discussed in (19) and (22).

1.4.3 Fatigue Under Varying Stress Amplitude; Cumulative Damage

The laws presented in the previous paragraphs refer to fatigue under constant stress amplitude. In practice most components are subjected in service to cyclic loadings of varying amplitude with the variation in stress level following either a regular or random pattern. A method for predicting life under such conditions is necessary. Fatigue under varying stress amplitude is known as cumulative damage.

The simplest empirical law for predicting cumulative damage is Miner's rule (26). Miner suggested that if cyclic stressing occurs at a series of stress amplitudes σ_{a1}, σ_{a2}, σ_{a3}.... which correspond to failure lifes of N_{f1}, N_{f2}, N_{f3}.... and the actual number of cycles at σ_{a1}, σ_{a2}, σ_{a3}..... is N_1, N_2, N_3..... then the damage will accumulate in such a way that

$$\frac{N_1}{N_{f1}} + \frac{N_2}{N_{f2}} + \frac{N_3}{N_{f3}} + \ldots\ldots = \sum_i \frac{N_i}{N_{fi}} = 1 \qquad (1.5)$$

However the results of cumulative damage tests often do not follow the linear damage law even in simple two level step tests.

The Miner rule used with correct forms of data and some engineering judgement may give a conservative design. The inaccuracy of this rule led to other methods for predicting life under varying stress amplitudes, including random loading. Much detailed design and research work is carried in these areas (22) which involve programme loading to simulate service conditions. The random loading is analysed using probability distributions.

1.4.4 Influence of Stress Concentrations

The presence of a stress concentration such as a fillet, a hole or an external groove or notch changes the fatigue behaviour of a specimen or component. For the same material and testing conditions the S-N curve for a notched specimen normally lies below that for a plain specimen. The ratio of the plain fatigue limit to the corresponding notched fatigue limit is called the fatigue-strength reduction factor, K_f. The conventional notched fatigue limits of some materials are greater than, and for others equal to or less than the corresponding plain fatigue limits divided by the elastic stress concentration factor K_t. Values of K_t for a wide variety of notch profiles loaded in tension, bending and torsion were collected by Peterson (27). A notch sensitivity factor q was defined as

$$q = \frac{K_f - 1}{K_t - 1} \qquad (1.6)$$

when $K_f = K_t$, $q = 1$ and the material is said to be fully notch sensitive; if $K_f = 1$, $q = 0$ and the material is said to be fully notch insensitive.

It has been suggested that q is a material constant, but from the experimental data in the literature it is clear that q depends on the material, specimen size and notch geometry.

Some other parameters must be taken into account when studying the stress concentration effect on fatigue behaviour. For example the material at a notch root may be subjected to a biaxial stress system even in a uniaxially loaded specimen. The effect of the stress gradient at the notch root is also important. The theoretical elastic stress distribution around a notch implies that the maximum stress occurs only at a point or line on the notch surface. For real materials this is not true because the subdivision of the material can not be carried out indefinitely. Neuber (28) has proposed an elementary structural unit measured from the notch root on the plane of minimum cross-sectional area where the average cyclic stress

must exceed the plain fatigue limit of the material before cracking can occur. A relationship between K_f and K_t was derived and by comparison with zero-mean-load fatigue data the sizes of the structural units were established for different materials.

Another important factor is the plasticity effect. If plastic deformation occurs at the notch root, as it may with a sharp root radius, the elastic stress concentration analysis is no longer applicable. The effect of plastic deformation in notches will be briefly discussed in the paragraph concerned with low-cycle fatigue.

Frost and Greenan (29) observed non-propagating cracks in wholly elastic notched specimens in a wide variety of materials. Frost (30) presented results for reversed direct-stress fatigue tests on notched specimens of different materials and for different values of K_t. These showed that below a certain K_t value the nominal stress for crack initiation is higher than the minimum propagation stress, and hence cracks will grow until complete failure. Above this K_t value the minimum propagation stress remains constant and independent of K_t, and the stress necessary to initiate a non-propagating crack is lower than the crack propagation stress, and higher than the plain fatigue limit divided by K_t. Frost's criteria for crack propagation in notched plates containing edge cracks (29) is such that the crack will grow if $\sigma_a^3 a > C_o$, where a is the edge crack length and C_o is a constant. If $\sigma_a^3 a < C_o$ the crack will not propagate. Frost and Greenan (31) verified that the constant C_o depended on the material and on the applied mean stress, reaching a minimum value above a certain value of σ_m/σ_a.

Recent work by Clark (32) and Barson and McNicol (33) conducted on notched steel specimens with different notch root radii showed the applicability of linear elastic fracture mechanics (LEFM) concepts (Appendix A) to the crack initiation problem. The number of cycles required for crack initi-

ation was related to the ratio $\Delta K/\sqrt{\rho}$ (32) where ΔK is the range of the stress intensity factor in the loading cycle (Appendix A) and ρ is the radius of curvature at the notch root. For crack initiation to occur both $\Delta K/\sqrt{\rho}$ and the maximum stress at the notch root σ_{max} must exceed a certain value (32,33). However the correlation with σ_{max} seems rather fortuitous because σ_{max} was obtained from a linear elastic stress analysis and the calculated σ_{max} greatly exceeded the yield stress of the material.

1.4.5 Influence of Complex Stress Systems

So far, discussion of the fatigue limit (or strength at long endurances) phenomenon has been restricted to specimens subjected to uniaxial cyclic loading. In many practical applications the components are stressed under biaxial stress systems such as combined bending and torsion, biaxial tension, biaxial bending, etc.

Most data relating to combined stresses have been obtained for combined bending and torsion. None of the usual theories of failure under combined stresses (Von Mises, maximum shear stress etc.) were found to represent all the results. The experimental results (19) could be represented by an ellipse gradient having as end points the fatigue limits in pure torsion and pure bending. The ellipse equation was

$$\frac{\sigma_b^2}{\sigma_{fb}^2} + \frac{\sigma_t^2}{\sigma_{ft}^2} = 1 \qquad (1.7)$$

where σ_{fb} and σ_{ft} are the fatigue limits in pure bending and torsion respectively, and σ_b and σ_t are the stress ranges due to bending and torsion respectively at the fatigue limit under combined stress loading. For brittle and notched specimens an ellipse arc given by

$$\frac{\sigma_t^2}{\sigma_{ft}^2} + \frac{\sigma_b^2}{\sigma_{fb}^2}\left(\frac{\sigma_{fb}}{\sigma_{ft}} - 1\right) + \frac{\sigma_b}{\sigma_{fb}}\left(2 - \frac{\sigma_{fb}}{\sigma_{ft}}\right) = 1 \qquad (1.8)$$

described the results better.

The effect of combined stresses on notched specimens is more complicated and less work has been published in this field. Some references may be found in (22).

1.4.6 Low-cycle Fatigue

The empirical laws for the fatigue limit or fatigue strength at long endurances have been presented in the previous sections. However some components may be designed for a finite life. This is particularly relevant when the frequency of load application is relatively small. Thus a knowledge of the life that may be expected from a specimen tested at a stress level greater than the fatigue limit is necessary. The region covering lives of components or specimens of up to about 10^5 cycles is known as low-endurance or low-cycle fatigue.

When a specimen is tested at stress levels above the fatigue limit gross plastic deformation usually occurs. A low-cycle fatigue failure may be achieved either with cycles of constant strain amplitude (strain-cycling) or with cycles of constant load amplitude (load-cycling).

(A) Strain Cycling

Constant strain amplitude tests may be performed either keeping the total strain range or the plastic strain range constant.

Benham (34) carried out early work in constant total strain amplitude tests on a wide range of materials and showed that the results can be represented by an equation of the type

$$\Delta\varepsilon_t N_f^{m_1} = C' \qquad (1.9)$$

where $\Delta\varepsilon_t$ is the total strain range, and C' and m_1 are material constants.

Manson (35) has shown that the resistance of a metal to total strain cycling can be considered as the summation of its plastic and elastic strain resistance. Thus

$$\Delta\varepsilon_t = \Delta\varepsilon_p + \Delta\varepsilon_e \qquad (1.10)$$

where $\Delta\varepsilon_p$ and $\Delta\varepsilon_e$ are the plastic and elastic strain ranges respectively. Since cyclic plastic strain is largely responsible for fatigue damage, the study of this variable will lead to a more important data correlation than the use of the total strain amplitude - despite the fact that for design purposes only the latter may be known.

Constant plastic strain amplitude data may be obtained either directly, from tests in which the hysteresis loop width is maintained constant, or from strain range tests, by subtracting the elastic strain range from the total strain range. Coffin (36) found that the plastic strain amplitude $\Delta\varepsilon_p/2$ was related to N_f in the form

$$\Delta\varepsilon_p/2 = \varepsilon_f' (2N_f)^c \qquad (1.11)$$

where ε_f', the fatigue ductility coefficient, is the plastic strain intercept at the first reversal ($2N_f = 1$), and c, the fatigue ductility exponent, is the slope of the logarithmic plastic strain amplitude-life plot. ε_f' may be related with the monotonic fracture ductility ε_f. Landgraf (37) has obtained some correlations among these variables. For the majority of metals $\varepsilon_f' = \varepsilon_f$ is a reasonably good approximation and the value of c ranges from -0.5 to -0.8 (37).

The response of metals when subjected to constant cyclic plastic strains may vary. Thus, generally in annealed metals the stress range initially increases with time, while some cold-worked materials may exhibit the opposite behaviour. The first phenomenon is called cyclic work-hardening and the second cyclic work-softening. After some time, however, a stable hysteresis loop is formed until crack initiation occurs. If the tips of stable hysteresis loops for specimens tested at different strain

amplitudes are connected, a curve called the cyclic stress-strain curve is obtained. For cyclic work-hardening materials the cyclic stress-strain curves lie above, and for cyclic work-softening materials below the monotonic stress-strain curves.

Morrow (38) expressed the cyclic stress-strain curve by a relationship of the form

$$\sigma_a = K'(\Delta\varepsilon_p/2)^{n'} \qquad (1.12)$$

where K' and n' are the cyclic strength coefficient and cyclic strain hardening exponent respectively. Through an energy argument it is possible to relate n' with the slope of the logarithmic stress amplitude-life plot and with the fatigue ductility exponent (38). The same author attempted to relate the cyclic plastic strain energy to the fatigue damage process. The plastic strain energy per cycle and the total plastic strain energy were calculated from the cyclic stress-strain equation and related with the fatigue life. Early work by Benham (39) and Benhan and Ford (40) has shown that for several materials a fundamental relationship exists between the total energy to fracture and the number of cycles to fracture.

In reversed strain cycling both the initial mean stress and the mean strain are zero and remain so throughout the test. However, if the initial mean strain is not zero and the specimen is subjected to a constant amplitude of alternating strain about a non-zero constant mean strain, a phenomenon of cycle-dependent stress relaxation occurs. This consists of the progressive decrease in mean stress with the number of load cycles. Morrow and Sinclair (41) have observed experimentally this relaxation of mean stress, which decreased as the strain amplitude about a constant mean strain was reduced. Assuming a stress-strain relationship they predicted the mean stress relaxation as a function of the strain amplitude and the number of cycles.

(B) Load Cycling

During load cycling large plastic strains may accumulate indefinitely. This phenomenon of plastic strain accumulation is usually described as cyclic creep, and several trends in the macroscopic behaviour have been recognized. This cyclic creep behaviour will be reviewed in some detail, since it was observed and computed in the elastic-plastic load-cycling fatigue crack propagation tests carried out in the present work (Chapter 6). Two important conclusions can be drawn from the relevant literature:

1. When prismatic members are subjected to periodic, uniaxial longitudinal stress σ, they exhibit an increment of permanent axial extensional strain in each cycle (38,40). Feltner and Sinclair (42) have observed that the rate of accumulation increases with the stress amplitude as well as with mean stress. Cyclic creep occurs during the entire life of the specimen and causes a necked-out type of fracture similar to a monotonic tensile failure in a ductile metal.

2. When the accumulated cyclic creep strain is plotted as a function of the number of cycles for different stress levels above the yield point, curves similar in shape to ordinary creep curves are obtained (39,40,42,43). After the initial extension (a short primary stage) during which the specimen hardens rapidly, the cyclic creep rate diminishes to attain a constant value (the secondary stage), and then rises abruptly towards fracture (tertiary stage) (39,40,42).

The secondary cyclic creep covers 80-90% of the specimen life and several relationships have been derived to correlate experimental data. The most successful (42) is a power law relating the cyclic creep strain ε_{cc} with the applied stress σ, in the form

$$\varepsilon_{cc} = C_1 N \sigma^m \qquad (1.13)$$

where C_1 and m are constants to be determined experimentally. If the mean stress is compressive the cyclic creep may be negative (43) and even with

zero mean stress slight cyclic creep occurs (39). When cyclic creep tests are conducted between zero and a maximum nominal stress range the peak value of true stress rises as the specimen extends due to its reduction in area. This effect can result in an apparent rapid increase in the rate of cyclic creep. Radon et al (44) used a true stress limit andreported that the cyclic creep rate decreased and remained constant. Oldroyd and Radon (45) found that the cyclic creep/cycle reached a maximum when the nominal mean stress was 20% of the stress range.

The field of cyclic creep has received comparatively little theoretical attention. Mulgahy (46) derived a plasticity model for cyclic creep under homogeneous plastic deformation but no attempt was made to relate it with experimental data.

A comparison between load and strain cycling conditions was made in (39,40). After the steady cyclic condition had been attained (work-hardening or softening occured)and without cyclic creep effects, close agreement was found between the stress and total energy to fracture against number of cycles curves in load cycling and strain cycling. One is led to conclude that each metal might have a particular cyclic condition achieved whatever the mode of cycling (40).

(C) The Effect of Notches

The influence of stress concentrations or notches on the fatigue limit has been reviewed in paragraph 1.4.4. In low-cycle fatigue plastic deformation often occurs either at the notch root or in the whole specimen. If the notch is sharp the life of the specimen is almost totally spent in crack propagation and will depend on the crack growth rate and the specimen dimensions. Here a fracture mechanics analysis is more appropriate as will be seen later. For cases in which the great majority of the life is spent in crack initiation, the Neuber relationship (47) between stress and strain concentration factors was applied by Topper et al (48) for the determination

of fatigue life of notched specimens. They concluded that

$$K_f^2 \overline{\Delta\sigma}\ \overline{\Delta\varepsilon} E = \Delta\sigma \Delta\varepsilon E \qquad (1.14)$$

where $\overline{\Delta\sigma}$ and $\overline{\Delta\varepsilon}$ are the nominal stress and strain ranges, $\Delta\sigma$ and $\Delta\varepsilon$ are the local stress and strain ranges at the notch root and E is the Young's Modulus. Using Eq. (1.14) it is possible to predict the fatigue life of notched specimens using data from smooth specimens of the same material. Wetzel (49) simulated the notch root stresses and strains in a notched specimen by tests on an unnotched specimen.

Wundt (50) published an extensive literature review on the effect of notches on low-cycle fatigue. It considers the application of the Neuber relationship to low-cycle fatigue, and the Stowell-Hardrath-Ohman equation (51) with its applications for the determination of the load stress-strain curves at the notch root and the stress and strain distributions with the number of cycles. Data on the fatigue strength reduction factors on a strain basis and in bending is also presented. Some criticism has been made in relation to the application of the Neuber and Stowell methods to predict the behaviour of notched specimens from plain specimens. For example data obtained by Bell (52) has shown that none of the prediction methods were satisfactory. Recent work by Mowbray et al (53) seems to indicate that finite element elastic-plastic analysis can accurately compute the notch root strains. Good agreement was found between these computed strains and the experimental values. The Stowell and Neuber formulae were found to overpredict notch root strains at stress levels beyond the initial plastic range. The finite element technique may provide the solution of the stress and strain distributions at the notch root during the fatigue life.

1.5 The Effect of Environment on Fatigue Strength

1.5.1 Phenomenological Trends

The environmental effect on the fatigue strength of specimens and

components is generally known as corrosion fatigue. The phrase implies that the presence of an environment that will chemically attack the material is necessary. In general terms for the same stress amplitude the fatigue strength for a specimen tested in an aggressive environment (water, salt solution etc.) is lower than that measured in air. Since the corrosion fatigue strength decreases continuously with increasing endurance it is often difficult to establish a corrosion fatigue limit. It is more reliable to quote the fatigue strength at a particular endurance. Because corrosive attack is a time dependent phenomenon, the corrosion fatigue strength at a given endurance tends to increase with the testing speed.

The first extensive review on corrosion fatigue was due to Gough (54) in 1932 and the first corrosion fatigue observations were reported by Haigh (55) as early as 1917. Generally metals which have high resistance to chemical attack from a particular corrosive environment exhibit higher corrosion fatigue strengths than those metals having a lower corrosion resistance. The combined actions of stress and corrosive attack enable a microcrack to develop at a lower stress level than in a test in air. In a corrosion fatigue test a much greater proportion of the total life is occupied by macrocrack growth than in a comparative test in air. Indeed it has been experimentally observed that specimens with a larger cross-section have greater fatigue strengths (56). The environmental influence on macrocrack growth will be reviewed later (Paragraph 1.7.5).

The effect of a corrosive environment on fatigue strength is most severe when the specimen is being cyclically stressed with free access from the atmosphere to the specimen surface due to the presence of oxygen. Thus if the corrosive fluid (e.g. salt solution) is dripped slowly on the specimen surface, the fatigue strength is lower than if the specimen is completely immersed in the fluid (54).
The dripping technique was used in the present work because it represents the most destructive conditions. Duquette (57) reviewed the effects of the salt

concentration and temperature on the fatigue strength. The damage tends to increase with the concentration and decrease with temperature.

In sharply notched specimens the cracks form rapidly at the notch root and the specimen life depends largely on the rate of crack growth. Some corrosion fatigue data from notched specimens in brine is presented in (22) and shows a marked decrease in the fatigue strength when compared with tests in air.

1.5.2 The Mechanism of Corrosion Fatigue

The exact mechanisms of corrosion fatigue are not clear since most proposed models fail to account for all the experimental observations reported. It is possible that no single mechanism is responsible for the corrosion fatigue behaviour of all metal/environment systems. Fracture mechanics may be used to describe crack growth in corrosive environments, and was successfully used in the present work to analyse fatigue crack growth data in different metals exposed to a 3.5% NaCl solution. Before the fracture mechanics techniques were available the mechanism or mechanisms of corrosion fatigue were studied by the conventional S-N test.

Early investigators of corrosion fatigue such as McAdam (58) assumed that the cracks were initiated in the bases of large hemispherical pits at the metal surface created by the corrosion process. Cyclic stressing accelerates the corrosion pitting and causes the development of crevices or fissures. McAdam's conclusions were based on the physical examination of broken specimens. However, Duquette (59) argued that the formation of pits is not a requirement for corrosion fatigue. Instead a crack initiation mechanism based on preferential local dissolution of the metal at emerging slip steps was proposed. The dissolution unlocks otherwise blocked slip

processes, accelerating the extrusion-intrusion phenomenon (see 1.3) which results in premature crack nucleation and growth. Crack propagation is accelerated by the corrosion created notch and by the preferential dissolution at the base of the growing crack. This mechanism was found to be operative in low carbon steels. Stubbington and Forsyth (60) performed rotating bending tests in salt spray on both high purity and commercial Al-Zn-Mg alloys and showed that corrosion fatigue cracking was a transcrystalline phenomenon. In the high-purity alloy, cracks developed from corrosion pits within the grains, while the transcrystalline cracks were initiated from intergranular pits in the Al-Zn-Mg alloy. Evans (61) in an electrochemical theory considers the corrosive attack of a specimen in a wet environment as an electrochemical process in which certain areas are anodic with respect to others. The whole surface consists therefore of a series of anodes and cathodes. This division might arise from electrochemical attack at plastically deformed areas in which the non-deformed metal acts as cathode. Based on this theory Whitwham and Evans (62) concluded that the failure process occurs when very fine cracks advanced by a combination of electrochemical-mechanical action. Surface film rupture was proposed by Duquette (57) as the principal mechanism of corrosion fatigue failure. A review of surface film rupture theories may be found in (57), together with theories that support the idea that the corrosion fatigue phenomenon is caused by a lowering of the surface energy of the metal due to absorption by the environment, especially of hydrogen, and the corresponding multiplication of pre-existing microcracks.

1.6 The Crack Propagation Process in Metals

1.6.1 Introduction

In paragraphs 1.2 to 1.5 crack initiation processes, empirical laws of fatigue behaviour and environmental influences on fatigue strength were briefly reviewed. We now reach the stage at which a surface microcrack has

formed and is penetrating the material . It is able to increase its size and grow as a macrocrack, that is, its growth behaviour is dictated by the amount that it opens and closes during the fatigue cycle.

Until recent years the fatigue crack propagation phenomenon has received little attention from scientists and engineers working in the fatigue field. The assessment of design stresses was largely based on the plain fatigue limit of the material obtained in the conventional S-N test. (Paragraphs 1.3 - 1.5). The purpose of this design approach was to prevent the initiation of any cracks. With the need to produce components of complex shape operating under conditions not precisely defined, together with the need for smaller dimensions and lower weight (as in the aircraft industry), has led to the possibility of crack formation in regions of stress discontinuity. The necessity to assume the existance of cracked members in engineering structures is now generally accepted. This knowledge of the crack growth rate characteristics of the material has become important in the design of high performance structures and components. Fatigue crack growth rate data may be used not only for material selection but also to determine inspection intervals. The design goal is to achieve low rates of crack propagation and a high residual static strength in the structure when a crack is present.

In the past twenty years or so the problem of brittle fracture has been studied extensively. Brittle fracture generally occurs in high strength materials (e.g. high strength aluminium alloys and steels), originating at cracks or flaws under nominal stresses below the yield stress of the material. Brittle fracture may also occur in more ductile metals at very low temperatures and/or very thick sections. The linear elastic fracture mechanics (LEFM) approach was developed to study the brittle fracture problem. The stress intensity factor, K, concept was derived to describe the stress field at the crack tip; when K reaches a critical value K_c the crack extends, often catastropically. If fracture occurs with large plastic de-

formations LEFM is no longer valid. The fracture behaviour under elastic-plastic conditions can, however, be explained in terms of the J contour integral and crack opening displacement (COD).

In view of its success in dealing with the static fracture problem it is logical to use Fracture Mechanics to analyse fatigue crack growth data. A review of the relevant definitions, concepts and equations of Fracture Mechanics is presented in Appendix A.

1.6.2 Mechanisms of Crack Propagation

It is now known that crack propagation in fatigue starts from the specimen surface and takes place in two stages (11). The first stage (Stage I) is characterized by propagation of the crack in a slip band. The crack grows along the slip plane with the highest resolved shear stress ($\approx$ 45 deg. to the stress axis) and it normally penetrates only a few tenths of milimeter into the specimen. At a critical crack length the crack turns and propagates along a plane at 90 deg. to the stress axis. This tensile mode is called Stage II propagation, and the change in the crack direction occurs when the local stress concentration at the crack tip reaches a critical value. The lower the stress or strain amplitude the more extensive is the Stage I process and the deeper Stage I cracks penetrate. Fatigue cracks initiating at second-phase particles, inclusions or twin-boundaries also follow the Stage I-II pattern, but the extent of Stage I is usually less. When a crack grows from a notch it usually starts its growth as a Stage II crack.

Because Stage II cracking is more extensive than Stage I, much more work has been done in the tensile mode and the microstructural mechanisms of Stage II are clearer. Laird (63) has suggested that the mechanism of propagation in Stage I is essentially the same as in Stage II, with the softness of the slip bands providing an easy path for crack propagation at 45 deg. to

the stress axis.

In Stage II crack propagation the mechanisms are related to the most pronounced microfracture modes:

1) Ductile striation formation

2) Brittle striation formation

3) Intergranular fracture

4) Clevage-like fracture

5) Stepwise growth

6) Rippled facet fracture

Striationshave been observed by many metallurgical researchers on fatigue crack propagation (63-65) using optical and scanning electron microscopes. Bowles (66) investigated the metal physics aspects of the structure associated with the fatigue crack tip with the transmission electron microscope to detect the local dislocation distribution.

The general characteristics and mechanism of formation of ductile striations have been studied in great detail (63). The mechanism may be as schematically indicated in Fig. 1. In this mechanism crack growth in each cycle occurs as the result of a repetitive process of crack tip blunting followed by resharpening. Crack tip blunting occurs when the load is increasing and resharpening in the unloading stage. Each load excursion is responsible for one striation and the striation spacing increases when both the maximum, K_{max}, and the range, ΔK, of the applied stress intensity factor increase. The ductile striation is characteristic of ductile metals under medium to large fatigue load amplitudes. It has, however, been observed in high strength aluminium alloys as reported by Fenney et al(67). In their extensive study they observed ductile striation formation in aluminium alloys 2024-T3 and 7878-T6 tested in 3.5% NaCl, at high ΔK values. Moreover in 2024-T3 the ductile striation formation was the predominant fracture process at high ΔK levels in four different environments (dry air, wet air, distilled water and 3.5% NaCl solution). The ductile striations

formed in 7178-T6 in 3.5% NaCl were characterized by a small height-to-spacing ratio, suggesting that their formation was strongly enhanced by the environment and accompanied by reduced plastic deformation.

The distinction between ductile and brittle striations was first made in (11). Brittle striations are characteristically brittle in appearance, less regular in spacing than ductile striations and are formed in association with river markings on very flat facets parallel to $\{100\}$ planes, and thus contain an element of cleavage. Ductile striations usually form on plateaus parallel to the general fracture plane and perpendicular to the axis of maximum tensile stress (63). The mechanism of brittle striation formation is not fully understood and is influenced by the chemical composition of the matrix.

Intergranular fracture is a microfracture mode in which the fracture has been observed to propagate along grain boundaries. Lattice irregularities at and near grain boundaries will, in general, have a tendency to make these boundaries weaker than the grain interiors. In addition, grain boundaries are often favourable sites for the segregation of various impurities or alloying elements to form either composition gradient zones or precipitate particles of secondary phases. If the constituent particles are numerous enough or large enough and possess properties that are sufficiently different from the grain interiors, fracture may nucleate and propagate along the grain boundaries to produce intergranular fractures. Intergranular fracture is the common microfracture mode for stress corrosion cracking of high strength aluminium alloys.

The multiplicity of slip systems, high dislocation density, and ease of cross slip are strong reasons against the occurence of cleavage fracture in fCC materials (63). Forsyth (11) has proposed that fatigue crack propagation always contains an element of cleavage.

Stepwise growth is a microfracture mode in which steps are present on the fracture surface, with extremely fine markings running almost perpen-

dicular to each step (11). It is possible that these markings are fine striations and that the steps represent different levels along which the crack propagates. The exact mechanism of stepwise growth is not fully understood.

Rippled facet fracture is a process attributed to wavy slip produced by a sliding-off process, i.e. rupture by alternating shear. Since the absence of oxidation is essential to this reversed slip process this type of fracture is observed in specimens tested in desiccated argon (67).

1.7 Fracture Mechanics Approach to Fatigue Crack Propagation

1.7.1 Introduction

The successful application of LEFM analysis in the description of the brittle fracture behaviour of metals under monotonically increasing loads has led to a logical extension of the same analysis to the study of slow crack growth under both static and fatigue loads, commonly termed subcritical crack growth. Subcritical crack growth covers all processes in which a crack slowly propagates at a K level below the critical value K_c corresponding to unstable and catastrophic failure. These may be stress corrosion cracking (SCC), creep cracking, fatigue crack propagation or any combination of these phenomena. The fracture mechanics approach to SCC in high strength aluminium alloys will be reviewed in Chapter 3. Here only the fracture mechanics approach to fatigue crack propagation will be considered.

It is known that the stress intensity factor K, or the strain energy release rate G, govern the intensity or magnitude of the stress field around the crack tip (Appendix A). Since crack extension occurs in this highly stressed region it is reasonable to assume that the intensity of the crack tip stress field as represented by K should control the rate of crack extension. The cyclic crack growth rate da/dN may be a function of the range of the stress intensity factor, ΔK, in the loading cycle. ΔK is given by

$$\Delta K = K_{max} - K_{min} \qquad (1.15)$$

and

$$K_{max} = \sigma_{max} Y \sqrt{\pi a} \qquad (1.16a) \qquad K_{min} = \sigma_{min} Y \sqrt{\pi a} \qquad (1.16b)$$

where K_{max} and σ_{max} are the maximum stress intensity factor and the maximum gross stress respectively and K_{min} and σ_{min} are the minimum values of the above variables in the loading cycle. Equations (1.16a) and (1.16b) are the general equations for the stress intensity factor under mode I conditions (Appendix A) where a is the crack length and Y is a dimensionless factor, a function of the crack length and specimen geometry.

da/dN will of course be dependent on many other variables, such as environment, frequency, mean stress, loading history etc. The applicability of LEFM to the fatigue crack propagation problem is limited by the amount of plastic deformation in the specimen. The specimen should be under linear elastic stresses and strains apart from the small plastic zone at the crack tip. However there is now some evidence, supported by the present work, that non-linear fracture mechanics (J contour integral) can be successfully used to analyse fatigue crack growth data under elastic-plastic conditions.

1.7.2 Fatigue Crack Growth Theories

Fatigue crack growth theories are now quite numerous. A comprehensive description of the more relevant ones is presented in (22). Early theories did not use fracture mechanics analysis.

The first crack propagation law to draw wide attention was that of Head (68). He employed a mechanical model which considered rigid-plastic work-hardening elements ahead of a crack tip and elastic elements over the remainder of the infinite sheet. The final equation obtained was

$$\frac{da}{dN} = \frac{C_2 \sigma_1^3 a^{3/2}}{(\sigma_{ys}-\sigma) w_o^{1/2}} \tag{1.17}$$

where C_2 is a constant and w_o is the size of the plastic zone near the crack tip (assumed constant during crack propagation). Head's law was later corrected by Paris (69) as

$$\frac{da}{dN} = \frac{C_3 \sigma_1^2 a}{(\sigma_{ys}-\sigma)} \tag{1.18}$$

where C_3 is a constant.

Frost and Dugdale (70) derived an equation using dimensional analysis. The result was

$$\frac{da}{dN} = \frac{\sigma^3 a}{C_4} \tag{1.19}$$

where C_4 is a constant.

The theory of McEvily and Illg (71) assumed the crack growth rate to be a function of the local stress σ_o and the stress σ_{net},

$$\frac{da}{dN} = F(\sigma_o) = F(K_t \sigma_{net}) \tag{1.20}$$

The function F was obtained empirically and the final value of da/dN was

$$\log_{10} \frac{da}{dN} = 0.00509\ K_t \sigma_{net} - 5.472 - \frac{34}{K_t \sigma_{net} - 34} \tag{1.21}$$

Liu (72) has restated Frost and Dugdale's (70) dimensional analysis and obtained the equation

$$\frac{da}{dN} = C_5 \sigma_1^2 a \tag{1.22}$$

where C_5 is a constant.

The first crack propagation law to incorporate the stress intensity factor was the well known Paris' law (69).

$$\frac{da}{dN} = C_6 (\Delta K)^{m_2} \tag{1.23}$$

where C_6 and m_2 are constants. It should be pointed out that using the definition of the stress intensity factor (Eqs.(1.16a,b)and Eq. A5-Appendix A) all the above mentioned laws can be reduced to the Paris' law by choosing appropriate values of the constants. The validity and limitations of the Paris' law will be discussed later.

Dislocation theories have been put forward. One example is that due to Weertman (73), giving a proportionality factor between da/dN and $(\Delta K)^4$.

Energy theories involve the computation of the energy associated with the plastic zone size. Rice (74) stated that the separation of the crack surfaces occurs when the total absorbed hysteresis energy U per unit of newly created surface area equals a postulated critical value U_c. da/dN is then obtained and is again proportional to $(\Delta K)^4$ as in the dislocation theory. The Griffith model (Appendix A) was used by Gallina et al (75) to derive a model of crack propagation. As a crude approximation, all the energy lost per cycle was considered to be expended in increasing the crack size. The energy agreement will be considered again in the discussion of the effect of mean stress on fatigue crack propagation.

Lehr (76) and Schwalbe (77) theories have assumed that crack propagation is caused by cumulative damage due to strain cycling of the material at the crack tip (76) or that a characteristic plastic displacement near the crack tip is equal to the crack propagation during each load cycle (77). In both Refs. (76) and (77) it was found that da/dN was dependent on $(\Delta K)^2$.

Frost and Dixon (78) and Tomkins (79) also obtained a dependence on $(\Delta K)^2$ in which the crack growth was considered to be a geometrical consequence of crack tip deformation, setting the incremental crack growth per cycle equal to the crack opening displacement (COD) (Appendix A). In Schwalbe's work (77) work-hardening in the plastic zone was taken into

account, while in (73-76, 78,79) an ideal plastic material was considered.

1.7.3 Phenomenological Analysis of the Fatigue Crack Propagation Curve

The most common technique for the experimental analysis of the fatigue crack propagation process is to plot da/dN against ΔK. Hahn and Simon (80) carried out a compilation of 22 different investigations of cyclic crack growth in high strength aluminium alloys. In steels extensive work was produced by Frost et al (81) and Crooker and Lange (82), apart from much other published data which will be analysed later in more detail.

Most of the crack propagation curves presented in the literature show three different regions of crack propagation as exemplified in Fig. 2. In Region I, for many materials, it has been shown that there exists a critical range of stress intensity ΔK_{th} below which crack propagation does not occur, or occurs extremely slowly ($da/dN < 10^{-7}$ mm /cycle). In this region da/dN depends strongly on ΔK. Region II is the intermediate region in which Paris' law seems to apply with da/dN depending on some power of ΔK of the order 2 to 10. In Region III da/dN is again strongly dependent on ΔK as K_{max} approaches the fracture toughness, K_c. The curve shown in Fig. 2 corresponds to a high-strength alloy in which subcritical crack growth occurs at K levels below, K_c and hence LEFM analysis is valid. It is known that for ductile metals fatigue crack propagation can occur with large plastic deformations. Fatigue crack growth under extensive plastic deformation is reviewed in 1.7.9.

The fatigue crack propagation curve may be affected by the mean stress, threshold behaviour, loading frequency, environment, and specimen thickness. The effect of these parameters on the crack propagation process will be reviewed in the next paragraphs.

1.7.4 The Effect of Mean Stress on Fatigue Crack Propagation - Crack Growth Laws

The fatigue crack growth theories presented in section 1.7.2 do not take into account the mean stress effect, threshold behaviour or the increase in crack growth rate as K_{max} approaches K_c. When these trends began to be experimentally observed crack growth laws predicting the above phenomena started to appear in the literature. Two recent extensive reviews on the subject are now available: Maddox's literature review on the effect of mean stress on fatigue crack propagation (83) and the compilation work carried out by the ASTM TASK force E 24.04 (84). In this paragraph only the more relevant "laws" will be presented, and will be divided into two categories: semi-empirical, those using fundamental parameters to produce relationships which fit experimental data, and theoretical.

(A) Semi-empirical Relationships

The Forman equation (85) was developed to consider the acceleration of crack growth rate in Region III (Fig. 2). The Forman equation has the form

$$\frac{da}{dN} = \frac{C_7(\Delta K)^{P_1}}{K_c(1-R)-\Delta K} \qquad (1.24)$$

where R is the stress ratio $\frac{\sigma_{min}}{\sigma_{max}} = \frac{K_{min}}{K_{max}}$,

and C_7 and p_1 are constants. The above equation has been extensively compared with crack growth rate data obtained by Hudson (86,87).

Erdogan and Ratwani (88) extended Forman's equation to consider Region I behaviour. The resulting equation was

$$\frac{da}{dN} = \frac{C_8(1+\beta_1)^{P_2}(\Delta K-\Delta K_{th})^{P_3}}{K_c(1+\beta_1)\Delta K} \qquad (1.25)$$

where $\beta_1 = (K_{max} + K_{min})/\Delta K$, and C_8, p_2 and p_3 are constants.

Pearson (89) investigated the effect of mean stress using thick specimens. The value of K_{1c} (Appendix A) was applied instead of K_c. Pearson modified Eq. 1.24 to give

$$\frac{da}{dN} = \frac{C_9 (\Delta K)^{p_4}}{\left[(1-R)K_{1c} - \Delta K\right]^{1/2}} \tag{1.26}$$

where C_9 and p_4 are constants. Equation 1.26 drew attention to the fact that K_{1c} (or K_c) may be a significant variable in fatigue crack propagation.

Recently Chu (90) has developed two equations to describe the stress ratio effect and predict the fatigue crack growth rate in the entire sub-critical range from ΔK_{th} to K_c. The equations are

$$\frac{da}{dN} = \frac{C_{10}(\Delta K^{p_5} - \Delta K_{th}^{p_6})}{\left[(1-R)K_c - \Delta K\right]^{p_7}} \tag{1.27a}$$

and

$$\frac{da}{dN} = \frac{C_{10}(\Delta K - \Delta K_{th})^{p_8}}{\left[(1-R)K_c - \Delta K\right]^{q_o}} \tag{1.27b}$$

where $C_{10}, p_5, p_6, p_7, p_8$ and q_o are constants.

Elber (91) has shown that a fatigue crack can be closed at its tip for a fraction of the loading amplitude. The stresses necessary for crack opening were obtained experimentally (91) and it was assumed that crack propagation can only occur when the crack is fully open. The crack closure phenomenon was attributed to the presence of compressive residual stresses as a result of the zone of tensile yielding (plastic zone) at the crack tip, left in the wake of the propagating crack. Elber measured crack closure stresses for different applied mean stresses and found that the proportion of the stress range during which the crack was open, U, was a linear function of R:

$$U = B_1 + B_2 R \tag{1.28}$$

where B_1 and B_2 are material constants. Thus an effective stress intensity factor ΔK_{ef} was defined as

$$\Delta K_{ef} = U\Delta K \tag{1.29}$$

and the crack growth rate expressed as

$$da/dN = B_3(\Delta K_{ef})^{q_1} = B_3(U\Delta K)^{q_1} \tag{1.30}$$

where B_3 and q_1 are constants. Since U_o increases with the stress ratio Eq. (1.30) is able to explain the increase in crack growth rate with the stress ratio. Elber found data in the literature to support his analysis.

The crack closure approach was also used to explain the experimental results obtained by Katcher and Kaplan (92), especially the existence of an R value called R_{cut} above which da/dN versus ΔK data does not shift to faster rates with increasing stress ratios. The R_{cut} is the R value above which the crack is always open ($U_o = 1$). Hence for $\Delta K > \Delta K_{th}$ and $R > R_{cut}$, ΔK_{ef} is the same irrespective of R and da/dN will no longer depend on R. Using a finite element analysis of an elastic-perfectly plastic material Newman (93) has computed the crack opening stresses under constant amplitude loading and found that agreement with Elber's results (91) was good. The importance of Newman's work (93) should be pointed out since it represents one of the first attempts to apply the finite element analysis to fatigue crack growth. Further research in this area might lead to the exact computation of the stresses and strains at the tip of the propagating crack. It is, however, difficult to believe that a program derived for an elastic-perfectly plastic material could give agreement with experimental results obtained in a real work-hardening material.

All the equations described so far were derived mainly to fit crack growth data in high strength aluminium alloys which are highly sensitive to mean stress.

For steels, in general, fatigue crack propagation is not so sensitive

to mean stress, although there has been some controversy in the literature about this point. It seems that high strength steels are more mean stress dependent than mild steels (82) but some mild and low alloy steels showed a comparatively strong mean stress influence (94-99). This effect will be discussed in more detail in Chapter 2. Barsom (100) has derived an equation to fit crack growth data in steels

$$da/dN = D_1 \Delta G \qquad (1.31)$$

where D_1 is a constant and ΔG is the range of the crack extension force G(Appendix A) in the loading cycle. Further equations predicting the mean stress influence on steels were obtained by Priddle (97) and Klesnil and Lukas (98). Other simple functional equations and multiparameter equations predicting the signoidal shape of the crack propagation rate curve may be found in (84).

In this department work by Arad et al (101) showed that the equation

$$\frac{da}{dN} = \beta\lambda^{n_1} = \beta(K^2_{max} - K^2_{min})^{n_1} = \beta(2\Delta K K_m)^{n_1} \qquad (1.32)$$

where β and n_1 are constants, could be applied with considerable success in the analysis of Region II crack propagation data in high strength aluminium-alloys and steels (101). The data was taken from Ref. (87), in the high strength aluminium alloys 2024-T3 and 7075-T6, producing a better plot than the Forman equation. The steel data analysed was taken from (82) and (95).

(B) Theoretical Analyses

The fatigue crack growth theories based on the energy approach presented in paragraph 1.7.2 do not predict any influence of mean stress. However some recent theoretical analyses are available in which this influence is considered. Thus Cherepanov and Halmanov (102) derived a crack propagation equation for an ideal elastic-plastic body using dimension-

analysis in the energy equation of crack propagation. This has two terms; the irreversible deformation work done by the plastic zone as it displaces in the direction of the crack extension as a rigid unit, and the irreversible deformation work due to the expansion of the plastic region during loading. The latter is not a function of crack length. The resulting expression for da/dN was

$$\frac{da}{dN} = -C_{11}\left(\frac{K_{max}^2 - K_{min}^2}{K_c^2} + \ell n \frac{K_c^2 - K_{max}^2}{K_c^2 - K_{min}^2}\right) \qquad (1.33)$$

where C_{11} is a constant.

Paris (103) adopted an energy approach for crack propagation. This was based on the assumption that the rate of change of elastic energy during fracture equals the rate of absorption of energy as plastic deformation. He suggested later (104) that the concept of an alternating plastic zone, cycling between compressive and tensile yield and proportional in size to $(\Delta K/2\sigma_{ys})^2$, within a larger pulsating plastic zone created in the first cycle and proportional to $(K_{max}/\sigma_{ys})^2$, was the relevant parameter for crack propagation. The Paris theory then predicts no influence of mean stress on the fatigue crack propagation rate, which is clearly not supported by the experimental data.

Each of the two plastic zones mentioned above was considered by Raju(105) as being split up into two parts with a neutral curve (106) on which the stress conditions do not vary with crack extension. Fig. 3 shows the four crack tip plastic zones considered. Zones A and D are within the pulsating plastic zone, whereas zones B and C are within the alternating plastic zone. Since reversed yielding occurs only in the alternating plastic zone a hysteresis stress-strain loop will only be obtained in zones B and C. The change in energy due to plastic deformation per cycle of crack extension was calculated, and it was found that in zones B and C it did not depend on da/dN since the energy increase in zone B was approximately the same as the decrease in zone C. In

zones A and D no hysteresis occurs and the energy change depends on da/dN, R and material constants. The equation of energy balance gives the crack growth rate as

$$\frac{da}{dN} = \frac{C_{12}(1-R)^{4-q_2} K_{max}^4}{K_c^2 - K_{max}^2} \qquad (1.34)$$

where C_{12} and q_2 are constants.

Erdogan (107) considered the crack propagation in terms of dislocation movement within the plastic zone and introduced the alternating and the pulsating plastic zones considered above. The equation obtained was

$$\frac{da}{dN} = C'_{12} K_{max}^{2\alpha_1} \Delta K^{2\alpha_2} \qquad (1.35)$$

where α_1, α_2 and C'_{12} are constants. Roberts and Kibler (108) introduced into equation (1.35) the increase in crack growth rate as K_{max} approaches K_c. The modified equation was

$$da/dN = \frac{C_{13}(1+\beta_1) \Delta K^3}{K_c (1+\beta_1) \Delta K} \qquad (1.36)$$

where C_{13} is a constant and β_1 is defined in Eq. (1.25).

Walker (109) introduced the effective range of the stress intensity factor $\Delta\bar{K}$ concept in the form $\Delta\bar{K} = (1-R)^{m_3} K_{max}$, where m_3 is a constant. Then

$$\frac{da}{dN} = f(\Delta\bar{K}) \qquad (1.37)$$

Kraft's tensile ligament instability model (TLIM) (110, 111) assumes that the instability necessary for fatigue crack propagation is caused by the separation of microstructural tensile ligaments at the tip of the crack. The equation for da/dN is rather extensive and may be found in (110).

None of the crack growth laws derived by theoretical analyses predict the threshold behaviour, which should be incorporated in any relationship intending to describe the experimental data. From the material point of view

Frost (112) suggested that materials such as mild steel or Cu having a definite yield point should not be sensitive to mean stress while materials such as aluminium alloys and high strength steels without a yield point would be. However much experimental data obtained on mild and low alloy steels (94-99) shows a strong mean stress effect. Ritchie and Knott (113) also found mean stress sensitivity in steel when the fracture mechanism changes from normal ductile striations to either void-coalescence or intergranular fracture.

1.7.5 The Effect of Environment on Fatigue Crack Propagation

Fatigue crack growth can be strongly affected by the test environment. The nature and magnitude of the effect depend on the particular material-environment system. Experimental information is most complete in the aluminium-water system. In this system the pattern of behaviour of the fatigue crack growth curve is as illustrated schematically in Fig. 2. The apparent threshold for crack growth is reduced by the presence of the environment, and the rate of fatigue crack growth is usually accelerated at any given K value. As K approaches K_c or K_{1c} the environmental influences are diminished as a result of either the rate limited nature of transport processes or other mechanical-chemical interaction. The effects of corrosive environment on fatigue crack growth are most fully developed at low values of the stress intensity factor where more time is spent on testing. At very high values of ΔK fast crack growth rates do not allow time for corrosive attack to intervene and the crack growth rate is then not significantly influenced by the environment.

In high strength Al-alloys Krupp et al (114) have grouped environments by their severity as follows; vacuum: no effect; dry gases, wet gases, water and salt solution: increasing effects of environment.

Speidel et al [115] observed that corrosion fatigue cracks can propagate either intergranularly or transgranularly depending on the orientation of the principal stress axis with respect to the preferred orientation of the grain boundaries. Wrought commercial high-strength Al-alloys generally have an elongated grain structure, the degree of orientation and its direction depending on the processing variables. In plate material, the grain boundaries are preferentially orientated parallel to the plane of the plate, i.e. the plane which contains the longitudinal, L, and the transverse, T, directions as seen in Fig. 4. Stress corrosion cracks in high strength Al-alloys exposed to aqueous solutions always grow along grain boundaries [116]. A meaningful comparison of stress corrosion cracking and corrosion fatigue is therefore only possible if both types of test are performed so that the material is stressed in the short transverse direction (S direction) and the crack grows along the rolling or longitudinal direction.

Referring to Fig. 2 three different regions may be considered in the environmental fatigue crack growth rate curve. For the particular case of aluminium alloys in salt solutions, which is of most concern in the present work, in Region I crack growth the da/dN versus ΔK curve is almost parallel to the crack growth rate axis, and there is a limiting stress intensity ΔK_{th} below which the corrosion fatigue crack growth rate is negligible. In Region II, crack growth is usually accelerated while in Region III crack growth rate is not significantly influenced by the environment. A possible explanation for this behaviour has been put forward above.

The acceleration of fatigue cracks in high strength aluminium alloys exposed to aqueous solutions has been the subject of many studies, and a number of hypotheses have been proposed to explain their behaviour. Among the phenomena responsible for this behaviour are anodic dissolution, specific absorption, hydrogen embrittlement, surface layer stresses etc. At the present stage very little is known about the microstructural mechanism

of corrosion fatigue crack propagation. An electrochemical model has been derived in (115) but the relationship da/dN against ΔK was not found. Cherepanov and Halmanov (117) found out that for high strength steels the mechanism of hydrogen embrittlement is the most plausible. Hartman (118) and Bradshaw and Wheeler (119), from their data on fatigue crack propagation in a series of aluminium alloys, suggested that the acceleration in the rate of fatigue crack growth with respect to a vacuum reference environment was caused by the superposition onto the applied stress field of stresses produced by high pressure hydrogen, driven into the crack tip region by the reaction of water with the freshly created aluminium crack surfaces. Wei (120) examined the effect of water and its constituents on the rate of crack growth in the high strength aluminium alloy 7075-T651 and confirmed the findings in (118,119). Water accelerated the rate of fatigue crack growth by a factor of 10 in relation to a dry argon environment, over a range of temperatues from 25°C to 90°C. Wei (120) found as well that fatigue crack propagation was controlled by a thermally activated process, with the apparent activation energy being strongly dependent on ΔK.

Reviews of the environmental fatigue crack propagation phenomenon were made by Wei (121) and McEvily and Wei (122). They concluded that despite the differences in fatigue crack growth the response of all of the aluminium alloys investigated appears to be similar. The accleration of growth rate in Region II depends on the test frequency (119). The frequency effect means that with lower frequencies the increase in crack growth rate would be greater than for higher frequencies, due to the increased testing time involved. The reduction in environment sensitivity at higher K levels (Region III) was explained (122) by a reduction in the effectiveness of the pressure mechanism of hydrogen embrittlement coupled with the plane strain to plane stress transition usually occuring in thin sheet specimens. This

transition phenomenon will be explained in more detail in paragraph 1.7.7. For the aluminium alloys 2024-T3 and 7075-T6 tested in a 3.5% NaCl solution, the onset of the transition corresponded to the K level at which the fatigue crack growth rate curves in air and in 3.5% NaCl become coincident(114). However in thicker specimens for which the transition from plane strain to plane stress is generally not verified the reduction in environmental sensitivity in Region III still occurs.

Fatigue crack growth data in high strength steels in water or salt solutions is more limited. The data available indicate that dependence on test frequency is very strong, as derived by Barsom (123), who expressed the crack growth rate as

$$\frac{da}{dN} = D(t)\,\Delta G \qquad (1.38)$$

D(t) is a function varying inversely with the frequency, attaining a constant minimum value for the frequency level at which fatigue crack growth is sufficiently fast to be unaffected by the environment. Spitzig et al (124) found no increase in crack propagation rate in a water vapour environment, probably due to crack tip blunting. Some experimental work investigating corrosion fatigue crack propagation in mild and low alloy steels has been reported by Jerram and Priddle (125) and Pook and Greenan (126). Oxidation at the crack tip leading to a slowing down or eventually cessation of crack growth may occur under specific conditions (125), but the mechanics of crack propagation in corrosion fatigue of mild steel are not fully understood.

1.7.6 Superposition Models for Environmental Fatigue Crack Propagation

Studies by Wei and Landes(127) have led to the suggestion of a simple quantitative method for estimating the effect of aggressive environments on fatigue crack growth in some ultra-high strength steels. This suggestion

was based on an accumulation of experimental evidence and fractographic observations, which seems to indicate that the mechanism for enhancement of fatigue crack growth is the same as that for crack growth under sustained loads (SCC). In the Wei and Landes model (127) the rate of fatigue crack growth in an aggressive environment is considered to be the sum of the rate of fatigue crack growth in an inert reference environment and an environmental component. The latter is to be computed from the load-profile and static load crack growth data obtained in an identical aggressive environment. The following expression has been derived for this approach

$$\left(\frac{\Delta a}{\Delta N}\right)_c = \left(\frac{\Delta a}{\Delta N}\right)_r + \int \frac{da}{dt} K(t)\, dt \qquad (1.39)$$

where $\left(\frac{\Delta a}{\Delta N}\right)_c$ is the rate of fatigue crack growth in an aggressive environment, $\left(\frac{\Delta a}{\Delta N}\right)_r$ is the rate of fatigue crack growth in an inert environment and the integral term is the environmental component computed from SCC. data obtained in the same aggressive environment. Such an approach is applicable when the threshold value of K in stress corrosion cracking K_{ISCC} is higher than ΔK_{th} in the aggressive environment.

The Wei and Landes superposition model has been applied with considerable success by Bucci (128) and Paris et al (129). However, fatigue crack growth may occur at stress intensities below K_{ISCC} both in high strength steels (123) and aluminium alloys in salt solutions (115) whereas from the superposition model no such influence of environment would be assumed possible. Moreover in aluminium alloys in salt solutions the accerlation of crack growth can occur above, around or below K_{ISCC} (115). This clearly indicates that SCC and corrosion fatigue in Region II are different phenomena. Since Region II crack growth is independent of SCC, corrosion fatigue crack growth rates can not be quantitatively estimated by the superposition referred to above. But it appears that in Region III in some materials the corrosion fatigue crack growth rate consists of the two additive components

of the Wei and Landes superposition model. In this case the onset of Region III in the $\frac{da}{dN}$ versus ΔK curve should always occur at stress intensities higher than K_{ISCC} and it is necessary that the SCC growth rate be comparable or higher than the fatigue crack growth rates. Nicholson (130) found that the superposition model was not applicable to fatigue crack growth data for a high strength steel in a sodium chloride solution.

Gerberich et al (131) derived a model based on that of Wei and Landes but instead of using the integral term in the stress corrosion component the mean value theorem was used to assess the average stress intensity in any one cycle. The model involves two other basic assumptions; the minimum stress intensity factor can be greater or less than K_{ISCC}, and $\Delta K_{th} < K_{ISCC}$ which is usually verified. Assuming that $K_{min} > \Delta K_{th}$ the stress corrosion contribution on the fatigue crack growth rate is given by

$$\left(\frac{da}{dN}\right)_{SCC} = \frac{1}{f(K_{max}-K_{min})} \int_{K_{min}}^{K_{max}} F(K)\,dK \qquad (1.40)$$

where f is the frequency of the loading cycle and F(K) is the stress corrosion crack growth rate. F(K) was determined separately and it was found that the crack growth rate was a thermally activated process with one unique activation energy that was independent of K. If $K_{min} > \Delta K_{th}$ Eq. (1.40) becomes

$$\left(\frac{da}{dN}\right)_{SCC} = \frac{1}{f}\left(\frac{K_{max} - \Delta K_{th}}{\Delta K}\right) \int_{\Delta K_{th}}^{K_{max}} F(K)\,dK \qquad (1.41)$$

When the model was applied agreement was found for the aluminium alloy 7178-T6.

From the above discussion it may be seen that the supperposition model has severe limitations. The agreement obtained in some cases might be considered as fortuitous since there is as yet no evidence suggesting that the stress conditions at the crack tip, the fracture mode and the environmental influence are the same under static and dynamic conditions.

1.7.7 The Threshold for Fatigue Crack Propagation

The existance of non-propagating cracks has been referred to before in paragraph 1.4.4 and in Refs. (29-31). Frost's expression $\sigma_a^3 a > C_o$ was one of the first relationships proposing a criterion for crack propagation. Later the same author (81) reanalysed the non-propagating crack growth data contained in Refs. (29-31) and others in terms of ΔK, and obtained values of ΔK_{th} at different stress ratios for a wide range of materials. Then in the last five years a great deal of data has been obtained for extremely slow fatigue crack propagation ($da/dN < 10^{-8}$ cm/cycle) and the existence of a threshold for crack propagation is now well established for a wide range of materials, loading conditions and environments.

As pointed out before, theoretically derived fatigue crack propagation models do not usually account for the threshold condition. A recent exception is provided by the work of Weiss (132) who derived a model on the basic assumption that da/dN is to extend over a distance over which the normal stress or strain exceeds a certain critical value σ_f or ε_f. The equation for da/dN is

$$\frac{da}{dN} = a\left(\frac{\sigma_a}{\sigma_f}\right)^{\frac{n+1}{n}} f(a,w) - \frac{\rho^*}{2} \qquad (1.42)$$

where n is the strain hardening exponent, ρ^* is the Neuber (28) micro-support effect constant, w is the specimen width and f(a,w) is a dimensionless correction factor for the finite width of the specimens. For the limiting threshold condition the equation for ΔK_{th} was derived in (132) as

$$\Delta K_{th} = \frac{3\pi}{2} (0.1E)^2 \rho^* \quad (R = 0) \qquad (1.43)$$

ΔK_{th} values obtained from Eq. (1.43) showed good agreement with extensive experimental ΔK_{th} values. However the above equation does not predict

any effect of the stress ratio on ΔK_{th}.

The effects of the load ratio and frequency on the magnitude of ΔK_{th} have been studied by Schmidt and Paris (133) for 2024-T3 aluminium alloy. It was found that ΔK_{th} decreased with increasing frequency above 300 Hz and with increasing stress ratio, reaching a constant value for R values greater than a critical value R_{cl}. The trend in variation of ΔK_{th} with R was explained by crack closure phenomena (91). In mild steels and low alloy steels data taken from Refs. 94-99 and analysed by Jerram and Priddle (134) showed that ΔK_{th} decreased linearly with R, but no limiting value seemed to be reached. Harrison (135) reanalysed data taken from several papers by Frost (e.g. refs. 29-31) and found that for R = 0 the ΔK_{th} value was normally greater than $1.5 \times 10^{-4} \times E(\sqrt{in})$. Grandt and Gallagher (136) analysed threshold data for several aluminium alloys and steels and described the results for $0 < R < 0.8$ with the equation.

$$\Delta K_{th} = (\Delta K_{th})_{R=0} (1-R^2) \qquad (1.44)$$

A more general equation has been put forward in (98)

$$\Delta K_{th} = (\Delta K_{th})_{R=0} (1-R^2)^{\gamma_1} \qquad (1.45)$$

where γ_1 is a material parameter. Cooke et al (137) obtained threshold data for EN24 steel and found that in a vacuum the value of γ_1 in equation (1.45) was 0 while for air it was 0.5. Thus there was no dependence on R in vacuum.

ΔK_{th} may be affected by the environment, decreasing for aluminium alloys in an aggressive environment. However, if crack blunting occurs ΔK_{th} is not significantly affected by the environment. In steels Bucci et al (138) did not observe any reduction in ΔK_{th} from air to a distilled water environment.

1.7.8 The Effect of Several Other Parameters on Fatigue Crack Propagation

(A) The Loading Frequency

The variation of crack growth rate with frequency is partly due to the environment. Thus tests in aluminium alloys performed by Bradshaw and Wheeler (139) showed no frequency effect in a vacuum for the materials tested. For other environments, including air, crack growth rate tends to increase with decreasing frequency as discussed in paragraph 1.7.5 and in the literature (114,121-123,127,128). Recent work by Yokobori and Sato (140) showed that in 2024-T3 aluminium alloy and SM-50 steel, both tested in air at room temperature, the crack growth rate and the striation spacing decreased with increasing frequency f according to the equations

$$\frac{da}{dN} = C_{14}(\Delta K)^{q_3}(f)^{-q_4} \quad (1.46a) \text{ and } s = C_{15}(\Delta K)^{q_5}(f)^{-q_6} \quad (1.46b)$$

where $C_{14}, q_3, q_4, C_{15}, q_5$ and q_6 are constants.

(B) The Specimen Thickness

The effect of specimen thickness (or more appropriately the ratio between thickness and some multiple of the crack tip plastic zone size) on fatigue crack growth is complicated. Fatigue behaviour is influenced by variations in the fracture toughness K_c, and in the plane strain plane stress transition.

Previous investigations by Plumbridge (141) and Frost (142) have demonstrated that higher crack growth rates are obtained with thicker specimens. Usually in plate specimens a phenomenon known as crack rotation occurs. The crack starts to propagate under plane strain condition but approaching the specimen free end it rotates 45° in relation to the tensile axis and specimen thickness, creating plane stress conditions. The rotat-

ion of the fracture plane occurs when the ratio plastic zone size/specimen thickness attains a critical value between 0.5 and 1. (141) which for high strength aluminium alloys corresponds to specimen thicknesses in the range 1-4 mm. Often the acceleration in fatigue crack growth rate occurs before the transition. In Appendix A the plastic zone size in a sheet specimen is shown schematically. The state of stress and the plastic zone change from plane strain and a small zone at the centre to plane stress and a large zone at the surface. The central portion of the crack point, that part in plane strain, increases in size as the thickness increases, and this increased plane strain plastic zone accounts for the faster crack growth rate in thicker specimens.

Specimens provided with side grooves show no plane strain-plane stress transition.

(C) Compressive Loading

Comparatively little experimental work has been carried out under load waves introducing compressive loading. Data obtained by Gurney (143) in mild steel subjected to alternating tension (R = -1) showed that part of the compressive portion of the alternating cycle appeared to be effective in propagating the crack. For one low alloy steel and two high strength steels (82) the rate of crack propagation for R = -1 was 50% higher than that for R = 0; that is, the compressive portion of the applied stress cycle contributed to crack propagation. More recent work by Sullivan and Crooker (144) in a high strength steel covered stress ratios from 0.75 to -2. It was found that compressive portion of the tension-compression cycle contributed to crack growth to a lesser degree than did the tensile portion. The fatigue crack growth for $0.75 < R < -2$ was expressed as

$$\frac{da}{dN} = C_{16} \frac{(1-b_1 R)}{(1-R)} \Delta K^{q_8} \qquad (1.47)$$

where b_1, q_8 and C_{16} are constants.

In high strength aluminium alloys the only experimental work conducted to date in which compressive loading has been applied has been performed by Illg and McEvily (145) on the aluminium alloys 2024-T3 and 7075-T6. It was found that the compressive part of the cycle did not contribute to fatigue crack growth. Future work should continue on other materials to obtain a more complete picture of the effect of compressive loading.

(D) The Loading History

The fatigue crack growth laws, theories and data discussed in the precedent paragraphs refer to constant amplitude loading; that is the cyclic maximum and minimum values of load are kept constant throughout the test. When cycles of varying amplitude are applied some complex interactions may occur. There is now considerable experimental evidence for the phenomenon of transient delay the period of abnormally low rate, or zero rate, of fatigue crack growth between a decrease in load level and the establishment of a rate of growth commensurate with that for constant amplitude loading at the prevailing lower load. The delay phenomenon, schematically illustrated in Fig. 5a, may occur after a single overload or when the K level is dropped. On the other hand early work by Matthews et al (146) reported a transient crack acceleration effect after the K level is increased (Fig. 5b). The transient acceleration has not been so extensively studied as the delay phenomenon.

One of the first crack propagation studies under variable load amplitude was carried out by Hudson and Hardrath (147). They found delay when the stress level was reduced this delay increasing as the initial stress was increased, but cracks propagated at the normal rate during the second stress application when this second stress was higher than the first. Later, extensive experimental work on the delay phenomena for a Ti-alloy

was reported by Wei and his co-workers (148,149,150). Preliminary work (149) showed that the number of cycles for delay N_D was a function of ΔK_1, ΔK_2, R_1, N_1 and f_1

$$N_D = f(\Delta K_1, \Delta K_2, R_1, R_2, N_1, N_2, f_1, f_2) \qquad (1.48)$$

where the subscripts 1 and 2 denote the preloading and the subsequent loading conditions respectively. In (149) it was found for example that for a constant value of $\Delta K_1/\Delta K_2$ delay increases with increasing ΔK_2. The phenomenon is highly complex with N_D found also to be dependent on R_2 and N_1.

The influence of the environment in the delay has been experimentally studied in (150). Comparison of delay data obtained in dehumidified argon, air and distilled water indicated that air and distilled water have little effect on delay. N_D increased with increasing K_{1max}/K_{2max} and N_1, decreased with increasing K_{2max}. It was observed that the variation of N_D with K_{2max} in the Ti-alloy tested was the reverse of that observed in a previous study by Von Euw et al (151) in 2024-T3 and 7075-T3 aluminium alloys. The results obtained in (150) in 3.5% NaCl solution were not understood due to the large amount of scatter involved. The effect of the sheet thickness on the delay obtained after a single peak overload was recently studied by Mills and Hertzberg (152). The results indicated that for the same overload N_D increased with decreasing specimen thickness, and the amount of crack growth affected by the delay (a_D in Fig. 5) agreed well with the plastic zone size left by the overload.

Several models have already been proposed to predict the value of N_D. The Wheeler model (153) is one example. It assumes that the extent of the residual stress region left by the previous higher load application is characterized by a load interaction zone considered equal to the plastic zone size under plane strain conditions which it created. Gray and Gallagher (154) applied this concept and modified it into a stress intensity factor formu-

lation. The modified model predicted, within a factor of two, the experimental data for the number of delay cycles following a single overload in 2024-T3 aluminium alloy, 4340 steel and Ti-6Al-4V titanium alloy. The crack closure concept (91) was used by Adams (155) to give a qualitative explanation of the delay phenomenon. The crack closure argument states that when the K level is reduced the crack does not propagate until the new crack opening level changes. However work by Richards and Lindley (156) showed that the fatigue crack delay caused by reduction was not due to crack closure.

Fatigue crack propagation under random loading has only received some attention recently despite its engineering importance. Dover and Boutle (157) have recently measured crack closure at positive stresses during random loading and concluded that thickness, mode of fracture and stress ratio all influenced the closure stress. Priddle (158) has shown that laws derived to fit constant amplitude fatigue crack growth data can be successfully applied to random load fatigue crack propagation results on a mild steel.

1.7.9 Fatigue Crack Growth at Large Plastic Strains

Fatigue crack growth can result from cycling with the maximum stress above or below the gross yield stress. The latter problem has been handled by applying LEFM and has already been reviewed. With the approach of gross yielding LEFM techniques are no longer applicable. There have been few studies of this aspect of fatigue crack propagation despite the engineering significance of fatigue crack growth resulting from plastic and strain cycling (low cycle fatigue crack propagation).

One of the first was performed by Laird and Smith (159). Their observations on the nature of crack tip blunting and resharpening provided a better understanding of the low cycle fatigue crack propagation phenomenon. Studies conducted by Crooker and Lange (160) have shown that for plate

bend specimens containing an embedded surface flaw the crack growth rate was described by

$$\frac{da}{dN} = C_{17}(\Delta\varepsilon_t)^{q_9} \qquad (1.49)$$

where C_{17} and q_9 are constants. The above equation described crack propagation under both elastic and plastic strain cycling.

McEvily (161) studied the low cycle fatigue of copper and used a strain concentration factor to describe his results in the form

$$\frac{da}{dN} = C_{18}(\Delta\varepsilon_t\sqrt{a})^{q_{10}} \qquad (1.50)$$

where C_{18} and q_{10} are constants. The parameter $\Delta\varepsilon_t\sqrt{a}$ was termed the "strain-intensity factor".

Solomon (162) performed low cycle fatigue crack propagation tests in a low carbon steel, keeping the plastic strain range constant. The relationship obtained was

$$\frac{da}{dN} = C_{19}a(\Delta\varepsilon p)^{q_{11}} \qquad (1.51)$$

where C_{19} and q_{11} are constants.

Tomkins (163,79) has proposed a model for crack propagation under the fully plastic situation of low cycle fatigue. The crack growth rate was expressed as a function of the cyclic strength coefficient K' and the cyclic strain hardening exponent n' (see Eq. 1.12) in the form

$$\frac{da}{dN} = \frac{\pi^2}{8\sqrt{2}}\left(\frac{K'}{2\sigma_{UTS}}\right)^2\frac{\Delta\varepsilon_p^{(2n'+1)}}{(2n'+1)}a \qquad (1.52)$$

It can be seen that Eq. (1.51) has the same form as 1.50 and, after integration between the initial crack length and the final crack length for unstable fracture gives the Coffin-Manson law Eq.(1.11).

Dover (164) reported results on crack growth rates in mild steel under constant COD (Appendix A) cycling, and found that the crack growth rate was

a power function of both the hysteresis loop width and the overall crack tip opening displacement range. A theoretical and experimental study of fatigue crack growth under elastic-plastic conditions using also the COD approach was reported recently by McEvily (165).

The energy interpretation of the J contour integral (Appendix A) was used by Dowling and Begley (166,167) to describe fatigue crack propagation data in the elastic and plastic regime. Preliminary work was carried out using compact tension specimens (166) and center cracked and compact tension specimens were used in (167). The material tested was steel A535B, and agreement was found between the results for both geometries when plotted as crack growth rate against the cyclic value of J,ΔJ. The value of J associated with the opening of fatigue crack surfaces was assumed to be the controlling parameter in the high growth rate regime. Crack growth rate was related to ΔJ as

$$\frac{da}{dN} = C_{20}(\Delta J)^{q_{12}} \qquad (1.53)$$

where C_{20} and q_{12} are material dependent constants. The experimental programme was conducted under decreasing load conditions. The cyclic creep behaviour of the specimens was not analysed, and the results are also only valid for long crack lengths.

Mowbray (168) has put forward a theoretical analysis relating the J integral with the strain cycling properties of the material. The equation derived was

$$N_f^{1/q_{12}} \Delta W = \text{const.} \qquad (1.54)$$

where W is the range in strain energy density and q_{12} is given by Eq.(1.53). Note that Eq. (1.54) has the same form as the Coffin-Manson equation with the plastic strain substituted by the applied strain energy density. Lamba (169) has applied the J integral analysis to determine the influence of notch geometry on the life to fatigue crack initiation. He found that the expression for the

strain concentration at the notch root when expressed in terms of J had the same form as that obtained from the Neuber approach. A life prediction for fatigue crack initiation was then proposed. Poulouse et al (170) have recently applied a non-linear energy toughness concept, G_{fc} to describe plastic cycling. In the aluminium alloy 2024-T3 it was found that G_{fc} decreased with the number of cycles to failure ($N_f < 100$) in a similar manner to the S-N curve.

Both COD and the J integral seem to be powerful tools for analysing fatigue crack growth under gross plastic strains. Much more work remains to be done in this area to establish the controlling variable in crack propagation both in load and strain cycling.

1.8 Fracture Mechanics Approach to Fatigue Crack Propagation in Components or Structures

1.8.1 Calculation of the Number of Cycles to Failure

If the life of the component or structure is totally spent in crack propagation the fracture mechanics approach may be used to estimate the number of cycles to failure, N_f, for certain structures or components. Assuming that an initial flaw of size a_i exists in the body, N_f will be the number of cycles necessary to propagate that crack of size a_i to a critical size, a_c, enough to cause unstable fracture. The value of a_i is conditioned by the non-destructive inspection technique available. A conservative figure is the minimum flaw size that that technique can detect. a_c is a function of stress, geometry and K_c and may be obtained from the Eq. (A.4b) as

$$a_c = \frac{K_c^2}{Y^2 \sigma_{max}^2 \pi} \tag{1.55}$$

N_f is then computed by integrating the appropriate crack growth rate equation, $da/dN = F(\Delta K)$. If $\Delta\sigma$ is the working stress range then N_f is obtained by

$$N_f = \int_{a_i}^{a_c} \frac{da}{F(Y\Delta\sigma\sqrt{\pi a})} \qquad (1.56)$$

with a_c obtained by Eq.(1.55) It should be pointed out that the function F might depend as well in ΔK_{th}, K_c and R. ΔK_{th} is usually known experimentally and the stress ratio influence can be expressed in terms of ΔK or K_{max} in which case the relationship with a is always possible. Some examples for the calculation of N_f were discussed by Crooker (171) and Frendentahl (172). The method described is applicable when the stress amplitude is constant. For variable amplitude loading the fatigue crack growth life can be worked out by a method proposed by Brussat (173)

1.8.2 Analysis in Components or Structures

Some work has been published in the study of fatigue crack propagation in welded structures. Maddox (174) has extensively studied the phenomenon of fatigue crack propagation in welded plates using the fracture mechanics approach. Different types of welding were tested and extensive testing was carried out both in the welded zone and the parent material. The fatigue behaviour of spot welds using a fracture mechanics analysis has been analysed by Pook (175). He treated the spot weld as a crack like flaw since virtually the whole life is occupied by fatigue crack growth. Different spot weld configurations were tested and a plot ΔK against the number of cycles to failure was obtained. A ΔK_{th} value was assumed from which the safe working stress can be established.

Hirt and Fisher (176) investigated fatigue crack growth in welded beams both theoretically and experimentally. A fracture mechanics model for cracks originating from the pores in the web-to-flange fillet weld was developed. Also the fatigue life of these welded beams was extremely dependent on the initial flaw-size. A crack growth equation was derived which exhibit the same trend as measured data from crack growth specimens.

Tanaka and Matsuoka (177) carried out more recent work in the fatigue strength of rolled welded beams with stiffeners welded to the web. They estimated the initial crack size and derived a theoretical crack growth equation for the evaluation of the fatigue strength of welded beams and transverse fillet welds. Gurney (178) produced extensive early work in this field compiling most of the work on both the S-N and fracture mechanics approach to the fatigue strength of welded structures.

A fracture mechanics analysis of fatigue crack propagation in several aircraft components may be found in some papers presented in the ASTM; STP 415, 486 and 495.

CHAPTER TWO

ENVIRONMENTAL FATIGUE CRACK PROPAGATION IN THE AL-ALLOYS RR58 AND LM30 AND MILD STEEL BS15

The propagation of cracks under fatigue conditions has been extensively studied in high-strength aluminium alloys due to the wide use of these materials in the aeronautical and aerospace industries. The design philosophy used in these industries recognizes that cracks may be present in the structure, or may initiate early in its service life. The selection of materials and inspection intervals is then based on the fatigue crack growth and fracture toughness properties of the material. One of the recently developed Cu-Al-alloys, RR58, which is being used in the Concorde design, was considered sufficiently important for the present study.

On the other hand, fewer studies have been made of the fatigue crack growth and fracture behaviour of other metals such as cast aluminium alloys and mild steels. These are true engineering materials with extensive applications (e.g motor car industry, structural engineering, pressure vessels etc.) . It was therefore decided to study fatigue crack propagation in one cast aluminium alloy (LM30) and also one mild steel (BS15) in two environments of practical interest. Corrosion fatigue failures may occur in engine blocks made of cast aluminium alloys such as LM 30; mild steel structures are also subject to the same type of failure (e.g. mild steel is widely used in the construction of the North Sea oil platforms).

2.1 Experimental Procedure

2.1.1 Material, Heat Treatment and Enviroment Selection

Aluminium alloy RR58 is an Al-Cu-Mg alloy belonging to the series 2000 (2618). The material was supplied in rolled plates 914 x 914 x 76mm. Precipitation hardening has been achieved after solution treatment at 530^{o}C

followed by water quenching. A further increase in strength has been obtained by straining 2.25% after the solution heat treatment.

Cast aluminium alloy LM30 is a chill cast Al-Si alloy (18% Si) developed from the early LM24 alloy. The addition of silicon facilitates the casting process and increases the abrasion resistance. It was supplied in plates 540 x 350 x 75mm in the cast condition.

Mild steel BS15 is a 0.19% carbon alloy steel which is largely used in welded structures. It was supplied in rolled plates 11.2 mm thick.

The composition and principal mechanical properties of these materials are given in Table 1.

Tests were conducted in two different environments: air (21°C and 50% R.H.) and a 3.5% NaCl solution in distilled water. The choice of 3.5% NaCl as a testing environment was based on the fact that these materials may be subjected to cyclic loading in salt solutions. Moreover the 3.5% NaCl solution is widely used as a standard testing environment, so that data obtained may readily be compared with similar data obtained in other materials and available in the literature.

2.1.2 Design and Selection of the Specimens

If a specimen is so designed that its compliance, C, changes linearly with crack length, a, then dC/da will have a constant value. The stress intensity factor K is related to dC/da through the equation (Appendix A)

$$K_I = P\left[\frac{E}{2B_n(1-\nu^2)}\ \frac{dC}{da}\right]^{1/2} \qquad (2.1)$$

where the subscript I refer to the tensile (opening) mode*. P is the applied load ν is Poisson's ratio and B_n is the crack width. From the above

*All the experimental programme presented in this work was carried out in mode I loading. Hence in the next paragraphs and chapters the subscript I will be ommited.

equation for a constant value of dC/da, the relationship between K and the load P will be independent of the crack length, and if fracture occurs at a constant load P_c the critical value of the stress intensity factor K_c will remain constant with the crack length.

Constant dC/da specimens were previously designed by Mostovoy et al (179). They are crack line loaded specimens giving large displacements at low loads and, consequently, large values of compliance - which is convenient for a simpler compliance determination. The specimen is analysed as a pair of cantilever beams built-in at the crack tip. Applying linear elastic beam theory a suitably contoured shape satisfies the condition dC/da = constant. This shape may be expressed by the relation

$$\frac{3a^2}{h^3} + \frac{1}{h} = m_o = \text{const.} \qquad (2.2)$$

where h is the specimen height at the crack tip. Srawley and Gross (180) have developed a more exact analysis whereby a constant K specimen was obtained with straight edges. The boundary collocation technique was used to compute K (see Appendix A). Johnson and Radon (181) have chosen a value of m_o, which was used in the present work, such that the tested geometry is very close to one of the geometries derived in (180).

The contoured double cantilever beam specimen (DCB) has great advantages in relation to other types of fracture mechanics specimens. It was selected for this study since it provides a constant stress intensity field along the crack path, as will be seen later (2.1.4). Therefore not only fatigue crack growth and stress corrosion cracking (SCC) can be studied under a constant K pattern but also the effects of loading history are properly assessed.

2.1.3 Specimen Dimensions and Preparation

The contoured DCB specimens (Fig. 6) used in the present test programme

all had the same overall dimensions and were provided with side grooves on both faces. These help to ensure that the crack grows along the specimen midplane, and enhance plane strain conditions.

Aluminium alloy RR58 specimens had 9.5 mm gross thickness, and were cut from the plate material so that the crack would propagate in the rolling direction and the loading direction coincided with the short transverse axis (plate thickness). As mentioned previously, this orientation (Fig. 4) is that for which the fracture toughness is lowest and susceptibility to environmental fatigue and stress corrosion cracking highest. Each specimen was aged in a salt bath at 190°C for 30 hours, to give a hardness (Hv) of 145±2. Side grooves 0.75 mm deep were milled on both sides of the specimens. This side groove depth was considered satisfactory for maintaining the crack propagation at the specimen midplane. A slot, approximately 40mm long, was machined from one end of each specimen on this midplane. Subsequently the ligament was cut to a swallow tail front (chevron) at the tip of this slot and indented with a razor blade to form a crack starter (Fig. 6). Finally, the side grooves were polished for ease of crack observation.

For LM30 the specimens had 28.5 mm gross thickness and were cut from the plate material so that the maximum specimen height coincided with the plate thickness (75mm). The side grooves were 9.5 mm deep, reducing the net specimen thickness almost to that of the RR58 specimens. It was necessary to use deep side grooves to keep the crack propagation in the specimen midplane. The crack was started from a saw cut approximately 65 mm long, extended with a 45° chevron notch and sharpened with a razor blade. Again the side grooves were polished for ease of crack tip observation.

Finally, the BS15 mild steel specimens were of 11.2 mm gross thickness the plate thickness) and were orientated to ensure that the crack subsequently grew along the rolling direction. This objective was achieved by providing

the specimens with 3.5mm deep grooves on both sides. The same notching technique was used.

2.1.4 Compliance Calibration and Calculation of K_c

In order to calculate K by Eq. (2.1) the appropriate dC/da values are necessary. Also K_c may thereby be obtained if unstable crack propagation occurs under linear elastic conditions. For BS15 it was found that such conditions were never met in a test under monotonically increasing load. The crack only propagated after gross plastic deformation had appeared in the specimen. The compliance calibration for this material was carried out later during fatigue tests in the linear elastic regime.

In aluminium alloys RR58 and LM30 the compliance calibration and calculation of K_c were obtained by precracking under monotonic load in air at 21°C, 50% R.H. The crack starter was extended by a further 25-30 mm by loading the specimens in an Instron TT-C testing machine, ±44 kN load capacity, at a constant crosshead speed of 0.05 mm/min.

The crack length was measured with a travelling microscope giving 10x magnification and reading to 0.01 mm. In RR58, after a sudden initial crack jump the load decreased and the crack slowly propagated at constant load. This is shown in Fig. 7 as a load versus deflection curve, where the deflection at the loading points corresponds to the crack length. A typical linear variation of compliance with crack length was recorded (Fig. 8). It may therefore be observed that this form of contoured DCB specimen satisfies experimentally the condition dC/da = const. Since P_c is assumed constant the fracture toughness K_c is obtained by substituting P by P_c in Eq. (2.1) and is proportional to P_c.

In the present fracture toughness tests K_c measured along the entire crack path did not vary more than ±2%. The cracking load variations were within ±1% and K_c values for various specimens ranged from 20.74 to 23.9 $MN/m^{3/2}$

as evidenced by the results presented in Table 2.

In LM30 the sudden crack jump was not noticeable. Instead, after the initial linear elastic extension of the specimen arms, the crack again propagated slowly at constant load (Fig. 7) giving a linear variation of compliance with crack length as shown in Fig. 9. K_c was obtained in the same way as for RR58, and, measured along the entire crack path, did not vary more than ±3%. Cracking load variations were within ±2% and the K_c values for various specimens are given in Table 2 and ranged from 18.59 $MN/m^{3/2}$ to 21.61 $MN/m^{3/2}$. Thus K_c is lower for LM30 than for RR58. Linear elastic conditions were met in these precracking tests: unloading the specimen during and after precracking produced a linear load-deflection trace passing through the origin (Fig. 7).

It should be pointed out that K_c values obtained for RR58 according to ASTM standard E399-72, using compact tension specimens (182), produced similar results. Thus the process of K_c evaluation described above may be regarded as a valid one.

2.1.5 Testing Programme

The purpose of this programme was to study the effects of the environment, loading frequency, range of load and mean load on fatigue crack propagation. Cyclic tensile fatigue tests at constant sinusoidal load amplitude were carried out on the previously described contoured DCB specimens according to the following programme:

1. Fatigue crack propagation in RR58 in air (21°C and 50% R.H.); and in a 3.5% NaCl solution; the effects of load range, mean load and loading frequency (0.15 and 35Hz).

2. Fatigue crack propagation in BS15 in air (21°C and 50% R.H.) and in a 35% NaCl solution; the effects of load range, mean load and loading frequency (0.25 and 35Hz).

3. Fatigue crack propagation in LM30 in air (21°C and 50% R.H.) and in a 3.5% NaCl solution at a frequency of 0.25Hz; the effects of load range and mean load.

2.1.6 Testing Apparatus

The tests in this programme were carried out using a Denison T42C2 Hydraulic Testing Machine, two Avery Hydraulic Fatigue Machines and a Dowty Electro Hydraulic Fatigue Machine.

The Denison T42C2 Hydraulic Universal Testing Machine was initially designed for monotonic tests but was later converted for cycling tests. The machine is fitted with limit switches to regulate the maximum and minimum loads. The operational frequency ranges from 0.1 to 0.5Hz, and the maximum load capacity is 100 kN.

The Avery Hydraulic Fatigue Machines have a maximum load capacity of 250 kN and 500 kN respectively and were capable of cycling up to 1Hz.

The Dowty is an electrohydraulic fatigue testing machine extensively described by Knight (183) with a range of frequency from 0.01 up to 100 Hz. The range of loading depends on the capacity of the load cell used, the maximum being 53.4 kN(12000 lb_f).

In all these machines it is possible to adjust the load while the test is in progress and automatic switch-off is provided when failure occurs i.e. when specimen deflection exceeds a certain amount. In the Dowty Machine the shape of the input load control waveform may be varied (sinusoidal, triangular, square, etc.).

2.1.7 Testing Procedure

Tests on RR58 at a frequency of 0.15Hz were performed using the Denison T42C2 machine. The tests on LM30 and BS15 at 0.25Hz were carried out on the

Avery machines, and the tests at 35Hz on the Dowty machine. The possibility of differences in the results arising purely from the use of two different testing machines (due to the stiffnesses of the testing assemblies) was checked and found to be negligible; the repeatability of the results obtained in both machines was within 5%.

The 3.5% NaCl solution was drip fed on to the crack surfaces through a hypodermic needle attached to an aspirator bottle provided with a flow regulator, maintaining a flow of about 6 drops per minute (0.5 litre per day). This experimental set up is schematically shown in Fig. 10. The crack length was monitored with a 50x magnification travelling microscope at an accuracy better than 0.0025mm. When observation of the crack tip became difficult due to corrosive attack the side grooves were cleaned and polished.

The applied ΔK values were calculated from Eq. (2.1). In RR58 and LM30 dC/da was obtained from the precracking test (Figs. 8 and 9). For BS15 dC/da was obtained on completion of each fatigue test by straining the specimen in the Instron tensile testing machine (type TT-C, 44 kN capacity) and measuring the compliance from the load extension chart as shown in Fig. 11, a constant value of dC/da was obtained.

From Eq. (2.1), and since dC/da is constant (Figs. 8, 9 and 11) it can be seen that

$$K_{max} \propto P_{max} \quad (2.3.a) \qquad \text{and} \qquad K_{min} \propto P_{min} \quad (2.3b)$$

As soon as K_{max} and K_{min} are selected (or P_{max} and P_{min}) the parameters K_m and ΔK remain constant while the crack is propagating.

2.2 Experimental Results

2.2.1 Fatigue Crack Propagation in RR58 in Air (21°C and 50% R.H.) and in 3.5% NaCl

The aim of this study was to assess the dependence of crack growth

rate on the range of the stress intensity factor, and also to reveal the combined effects of the environment, loading frequency and mean load (represented by the mean value of the stress intensity factor K_m. The experimental programme covered the full subcritical range.

At 0.15Hz tests were conducted with R = 0 (various K_m and ΔK values), at specific K_m values (5.5, 8.25, 12.1, 16.5 and 18.15 $MN/m^{3/2}$) and, in some isolated tests, at specific ΔK values. For 35Hz only three K_m values were selected (5.5, 12.1 and 16.5 $MN/m^{3/2}$) together with tests at R = 0, various K_m and ΔK values, and some tests at specific ΔK values.

(A) The da/dN-ΔK Relation and the Effects of K_m and ΔK in Air, at 0.15Hz

A typical linear relationship between crack length and number of cycles for tests at R = 0 is shown in Fig. 12. Crack speed da/dN increased with increasing values of applied ΔK. There is a markedly steep increase in growth rate when ΔK was increased from 18.43 to 21.81 $MN/m^{3/2}$. Additional data for R = 0 may be found in a previous work by the author (184).

Some results for low values of ΔK and still at R = 0 are presented in Fig. 13. These tests were conducted to verify the existence of a threshold for crack propagation. One observes that a large decrease in crack growth rate ocurred when ΔK changed from 6.17 to 5.63 $MN/m^{3/2}$ at which the crack growth rate obtained was 3.3×10^{-7} mm/cycle (Table 3). The crack growth pattern presented in Fig. 13 suggests that in that ΔK region (7.74 to 5.63 $MN/m^{3/2}$) the crack growth rate is rapidly decreasing towards the threshold level.

Crack growth rate, da/dN, was obtained for each test and all the data obtained under R = 0 conditions is presented in Table 3. Fig. 14 shows da/dN plotted against ΔK with curve 1 fitting the data for R = 0 loading.

It should be remembered that the results of tests in which ΔK is varied at R = 0 inevitably include the influence of the mean value of stress

intensity as well, since K_m increases proportionately with increasing ΔK. Thus the results of tests in which R = 0 and K_m (and hence ΔK) is varied (curve 1 Fig. 14) may be described (in the linear region) by a crack propagation law such as Eq. (1.23), but they cannot indicate the separate effects of ΔK and K_m.

In order to separate these individual effects, the two other series of tests were conducted. Thus for a specific value of K_m (12.1 $MN/m^{3/2}$) and with ΔK varying between 2.86 and 17.27 $MN/m^{3/2}$, all the results showed a linear dependence of crack growth on the number of cycles. Crack growth rate increased with ΔK, as shown in Fig. 15 for three consecutive tests.

The numerical values of $\frac{da}{dN}$ corresponding to the tests performed under K_m = constant conditions are given in Table 3, and are plotted against ΔK in Fig. 14. A family of curves (2-6) was drawn to represent the K_m = const. data.

In the second series of tests (Fig. 16) ΔK was maintained with the same value whilst K_m was varied. Again a linear relationship between the crack growth and the number of load cycles was obtained, but the rate of increase of crack growth was not proportional to K_m. These two series of tests indicate that both K_m and ΔK exert a distinct influence on the crack growth rates in aluminium alloy RR58.

The slopes of the crack growth rate curves in Fig. 14 tend to decrease with increasing values of mean stress intensity, K_m. In tests performed at constant values of ΔK and varying mean stress intensity, K_m, the crack growth rate may be expected to vary within wide limits, and this was indeed the case. In tests at $\Delta K = 5.5$ $MN/m^{3/2}$ increasing K_m (from 2.75 to 18.15 $MN/m^{3/2}$) increased the crack growth rate by three orders of magnitude (from 2.5×10^{-7} mm/cycle to 2.5×10^{-4} mm/cycle). However, this rate of increase did not remain constant but decreased with increasing ΔK.

A fatigue crack growth curve (e.g. curve 1, Fig. 14) may be divided into three parts. Region I represents a fatigue threshold below which cracks do not propagate; in this region, at very low crack growth rates, ΔK reaches a threshold value, ΔK_{th}. The higher crack growth rate in Region II can be described by basic equations such as the Paris equation. An even faster rate is observed in Region III, culminating in a 1/2 cycle loading when K_{max} will reach its critical value K_c.

The steep downward trend in Region I observed in the present tests (Fig. 14) suggests that the threshold values, ΔK_{th} can be confidently established at crack speeds around 2.5×10^{-7} mm/cycle. Data obtained in the present programme for values of ΔK at R = 0 form the typical sigmoidal curve 1 in Fig. 14, having a threshold value 5.5 $MN/m^{3/2}$ - which may be read directly from the figure. Similarly values of ΔK_{th} for curves 2-6 may be taken from the same figure the curves being extrapolated to 10^{-7} mm/cycle as indicated. Other tests conducted at values of ΔK below the quoted ΔK_{th} failed to produce any growth and were discontinued . The threshold data presented herein indicates that the value of ΔK_{th} is dependent upon K_m, ΔK_{th} decreasing as K_m increases.

(B) The $\frac{da}{dN}$ ΔK Relation and the Effects of K_m and ΔK in Air at 35 Hz.

Four typical tests at a constant value of K_m = 12.1 $MN/m^{3/2}$ produced the results given in Fig. 17. It can be seen that the crack growth relation is linear and its rate decreases with ΔK. Fig. 18 shows the results of three consecutive tests at a constant value of ΔK = 6.6 $MN/m^{3/2}$ and with K_m decreasing. The crack growth rate decreases by a factor of one order of magnitude as K_m is reduced from 16.5 to 5.5 $MN/m^{3/2}$.

Crack growth rates were obtained for each test, numerical values given in Table 4 and plotted against ΔK in Fig. 19. These results for given

K_m values at $R \neq 0$ together with curve 1 obtained from the $R = 0$, variable K_m tests, form a family of curves. These curves (1-4) have a similar shape to those presented in Fig. 14 showing curves 1, 3 and 4 the three different regions of crack growth.

The threshold values, ΔK_{th}, were taken from Fig. 19 by considering the interception of the curves (1-4) with $da/dN = 10^{-7}$ mm/cycle. This task is facilitated by the existence of a few tests in which crack growth did not occur even after 10^7 cycles. These points of zero crack growth are indicated by arrows in Fig. 19.and were obtained for all the four curves considered. ΔK_{th} has a maximum value of 4.5 $MN/m^{3/2}$ for $R = 0$ and then decrease as K_m increases.

The fracture surface appearance of one of the specimens can be seen in Fig. 20. (Spec. 1) A predominantly flat fracture surface was obtained which shows that the crack propagation process was under plane strain conditions. The difference in fracture surface appearance from the static precracking zone to the fatigue crack propagation zone can clearly be noticed.

(C) The da/dN- ΔK Relation and the Effect of K_m and ΔK in 3.5% NaCl

A typical crack growth plot for tests conducted under $R = 0$ conditions and at various ΔK values is given in Fig. 21 together with crack growth data under the same ΔK values obtained in air. Each set of lines refer to one specimen and it may be noticed that the crack growth rate increased substantially in the 3.5% NaCl solution in the tests performed at comparatively low values of ΔK; i.e. curve 4, Fig. 21. However no increase was recorded when the value of $\Delta K = K_{max}$ reached 19.66 $MN/m^{3/2}$. Thus the crack growth rate in the fatigue tests performed at K_{max} values higher than 19.66 $MN/m^{3/2}$ remained nearly the same for both environments.

Typical results from tests performed under the same K_m value of 8.25 $MN/m^{3/2}$ are shown in Fig. 22. All the data in Fig. 22 also indicate a linear dependence of crack growth on number of cycles the crack growth rate increasing with ΔK, and accelerating in the 3.5% NaCl solution when compared with tests in air at the same K_m and ΔK values.

Typical tests performed at a constant ΔK value of 5.5 $MN/m^{3/2}$, produced the results given in Fig. 23. Again a linear relationship between crack growth and number of load cycles was obtained but the crack growth rate was not proportional to K_m. These results indicate that in this environment too the Paris equation does not entirely explain the crack propagation phenomena in this material, and that both K_m and ΔK have separate influences on the crack growth rate similar to those obtained in air.

Crack growth rate was calculated from the linear relationship obtained between crack growth and number of cycles and the complete numerical results are listed in Tables 3 and 4.

The variation of da/dN with ΔK is illustrated in Fig. 24 for loading frequency of 0.15 Hz. The family of curves presented shows the three different regimes of crack propagation and bare a similar shape to the da/dN - ΔK plots in air (Figs. 14 and 19).

Some tests were performed in which no crack growth was detected. ΔK_{th} was obtained as the ΔK value for which da/dN is below 10^{-7} mm/cycle and each curve in Fig. 24 produced a different value. The ΔK_{th} value in 3.5% NaCl for R = 0 loading was assumed to be 4.8 $MN/m^{3/2}$ and ΔK_{th} is seen to decrease as K_m increases (Figs. 19 and 24), repeating the trend observed in air.

One of the broken specimens is shown in Fig. 20 (Spec. 2). A predominantly plane strain fracture surface was obtained with the corrosion products covering it.

2.2.2 Fatigue Crack Propagation in BS15 Mild Steel in Air (21°C and 50% R.H.) and in 3.5% NaCl

In the literature review presented in Chapter 1 it was noted that fewer fatigue crack propagation studies of mild steels have been reported, despite the engineering significance of these materials.

The effects on the fatigue crack propagation of mean stress and frequency are not clear with some authors reporting strong mean stress effects and frequency dependence absent in other studies. These discrepancies have been discussed in Chapter 1 (1.7.4 and 1.7.8a). Moreover the environmental effect on fatigue crack propagation is scarcely known (see Paragraph 1.7.5) It was therefore decided to extend the experimental programme by a series of similar tests on this material.

Tests were conducted in the full subcritical range at two different loading frequencies (0.25 and 35 Hz) under R = 0, variable K_m conditions; at specific constant values of K_m (15.8, 31.6 and 47.5 $MN/m^{3/2}$) and at various constant values of ΔK.

(A) The da/dN- ΔK Relation and the Effect of K_m and ΔK in Air.

Early tests were conducted at R = 0 and at various K_m and ΔK values. Results presented in Tables 5 and 6 show da/dN increasing both with ΔK and with K_m.

The crack growth curves obtained from tests at 35 Hz, in which K_m was maintained constant at 31.6 $MN/m^{3/2}$ and ΔK was fixed at specific levels between 15.8 and 57 $MN/m^{3/2}$, are shown in Fig. 25. There is a typical linear relationship in each case and the growth rate increases with ΔK. Tests at ΔK equal to 57 $MN/m^{3/2}$ and 31.6 $MN/m^{3/2}$ were repeated at a frequency of 0.25 Hz, and the results are shown superimposed on the same line. Clearly there is no frequency effect under these conditions. Numerical results

appertaining to all the tests are given in Table 5 (0,25 Hz) and Table 6 (35 Hz).

Crack growth rate data for both frequencies are plotted as a function of ΔK in Fig. 26; a family of K_m = constant curves, corresponding to K_m = 15.8, 31.6 and 47.5 $MN/m^{3/2}$, is shown together with the curve corresponding to R = 0 and various K_m conditions. Data for K_m = 23.7 $MN/m^{3/2}$ at 0.25 Hz was also obtained but is omitted from Fig. 26 for clarity

The present results for R = 0 agree well with the Maddox data (174) Fig. 26 obtained in what is usually described as Region II of crack propagation. In general the effect of frequency is negligible (Fig. 26), and for a given ΔK value crack growth rate increases with K_m although as ΔK increases the relative differences in crack growth rates become smaller. Hence the early Paris law again fails to explain the large variations in crack growth rates in tests at constant, but different ΔK levels.

Threshold data in the form of ΔK_{th} have been obtained from each curve in Fig. 26 by repeating the procedure previously adopted in RR58. It can be seen that ΔK_{th} decreases as K_m increases in the same way as reported earlier for RR58.

(B) The da/dN- ΔK Relation and the Effects of K_m and ΔK in 3.5% NaCl

Crack growth rate is plotted against ΔK in Fig. 27 for tests conducted at 35 Hz. The curves for the same frequency obtained in air (Fig. 26) are also plotted. In this particular loading frequency (35Hz) the effect of the environment is negligible.

The numerical values of ΔK_{th} have been obtained in the same way as in RR58 and were not affected by the environment (Fig. 27). The maximum value of ΔK_{th} is for R = 0 and was assumed to be 6.33 $MN/m^{3/2}$. Each curve in Fig. 27 has produced a different ΔK_{th} value which is seen to decrease

as the applied K_m increases. Some tests conducted at applied ΔK values below the assumed ΔK_{th} values failed to produce any growth after 10^7 cycles and were discontinued (see Figs. 26 and 27).

Tests at the lower frequency (0.25 Hz) revealed a crack growth pattern for some values of ΔK not observed either in RR58 or in this material at the higher frequency. During each constant ΔK test the crack growth rate was initially constant, increasing with ΔK (Fig. 28). At a later stage blunting occurred and finally the crack arrested. The arrest points are indicated by the letter A in Fig. 28 and it was observed that the time for crack arrest, t_a, (or the corresponding number of cycles) is increasing with ΔK and with the crack growth rate for the initially sharp crack. The tests performed at the three different constant values of K_m (15.8, 31.6 and 47.5 $MN/m^{3/2}$) showed a similar trend (Fig. 29). Each curve produced a limiting value of ΔK at which the crack does not arrest, and the time to crack arrest increases with K_m.

The crack arrest phenomenon is dependent on the crack growth rate as illustrated in Fig.30. Crack blunting and subsequent arrest were not obtained above a certain value $(da/dN)_b$ which for this material and environment is about 3.2×10^{-4} mm/cycle. A typical example is given in Fig. 31 for two tests under R = 0 loading in which it is seen that no crack blunting and arrest occurred in test 1 for a ΔK value of 23.73 $MN/m^{3/2}$. However in test 2, performed in the same specimen and following test 1 blunting has occurred after 130 h approximately for an applied ΔK value of 19 $MN/m^{3/2}$. This latter value is below the limiting value of ΔK = 22.4 $MN/m^{3/2}$ obtained for crack arrest under R = 0. (Fig. 29).

It should be noted that the time interval selected for the tests in which blunting has not occurred is conditioned by the length available for crack growth. For example the duration of test 1 was about 200 hours and since a constant crack growth rate was being obtained and also visual inspect-

ion revealed a sharp crack the test was therefore discontinued. Other tests in which blunting was not detected were extended for more than 175 hours (Fig. 29) and the crack growth rate did not show signs of diminishing.

Crack growth rate data is presented in Table 6 and the respective plot $\frac{da}{dN}$ against ΔK in Fig. 32 including the curves representing the results in air at thesame frequency, and taken out from Fig. 26. A family of curves can be drawn from the data points with curve 1 corresponding to the R = O, (various K_m and ΔK) tests and curves (2-4) to the constant K_m tests.

The effect of K_m on the crack growth rate for a sharp crack and at a given ΔK value is similar to that previously reported for RR58. However only two different regions of crack propagation were obtained and are identified in Fig. 32. The crack growth rate is faster in 3.5% NaCl than in air, by a factor of 2 approximately.

The threshold values, ΔK_{th} were obtained from the extrapolation of the lower crack growth rate data to 10^{-7}mm/cycle. Each curve in Fig. 32 produced a ΔK_{th} value which is not influenced by the 3.5% NaCl solution but decrease as K_m increases with a maximum value for R = O loading of 6.33 $MN/m^{3/2}$.

When cycling at ΔK values below ΔK_{th} no growth was observed and after approximately 72 hours a blunt crack was formed with a tip radius approximately equal to that observed at arrest for $\Delta K > \Delta K_{th}$. These threshold points characterized by zero growth and progressive blunting are identified by the letter T in Figs. 29 and by arrows in Fig. 31.

2.2.3 Fatigue Crack Propagation in LM30 in Air and in 3.5% NaCl

To the author's knowledge there is no published fatigue crack growth data for cast aluminium alloys.

The main objectives of this investigation were to obtain fatigue

crack propagation data in the entire subcritical range (from threshold to fast fracture) and to compare the behaviour of a cast aluminium alloy (LM30) with that of a high strength aluminium alloy (RR58).

(A) The da/dN- ΔK Relation and the Effect of K_m and ΔK in Air

The experimental programme included tests at R = 0, various K_m and ΔK values, and tests at constant values of K_m namely 5.5 and 12.1 $MN/m^{3/2}$. In all the tests a linear relationship between crack growth and number of cycles was obtained with da/dN increasing with ΔK and K_m. The complete crack growth rate data on this material is presented in Table 7.

The crack growth rates da/dN are plotted against ΔK in Fig. 33. The pattern of the results is the same as that observed for RR58 and BS15. The family of curves in Fig. 33 (curves 1-3) shows these distinct regions of crack propagation. Curve 1 represents the R = 0, variable K_m tests and curves 2 and 3 the tests at constant K_m values (R > 0). Extremely high crack growth rates were obtained in Region III (up to 1.2 mm/cycle) which were not observed in the other materials. Also Region III is more extensive in this alloy.

Threshold data was obtained in the usual way ($\frac{da}{dN} < 10^{-7}$ mm/cycle) and in some tests no measurable crack growth was detected (Fig. 33 and Table 7). ΔK_{th} was obtained for each curve with a maximum value for R = 0 of 7.4 $MN/m^{3/2}$.

(B) The $\frac{da}{dN}$ - ΔK Relation and the Effect of K_m and ΔK in 3.5% NaCl

In this environment the tests were performed at the same K_m and ΔK values as the tests in air. Hence a direct comparison can be made between corresponding tests by analysing the results presented in Table 7.A linear relationship between crack growth and number of load cycles was obtained with da/dN increasing with ΔK and K_m.

The obtained crack rates, $\frac{da}{dN}$ are plotted against ΔK in Fig. 33 presenting a similar pattern to that of the results in air. Crack growth rate is accelerated in 3.5% NaCl with the difference increasing as ΔK decreases. In Region III very high crack growth rates were obtained repeating the pattern observed in air.

ΔK_{th} values were obtained with a maximum value of 6.9 $MN/m^{3/2}$ for $R = 0$.

One LM30 broken specimen is shown in Fig. 20 (Spec. 3). The fracture surface is macroscopically flat produced by the largely developed plane strain conditions already observed in RR58. However the fracture surface appearance is considerably different, very irregular, showing fracture planes at various angles and depths.

2.3 Discussion of Results

2.3.1 The Threshold Results

It is recognised that the threshold determination might be sensitive to the test method used (as discussed by Bucci (185)). However, careful precautions, such as adequate precracking, avoidance of overloading and of residual stresses etc. have been taken in the present tests. All threshold data were obtained either by extrapolation of lower rate data to 10^{-7} mm/cycle, or from zero growth tests, and the ΔK levels corresponding to the threshold points are on average 10-20% above or below the ΔK level in the immediately preceding test. (Tables 3-7). Hence any delay or transient acceleration phenomenon is effectively eliminated (See Para. 1.7.8D)

(A) Theshold Results in RR58 and LM30

The threshold results for RR58 will be analysed first. In Fig. 19

and for R = 0 in laboratory air at a frequency of 35 Hz the value of ΔK_{th}, obtained by extrapolation of the lower rate data, is 4.37 $MN/m^{3/2}$. Testing at still lower crack growth rates is very time-consuming. This value is higher than the 1.65$MN/m^{3/2}$ for pure aluminium and 2.09$NM/m^{3/2}$ for a 4.5% Cu-Al alloy (BSL65) quoted by Frost(81). Both materials have been tested at frequencies between 25 and 30Hz(186). In 2024-T3 Hudson(86) obtained a threshold value of 2.75 $MN/m^{3/2}$, but data presented by Donahue et al (187) gives 5.5 $MN/m^{3/2}$, for the same alloy and test frequency. It should be pointed out that all the data for 2024-T3 were obtained on specimens with about 2.5 mm thickness while Frost's work (81) was on 6.5 mm thick specimens, which seems to indicate a thickness dependence. Although comparable threshold data at a range of frequencies and R-ratios for RR58 are not available, the present result is considered to be high even when compared with the values of 4 $MN/m^{3/2}$ (R = 0) reported by Schmidt and Paris (133) for 2024-T3 alloy (the same series as RR58) at a very high frequency (300 Hz).

ΔK_{th} values obtained from Figs. 14 and 24 are presented in Table 8 and plotted against K_m in Fig. 34. ΔK_{th} decreases linearly with K_m for both frequencies and environments. ΔK_{th} is only 12% lower in the 3.5% NaCl solution than in air and is 20% lower at 35 Hz than at 0.15 Hz.

There is no measurable difference between ΔK_{th} values at 35Hz in air and in 3.5% NaCl. Data from Feeney et al (67) obtained in 2024-T3 with the same crack orientation as in the present tests and at a testing frequency of 2 Hz are superimposed on Fig. 34 and agree well with the present results.

The above results seem to indicate a frequency dependence of the threshold for crack propagation in these alloys, ΔK_{th} decreasing with increasing frequency.

In LM30 the threshold values of ΔK are presented in Table 8 and plotted against K_m in Fig. 34. The value of ΔK_{th} for R = 0 (7.4 $MN/m^{3/2}$) is higher than the comparative threshold results presented by Weiss (132).

and Donahue et al (187) for high strength aluminium alloys. Donahue et al (187) reported an increase in ΔK_{th} with decreasing yield stress. Since LM30 has considerable lower yield stress than RR58 this may explain the difference.

An alternative plot of $\Delta K_{th}/E$ against R is shown in Fig. 35. Tests at very high stress ratios (above 0.9) have not been completed, but the results obtained below that value provide a good fit to a smooth curve Fig. 35. The curve may be expressed by the relation

$$\frac{\Delta K_{th}}{E} = \left[\frac{\Delta K_{th}}{E}\right]_{R=0} (1-R^2)^{\alpha'} \qquad (2.4)$$

with $\alpha' = 0.55$ for RR58 at 35 Hz; $\alpha' = 0.73$ for RR58 at 0.15 Hz in air and 0.65 in 3.5% NaCl. For LM30 $\alpha' = 1.1$ in air and 3.5% NaCl. The above equation is more general than the Grandt and Gallagher expression (136) in which $\alpha' = 1$.

A sudden change in the shape of similar curves observed by Schimdt and Paris (133) for 2024-T3 aluminium and A533 steel (albeit at lower values of R than those investigated here) was explained by a crack closure originally discussed by Elber (91) but it is doubtful that such a change would occur in RR58 and LM30. It should be mentioned here that the analysis of the fatigue tests on RR58 performed by Pearson (89) led to unexpected discrepancies; thus the possibility of behaviour different from that commonly observed in class 2000 aluminium alloys should not be ruled out.

(B) Threshold Results in Mild Steel BS15

Threshold data in the form of ΔK_{th} are presented in Table 8 and plotted against K_m in Fig. 36. Other threshold data included in Fig. 36 was obtained from four different steels (94-97) whose crack growth rate characteristics will be analysed in more detail later. The threshold data varies between stress ratios of 0 to about 0.95, as evidenced by the four

constant R lines drawn in the figure. The BS15 threshold results agree well with Frost's for cold rolled mild steel. At stress ratios near 0, A533 B-1 and EN3A mild steel have better threshold behaviour than the other steels, but when $0.5 < R < 0.95$ the best results are those for cold rolled mild steel and BS15.

In Fig. 37 the factor $\Delta K_{th}/E$ is shown as a function of the stress ratio at the threshold points. This curve is significant since it has been suggested that for a given stress ratio the factor $\Delta K_{th}/E$ may be material dependent (135). When plotted on this basis it may be seen that for the present steels data does not fall on one single line. Hence, at least for these materials, the ratio $\Delta K_{th}/E$ is not material independent. For cold rolled mild steel and BS15 Eq. (2.4) fits the threshold data well with $\alpha' = 0.5$. This equation gives better correlation of these results than the Grandt and Gallagher expression (136) shown superimposed on Fig. 37.

A crack closure approach shows a reasonable correlation with data obtained for A533 B-1 steel (133) as indicated in Fig. 37 but no such agreement was obtained for BS15, the crack closure estimate for which is also shown in the figure. This curve may be established since crack growth does not occur for cycling conditions in which $K_{min} < K_{cl}$ when

$$K_{max} = K_{cl} + \Delta K_o = \text{constant} \qquad (2.5)$$

where K_{cl} is the value of the stress intensity factor necessary to open the crack and ΔK_o is the stress intensity range above K_{cl} which must be exceeded for crack growth to occur. These definitions of K_{cl} and ΔK_o follow the ones proposed by Elber (91). Hence from Eq. (25).

$$\Delta K_{th} = K_{max} - K_{min} = (K_{cl} + \Delta K_o)(1-R) \qquad (2.6)$$

Also, for $K_{min} > \Delta K_{cl}$, crack growth does not occur when $\Delta K_{th} = \Delta K_o = \text{constant}$.

Thus when R = O

$$[\Delta K_{th}]_{R=O} = K_{cl} + \Delta K_O \qquad (2.7a)$$

and when $K_{min} > K_{cl}$

$$\Delta K_{th} = (\Delta K_{th})_{min} \qquad (2.7b)$$

This condition is met when R = 0.5, and enables the two straight lines forming the curve for BS15 to be drawn. The inference is then that for all values of R > 0.5, $\Delta K_{th}/E$ should remain constant. That this is not the case is clearly indicated by the data shown in Figs. 35 and 37. The crack closure approach is not appropriate for cold rolled mild steel nor BS15, and any attempt to use it will lead to a very conservative estimate of ΔK_{th}.

2.3.2 The Effect of Environment and loading Frequency

(A) Environmental and Loading Frequency Effects in RR58 and LM30

Two K_m = constant curves were taken from Figs. 14 and 24 and a comparison between them is made in Fig. 38 together with the R = O curves, to assess the effect of 3.5% NaCl solution on crack growth rate.

In comparison with laboratory air the 3.5% NaCl solution lowers the threshold value for crack propagation and causes an increase in fatigue crack growth rate which varies from a factor of 2 in Region II and about one order of magnitude in Region I (Fig. 38). However at higher K_{max} values e.g. 21 $MN/m^{3/2}$ (Region III), no significant difference between the crack growth rates was observed. However at 35 Hz (Fig. 19) the crack growth rates were not significantly affected by the environment.

Acceleration of crack growth rate in a 3.5% NaCl solution is usual for aluminium alloys as extensively discussed in section 1.7.5 and in Refs. (67, 114-122). The above results indicate that corrosion fatigue is a time dependent phenomenon and environments that can corrode and embrittle

the material at the crack tip will increase the rate of crack growth with the effect being most pronounced at low crack growth rates (Region I) and at low frequencies (0.15Hz). Extensive dissolution not accompanied by material embrittlement at the crack tip leads to crack blunting (e.g. mild steel BS15). Local dissolution was experimentally observed in the crack tip region but it did not affect the geometry of the crack tip, i.e. the crack remained sharp during propagation.

The effect of K_m is similar for both environments when compared with the R = 0 curves (Fig. 38).

A frequency effect was observed in the tests conducted in laboratory air. Rates of crack propagation in air are shown in Fig. 39 for comparative purposes. In Region II the crack growth rate increases as frequency decreases, but for lower ΔK values (Region I) the corresponding curves for the two frequencies cross (points A and B, Fig. 39) and the crack growth rate is higher and the threshold is lower at .35 Hz. As mentioned above, the frequency effect on crack growth rate in high strength aluminium alloys has only been studied in limited crack growth rate regions, usually in Region II (80, 114, 121, 122, 139, 140). In Region III it is seen that the results are strongly dependent on K_c. Hence in specimens with lower K_c values the transition from Region II to III occurs at lower ΔK values and the crack growth rate may be higher at 35 Hz (curves 3, Fig. 39).

Data presented by Bradshaw and Wheeler (139) for 5070A aluminium alloy shows that the crack growth rate curves for loading frequencies of 100 and 1 Hz cross at $\Delta K = 5.5$ MN/m$^{3/2}$. The data also strongly suggests a higher threshold value at the lower frequency. The present results support this trend with the crossover point (point A) occurring at a ΔK value of about 7 MN/m$^{3/2}$.

The increase in crack growth rate with decreasing frequency was explained by Bradshaw and Wheeler (139) as being caused by an environmental

effect obtained in the reaction between the surrounding gas(air) and the freshly exposed metal at the crack tip. Thus at the lower frequency there is more time available for the reaction between the constituents of ordinary air such as oxygen, nitrogen and water vapour and the metal. Therefore this effect should be more pronounced at lower ΔK levels. The results presented in his work (139), and the present results do not support the above conclusion. Indeed, for ΔK values below those at points A and B (Fig. 39) the crack growth rate is higher at the higher frequency. It is thought that some of the acceleration of crack growth rate in air is due to an environmental effect (presence of oxygen and water vapour in air) but that is largely due to an intrinsic frequency effect of the material which may be detected by performing tests in a vacuum. Further study of the frequency effect is necessary to clarify these points.

For the LM30 cast aluminium alloy the data presented in Fig. 33 indicates that the 3.5% NaCl solution accelerates the crack growth rate with respect to that in air and lowers the threshold value for crack propagation producing a similar effect to that on RR58. Thus $\frac{da}{dN}$ is accelerated by a factor of 7 at lower ΔK values (Region I), by a factor of about 2 in the top of Region II and finally in Region III the results from both environments are practically coincident.

(B) Environmental and Loading Frequency Effects on BS15

The frequency and threshold behaviour observed in BS15 is in line with the behaviour of high strength steels (122, 123,127 and 128). However crack blunting has not been reported in these latter materials.

Crack blunting and subsequent arrest are known to occur in stress corrosion, as investigated by Creager and Paris (188) but neither in stress corrosion nor in corrosion fatigue has the infleunce of external variables been fully investigated.

The existance of a critical value $(\frac{da}{dN})_b$ above which blunting does not occur (Fig. 30) can be explained by a combination of dissolution and crack propagation. The dissolution and oxidation processes contribute not only to the crack advance per cycle but also to increase its radius of curvature. The latter effect may be obtained if the environmental effect does not cause enough material embrittlement.

If the rate at which the crack propagates exceeds the rate at which its radius of curvature increases then the crack tip will remain sharp and blunting and arrest will not occur. Hence a critical rate of crack propagation may be obtained so that blunting and crack arrest will be observed if the crack growth rate is below that value.

When the initial crack growth rate (sharp crack) is below $(\frac{da}{dN})_b$ the crack is being widened at a faster rate than it advances. As the radius of curvature increases the crack growth rate will be reduced until a radius of curvature is reached where arrest occurs. This provides a qualitative explanation of the shape of the curves presented in Fig. 28. Additionally with increasing crack growth rate (below $(\frac{da}{dN})_b$) more time will be necessary to reach that critical radius of curvature responsible for crack arrest, since a larger volume of material will have to be removed. Hence the crack growth rate will increase with the time to crack arrest which is supported by the results presented in Fig. 30.

The dissolution process also contributes to increase in crack growth rate in relation to comparative tests in air in the absence of any blunting effects i.e. in the early stages of cracking when $(\frac{da}{dN}) < (\frac{da}{dN})_b$ and in the overall test if $\frac{da}{dN} > (\frac{da}{dN})_b$.

The stress conditions at the crack tip leading to deceleration and arrest of blunt cracks are discussed in (188). The tangential stress σ_t at a crack tip having a radius of curvature ρ may be qualitatively expressed by the equation derived by Heckel and Wagner (189).

$$\sigma_t \simeq \frac{\Delta K}{\rho^{\frac{1}{2}}} \qquad (2.8)$$

which shows that as ρ increases σ_t decreases. It is also assumed that the decreasing value of σ_t reduces the local value of ΔK. The effective value of ΔK, ΔK_{ef}, may characterize the stress distribution at the crack tip. ΔK_{ef} decreases as ρ increases and at arrest ΔK_{ef} might be equal to ΔK_{th}, the threshold value of ΔK in the same environment and for a sharp crack.

Further analytical work is necessary to establish the appropriate stress distribution at the crack tip for different geometries and ρ values. The data presented in Figs. 29 and 30 may be of interest for design purposes as at some subcritical ΔK values a corrosive environment may be beneficial and ultimately lead to the arrest of a crack. In such a situation an initial corrosive crack propagation may be tolerated.

2.3.3 A Semi-Empirical Fatigue Crack Propagation Model

(A) Proposed Model

All the data collected in the experimental programme showed that both ΔK and K_m have a significant influence on the fatigue crack growth process. The above influence is similar to that reported in the study of Region II fatigue crack propagation in high strength aluminium alloys and steels carried out by Arad et al (101) in this department. Thus Eq. (1.32) has been applied with considerable success for predicting the mean stress effect in those materials. It seems therefore appropriate to study the behaviour of the function $\frac{da}{dN} = F(\lambda)$ and considering Eq. (1.32) $\frac{da}{dN}$ may be expressed in the form

$$\frac{da}{dN} = \beta\lambda^{n_1} = \beta(K_{max}^2 - K_{min}^2)^{n_1} = \beta(2\Delta K K_m)^{n_1} = \beta'(\Delta K K_m)^{n_1} \qquad (2.9)$$

with the constant $\beta' = \beta 2^{n_1}$. Plotting log $(da/dN)/\beta'$ against log ΔK for

different K_m values with a hypothetical value of $n_1 = 1$ produced the curves shown in Fig. 40 showing that this predicted mean stress effect corresponds to the experimental results for Region II crack propagation (see Figs. 14, 19,24,26,27,32,33,38 and 39).

The numerical values of λ are given in Tables 3-7 and the plots $\frac{da}{dN}$ against λ are shown in Figs. 41, 42 and 43 for RR58, BS15 and LM30 respectively. In the case of RR58 (Fig. 41) and LM30 (Fig. 43) and as already observed in the study of aluminium alloys 2024-T3 and 7075-T6 (101) the agreement with λ in Region II is good between 10^{-4} mm/cycle and 10^{-2} mm/cycle. In BS15 (Fig. 42) the agreement with λ was obtained from 5.0×10^{-5} mm/cycle to 2.0×10^{-3} mm/cycle - well inside the range of agreement with λ for cold rolled mild steel and 6N$_i$-4CO-0.25C steel (101). It is apparent that the use of this parameter has the effect of bringing all the experimental data onto a single curve in Regions II and III, although in Region I λ is dependent on K_m. This latter region is approaching threshold conditions and a rapid increase in crack growth rate occurs at higher values of λ in Region III.

To predict behaviour in Regions I and III, and also to normalise crack growth data in the entire subcritical range a modification of the early Arad equation, Eq. (1.32) may therefore be described as follows:

For lower crack growth rates ($<2.5 \times 10^{-5}$ mm/cycle) λ is strongly dependent on K_m and its threshold value $\lambda_{th} = 2\Delta K_{th} K_m$ influences crack growth in this region (Region I). A sharp increase in growth rate occurs for higher values of K_{max} approaching the critical value K_c. These two values provide the limiting conditions of the model

$$\lim_{\lambda - \lambda_{th}} \frac{da}{dN} = 0 \qquad \text{and} \qquad \lim_{K_{max} \to K_c} \frac{da}{dN} = \infty \qquad (2.10)$$

Hence in the modified model the term $\lambda - \lambda_{th}$ should figure in the

numerator and $K_c - K_{max}$ in the denominator. A generalised equation may be chosen as

$$\frac{da}{dN} = A_c \Phi^{\alpha} \tag{2.11}$$

where $$\Phi = \frac{\lambda - \lambda_{th}}{K_c^2 - K_{max}^2} = \frac{2K_m(\Delta K - \Delta K_{th})}{K_c^2 - K_{max}^2} \tag{2.12}$$

and A_c and α are constants.

In LEFM (Appendix A) the stress intensity factor K is related to the crack tip opening displacement (COD) and the J contour integral or crack extension force G (Appendix A). Hence Eq. (2.11) may be re-written in terms of the crack opening displacement and crack extension force as

$$\frac{da}{dN} = A_c\left(\frac{\Delta v - \Delta v_{th}}{v_c - v_{max}}\right)^{\alpha} = A_c\left(\frac{\Delta G - \Delta G_{th}}{G_c - G_{max}}\right)^{\alpha} \tag{2.13}$$

where $\Delta v = v_{max} - v_{min}$, $\Delta G = G_{max} - G_{min}$, v_{max} and v_{min}, G_{max} and G_{min} are the maximum and minimum values of v and G respectively, Δv_{th} is the threshold value of Δv for crack extension, v_c and G_c are the critical values of v and G for unstable fracture and ΔG_{th} is the threshold value of ΔG. For plane stress conditions ΔG_{th} is given by

$$\Delta G_{th} = \frac{(K_{max}^2)_{th} - (K_{min}^2)_{th}}{E} \tag{2.14}$$

where $(K_{max})_{th}$ and $(K_{min})_{th}$ are the maximum and minimum values of K at the threshold point. ΔG_{th} represents the variation in cyclic potential energy with crack length, assuming that crack growth is still obtained at the threshold point (which is approximately true since $da/dN < 10^{-7}$ mm/cycle).

The parameter Φ is an energy or crack opening displacement ratio. It has the same dimensionless value whether expressed in terms of K, G or COD. Crack growth rate increases as $(\Delta v - \Delta v_{th})$ increases and as v_{max} approaches to v_c. These relations, Eqs. (2.11, 2.13) imply that

crack growth will occur when a certain level of $\Delta v > \Delta v_{th}$ is attained and when $v_{max} \rightarrow v_c$ or $G_{max} \rightarrow G_c$ unstable fracture is obtained.

(B) The use of the Proposed Model for Representing Experimental Data

In this section da/dN will be plotted against Φ not only for the investigated materials but also for relevant data on steel taken from the literature.

In calculating Φ appropriate values of K_c were taken. Thus for RR58 and LM30 the K_c value for the particular specimen being tested was assumed in the calculation (Table 2). For BS15 K_c was taken as 98 $MN/m^{3/2}$ (190). In tables 3-7 the numerical values of Φ are given. In RR58 at 0.15Hz da/dN is plotted against Φ in Fig. 44. A linear relationship is apparent. The Φ plot for RR58 at 35 Hz is shown in Fig. 45 and for LM30 in Figs. 46 and 47. The corresponding data in mild steel BS15 is presented in Fig. 48 for laboratory air and Fig. 49 for the 3.5% NaCl solution. All the data presented in Figs. 44-49 show a linear relation over the complete range from threshold to rapid fracture conditions.

In appropriate cases for which the literature (94-97) gave sufficient data over a wide range of crack growth rates, the model has been applied to other materials. Relevant threshold data has been indicated in Figs. 36 and 37 and the variations in crack growth rates with Φ are shown in Figs. 50-52 for tests in which the stress ratio R was constant. In these cases the parameter Φ could be calculated as

$$\Phi = \frac{(1-R^2)\left(K_{max}^2 - (K_{max}^2)_{th}\right)}{K_c^2 - K_{max}^2} \qquad (2.15)$$

where K_c was assumed to be the same as in BS15 except for A533 B-1 where a value of 125 $MN/m^{3/2}$ had been established (96).

Φ may be considered a valid crack growth parameter for each of the

materials over the range tested e.g. for mild steel (95), Fig. 50 a range of crack growth rates of 10^{-7} to 10^{-3} mm/cycle, for cold rolled mild steel (94), Fig. 51, 10^{-7} to 10^{-2} mm/cycle and for A533 B-1 steel (96), Fig. 52 10^{-7} to 10^{-2} mm/cycle approximately. In each of the above cases the parameter Φ may be considered valid over the full subcritical range. In the case of EN3A mild steel (97), Fig. 53 the parameter appears equally valid, although in this case the maximum crack growth rate had been restricted to 10^{-3} mm/cycle and the full range of Region III may not therefore have been explored. It should be noted that in Figs. 50 and 53 the authors' actual data points are indicated, but in Figs. 51 and 52 it was necessary to indicate the mid points of scatter bands at randomly chosen $\frac{da}{dN}$ values, since only scatter bands were available.

The above results clearly demonstrate that for mild and low alloy steels the parameter Φ is capable of expressing by a single line data obtained at any values of ΔK, R or K_m. Similar checks on other materials like high strength aluminium alloys and steels must be made before the relationship is generally considered to be a good predictor of crack growth rates in metals. The satisfactory agreement given by the parameter Φ in all these metals is particularly encouraging, especially if the relationship is used for material selection and design purposes.

The relation (2.13) offers to the designer a single expression covering the full subcritical range and normalising the stress ratio effect and threshold behaviour which are not fully accounted for by other expressions mentioned earlier (Paragraph 1.7.4). The selection of materials can be most conveniently performed by using the parameter Φ without the inconvenience of the use of different equations for different stress ratios and in different regions of crack propagation.

(C) Trends of Variation in α and A_c Coefficients

The numerical values of α and A_c are given in Table 9. The inference taken from those values is that α and A_c are dependent on material, frequency and environment.

For RR58 tested in laboratory air when the frequency increased both α and A_c decreased. However in 3.5% NaCl A_c decreased but α remained practically constant (frequency independent). Hence the frequency effect for RR58 in air is such that the crack growth rate curve for the lower frequency will lie above the curve for the higher frequency (Fig. 45) with the difference increasing for higher values of Φ.

On the other hand the 3.5% NaCl environment causes a decrease in α and an increase in A_c at 0.15 Hz when compared to the results in air. Consequently the data presented in Fig. 44 converge with increasing values of Φ, the accelerating effect of 3.5% NaCl being practically non-existent for Φ values greater than 10. ($da/dN > 2.5 \times 10^{-2}$ mm/cycle). At 35 Hz α and A_c are not dependent on the environment.

For LM30 (Figs. 46 and 47) both α and A_c showed the same trend as for RR58. However the increase in A_c from air to 3.5% NaCl is smaller than that for RR58 (30% increase compared to a factor of about 2.5). The Φ plot shows, therefore, a considerable minor effect of the 3.5% NaCl solution on the crack growth rate for LM30.

In BS15 and at 0.25 Hz α decreased and A_c increased when the environment was changed from air to 3.5% NaCl (Figs. 48 and 49 and Table 9). The frequency effect in 3.5% NaCl led to a decrease in A_c and an increase in α on increasing the frequency from 0.25 to 35 Hz (Fig. 49 and Table 9). BS15 therefore shows the opposite trend to that reported for RR58.

Values of α and A_c for the other data on steel selected from the literature [94-97] are also shown in Table 9. α and A_c varied from material to material, with Frost's mild steel (Fig. 49) giving the minimum values. If

any steel selection was to be carried out in terms of crack growth rate resistance this material would be the obvious choice.

Another immediate advantage of the law described by Eq. (2.11) is illustrated by the fact that when plotting da/dN against Φ it is possible to say that RR58 has better crack growth rate characteristics than LM30 in both environments (Figs. 46 and 47).

2.3.4 An Example of the Application of the Proposed Model to Calculate the Number of Cycles to Failure

The semi-empirical model described by Eq. (2.11) can be used to calculate the number of cycles to failure, N_f spent in crack propagation Thus Eq. (2.11) may be expressed in terms of the stress ratio as

$$\frac{da}{dN} = A_c \left[\frac{(1-R^2)(K_{max}^2 - (K_{max}^2)_{th})}{K_c^2 - K_{max}^2} \right]^{\alpha} \tag{2.16}$$

By its turn and using the definition of K (Appendix A).

$$K_{max}^2 = Y^2 \sigma_{max}^2 \pi a \ , \tag{2.17a}$$

$$(K_{max}^2)_{th} = Y^2 \sigma_{max}^2 \pi a_i \tag{2.17b}$$

and $$K_c^2 = Y^2 \sigma_{max}^2 \pi a_c \tag{2.17c}$$

Substituting Eqs. (2.17a,c) in Eq. (2.16) and simplifying N_f may be obtained by integrating the equation

$$N_f = \frac{1}{A_c(1-R^2)} \left[\int_{a_o}^{a_c} \left(\frac{a_c - a}{a - a_i} \right)^{\alpha} da \right] \tag{2.18}$$

where a_o is the initial flaw size.

If $\alpha \neq 1$ analytical integration of Eq. (2.18) is extremely difficult, but a numerical integration can be easily carried out in a very small

computer program. On the other hand the derived equation offers two great advantages. First is valid in the entire subcritical range, and the second is valid for any positive values of R.

When $\alpha = 1$ integration of Eq. (2.18) is straightforward and gives

$$N_f = \frac{1}{A_c(1-R^2)} \left[(a_o - a_c) + (a_c - a_i) \left(\ell n (a_c - a_i) - \ell n (a_o - a_i) \right) \right] \qquad (2.19)$$

The plot N_f against a_o is presented in Fig. 54 for BS15 mild steel in air at R = 0. Two different curves are showed corresponding to usual working stress ranges ($\frac{2}{3}\sigma_{ys}$ and $\frac{1}{2}\sigma_{ys}$). The values of a_i and a_c were calculated from Eqs. (2.17b) and (2.17c) with $(K_{max})_{th} = 6.33$ MN/m$^{3/2}$ and the geometry considered in the example is that for which Y = 1, value often used for engineering purposes. The curves presented in Fig. 54 allow the designer to predict the number of cycles to failure in the component assuming that life is totally spent in propagating a crack having an initial size a_o to the critical size a_c. N_f increases when both the working stress and the initial crack length decrease and tend to infinite when $a_o \to a_i$.

CHAPTER THREE

A SHORT REVIEW ON STRESS CORROSION CRACKING IN ALUMINIUM ALLOYS - A FRACTURE MECHANICS APPROACH

3.1 Introduction

Almost all Al-alloys are susceptible to stress corrosion cracking (SCC) in a hostile environment. They usually show intergranular cracking under the simultaneous action of a corrosive environment and applied (or residual) tensile stress. It is known that the degree of corrosion susceptibility is influenced by metallurgical variables such as chemical composition, processing heat treatment and microstructure as well as by the direction of applied stress and the temperature.

Traditionally, SCC data for aluminium alloys have been obtained by exposing suitably stressed smooth unnotched specimens to a corrosive environment. Time to failure (TTF) was then recorded as a function of the applied gross stress, this being usually below the nominal yield stress of the material tested. Smooth specimens are also used to determine a threshold stress σ_{SCC} below which SCC is not observed within a given time. An extensive collection of σ_{SCC} data was presented by Sprowls and Brown (191). The same authors (192) published the contribution of smooth specimen testing (TTF tests) to the understanding of the SCC phenomenon in aluminium alloys.

In the time to failure test it is often difficult to define the applied stress with sufficient accuracy, since it can be highly localised by a surface defect, an internal defect or a corrosion pit. Furthermore, data obtained on nominally smooth specimens included both the initiation and propagation phases of the stress corrosion process and these could not easily be separated. The initiation phase consists of the nucleation and growth of the corrosion pits, while the propagation phase covers the crack growth from microscopic dimensions to critical size. Natural initiation of a crack may conveniently be substituted by the introduction of a very sharp notch, allowing investigation of the

crack propagation phase alone. Since, furthermore, SCC occurs below gross yielding, it is appropriate to use an LEFM analysis.

3.2 The SCC Process in Aluminium Alloys and Parameters which Influence it

3.2.1 The Specimen Orientation in the Plate Material

It was reported by Prestley (193) that aluminium alloys are more susceptible to SCC when tested in the S-L* orientation. Due to the intergranular nature of the SCC process, susceptibility to stress corrosion is a function of the resolved stress component acting normally to the grain boundaries which, in the S-L orientation offer a much larger number of nucleation sites than in other directions. Consequently the degree of SCC is substantially lower in T-L and L-S orientations. It may be noted that tensile tests as well as fracture toughness tests performed on specimens in these orientations show corresponding changes in the respective values of hardness, elongation, tensile stress, yield stress and stress intensity factor.

3.2.2 The Effect of Stress

(A) The Stress Intensity Factor and Testing Techniques.

The similarity concept applied by Schjive (194) shows that similar values of the stress intensity factor, K, characterising the stress field around a sharp crack, should produce similar rates of crack growth. The level of K to cause stable cracking is substantially less than the critical toughness K_c for unstable fracture under statically applied load. Hence in the LEFM approach SCC could be defined as environmentally induced subcritical crack growth under

*A two letter system is used here to identify the testing conditions. The first letter identifies the stressing direction and the second letter the direction of crack propagation in the plate material. The letters are S for the short transverse direction, T for the long transverse and L for the longitudinal (or rolling) direction (Fig. 4).

static tensile stress. LEFM can then predict whether cracks can propagate by SCC, thus overcoming some of the difficulties of the TTF technique.

Knowledge of the stress corrosion crack velocity, da/dt, as a function of K would constitute valuable information for alloy development as well as for the determination of a possible threshold value of K, K_{ISCC}, below which cracks would not propagate or propagate extremely slowly.

A flawed structure can be conveniently represented in the laboratory by a specimen containing an initial sharp crack, appropriately loaded in a hostile environment such as a solution of NaCl in water. Crack growth rate or any other related variable may then be measured and analysed as a function of the applied stress intensity factor K.

Brown (195) has reviewed the application of fracture mechanics to stress corrosion cracking. This included details of specimen designs practically suitable for SCC studies, methods for the determination of K_{ISCC}, experimental techniques of monitoring stress corrosion crack growth and the translation of laboratory data into practical service applications. One of the first test techniques to be used in fracture mechanics SCC studies was also due to Brown (196). A precracked bar stressed in bending as a cantilever beam was used and the propagation of the stress corrosion crack was detected by a standard dial gauge. Chu and Wacker (197) have investigated SCC of 7079-T6 aluminium alloy in sea water using smooth and precracked specimens. They found a general agreement between the results from the two methods.

The DCB specimen is now widely used in SCC studies of aluminium alloys. Its geometry is particularly indicated for the experimental determination of crack growth rates in the S-L orientation. Also another advantage of the DCB specimen is the ease with which SCC data can be obtained from a reduced number of specimens. The first extensive experimental work using this geometry was carried out by Hyatt (198). The environment was a 3.5% NaCl solution and ten high strength aluminium alloys in a variety of heat treatment conditions were tested.

Jacobs and Marcus (199) have recently published the results of a "round robin" stress corrosion testing programme on aluminium alloys in the USA to evaluate and compare techniques for stress corrosion susceptibility testing. Crack growth measurements were performed with several types of fracture mechanics specimens including some parallel and tapered DCB tests. Subsequently a similar programme has been initiated in England (200).

(B) The da/dt-K Diagram

The effects of stress, environment and metallurgical factors are most conveniently studied by analysing the da/dt-K diagram for the investigated material. For the aluminium alloys tested this often shows two different regions of crack propagation. However in some material-environment combinations, such as alumina in water, Evans (201) has observed three different regions.

Speidel and Hyatt (116) have compiled extensive da/dt-K data and characterised the phenomenological trends in both Regions. Thus in Region I da/dt is strongly dependent on K, tending towards the threshold value K_{ISCC}. In Region II there is a plateau velocity (da/dt independent of K); its extent depends on the material and environment. For most alloy-environment combinations Region II extends to K_c. In a few cases, however, as the applied K approaches K_c a sharp acceleration of crack growth occurs, forming what is called Region III.

In some alloys having an equiaxed grain structure macroscopic crack branching is possible. This phenomenon was studied by Speidel (202) who proposed that crack branching may occur if a plateau region (K-independent) exists and the crack tip stress intensity at the point of branching is at least 1.4 times the stress intensity at which Region II begins. These conditions were considered necessary but not sufficient for crack branching. Crack branching in high strength steels was investigated by Carter (203) who stated that the onset of twinning is characterized by a critical stress intensity factor K_{1b}. Later an elaborate theoretical treatment of crack twinning was carried out by

Cherepanov and Kuliev (204). The analysis was based on perturbation theory. The stress intensity factor of each branch was calculated as a function of the applied stress intensity factor and the angle ψ between the branches. To calculate these stress intensity factors, theory of elasticity was applied for a semi-infinite straight slit with two symmetric straight branches. A value K_{1b} was identified, below which (and above K_{ISCC}) the crack propagated at a constant rate and above which it branched. This value was predicted on the assumption that for $\psi = 45^{o}K$ at the tip of one branch attains K_{1C}, to be that at which $K_{1C}/K_{1b} = 1.31$ - comparing well with the experimental value 1.46.

3.2.3 The Effect of Environment

The environment has a most important effect on the nucleation and growth of cracks in aluminium alloys. The measured crack tip velocities can vary by several orders of magnitude depending on the environment that fills the crack.

SCC may occur in gaseous environments, due to the pressure of water vapour; hence crack growth rate increases with humidity. Neither initiation nor propagation of stress corrosion cracks has been observed in a very wide range of aluminium alloys exposed to dry air. Furthermore, crack growth caused by room temperature creep effects has not been observed. The crack growth rates obtained in gaseous environments with very high humidity percentages are considerably less than the crack growth rates obtained in gaseous solutions. In distilled water many aluminium alloys exhibit almost identical crack growth rates to those obtained in gaseous atmospheres of 100% relative humidity (116).

It is of considerable practical importance to investigate SCC in aluminium alloys exposed to aqueous solutions containing chloride and other halides. These halides exist in marine environments and their influence in the cracking process must therefore be known if susceptible alloys are to be used in those

environments. One of the most widely used laboratory simulations of sea water is the 3.5% NaCl solution which was used in the present work.

Data presented in (116) shows that in aqueous solutions the crack growth rate is considerably accelerated in comparison with a distilled water environment. It is realised that this acceleration depends on the metallurgical, mechanical, electrochemical and other parameters which must be controlled if a valid quantitative test is to be attempted.

Usually the crack velocity in aqueous solutions is increased if the salt concentration is increased above a certain critical value. Below this value the crack velocity is not influenced by the concentration. However K_{ISCC} seems not to depend on the concentration, which is somewhat surprising. Some typical examples of the concentration effect on crack velocity may be found in(116). The electric potential and the pH of the solution also influence the crack growth rate. The effect of pH was found to be negligible in Region II and Region I was shifted to lower K values when the solution was acidified.

The effect of temperature in the SCC of aluminium alloys is also of great importance. It is known that in many applications components are subjected to SCC above room temperature. TTF data obtained by Helfrich (205) has shown that higher temperatures can cause a decrease of the time to failure

Speidel (202) has investigated the effect of temperature in 7979-T651 aluminium alloy exposed to a solution of KI. K_{ISCC} decreased when the temperature was increased from $-11^{o}C$ to $105^{o}C$. The plateau velocity in Region II crack propagation increased by one order of magnitude in the same temperature range. The crack velocity da/dt in Region II was approximated by the equation:

$$da/dt = V_o \exp(-Q/R_g T) \qquad (3.1)$$

where V_o is an experimental constant, Q is the activation energy, R_g is the gas constant and T is temperature. In Region I da/dt was given by the empirical equation:

$$da/dt = V_o \exp (-Q+bK)/RT \qquad (3.2)$$

where b is a constant. The crack growth process was found to be thermally activated with constant but different activation energies in Region II and Region I. However in other alloys K_{ISCC} is not influenced by the temperature and even in similar alloys large differences in activation energy were obtained (201). This temperature influence requires further study.

3.2.4 Metallurgical Factors

The stress corrosion resistance of high strength Al-alloys is largely dependent on their composition and heat treatment. No systematic quantitative work has been carried out on the effect of composition excepting a short note on the main metallurgical aspects of aluminium alloys in (116).

Precipitation hardening is of the utmost importance for high strength aluminium alloys (116); in particular the initial stages of precipitation hardening decrease the resistance to SCC while overaging can increase it. The selection of the proper heat treatment may be aided by testing precracked DCB specimens containing ageing gradients along their lengths. This procedure has been used by Hyatt (206).

The quench rate is also a very important factor in stress corrosion resistance. Its influence on K_{ISCC} and other mechanical properties is extensively presented and discussed in (116).

The quenching operation may, however, introduce residual stresses which can lead to extensive crack bowing. Hyatt (207) investigated this residual stress problem and found that crack bowing was caused by residual compressive stresses on the surfaces of the re-heat-treated DCB specimens. The residual stresses can be eliminated by plastically deforming the specimen after quenching. Residual quenching stresses not only increase the chances of initiating stress corrosion cracks but also contribute to an acceleration in the average growth rate. This results from the increased COD and K levels at the crack

tip due to deflections caused by residual stresses. If any comparison is to be made between aluminium alloys care must be taken to verify that the alloys have been similarly heat treated and thus contain equivalent residual stress patterns.

No references to any SCC studies on cast aluminium alloys have been found by the author. Since these alloys usually contain large percentages of silicon it is thought that their stress corrosion resistance is poor (116).

3.3 Stress Corrosion Cracking Theories

It is now widely accepted that SCC is a rather complex phenomenon involving mechanical, chemical and metallurgical aspects. This complexity has made the task of presenting a valid SCC theory extremely difficult. Some of the theories already proposed analyse the problem mainly in one field (fracture mechanics, metallurgical or electrochemical) and do not attempt to relate all the mechanisms involved. Some theoretical treatments of SCC attempt to understand the basic mechanisms near the crack tip at the scale of atomic dimensions - at which, however, observations are extremely difficult to undertake.

Extensive quantitative experimental SCC data have only become available in recent years (116,195,198,200,202,206,207); thus this approach is still comparatively new. Speidel (116) has recently reviewed the available SCC theories prior to 1972. A similar presentation herein will extend to work published since this date.

3.3.1 Activation Energy Theories

In this group are included those theories based on the assumption that da/dt is controlled by the kinetics of a chemical reaction between the metal and the environment. Wiederhorn (208) proposed that stress corrosion should be a thermally activated process and the activation energy was assumed to be stress sensitive. Thus the most rapid reaction between the metal and the

environment (stress activated dissolution) is at the crack tip. By calculating the elastic stress field for blunt cracks (188) it was concluded that to avoid crack blunting the dissolution velocity should be more strongly dependent on stress than a one-half power law. Wiederhorn and Bolz (209) developed the above ideas into a quantitative theory of SCC in which the crack growth rate is given by an equation of the same type as Eq. (3.2) with

$$Q = Q_o + \frac{V_m \gamma_s}{\rho} \tag{3.3}$$

and

$$b = \frac{2V_u}{(\pi\rho)^{\frac{1}{2}}} \tag{3.4}$$

In the above equations Q_o is the stress-free activation energy, V_m is the molar volume, γ_s is the fracture surface energy and V_u is the activation volume.

The model predicted very well the experimental results for Region I crack propagation obtained in (202). Moreover, the slopes of Region I crack growth curves of high strength aluminium alloys are very closely approximated by Eqs. (3.2), (3.3) and (3.4). However, in Region II the equation did not produce satisfactory results. Some of the objections of the model are the extremely difficult task of measuring directly the radius of curvature at the crack tip and the influence of plastic deformation at the crack tip on the fracture energy.

3.3.2 Strain-Enhanced Theories

Two basic models for stress corrosion crack growth are included in this section. Kraft and Mulherin (210), tensile ligament instability model (TLIM) and the recent work by Vermilyea and Diegle (211) on strain enhanced corrosion mechanisms.

The TLIM model (210) postulates that tiny ligaments of size d_T form the bulk metal at the crack tip. During crack growth a critical strain ε_c is reached such that the ligaments are ruptured. i.e. when

$$\varepsilon_c = \frac{K_{1c}}{E(2\pi d_T)^{\frac{1}{2}}} \qquad (3.5)$$

The model assumes that a corrosive environment can reduce the value of ε_c by attacking chemically the outer perimeter of each ligament, but no prediction of the da/dt - K curve is made . K_{ISCC} is estimated to occur when the K level is such that the plastic zone size created equals d_T i.e.

$$K_{ISCC} = \frac{\sigma_{ys}(2\pi d_T)^{\frac{1}{2}}}{1-2\nu} \qquad (3.6)$$

K_{ISCC} is then independent of the environment and is only influenced by metallurgical factors. This conclusion is clearly not supported by the experimental results (116).

The strain enhanced mechanism (211) is based on the assumptions that stress corrosion crack growth can only occur if the ratio between da/dt and the crack tip strain rate $d\varepsilon/dt$ exceeds a critical value which is a function of the crack tip radius, and that each increment of strain must cause sufficient crack advance by stress corrosion to produce another increment of strain. The model was applied to data for steel but the determination of the appropriate strain rates in an elastic-plastic material at the crack tip is, at this stage, far from being satisfactory.

3.3.3 Hydrogen Embrittlement Theories

The hydrogen embrittlement phenomenon has been extensively studied. Hirth and Johnson (212) have recently published a review paper on the subject. In SCC hydrogen embrittlement is more likely to occur in high strength steels.

Leeuwen (213) obtained an equation for Region II of the $\frac{da}{dt}$ - K curve which fitted data for 4340 steel. Cherepanov (214) derived a crack growth theory on the assumption that hydrogen atoms penetrate the material mainly through the fresh crack surfaces. The diffusion of protons forms a zone of embrittled metal near the crack tip. The concentration of protons was calculated and, using an LEFM analysis, a linear relationship between da/dt and K was predicted. The model was successfully applied to Region I data for some high strength steels and one aluminium alloy.

Gest and Troiano (215)demonstrated that for the high strength aluminium alloy 7075 T651 the stress corrosion process was caused by a strain ageing type of reversible hydrogen embrittlement.

3.3.4 Other Stress Corrosion Theories

In this section a brief description of various SCC theories which are not classifiable in the previous sections will be presented.

Cherepanov (216) derived a theoretical model of stress corrosion crack growth based on electrochemical processes. It involves an electrochemical dissolution of the anodic metal at the crack tip and its subsequent failure. Using electrochemical theory an equation for the crack growth rate was obtained indicating a constant rate of crack growth and crack branching at a certain, sufficiently large, value of the applied stress intensity factor. Thus the model only predicts the behaviour in Region II crack propagation.

Theories predicting the stress corrosion performance of high strength aluminium alloys based on metallurgical factors (e.g. microstructure and composition) are scarce. Nielsen (217) has adequately reviewed the main metallurgical factors involved, and Meyn (218) has published a fractographic study of SCC in Al-Zn-Mg alloys.

Smith (219) developed a capillary model specifically taking into account the crack growth rate as a function of crack length, fluid viscosity and surface tension, contact angle and temperature. The capillary flow within the crack was theoretically analysed and was found to be related with the contact angle between the fluid and the crack surfaces.

Liu (220) has proposed that SCC may be caused by stress-induced diffusion of hydrogen or chloride ions in solid solution. The solute atoms are assumed to concentrate at the elastic-plastic boundary. The high concentration of solute atoms near the crack tip will then enhance the reaction between solute and solvent atoms and the low fracture strength of the reaction product may cause crack growth. Because of the mismatch in solute and solvent atomic sizes an elastic interaction field is created. The steady state solute concentration in the presence of this stress field was calculated and was found to increase rapidly near the crack tip. Assuming that the crack growth rate is proportional to the reaction rate between the highly concentrated solute atoms and the bulk material a crack growth rate equation was obtained:

$$\log \left(\frac{da}{dt}/C_o'\right) = \gamma' + \left(\frac{M_o K}{k_c T \delta_2^{\frac{1}{2}}}\right) \qquad (3.7)$$

where C_o' is the solute concentration on crack surfaces, γ' is a constant at a given temperature, M_o is a parameter that determines the magnitude of the elastic interaction, k_c is the Boltzmann constant and δ_2 is a material structural size parameter.

A comparison of Eq. (3.7) with Eq. (3.2) shows that the da/dt-K relation is correctly predicted in Region I.

West (221) put forward a theory based on the energy balance approach. Thus an additional electrochemical energy component is added to the elastic strain energy, reducing the overall energy required for fracture. No experimental data has been presented with which to verify the model.

CHAPTER FOUR

STRESS CORROSION CRACKING IN THE ALUMINIUM ALLOYS RR58 and LM30

In Chapter Two a LEFM approach to an environmental fatigue crack propagation study on the aluminium alloys RR58 and LM30 was described. A logical extension of this study was to undertake a similar investigation of the same materials and corrosive environment (3.5% NaCl) but under static loading conditions (SCC).

The main objectives of this study were to obtain K_{ISCC} and the da/dt-K curve using two different wetting methods and to assess the effect of loading history on crack growth rate. The investigation of the latter two factors is usually absent from the relevant literature although the loading history effect on fatigue crack growth has been extensively studied. (See Chapter 1, Paragraph 1.7.8). Furthermore no stress corrosion studies of cast aluminium alloys have been reported despite the engineering significance of these alloys (e.g. in the car industry) in applications where SCC failures may occur. Thus a comparative study of one cast aluminium alloy (LM30) with respect to the behaviour in high strength aluminium alloys was considered of primary importance.

4.1 Experimental Procedure

4.1.1 Test Rigs.

The test rigs were specially built for the present programme and a unit comprising two of these is shown in Fig. 55. These rigs have a high mechanical advantage (28.2) achieved by a double lever system. They are adaptable to perform tests with the specimens positioned either horizontally or vertically.

4.1.2 Material and Environment Selection

The materials selected for this study were the high strength aluminium alloy RR58 and the cast aluminium alloy LM30. Their composition and principal mechanical properties are presented in Table 1. The plate dimensions and a description of the heat treatment for RR58 are described in 2.1.1.

The environment selected in this experimental programm was 3.5% NaCl solution, allowing a direct comparison with the fatigue crack propagation results. A very small percentage of nitric acid (0.5%) was added to the solution to release any copper which could delay crack growth.

4.1.3 Specimens

The specimens used were the contoured DCB specimens (Fig. 6) whose design, dimensions and preparation were previously described in 2.1.2 and 2.1.3.

4.1.4 Compliance Calibration and Calculation of K_c

The compliance and calculation of K_c are described in 2.1.4 K_c values obtained from the specimens used in the stress corrosion programme are presented in Table 2. After the precracking operation to calculate the compliance and K_c, the specimen could be used for SCC tests at any required stress corrosion load $P_{SCC}<P_c$, producing a constant stress intensity field along the crack path.

4.1.5 Testing Procedure

The test rigs were individually calibrated with strain gauge load cells and the weight of the lever arms and loading pans accurately determined. Careful calibration was of importance since it could be one of the sources of error during actual SCC testing. The accuracy of load measurement was within ±0.5% of the maximum load.

In order to reduce surface corrosion all the specimens were painted with a suitable aluminium paint. It is important to minimise general corrosion of the specimen since it could change the compliance and influence the results.

The specimens were next assembled in the loading jaws, load was carefully applied and corrodent introduced.Initial load application time was not longer than 60 sec, during which time the weight-pan was supported to ensure smooth and steady loading. The corrodent was brought close to the tip of the crack through a rubber capillary tube to effect a continuous drip feed. The flow rate was adjusted so that in each test the specimen received 1 litre of corrodent every 24 hours. The loading of a horizontal specimen and corrodent feeding arrangements are shown in Fig. 10.

In the first series of testson horizontally positioned specimens crack growth rates at different, constant, applied K values were established. As each test progressed crack opening deflection values along the loading axis were measured as a function of time by dial gauges firmly attached to the base of the rig. After each specimen was removed from the rig, its entire surface was thoroughly cleaned. It was then re-inserted into the rig,, reloaded, and the final crack length rechecked using the travelling microscope

A second series of similar tests was conducted but with the specimens fitted vertically in the rigs in order to increase the wetting efficiency of the corrodent on the crack surface while applying the same flow rate.

4.2 Experimetal Results

4.2.1 Stress Corrosion Cracking in RR58 in 3.5% NaCl

A typical increase of deflection, δ, with time for a test performed immediately after initial precracking at K_c = 23.82 $MN/m^{3/2}$ is shown in Fig.56. Crack growth stabilised to a constant rate of 3.1 x 10^{-5} rm/s after a primary

incubation period, t_i, of 28 hours. This curve pattern was very often observed when the K level was reduced from the preceeding test on the same specimen. From this linear variation in deflection, δ, with time, t, $d\delta/dt$ was calculated and used to obtain the crack growth rate da/dt as follows:

$$\frac{dC}{da} = \frac{d}{da}\left(\frac{\delta}{P_{SCC}}\right) = \frac{1}{P_{SCC}} \frac{d\delta}{da} \qquad (4.1)$$

and

$$\frac{da}{dt} = \frac{d\delta}{dt} \Big/ \frac{d\delta}{da} = \frac{\frac{d\delta}{dt}}{P_{SCC}\frac{dC}{da}} \qquad (4.2)$$

Following the terminology used in a previous study by Radon and Culver(222) it was found convenient to describe the primary incubation period, t_i, as the time necessary to reach a constant (secondary) crack growth rate. The incubation period recorded in Fig. 56 was observed in a test with an applied K value (12.76 $MN/m^{3/2}$) lower than that applied in the immediately preceding test (23.82 $MN/m^{3/2}$) on the same specimen. Further typical examples are presented in Fig. 57, in which tests 1 and 4 show comparable (long) incubation times. In test 1 the value of K applied was reduced from the precracking K_c value of 23.60 $MN/m^{3/2}$ to 13.26 $MN/m^{3/2}$ with t_i = 58h, while in test 4, performed at the same K value, the previous K level was only 19.8 $MN/m^{3/2}$, resulting in a shorter incubation time, t_i = 45h.

The complete set of incubation time results is presented in Table 10 for the horizontally aligned specimens and Table 11 for the vertically aligned specimens. In these tables K_r is the K value in the immediately preceeding test and K_s the actual K value subsequently applied.

It was observed that the steady state (secondary) crack growth rate was not significantly affected by the prior stress corrosion history. Tests with the same K values but performed in different specimens will produce different crack growth rate values (see Tables 10 and 11). However this diff-

erence is due to the variation in material homogeneity and heat treatment from specimen to specimen and not to any loading history effect. Crack growth rate is then a function of the alloy, heat treatment, environment and current stress intensity. Several tests were conducted to illustrate this point and a typical example is shown in Fig. 57 where tests 1 and 4 were performed under the same K value (13.2 $MN/m^{3/2}$) using the same specimen and showed practically the same crack growth rates despite different prior values of K.

The effect of increasing the K level was also studied. Test 3 in Fig. 57 and also tests 2 and 3 in Fig. 58 illustrate the observation that on increasing K a temporary and substantial increase in crack growth rate occured, followed by a reduction to a lower rate in the steady regime. In these tests the incubation times were much shorter than those observed previously in tests 1 and 4 Fig. 57. Other tests showed that the incubation period in increasing K tests was always much shorter than in tests under decreasing K, (Tables 10 and 11). The two types of incubation period are identified in Fig. 58 (t_i' under decreased K and t_i'' under increased K).

Crack growth rates, da/dt, in the constant (secondary) rate regime for each test are plotted against the applied stress intensity factor K in Fig. 59. The crack growth rate results are presented in Table 10 for the horizontal specimens and Table 11 for the vertical specimens. Fig.59 shows that results for the specimens tested in the vertical position are above those obtained for the horizontal specimens, and the "threshold" K_{ISCC} was found to be about 6 $MN/m^{3/2}$ for the vertical specimens while it appears to be nearly 7.5 $MN/m^{3/2}$ for the horizontal ones. The da/dt-K curves show three different regions of crack propagation. Region I extends from the threshold to about 17 $MN/m^{3/2}$ (Fig. 59). Note that K_{ISCC} has been established at crack growth rates close to 10^{-7} mm/s (testing times in excess of 30 days) and that all tests were repeated. Region II consists of

a short plateau (K independent region) extending from 17 to 21 $MN/m^{3/2}$ in which the growth rate for the vertical specimens is a factor of 2 above that for the horizontal ones (4.0×10^{-5} to 8.0×10^{-5} mm/s). In Region III the crack growth rate accelerates increasingly as the K_c value is approached, with no measurable difference between the horizontal and vertical results.

4.2.2. Stress Corrosion Cracking in LM30 in 3.5% NaCl

Tests on this alloy were only carried out using horizontally aligned specimens. Typical deflection against time curves for one of the specimens are presented in Fig. 60. The pattern of behaviour is similar to that for RR58, with an incubation time t_i=90h in test 1 ($K = 7.91 MN/m^{3/2}$) corresponding to a reduction in K from the precracking K_c value ($K_c = 21.51 MN/m^{3/2}$ to $K = 7.91 MN/m^{3/2}$. When K was next increased from 7.91 to $9.5 MN/m^{3/2}$ a temporary increase in crack growth rate occurred, repeating the phenomenon already observed in RR58 (Tests 2 and 3, Fig. 58). The incubation times obtained in the test programme are presented in Table 12.

Crack growth rates in the constant rate stage were calculated for each test using Eq. (4.2) and are plotted against K in Fig. 61. The numerical results of tests on LM30 are presented in Table 12.

The da/dt-K curve for LM30 also shows three distinct regions of crack propagation. K_{ISCC} obtained in the same experimental conditions as in RR58 is about $5.5 MN/m^{3/2}$ and Region II shows the K-independent plateau from 8.7 to $18.35 MN/m^{3/2}$ at crack growth rates close to 5.0×10^{-5} mm/s. Region III covers the range of K values from $18.35 MN/m^{3/2}$ to K_c, with a sharp acceleration of crack growth rate towards the K_c value.

4.3 Discussion of Results

4.3.1 The Influence of Load History

(A) Prediction of the Incubation Time Under Decreasing K

Stress corrosion curves of the same type as in Figs. 56,57,58 and 60 are

absent from the literature on SCC in aluminium alloys. Instead similar curves have been obtained by Harrigan et al (223) and Landes and Wei (224) from SCC tests of AlSl 4340 and D6AC steels in distilled water, with an incubation time defined as the time of zero crack growth.

In the present study it is more convenient to consider the effect of the plastic zone size at the crack tip.

When the level of applied K is reduced from K_r, applied in the immediately preceding test, to K_s, a larger plastic zone size exists at the crack tip corresponding to K_r. Its size, r_r, can be calculated for plane strain conditions using Eq. (A.10)

$$r_r = \frac{1}{6\pi} \frac{K_r^2}{\sigma_{ys}^2} \qquad (4.3)$$

The prior load caused a residual stress state at the crack tip. Here it has been assumed that the plastic zone size created by the previous load application under plane strain conditions, may sufficiently characterize the maximum extent of the generated residual stress state. A similar parameter, described as a localised load interaction zone, has been considered in (153, 154) for a special case of fatigue crack growth following a single overload.

However the present approach is more general. While the crack tip remains enveloped by the material plastically deformed(work hardened) during the previous load, the crack growth rate will be reduced. The crack length corresponding to the incubation stage, a_i, would be of the same order of magnitude as r_r. Experimental evidence is presented in Tables 10, 11 and 12 in which a_i is compared with r_r as calculated from Eq. (4.3). The plastic zone size values for LM30 (Table 12) are, in general, 5 times greater than those for RR58 (Tables 10 and 11). The difference is due to the lower yield stress of LM30 (150 N/mm^2) compared with that for RR58 (367 N/mm^2). The corresponding experimental values of a_i do indeed show a similar variation.

The incubation time will be primarily dependent upon the plastic zone

created by the previous load application and the actual level of K applied. Additionally, electrochemical and metallurgical factors may affect the magnitude of t_i. While the emphasis of the current work is on LEFM analysis, a deeper understanding of these aspects involved in the incubation time is necessary.

It is then suggested that

$$t_i = f\left(\frac{K_r - K_s}{K_s}\right) \tag{4.4}$$

where f is an increasing function, since t_i will increase with the difference $K_r - K_s$ and reduce with increasing K_s. The present incubation time results (Tables 10,11 and 12) were plotted in the form of

$$\frac{K_r^2 - K_s^2}{K_s^2} = \frac{r_r - r_s}{r_s} \tag{4.5}$$

in Fig. 62. It should be pointed out that while the crack tip is inside the plastic zone, r_r, r_s will not physically exist, but the incubation time will depend on K_s, which in turn can be expressed in terms of r_s. A good correlation was obtained in Fig. 62 by applying a power function

$$t_i = C_i\left[\frac{K_r^2 - K_s^2}{K_s^2}\right]^{n_i} = C_i \psi^{n_i} \tag{4.6}$$

with C_i= 24.58h and n_i= 1.203 for the horizontally aligned RR58 specimens, and C_i= 11.549h and n_i= 1.1562 for the vertical orientation. For LM30 C_i= 33.79h and n_i= 0.623. The constants C_i and n_i depend on the material, Fig. 62) environment, wetting conditions (Fig. 62) and possibly on the strain hardening behaviour of the material investigated.

Considering now the tests performed immediately after precracking (Tables 10, 11 and 12), K_s/K_c was plotted against t_i in Fig. 63. This relationship has two limiting conditions, namely for

$$K_s/K_c \rightarrow 1 \qquad t_i \rightarrow 0 \tag{4.7a}$$

and for

$$K_s/K_c \rightarrow K_{ISCC}/K_C \qquad t_i \rightarrow \infty \tag{4.7b}$$

In RR58 two curves, for horizontal and vertical orientation of the specimen, were obtained. Both are concave upwards and the curve for the horizontal specimen alignment again lies above the vertical results. The LM30 results are also included in Fig. 63 and lie below the corresponding curve for RR58. Thus, despite the fact that a_i is longer in LM30, the incubation time is shorter. This means that in LM30 the crack growth rate is faster in the incubation period. Fig. 63 provides an indication of the incubation period in the SCC tests. This influence increases with the decreasing total testing time.

(B) The Incubation Time Under Increasing K

Equation (4.6) can not be applied to predict incubation times when K is increased, since the crack tip in this condition does not pass through a more hardened zone. The typical test 3 in Fig. 57, tests 2 and 3 in Fig. 58 and also test 2 in Fig. 60 indicate that the incubation times t_i'' were much shorter than those observed under decreasing K and discussed in the preceeding section. It is thought that the substantial increase in crack growth rate observed during the incubation times under increasing K is due to a process of local rupture which occurs when the already damaged material at the crack tip is subjected to a higher load. A theoretical explanation for the phenomenon may not be supplied within LEFM analysis alone.

4.3.2 The da/dt-K Curves

(A) The Influence of Specimen Orientation

The data presented in Fig. 59 indicates that the crack growth rate results for the specimens tested in the vertical position are above those obtained for the horizontal specimens, and K_{ISCC} is reduced from 7.5 to 6 $MN/m^{3/2}$. The

difference in K_{ISCC} is attributed to the vertical drip feed action being more efficient in wetting the crack tip and in removing the corrosion products. Care must be taken in comparative interpretation of SCC data since the results depend on the testing method as well as the amount of corrodent applied to the specimen.

The accelerated crack growth rate in the vertical alignment is thought to be due to a more effective dissolution process. In Region III which is very rarely observed in SCC studies of aluminium alloys, the difference between the horizontal and vertical crack alignment results is virtually non-existent, suggesting that at high K values the cracking process is mainly of mechanical origin although the presence of the corrosive environment is necessary. This is confirmed by the fact that some static tests conducted in laboratory air at K levels very close to K_c(95-98%) failed to produce any crack growth after more than 30 days of load application.

(B) Comparisons between Materials and between Wetting Techniques

A direct comparison between the $\frac{da}{dt}$-K curves for RR58 and LM30 can be seen in Fig. 61. K_{ISCC} is lower in LM30 (5.5 $MN/m^{3/2}$ compared to 7.5 $MN/m^{3/2}$ for RR58). The plateau (K independent region) occurs at approximately the same crack growth rate despite the fact that in LM30. Region II is more extensive than in RR58. Region III starts at lower K values in LM30, due to its lower K_c values.

The scatter bands bounding all the RR58 and LM30 results are shown in Fig. 64, together with the SCC results of six other 2000 series Al-alloys (116) tested in the same environment and having identical crack orientation as in RR58, the only difference being in the application of the environment. The series 2000 alloys were subjected to intermittent wetting (3 times a day). Hence it may be expected that the corrosive action would be more effective in the present tests. The RR58 and LM30 scatter bands lie substantially

above those for the other Al-alloys. It is interesting to note that data obtained on RR58 by Baxter (225) yielded a rather high K_{ISCC} value (14 $MN/m^{3/2}$) while the maximum crack growth rates were closely comparable to those presented here. The present K_{ISCC} value (6-7.5 $MN/m^{3/2}$) does not differ substantially from the results quoted in the literature on 2000 series. Al-alloys. It is possible that in Region I the level of K_{ISCC} might be associated with blunt cracks (188) which have formed after the long exposure times associated with very low K and da/dt values. Since the results obtained in (224) were obtained by daily wetting of the specimens with 3.5% NaCl solution, it may be concluded that the more severe corrosive conditions obtained in the present tests are responsible for the low K_{ISCC} results. Thus K_{ISCC} should not be classified as a true material property, since it may be strongly influencedby the testing method.

In Fig. 64 it is apparent that the cast aluminium alloy LM30 has inferior SCC properties to those of the 2000 series aluminium alloys considered; its K_{ISCC} is lower and the plateau velocity is about one order of magnitude greater. As mentioned in Chapter 3 high percentages of silicon (as in LM30) cause comparatively poor stress corrosion resistance. Extensive silicon dissolution was experimentally observed in this alloy, confirming the importance of this element in the cracking process. Future studies on cast aluminium alloys should include tests in alloys with different silicon contents. Eventually an optimum silicon content may be obtained for the best stress corrosion performance.

Clearly, more work is necessary in this field to draw definite conclusions. This would include the investigation of different wetting conditions, corrodents and temperatures. It is expected that increasing the wetting frequency and temperature (116) would increase corrosive action. Tests on thicker specimens will produce a lower K_c value (181) and the crack growth rate might

increase due to the more developed plane strain conditions obtained in thicker specimens.

4.3.3 Comparison between Static and Dynamic Crack Propagation

The fatigue crack growth rate curve for RR58 under R = 0 loading in 3.5% NaCl (Fig. 24) is replotted in Fig. 61. The crack growth rates were converted to a time basis ($\frac{da}{dt} = f \frac{da}{dN}$) so that a direct comparison with the stress corrosion curve can be made. The result of this exercise clearly shows that under dynamic conditions the crack growth rate is considerably greater, and the threshold value lower. The difference in crack growth rate varies from one order of magnitude at lower K values to two for higher K values.

The superposition models described in Chapter 1 (1.7.6) are not applicable to the present data. Firstly K_{ISCC} is considerably higher than ΔK_{th} (Fig. 61), contradicting the superposition theory and secondly for K values greater than K_{ISCC} the SCC growth rate must be comparable to or higher than the fatigue crack growth rate, which is clearly not the case. A similar analysis carried out for LM30 produced the same conclusions.

The present results offer support to the criticism of the superposition principle. In order for the latter to be applicable, extremely high stress corrosion crack growth rates are necessary and the K_{ISCC} value must be very low.

CHAPTER FIVE

THE J INTEGRAL APPROACH TO SLOW CRACK GROWTH UNDER MONOTONIC LOADING

In Chapter 2 a procedure for calculating the critical value of the stress intensity factor for unstable crack propagation, K_c, was described. Using the contoured double cantilever beam specimen (a constant K specimen), K_c was evaluated for the aluminium alloys RR58 and LM30 within the range of applicability of LEFM. However, in the case of BS15 mild steel this approach could not be used since slow crack growth and extensive plastic deformation occurred before sudden crack propagation.

In this Chapter non-linear fracture mechanics theory (J contour integral) will be applied to obtain a critical value of J, J_c, for crack propagation. Firstly a theoretical method to calculate the J integral in the contoured DCB specimen will be derived. Secondly, the experimental determination of J_c for BS15 mild steel in two different specimen geometries (contoured DCB and compact tension) using the resistance curve test technique (J against crack extension) will be reported. Finally the results will be compared and discussed in the light of the non-linear fracture mechanics approach.

5.1 Theoretical Analysis

5.1.1 The Energy Definition of the J Contour Integral for Monotonic Loading

The energy interpretation of J is illustrated in Fig. 65 for the case of monotonic loading. Line OABC represents the load-deflection or load extension curve for a specimen in which the loading is linear elastic from O to A, work hardening occurs from A to B, and along BC the crack extends an amount da at a constant load P causing an increment of deflection $d\delta$. The curve is typical for mild steel. For other metals non-linear be-

haviour may be apparent from point O. The line OA_1C is the equivalent load-deflection curve for an initial crack length (a+da). The shaded area therefore represents the potential energy lost in propagating the crack from a to (a+da).

For a crack of width B_n J is defined by Eq.(A.20). The potential energy U is obtained from the equation

$$U = -\int \delta dP = U_1 + U_2 \tag{5.1}$$

U_1 being the linear elastic term

$$U_1 = \frac{P_{ys}\delta_{el}}{2} \tag{5.2}$$

where P_{ys} is the yield load of the specimen and δ_{el} is the elastic deflection corresponding to P_{ys}. The plastic (non-linear elastic) energy term, U_2 is given by

$$U_2 = P_{pl}\delta_{el} + \int_0^{P_{pl}} \delta_{pl}\, dP \tag{5.3}$$

where $P_{pl} = (P-P_{ys})$ and $\delta_{pl} = (\delta - \delta_{el})$.
It is then assumed that after P_{ys} has been attained the material follows a stress-strain law

$$\varepsilon_{pl} = A\sigma_{pl}^{\,n} \tag{5.4}$$

where ε_{pl} is the plastic strain, $\sigma_{pl} = (\sigma - \sigma_{ys})$, n is the strain hardening exponent and A is a constant. It can be shown using elementary relations that

$$\delta_{pl} \propto P_{pl}^{\,n} \tag{5.5}$$

and substituting Eq. (5.5) into Eq. (5.3) and integrating the second term in Eq. (5.3), the energy U is given by

$$U = \frac{P_{ys}\delta_{el}}{2} + P_{pl}\left(\delta_{el} + \frac{\delta_{pl}}{(n+1)}\right) \tag{5.6}$$

consequently

$$J = -\frac{1}{B_n}\left[P\left(\frac{d\delta_{el}}{da} + \frac{d\delta_{pl}}{da}\ \frac{1}{(n+1)}\right) - P_{ys}\left(\frac{1}{2}\ \frac{d\delta_{el}}{da}\right.\right.$$

$$\left.\left. + \frac{d\delta_{pl}}{da}\ \frac{1}{(n+1)}\right) - \frac{dP_{ys}}{da}\left(\frac{\delta_{el}}{2} + \frac{\delta_{pl}}{(n+1)}\right)\right] \tag{5.7}$$

Provided that the boundary conditions are prescribed in terms of fixed loads, Eq. (5.7) allows the determination of the J values for any specimen geometry. δ_{el}, δ_{pl}, P_{ys} and their derivatives with respect to a may also be obtained at the loading points using the usual stress analysis methods.

5.1.2 Application to the Contoured DCB geometry

In the present case the deflections δ_{el} and δ_{pl} can be calculated with the assumption that each leg of the DCB specimen (Fig. 6) is built-in at the crack tip and the crack propagates along the direction of the bending stresses. Beam theory may be used to calculate deflections. A short note on the relevant definitions and equations of linear and non-linear elastic beam theory is presented in Appendix B.

(A) The Effect of the Bending Moment on Deflections

The elastic deflection due to the bending moment δ^M_{el} is obtained by integration of the differential equation relating the curvature and the deflection of a beam :

$$k_{el} = -\frac{d^2\,\delta^M_{el}/dx^2}{\left[1 + \left(\frac{d\,\delta^M_{el}}{dx}\right)^2\right]^{3/2}} \tag{5.8}$$

where k_{el} is the elastic bending moment curvature given by Eq. (B.3) in

Appendix B.

The contour of the DCB specimen may be closely approximated by a straight line. The specimen used in the present analysis one half is shown in Fig. 66. The beam height h is then a linear function of x. For $x > 30$ mm

$$h = h_o + h_1(x - 30) \tag{5.9}$$

and for $x < 30$ mm the height was assumed to be constant (1st beam element, Fig. 66) where $h = h_o = 12.4$ mm, and $h_1 = 0$. The heights were considered to be the mean of the value corresponding to the crack plane and that corresponding to the longitudinal line limiting the side groove. This mean value of height produces the same moment of inertia as a single beam of constant gross thickness B. Consequently Eq. (5.9) is substituted into the curvature equation (Eq. (B.3)) to render it a function of x only.

Numerical methods were applied to integrate the second order differential equation, (Eq. 5.8). The method presently used involved reduction of the order of the equation by putting

$$\frac{d\delta_{el}^{M}}{dx} = Z_1 \tag{5.10}$$

Eq. (5.8) then becomes

$$k_{el} = \frac{dZ_1/dx}{(1+Z_1^2)^{3/2}} \tag{5.11}$$

Thus Eq. (5.11) was integrated between 0 and the crack length $x = a$ in a computer program using the modified Euler method and also the Runge-Kutta method, both methods yielding very similar results. Finally, integration of Eq. (5.10) was carried out in the same program, using Simpson's rule with the Z_1 values previously obtained in the first integration. The accuracy of the numerical method depended on the step interval; after several trials 0.5 mm was chosen. Crack length values ranged from 70 to 160 mm in 10 mm intervals. The computer program used in the present analysis is listed in

Appendix B.

The plastic deflection caused by the bending moment, δ^{M}_{pl}, was calculated by a similar process, the only difference being that the curvature equation used is that for a beam of a non-linear elastic material (second term in Eq. (B.4).

The yield load, P_{ys}, obtained from elementary beam theory, increased with crack length, (Fig. 67) for crack lengths in the range of practical interest (70 to 160 mm). The appropriate value of P_{ys} was substituted in the curvature equations before integration was carried out between 0 and a crack length a.

Neglecting the crack tip singularity the maximum bending stress in the beam is given by Eq. (B.11)

$$\sigma_{max} = \sigma_{ys} + \frac{2P_{pl}(2n+1)}{Bh^2 n} \qquad (5.12a)$$

for $\sigma_{max} > \sigma_{ys}$ and

$$\sigma_{max} = \frac{6Pa}{Bh^2} \qquad (5.12b)$$

for $\sigma_{max} < \sigma_{ys}$. Eq. (5.12a) corresponds to non-linear elastic behaviour ($P > P_{ys}$) and Eq. (5.12b) to the linear elastic stage ($P < P_{ys}$).

In Fig. 68 curves for σ_{max} (given by Eqs.(5.12a,b)) are plotted for six load values (4.5 to 7.0kN) The values of n and σ_{ys} taken are those for BS15 mild steel (Table 1). It can be seen that σ_{max} increases with applied load and decreases with crack length. With increasing load linear elastic conditions are attained at increasing crack lengths. Plastic deformation will be obtained in the specimen for any monotonic loading to greater than 5.5kN for crack lengths between 70 and 160 mm. For loads below 5.5 kN the linear elastic stage is being obtained with increasing crack lengths as the load increases.

In Table 13 the calculated values of δ^M_{el} and δ^M_{pl} for BS15 mild steel (Table 1) at 5.5 kN load are presented for crack length values ranging from 70 to 160 mm. Similar results have been obtained for the other load values (4.5, 5,6, 6.5 and 7 kN); they show that δ^M_{el} increases with crack length while δ^M_{pl} decreases. This trend originates from an increase in P_{ys} with crack length (Fig. 67) and a corresponding decrease in P_{pl} and σ_{max} (Fig. 68). For the crack length of 160 mm $\delta^M_{pl} = 0$, i.e. the load-deflection curve for the specimen is linear elastic, a result confirmed by Figs. 67 and 68.

(B) The Effect of Shear Force and Rotation at the Crack Tip on the Deflection Values

The effect of the shear force on the deflection was also considered. The elastic shear force deflection δ^S_{el} is obtained by integrating the following equation

$$\frac{d\delta^S_{el}}{dx} = \frac{(\tau^{el}_{yx})_{y=0}}{G'} \qquad (5.13a)$$

where τ^{el}_{yx} is the linear elastic shear stress and G' is the shear modulus. The plastic (non-linear elastic) shear force deflection, δ^S_{pl} is obtained by integrating the equation:

$$\frac{d\delta^S_{pl}}{dx} = D(\tau^{pl}_{yx})^n_{y=0} \qquad (5.13b)$$

where D is a constant and equal to $A\left(3\ \frac{n+1}{2}\right)$, and τ^{pl}_{yx} is the plastic shear stress. In Appendix B the shear stress distribution in a variable height beam (DCB specimen) is derived for both linear elastic and non-linear elastic materials. Hence $(\tau^{el}_{yx})_{y=0}$ is given by Eq. (B.23b) and $(\tau^{pl}_{yx})_{y=0}$ by Eq. (B.23a).

Subsequently the rotational effect at the crack tip was computed, assuming that the beam would rotate around the crack tip, with the end of

the specimen being built-in. In Appendix B section B.5 the deflection δ^R due to the rotation effect is calculated.

The total theoretical deflection δ_t is then the superposition of all the calculated deflections:

$$\delta_t = \delta^M_{el} + \delta^M_{pl} + \delta^S_{el} + \delta^S_{pl} + \delta^R \qquad (5.14)$$

with δ^R given by the last term in Eq. (B.25).

A comparison between the computed bending moment deflections, δ^M, (elastic + plastic), shear force deflections δ^S (elastic + plastic) and rotational deflections is presented in Table 13. It may be seen that δ^S is between 2-3% of δ^M and δ^R varies between 5-8% of δ^M. From the above results it is clear that the effect of shear force and rotation can not be simply discarded in calculation of the deflections.

(C) Theoretical Results for Deflections, Potential Energy and J Contour Integral

Fig. 69 shows the theoretical load-total deflection curves for three crack length values 70, 100 and 130 mm and for an applied load of 6kN. The yield points are indicated in the figure and were taken from Fig. 67. These curves were constructed using Eq. (5.14) with deflection values obtained in the computer program at 4.5, 5, 5.5 and 6kN load values.

Fig. 70 also includes two theoretical load-deflection curves corresponding to an applied load of 7kN and crack length values of 70 and 160 mm (maximum and minimum values of crack length).

Eq. (5.6), with the appropriate values of δ_{el} and δ_{pl}, yields the potential energy, which is plotted against crack length in Figs. 71a and 71b. The amount of potential energy sufficient to cause linear elastic deformation for the same applied load has also been recorded and, as expected, the elastic-plastic potential energy is greater than the linear elastic

counterpart. The difference between the two energies, which increases as load increases and decreases as crack length increases, is due to the increase in yield load with crack length (Fig. 67) which causes the plastic energy term to decrease with crack length. The potential energy curves presented in Fig. 71b show two cases for which the load is high enough to rule out the possibility of obtaining any linear elastic load deflection curve for this geometry.

The slopes of the curves presented in Figs. 71a and 71b gave the J values, which were also obtained using the general Eq. (5.7). The required derivatives were obtained by the computer program, using a central difference formula. The theoretical J curves are plotted against crack length in Fig. 72. J increases slightly with crack length, and in tests in which the applied loads were 4.5, 5 and 5.5 kN it attained a constant value corresponding to linear elastic loading (Fig. 68). Under such conditions the value of J is expected to be constant in a constant K test piece.

5.2 Experimental Procedure

5.2.1 Material and Specimens

The material used was 11.2 mm thick BS15 mild steel plate. The composition and principal mechanical properties are presented in Table 1.

The specimens used were of two types: the contoured double cantilever beam (DCB) test piece with a constant stress intensity factor characteristic (Fig. 6) and compact tension specimens with dimensions shown in Fig. 73. Both types of specimen were cut so that the crack propagated along the rolling direction.

The notching technique used in the contoured DCB specimen has been previously described (2.1.3). In the compact tension specimens a slot was machined along the specimen midplane (Fig. 73) and sharpened with a ground hacksaw blade approximately 0.5 mm thick. These latter specimens were pro-

vided with side grooves 3.5 mm deep (as in the contoured DCB specimen) which were polished for ease of crack tip observation.

5.2.2 Testing Procedure

(A) Tests for the Determination of A and n

These were tensile tests performed in air at room temperature on 6.25 mm diameter round specimens of 25 mm gauge length, stressed in the rolling direction. The load extension curves were plotted on a U-V recorder directly connected to the load cell of an Instron TT-C type testing machine of 44 kN load capacity. In these tests the extension record was corrected for deformation of the fittings and other machine parts (shackles).

The value of the constant A and the strain hardening exponent n were obtained by plotting the true plastic stress against true plastic strain, on a logarithmic scale, up to the necking point only. A straight line was obtained, verifying Eq. (5.4), from which the values of A and n were taken. These are presented in Table 1.

(B) Precracking Tests

The fatigue precracking of the contoured DCB specimens was accomplished using the 500 kN Avery hydraulic fatigue machine briefly described in 2.1.5. A load amplitude of 1.2 kN was used and the test was stopped when the crack length reached 70 mm. The crack length was monitored with a travelling microscope of 10x magnification reading to 0.005 mm.

The compact tension specimens were fatigue precracked in a Schenck pulsator fatigue machine at a frequency of 20Hz and at a load range of 2kN (one third of its yield load). Crack propagation was followed with a magnifying glass and a graduated scale drawn on the specimen. The test was stopped when $a/w = 0.6$. All the tests were conducted at 21°C in laboratory air, 50% R.H.

(C) Tests for the Determination of J_c

Tests on contoured DCB test pieces were performed in the 500 kN Avery hydraulic machine. The initial crack length in all specimens was 70 mm and the crack extension at maximum load was recorded with a travelling microscope of 10x magnification reading to 0.005 mm. The maximum loads used were 4.5, 5, 5.5, 6, 7 and 8 kN, using one specimen for each load. The specimens were then unloaded, and load-cycling tests were performed at 0.1 Hz frequency as part as part of an experimental programme on the application of the J integral to elastic-plastic load cycling (Chapter 6).

The load point deflections were measured with a strain gauge clip gauge which was previously calibrated with a micrometer reading to 0.002mm. The load signal, obtained through a D.C. potentiometer coupled to the loading mechanism, was used to plot load-deflection curves on a Bryans (U.K.) X-Y plotter.

In the series of tests performed on the compact tension specimens (a/w = 0.6) each specimen was loaded to a particular deflection value using an Instron tensile testing machine type TT-C of 44 kN load capacity. The deflections were measured at the knife edges, shown in Fig. 73, with the clip gauge. The load signal was taken directly from the load-extension plotter of the machine and the load-deflection curves monitored on the Bryans (U.K.) X-Y plotter. Crack extension was measured with a travelling microscope. A total of five specimens were tested.

Compact tension specimens were subsequently broken by fatigue so that the crack extension value read by the travelling microscope could be checked with the value obtained by fracture surface measurement. This task was facilitated by the clear distinction between the two fracture surface appearances (monotonic loading and fatigue).

5.3 Experimental Results

5.3.1 Contoured DCB Results on BS15

In Fig. 67 experimental yield load values are presented for the six specimens tested at a crack length of 70 mm, together with a few values obtained at other crack lengths. These latter results were obtained from the linear elastic tests on BS15 described in Chapter 2. At a crack length of 70 mm the yield load values were between 3.8 and 4.2 kN, varying from specimen to specimen.

The experimental load-deflection curve for the specimen loaded up to 7kN and with 70 mm crack length is shown in Fig. 70. The maximum deflection obtained was 24.85 mm, a value which may be compared with that of 14.5mm obtained in a specimen with 160 mm crack length. Particularly noticeable was the large decrease in plastic deformation obtained when the 160 mm crack length specimen was loaded.

Some experimental potential energy values are also plotted in Figs. 71a and 71b, corresponding to the present experimental programme for crack lengths of 70 mm. Linear elastic values of potential energy obtained from the tests described in Chapter 2 are superimposed on the same figures.

The J against crack extension curve (resistance curve) is shown in Fig. 74. The J values at the appropriate crack lengths were taken from Fig. 72. The curve shows two regions, data in the first lying near the vertical axis and in the second region forming a slightly concave-upwards curve. J_c was calculated using the Begley and Landes (226) resistance curve technique (Appendix A), which uses the interception of the second curve with the line $J/2\sigma_{flow}$ where σ_{flow} is the mean value between yield stress and the ultimate tensile stress. A room temperature J_c value of 42N/mm was obtained.

5.3.2 Results from Compact Tension Specimens

In the series of tests on compact tension specimens, J values were obtained from Eq. (A.21) (Appendix A)

$$J = \frac{2A_L}{B_n b} \qquad (5.15)$$

where A_L is the area under the load-deflection curve at the displacement of interest, B_n is the crack width and b is the uncracked ligament length, which is equal to (w-a). To calculate A_L, the deflection values have to be referred to the loading points. The location of the clip gauge was at 19mm from the loading points; hence, assuming that the crack rotates about a point one quarter of the respective uncracked ligament length (227) from the crack tip, it was found that the deflection at the loading points was on average 29% less than the experimental values, this factor varying ±1% over the measured crack lengths.

Assuming that B_n is the net thickness the J values are plotted against-crack extension in Fig. 74. The results of the multiple specimen technique also produced a J_c value estimated as 42 N/mm .

5.4 Discussion of Results

5.4.1 Results for the DCB Specimen

The agreement between the experimental and theoretical values of the yield load P_{ys} is good, as shown in Fig. 67. A greater quantity of data is available for the crack length of 70 mm, and it can be seen that the maximum difference between the experimental and theoretical yield loads is in the order of 5%.

The results presented in Table 13 (in which δ_{exp} are the experimental values) and the theoretical and experimental load-deflection curves in Fig. 70 show that very close agreement was obtained between the theoretical and experimental deflection values. The maximum difference is in the order

of 1% with the experimental results usually exceeding the theoretical ones. The same sort of agreement was obtained between potential energy values (Figs. 71a and 71b).

The theoretical linear elastic J values are compared with the experimental values in Fig. 72. The latter were obtained from the equation

$$J = G = \frac{P^2}{2B_n} \frac{dC}{da} \qquad (5.16)$$

where $\frac{dC}{da}$ is constant in this geometry (Fig. 11), and the selected load values were 4.5, 5 and 5.5 kN. The agreement with the theoretical values is good, differences being in the order of 2% with the experimental results often the greater. The maximum linear elastic J value obtained for a load value of 5.5 kN was 44 N/mm .

5.4.2 The J_c Determination in DCB and Compact Tension Specimens

In Fig. 74 it can be seen that the same resistance curve (J against crack extension) fits data points for the two investigated geometries. The results strongly suggest a geometry independence of the J value.

The experimental value assumed for the crack extension can significantly influence the shape of the resistance curve (Fig. 74) and the value of J_c. Crack extension values for the contoured DCB specimens were measured with the travelling microscope only, while in the compact tension specimen tests crack extension was also measured on the fracture surface using fatigue marking. In the latter specimens some difference (20%) was found between values obtained using these two techniques. The crack extension values in Fig. 74 are their respective mean values.

The value of J_c is only slightly influenced by the slope of the line $\frac{J}{2\sigma_{flow}}$. Thus in (226) it is also recommended that instead of the line $J/2\sigma_{flow}$ a line $\frac{J}{2\sigma_{ys}}$ may be used. The J_c value will be considerably different if the slopes of these lines are not high. In the present results

the slope is very high and any variation will not significantly affect the J_c value.

The numerical value obtained for J_c (42 N/mm) on BS15 agrees well with that obtained for mild steel (47 N/mm) (190). Recently Garwood (228) has obtained a value of 40 N/mm on EN32B mild steel using three point specimens 12.5 mm thick with 3 mm deep side grooves, a geometry very similar to that investigated here.

CHAPTER SIX

A STUDY OF ELASTIC-PLASTIC FATIGUE CRACK GROWTH UNDER LOAD-CYCLING

As referred to in Chapter 1(1.7.9) low and intermediate strength alloys such as mild or other low alloy steels may exhibit fatigue crack growth with relatively large nominal plastic specimen deformation. The data discussed in Chapter 2 was obtained at stress levels below the yield point. If large plastic deformations are present during fatigue crack growth, LEFM can no longer characterize the local stress distribution at the crack tip. The fracture toughness of these highly ductile materials can however be expressed in terms of the J contour integral and COD.

The work published to date on the application of J contour integral and COD concepts to fatigue crack growth has been reviewed in Chapter 1 (1.7.9) It is clear that a lot of work remains to be done in this area. Thus fracture mechanics analyses of load and strain-cycling fatigue crack propagation are almost totally absent from the literature. It was therefore decided that a theoretical and experimental investigation of fatigue crack propagation under load-cycling conditions would be of great interest.

In this Chapter a theoretical and experimental method, based on the energy interpretation of the J integral, for computing cyclic J values for load-cycling is proposed. The method may be used for any geometry provided that cyclic creep occurs, and it has been applied to the contoured DCB specimen geometry used in the experimental programme described in Chapters 2 and 4. The material selected for this investigation was mild steel BS15 for which linear elastic fatigue crack propagation data has previously been obtained in Chapter 2.

6.1 Theoretical Analysis

6.1.1 Operational Definition of ΔJ for Elastic-Plastic Load Cycling

When a fully tensile load is applied to a specimen or component having

an initial crack of length a_o the load-deflection curves at the loading point are as illustrated in Fig. 75a for a linear elastic material and Fig. 75b for load cycling above the yield point. In both cases the crack has grown from a_o to $(a_o + da)$ in the first cycle and from a_o to a after N cycles. The area illustrated represents the decrease in total potential energy ΔU after N cycles. For the linear elastic case a cyclic value ΔG of the monotonic crack extension force can be defined as

$$\Delta G = -\frac{1}{B_n}\frac{d(\Delta U)}{da} = -\frac{\Delta P}{2B_n}\frac{d(\Delta\delta)}{da} \qquad (6.1)$$

where $\Delta G = (G_{max} - G_{min})$, G_{max} and G_{min} are the maximum and minimum values of G in the loading cycle, $\Delta P = (P_{max} - P_{min})$, P_{max} and P_{min} are the cyclic tensile load limits and $\Delta\delta$ the corresponding range of deflection δ at the loading points.

In Fig. 75b (OABFO) represents the load-deflection curve obtained in the first loading cycle of an elastic-plastic material. The curve is linear elastic from O to A and plastic deformation occurs from A to B. This type of loading curve is typical for mild steel. For other metals a non-linear curve starting at O may be more appropriate. BC (Fig. 75b) represents the accumulated deflection caused by cyclic creep and crack growth after N cycles at a constant load range ΔP.

This cyclic creep phenomenon has been extensively studied in the literature and a review is presented in Chapter 1 (1.4.6). It consists basically of strain accumulation caused by load-cycling at stress levels above the yield point. In general, the cyclic creep curve (accumulated strain against number of cycles) has a shape analogous to that of the ordinary creep curve. An initial primary stage is followed by a well-defined secondary stage with a constant cyclic creep strain rate, covering 80-90% of the specimen life, and finally a very short tertiary stage near fracture. Consequently the cyclic creep deflection represented by the quantity (BC) in Fig. 75b is here considered

to consist basically of the secondary stage, since experimental evidence [40,42,44,45] indicates that the primary stage is virtually completed during the first loading cycle and is thus represented by (BB) in Fig. 75b.

The potential energy of the first cycle, ΔU_1, obtained by loading a specimen with crack length a_o and zero initial deflection, is represented by the area (OABHO) in fig. 75b. The total accumulated potential energy after N cycles, ΔU_N, is given by the area (OECHO) . . ΔU_N is obtained by elastically loading from E to C a specimen having a crack length a and with a permanent initial deflection, indicated by (OE); it is numerically equal to the real permanent deflection after N cycles. It should be pointed out that (OE) represents the accumulated cyclic creep deflection after N cycles and, if crack growth had not occurred, the trace (EC) would have been parallel to (BF). The elastic loading condition for (EC) is closely true since the yielding has been largely accomplished between points A and B.

Because only loading conditions were assumed the energy interpretation of the J contour integral (Appendix A, Eq. (A.20)) can be extended to cyclic loading of an elastic-plastic material to define a cyclic ΔJ value after N loading cycles as

$$\Delta J = \frac{1}{B_n} \frac{d(\Delta U)}{da} \qquad (6.2)$$

where $\Delta U = \Delta U_N - \Delta U_1$.

It should be noted that in the strict mathematical sense the above definition and Eq. (6.2) are valid only if unloading phenomena are not considered (deformation theory of plasticity - non-linear elasticity). However the present approach may have more general applicability than the mathematical definition. The operational definition of ΔJ put forward is equivalent to saying that ΔJ defines the stress and strain fields near the crack tip during the loading half of the cycle.

Therefore this equivalent analysis does not take account of a slight overlapping effect (anelastic deformation) usually occurring between the unloading and loading lines on consecutive load-deflection loops. This overlapping is only noticeable in the first few loading cycles and is practically eliminated thereafter. Also, unloading might cause a yield stress increase due to cyclic work hardening which, again, is not considered here.

The second term in Eq. (6.2) $\frac{d(\Delta U)_1}{da} = 0$ because ΔU_1 depends on a_o but not on a. From Fig. 75b ΔU_N can be expressed as

$$\Delta U_N = \Delta \delta_N \Delta P - \frac{\Delta P}{2} \Delta \delta_{el} \tag{6.3}$$

where $\Delta \delta_{el}$ is the elastic loading deflection (ED) and $\Delta \delta_N$ is the total deflection (HC) at load P_{max}. Substitution of Eq. (6.3) into Eq. (6.2) leads finally to a generalised equation valid for any specimen geometry

$$\Delta J = - \frac{1}{B_n} \left[\frac{d(\Delta \delta_N)}{da} \Delta P - \frac{\Delta P}{2} \frac{d(\Delta \delta_{el})}{da} \right] \tag{6.4}$$

The total deflection $\Delta \delta_N$ in Eq. (6.4) is obtained from

$$\Delta \delta_N = \Delta \delta_1 + \Delta \delta_{cc} \tag{6.5}$$

where $\Delta \delta_1$ is the maximum deflection of the first "specimen" (HB) and $\Delta \delta_{cc}$ is the accumulated deflection due to cyclic creep and crack growth after the first loading cycle, (BC). The separation of $\Delta \delta_N$ into two terms was considered more convenient for reasons which will be seen in the next section.

6.1.2 Application of ΔJ for the Contoured DCB Specimen

(A) Analysis for Small Deflections

Equation (6.4) may be used to compute ΔJ in any specimen geometry provided that the deflection or extension at the loading points is known under load-cycling conditions. Theoretically $\Delta \delta_N$ and $\Delta \delta_{el}$ may be calculated

for beam specimens using non-linear beam theory derived by Timoshenko (Appendix B). It is assumed here, as in Chapter 5, that the crack grows in the direction of the bending stresses, and the specimen is treated as a pair of variable height beams built-in at the crack tip.

It is known from beam theory that $\Delta\delta_1$ may be expressed as

$$\Delta\delta_1 = 2 \int_o^{a_o} x\, k_o\, dx \qquad (6.6)$$

where x is the co-ordinate along the beam length and k_o is the curvature caused by the maximum load at point B in the first cycle, Fig. 75b, and given by Eq. (B.4), Appendix B. Similarly the expression for $\Delta\delta_{cc}$ is

$$\Delta\delta_{cc} = 2 \int_o^{a} x\, k_{cc}\, dx \qquad (6.7)$$

where k_{cc} is the curvature caused by the secondary cyclic creep (Eq. B.5). Therefore, considering Eq. (6.5), $\Delta\delta_N$ will be obtained by a simple addition of equations (6.6) and (6.7).

In order to carry out the integrations indicated in these latter equations, the contoured shape of the DCB specimen may be closely approximated by a straight line. The beam height h is then given by Eq. (5.9) which was substituted in the curvature equations for k_o and k_{cc} (see Appendix B) and the integrations performed in a computer program using Simpson's rule. The step interval was 0.125 mm with a_o = 70 mm and the crack length, a, and number of cycles, N, values were those obtained in the fatigue crack growth tests at 4.5 and 5 kN. The appropriate values of A and n obtained experimentally for BS15 mild steel were used in the curvature equation for $\Delta\delta_1$ and are presented in Table 1. The secondary cyclic creep law used for the evaluation of C_1 and m in the equation for k_{cc} has the form given by Eq. (B.1b).

The theoretical curves of $\Delta\delta_N$ for load ranges ΔP = 4.5 kN and 5.0 kN are presented in Fig. 76 and the respective numerical values are listed in Table 14. $\Delta\delta_N$ increases with the applied load range and crack length. The cyclic creep deflection rate decreases with crack length as expected, since bending stress σ_{max} also decreases with crack length. Elastic conditions

are respectively attained at points A and B in Fig. 76 at which the crack length values are 105 and 125 mm. This happens when $\Delta P = P_{ys}$ (Fig. 67), at which point cyclic creep stops.

(B) Analysis for Large Deflections

The analysis presented in the previous section is valid for small deflections only i.e. when the appropriate curvature is assumed to be equal to the second derivature of the deflection. The exact analytical solution is provided by the solution of the differential equations (B.8a) and (B.8b). In Chapter Five a similar differential equation was used to calculate the elastic and plastic deflections for monotonic loading (Eq. 5.8). Additionally, some rotation at the crack tip may occur. This latter effect has also been computed, following the procedure explained in Section B.5 (Appendix B); deflections, δ^R, caused by crack tip rotation are presented in Table 15.

The determination of the error factor introduced by the assumption of equality between the curvature and the second derivative of deflection is presented in Appendix B (Section B.3). It was found that when the load range exceeded 5 kN the deflections were so large that the accuracy of the approximate analysis was no longer satisfactory.

For load range values of 5.5, 6 and 6.5 kN respectively it was decided to calculate $\Delta\delta_N$ by integrating Eqs. (B.8a) and (B.8b). It should be pointed out that $\Delta\delta_1$ has already been calculated in Chapter Five, including the shear force and crack tip rotation effects, and since a_o = 70 mm the theoretical load-deflection curve may be seen in Fig. 70. The method employed to calculate $\Delta\delta_{cc}$ was basically the same as that for the monotonic loading case described in section 5.1.2A. Thus the order of the differential equation (B.8b) has been reduced by putting

$$\frac{d\Delta\delta_{cc}}{dx} = z_2 \tag{6.8}$$

Eq. (B.8b) then becomes

$$k_{cc} = \frac{dz_2/dx}{(1+z_2^2)^{3/2}} \tag{6.9}$$

Eq. (6.9) was integrated between O and the crack length x = a by a computer program applying the modified Euler method. Finally, integration of Eq. (6.8) was carried out in the same program using Simpson's rule with the Z_2 values previously obtained in the first integration. The step interval chosen was 0.125 mm and the crack length and number of cycles values were those obtained in fatigue crack propagation tests at the appropriate load range values. The computer program is listed in Appendix B.

The computed $\Delta\delta_N$ curves are plotted against crack length in Fig. 77, and numerical values are presented in Table 15. $\Delta\delta_N$ values, which include the deflection δ^R caused by crack tip rotation (Eq. B.25), increase with the applied load range and crack length, showing the same trend as observed in Fig. 76. Linear elastic conditions were only obtained for 5.5 kN at crack length values greater than 152 mm, since the two other load range values (6.0 and 6.5 kN) exceed the yield load of the specimen (Fig. 67).

(C) The ΔJ Results

Using linear elastic beam theory the value of the derivative $d(\Delta\delta_{el})/da$ in Eq. (6.4) caused solely by the bending moment is given by

$$\frac{d(\Delta\delta_{el})}{da} = \frac{24\Delta P}{EB} \frac{a^2}{(h_o + h_1 a)^3} \qquad (6.10)$$

Furthermore, numerical differentiation of the $\Delta\delta_N$ values, Eq. (6.5), with respect to a, using a central difference formula inserted in the computer program, gave $\frac{d(\Delta\delta_N)}{da}$. Theoretical values of ΔJ were then calculated by substituting the numerical values of both terms, $d(\Delta\delta_N)/da$ and $d(\Delta\delta_{el})/da$, into the general equation (Eq. (6.4)). The theoretical ΔJ against crack length curve is shown in Fig. 78 for the load range 5.0 kN, and in Fig. 79 for load ranges of 5.5, 6.0 and 6.5 kN. The numerical values are shown in Tables 14 and 15.

ΔJ decreases with the crack length corresponding to the decrease in $d(\Delta\delta_N)/da$ values with crack length. For the load range $\Delta P = 5.0$ kN J is constant for crack lengths greater than 115 mm, a result which would be expected from the early deflection analysis in Fig. 76.

6.2 Experimental

6.2.1 Material

The material used was BS15 mild steel plate, 11.2 mm thick. The composition and mechanical properties are presented in Table 1.

6.2.2 Specimens

The specimens were contoured DCB test pieces with a constant K characteristic, as previously described in detail in (2.1.4). They were cut so that the crack propagated along the rolling direction. Side grooves 3.5 mm deep were cut on both sides of the specimen to enhance plane strain conditions and to help confine crack propagation to the specimen midplane. The side grooves were polished for ease of crack tip observation. A machined slot approximately 65 mm long with a chevron front sharpened with a razor balde to form a crack starter was provided in each specimen.

6.2.3 Cyclic Creep Tests

The cyclic creep tests were performed on 6.25 mm diameter specimens, 25 mm gauge length, stressed in the rolling direction.

An Instron TT-C type testing machine of 44 kN load capacity was used, the cyclic creep strain (longitudinal extension of the specimen) being obtained on the machine load-extension recorder. The tests were conducted until failure occured, which was by the necked-out type of fracture, producing deformations in the order of 40%. The final length of the specimen was measured

with a micrometer and, if the extension record was corrected for machine deformations, this value agreed with that obtained by the machine load-extension recorder.

6.2.4 Fatigue Crack Growth Tests

The fatigue crack growth tests were conducted at 21°C in laboratory air of 50% R.H., at a loading frequency of 0.1 Hz in a 500 kN capacity Avery hydraulic machine. The crack was initially extened to a length of 70 mm by fatigue pre-cracking under 2 kN tensile load in the same machine, and the tests at five load levels (4.5, 5.0, 5.5, 6.0 and 6.5 kN) were then performed, load-deflection loops being monitored regularly using an X-Y plotter. The load signal was obtained from a potentiometer directly attached to the loading mechanism. Deflections were measured along the loading axis with a standard clip gauge, (30 mm range) the signal being converted via a transducer converter into the X-Y plotter, (Bryans, UK). Crack length was measured with a 20 x magnification travelling microscope. Fig. 80 shows one of the specimens being tested. The large deflection at the loading points can be seen clearly. After each test the specimen was pulled apart and the final crack length measured on the fractured surface of the specimen.

6.3 Experimental Results

6.3.1 Cyclic Creep Results

The results of the tensile cyclic creep tests are presented in Fig. 81, the curves being similar in form to those reported in earlier literature (40, 42, 44, 45). The usual three regions of the cyclic creep curve were obtained with the primary stage practically confined to initial loading and the secondary stage obtained at constant cyclic creep strain rate. Thus the assumption put forward in the theoretical analysis, that the constant rate cyclic creep region immediately followed initial loading, is well justi-

fied by the experimental results. The total cyclic creep strain $\Delta\varepsilon_{cct}$ is very closely given by

$$\Delta\varepsilon_{cct} = \Delta\varepsilon_{o} + \Delta\varepsilon_{cc} \qquad (6.11)$$

where $\Delta\varepsilon_{o}$ is the initial elastic and plastic straining (Fig. 81) (primary stage), while the second term represents the secondary creep stage defined by Eq.(B.1b).

6.3.2 Fatigue Crack Propagation Results

Figs. 82 and 70 exemplify load-deflection loops obtained in fatigue crack growth tests at ΔP = 5.0 and 5.5 kN respectively. Similar records were obtained in the other tests. The variation of crack length with number of cycles, presented in Fig. 83, shows that for ΔP = 5.0 kN a constant crack growth rate region starts at a crack length of about 115 mm, whilst for ΔP = 4.5 kN it starts at approximately 100mm and for ΔP = 5.5 kN at 142 mm (Fig. 84). For shorter cracks, crack growth is faster and non-linear. In Fig. 85 the linear region was not attained for load ranges of 6.0 and 6.5 kN. The load-deflection loops for linear elastic loading are numbered 13, 14 and 15 in Fig. 82, and correspond to crack lengths exceeding 125 mm. Their unloading lines converge to point S. Similar behaviour was recorded for the second specimen cyclically loaded to 4.5 kN, the difference being that the transition point from plastic to linear elastic conditions occured at a shorter crack length, as predicted by Fig. 67, amounting to about 105 mm.

The experimentally determined total potential energy ΔU, which is the area within the load-deflection loops, is plotted against crack length in Fig. 86 for the load range of 5.0 kN and in Fig. 87 for 5.5 and 6.0 kN. The slopes of these curves are the experimental ΔJ values, which are superimposed on the theoretical curves in Figs. 78 and 79.

The relationship between da/dN and ΔJ (or K^2/E, where K^2/E refers to the linear elastic results quoted in Fig. 26) is shown in Fig. 88. The present experimental crack growth rate values under elastic-plastic cyclic

conditions increased by about 2 orders of magnitude from 4.5×10^{-3} mm/cycle to 2.5×10^{-1} mm/cycle, and the maximum ΔJ reached 1100 N/mm.

6.4 Discussion of Results

Both theoretical and experimental ΔJ values decrease with crack length and reach the linear elastic value ΔG(Fig. 78). The crack growth rate also decreases (Figs. 83, 84 and 85) suggesting that the crack growth process may be controlled by ΔJ. The experimental values of ΔJ(Fig. 78) are greater than the theoretical ones, differences ranging from 5% for short crack lengths to 10% for long crack lengths. These discrepancies may be explained in terms of deflection differences. The deflections calculated from equations (6.6) and (6.7) are due to the bending moment only, whereas the experimental deflection values include the shear force effect together with some rotation occurring at the crack tip. Thus the experimental deflection values might well be expected to lie somewhat above the theoretical ones as observed, Fig. 76. Consequently the experimental values of ΔJ must also be higher than the theoretical ones, Fig. 78. However, when the effect of crack tip rotation is considered the above differences between the theoretical and experimental deflection and ΔJ values are considerably reduced. Thus it is seen in Table 15 and in Figs. 77 and 79 that the difference between theoretical and experimental deflection and ΔJ values are in the order of 1-2%.

In Fig. 70 (Chapter 5) the experimental and theoretical monotonic load-deflection curves have also been plotted. Plotting the load-deflection loops for $\Delta P \simeq 5.5$ kN in the same figure clearly shows that in the load-cycling case the total potential energy increases and, for the same crack length (e.g. 160 mm), is considerably greater under cyclic conditions than in monotonic loading. This effect is due to cyclic creep, which is not observed in monotonic loading.

The variation of the cyclic J value with the crack length is also presented, Fig. 72. The load range $\Delta P = 4.5$ kN was chosen for comparative purposes. For the same crack length the cyclic J value is higher than the corresponding monotonic value until linear elastic conditions are reached;

thereafter both quantities are the same. Fig. 88 shows that the present elastic plastic results are in good agreement with the previous linear elastic results Fig. 26. The evidence indicates that linear elastic results at long crack lengths give the same values of ΔJ and crack growth rate as plastic results at short crack lengths. Fig. 67 shows that with the current specimen geometry, linear elastic tests can still be performed at loads up to 58 kN, corresponding to a $\Delta G = \Delta J$ value of 48 N/mm . If larger specimens were used, ΔG values would increase and would allow additional tests to be carried out to obtain linear elastic data at greater values of ΔG.

The present results show that the crack growth rate is controlled as herein defined ΔJ (Fig. 88), confirming the correlation found by Dowling and Begley (166, 167) for the compact tension and centre cracked geometries. The relationship between the crack growth rate and ΔJ is similar to Eq. (1.53) despite the fact that ΔJ was calculated by a different process and under different loading conditions. It can be shown that there is a direct relationship between ΔJ and the parameter $\lambda = K_{max}^2 - K_{min}^2$ correlating linear elastic fatigue crack growth data for a range of Al-alloys and steels. This relationship has the form

$$\Delta J = \frac{\lambda}{E} \qquad (6.12)$$

Substituting Eq. (6.12) in Eq. (1.32) and incorporating E into the constant β Eqn. (1.32) becomes

$$\frac{da}{dN} = C_{pl}(\lambda)^{n_1} \qquad (6.13)$$

Therefore a crack growth rate correlation with λ in the linear elastic range implies a similar correlation with ΔJ in the elastic-plastic range.

CONCLUSIONS

The concepts of linear elastic fracture mechanics (LEFM) can be successfully used to characterize the fatigue crack propagation process in metals whose mechanical behaviour under small scale yielding conditions can be assumed to be linear. The results of a comprehensive programme of studies on two aluminium alloys (RR58 and LM30) and a mild steel (BS15) using a contoured double cantilever beam geometry with a constant stress intensity field, K, along the crack path, have shown that variations in parameters such as the amplitude and mean level of K (ΔK and K_m respectively), frequency, and environment may have a significant effect on the rate of crack propagation, $\frac{da}{dN}$. An increase in the level of ΔK or K_m leads to an increased $\frac{da}{dN}$, this effect being more pronounced at low values of $\frac{da}{dN}$. The threshold value of ΔK, ΔK_{th}, was found to decrease linearly with increasing K_m.

Investigation of the combined effects of environment and frequency has shown that in RR58 tested at low frequency fatigue crack growth was accelerated in 3.5% NaCl in comparison to a laboratory air environment, but for higher values of the maximum stress intensity factor in the loading cycle K_{max}, this effect was non-existent. ΔK_{th} decreased in 3.5% NaCl in comparison with laboratory air. Similar behaviour was observed in the cast aluminium alloy LM30, the acceleration effect being slightly less pronounced. At high frequency (35Hz) no environmental effect was observed on RR58 or BS15, but at low frequency the latter material exhibited crack blunting when the crack growth rate for the initially sharp crack was below a certain critical value $(\frac{da}{dN})_b$. This phenonmenon was extensively studied and the time necessary to produce crack arrest was investigated in terms of ΔK, K_m and $\frac{da}{dN}$, and was found to increase with each of these parameters.

Considerations of the data obtained in the experimental programme showed that the following model predicted the crack growth rate:

$$\frac{da}{dN} = A_c \Phi^{\alpha}$$

where $\Phi = \frac{2K_m(\Delta K - \Delta K_{th})}{K_c^2 - K_{max}^2}$, K_c is the critical value of K and A_c and α are constants. The model was successfully applied for all the investigated materials in the full subcritical range (from threshold to fast fracture) and an analysis of data published by other authors has shown this model to be equally satisfactory for a range of mild steels. This equation was used to compare the fatigue crack growth performance of the materials investigated and an example of the prediction of the number of cycles spent in crack propagation in a particular engineering component was presented. The form of the model enables it to be related to the crack opening displacement (COD) and the J contour integral, and the threshold and critical values of these parameters.

The fatigue threshold behaviour in BS15, RR58, LM30 and other materials was not found to be satisfactorily explained by the crack closure approach.

The application of LEFM and of the contoured DCB specimen can successfully describe the stress corrosion process in aluminium alloys. Stress corrosion cracking (SCC) data was obtained for alloys RR58 and LM30 in a 3.5% NaCl solution. It was shown in RR58 that the crack growth rate is faster in vertically aligned than in horizontally aligned specimens; this is thought to be due to a more vigorous dissolution process, caused mainly by the environment at the crack tip. The threshold value of K, K_{ISCC}, was found to be lower for vertical alignment. Cast aluminium alloy LM30 has shown inferior SCC properties to those of RR58 due to its high silicon content. The data was compared with other results obtained for similar aluminium alloys and the differences in crack growth rate and threshold values have been explained in terms of the corrodent application. A strong dependence of crack growth rate on very high values of applied K was recorded and described as Region III of the crack growth rate - K diagram.

In the stress corrosion tests it was observed that a decrease in the stress intensity factor resulted in a marked reduction in the subsequent

crack growthrate. The time interval during which this reduction occured is termed incubation time. There is some evidence that the incubation time is dependent on the size of the plastic zone formed during previous loading. An equation relating the incubation time to the two levels of K applied was proposed. With increasing K a faster crack growth rate may be observed before the steady state is attained. This incubation time is, however, much shorter than that resulting from a decreasing-K history.

Non-linear fracture mechanics parameters (J contour integral) can be used to characterize the fatigue crack propagation phenomeneon for metals in which extensive nominal plastic deformation occurs. In the present work elastic-plastic fatigue crack growth under load cycling has been studied;: and on the basis of the energy interpretation of the J contour integral the variation of the total potential energy with crack length was adopted as a definition of the cyclic value of J, ΔJ. An analytical method based on non-linear beam theory was derived to compute ΔJ values for situations in which cyclic creep occurs under tensile load cycling above the yield load. Application of the method to contoured DCB specimens showed that the derived relation for ΔJ is a function of load, crack length, number of cycles, and the strain hardening and cyclic creep properties of the material. ΔJ was found to decrease with the crack length, reaching a constant value if linear elastic conditions were met. The method described is applicable to any geometry for which cyclic creep occurs.

Experimental investigation of fatigue crack growth phenomena in BS15, under conditions of cyclic tensile load and under elastic-plastic conditions showed that the cyclic values of J determined from the variation of the total cyclic potential energy with the crack length are in good agreement with the theoretical values of ΔJ.

Elastic-plastic fatigue crack growth rates correlated with ΔJ and with previous linear elastic results yielding an equation of the form

$$\frac{da}{dN} = C_{pl}(\Delta J)^{n_1}$$

where C_{pl} and n_1 are constants.

The J contour integral was also successfully evaluated, both theoretically and experimentally, for the constant K contoured DCB specimen of BS15 under monotonic loading conditions. J increased with crack length until a constant value was attained for linear elastic loading. ΔJ values under load cycling are greater than the monotonic values, the difference being due to the increase in potential energy caused by cyclic creep in load cycling. A critical value of J for crack propagation, J_c, was obtained for this material using compact tension and contoured DCB specimens. Using the R-curve technique J_c was shown not to vary in these specimen geometries.

PROPOSALS FOR FUTURE WORK

The discussion presented in this thesis in relation to the applicability of fracture mechanics concepts to the characterisation of fatigue and stress corrosion failure processes in metals, has clearly indicated the need for further studies in this field.

The fatigue crack propagation process under linear elastic conditions is, at this stage, fairly well established. Work in this field should explore other materials, the tension-compression loading pattern and the effect of temperature. The latter parameter should be studied, in an interrelated programme, with creep. Thus the possibility of any creep and fatigue superposition effects should be investigated.

Environmental fatigue crack propagation requires further study; in particular, an analytical treatment of the crack blunting process is necessary. The blunt crack can be treated as a notch, and such theoretical and experimental studies undoubtedly have great engineering interest. Other alloy-

environment systems should be tested and the applicability of the proposed model to them should be checked. Also, in the same programme, threshold studies are highly recommended.

In the stress corrosion field an immediate extension of the present programme of research should include the investigation of different wetting conditions, corrodents and temperatures. The effect of specimen thickness on the crack growth rate requires investigation. The loading history study initiated in this work should develop into a more detailed theoretical analysis, particularly in the case of the increasing-K pattern.

The fatigue crack propagation process under elastic-plastic conditions is still a comparatively new field. The work presented herein should be extended in the following directions:

Theoretical and experimental work under load cycling conditions for different mean load values, either tensile or compressive. The cyclic creep behaviour of the material should then be investigated. The analytical method presented in this work can be extended or modified for other geometries and cycling conditions. The programme may include tests both at room and high temperatures.

Theoretical and experimental work under strain or controlled-deflection cycling is recommended. Load and strain cycling fatigue crack propagation at room and high temperatures should be compared due to the great importance of low cycle fatigue failures in certain engineering components.

Slow crack growth under elastic-plastic monotonic loading is another area requiring further study. Other geometries, materials and environmental conditions are particularly worthy of investigation. The trend in variation of the critical value of J, J_c, for crack propagation with the above parameters must be sought.

References

1. Ewing, J.A. and Humphrey, J.C.W., "The Fracture of Metals Under Repeated Alternations of Stress", Phil. Trans. Vol. A200, p.241 (1903).

2. Thompson, N., Wadsworth, N.J. and Louat, N., "The Origin of Fatigue Fracture in Copper" Phil. Mag. Vol. 1, p. 113 (1956).

3. Stubbington, C.A. and Forsyth, P.J.E., "Some Metallographic Observations on the Fatigue Behaviour of Copper and Nickel and Certain of their Alloys", J. Inst. Metals, Vol. 86, p. 90 (1957-58).

4. Klesnil, M. and Lukas, P., "Dislocation Arrangement in the Surface Layer of α-iron Grains During Cyclic Loading", J. Iron Steel Inst. Vol. 203, p. 1043 (1965).

5. Plumbridge, W.J. and Ryder, D.A., "The Metallography of Fatigue", Metallurgical Rev. Vol. 14, p. 119 (1969).

6. Grosskreutz, J.C., "The Mechanisms of Metal Fatigue - Part II", Physica Status Solidi (B) Vol. 47, p. 359 (1971).

7. Cottrell, A.H., "Mechanical Properties of Matter", p. 373 (1964) Ed. by John Wiley and Sons (New York).

8. Lynch, S.P., "A New Model for Initiation and Growth of Fatigue Cracks", Metal Sci., Vol. 9, p. 401 (1975).

9. Wood, W.A., Consland, S. and Sargent, K.R., "Systematic Microstructural Changes Peculiar to Fatigue Deformation", Acta Metal., Vol. 11, p. 643 (1963).

10. Dover, W.D. and Jones, W.J.D., "The Initiation of Fatigue Cracks in Copper", Brit. J. Appl. Phys., Vol. 18, p. 1257 (1967).

11. Forsyth, P.J.E., "Fatigue Damage and Crack Growth in Aluminium Alloys", Acta Metal., Vol. 11, p. 703 (1963).

12. Lynch, S.P., "Tensile Deformation and Fracture in High-Strength Al-Zn-Mg Alloys", Metal Sci. Journal, Vol. 7, p. 93 (1973).

13. Pearson, S., "Initiation of Fatigue Cracks in Commercial Aluminium Alloys

and the Subsequent Propagation of Very Short Cracks", Eng. Fract. Mech., Vol. 7, p. 235 (1975).

14. Grosskreutz, J.C. and Shaw, C.G., "Critical Mechanisms in the Development of Fatigue Cracks in 2024-T4 Aluminium", Proc. 2nd Int. Conf. on Fracture, Brighton, p. 620 Edited by Chapman and Hall Ltd. London (1969).

15. Yokobori, T., Nanbu, M. and Takeuchi, N., "Observations of Initiation and Propagation of Fatigue Cracks by Plastic Replication Method", Rep. of Inst. for Strength and Fracture of Mater., Vol. 5, p. 1 (1969).

16. Delange, R.G., "Plastic Replica Methods Applied to a Study of Fatigue Crack Propagation in Steel 34CD4 and 26ST Aluminium Alloy", Trans. Met. Soc. AIME, Vol. 230, p. 644 (1964).

17. Wohler, A.Z., Engineering, Vol. 11, p. 199 (1871).

18. Cazaud, R., "Fatigue of Metals", Ed. by Chapman and Hall, London (1953).

19. Forrest, P.G., "Fatigue of Metals", Ed. by Pergamon Press, Oxford (1970).

20. Wilson, D.V., Phil. Mag., Vol. 22, p. 643 (1970).

21. Tetelman, A.S. and McEvily, A.J., "Fracture of Structural Materials", p. 348, Ed. by John Wiley, England (1967).

22. Frost, N.E., Marsh, K.J. and Pook, L.P., "Metal Fatigue", p. 47, Ed. by Oxford University Press, London (1974).

23. Goodman, J., "Mechanics Applied to Engineering", Longman, Green and Company, London (1899).

24. Gerber, W.Z. bayer. Archit. Ing. Ver. Vol. 6, p. 101 (1874).

25. Heywood, R.B., "Designing Against Fatigue", Ed. by Chapman and Hall, London (1962).

26. Miner, M.A., "Cumulative Damage in Fatigue", J. Appl. Mech., Vol. 12, p. A159 (1945).

27. Peterson, R.E., "Stress Concentration Design Factors", Ed. by John Wiley, New York (1974).

28. Neuber, H. "Theory of Notch Stresses", Ed. by Edwards, London (1946).

29. Frost, N.E., and Greenan, A.F., "Cyclic Stress Required to Propagate Edge Cracks in Eight Materials", J. Mech. Eng. Sci., Vol. 6, No. 3, p. 203 (1964).

30. Frost, N.E., "Notch Effects and The Critical Alternating Stress Required to Propagate a Crack in an Aluminium Alloy Subject to Fatigue Loading", J. Mech. Eng. Sci., Vol. 2, No. 2, p. 109 (1960).

31. Frost, N.E., and Greenan, A.F., "Effect of a Tensile Mean Stress on the Alternating Stress Required to Propagate an Edge-Crack in Various Materials", J. Mech. Eng. Sci., Vol. 12, No. 3, p. 159 (1970).

32. Clark, Jr., W.G., "Evaluation of the Fatigue Crack Initiation Properties of Type 403 Stainless Steel in Air and Steam Environments", Fracture Toughness and Slow-Stable Cracking ASTM STP 559, p. 205 (1974).

33. Barson, J.M. and McNicol, R.C., "Effect of Stress Concentration on Fatigue-Crack Initiation in HY-30 Steel", Fracture Toughness and Slow-Stable Cracking, ASTM STP 559, p. 183 (1974).

34. Benhan, P.P., "Fatigue of Metals Caused by a Relatively Few Cycles of High Load or Strain Amplitude", Metall. Rev., Vol. 3, p. 203 (1958).

35. Manson, S.S., "Fatigue: A Complex Subject - Some Simple Approximations", Exp. Mech., Vol. 22, No. 2, p. 193 (1965).

36. Coffin, Jr., L.F., "Low Cycle Fatigue: A Review", Appl. Mat. Res., Vol. 1, No. 3, p. 129 (1962).

37. Landgraf, R.W., "The Resistance of Metals to Cyclic Deformation", Achievement of High Fatigue Resistance in Metals and Alloys, ASTM STP 467, p. 3 (1970).

38. Morrow, J.D., "Cyclic Plastic Strain Energy and Fatigue of Metals", Internal Friction, Damping and Cyclic Plasticity, ASTM STP 378, p. 45 (1965).

39. Benhan, P.P., "Axial-Load and Strain-Cycling Fatigue of Copper at

Low Endurance", J. Inst. Metals, Vol. 89, p. 328 (1961).

40. Benhan, P.P. and Ford, H., "Low Endurance Fatigue of a Mild Steel and an Aluminium Alloy", J. Mech. Eng. Sci., Vol. 3, No. 2, p. 119 (1961).

41. Morrow, J.D. and Sinclair, G.M., "Cycle-Dependent Stress Relaxation", Symposium on Basic Mechanisms of Fatigue, ASTM STP 237, p. 83 (1958).

42. Feltner, C.E. and Sinclair, G.M., "Cyclic Stress Induced Creep of Packed Metals", Proc. of Joint Int. Conf. on Creep, Inst. Mech. Engrs., London, p. 319 (1965).

43. Coffin, L.F., "The Influence of Mean Stress on the Mechanical Hysteresis Loop Shift of 1100 Aluminium", J. Bas. Eng., Trans. Am. Soc. Mech. Engs. (Series D), Vol. 86, p. 673 (1964).

44. Radon, J.C., Oldroyd, P.W.J. and Burns, D.J., "Mean Strain and Hardness Changes in Uniaxial Stress Cycling", Proc. 1st Int. Conf. Mechanical Behaviour of Materials, Kyoto, Vol. II, p. 285, Soc. Mat. Sci. Japan, (1972).

45. Oldroyd, P.W.J. and Radon, J.C., "Behaviour of Aluminium in Uniaxial Stress Cycling", Proc. 1973 Symp. Mechanical Behaviour of Materials, p. 251, Soc. Mat. Sci. Japan (1974).

46. Mulgahy, T.M., "A Plasticity Model for Cyclic Strain Accumulation", J. Appl. Mech., p. 869 (1971).

47. Neuber, H., "Theory of Stress Concentration for Shear-Strained Prismatical Bodies with Arbitrary Nonlinear Stress-Strain Law", J. Appl. Mech. p. 544, (1961).

48. Topper, T.H., Wetzel, R.M. and Morrow, J.D., "Neuber's Rule Applied to Fatigue of Notched Specimens", J. Mat., Vol. 4, No. 1, p. 200 (1969).

49. Wetzel, R.M., "Smooth Specimen Simulation of Fatigue Behaviour of Notches", J. of Mat., Vol. 3, No. 3 p. 646 (1968).

50. Wundt, B.M., "Effect of Notches on Low-Cycle Fatigue", Metals Properties Council, ASTM STP 490 (1972).

51. Hardrath, H.F. and Ohman, L., "A Study of Elastic and Plastic Stress Concentration Factors Due to Notches and Fillets in Flat Plates", NASA Rep. 1117 (1953).

52. Bell, W.J. and Benham, P.P., "The Effect of Mean Stress on the Fatigue of Plain and Notched Stainless Steel Sheet in the Range from 10 to 10^7 Cycles", quoted by Wundt, B.M. (Ref. 50).

53. Mowbray, D.F. and McConnelee, J.E., "Applications of Finite Element Stress Analysis and Stress-Strain Properties in Determining Notch Fatigue Specimen Deformation and Life", Cyclic Stress-Strain Behaviour - Analysis, Experimentation and Failure Prediction, ASTM STP 519, p. 151 (1973).

54. Gough, H.J., J. Inst. Metals, Vol. 49, p. 17 (1932).

55. Haigh, B.P., J. Inst. Metals, Vol. 18, p. 55 (1917).

56. Hara, S., Hoshino, J. and Arai, J., Proc. of the 10th Japanese National Congress for Applied Mechanics, p. 187 (1958).

57. Duquette, D.J., "An Historical Review of Corrosion Fatigue", Proc. Int. Conf. on Corrosion Fatigue NACE, University of Connecticut, p. 33/2 (1971).

58. McAdam, Jr., D.J. and Geil, G.W., Proc. Am. Soc. Test, Mat., Vol. 41, p. 696 (1941).

59. Duquette, D.J. and Uhlig, H.H., Trans. ASM, Vol. 62, p. 839 (1969).

60. Stubbington, C.A. and Forstyh, P.J.E., J. Inst. Metals, Vol. 90, p. 347 (1962).

61. Evans, W.R., "The Corrosion and Oxidation of Metals", Ed. by Edward Arnold, London (1960).

62. Whitwham, D. and Evans, W.R., J. Iron and Steel Institute, Vol. 165, No.1, p. 72 (1950).

63. Laird, C., "The Influence of Metallurgical Structure on the Mechanisms of Fatigue Crack Propagation", Fatigue Crack Propagation, ASTM STP 415, p. 131 (1967).

64. Hertzberg, R.W., "Fatigue Fracture Surface Appearance", Fatigue Crack Propagation, ASTM STP 415, p. 205 (1967).

65. McMillan, J.C. and Pelloux, R.M.N., "Fatigue Crack Propagation Under Program and Random Loads", Fatigue Crack Propagation, ASTM STP 415, p. 505 (1967).

66. Bowles, C.Q., "On the Formation of Fatigue Striations", Int. J. of Fract. Mech., Vol. 8, No.1, p. 75 (1972).

67. Feeney, J.A., McMillan, J.C. and Wei, R.P., "Environmental Fatigue Crack Propagation of Aluminium Alloys at Low Stress Intensity Levels", Met. Trans., Vol. 1, p. 1741 (1970).

68. Head, A.K., "The Growth of Fatigue Cracks", Phil. Mag., Vol. 44, Series 7 p. 925 (1953).

69. Paris, P.C. and Erdogan, F., "A Critical Analysis of Crack Propagation Laws", J. Bas. Eng., Trans. ASME, Series D, Vol. 85, p. 528 (1963).

70. Frost, N.E. and Dugdale, D.S., "The Propagation of Fatigue Cracks in Sheet Specimens", J. Mech. Phys. of Solids, Vol. 6, No. 2, p. 92 (1958).

71. McEvily, A.J. and Illg, W., "The Rate of Crack Propagation in Two Aluminium Alloys", NACA Technical Note 4394 September 1958.

72. Liu, H.W., "Fatigue Crack Propagation and Applied Stress Range - An Energy Approach", J. Bas. Eng., Trans. ASME, Series D, Vol. 83, p. 23 (1961).

73. Weertman, J., "Rate of Growth of Fatigue Cracks Calculated from the Theory of Infinitesimal Dislocations Distributed in a Plane", Proc. Int. Conf. on Fracture, Sendai, p. 153 (1965).

74. Rice, J.R., "Mechanics of Crack Tip Deformation and Extension by Fatigue", Fatigue Crack Propagation, ASTM STP 415, p. 247 (1967).

75. Gallina, V., Galotto, C.P. and Omini, M., "On a Possible Model of Crack Propagation in a Solid Subjected to a Cyclic Loading". Int. J. of Fract. Mech., Vol. 3, No. 1, p. 37 (1967).

76. Lehr, K.R. and Liu, H.W., "Fatigue Crack Propagation and Strain Cycling Properties", Int. J. of Fract. Mech., Vol. 5, No. 1, p. 45 (1969).

77. Schwalbe, K.H., "Approximate Calculation of Fatigue Crack Growth", Int. J. of Fract., Vol. 9, No. 4, p. 381 (1973).

78. Frost, N.E. and Dixon, J.R., "A Theory of Fatigue Crack Growth", Int. J. of Fract. Mech., Vol. 3, No. 3, p. 301 (1967).

79. Tomkins, B., "Fatigue Crack Propagation - An Analysis", Phil. Mag., Vol. 17, p. 1041 (1968).

80. Hahn, C.T. and Simon, R., "A Review of Fatigue Crack Growth in High Strength Aluminium Alloys and the Relevant Metallurgical Factors", Eng. Fract. Mech., Vol. 5, No. 3, p. 523 (1973).

81. Frost, N.E., Pook, L.P. and Denton, K., "A Fracture Mechanics Analysis of Fatigue Crack Growth Data for Various Materials", Eng. Fract. Mech., Vol. 3, p. 109 (1971).

82. Crooker, T.W. and Lange, E.A., "Fatigue Crack Propagation in a High Strength Steel Under Constant Cyclic Load with Various Mean Loads", Naval Research Laboratory, USA, NRL Report No. 6805 November (1968).

83. Maddox, S.J., "The Effect of Mean Stress on Fatigue Crack Propagation, A Literature Review", Int. J. of Fract., Vol. 11, No. 3, p. 389 (1975).

84. "Fatigue Crack Growth Rate Laws Accounting for Stress Ratio Effects", ASTM Task Force E24.04.04 Report No. 1, Chairman J.P. Gallagher (1975).

85. Forman, R.G., Kearney, V.E. and Engle, R.M., "Numerical Analysis of Crack Propagation in Cyclically Loaded Structures", J. of Bas. Eng., Trans. ASME, Vol. 89, Series D, p. 459 (1967).

86. Hudson, C.M., "Effect of Stress Ratio on Fatigue Crack Growth in 7075-T6 and 2024-T3 Aluminium Alloy Specimens", NASA TN D-5390 August 1969.

87. Hudson, C.M. and Newman, J.C., Jr., "Effect of Specimen Thickness on Fatigue Crack Growth Behaviour and Fracture Toughness of 7075-T6 and 7178-T6 Aluminium Alloys", NASA TN D 7173, April 1973.

88. Erdogan, F. and Ratwani, M., "Fatigue and Fracture of Cylindrical Shells Containing Circumferential Cracks", Int. J. of Fract. Mech. Vol. 6, No. 4, p. 379 (1970).

89. Pearson, S., "The Influence of Mean Stress on Fatigue Crack Growth in 1/2 in. Thick Specimens of Al-alloys of High and Low Fracture Toughness", Eng. Fract. Mech. Vol. 4, No. 1, p. 9 (1972).

90. Chu, H.P. "Effect of Mean Stress Intensity on Fatigue Crack Growth in a 5456-H117 Al-alloy", Fracture Toughness and Slow Stable Cracking ASTM STP 559, p. 245 (1974).

91. Elber, W., "The Significance of Fatigue Crack Closure", Damage Tolerance in Aircraft Structures, ASTM STP 486, p. 230 (1971).

92. Katcher, M. and Kaplan, M., "Effects of R-Factor and Crack Closure on Fatigue Crack Growth for Aluminium and Titanium Alloys", Fracture Toughness and Slow Stable Cracking, ASTM STP 559, p. 264 (1974).

93. Newman, J.C., "A Finite Element Analysis of Fatigue Crack Closure", Proc. ASTM 8th Nat. Symp. Fract. Mech. to appear in Mechanics of Crack Growth, ASTM STP 590, (1976).

94. Frost, N.E., Pook, L.P. and Denton, K., "A Fracture Mechanics Analysis of Fatigue Crack Growth Data for Various Materials", National Engineering Laboratory NEL Report No. Z2/1/69 September 1969.

95. Pook, L.P., "Fatigue Crack Growth Data for Various Materials Deduced from the Fatigue Lives of Pre-cracked Plates", Stress Analysis and Growth of Cracks, ASTM STP 513, p. 106 (1972).

96. Paris, P.C., Bucci, R.J., Wessel, E.T., Clark, W.G. and Magu, T.R. "An Extensive Study of Low Fatigue Crack Growth Rates in A533 and A508 Steels", Stress Analysis and Growth of Cracks, ASTM STP 513, p. 141 (1972).

97. Priddle, E.K., "Some Equations Describing the Constant Amplitude Fatigue Crack Propagation Characteristics of a Mild Steel", Central Electricity

Generating Board, CEGB Report RD/B/N2390 (1972).

98. Klesnil, M. and Lukas, P., "Effect of Stress Cycle Asymmetry on Fatigue Crack Growth", Mat. Sci. and Eng., Vol. 9, p. 231 (1972).

99. Cooke, R.J. and Beevers, C.J., "The Effect of Load Ratio on the Threshold Stresses for Fatigue Crack Growth in Medium Carbon Steels", Eng. Fract. Mech., Vol. 5, p. 1061 (1973).

100. Barsom, J.M., "The Dependence of Fatigue Crack Propagation on Strain Energy Release Rate and Crack Opening Displacement", Damage Tolerance in Aircraft Structures, ASTM STP 486, p. 1 (1971).

101. Arad, S., Radon, J.C. and Culver, L.E., "Growth of Fatigue Cracks in Metals and Polymers", Eng. Fract. Mech., Vol. 6, No. 1, p. 195 (1974).

102. Cherepanov, G.P. and Halmanov, H., "On the Theory of Fatigue Crack Growth", Eng. Fract. Mech., Vol. 4. p. 219 (1972).

103. Paris, P.C., "The Fracture Mechanics Approach to Fatigue, Fatigue - an Interdisciplinary Approach", 10th Syracuse Army Materials Research Conference, Syracuse University Press (1964).

104. Johnson, H.H. and Paris, P.C., "Subcritical Flaw Growth", Eng. Fract. Mech. Vol. 1, No. 1, p. 3 (1968).

105. Raju, K.N., "An Energy Balance Criterion for Crack Growth Under Fatigue Loading from Considerations of Energy of Plastic Deformation", Int. J. of Fract. Mech., Vol. 8, No. 1, p. 1 (1972).

106. Raju, K.N., "On the Calculation of Plastic Energy Dissipation Rate During Stable Crack Growth", Int. J. of Fract. Mech., Vol. 5, No. 2 p. 101 (1969).

107. Erdogan, F., "Crack Propagation Theories", Fracture - an advanced treatise, Vol. II Ed. by Harold Liebowitz, Academic Press, New York (1968).

108. Roberts, R. and Kibler, J.J., "Some Aspects of Fatigue Crack Propagation", Eng. Fract. Mech., Vol. 2, No. 3, p. 243 (1971).

109. Walker, K., "The Effect of Stress Ratio During Crack Propagation and Fatigue for 2024-T3 and 7075-T6 Aluminium", Effects of Environment and Complex Load History on Fatigue Life, ASTM. STP 462, p. 1, (1970).

110. Krafft, J.M., "Correlation of Plane-Strain Toughness with Strain Hardening Characteristics of a Low, a Medium and a High Strength Steel", Appl. Mat. Res., Vol. 3, (1964).

111. Krafft, J.M., "Method for Relating Plastic Flow Properties to Fatigue Crack Propagation Including Effects of Stress Ratio", Naval Research Laboratory, NRL Report 2980, January 1975.

112. Frost, N.E., "Effect of Mean Stress on the Rate of Growth of Fatigue Cracks in Sheet Materials", J. Mech. Eng. Sci., Vol. 4, No. 1, p. 22 (1962).

113. Ritchie, R.O. and Knott, J.F., "Mechanism of Fatigue Crack Growth in Low Alloy Steel", Acta Met., Vol. 21 (1973).

114. Krupp, W.E., Hoeppner, D.W. and Walker, E.K., "Crack Propagation of Aluminium Alloys in Corrosive Environments", Proc. Int. Conf. on Corrosion Fatigue, University of Connecticut, p. 468 (1972).

115. Speidel, M.O., Blackburn, M.J., Beck, T.R. and Feeney, J.A., "Corrosion Fatigue and Stress Corrosion Crack Growth in High Strength Aluminium Alloys Magnesium Alloys and Titanium Alloys Exposed to Aqueous Solutions", Proc. Int. Conf. on Corrosion Fatigue. University of Connecticut, p. 324 (1972).

116. Speidel, M.O. and Hyatt, M.V., "Stress Corrosion Cracking of High Strength Aluminium Alloys", Chapter 3 in Advances in Corrosion Science and Technology, Plenum Press, New York (1972).

117. Cherepanov, G.P. and Halmanov, H., "Fatigue Crack Growth Below K_{ISCC}", Eng. Fract. Mech., Vol. 6, p. 551 (1974).

118. Hartman, A., "On the Effect of Oxygen and Water Vapour on the Propagation of Fatigue Cracks in 2024-T3 Alclad Sheet,", Int. J. of Fract. Mech., Vol. 1, No. 3, p. 167 (1965).

119. Bradshaw, F.J. and Wheeler, C., "The Effect of Environment on Fatigue Crack Growth in Aluminium and Some Aluminium Alloys", Appl. Mat. Res., Vol. 5, p. 112 (1966).

120. Wei, R.P., "Fatigue Crack Propagation in a High Strength Aluminium Alloy", Int. J. of Fract. Mechs. Vol. 4, No. 2, p. 159 (1968).

121. Wei, R.P., "Some Aspects of Environment Enhanced Fatigue Crack Growth", Eng. Fract. Mech., Vol. 1, p. 633, (1970).

122. McEvily, A.J. and Wei, R.P., "Fracture Mechanics and Corrosion Fatigue", Proc. Int. Conf. on Corrosion Fatigue, University of Connecticut, p. 381 (1972).

123. Barsom, J.M., "Corrosion Fatigue Crack Propagation Below K_{ISCC}", Eng. Fract. Mech., Vol. 3, p. 15 (1971).

124. Spitzig, W.A., Talda, P.M. and Wei, R.P., "Fatigue Crack Propagation and Fractographic Analysis of $18N_i$(290) Maraging Steel Tested in Argon and Hydrogen Environments", Eng. Fract. Mech., Vol. 1, p. 155 (1968).

125. Jerram, K. and Priddle, E.K., "The Development and Evaluation of a Fatigue Crack Length Monitoring System for Liquid Environments", Central Electricity Generating Board, CEGB Report RD/B/N2703, (1973).

126. Pook, L.P. and Greenan, A.F., "Fatigue Crack Growth Threshold for Mild Steel, a Low Alloy Steel and a Grey Cast Iron", National Engineering Laboratory NEL Report, No. 571 (1974).

127. Wei, R.P., and Landes, J.D., "Correlation Between Sustained-Load and Fatigue Crack Growth in High-Strength Steels", Mats. Res. Stand., Vol. 9, No. 7, p. 25 (1969).

128. Bucci, R., "Environment Enhanced Fatigue and Stress Corrosion Cracking of a Titanium Alloy Plus a Simple Model for Assessment of Environmental Influence of Fatigue Behaviour", Ph.D. dissertation, Lehgih University,

USA (1970).

129. Paris, P.C., Bucci, R.J., and Little, R.E., "Fatigue Crack Propagation of D6ac Steel in Air and Distilled Water", Stress Analysis and Growth of Cracks, ASTM STP 513, p. 196 (1971).

130. Nicholson, C.E. "Influence of Mean Stress and Environment on Crack Growth", Mechanics and Mechanisms of Crack Growth, Proc. Conf. BSC, Cambridge, p. 226 (1973).

131. Gerberich, W.W., Birat, J.P., and Zackay, V.F., "On the Superposition Model for Environmentally Assisted Fatigue Crack Propagation", Proc. Int. Conf. on Corrosion Fatigue, University of Connecticut, p. 396 (1972).

132. Weiss, V. and Lal, D.N., "A Note on the Threshold Condition for Fatigue Crack Propagation", Met. Trans. Vol. 5, p. 1946 (1974).

133. Schmidt, R.A. and Paris, P.C., "Threshold for Fatigue Crack Propagation and the Effects of Load Ratio and Frequency", Progress in Flaw Growth and Fracture Toughness Testing, ASTM STP 536, p. 79 (1973).

134. Jerram, K. and Priddle, E.K., "System for Determining the Critical Range of Stress-Intensity Factor Necessary for Fatigue Crack Propagation", J. Mech. Eng. Sci., Vol. 15, No. 4, p. 271 (1973).

135. Harrison, J.D., "An Analysis of Data on Non-Propagating Cracks on a Fracture Mechanics Basis", The Welding Institute Research Report, No. E20/3/69, The Welding Institute, Cambridge, March 1969.

136. Grandt, Jr., A.F., and Gallagher, J.P. "Proposed Fracture Mechanics Criteria to select Mechanical Fasteners for Long Service Lifes", Fracture Toughness and Slow Stable Cracking, ASTM STP 559, p. 283 (1974).

137. Cooke, R.J., Irwing, P.E., Booth, G.S. and Beevers, C.J. "The Slow Fatigue Crack Growth and Threshold Behaviour of a Medium Carbon Alloy Steel in Air and Vacuum", Eng. Fract. Mech.,Vol.7, No.1, p. 69(1975).

138. Bucci, R.J., Clark, Jr., W.G. and Paris, P.C., "Fatigue Crack Propagation Growth Rates Under a Wide Variation of ΔK for an ASTM A517

Grade F(T-1)Steel", Stress Analysis and Growth of Cracks ASTM STP 513, p. 177 (1972).

139. Bradshaw, F.J. and Wheeler, C.,"The Influence of Gaseous Environments and Fatigue Frequency on the Growth of Fatigue Cracks in some Aluminium Alloys", Int. J. of Fract. Mech., Vol. 5, No. 4, p. 225 (1969).

140. Yokobori, T. and Sato, K., "The Effect of Frequency on Fatigue Crack Propagation Rate and Striation Spacing in 2024-T3 Aluminium Alloy and SM-50 Steel", Eng. Fract. Mech., Vol. 8, No. 1, p. 81 (1976).

141. Plumbridge, W.J., "The Influence of Specimen Thickness on Fatigue Crack Propagation in Aluminium and Aluminium Alloys", Proc. Int. Conf. Quantitative Relation Between Properties and Microstructure, Haifa, Israel, p. 399 (1969).

142. Frost, N.E. and Denton, K., "The Effect of Sheet Thickness on the Rate of Growth of Fatigue Cracks in Mild Steel", J. of Mech. Eng., Vol. 3, p. 295 (1961).

143. Gurney, T.R., "The Effect of Mean Stress and Material Yield Stress on Fatigue Crack Propagation in Steels, Metal Constr., Vol. 1, No. 2, p. 91 (1969).

144. Sullivan, A.M. and Crooker, T.W., Analysis of Fatigue Crack Growth in a High Strength Steel - Part I: Stress Level and Stress Ratio Effects at Constant Amplitude", J. of Pres. Vessel Tech., Trans. ASME, Paper No. 75-WA/PVP-22 (1975).

145. Illg, W., and McEvily, A.J., "The Rate of Fatigue Crack Propagation for Two Aluminium Alloys Under Completely Reversed Loading", NASA TND-52 (1959).

146. Matthews, .W.T., Barata, F.I. and Driscoll, G.W., "Experimental Observation of a Stress Intensity History Effect Upon Fatigue Crack Growth Rate", Int. J. of Fract. Mech., Vol. 7, p. 224 (1971).

147. Hudson, C.M. and Hardrath, H.F., "Effects of Changing Stress Amplitude on the Rate of Fatigue Crack Propagation in Two Aluminium Alloys", NASA TND960 (1961).

148. Jonas, D. and Wei, R.P., "An Exploratory Study of Delay in Fatigue Crack Growth", Int. J. of Fract. Mech., Vol. 7, p. 116 (1971).

149. Wei, R.P. and Shih, T.T., "Delay in Fatigue Crack Growth", Int. J. of Fract., Vol. 10, No. 1, p. 77 (1974).

150. Shih, T.T. and Wei, R.P., "Load and Environment Interactions in Fatigue Crack Growth", Presented at the Conference on the Prospects of Advanced Fracture Mechanics, Delft, The Netherlands, June 1974.

151. Von Euw, E.F.J., Hertzberg, R.W. and Roberts, R., "Delay Effects in Fatigue Crack Propagation", Stress Analysis and Growth of Cracks, ASTM STP 513, p. 230 (1972).

152. Mills, W.J. and Hertzberg, R.W., "The Effect of Sheet Thickness on Fatigue Crack Retardation in 2024-T3 Aluminium Alloy", Eng. Fract. Mech., Vol. 7, No. 4, p. 705, (1975).

153. Wheeler, O.E., "Spectrum Loading and Crack Growth", J. of Bas. Eng., Trans. ASME, Series D, Vol. 94, No. 1, p. 181 (1972).

154. Gray, T.D. and Gallagher, G.P., "Predicting Fatigue Crack Retardation Following a Single Overload Using a Modified Wheeler Model", Presented at the 8th Nat. Symp. on Fracture Mechanics, Providence, R.I. August 1974.

155. Adams, N.J.I., Int. J. of Fract. Mech., Vol. 8, p. 121 (1972).

156. Richards, C.E. and Lindley, T.C., "The Relevance of Crack Closure to Fatigue Crack Propagation", Mechanics and Mechanisms of Crack Growth, Proc. Int. Conf. BSC, Cambridge, p. 184 April 1973.

157. Dover, W.D. and Boutle, N.F., "Crack Closure at Positive Stresses During Random Load Fatigue Crack Growth", J. of Strain Anal., Vol. 11, No. 1, p. 32 (1976).

158. Priddle, E.K., "High Cycle Fatigue Crack Propagation under Random and Constant Amplitude Loadings", Int. J. Pres. Ves. and Piping, Vol. 4, p. 89 (1976).

159. Laird, C. and Smith, G.C., Phil. Mag., Vol. 7, p. 847 (1961).

160. Crooker, T.W. and Large, E.A., "Low Cycle Fatigue Crack Propagation Resistance of Materials for Large Welded Structures", Fatigue Crack Propagation, ASTM STP 415, p. 94 (1967).

161. McEvily, A.J., "Fatigue Crack Growth and the Strain Intensity Factor", Proc. Air Force Conference on Fatigue and Fracture of Aircraft Structures and Materials, Florida, p. 451 (1970).

162. Solomon, H.D., "Low Cycle Fatigue Crack Propagation in 1018 Steel", Journal of Materials, Vol. 7. No. 3, p. 299 (1972).

163. Tomkins, B., "Plastic and Elastic-Plastic Models for Fatigue Crack Growth", Mechanics and Mechanisms of Crack Growth, Proc. Int. Conf. BSC, Cambridge, p. 184 (1973).

164. Dover, W.D., "Fatigue Crack Growth under COD Cycling", Eng. Fract. Mech., Vol. 5, No.1, p. 11 (1973).

165. McEvily, A.J., Beukelmann, D. and Tanaka, K., "On Large Scale Plasticity Effects in Fatigue Crack Propagation", Presented at the Mechanical Failures Prevention Group, Symp. on Mechanical Failures National Bureau of Standards, May 1974.

166. Dowling, N.E. and Begley, J.A., "Fatigue Crack Growth During Gross Plasticity and the J. Integral", Scientific Paper 74-1E7 Creep P1, Westinghouse Research Laboratories, Pittsburgh, Pa., August 1974.

167. Dowling, N.E., "Geometry Effects and the J.Integral Approach to Elastic-Plastic Fatigue Crack Growth", Presented at the ASTM 9th Nat. Symp. on Fracture Mechanics, University of Pittsburgh, Pittsburgh, Pa., August 1975.

168. Mowbray, D.F., "Derivation of a Low-Cycle Fatigue Relationship Employing Recent Developments in Non-Linear Fracture Mechanics", Materials and Processes Laboratory, General Electric Company, New York (1975).

169. Lamba, H.S., "The J-integral Applied to Cyclic Loading", Eng. Fract. Mech, Vol. 7, No. 4, p. 693 (1975).

170. Poulouse, P.K., Jones, D.L. and Liebowitz, H., "Determination of

Nonlinear Energy Toughness Values for Cyclic Loading Applications", Eng. Fract. Mech., Vol. 8, No. 1, p. 293 (1976).

171. Crooker, T.W., "Basic Concepts for Design Against Structural Failure by Fatigue Crack Propagation", Naval Research Laboratory, NRL Report 7347 (1972).

172. Freudenthal, A.M., "Fatigue and Fracture Mechanics", Eng. Fract. Mech., Vol. 5, p. 403 (1973).

173. Brussat, T.R., "Rapid Calculation of Fatigue Crack Growth by Integration", Fracture Toughness and Slow Stable Cracking, ASTM STP 559, p. 298 (1974).

174. Maddox, S., "Fatigue Strength of Welded Joints", Ph.D. Thesis, University of London (1972).

175. Pook, L.P., "Fracture Mechanics Analysis of the Fatigue Behaviour of Spot Welds", Int. J. of Fract. Vol. 11, No. 1, p. 173 (1975).

176. Hirt, M.A. and Fisher, J.W., "Fatigue Crack Growth in Welded Beams", Eng. Fract. Mech., Vol. 5, p. 415 (1973).

177. Tanaka, K. and Matsuoka, S., "Fatigue Strength of Rolled JIS SM50A Beams", Eng. Fract. Mech., Vol. 7, No. 1, p. 79 (1975).

178. Gurney, T.R., "Fatigue of Welded Structures", Ed. by Cambridge University Press (1968).

179. Mostovoy, S. Crosley, P.B., and Ripling, E.J., "Use of Crack Line Loaded Specimens for Measuring Plane Strain Fracture Toughness", J. of Mat., Vol. 2, No. 3, p. 661 (1967).

180. Srawley, J.E. and Gross, B., "Stress Intensity Factors for Crack Line Loaded Edge Crack Specimens", NASA TN D-3820 (1967).

181. Johnson, F.A. and Radon J.C., "Mechanical and Metallurgical Aspects of Fracture Behaviour of an Al-alloy", Int. J. of Fract. Mech., Vol. 8, No. 1, p. 21 (1972).

182. Johnson, F.A. and Radon, J.C., "Fracture Toughness Data on Aluminium Alloys", Internal Report. Imperial College (1976).

183. Knight, R.N., "The Dowty Rotol 20 Ton Fatigue Machine", Proc. Inst. Mech Eng., Vol. 170, p. 170 (1965-66).

184. Branco, C.M., "Corrosion Fatigue of Al-alloy RR58 – A Fracture Mechanics Approach", M.Sc. Thesis, University of London, October 1973.

185. Bucci, .R.J., Discussion to Chu, H.P. Paper, see (Ref. 90).

186. Frost, N.E., Private Communication (1974).

187. Donahue, R.J., Clark, H.Mc I., Atanmo P., Kumble, R. and McEvily, A.J., "Crack Opening Displacement and the Rate of Fatigue Crack Growth", Int. J. of Fract. Mech., Vol. 8, No. 2, p. 209 (1972).

188. Creager, M. and Paris, P.C., "Elastic Field Equations for Blunt Cracks with Reference to Stress Corrosion Cracking", Int. J. of Fract. Mech., Vol. 3, No. 4, p. 247 (1967).

189. Heckel, K. and Wagner, R., "The Tensile Fatigue Behaviour of CT-Specimens with Small Notch Root Radius", Int. J. of Fract. Vol. 11, No. 1, p. 135 (1975).

190. Bellorin, N. "J_{1c} Tests in Mild Steel" M.Sc. Thesis, University of London, Imperial College (1974).

191. Sprowls, D.O. and Brown, R.H., "What Every Engineer Should Know About Stress Corrosion of Aluminium", Metals Progr., Vol. 81, No. 4, p. 79 (1962).

192. Sprowls, D.O. and Brown, R.H., "Stress Corrosion Mechanisms for Aluminium Alloys", Proc. of the Int. Conf. Fundamental Aspects of Stress Corrosion Cracking, Ohio State University, NACE, p. 466 (1969).

193. Prestley, J.S., "Effect of Stress Orientation on Resistance to SCC of Wrought Aluminium Products", MRD 35-901-3-1, Reynolds Metal Company, (1965).

194. Schijve, D., "Fatigue Crack Propagation and the Stress Intensity Factor", Memorandum. M-191, Delft University of Technology, Holland (1973).

195. Brown,B.F., "The Application of Fracture Mechanics to Stress Corrosion Cracking", Met. Rev., Review 129, p. 171 (1969).

196. Brown, B.F., "A New Stress Corrosion Cracking Test for High Strength Alloys", Mat. Res. and Stand., Vol. 6, No. 3, p. 120 (1966).

197. Chu, H.P. and Wacker, G.A., "Stress Corrosion Testing of 7079-T6 Aluminium Alloy in Seawater Using Smooth and Precracked Specimens", Trans. ASME, J. of Bas. Eng., p. 565 (1969).

198. Hyatt, M.V., "Use of Precracked Specimens in Stress Corrosion Testing of High Strength Aluminium Alloys", Corrosion (NACE), Vol. 26, No. 11, p. 487 (1970).

199. Jacobs, A.J. and Marcus, H.L., "Evaluation of Stress Corrosion Cracking Testing Methods", Corrosion (NACE), Vol. 30, No. 9, p. 305 (1974).

200. "Results of the Collaborative Testing Programme of the Stress Corrosion Cracking Working Group", BISRA, Sheffield, U.K. (1973).

201. Evans, A.G., "A Simple Method for Evaluating Slow Crack Growth in Brittle Materials", Int. J. of Fract., Vol. 9, No. 3, p. 267 (1973).

202. Speidel, M.D., "Current Understanding of Stress Corrosion Crack Growth in Al-alloys", Proc. of the Conf. on Theories of Stress Corrosion Cracking in Alloys, NATO Science Committee, Portugal (1971).

203. Carter, C.S., "Stress Corrosion Crack Branching in High Strength Steels", Eng. Fract. Mech., Vol. 3, No. 1, p.1 (1971).

204. Cherepanov, G.P. and Kuliev, V.D., "On Crack Twinning" Int. J. of Fract., Vol. 11, No. 1, p. 29 (1975).

205. Helfrich, W.F., "Influence of Stress and Temperature on Short Transverse Stress Corrosion Cracking of an Al-4.2 Zn-2.5 Mg Alloy", Stress Corrosion Testing Methods, ASTM STP 425, p.203 (1967).

206. Hyatt, M.V., "Use of Precracked Specimens in Selecting Heat Treatments for Stress Corrosion Resistance in High Strength Aluminium Alloys", Corrosion (NACE), VOl. 27, No. 1, p. 49 (1971).

207. Hyatt, M.V., "Effects of Residual Stresses on Stress Corrosion Crack Growth Rates in Aluminium Alloy", Corrosion (NACE), Vol. 26, No. 12, p. 547 (1970).

208. Wiederhorn, S.M., "Influence of Water Vapour on Crack Propagation in Soda-Lime Glass", J. Am. Ceramic Soc., Vol. 50, No. 8, p. 407 (1967).

209. Weiderhorn, S.M. and Bolz, L.B., "Stress Corrosion and the Static Fatigue of Glass", J. Am. Ceramic Soc. Vol. 53, p. 543 (1970).

210. Kraft, J.M. and Mulherin, J.H., "Tensile Ligament Instability and the Growth of Stress Corrosion Cracks in High Strength Alloys", Trans. ASM, Vol. 62, p. 64 (1969).

211. Vermilyea, D.A. and Diegle, R.B., "Concerning Strain Enhanced Corrosion Mechanisms of SCC", Corrosion (NACE), Vol. 32, No. 1, p. 26 (1976).

212. Hirth, J.P. and Johnson, H.H., "Hydrogen Problems in Energy Related Technology", Corrosion (NACE), Vol. 32, No. 1, p. 3(1976).

213. Van Leeuwen, H.P., "Plateau Velocity of SCC in High Strength Steel - a Quantitative Treatment" Corrosion (NACE), Vol. 31, No. 2, p. 42 (1975).

214. Cherepanov, G.F., "On the Theory of Crack Growth Due to Hydrogen Embrittlement", Corrosion (NACE), Vol. 29, No. 8, p. 305 (1973).

215. Gest, R.J. and Troiano, A.R., "Stress Corrosion and Hydrogen Embrittlement in an Aluminium Alloy", Corrosion (NACE), Vol. 30, No. 8, p. 274 (1974).

216. Cherepanov, G.P., Ershov, L.V. and Kuzmin, G.G., "On the Growth of Corrosion Cracks", Corrosion (NACE), Vol. 29, No. 3, p. 100 (1973).

217. Nielsen, N.A., "Observations and Thoughts on Stress Corrosion Mechanisms", ASTM 1970 Gillett Memorial Lecture, Corrosion (NACE), Vol. 27, No. 5, p. 173 (1971).

218. Meyn, D.A., "Fractographic Diagnosis of SCC in Al-Zn-Mg Alloys", Corrosion (NACE), Vol. 26, No. 10, p. 427 (1970).

219. Smith, T., "A Capillary Model for SCC of Metals in Fluid Media", Corr. Sci., Vol. 12, p. 45 (1972).

220. Liu, H.W., "Stress Corrosion Cracking and the Interaction Between Crack Tip Stress Field and Solute Atoms", Trans. ASME, J. Bas. Eng. p. 633 (1970).

221. West, J.M., "A General Model for Stress Corrosion Crack Propagation", Met. Sci. Journal, Vol. 7, p. 169 (1973).

222. Radon, J.C. and Culver, L.E., "Intergranular Stress Corrosion - A Fracture Mechanics Approach", Proc. Symp. on Mechanical Behaviour of Materials, Kyoto, Japan, Paper C3(b), (1974).

223. Harrigan, H.C., Dull, D.L. and Raymond, L., "Effect of a Loading Sequence on Threshold Stress Intensity Determination", Progress in Flaw Growth and Fracture Toughness Testing, ASTM STP 536, p. 171 (1973).

224. Landes, J.D. and Wei, R.P., "The Kinetics of Subcritical Crack Growth under Sustained Loading", Int. J. of Fract., Vol. 9, No. 3, p. 277 (1973).

225. Baxter, D.C. (High-Duty Alloys Ltd., Slough, Bucks., England), private communication, June 1970.

226. Begley, J.A. and Landes, J.D., "Tentative J_{1c} Test Method", Presented to the ASTM Committee E-24.01 on the Fracture of Metals, Philadelphia, Pa. Oct. 1973.

227. Smith, R.F., Ph.D. Thesis, Department of Metallurgy and Materials Science, University of Cambridge (1972).

228. Garwood, S.J., Robinson, J.N. and Turner, C.E., The Measurement of Crack Growth Resistance Curves (R-Curves) Using the J Integral", Dept. of Mech. Eng. Imperial College, (1975).

APPENDIX A

A BRIEF REVIEW ON FRACTURE MECHANICS

A.1 Elastic Stress Distribution at the tip of a Crack - the Elastic Stress Intensity Factor K

Inglis (A.1) was the first to derive an equation for the maximum stress σ_{yy} at the tip of an elliptical notch with major axis a and minor axis b' under a stress

$$(\sigma_{yy})_{max} = \sigma\left(1 + (\frac{2a}{b'})\right) \qquad (A.1)$$

As the ellipse becomes long and narrow σ_{yy} becomes very large and is given approximately by

$$(\sigma_{yy})_{max} = 2\sigma(\frac{a}{\rho})^{\frac{1}{2}} \qquad (A,2)$$

where $\rho = b'^2/a$ is the radius of curvature.

Many years later, using the Westergaard (A.2) solutions for a number of configurations involving cracks in tensile stress fields, a general solution for the stress system at the tip of an infinitely sharp crack was derived by Irwin (A.3) and Williams (A.4). The near crack tip stresses and displacements could be written in the form

$$\begin{bmatrix} \sigma_{xx} \\ \sigma_{yy} \\ \tau_{xy} \end{bmatrix} = \frac{K_I}{\sqrt{2\pi r}} \begin{bmatrix} \cos\frac{\theta}{2}\left(1 - \sin\frac{\theta}{2}\sin\frac{3\theta}{2}\right) \\ \cos\frac{\theta}{2}\left(1 + \sin\frac{\theta}{2}\sin\frac{3\theta}{2}\right) \\ \cos\frac{\theta}{2}\sin\frac{\theta}{2}\cos\frac{3\theta}{2} \end{bmatrix} \qquad (A.3a)$$

$$\begin{bmatrix} u \\ v \end{bmatrix} = \frac{K_I}{8\mu}(\frac{2r}{\pi})^{\frac{1}{2}} \begin{bmatrix} (2\mu - 1)\cos\theta/2 - \cos 3\theta/2 \\ (2\mu + 1)\sin\theta/2 - \sin 3\theta/2 \end{bmatrix} \qquad (A.3b)$$

where $\mu = 3-4\nu$ in plane strain, $= (2-\nu)/(1+\nu)$ in plane stress, and r,θ is

a co-ordinate system centred at the crack tip,

K_I, the stress intensity factor, is independent of r and θ. It dictates the magnitude but not the distribution of the stress fields in different crack configurations. For an infinite plate containing a crack of length 2a, subjected to a remote tensile stress field σ, the Westergaard solution gives

$$K_I = \sigma\sqrt{\pi a} \tag{A.4a}$$

For more complex cases K_I is given by

$$K_I = Y\sigma\sqrt{\pi a} \tag{A.4b}$$

where Y is a dimensionless parameter accounting for such variables as proximity of a free surface, crack shape and distribution of load. K_I can be related with the elastic stress concentration factor K_t

$$K_I = \lim_{\rho \to 0} \frac{K_t \sigma \rho^{\frac{1}{2}}}{2} \tag{A.5}$$

The above equation, derived by Irwin (A.3), implies that K_I is valid only when a sharp crack is considered.

Thus far attention has been centred on the case of a crack in a tensile stress field. Results analogous to Equation (A.3) can also be obtained for the case of cracks subjected to in-plane shear.

$$\begin{bmatrix} \sigma_{xx} \\ \sigma_{yy} \\ \tau_{xy} \end{bmatrix} = \frac{K_{II}}{\sqrt{2\pi r}} \begin{bmatrix} -\sin\frac{\theta}{2}\left(2 + \cos\frac{\theta}{2}\cos\frac{3\theta}{2}\right) \\ \sin\frac{\theta}{2}\cos\frac{3\theta}{2}\cos\frac{3\theta}{2} \\ \cos\frac{\theta}{2}\left(1 - \sin\frac{\theta}{2}\sin\frac{3\theta}{2}\right) \end{bmatrix} \tag{A.6}$$

and out of plane shear

$$\begin{bmatrix} \tau_{xz} \\ \tau_{yz} \end{bmatrix} = \frac{K_{III}}{\sqrt{2\pi r}} \begin{bmatrix} -\sin \theta/2 \\ \cos \theta/2 \end{bmatrix} \qquad (A.7)$$

K_I, K_{II} and K_{III} are usually referred to as the mode I, mode II and mode III stress intensity factors (Fig. A.1). However, the present analysis will be concerned only with mode I.

A.2 Methods of Determining Stress Intensity Factors

Essentially the problem is that of obtaining the values of Y in Eq. (A.4b). Four different methods are available:

1. The direct application of Muskhelishvili's analysis of the elastic stress field: This method provides a solution which completely satisfies the boundary conditions and provides an exact value of the stress intensity factor. However the labour involved in most cases makes it unsuitable for general use.

2. The boundary collocation method: This is relatively easy to apply. The method is based on the Williams (A.4) polynomial expansion of the stress field, for which the constants are obtained by matching boundary conditions at discrete points. Boundary collocation has been used to determine the stress intensity factor for standard specimens recommended by ASTM (A.5).

3. The finite element method: This provides an easily handled approach for any arbitrary two dimensional geometry and loading system. There is a slight loss of accuracy compared with other methods.

4. The compliance method: This method is used when numerical or analytical solutions are unobtainable, and also to verify numerical solutions previously obtained by other methods. It is based on the Irwin and Kies (A.6) compliance equation for the elastic strain energy release rate, which will be considered later.

Compendia of known solutions are now beginning to appear (A.7). One

of the reasons for linear elastic fracture mechanics (LEFM) not yet having achieved widespread use is the lack of known solutions to calculate K values for more complicated geometries which often occur in practice.

A.3 Fracture Analysis Using K - Linear Elastic Fracture Mechanics

The field values at the tip of a crack in a purely linear elastic body are completely specified once the stress intensity factor K is known. On the assumption that fracture is governed by conditions at the crack tip, it must be expected that fracture will occur when K reaches a critical value K_c. K_c may be obtained from a laboratory test in which failure stress crack length and geometry factor are determined. The difficulty in applying LEFM lies in ensuring that K_c is obtained under crack tip conditions which are reproduced in the structure to be analysed. For purely elastic behaviour this is no problem, since the stress-strain field at the crack tip is completely specified by K for all configurations. However for a real material perfect elasticity is never completely realised.

Equation (A.3) indicates that as $r \to 0$ crack tip stresses would become infinite for any value of the applied stress. Hence plastic deformation will occur at the crack tip. The order of magnitude of the plastic zone, r_y, can be estimated from Eq. (A.3) by settting $\sigma_y = \sigma_{ys}$, the yield strength of the material, leading to

$$r_y = \frac{1}{2\pi}\left(\frac{K_I}{\sigma_{ys}}\right)^2 \qquad (A.8)$$

for plane stress conditions.

An elastic stress distribution with a singularity at the crack tip describes the stress field ahead of the crack where plastic yielding occurs. If the extent of the plastic zone is small in comparison with the dimensions

of the elastically stressed region of the structure, the inaccuracy of the elastic model will be negligible. Since LEFM provides a method of measuring the fracture strength of a brittle material, one must ensure that the errors introduced by plastic yielding are minor or can be corrected. For plasticity effects to be negligible, the plastic zone must be small in comparison with the crack length or the remaining cross section. At the onset of fracture, at which $K = K_c$, the error introduced by plastic yielding may be estimated from the ratio.

$$\frac{r_y}{a} = \frac{1}{2\pi a}\left(\frac{K_c}{\sigma_{ys}}\right)^2 = \frac{1}{2}\left(\frac{\sigma_f}{\sigma_{ys}}\right)^2 \qquad (A.9)$$

where σ_f is the gross fracture strength. Thus the LEFM approach is acceptable as long as the gross fracture stress is small compared to the yield strength of the material.

The elastic stress singularity and the plastic zone size are illustrated in Fig. A.1 for mode I loading, in plane stress and plane strain conditions. For plane strain allowance must be made for the elevation of yield stress ahead of the crack. This is conventionally done by substituting $\sqrt{3}\sigma_{ys}$ for σ_{ys} in Eq. (A.9). For plane strain

$$r_y = \frac{1}{6\pi}\frac{K_c^2}{\sigma_{ys}^2} \qquad (A.10)$$

To correct the small scale plastic yielding effect it was suggested by Irwin that the effective length of the crack be increased by an amount r_y.

The fracture toughness K_c is dependent on, among other factors, thickness. The role of thickness is to provide a triaxial stress field ahead of the crack, which elevates the hydrostatic stress and reduces the plastic zone size. Experimentally it has been verified that K_c decreases as thickness increases (Fig. A.2) and a minimum value, K_{1c}, is attained correspond-

ing to plane strain conditions, The major effect explaining the above trend is the tensile stress elevation occuring as thickness is increased. This favours the cleavage mode of fracture over the shear mode, with consequential reduction in K_c, and indeed the percentage of square fracture increases with the thickness (Fig. A.2). Therefore a plane strain fracture corresponds to a macroscopically flat fracture surface, whereas a large percentage of a plane stress fracture surface is occupied by shear lips.

As a final comment one can say that LEFM may be applicable to the determination of fracture toughness when r_y is negligible in comparison with other characteristic dimensions of the body, such as crack length or thickness. This is the case where a crack or flaw is present in high-strength aluminium, steel and titanium alloys. These materials have limited ductility and generally fail without gross yielding under the above conditions. LEFM can also be applied in more ductile metals, e.g. mild steel, but only at very low temperatures or in very thick plates.

A.4 Test Techniques to Evaluate K_c

As a result of extensive experimental investigation (A.5) it has been shown that to obtain a valid K_{1c} test crack length a, specimen thickness B and the uncracked ligament should all exceed $2.5\,(K_Q/\sigma_{ys})^2$ where K_Q is the apparent fracture toughness value. If these conditions are satisfied K_Q is a valid K_{1c} value within LEFM analysis. The stated criterion is proportional to the plastic zone size r_y.

$$\frac{r_y}{2.5(K_Q/\sigma_{ys})^2} \simeq 0.132 \qquad \text{(A.11)}$$

Therefore the range of applicability of LEFM is limited by the existence of a plastic zone size at the crack tip, which can not be more than 13% greater than the crack length, specimen thickness or uncracked ligament length.

K_Q can be obtained using many different types of specimen (A.5). The most popular of these are the single-edge notch, three point bend and compact tension. Experimentally, the procedure would be to record the applied load against some function of crack length. The requirements of the test (A.8) include a sharp initial fatigue crack, a limited deviation from linearity in the overall load-deflection curve and the correct detection of the first increment of crack extension ("pop-in" phenonmenon). The load corresponding to crack initiation is evaluated. Full details are given in the ASTM STP410 (A.8). Provided all the above conditions are satisfied, the K_Q obtained may be regarded as a material parameter, K_{1c}, the plane strain fracture toughness value.

A.5 Energy Balance Criteria

A more direct explanation of the fracture process is provided by the use of an energy balance criterion. This was first suggested by Griffith (A.9). Using Inglis (A.1) results, Griffith calculated the release of energy caused by the introduction of a centre crack, of length 2a, into a plate, boundary conditions remaining fixed. He compared the energy released with that required to create the new crack surface, postulating that this had a surface energy γ_s/unit area. Instability occurs when an additional release of energy equal to, or in excess of, that absorbed as surface energy. The critical stress at fracture, σ_c was thus found to be

$$\sigma_c = \sqrt{\frac{2\gamma_s E}{\pi a}} \qquad (A.12)$$

Griffith measured γ_s for glass, and applied the above equation to obtain the value σ_c, which was found to agree with the experimental value.

When applying the Griffith theory to metals, difficulty arises over the identity of the term γ_s. Irwin (A.10) and Orowan (A.11) suggested that γ_s

in Eq. (A.12) be replaced by $\gamma_s + \gamma_p$, where γ_p represents the localised plastic energy dissipation/unit area at the crack tip. More generally, $\gamma_s + \gamma_p$ can be regarded as the total work required to open unit area of the crack. The problem is that γ_p cannot be measured directly. This difficulty was overcome by Irwin and Kies (A.6) who suggested an experimental method for calculating energy release rate in an arbitrary body. The energy release rate or change in strain energy dU/da was shown to be

$$\frac{dU}{da} = \frac{P^2}{2} \quad \frac{dC}{da} \tag{A.13}$$

where P is the applied load and C is the compliance. dC/da can be found from a series of load displacement curves for different crack lengths in the same geometry. The critical value of energy release rate and hence $2\gamma_s$ can be found by substituting the fracture load and the appropriate value of dC/da in Eq. (A.13).

Irwin (A.3) suggested the equivalence between the parameter G, which he defined as the crack extension force, and the stress intensity factor.

$$G = \frac{K^2}{E'} \tag{A.14}$$

where $E' = E$ for plane stress and $E' = E(1-\nu^2)$ for plane strain. Eq. (A.14) establishes the analogy between the stress intensity and energy balance theories of fracture.

The most complete mathematical treatments of the energy balance for crack propagation in an elastic body were provided by Rice (A.12) and Cherepanov (A.13). They found that G can be expressed as

$$G = - \frac{dU}{da} \tag{A.15}$$

where U is the potential energy of an elastic body. G is then more generally defined as the rate at which potential energy decreases with crack

length. A convenient way of visualising the potential energy decrease is as the area between the overall load deflection curves before and after crack extension. This holds true for non-linear elastic as well as linear elastic behaviour.

A.6 Elastic-Plastic Stress Analysis of Cracks

Non-Linear Fracture Mechanics

The stress-strain field at the tip of a crack in an elastic medium is completely described by the value of K. This holds true if the extent of plastic deformation is such that $r_y/a < 0.02$. If extensive plastic deformation occurs the linear elastic approach is no longer valid and an elastic plastic (non-linear) fracture parameter must be sought.

A large number of possible fracture criteria have been suggested, but the two parameters which have recieved most attention in recent years are crack opening displacement (COD) and the J integral.

A.6.1 The Dugdale Model and the Crack Opening Displacement

Dugdale (A.14) considered an isolated straigth crack of length 2a in an infinite sheet with remotely applied stress σ normal to the crack plane; yielding is confined to a narrow band along the line of the crack, extending to a distance x from the crack tip. He assumed that σ_{ys} was constant over this distance, and that all stresses in the plate were to remain finite.

Although the Dugdale model was originally suggested to correlate experimentally observed plastic zone sizes in mild steel, it can also be used to obtain the COD at the crack tip, as

$$v = \frac{8\sigma_y a}{\pi E} \left(\log_e \sec \frac{\pi\sigma}{2\sigma_y}\right) \qquad (A.16)$$

where v is the crack opening displacement, Expanding Eq. (A.16) as a series and considering the first term only

$$v = \frac{\sigma^2 \pi a}{E\sigma_y} = G\sigma_y \qquad (A.17)$$

The COD may be used as a failure criterion in materials which exhibit extensive plastic deformation at the crack tip, i.e. failure occurs when COD reaches a critical value. This was initially proposed by Wells (A.15).

Early experimental COD measurement was performed using a rotating paddle meter. This technique was developed by Burdekin and Stone (A.16). Due to the large experimental errors involved, this technique was abandoned and substituted by the measurement of the notch opening using a clip gauge. This quantity can be related to the COD by assuming that the crack opens about a center of rotation a distance r(w-a) beyond its tip. Wells (A.17) suggested an analytical relationship between v and the notch opening, and more recently Sumpter (A.18) has computed COD for a large variety of geometries, using the finite element method.

A.6.2 The J Contour Integral

The fracture toughness of ductile materials can be expressed in terms of the J contour integral. The energy line integral, J, is applicable to elastic or elastic-plastic materials when these can be treated by a deformation theory of plasticity (i.e. unloading is not permitted). It was defined by Rice (A.19) for two-dimensional problems as:

$$J = \int_r W dy - T\left(\frac{\partial u}{\partial x}\right) ds \qquad (A.18)$$

where r is any contour surrounding the crack tip, W is the strain energy density, and T, u are traction and displacement vectors defined by the outward normal to r, and s is the arc length along r. The path independence of the

J integral was proven by Rice (A.19).

McClintock (A.20) has shown that by combining the work of Hutchinson (A.21) and Rice and Rosengren (A.22) the crack tip plastic stress and strain singularities can be expressed as functions of J. In McClintock's work (A.20) it was assumed that the material followed a relationship between equivalent stress σ_{eq} and equivalent plastic strain ε_{pl} of the form

$$\sigma_{eq} = \left(\frac{\varepsilon_{pl}}{A}\right)^{1/n} \tag{A.19}$$

where n is the strain hardening exponent. From the above, one may assume that fracture will be governed by J, since J characterizes the near tip deformation field in an elastic-plastic material.

The J integral has an energy interpretation (A.23) which leads to a straightforward experimental determination:

$$J = -\frac{1}{B_n}\frac{dU}{da} \tag{A.20}$$

where B_n is the net fracture width, U is the potential energy and a is the crack length. In the linear elastic case J is therefore equal to G, the crack extension force.

Equation (A.20) has been applied to the experimental determination of J values using a compliance type procedure on several specimens of varying crack lengths (A.24, A.25). However, for certain geometries, such as deeply notched compact tension and three point bend specimens, Rice et al (A.26) developed a method which allows J values to be estimated from a single experimental load-displacement curve. In this technique the specimen with a deep crack ($a/w > 0.6$) is loaded to the displacement of interest and J is determined as a function of displacement from the expression

$$J = \frac{2A_L}{Bb} \tag{A.21}$$

where A_L is the area under the load-displacement curve taken at the displacement of interest, B is the thickness, b is the uncracked ligament (w-a) and w is the width of the specimen.

Critical values of $J(J_{1c})$ are obtained at zero crack extension, but defining crack initiation and determining its onset is perhaps the most difficult part of the J_{1c} evaluation. To overcome this problem J was plotted against crack extension by Landes and Begley (A.27), in the form of a resistance, R, curve (A.28). J_{1c} is taken at the intersection of the stretch zone line ($J/2\sigma_{flow}$) and the J versus crack extension curve where σ_{flow} is the mean of the yield stress and the ultimate tensile stress. The stretch zone takes into account the crack front geometry change usually occuring before actual material separation. This stretch zone is associated with the "crack opening stretch", COS. Recent work by Robinson and Tetelman (A.29) has shown experimentally that the COS is equal to J/σ_{ys} where σ_{ys} is the yield stress of the material. However, the criterion $J/2\sigma_{flow}$ accounts for other cases in which the material has a high strain hardening exponent.

A tentative J_{1c} test method based on the above considerations has already been put forward by Begley and Landes (A.30) and extensively applied by Logsdon (A.31) for various materials. It has also been shown by Clarke et al (A.32) that J results are unaffected by unloading of less than 10% of the maximum load.

References

A.1 Inglis, C.E., "Stresses in a Plate due to the Presence of Cracks and Sharp Corners", Trans. Inst. Naval Architects, Vol. 60, p. 219 (1913).

A.2 Westergaard, H.M., "Bearing Pressures and Cracks", J. Appl. Mech., p. A49 (1939).

A.3 Irwin, G.R., "Analysis of Stresses and Strains near the End of a Crack Traversing a Plate", J. Appl. Mech., Vol. 24, p. 361 (1957)

A.4 Williams, M.L., "On the Stress Distribution at the Base of a Stationary Crack", J. Appl. Mech., Vol. 24, p. 109 (1957).

A.5 ASTM STP 463, "Review of Developments in Plane Strain Fracture Toughness Testing" (1970).

A.6 Irwin, G.R. and Kies, J.A., "Fracturing and Fracture Dynamics", Weld. J. Res. Suppl., Vol. 17, p. 95 (1952).

A.7 Cartwrigth, D.J. and Rooke, D.P., "Methods of Determining Stress Intensity Factors", Royal Aircraft Establishment, RAE Tech. Rep. 13031 (1973).

A.8 ASTM STP 410, "Plane Strain Fracture Toughness Testing of High Strength Materials" (1966).

A.9 Griffith, A.A., "Phenomena of Rupture and Flow in Solids", Phil. Trans., Vol. 221, Series A, p. 163 (1920).

A.10 Irwin, G.R., "Fracture Dynamics. Fracturing of Metals". Am. Soc. of Metals, Cleveland (1948).

A.11 Orown, E., "Fracture and Strength of Solids", Rep. Prog. Phys., Vol. 12, p. 85 (1949).

A.12 Cherepanov, G., "Cracks in Solids", Int. J. Solids and Structures, Vol. 4, p. 811 (1968).

A.13 Rice, J.R., "An Examination of the Fracture Mechanics Energy Balance from the Point of View of Continuum Mechanics", Proc. 1st Int. Conf. on Fracture, Vol. 1, p. 283 (1965).

A.14 Dugdale, D.S., "Yielding of Steel Sheets Containing Slits", J. Mech. and Phys. of Solids, Vol. 8, p. 100 (1960).

A.15 Wells, A.A., "Application of Fracture Mechanics at and Beyond General Yielding", Brit. Weld. J., p. 563 (1963).

A.16 Burdekin, F.M. and Stone, D.E.W., "The Crack Opening Displacement Approach to Fracture Mechanics in Yielding Materials", J. Strain Anal., Vol. 1, p. 145 (1966).

A.17 Wells, A.A., "The Status of COD in Fracture Mechanics", 3rd Canadian Congress of Applied Mechanics (1971).

A.18 Sumpter, J.D.G., "Elastic-Plastic Fracture Analysis and Design Using the Finite Element Method", Ph.D. Thesis, University of London, December 1973.

A.19 Rice, J.R., "A Path Independent Integral and the Approximate Analysis of Strain Concentrations by Notches and Cracks", Trans. ASME, J. Appl. Mech., Vol. 35, p. 379, (1968).

A.20 McClintock, F.A., "Plasticity Aspects of Fracture", Chapter 2 in Fracture, H. Liebowitz, editor, Vol. III, Academic Press, New York, p. 47, (1968).

A.21 Hutchinson, J.W., "Singular Behaviour at the End of a Tensile Crack in a Hardening Material", J. Mech. and Phys. of Solids, Vol. 16, p. 13, (1968).

A.22 Rice, J.R. and Rosengren, G.F., "Plane-Strain Deformation near a Crack Tip in a Power-Law Hardening Material", J. Mech. and Phys. of Solids, Vol. 16, p. 1, (1968).

A.23 Rice, J.R., "Mathematical Analysis in the Mechanics of Fracture", Chapter 3 in Fracture, H. Liebowitz, editor, Vol. III, Academic Press, New York, p. 191, (1968).

A.24 Landes, J.D. and Begley, J.A., "The Effect of Specimen Geometry on J_{1c}", Fracture Toughness, ASTM STP514, p. 24, (1972).

A.25 Bucci, R.J., Paris, P.C., Landes, J.D. and Rice, J.R., "J Integral Estimation Procedures", Fracture Toughness, ASTM STP 514, p. 40, (1972).

A.26 Rice, J.R., Paris, P.C. and Merkle, J.G., "Some Further Results of J-Integral Analysis and Estimates", Progress in Flaw Growth and Fracture Toughness Testing, ASTM STP 536, p. 231, (1973).

A.27 Landes, J.D. and Begley, J.A., "Test Results from J-Integral Studies: an attempt to Establish a J_{1c} Testing Procedure", Fracture Analysis, ASTM STP 560, p. 110, (1974).

A.28 "Fracture Toughness Evaluation by R-Curve Methods", ASTM STP 527, (1973).

A.29 Robinson, J.N. and Tetelman, A.S., "Measurement of K_{1c} on Small Specimens Using Critical Crack Tip Opening Displacement", Fracture Toughness and Slow-Stable Cracking, ASTM STP 559, p. 139, (1974).

A.30 Begley, J.A. and Landes, J.D., "Tentative J_{1c} Test Method", presented to the ASTM Committee E-24.01 on the Fracture of Metals, Oct. 1973, Philadelphia, Pa.

A.31 Logsdon, W.A., "Elastic Plastic (J_{1c}) Fracture Toughness Values: Their Experimental Determination and Comparison with Conventional Linear Elastic (K_{1c}) Fracture Toughness Values for Five Materials", presented at the Eighth National Symposium on Fracture Mechanics, ASTM, Brown Univ., Providence, R.I., Aug. 1974.

A.32 Clarke, G.A., Andrews, W.R., Paris, P.C. and Schmidt, D.W., "Single Specimen Tests for J_{1c} Determination", to be published in Mechanics of Crack Growth, ASTM STP 590 1976.

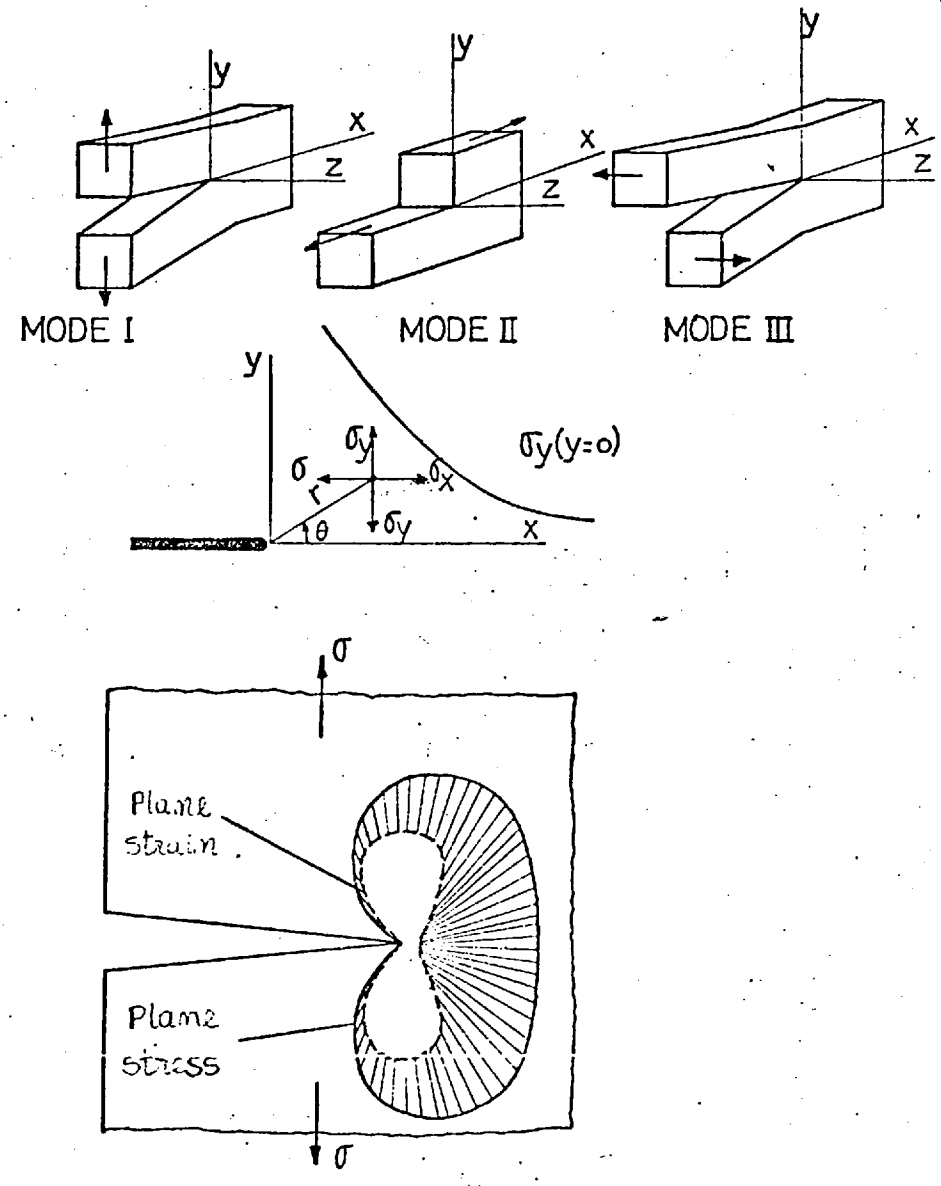


FIG. A1 The Loading Modes and the Plastic Zone Size at the Crack Tip

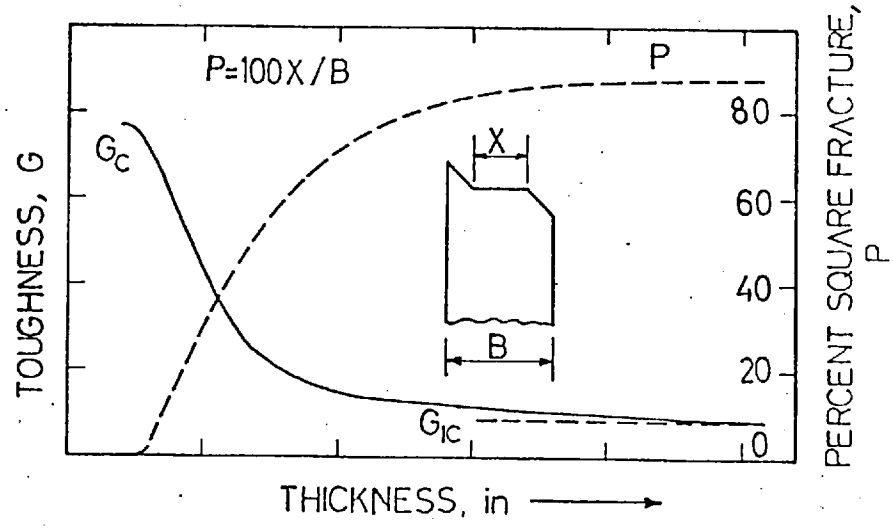


FIG. A2 The Variation of G with the Thickness

APPENDIX B

NON-LINEAR BEAM THEORY USED IN THE PRESENT ANALYSIS

The contoured DCB specimen used in this analysis was treated as a pair of variable-height rectangular cross-section beams built-in at the crack tip. The contoured shape is closely approximated by a straight line (Fig. 66) with an angle of approximately 10^{o}. This angle is sufficiently small for equations developed for beams of constant cross-section to be applicable with adequate accuracy in the variable cross-section area.

B.1 The General Curvature Equations

The stress-strain law for a given material may be expressed as

$$\varepsilon = A\sigma^{\alpha}F(t) \qquad \text{(B.1)}$$

where ε is the strain, σ is the applied stress and A, F(t) and α are constants for each loading condition. Equation (B.1) can have two main applications:

a) Strain-hardening behaviour - where A is the Strain hardening constant, F(t) = 1, α is the strain hardening exponent n. (Table 1), and hence $\varepsilon = A\sigma_{pl}^{n}$ (B.1a)

b) Secondary stage of creep and cyclic creep - where A is the creep of cyclic creep constant C_1, F(t) is time or number of cycles N, depending on the load application method, and α is the creep or cyclic creep exponent m, (Table 1), and therefore $\varepsilon = C_1 N\sigma_{pl}^{m}$ (B.1b)

Considering solely the bending moment effect on the deflections, the curvature k in a beam of rectangular cross-section is given by a general equation

$$k = - AF(t) \left[\frac{P(2\alpha+1)}{2\alpha B}\right]^{\alpha} \frac{x^{\alpha}}{(h/2)^{2\alpha+1}} \qquad \text{(B.2)}$$

derived in Ref. (B.1) where x is the co-ordinate along the beam length, B is the beam thickness, P is the applied load and h the beam height. The effect of the shear force on the curvature is not taken into account in the above equation since the increase in deflection due to shear force is very small (3 or 4%) when small deflections or loads are considered. When $\alpha = 1$ and $A = \frac{1}{E}$ (where E is Young's modulus) Eq. (B.2) reduces to the linear elastic curvature k_{el}

$$k_{el} = -\frac{12P}{EB}\frac{x}{h^3} \tag{B.3}$$

For an elastic-plastic material showing a linear elastic regime from zero to the yield load the total curvature is given by

$$k_o = \frac{12P_{ys}}{EB}\frac{x}{h^3} + A\left(\frac{P_{pl}(2n+1)}{2nB}\right)^n \frac{x^n}{(h/2)^{2n+1}} \tag{B.4}$$

where $P_{pl} = P_{max} - P_{ys}$, P_{max} the maximum load and P_{ys} the yield load. The second term in Eq. (B.4) represents the plastic curvature, assuming that after P_{ys} has been reached the material follows a non-linear stress strain law given by Eq. (B.1a).

B.2 The Curvature Due to Cyclic Creep in Load Cycling

For a material exhibiting cyclic creep (e.g. load cycling in the contoured DCB specimen) the curvature k_{cc} is

$$k_{cc} = C_1 N\left(\frac{P_{cc}(2m+1)}{2mB}\right)^m \frac{x^m}{(h/2)^{2m+1}} \tag{B.5}$$

where $P_{cc} = P_{ef} - P_{ys}$, C_1 and m are defined by the cyclic creep law, Eq. (B.1b), and P_{ef} is the load component normal to the tangent to the deformed beam at the loading points. P_{ef} is then given by

$$P_{ef} = P_{max} \cos \text{arc tg}(d\delta_N/dx)_{x=0} = P_{max}\cos\theta' \tag{B.6}$$

where δ_N is the total deflection after N loading cycles and θ' is the angle schematically shown in Fig. 66. It was assumed that the total deflection is the sum of that caused in the first load cycle (δ_1) when the crack length is a_o and that accumulated due to cyclic creep (δ_{cc}) in subsequent cycles. Thus $(\frac{d\delta_N}{dx})_{x=0}$ is given by

$$(\frac{d\delta_N}{dx})_{x=0} = \int_0^{a_o} k_o dx + \int_0^{a} k_{cc}\, dx \qquad (B.7)$$

This equation was integrated using Simpson's rule.

B.3 Determination of the Error Factor for Large Deflections

It is known that for small deflections the curvature is approximately equal to the second derivative of the deflection. However the accuracy of this approximate analysis may be checked against the exact analytical solution,

$$k_o + k_{cc} = \frac{d^2(\delta_1+\delta_{cc})/dx^2}{\left[1 + \left(\frac{d(\delta_1+\delta_{cc})}{dx}\right)^2\right]^{3/2}} \quad \text{when } x < a_o \qquad (B.8a)$$

and

$$k_{cc} = \frac{d^2\,\delta_{cc}/dx^2}{\left[1 + \left(\frac{d\,\delta_{cc}}{dx}\right)^2\right]^{3/2}} \quad \text{when } x > a_o \qquad (B.8b)$$

With both equations applicable for large deflections.

The approximate method is accurate when $d\delta_N/dx$ is sufficiently small. The accuracy of the present solution has been checked by choosing at random the point x=30 by integrating (Simpson's rule) the curvature equations at crack length values ranging from 70 to 160 mm and substituting this $d\delta_N/dx$ value into

$$r = \frac{k}{d^2\delta_N/dx^2} \tag{B.9}$$

to evaluate the ratio r. The method is accurate when $r \simeq 1$. It was found that for loads less than 5kN and for short crack lengths, $d\delta_N/dx$ was such as to give r values greater than 0.95 (i.e. less than 5% error). This value was considered to be the limit of acceptability.

B.4 Shear Stress Distribution in Variable Height Beams for Linear and Non-Linear Elastic Materials

Considering an element of a variable height beam of length x having heights h and h-dh, the equilibrium equation for the element dx is

$$B\int_y^{\frac{h-dh}{2}} (\sigma_x + d\sigma_x)\,dy - B\int_y^{h/2} \tau_{xy}\,dy = B\tau_{yx}\,dx \tag{B.10}$$

where τ_{yx} is the shear stress and σ_x is the bending stress. It is assumed that the origin is on the neutral axis and that the bending stress distribution is the same as that for a constant height beam; this is sufficiently accurate as the included angle of the beam is typically less than 20° (9° in present design). Hence Timoshenko (B.1) gives σ_x as

$$\sigma_x = \frac{2}{Bh^2}\frac{PL(2n+1)}{n}\left(\frac{2y}{h}\right)^{1/n} \tag{B.11}$$

where L = a - x and n is the strain hardening exponent in the stress-strain law $\varepsilon = A\sigma_x^n$. Differentiating Eq. (B.11) we obtain

$$\frac{d\sigma_x}{dx} = \frac{2(2n+1)2^{1/n}P^{1/n}y^{1/n}}{Bn}\frac{d}{dx}\left(\frac{L}{h^2h^{1/n}}\right)dx \tag{B.12}$$

After splitting the integral terms Eq. (B.10) may be written as

$$\int_{y}^{h/2} \sigma_x dy + \int_{y}^{h/2} \frac{d\sigma_x dx dy}{dx} - \int_{\frac{h-dh}{2}}^{h/2} \sigma_x dy = \tau_{yx} dx \qquad (B.14)$$

Substituting Eq. (B.12) in (B.14) the first integral term becomes

$$\frac{2^{\frac{n+1}{n}}(2n+1)P}{Bn} \frac{d}{dx}\left(\frac{L}{h^{2}h^{1/n}}\right) \int_{y}^{h/2} y^{1/n} dy \qquad (B.15)$$

If h is a function of x, such as $h = h_o + h_1 L$ then

$$\frac{d}{dx}\left[\frac{L}{h^{\frac{2n+1}{n}}}\right] = \frac{\frac{2n+1}{n} h_1 L - h}{h^{\frac{3n+1}{n}}} = M \qquad (B.16)$$

The second integral term of Eq. (B.14) can be calculated as

$$\left[\frac{2^{\frac{n+1}{n}}(2n+1)\,PL}{\left(h^{\frac{2n+1}{n}}\right)(n+1)B} y^{\frac{n+1}{n}}\right]_{\frac{h-dh}{2}}^{h/2} = \frac{\left(2^{\frac{n+1}{n}}\right)(2n+1)PL}{B(n+1)\left(h^{\frac{2n+1}{n}}\right)} \left[\left(\frac{h}{2}\right)^{\frac{n+1}{n}} - \left(\frac{h-dh}{2}\right)^{\frac{n+1}{n}}\right] \qquad (B.17)$$

The second term in the RHS brackets may be expressed as a power series and becomes

$$\left(\frac{h-dh}{2}\right)^{\frac{n+1}{n}} = \left(2^{\frac{n}{n+1}}\right)\left(h^{\frac{n+1}{n}}\right)\left[1-\left(\frac{n+1}{n}\right)\frac{dh}{h} + \left(\frac{n+1}{2n^2}\right)\left(\frac{dh}{h}\right)^2 + \cdots\right] \qquad (B.18)$$

$$= \left(2^{\frac{n}{n+1}}\right) h^{\frac{n+1}{n}} \left(1- \left(\frac{n+1}{n}\right)\frac{dh}{h}\right)$$

after neglecting the higher order terms.

Substituting Eq. (B.18) in (B.17) the second integral term T_2 of Eq. (B.14) is finally obtained as

$$T_2 = - \frac{(2n+1)PL}{Bnh^2} \, dh \qquad (B.19)$$

Then the plastic (non-linear elastic) shear stress distribution τ_{yx}^{pl} is given by the following equation

$$\tau_{yx}^{pl} = \frac{(2n+1)PL}{Bnh^2} h_1 + \frac{\left(\frac{n+1}{n}\right)(2n+1)P}{B(n+1)} M \left[\left(\frac{h}{2}\right)^{\frac{n+1}{n}} - y^{\frac{n+1}{n}}\right] \qquad (B.20a)$$

It should be noted that for both the beam elements considered in the DCB specimen (Fig. 66) Eq. (B.20a) should be used with $P = P_{pl} = P_{max} \rightarrow P_{ys}$, since between P_{ys} and P_{max} the material follows a non-linear stress strain law given by Eq. (B.1a).

For the linear elastic case n = 1 and in the present application $P = P_{ys}$, so that Eq. (B.20a) becomes

$$\tau_{yx}^{el} = \frac{3P_{ys}L}{Bh^2} h_1 + \frac{6P_{ys}}{B}\left(\frac{h^2}{4} - y^2\right)\left(\frac{3h_1L-h}{h^4}\right) \qquad (B.20b)$$

When the height is constant (1st beam element, Fig.66), $h = h_o$ and $h_1 = 0$ and hence Eqs. (B.20a) and (B.20b) simplify to

$$\tau_{yx}^{pl} = \frac{(2)^{\frac{n+1}{n}}(2n+1)P_{pl}}{B(n+1)}\left(h_o\right)^{\frac{-2n-1}{n}}\left[\left(\frac{h_o}{2}\right)^{\frac{n+1}{n}} - y^{\frac{n+1}{n}}\right] \qquad (B.21a)$$

and

$$\tau_{yx}^{el} = \frac{6P_{ys}}{Bh_o^3}\left(\frac{h_o^2}{4} - y^2\right) \qquad (B.21b)$$

The latter equation agrees with the standard solution for linear elastic beam theory (B.1). The positive sign is obtained in Eqs. (B.21a) and (B.21b) since for a constant height beam the bending stress increases with x, reversing the integral terms in Eq. (B.10). Note that Eq. (B.10)

has been derived for σ_x decreasing with x; this is true for the contoured DCB specimen analysed.

The deflections δ^s_{el} and δ^s_{pl} due to the shear force are obtained by integrating the following equations

$$\frac{d\delta^s_{el}}{dx} = \frac{(\tau^{el}_{yx})_{y=0}}{G'} \tag{B.22a}$$

for the linear elastic region where G' is the shear modulus and

$$\frac{d\delta^s_{pl}}{dx} = D(\tau^{pl}_{yx})^n_{y=0} \tag{B.22b}$$

where $D = A(3)^{\frac{n+1}{2}}$, A being the strain hardening constant for the non-linear (plastic) region.

This relation was obtained from the equivalent stress-equivalent strain curve in tension and shear.

Equations (B.22a) and (B.22b) were integrated for both beam elements using Simpson's rule with $h_1 = 0$ in the first element and the appropriate limits of integration. For this purpose Eq. (B.20a), with y = 0 and the appropriate value of M substituted, simplifies to:

$$(\tau^{pl}_{yx})_{y=0} = \frac{(2n+1)P_{pl}}{n(n+1)Bh^2}\left((3n+2)\,Lh_1 - nh\right) \tag{B.23a}$$

and for the linear elastic regime Eq. (B.20b) or (B.23a) gives

$$(\tau^{el}_{yx})_{y=0} = \frac{3P_{ys}}{2Bh^2}(5Lh_1 - h) \tag{B.23b}$$

For the constant height element δ^s_{el} and δ^s_{pl} can however be obtained by direct integration, i.e.

$$\delta^{s}_{el} = \frac{3P_{ys}}{Bh_o G'} x \qquad (B.24a)$$

and

$$\delta^{s}_{pl} = \frac{2(2n+1)DP_{pl}}{(n+1)Bh_o} x \qquad (B.24b)$$

In the latter equations, and also in all the numerical deflection values obtained, a factor of 2 was included for a pair of beams representing the contoured DCB specimen.

B.5 The Deflection Caused by Rotation at the Crack Tip

In the DCB specimen analysed some rotation at the crack tip occurs. Thus the initial assumption of the beam being built-in at the crack tip should be corrected to take this into account. Deflection at the loading points due to rotation was computed, assuming that the beam would freely rotate at the crack tip and being built-in at the end of the specimen. The uncracked ligament was supposed to behave entirely within linear elastic conditions; this is a good approximation since plastic deformation is confined to the divided part of the beam and the crack tip.

It can be shown (B.1) that under these conditions the total deflection at the loading points is given by

$$\delta_t = \delta^M + \delta^S + \delta^R = \delta^M + \delta^S + \frac{6Pa^2(w-a)}{EBh_u^3} \qquad (B.25)$$

The first and second terms represent the bending moment and shear stress deflections respectively for a built-in beam, and the last term δ^R is the deflection due to rotation at the crack tip, where h_u is the uncracked ligament height.

References

B.1 Timoshenko, S., "Strength of Materials", Part II, Advanced, Ed. by Van Nostrand and Reinhold (1970).

```
      PROGRAM MONJ(INPUT,OUTPUT,TAPE5=INPUT,TAPE6=OUTPUT)
      REAL  LL0
      COMMON PY(40),SIGMA(40),X0(1500),AK0(1500),DYDXES(1500),PPL(40),
     1DYDXS(1500),DYDX0(1500),DYDXEL(1500),DZDXEL(1500),DZDX(1500),
     2Y0(40),YOEL(40),U(40),SEL(40),YR0(40),YST(40),DELTAJ(40),YJST(40),
     3AKEL(1500)
C     PROGRAM TO COMPUTE THE J INTEGRAL IN THE DCB SPEC. FOR MONOTONIC
C     LOADING
C     P IS THE LOAD ,B IS THE GROSS THICKNESSAND ENO IS THE STRAIN
C     HARDENING EXPONENT
      READ(5,1)   B
    1 FORMAT(20X,F6.1)
      READ(5,9)   B
    9 FORMAT(20X,F4.1)
      WRITE(6,5)     B,B
    5 FORMAT(1H1,15X,3HP =,F6.1,45X,3HB =,F4.1,////////)
      SY=401.0
      HMAX=36.7
      BN=3.6
C     SY IS THE YIELD STRESS,HMAX IS THE MAXIMUM HEIGHT ,BN IS THE NET
C     THICKNESS,AND HO A GEOMETRIC CONSTANT
      HO=7.1
C     AO IS THE STRAIN HARDENING CONSTANT,B1 IS THE NET THICKNESS
C     EY IS THE YOUNGS MODULUS AND H1R IS A GEOMETRIC CONSTANT
      EY=2.07E+5
      H1R=0.1775
C     HO2 IS A GEOMETRIC CONSTANT AND H IS THE STEP INTERVAL FOR THE
C     INTEGRATION
      H=0.5
      G=8.0E+4
      W=216.0
C     G IS THE SHEAR MODULUS AND W IS SPECIMEN LENGTH
      M=0
C     LL0 IS THE INITIAL CRACK LENGTH AND H1 IS THE SLOPE OF THE SHAPE
      LL0=65.
      WRITE(6,87)
   87 FORMAT(28X,30HROTATION AT THE LOADING POINTS,/////)
   81 M=M+1
      LL0=LL0+5.
      IF(M.EQ.23)     GO TO 99
      H1=1.72E-1
      H20=HO+H1*LL0
C     M IS THE NUMBER OF CRACK LENGTHS CONSIDERED AND PY IS THE YIELD
C     LOAD
      PY(M)=(B*(H20**2)*SY)/(6.*LL0)
      PPL(M)=P-PY(M)
      IF(PPL(M).LE.0.)      GO TO 98
      ENO=2.459
      AO=5.554E-3
      C=(2.*ENO+1.)/ENO
      SIGMA(M)=SY*(2.*PPL(M)*LL0*C)/(B*(H20**2))
      DJ=C*ENO
      CJ=(ENO+1.)/2.
      EJ=AO*(3.**CJ)
      EM=ENO
      D1=(2.*ENO+1.)/(ENO*(ENO+1.))
      D2=3.*ENO+2.
      VAL2J=(PPL(M)*(2.*ENO+1.))/(2.*ENO*B)
      VAL1J=AO*(VAL2J**ENO)
      GO TO 99
   98 SEL(M)=(6.*LL0*P)/(B*(H20**2))
      PPL(M)=0.
      PY(M)=0
      SIGMA(M)=SEL(M)
   99 NSTO=IFIX(LL0/H)
      LIMO=NSTO+1
C     PPL IS THE PLASTIC LOAD AND SIGMA IS THE STRESS
      DO 3 I=1,LIMO
      X0(I)=H*FLOAT(I-1)
      XXO=LL0-X0(I)
      H2=H1*(XXO)-30.)
      IF(XXO.LE.30.)     H2=0.
      HO2=11.5
      H21=H2+HO2
      AKEL(I)=(12.*PY(M)*XXO)/(EY*B*(H21**3))
      IF(XXO.LE.30.)      AKEL=0.
      TXYEL=(1.5-PY(M)/(B*(H21**2)))*(5.*XXO*H1-H21)
      IF(H2.EQ.0.)      TXYEL=-TXYEL
      DYDXES(I)=TXYEL/G
      HO2=12.4
      H21=H2+HO2
      AK0(I)=VAL2J*(XXO**EMO)/((H21/2.)**DO)
      VAL3=D1*(PPL(M)/(B*(H21**2)))
      TXY=VAL3*(D2-XXO*H1-ENO*H21)
      IF(H2.EQ.0.)      TXY=-TXY
```

```
      DYDXS(I)=(TXY**EM)*C0
    3 CONTINUE
C     XJ IS THE COORDINATE ALONG THE BEAM LENGTH
C     AKEL IS THE ELASTIC CURVATURE AND TXYEL ISTHE ELASTIC SHEAR STRES
C     DYDXES IS THE SHEAR STRESS ROTATION(ELASTIC) AND TXY IS THE
C     PLASTIC SHEAR STRESS
C     AK0 IS THE PLASTIC CURVATURE(BENDING MOMENT)AND DYDXS IS THE
C     PLASTIC SHEAR STRESS ROTATION
C     DYDXEL IS THE ELASTIC BENDING MOMENT ROTATIONAND DYDX0 IS THE
C     PLASTIC BENDING MOMENT ROTATION
C     AL IS THE UNCRACKED LIGAMENT LENGTHAND YR0 IS THE DEFLECTION DUE
C     TO THE ROTATION AT THE CRACK TIP
      AL=W-LL0
      H31=HMAX-H1*(AL-41.)
      IF(LL0.GE.156.0)     H31=HMAX
      H31=(H31+HMAX)/2.
      YR0(M)=6.*P*(LL0**2)*AL/(EY*B*(H31**3))
      DYDXEL(1)=(3.*P*LL0*AL)/(EY*B*(H31**3))
      DYDX0(1)=0.
C     FIRST INTEGRATION WITH EULERS RULE
      DO 6 I=1,NSTO
      DZDXEL(I)=AKEL(I)*(1.+DYDXEL(I)**2)**1.5
      DZDX(I)=AK0(I)*(1.+DYDX0(I)**2)**1.5
      DYDXEL(I+1)=DYDXEL(I)+H*DZDXEL(I)
      DYDX0(I+1)=DYDX0(I)+H*DZDX(I)
    6 CONTINUE
      SDEL1=DYDXEL(1)+DYDXEL(LIM0)
      SDEL2=DYDXES(1)+DYDXES(LIM0)
      SD1=DYDX0(1)+DYDX0(LIM0)
      SD2=DYDXS(1)+DYDXS(LIM0)
      SD3=0.
      SD4=0.
      SD5=0.
      SD6=0.
      SDEL3=0.
      SDEL4=0.
      SDEL5=0.
      SDEL6=0.
C     SECOND INTEGRATION WITH SIMPSONS RULE
      DO 31 I=2,LIM0-1,2
      SD3=SD3+DYDX0(I)
      SD4=SD4+DYDXS(I)
      SDEL3=SDEL3+DYDXEL(I)
      SDEL4=SDEL4+DYDXES(I)
   31 CONTINUE
      DO 41 I=3,LIM0-2,2
      SD5=SD5+DYDX0(I)
      SD6=SD6+DYDXS(I)
      SDEL5=SDEL5+DYDXEL(I)
      SDEL6=SDEL6+DYDXES(I)
   41 CONTINUE
C     Y/M IS THE PLASTIC BENDING MOMENT DEFLECTION
C     YDS IS THE PLASTIC SHEAR STRESS DEFLECTION
C     YDMEL IS THE ELASTIC BENDING MOMENT DEFLECTION
C     YDSEL IS THE ELASTIC SHEAR STRESS DEFLECTION
      YDM=2.*H*(SD1+4.*SD3+2.*SD5)/3.
      YDS=2.*H*(SD2+4.*SD4+2.*SD6)/3.
      YDMEL=2.*H*(SDEL1+4.*SDEL3+2.*SDEL5)/3.
      YDSEL=2.*H*(SDEL2+4.*SDEL4+2.*SDEL6)/3.
      YDST(M)=YDSEL+YDS
C     YDEL IS THE TOTAL ELASTIC DEFLECTION
      YDEL(M)=YDMEL+YDSEL
C     YD IS THE TOTAL PLASTIC DEFLECTION
      YD(M)=YDM+YDS
C     U IS THE ENERGY AND DMAX IS THE ROTATION AT THE LOADING POINTS
      DMAX=DYDX0(LIM0)+DYDXS(LIM0)+DYDXEL(LIM0)+DYDXES(LIM0)
      WRITE(6,79)    DMAX
   79 FORMAT(38X,F6.4,///)
      U(M)=PY(M)*YDEL(M)/2.+PEL(I)*(YD(M)/(EN0+1.))+PPL(M)*YD(M)+YR0(M)*
     1P/2.
C     YDT IS THE TOTAL DEFLECTION IN THE SPECIMEN
      YDT(M)=YDEL(M)+YD(M)+YR0(M)
      GO TO 81
   80 WRITE(6,75)
   75 FORMAT(15X,12HCRACK LENGTH,15X,11HDEFLECTION,15X,6HENERGY,15X,19HE
     1LASTIC DEFLECTIONS,//////)
      DO 77 M=2,21
      MM=5*(M-2)
      LL0=70.+FLOAT(MM)
      WRITE(6,78)    LL0,YDT(M),U(M),YDEL(M)
   78 FORMAT(20X,F5.1,20X,F6.3,13X,F9.1,17X,F7.2,///)
   77 CONTINUE
      WRITE(6,88)
   88 FORMAT(20X,12HCRACK LENGTH,20X,6HSTRESS,6X,24HSHEAR STRESS DEFLECT
     1IONS,15X,21HROTATION DEFLECTIONS,//////)



      DO 91 M=1,22
      MM=5*(M-1)
      LL0=65.+FLOAT(MM)
C     YDST IS THE TOTAL SHEAR STRESS DEFLECTION
      WRITE(6,93)    LL0,SIGMA(M),YDST(M),YR0(M)
   93 FORMAT(25X,F5.1,20X,F6.2,23X,F4.2,24X,F4.2,///)
   91 CONTINUE
      STOP
      END
```

```
      PROGRAM LOLF(INPUT,OUTPUT,TAPE5=INPUT,TAPE6=OUTPUT)
      REAL LLO,LL
      COMMON X0(1000),AK0(1000),DYDXS(1000),DYDXJ(1000),DZDX(1000),
     1Y1(40),Y2(40),Y(40),LL(40),M(40),REF(40),AK(1500),DMAX(40),A(40),
     2X(1500),DYDX(1500),DZDXT(1000),DYDA(41),DELTAJ(40),SIGMA(40)
C     PROGRAM TO COMPUTE DELTAJ IN THE DCB SPECIMEN FOR LARGE DEFLECTIONS
C     P IS THE LOAD AND HO2 AND HO1 ARE GEOMETRIC CONSTANTS
C     H IS THE BEAM HEIGHT              H=HO+H1*X
C     ENO IS THE STRAIN HARDENING EXPONENT AND B IS THE GROSS THICKNESS
C     EN IS THE CYCLIC CREEP EXPONENT
      READ(5,1)   B
    1 FORMAT(20X,F6.1)
      READ(5,9)   B
    9 FORMAT(20X,F4.1)
      READ(5,4)   EN
    4 FORMAT(20X,F5.2)
      READ(5,21)    ENO
   21 FORMAT(20X,F4.2)
      WRITE(6,5)      P,B,EN,ENO
    5 FORMAT(1H1,11X,3HP =,F6.1,20X,3HB =,F4.1,20X,4HEN =,F5.2,20X,5HENO
     1 =,F5.2,////////)
C     SY IS THE YIELD STRESS AND LLO IS THE INITIAL CRACK LENGTH
      SY=401.
      LLO=70.
C     A0 AND A ARE THE STRAIN HARDENING AND CYCLIC CREEP CONSTANTS
      HMAX=37.8
      HO=7.1
      HO1=14.3
      A0=4.421E-19
C     BN IS THE NET THICKNESS AND EY IS THE YOUNGS MODULUS
      BN=3.6
      EY=2.07E+5
      H1=0.16952
      HO2=12.4
      H1=1.72E-1
C     THE INITIAL DEFLECTION(ELASTIC+PLASTIC) IS TO BE COMPUTED
C     AKO IS THE INITIAL PLASTIC CURVATURE DUE TO THE BENDING MOMENT
C     AKEL IS THE INITIAL ELASTIC CURVATURE DUE TO THE BENDING MOMENT
C     THE DEFLECTIONS ARE OBTAINED FROM EULER AND SYMPSONS RULE INTEGRA
      DO=2.*ENO+1.
C     H IS THE INTEGRATION STEP AND PY IS THE EXPERIMENTAL YIELD LOAD
      H=0.25
      PY=4000.0
C     PPL IS THE PLASTIC LOAD
      PPL=P-PY
      NSTO=IFIX(LLO/H)
      LIMO=NSTO+1
C     DYDXO IS THE DERIVATIVE OF THE INITIAL DEFLECTION
C     SO IS THE SHEAR STRESS CONSTANT AND EN IS THE SHEAR STRESS EXPONE
C     TXYEL IS THE ELASTIC SHEAR STRESS AND G IS THE SHEAR MODULUS
C     DYDXS ARE THE SHEAR STRAIN ROTATIONS(ELASTIC+PLASTIC)
      G=8.0E+4
      SO=(ENO+1.)/2.
      EO=AO*(2.**ENO)
      EN=ENO
      D1=(2.*ENO+1.)/(ENO*(ENO+1.))
      D2=3.*ENO+2.
      VAL20=(PPL**2.*ENO+1.))/(2.*ENO*B)
      VAL10=AO*(VAL20**ENO)
      DO 3 I=1,LIMO
      X0(I)=H*FLOAT(I-1)
      XX0=LLO-X0(I)
      H2=H1*(XX0-30.)
      IF(XX0.LE.30.)      H2=0.
      H21=H2+HO2
      AKEL=(12.*PY*XX0)/(EY*B*(H21**3))
      AK0(I)=VAL10*(XX0**ENO)/((H21/2.)**DO)+AKEL
      IF(XX0.LE.30.)    H1=0.
      H2=H1*(XX0-30.)
      H21=H2+HO2
      TXYEL=(1.5*PY/(B*(H21**2)))*(5.*XX0*H1-H21)
      IF(H2.EQ.0.)      TXYEL=-TXYEL
      DYDXES=TXYEL/G
      VAL30=D1*(PPL/(B*(H21**2)))
      TXY=VAL30*(D2*XX0*H1-ENO*H21)
      IF(H2.EQ.0.)      TXY=-TXY
      SR=(TXY**EN)*EO
      DYDXS(I)=SR+DYDXES
    3 CONTINUE
C     FIRST INTEGRATION TO GET DYDXO DUE TO THE BENDING MOMENT
      DYDXO(1)=0.
      DO 6 I=1,NSTO
      DZDX(I)=AK0(I)*(1.+DYDXO(I)**2)**1.5
      DYDXO(I+1)=DYDXO(I)+H*DZDX(I)
    6 CONTINUE
```

```
C       SYMPSONS RULE TO CALCULATE THE INITIAL DEFLECTIONS(S.FORCE+L.MOMENT
        S01=DYDX0(1)+DYDX0(LIM0)
        S02=DYDXS(1)+DYDXS(LIM0)
        S03=0.
        S04=0.
        S05=0.
        S06=0.
        DO 31 I=2,LIM0-1,2
        S03=S03+DYDX0(I)
        S04=S04+DYDXS(I)
   31   CONTINUE
        DO 41 I=3,LIM0-2,2
        S05=S05+DYDX0(I)
        S06=S06+DYDXS(I)
   41   CONTINUE
C       Y0M ARE THE INITIAL BENDING MOMENT DEFLECTIONS
C       Y0S ARE THE INITIAL SHEAR FORCE DEFLECTIONS
        Y0M=2.*H*(S01+4.*S03+2.*S05)/3.
        Y0S=2.*H*(S02+4.*S04+2.*S06)/3.
C       THE DEFLECTIONS DUE TO THE ROTATION AT THE CRACK TIP ARE
CC      CALCULATED NEXT
CC      W IS THE SPECIMEN WIDTH MEASURED FROM THE LOADING POINTS
C       AL IS THE UNCRACKED LIGAMENT
        W=216.0
        AL=W-LL0
        H31=20.0
C       Y0R IS THE DEFLECTION DUE TO THE ROTATION AT THE CRACK TIP
        Y0R=(6.*P*(LL0**2)*AL)/(EY*B*(H31**3))
C       Y0T IS THE TOTAL INITIAL DEFLECTION
        Y0T=Y0M+Y0S+Y0R
        WRITE(6,49)     Y0M,Y0S
   49   FORMAT(39HINITIAL BENDING MOMENT DEFLECTION Y0M =,F6.3,//////,10X,
     136HINITIAL SHEAR FORCE DEFLECTION Y0S =,F6.3,//////)
        WRITE(6,50)     Y0T
   50   FORMAT(10X,30HINITIAL TOTAL DEFLECTION Y0T =,F6.3,//////////////)
C       THE CALCULATIONS FOR THE NEXT CYCLES ARE NOW FOLLOWING
        S2=0.
        S3=0.
C       DYDX0T IS THE TOTAL INITIAL ROTATION(LOADING POINTS)
        DYDX0T=DYDX0(LIM0)+DYDXS(LIM0)
C       TETA IS THE ROTATION ANGLE
        DMAX(1)=DYDX0T
        TETA=ATAN(DMAX(1))
        PEF(1)=P*COS(TETA)
        WRITE(6,55)     DYDX0T
   55   FORMAT(10X,47HINITIAL ROTATION AT THE LOADING POINTS DYDX0T =,F6.4
     1,///////)
        A4=0.823
C       READ INPUT DATA
        NX=22
C       LL ARE THE CRACK LENGTHS AND N IS THE NUMBER OF CYCLES
        READ(5,14)      (LL(J),J=1,12)
   14   FORMAT(6F5.3,6F7.3)
        READ(5,15)      (LL(J),J=13,NX)
   15   FORMAT(12F7.3)
        READ(5,16)      (N(J),J=1,NX)
   16   FORMAT(I1,2I2,8I3.1,4I4)
        READ(5,17)      (A(J),J=1,13)
   17   FORMAT(F3.1,8F7.3,7F6.3)
        READ(5,23)      (A(J),J=14,NX)
   23   FORMAT(9F8.3)
C       YM IS THE FINAL BENDING MOMENT DEFLECTION
CC      YR IS THE FINAL ROTATION DEFLECTION AND Y IS THE FINAL TOTAL
C       DEFLECTION
        YM(1)=0.
        YR(1)=0.
        Y(1)=0.
        D=2.*EN+1.
        C=(2.*EN+1.)/EN
        H1=1.72E-1
        H0=7.1
        SIGMA(1)=0.
        DO 10 J=2,NX
        A(J)=A(J)*1.0E-13
        NST=IFIX(LL(J)/H)
        LIM=NST+1
        T=A(J)*FLOAT(N(J))
C       H22 IS THE CURRENT SPECIMEN HEIGHT H1 AND H0 ARE GEOMETRIC
C       CONSTANTS
        H22=H1*LL(J)+H0
C       PCC IS THE CYCLIC CREEP LOAD AND PY1 IS THE THEORETICAL YIELD LOAD
        PY1=(B*(H22**2)*SY)/(6.*LL(J))+750.
        PCC=PEF(J-1)-PY1
        SIGMA(J)=(3.*PCC*LL(J)*C)/(B*(H22**2))+435.5
        IF(PCC.LE.0.)   GO TO 8
```

```
      VAL2=(PCC*(2.*EN+1.))/(2.*EN*B)
      VAL1=T*(VAL2**EN)
C     DYDX IS THE ROTATION AND AK IS THE CURVATURE
      DO 60 K=1,LIM
      X(K)=H*FLOAT(K-1)
      XX=LL(J)-X(K)
      H2=H1*(XX-3.)
      IF(XX.LT.3.)       H2=0.
      H21=H2+H0
      AK(K)=VAL1*(XX**EN)/((H21/2.)**D)
   60 CONTINUE
      DYDX(1)=0.
      DO 70 K=1,LIM-1
      DZDXT(K)=AK(K)*(1.+DYDX(K)**2)**1.5
      DYDX(K+1)=DYDX(K)+H*DZDXT(K)
   70 CONTINUE
      S1=DYDX(1)+DYDX(LIM)
C     INTEGRATION CARRIED OUT WITH SIMPSON AND EULERS RULE
      DO 30 K=2,LIM-1,2
      S2=S2+DYDX(K)
   30 CONTINUE
      DO 40 K=3,LIM-2,2
      S3=S3+DYDX(K)
   40 CONTINUE
      DMAX(J)=DYDX(LIM)
      TETA=ATAN(DMAX(J))
      PEF(J)=P*COS(TETA)
      DD=DMAX(J)
      YM(J)=2.*H*(S1+4.*S2+2.*S3)/3.
      AL=W-LL(J)
      H31=HMAX-H1*(AL-41.)
      IF(LL(J).GT.155.0)       H31=HMAX
      YR(J)=6.*PEF(J)*(LL(J)**2)*AL/(EY*B*(H31**3))
      GO TO 22
    8 DYDXEL=(6.*PEF(J-1)*(LL(J)**2))/(EY*B*HC*(H22**2))
      TETA=ATAN(DD+DYDXEL)
      PEF(J)=P*COS(TETA)
      YM(J)=YM(J-1)+(24.*PEF(J)*AM*(LL(J)-LL(J-1)))/(EY*B)
      AL=W-LL(J)
      H31=HMAX-H1*(AL-41.)
      IF(LL(J).GT.155.0)       H31=HMAX
      YR(J)=6.*PEF(J)*(LL(J)**2)*AL/(EY*B*(H31**3))
   22 Y(J)=YM(J)+YR(J)
   10 CONTINUE
      WRITE(6,57)
   57 FORMAT(28X,30HROTATION AT THE LOADING POINTS,////)
      DO 18 J=2,NX
      WRITE(6,66)      DMAX(J)
   66 FORMAT(30X,F6.4,//)
   18 CONTINUE
      DO 12 J=2,NX-1
      HN=LL(J)-LL(J-1)
      HM=LL(J+1)-LL(J)
      BK=1./(2.*HN*HM)
      DYDA(J)=BK*(HN*(YM(J+1)-YM(J))+HM*(YM(J)-YM(J-1)))
      GEL=(12.*PEF(J)**2)*AM/(EY*B)
      DELTAJ(J)=1./BN*(DYDA(J)*PEF(J)-GEL)
   12 CONTINUE
      WRITE(6,51)
   51 FORMAT(15X,12HCRACK LENGTH,12X,16HNUMBER OF CYCLES,12X,10HDEFLECTI
     1ON,12X,4HDYDA,12X,16HJ CONTOUR INTEGRAL,///////)
      DO 13 J=2,NX-1
      WRITE(6,52)      LL(J),N(J),YM(J),DYDA(J),DELTAJ(J)
   52 FORMAT(15X,F7.3,18X,I5,19X,F6.3,15X,F6.4,17X,F7.2,////)
   13 CONTINUE
      WRITE(6,58)
   58 FORMAT(15X,12HCRACK LENGTH,20X,6HSTRESS,20X,14HEFFECTIVE LOAD,16X,
     1 13HROTATIONS DEFLECTIONS,/////)
      DO 19 J=2,NX
      WRITE(6,59)      LL(J),SIGMA(J),PEF(J-1),YR(J)
   59 FORMAT(20X,F7.3,20X,F8.3,20X,F7.2,26X,F5.3,///)
   19 CONTINUE
      STOP
      END
```

TABLE 1

1. Composition and Mechanical Properties of the Aluminium Alloy RR58

Element	Cu	Mg	M_n	S_i	F_e	T_i	Z_n	N_i
Weight %	2.64	1.65	0.03	0.23	1.15	0.06	0.06	0.10

$E = 75.0 \times 10^3$ N/mm^2 (Young's Modulus)

$\nu = 0.33$ (Poisson's Ratio)

$\sigma_{UTS} = 450$ N/mm^2 (Ultimate Tensile Stress)

$\sigma_{ys} = 367$ N/mm^2 (0.1% Yield Stress)

$\varepsilon_r = 6\%$ (Minimum Elongation)

2. Composition and Mechanical Properties of the Mild Steel BS15

Element	C	M_n	S_i	P	N_i	C_r	M_o	N_b
Weight %	0.19	0.59	0.028	0.021	0.02	0.01	0.02	0.005

$E = 2.07 \times 10^5$ N/mm^2

$\nu = 0.3$

$\sigma_{UTS} = 585$ N/mm^2

$\sigma_{ys} = 401$ N/mm^2

$\varepsilon_r = 28\%$

$A = 5.54 \times 10^{-8}$ mm^2/N

$n = 2.46$

$\sigma_V = 660$ N/mm^2 (True Stress at the Maximum Load)

$C_1 = 1.34 \times 10^{-11}$ mm^2/N

$m = 3.05$

3. Composition and Mechanical Properties of the Cast Aluminium Alloy LM30

Element	Cu	Mg	S_i	F_e	M_n	N_i	Z_n	P_b	S_n	T_i
Weight%	4.5	0.6	18	1.1	0.3	0.1	0.2	0.1	0.1	0.2

$E = 82.0 \times 10^3$ N/mm^2

$\nu = 0.33$

$\sigma_{UTS} = 160$ N/mm^2

$\sigma_{ys} = 150$ N/mm^2

TABLE 2

Fracture Toughness Data for RR58 and LM30

(DCB Specimen - 9.5 mm net thickness)

All the data at room temperature

RR58 K_c in MN/m$^{3/2}$		RR58 MN/m$^{3/2}$		LM30 MN/m$^{3/2}$	
D60*	22.02	C79*	22.06	F10*	21.27
C28*	20.74	C83*	22.28	F11*	21.61
C46*	21.34	C68*	22.36	F17*	18.59
C45*	21.56	C30**	21.45	F18*	19.08
C18*	21.26	C29**	22.19	F19*	20.25
C48*	22.02	C31**	20.84	F16*	20.57
C27*	22.77	C32**	22.76	F12**	21.52
C21*	22.88	C33**	22.242	F13**	21.36
C29*	22.0	D31**	22.44	F14**	20.90
C47*	22.71	D28**	21.34		
C44*	22.88	C62**	22.02		
C60*	22.55	C78**	22.42		
C50*	22.67	C82**	22.94		
C37*	23.65	C80**	23.60		
C36*	23.70	C84**	23.21		
D30*	22.44	C85**	23.75		
C61*	24.03	C69**	20.79		
C70*	23.76	C51**	23.82		
C73*	23.98	C66**	22.72		
C64*	22.44	C67**	22.10		
C63*	22.99	C81**	23.75		
C72*	22.55				
C71*	22.39				
C74*	22.29				

* - Specimens used in fatigue crack propagation tests

** - Specimens used in stress corrosion tests

TABLE 3

Cyclic Crack Growth Data for RR58 In Laboratory Air and 3.5% NaCl at a Frequency of 0.15 Hz

Spec. No.	Env.	R	ΔK $MN/m^{3/2}$	K_m $MN/m^{3/2}$	da/dN mm/cycle	λ MN^2/m^3	Φ
D60	Air	0	16.15	8.07	1.4×10^{-3}	260.82	1.029
D60	Air	0	18.45	9.22	2.65×10^{-3}	340.40	2.145
D60	Air	0	21.84	10.92	1.85×10^{-1}	476.98	55.98
C28	Air	0	15.31	7.65	1.19×10^{-3}	234.39	1.044
C28	Air	0	17.27	8.64	2.0×10^{-3}	298.25	2.035
C28	Air	0	18.71	9.35	3.2×10^{-3}	350.06	4.072
C28	Air	0	19.78	9.89	2.9×10^{-3}	391.24	9.653
C46	Air	0	10.71	5.35	1.03×10^{-4}	114.70	0.248
C46	Air	0	12.83	6.42	2.9×10^{-4}	164.60	0.460
C46	Air	0	14.40	7.20	5.5×10^{-4}	207.36	0.710
C45	Air	0	16.46	8.23	8.3×10^{-4}	270.93	1.245
C45	Air	0	17.61	8.80	1.63×10^{-3}	310.11	1.805
C45	Air	0	18.92	9.46	3.45×10^{-3}	357.96	3.080
C18	Air	0	16.76	8.38	1.72×10^{-3}	280.89	1.395
C18	Air	0	18.03	9.02	2.69×10^{-3}	325.08	2.350
C18	3.5% NaCl	0	18.03	9.02	6.5×10^{-3}	325.08	2.381
C48	Air	0	13.73	6.86	3.05×10^{-4}	188.60	0.538
C48	3.5% NaCl	0	13.73	6.86	8.05×10^{-4}	188.60	0.558
C48	3.5% NaCl	0	15.97	7.98	2.59×10^{-3}	255.04	1.015
C48	3.5% NaCl	0	17.36	8.68	5.2×10^{-3}	301.36	1.543
C48	3.5% NaCl	0	20.05	10.02	8.7×10^{-3}	402.00	4.588
C27	Air	0	19.66	9.83	1.18×10^{-2}	386.68	2.732
C27	3.5% NaCl	0	19.66	9.83	1.18×10^{-2}	386.68	2.721
C21	3.5% NaCl	0	13.10	6.55	8.75×10^{-4}	171.66	0.423
C21	3.5% NaCl	0	14.68	7.34	2.2×10^{-3}	215.41	0.625
C21	3.5% NaCl	0	21.08	10.54	2.9×1.0^{-2}	444.28	5.528
C21	3.5% NaCl	0	13.73	6.86	1.26×10^{-3}	188.60	0.493
C21	3.5% NaCl	0	21.34	10.67	7.7×10^{-2}	455.57	15.92
C29	3.5% NaCl	0	11.89	5.95	4.2×10^{-4}	141.47	0.324
C29	3.5% NaCl	0	15.73	7.86	3.3×10^{-3}	247.43	0.960
C29	3.5% NaCl	0	15.73	7.86	3.55×10^{-3}	247.43	0.960

TABLE 3 (cont.)

Spec. No.	Env.	R	ΔK $MN/m^{3/2}$	K_m $MN/m^{3/2}$	da/dN mm/cycle	λ MN^2/m^3	Φ
C29	3,5% NaCl	0	11,65	5.83	$4,4 \times 10^{-4}$	135,77	0,324
C47	3,5% NaCl	0	15,22	7.61	$1,76 \times 10^{-3}$	231,69	0,741
C47	3,5% NaCl	0	17,30	8.65	$5,0 \times 10^{-3}$	299,39	1,285
C47	3.5% NaCl	0	18.90	9.45	$8,29 \times 10^{-3}$	357.21	2,132
C47	3,5% NaCl	0	20,09	10.05	1.44×10^{-2}	403.44	3.408
C44	Air	0	18.03	9.02	3.85×10^{-3}	325.04	1.492
C44	Air	0	21.48	10.74	7.3×10^{-2}	461.27	36.18
C44	3.5% NaCl	0	16.58	8.29	3.7×10^{-3}	274.79	0.992
C44	Air	0	11.23	5.62	1.53×10^{-4}	126.07	0.242
C60	Air	0.482	8.47	12.1	4.39×10^{-4}	204.97	0.565
C60	Air	0.409	10.14	12.1	6.71×10^{-4}	245.38	0.835
C60	Air	0.35	11.63	12.1	1.82×10^{-3}	281.44	1.14
C60	Air	0.285	13.48	12.1	2.74×10^{-3}	326.21	1.69
C60	Air	0.228	15.2	12.1	3.45×10^{-3}	367.84	2.48
C60	Air	0.187	16.4	12.1	5.61×10^{-3}	396.88	3.41
C60	Air	0.167	17.27	12.1	2.0×10^{-2}	417.93	4.43
C60	Air	0.554	8	13.95	6.22×10^{-4}	223.2	-
C60	Air	0.619	8	17.04	1.4×10^{-3}	272.64	-
C60	Air	0.158	8	5.5	5.03×10^{-5}	88	0.0728
C50	Air	0	7.74	3.87	4.45×10^{-5}	59.97	0.074
C50	Air	0	6.59	3.29	952×10^{-6}	43.49	0.028
C50	Air	0	6.17	3.08	2.39×10^{-6}	38.08	0.015
C50	Air	0	5.63	2.82	3.3×10^{-7}	31.66	0.0026
C37	Air	0.594	6.16	12.1	1.21×10^{-4}	149.07	0.246
C37	Air	0.759	4.51	16.5	1.29×10^{-4}	148.83	0.330
C37	Air	0.617	7.81	16.5	6.1×10^{-4}	257.73	1.075
C37	Air	0.463	12.1	16.5	4.83×10^{-3}	399.30	6.80
C37	Air	0.429	13.2	16.5	1.88×10^{-2}	435.60	13.65
C36	Air	0.630	5.5	12.1	1.6×10^{-4}	133.10	0.190
C36	Air	0.705	4.18	12.1	2.18×10^{-5}	101.15	0.089
C36	Air	0.814	3.41	16.5	2.24×10^{-5}	112.53	0.143
C36	Air	0.754	3.41	12.1	8.02×10^{-6}	82.52	0.0357
C36	Air	0.789	2.86	12.1	1.75×10^{-6}	69.21	0.00705
C36	Air	0.841	2.86	16.5	8.76×10^{-6}	94.38	0.061
C36	Air	0.860	2.48	16.5	1.13×10^{-6}	81.84	0.0074
C36	Air	0.250	6.6	5.5	2.27×10^{-5}	72.60	0.0462
C36	Air	0.325	5.5	5.5	7.87×10^{-6}	60.50	0.0208
C36	Air	0.375	4.95	5.5	1.83×10^{-6}	54.45	0.00851

TABLE 3 (cont.)

Spec. No.	Env.	R	ΔK $MN/m^{3/2}$	K_m $MN/m^{3/2}$	da/dN mm/cycle	λ MN^2/m^3	Φ
C36	Air	0.398	4.73	5.5	6.35×10^{-7}	52.03	0.00364
C36	Air	0.605	4.07	8.25	1.23×10^{-6}	67.16	0.010
C36	Air	0.500	5.5	8.25	1.96×10^{-5}	90.75	0.0612
D30	Air	0.578	4.4	8.25	4.01×10^{-6}	72.60	0.0184
D30	Air	0.304	8.8	8.25	1.8×10^{-4}	145.20	0.232
D30	Air	0.200	11.0	8.25	4.34×10^{-4}	181.50	0.368
D30	Air	0.111	13.2	8.25	5.69×10^{-4}	217.80	0.540
D30	Air	0.034	15.4	8.25	9.35×10^{-4}	254.10	0.756
D30	Air	0	20.57	10.29	7.49×10^{-3}	423.12	30.83
D30	Air	0.553	10.45	18.15	3.73×10^{-2}	379.33	18.21
D30	Air	0.642	7.92	18.15	2.53×10^{-3}	287.49	2.902
D30	Air	0.692	6.6	18.15	7.32×10^{-4}	239.58	1.642
D30	3.5% NaCl	0.622	7.7	16.5	2.06×10^{-3}	254.10	1.293
D30	3.5% NaCl	0.500	11	16.5	6.83×10^{-3}	363	3.344
D30	3.5% NaCl	0.200	11	8.25	7.87×10^{-4}	181.50	0.334
C61	Air	0.808	3.85	18.15	1.55×10^{-4}	139.75	0.447
C61	Air	0.833	3.3	18.15	8.03×10^{-5}	119.79	0.3
C61	Air	0.847	2.97	18.15	4.01×10^{-5}	107.81	0.188
C61	Air	0.864	2.64	18.15	6.1×10^{-6}	95.83	0.038
C61	Air	0.886	2.2	18.15	2.26×10^{-6}	79.86	0.00021
C61	3.5% NaCl	0	10.67	5.33	3.0×10^{-4}	113.84	0.194
C61	3.5% NaCl	0	9.68	4.84	2.0×10^{-4}	93.70	0.145
C61	Air	0	9.68	4.84	5.0×10^{-5}	93.70	0.145
C61	3.5% NaCl	0	8.12	4.06	6.75×10^{-5}	65.90	0.055
C61	3.5% NaCl	0	7.04	3.42	3.95×10^{-5}	49.56	0.035
C61	3.5% NaCl	0	6.22	3.11	1.85×10^{-5}	38.63	0.016
C61	3.5% NaCl	0	5.17	2.58	3.8×10^{-6}	26.73	0.0059
C61	3.5% NaCl	0	4.92	2.46	5.1×10^{-7}	24.19	0.0013
C70	3.5% NaCl	0.333	5.5	5.5	4.78×10^{-5}	60.50	0.0238
C70	3.5% NaCl	0.5	5.5	8.25	1.13×10^{-4}	90.75	0.0778
C70	3.5% NaCl	0.629	5.5	12.1	2.53×10^{-4}	133.10	0.334
C70	3.5% NaCl	0.714	5.5	16.5	9.02×10^{-4}	181.50	0.63
C70	3.5% NaCl	0.449	4.18	5.5	2.41×10^{-6}	45.98	0.00378
C70	3.5% NaCl	0.05	9.9	5.5	2.29×10^{-4}	108.90	0.144
C70	3.5% NaCl	0.638	3.52	8.25	4.52×10^{-6}	58.08	0.00651
C70	3.5% NaCl	0.03	15.4	8.25	2.41×10^{-3}	254.10	1.045

TABLE 3 (cont.)

Spec. No.	Env.	R	ΔK $MN/m^{3/2}$	K_m $MN/m^{3/2}$	da/dN mm/cycle	λ MN^2/m^3	Φ
C70	3.5% NaCl	0.222	15.4	12.1	4.52×10^{-3}	341.88	1.81
C73	3.5% NaCl	0.379	4.95	5.5	2.36×10^{-5}	54.45	0.0337
C73	3.5% NaCl	0.176	7.7	5.5	1.35×10^{-4}	84.70	0.0955
C73	3.5% NaCl	0.100	19.8	12.1	4.01×10^{-2}	479.76	11.96
C73	3.5% NaCl	0.375	11	12.1	2.13×10^{-3}	255.20	0.92
C73	3.5% NaCl	0.796	2.75	12.1	1.37×10^{-5}	66.55	0.0164
C73	3.5% NaCl	0.807	2.59	12.1	1.75×10^{-6}	62.56	0.0028
C73	3.5% NaCl	0.596	4.18	8.25	3.1×10^{-5}	68.97	0.0308
C73	3.5% NaCl	0.517	7.7	12.1	8.0×10^{-4}	186.34	0.470
C73	3.5% NaCl	0.846	2.75	16.5	1.14×10^{-4}	90.75	0.152
C73	3.5% NaCl	0.875	2.2	16.5	4.52×10^{-5}	72.60	0.044
C73	3.5% NaCl	0.887	1.98	16.5	6.6×10^{-6}	65.34	0.0134
C73	3.5% NaCl	0.892	1.87	16.5	1.31×10^{-6}	61.71	0.0021
C73	3.5% NaCl	0.463	12.1	16.5	8.64×10^{-3}	399.30	5.13
C73	3.5% NaCl	0.429	13.2	16.5	3.05×10^{-2}	435.60	9.15
C73	3.5% NaCl	0.397	14.3	16.5	9.91×10^{-2}	471.90	25.36

TABLE 4

Cyclic Crack Growth Data for RR58 at a Frequency of 35 Hz.

Spec. No.	Env.	R	ΔK $MN/m^{3/2}$	K_m $MN/m^{3/2}$	da/dN mm/cycle	λ MN/m^{2}	Φ
C64	Air	0	3.45	1.72	-	11.9	-
C64	Air	0	4	2	-	16	-
C64	Air	0	4.51	2.25	5.27×10^{-7}	20.34	0.00559
C64	Air	0	5.06	2.53	1.33×10^{-6}	25.60	0.0167
C64	Air	0	5.83	2.91	3.9×10^{-6}	33.99	0.0348
C64	Air	0	6.6	3.3	5.03×10^{-6}	43.56	0.0563
C64	Air	0	7.7	3.85	1.28×10^{-5}	59.29	0.0938
C64	Air	0	8.8	4.4	4.95×10^{-5}	77.44	0.1403
C64	Air	0	9.9	4.95	3.02×10^{-5}	98.01	0.198
C64	Air	0	11	5.5	5.45×10^{-5}	121	0.270
C64	Air	0	12.1	6.05	6.3×10^{-5}	146.41	0.361
C64	Air	0	13.2	6.6	1.24×10^{-4}	174.24	0.476
C64	Air	0	14.3	7.15	1.1×10^{-4}	204.49	0.625
C64	Air	0	15.4	7.7	1.68×10^{-4}	237.16	0.824
C63	Air	0	16.5	8.25	2.0×10^{-4}	272.25	0.993
C63	Air	0	17.6	8.8	4.26×10^{-4}	309.76	1.336
C63	Air	0	18.15	9.07	2.95×10^{-4}	329.42	1.566
C63	Air	0	18.7	9.35	4.2×10^{-4}	349.69	1.857
C63	Air	0	18.15	9.07	3.14×10^{-4}	329.42	1.566
C63	Air	0	19.8	9.9	6.5×10^{-4}	392.04	2.743
C63	Air	0	20.35	10.17	1.16×10^{-3}	414.12	3.465
C63	Air	0	20.9	10.45	1.72×10^{-3}	436.81	4.57
C72	Air	0.1	19.8	12.1	2.87×10^{-3}	479.16	6.296
C72	Air	0.158	17.6	12.1	1.05×10^{-3}	425.92	5.185
C72	Air	0.222	15.4	12.1	2.8×10^{-4}	372.68	2.035
C72	Air	0.333	12.1	12.1	1.63×10^{-4}	292.82	1.333
C72	Air	0.571	6.6	12.1	6.85×10^{-5}	159.72	0.389
C72	Air	0.666	6.6	16.5	1.35×10^{-4}	217.80	1.016
C72	Air	0.250	6.6	5.5	1.26×10^{-5}	72.60	0.0758
C72	Air	0.692	4.4	12.1	2.5×10^{-5}	106.48	0.171
C72	Air	0.111	8.8	5.5	2.38×10^{-5}	96.80	0.139
C72	Air	0.463	11.0	16.5	3.87×10^{-3}	363.0	12.66

TABLE 4 (cont.)

Spec. No.	Env.	R	ΔK $MN/m^{3/2}$	K_m $MN/m^{3/2}$	da/dN mm/cycle	λ MN^2/m^3	Φ
C72	Air	0	22	11.0	5.65×10^{-3}	484	19.04
C71	Air	0.765	4.4	16.5	7.95×10^{-5}	145.2	0.609
C71	Air	0.818	3.3	16.5	$4.x \times 10^{-5}$	108.9	0.326
C71	Air	0.760	3.3	12.1	1.6×10^{-5}	79.86	0.0823
C71	Air	0.429	4.4	5.5	2.12×10^{-6}	48.40	0.0192
C71	Air	0.795	2.75	12.1	4.7×10^{-6}	66.55	0.0387
C71	Air	0.814	2.48	12.1	2.0×10^{-6}	60.02	0.0181
C71	Air	0.825	2.31	12.1	7.1×10^{-7}	55.90	0.00529
C71	Air	0.835	2.2	12.1	No growth	53.24	-
C71	Air	0.860	2.48	16.5	1.68×10^{-5}	81.84	0.155
C71	Air	0.875	2.2	16.5	1.41×10^{-5}	72.60	0.103
C71	Air	0.905	1.65	16.5	1.68×10^{-6}	54.45	0.00771
C71	Air	0.908	1.58	16.5	No growth	52.14	-
C71	Air	0.471	3.96	5.5	3.55×10^{-7}	43.56	0.00813
C71	Air	0.497	3.70	5.5	No growth	40.7	-
C71	Air	0.538	9.9	16.5	1.73×10^{-3}	326.7	6.64
C71	Air	0.579	8.8	16.5	7.98×10^{-4}	290.4	3.68
C71	3.5% NaCl	0	3.45	1.72	No growth	11.9	-
C71	3.5% NaCl	0	4	2	No growth	16	-
C71	3.5% NaCl	0	4.51	2.25	5.07×10^{-7}	20.34	0.00487
C71	3.5% NaCl	0	5.06	2.53	1.55×10^{-6}	25.60	0.0167
C71	3.5% NaCl	0	5.83	2.91	4.32×10^{-6}	33.99	0.035
C71	3.5% NaCl	0	6.6	3.3	8.46×10^{-6}	43.56	0.0566
C71	3.5% NaCl	0	7.7	3.85	1.15×10^{-5}	59.29	0.0942
C74	3.5% NaCl	0	8.8	4.4	2.41×10^{-5}	77.44	0.141
C74	3.5% NaCl	0	9.9	4.95	3.57×10^{-5}	98.01	0.199
C74	3.5% NaCl	0	11	5.5	5.34×10^{-5}	121	0.272
C74	3.5% NaCl	0	12.1	6.05	5.98×10^{-5}	146.41	0.363
C74	3.5% NaCl	0	13.2	6.6	1.34×10^{-4}	174,24	0.479
C74	3.5% NaCl	0	14.3	7.15	1.33×10^{-4}	204.49	0.629
C74	3.5% NaCl	0	15.4	7.7	1.58×10^{-4}	237.16	0.831
C74	3.5% NaCl	0	16.5	8.25	2.18×10^{-4}	272.25	1.112
C74	3.5% NaCl	0	17.6	8.8	3.37×10^{-4}	309.76	1.525
C79	3.5% NaCl	0	18.15	9.07	3.76×10^{-4}	329.42	1.983
C79	3.5% NaCl	0	18.7	9.35	4.9×10^{-4}	349.69	2.425
C79	3.5% NaCl	0	19.8	9.9	7.67×10^{-4}	392.04	3.958

TABLE 4 (cont.)

Spec. No.	Env.	R	ΔK $MN/m^{3/2}$	K_m $MN/m^{3/2}$	da/dN mm/cycle	λ MN^2/m^3	Φ
C79	3.5% NaCl	0	20.35	10.17	1.03×10^{-3}	414.12	5.457
C79	3.5% NaCl	0	20.9	10.45	2.13×10^{-3}	436.81	8.412
C83	3.5% NaCl	0.1	19.8	12.1	3.57×10^{-3}	479.16	34.3
C83	3.5% NaCl	0.158	17.6	12.1	9.02×10^{-4}	425.92	6.239
C83	3.5% NaCl	0.222	15.4	12.1	2.9×10^{-4}	372.68	3.023
C83	3.5% NaCl	0.333	12.1	12.1	1.83×10^{-4}	292.82	1.52
C83	3.5% NaCl	0.571	6.6	12.1	6.0×10^{-5}	159.72	0.407
C83	3.5% NaCl	0.25	6.6	5.5	1.34×10^{-5}	72.6	0.0779
C83	3.5% NaCl	0.666	6.6	16.5	1.45×10^{-4}	217.8	1.08
C83	3.5% NaCl	0.765	4.4	16.5	6.68×10^{-5}	145.2	0.629
C83	3.5% NaCl	0.818	3.3	16.5	3.65×10^{-5}	108.9	0.335
C83	3.5% NaCl	0.86	2.48	16.5	2.1×10^{-5}	81.84	0.159
C83	3.5% NaCl	0.875	2.2	16.5	1.19×10^{-5}	72.6	0.106
C83	3.5% NaCl	0.905	1.65	16.5	8.71×10^{-7}	54.45	0.00789
C83	3.5% NaCl	0.908	1.58	16.5	-	52.14	-
C68	3.5% NaCl	0.463	11	16.5	5.68×10^{-3}	363	19.38
C68	3.5% NaCl	0.538	9.9	16.5	2.15×10^{-3}	326.7	7.25
C68	3.5% NaCl	0.579	8.8	16.5	5.06×10^{-4}	290.4	3.759
C68	3.5% NaCl	0.111	8.8	5.5	2.6×10^{-5}	96.8	0.141
C68	3.5% NaCl	0.429	4.4	5.5	2.32×10^{-6}	48.4	0.0192
C68	3.5% NaCl	0.471	3.80	5.5	3.25×10^{-7}	41.10	0.00415
C68	3.5% NaCl	0.497	3.70	5.5	-	40.7	-
C68	3.5% NaCl	0.76	3.3	12.1	1.43×10^{-5}	79.86	0.0815
C68	3.5% NaCl	0.795	2.75	12.1	6.53×10^{-6}	66.55	0.0369
C68	3.5% NaCl	0.814	2.48	12.1	2.07×10^{-6}	60.02	0.0181
C68	3.5% NaCl	0.825	2.31	12.1	5.89×10^{-7}	55.90	0.00336

TABLE 5

Cyclic Crack Growth Data for BS15 at a Frequency of 35 Hz

Spec. No.	Env.	R	ΔK $MN/m^{3/2}$	K_m $MN/m^{3/2}$	da/dN mm/cycle	λ MN^2/m^3	Φ
MS5	Air	0	45.4	22.7	5.7×10^{-4}	2060	0.261
MS5	Air	0	50	25	8.05×10^{-4}	2500	0.335
MS5	Air	0	54.46	27.23	1.18×10^{-3}	2966	0.427
MS5	Air	0	59.02	29.51	1.46×10^{-3}	3483	0.542
MS5	Air	0	40.89	20.45	5.9×10^{-4}	1672	0.202
MS5	Air	0	35.33	18.16	3.52×10^{-4}	1320	0.151
MS5	Air	0	27.25	13.63	1.96×10^{-4}	743	0.0775
MS5	Air	0	24.24	12.12	1.5×10^{-4}	588	0.0595
MS5	Air	0	21.20	10.60	1.27×10^{-4}	449	0.0438
MS5	Air	0	18.2	9.1	6.1×10^{-5}	331	0.0253
MS5	Air	0	12.15	6.08	1.88×10^{-5}	148	0.0112
MS6	Air	0	7	3.5	9.65×10^{-7}	49	0.00094
MS6	Air	0	6.22	3.11	No growth	38.7	-
MS6	Air	0	77.85	38.92	4.42×10^{-3}	6060	1.61
MS6	Air	0	68.35	34.17	2.32×10^{-3}	4672	0.896
MS6	Air	0	49.68	24.84	7.25×10^{-4}	2468	0.33
MS6	Air	0.052	56.9	31.6	1.52×10^{-3}	3600	0.54
MS6	Air	0.142	47.5	31.6	1.01×10^{-3}	3000	0.41
MS6	Air	0.333	31.6	31.6	5.25×10^{-4}	2000	0.232
MS6	Air	0.6	15.8	31.6	2.25×10^{-4}	1000	0.0915
MS6	Air	0.818	6.33	31.6	6.0×10^{-5}	400	0.018
MS6	Air	0	47.5	23.75	1.06×10^{-3}	2256	0.292
MS6	Air	0.86	4.75	31.6	1.17×10^{-5}	300	0.00625
MS6	Air	0.11	25.32	15.8	1.58×10^{-4}	800	0.07
MS6	Air	0.333	15.8	15.8	9.0×10^{-5}	500	0.0356
MS6	Air	0.538	9.49	15.8	2.7×10^{-5}	300	0.0139
MS6	Air	0.6	7.9	15.8	1.61×10^{-5}	250	0.0085
MS6	Air	0.666	6.33	15.8	5.2×10^{-6}	200	0.00318
MS6	Air	0.694	5.7	15.8	7.4×10^{-7}	180	0.00106
MS6	Air	0	8.7	4.35	7.6×10^{-6}	75.6	0.00365
MS6	Air	0.878	4.11	31.6	2.15×10^{-6}	260	0.00164
MS6	Air	0.932	3.36	47.5	1.59×10^{-6}	319	0.00202
MS6	Air	0.917	4.11	47.5	2.81×10^{-5}	390	0.0123
MS7	Air	0	88.61	44.30	1.48×10^{-2}	7852	3.98
MS7	Air	0	81.80	40.90	6.65×10^{-3}	6691	2.15

TABLE 5 (cont.)

Spec. No.	Env.	R	ΔK $MN/m^{3/2}$	K_m $MN/m^{3/2}$	da/dN mm/cycle	λ MN^2/m^3	Φ
MS7	Air	0	85.13	42.56	9.1×10^{-3}	7247	2.83
MS7	Air	0.887	3.80	31.6	No growth	240	-
MS7	Air	0	7.75	3.87	4.05×10^{-6}	60	0.00206
MS7	Air	0	72.47	35.23	2.21×10^{-3}	5250	1.145
MS7	Air	0.5	31.6	47.5	9.25×10^{-4}	3000	0.465
MS7	Air	0.396	41.14	47.5	1.14×10^{-3}	3960	0.683
MS7	Air	0.765	12.66	47.5	2.69×10^{-4}	1200	0.13
MS7	Air	0.875	6.33	47.6	1.37×10^{-4}	600	0.0415
MS7	Air	0.25	57	47.5	2.32×10^{-3}	5400	1.27
MS7	Air	0.09	79.1	47.5	1.18×10^{-2}	7500	3.25
MS7	Air	0.05	85.44	47.5	1.81×10^{-2}	8100	4.65
MS7	Air	0.882	3.96	31.6	5.08×10^{-7}	250	0.00048
MS7	Air	0.932	3.32	47.5	2.6×10^{-7}	315	0.00021
MS7	Air	0.935	3.17	47.5	No growth	300	-
MS8	3.5% NaCl	0	72.31	36.16	3.35×10^{-3}	5229	1.186
MS8	3.5% NaCl	0	50.63	25.32	9.15×10^{-4}	2560	0.357
MS8	3.5% NaCl	0	79.11	39.55	5.45×10^{-3}	6250	1.848
MS8	3.5% NaCl	0	86.71	43.35	1.6×10^{-2}	7519	3.577
MS8	3.5% NaCl	0	42.72	21.36	5.85×10^{-4}	1825	0.299
MS8	3.5% NaCl	0.091	79.11	47.5	1.22×10^{-2}	7500	3.538
MS8	3.5% NaCl	0.666	6.33	15.8	5.6×10^{-6}	200	0.00262
MS8	3.5% NaCl	0	9.49	4.75	1.19×10^{-5}	90	0.00525
MS8	3.5% NaCl	0	15.8	7.9	3.6×10^{-5}	250	0.0224
MS8	3.5% NaCl	0	25.32	12.66	1.41×10^{-4}	640	0.0668
MS8	3.5% NaCl	0	31.61	15.30	2.98×10^{-4}	1000	0.115
MS8	3.5% NaCl	0.11	25.32	15.8	1.6×10^{-4}	800	0.071
MS8	3.5% NaCl	0.33	15.8	15.8	8.0×10^{-5}	500	0.0359
MS9	3.5% NaCl	0	18.99	9.5	3.5×10^{-5}	360	0.0346
MS9	3.5% NaCl	0	37.97	18.98	4.4×10^{-4}	1440	0.171
MS9	3.5% NaCl	0	7.91	3.95	2.5×10^{-6}	552.5	0.0013
MS9	3.5% NaCl	0	6.96	3.48	1.25×10^{-6}	48.4	0.000871
MS9	3.5% NaCl	0	57	28.5	1.02×10^{-3}	3240	0.502
MS9	3.5% NaCl	0.305	50.63	47.5	1.2×10^{-3}	4800	1.041
MS9	3.5% NaCl	0	63.2	31.6	1.97×10^{-3}	4000	0.706
MS9	3.5% NaCl	0.396	41.14	47.5	$1.0 \times 1 \times 10^{-3}$	3900	0.720
MS9	3.5% NaCl	0.211	41.14	31.6	6.7×10^{-4}	2600	0.349
MS9	3.5% NaCl	0.5	31.6	47.5	8.9×10^{-4}	3000	0.479
MS9	3.5% NaCl	0.33	31.6	31.6	5.5×10^{-4}	2000	0.238

TABLE 5 (cont.)

Spec. No.	Env.	R	ΔK $MN/m^{3/2}$	K_m $MN/m^{3/2}$	da/dN mm/cycle	λ MN^2/m^3	Φ
MS9	3.5% NaCl	0.715	15.8	47.5	3.5×10^{-4}	1500	0.181
MS9	3.5% NaCl	0.6	15.8	31.6	2.4×10^{-4}	1000	0.0932
MS9	3.5% NaCl	0.875	6.33	47.5	1.43×10^{-4}	600	0.0405
MS9	3.5% NaCl	0.818	6.33	31.6	7.1×10^{-5}	400	0.0179
MS9	3.5% NaCl	0.428	12.66	15.8	4.45×10^{-5}	400	0.0247
MS9	3.5% NaCl	0.911	4.43	47.5	2.53×10^{-5}	420	0.0147
MS9	3.5% NaCl	0.861	4.75	31.6	1.3×10^{-5}	300	0.00591
MS9	3.5% NaCl	0.878	4.11	31.6	2.25×10^{-6}	260	0.00118
MS10	3.5% NaCl	0.666	12.66	31.6	3.55×10^{-4}	800	0.0673
MS10	3.5% NaCl	0.9	5	47.5	3.13×10^{-5}	475	0.0225
MS10	3.5% NaCl	0.923	3.8	47.5	1.16×10^{-5}	361	0.00642
MS10	3.5% NaCl	0.935	3.2	47.5	No growth	304	-
MS10	3.5% NaCl	0.143	71.2	47.5	2.44×10^{-3}	6764	2.354
MS10	3.5% NaCl	0.929	3.5	47.5	3.65×10^{-6}	332	0.00237
MS10	3.5% NaCl	0	6.68	3.34	3.57×10^{-7}	44.62	0.000476
MS10	3.5% NaCl	0	6.2	3.1	No growth	38.44	-
MS10	Air	0	17.78	8.89	4.5×10^{-5}	316.12	0.0297
MS10	Air	0	13.18	6.59	1.93×10^{-5}	173.71	0.0142
MS10	Air	0	11.22	5.56	1.33×10^{-5}	125.88	0.0905
MS10	Air	0	8.32	4.16	5.87×10^{-6}	69.22	0.00306
MS10	Air	0.584	8.32	15.8	1.46×10^{-5}	262.91	0.00454
MS10	Air	0	93.34	46.67	5.12×10^{-2}	8712	9.657
MS10	3.5% NaCl	0.685	5.9	15.8	1.95×10^{-6}	186.44	0.00124
MS10	3.5% NaCl	0.881	4	31.6	3.5×10^{-7}	252.8	0.00033
MS10	3.5% NaCl	0.884	3.9	31.6	No growth	246.48	-

TABLE 6

Cyclic Crack Growth Data for BS15 at a Frequency of 0.25 Hz

Spec. No.	Env.	R	ΔK $MN/m^{3/2}$	K_m $MN/m^{3/2}$	da/dN mm/cycle	λ MN^2/m^3	Φ
MS1	Air	0	11.39	5.69	1.49×10^{-5}	129.73	0.0093
MS1	Air	0	17.72	8.86	4.8×10^{-5}	314	0.029
MS1	Air	0	22	11	9.4×10^{-5}	483.7	0.0475
MS1	Air	0	23.58	11.79	1.18×10^{-4}	555.79	0.0559
MS1	Air	0	24.62	12.31	1.86×10^{-4}	606.14	0.061
MS1	Air	0	39.87	19.94	4.3×10^{-4}	1590	0.188
MS1	Air	0	43.67	21.84	5.2×10^{-4}	1907	0.237
MS1	Air	0	45.89	22.95	6.33×10^{-4}	2106	0.267
MS1	Air	0	53.8	26.9	8.35×10^{-4}	2894	0.415
MS1	Air	0	63.29	31.65	1.4×10^{-3}	4006	0.682
MS2	Air	0	8.13	4.07	6.33×10^{-6}	66.10	0.00266
MS2	Air	0	12.85	6.43	1.93×10^{-5}	165.12	0.013
MS2	Air	0	20.87	10.43	5.6×10^{-5}	435.65	0.0424
MS2	Air	0	23.04	11.52	1.04×10^{-4}	530.72	0.053
MS2	Air	0	25.7	12.85	1.58×10^{-4}	660.28	0.0679
MS2	Air	0	27.9	13.95	1.9×10^{-4}	779.03	0.082
MS2	Air	0	30.38	15.19	3.4×10^{-4}	922.94	0.0995
MS2	Air	0	32.9	16.45	3.62×10^{-4}	1083	0.120
MS2	Air	0	35.4	17.7	4.48×10^{-4}	1253	0.142
MS2	Air	0	50.63	25.32	6.9×10^{-4}	2564	0.348
MS2	Air	0.433	25	31.6	3.65×10^{-4}	1580	0.17
MS2	Air	0.333	31.6	31.6	7.05×10^{-4}	1997	0.232
MS2	Air	0.2	63.25	47.5	3.5×10^{-3}	6009	1.602
MS2	Air	0	57.87	28.98	1.02×10^{-3}	3349	0.512
MS2	Air	0	63.2	31.6	6.0×10^{-3}	3994	1.012
MS3	Air	0	7.09	3.05	2.12×10^{-6}	50.97	0.00102
MS3	Air	0.428	12.66	15.8	5.95×10^{-5}	400	0.0247
MS3	Air	0.666	6.33	15.8	5.93×10^{-6}	200	0.00318
MS3	Air	0.11	25.32	15.8	1.71×10^{-4}	800	0.07
MS3	Air	0	31.6	15.8	2.16×10^{-4}	1000	0.0858
MS3	Air	0.2	31.6	23.7	5.8×10^{-4}	1500	-
MS3	Air	0.765	6.33	23.7	1.32×10^{-5}	300	-
MS3	Air	0.304	25.3	23.7	3.6×10^{-4}	1200	-
MS3	Air	0.111	37.95	23.7	4.82×10^{-4}	1800	-

TABLE 6 (cont.)

Spec. No.	Env.	R	ΔK $MN/m^{3/2}$	K_m $MN/m^{3/2}$	da/dN mm/cycle	λ MN^2/m^3	Φ
MS3	Air	0.034	44.28	23.7	5.75×10^{-4}	2100	-
MS3	Air	0.666	2.66	31.6	1.62×10^{-4}	800	0.0655
MS3	Air	0.739	9.49	31.6	4.1×10^{-5}	600	0.0418
MS3	Air	0.05	56.96	31.6	1.47×10^{-3}	3600	0.542
MS3	Air	0.155	69.58	47.5	5.45×10^{-3}	6600	2.06
MS4	Air	0.428	18.98	23.7	1.97×10^{-4}	900	-
MS4	Air	0.645	10.24	23.7	2.64×10^{-5}	485.37	-
MS4	Air	0.562	8.86	15.8	2.03×10^{-5}	280	0.0117
MS4	Air	0.875	6.33	47.5	1.1×10^{-4}	600	0.0414
MS4	Air	0.686	5.88	15.8	1.4×10^{-6}	186	0.000424
MS4	Air	0.836	4.63	31.6	2.65×10^{-5}	356	0.0128
MS4	Air	0.85	5.12	31.6	2.37×10^{-6}	324	0.0090
MS4	3.5% NaCl	0	56.92	28.46	2.03×10^{-3}	3240	0.488
MS4	3.5% NaCl	0	86.97	43.48	9.22×10^{-3}	7564	3.411
MS4	3.5% NaCl	0.305	50.6	47.5	4.98×10^{-3}	4807	0.989
MS4	3.5% NaCl	0.2	63.2	47.5	6.53×10^{-3}	6000	1.581
MS4	3.5% NaCl	0.429	37.95	47.5	2.6×10^{-3}	3600	0.61
MS4	3.5% NaCl	0.517	31.6	47.5	2.03×10^{-3}	3000	0.463
MS4	3.5% NaCl	0.579	25.3	47.5	1.68×10^{-3}	2400	0.337
MS4	3.5% NaCl	0	23.72	11.86	3.85×10^{-4}	562.5	0.0566
MS4	3.5% NaCl	0	18.98	9.99	2.8×10^{-4}	360	0.0339
MS4	3.5% NaCl	0	11.07	5.53	7.56×10^{-5}	122.5	0.00853
MS4	3.5% NaCl	0	9.49	4.74	3.78×10^{-5}	90	0.00515
MS4	3.5% NaCl	0	7.91	3.95	2.24×10^{-5}	62.5	0.00231
MS4	3.5% NaCl	0	6.96	3.48	9.1×10^{-6}	48.4	0.000862
MS4	3.5% NaCl	0	6.33	3.16	No growth	40	-
MS4	3.5% NaCl	0.666	6.33	15.8	1.82×10^{-5}	200	0.00234
MS4	3.5% NaCl	0.695	5.69	15.8	5.79×10^{-6}	180	0.00052
MS11	3.5% NaCl	0	29.73	14.86	7.264×10^{-4}	883.75	0.09461
MS11	3.5% NaCl	0	44.28	22.14	1.4×10^{-3}	1960	0.245
MS11	3.5% NaCl	0	63.3	31.65	3.27×10^{-3}	4000	0.683
MS11	3.5% NaCl	0	37.95	18.98	1.05×10^{-3}	1440	0.1675
MS11	3.5% NaCl	0	25.3	12.65	4.72×10^{-4}	640	0.0655
MS11	3.5% NaCl	0	47.44	23.72	2.84×10^{-3}	2250	0.293
MS11	3.5% NaCl	0	12.65	6.32	4.76×10^{-5}	1600	0.0125
MS11	3.5% NaCl	0	17.39	8.70	1.67×10^{-4}	302.41	0.0279
MS11	3.5% NaCl	0.111	50.6	31.6	4.65×10^{-3}	3200	0.449

TABLE 6 (cont.)

Spec. No.	Env.	R	ΔK $MN/m^{3/2}$	K_m $MN/m^{3/2}$	da/dN mm/cycle	λ MN^2/m^3	Φ
MS11	3.5% NaCl	0.25	37.95	31.6	1.41×10^{-3}	2400	0.315
MS11	3.5% NaCl	0.333	31.6	31.6	1.25×10^{-3}	2000	0.232
MS11	3.5% NaCl	0.428	25.3	31.6	1.02×10^{-3}	1600	0.172
MS11	3.5% NaCl	0.	15.8	7.9	1.05×10^{-4}	250	0.0211
MS12	3.5% NaCl	0	28.46	14.23	5.02×10^{-4}	810	0.0857
MS12	3.5% NaCl	0	6.64	3.32	1.51×10^{-6}	44.00	0.00017
MS12	3.5% NaCl	0.873	4.27	31.6	2.23×10^{-6}	269.86	0.00029
MS12	3.5% NaCl	0.704	5.5	15.8	1.23×10^{-6}	173.8	0.00019
MS12	3.5% NaCl	0.708	5.4	15.8	No growth	170.64	-
MS12	Air	0	6.5	3.25	1.06×10^{-6}	42.25	0.00079
MS12	Air	0	70	35	6.1×10^{-3}	4900	2.46
MS23	3.5% NaCl	0.667	18.98	47.5	1.2×10^{-3}	1800	0.227
MS23	3.5% NaCl	0.765	12.65	47.5	7.5×10^{-4}	1200	0.128
MS23	3.5% NaCl	0.538	18.98	31.6	7.02×10^{-4}	1200	0.117
MS23	3.5% NaCl	0.666	12.65	31.6	4.62×10^{-4}	800	0.0658
MS23	3.5% NaCl	0.111	25.3	15.8	4.1×10^{-4}	800	0.0695
MS23	3.5% NaCl	0.25	18.98	15.8	3.35×10^{-4}	600	0.0464
MS23	3.5% NaCl	0.428	12.65	15.8	1.95×10^{-4}	400	0.0271
MS23	3.5% NaCl	0.778	7.9	31.6	2.33×10^{-4}	500	0.0292
MS23	3.5% NaCl	0.538	9.49	15.8	6.84×10^{-5}	300	0.0133
MS23	3.5% NaCl	0.818	6.33	31.6	8.46×10^{-5}	400	0.0175
MS23	3.5% NaCl	0.875	6.33	47.5	2.6×10^{-4}	600	0.041
MS23	3.5% NaCl	0.936	3.16	47.5	No growth	300	-
MS23	3.5% NaCl	0.905	4.74	47.5	7.63×10^{-5}	450	0.0185
MS23	3.5% NaCl	0.923	3.8	47.5	4.76×10^{-5}	360	0.00614
MS23	3.5% NaCl	0.927	3.61	47.5	7.45×10^{-6}	342	0.000814
MS23	3.5% NaCl	0.86	4.74	31.6	5.79×10^{-5}	300	0.00585
MS23	3.5% NaCl	0.878	4.11	31.6	1.26×10^{-5}	260	0.00115
MS23	3.5% NaCl	0.887	3.8	31.6	No growth	240	-

TABLE 7

Cyclic Crack Growth Data for LM30 in Laboratory Air and 3.5% NaCl at a Frequency of 0.25 Hz

Spec. No.	Env.	R	ΔK $MN/m^{3/2}$	K_m $MN/m^{3/2}$	$\frac{da}{dN}$ mm/cycle	λ MN^2/m^3	Φ
F10	Air	0	18.99	9.5	1.53×10^{-1}	360.62	3.322
F10	Air	0	17.41	8.7	2.28×10^{-2}	303.1	1.657
F10	Air	0	16.61	8.3	1.38×10^{-2}	275.89	1.248
F10	Air	0	15.82	7.91	8.61×10^{-3}	250.27	0.962
F10	Air	0	14.24	7.12	2.83×10^{-3}	202.77	0.589
F10	Air	0	13.45	6.72	1.65×10^{-3}	180.9	0.461
F10	Air	0	12.66	6.33	1.02×10^{-3}	160.27	0.317
F10	Air	0	11.87	5.94	3.25×10^{-4}	140.89	0.274
F10	Air	0	11.08	5.54	2.44×10^{-4}	122.76	0.204
F10	Air	0	10.28	5.14	1.22×10^{-4}	105.67	0.144
F10	Air	0	9.49	4.75	7.72×10^{-5}	90.06	0.0634
F10	Air	0	8.70	4.35	3.09×10^{-5}	75.69	0.0531
F10	Air	0	7.91	3.96	5.69×10^{-6}	62.57	0.0179
F10	Air	0	7.12	3.56	No growth	50.69	-
F10	Air	0	6.33	3.17	No growth	40.07	-
F11	Air	0	11.0	5.5	2.41×10^{-4}	121	0.140
F11	Air	0.05	10	5.5	1.06×10^{-4}	110	0.105
F11	Air	0.158	8	5.5	2.14×10^{-5}	88	0.0409
F11	Air	0.222	7	5.5	1.64×10^{-6}	77	0.0114
F11	Air	0.333	5.5	5.5	No growth	60.5	-
F17	3.5% NaCl	0	7.91	3.96	8.9×10^{-5}	62.57	0.0519
F17	3.5% NaCl	0	8.7	4.35	1.4×10^{-4}	75.69	0.103
F17	3.5% NaCl	0	9.49	4.75	2.68×10^{-4}	90.06	0.165
F17	3.5% NaCl	0	10.28	5.14	7.85×10^{-4}	105.67	0.241
F17	3.5% NaCl	0	11.08	5.54	9.56×10^{-4}	122.76	0.336
F18	3.5% NaCl	0	10.28	5.14	8.35×10^{-4}	105.67	0.224
F18	3.5% NaCl	0	11.08	5.54	1.12×10^{-3}	122.76	0.310
F18	3.5% NaCl	0	7.37	3.68	3.0×10^{-5}	54.32	0.0208
F18	3.5% NaCl	0	6.33	3.17	No growth	40.07	-
F18	3.5% NaCl	0	5.54	2.77	No growth	30.69	-
F18	3.5% NaCl	0	11.87	5.94	1.84×10^{-3}	140.89	0.417
F18	3.5% NaCl	0	12.66	6.33	3.29×10^{-3}	160.27	0.552
F18	3.5% NaCl	0	13.45	6.72	4.68×10^{-3}	180.9	0.726
F18	3.5% NaCl	0	14.24	7.12	6.46×10^{-3}	202.77	0.960

TABLE 7 (cont.)

Spec. No.	Env.	R	ΔK $MN/m^{3/2}$	K_m $MN/m^{3/2}$	da/dN mm/cycle	λ MN^2/m^3	Φ
F18	3.5% NaCl	0	15.82	7.91	1.29×10^{-2}	250.27	1.779
F18	3.5% NaCl	0	17.41	8.7	2.46×10^{-2}	303.1	4.188
F17	3.5% NaCl	0.671	4.75	12.1	3.27×10^{-4}	114.95	0.222
F17	Air	0.627	5.554	12.1	9.33×10^{-4}	134.06	0.397
F17	Air	0.585	6.33	12.1	2.08×10^{-3}	153.18	0.608
F17	Air	0.507	7.91	12.1	6.17×10^{-3}	191.42	1.215
F17	Air	0.437	9.49	12.1	1.67×10^{-2}	229.65	2.344
F17	Air	0.294	11.87	12.1	1.75×10^{-1}	287.25	9.968
F19	3.5% NaCl	0	19.93	9.96	1.22	397.2	26.91
F19	3.5% NaCl	0	18.99	9.5	1.25×10^{-1}	360.62	6.314
F19	3.5% NaCl	0.209	15.82	12.1	8.22×10^{-1}	382.84	31.68
F19	3.5% NaCl	0.233	15.03	12.1	1.96×10^{-1}	363.72	11.351
F19	3.5% NaCl	0.259	14.24	12.1	9.33×10^{-2}	344.6	6.612
F19	3.5% NaCl	0.341	11.87	12.1	2.77×10^{-2}	287.25	2.499
F19	3.5% NaCl	0.437	9.49	12.1	1.13×10^{-2}	229.65	1.223
F19	3.5% NaCl	0.508	7.91	12.1	5.5×10^{-3}	191.42	0.764
F19	3.5% NaCl	0.585	6.33	12.1	2.14×10^{-3}	153.18	0.441
F19	3.5% NaCl	0.627	5.54	12.1	1.24×10^{-3}	134.06	0.312
F19	3.5% NaCl	0.671	4.75	12.1	5.11×10^{-4}	114.95	0.1
F16	Air	0.259	14.24	12.1	8.46×10^{-2}	344.6	4.839
F16	Air	0.233	15.03	12.1	1.42×10^{-1}	363.72	7.271
F16	Air	0.209	15.82	12.1	5.13×10^{-1}	382.84	13.122
F16	3.5% NaCl	0	11.0	5.5	7.78×10^{-4}	121	0.186
F16	3.5% NaCl	0.05	10	5.5	4.55×10^{-4}	110	0.144
F16	3.5% NaCl	0.158	8	5.5	1.52×10^{-4}	88	0.0694
F16	3.5% NaCl	0.222	7	5.5	5.26×10^{-5}	77	0.0354
F16	3.5% NaCl	0.333	6	5.5	1.22×10^{-6}	60	0.00314
F16	3.5% NaCl	0.719	3.96	12.1	1.81×10^{-4}	95.83	0.0925
F16	Air	0.719	3.96	12.1	2.45×10^{-5}	95.83	0.0495
F16	Air	0.739	3.64	12.1	3.27×10^{-6}	88.09	0.0148
F16	3.5% NaCl	0.739	3.64	12.1	9.88×10^{-5}	88.09	0.0569
F16	3.5% NaCl	0.769	3.16	12.1	5.07×10^{-6}	76.47	0.00615
F16	3.5% NaCl	0.270	6.32	5.5	9.52×10^{-6}	69.52	0.0132
F16	Air	0	20.25	10.13	1.42×10^{0}	410.06	27.136
F16	Air	0	18.20	9.1	3.85×10^{-2}	331.09	2.993

TABLE 8

Fatigue Crack Growth Threshold Data

Material	Env.	f (Hz)	K_m ($MN/m^{3/2}$)	R	ΔK_{th} ($MN/m^{3/2}$)	$\Delta K_{th}/E$ ($mm^{1/2}$)
RR58	Air	0.15	2.75	0	5.5	2.32×10^{-3}
RR58	Air	0.15	5.5	0.4	4.73	1.99×10^{-3}
RR58	Air	0.15	8.25	0.622	3.85	1.62×10^{-3}
RR58	Air	0.15	12.1	0.796	2.75	1.16×10^{-3}
RR58	Air	0.15	16.5	0.879	2.11	8.89×10^{-4}
RR58	Air	0.15	18.15	0.905	1.82	7.67×10^{-4}
RR58	Air	35	2.18	0	4.37	1.84×10^{-3}
RR58	Air	35	5.5	0.478	3.89	1.64×10^{-3}
RR58	Air	35	12.1	0.832	2.22	9.36×10^{-4}
RR58	Air	35	16.5	0.906	1.62	6.83×10^{-4}
RR58	3.5% NaCl	0.15	2.42	0	4.84	2.04×10^{-3}
RR58	3.5% NaCl	0.15	5.5	0.471	3.96	1.67×10^{-3}
RR58	3.5% NaCl	0.15	8.25	0.653	3.46	1.46×10^{-3}
RR58	3.5% NaCl	0.15	12.1	0.811	2.53	1.07×10^{-3}
RR58	3.5% NaCl	0.15	16.5	0.895	1.82	7.67×10^{-4}
RR58	3.5% NaCl	35	2.18	0	4.36	1.84×10^{-3}
RR58	3.5% NaCl	35	5.5	0.487	3.80	1.6×10^{-3}
RR58	3.5% NaCl	35	12.1	0.829	2.26	9.53×10^{-4}
RR58	3.5% NaCl	35	16.5	0.908	1.60	6.75×10^{-4}
LM30	Air	0.25	3.7	0	7.4	2.85×10^{-3}
LM30	Air	0.25	5.5	0.25	6.6	2.55×10^{-3}
LM30	Air	0.25	12.1	0.747	3.5	1.35×10^{-3}
LM30	3.5% NaCl	0.25	3.45	0	6.9	2.66×10^{-3}
LM30	3.5% NaCl	0.25	5.5	0.302	5.9	2.28×10^{-3}
LM30	3.5% NaCl	0.25	12.1	0.773	3.1	1.19×10^{-3}
BS15	Air	0.25	3.16	0	6.33	9.67×10^{-4}
BS15	Air	0.25	15.8	0.704	5.50	8.4×10^{-4}
BS15	Air	0.25	23.7	0.82	4.69	7.15×10^{-4}
BS15	Air	0.25	31.6	0.884	3.89	5.94×10^{-4}
BS15	Air	0.25	47.5	0.933	3.28	5.01×10^{-4}
BS15	3.5% NaCl	0.25	3.16	0	6.33	9.67×10^{-4}
BS15	3.5% NaCl	0.25	15.8	0.703	5.54	8.46×10^{-4}
BS15	3.5% NaCl	0.25	31.6	0.882	3.96	6.05×10^{-4}
BS15	3.5% NaCl	0.25	47.5	0.931	3.35	5.12×10^{-4}

TABLE 8 (cont.)

Material	Env.	f (Hz)	K_m ($MN/m^{3/2}$)	R	ΔK_{th} ($MN/m^{3/2}$)	$\Delta K_{th}/E$ ($mm^{1/2}$)
BS15	Air	35	3.16	0	6.33	9.67×10^{-4}
BS15	Air	35	15.8	0.701	5.62	8.59×10^{-4}
BS15	Air	35	31.6	0.88	4.02	6.14×10^{-4}
BS15	Air	35	47.5	0.927	3.41	5.21×10^{-4}
BS15	3.5% NaCl	35	3.16	0	6.33	9.67×10^{-4}
BS15	3.5% NaCl	35	15.8	0.703	5.54	8.46×10^{-4}
BS15	3.5% NaCl	35	31.6	0.882	3.96	6.05×10^{-4}
BS15	3.5% NaCl	35	47.5	0.931	3.35	5.12×10^{-4}

TABLE 9

Values of the constants α and A_c in the equation $\frac{da}{dN} = A_c \Phi^{\alpha}$

Material	Environment	Loading frequency (Hz)	A_c (mm/cycle)	α
RR58	Lab. air	0.15	9.71×10^{-4}	1.36
RR58	3.5% NaCl	0.15	2.5×10^{-3}	1.1
RR58	Lab. air	35	2.05×10^{-4}	1.148
RR58	3.5% NaCl	35	2.12×10^{-4}	1.151
BS15	Lab. air	0.25	2.1×10^{-3}	1.10
BS15	3.5% NaCl	0.25	4.41×10^{-3}	0.89
BS15	Lab. air	35	2.1×10^{-3}	1.10
BS15	3.5% NaCl	35	2.1×10^{-3}	1.10
LM30	Lab. air	0.25	5.173×10^{-3}	1.72
LM30	3.5% NaCl	0.25	6.49×10^{-3}	1.45
Mild steel	Air	25-30	2.21×10^{-4}	0.81
Cold rolled	Air	24-30	2.17×10^{-3}	1.36
Mild steel	-	-	-	-
A533 B-1	Air	160	1.04×10^{-3}	1.07
EN3A	Air	100	6.53×10^{-4}	1.40

TABLE 10

Stress Corrosion Data for RR58 (Horizontal Specimen Orientation)

Spec. No.	t_i h	K_r $MN/m^{3/2}$	K_s $MN/m^{3/2}$	K_s/K_c	da/dt mm/s	ψ	a_i mm	r_r mm	a_i/r_r
C30	53	21.45	12.21	0.569	8.35×10^{-6}	2.086	0.182	0.1812	1.004
C30	0	12.21	14.58	-	2.45×10^{-5}	-	-	-	-
C30	0	14.58	15.07	-	1.46×10^{-5}	-	-	-	-
C30	0	15.07	15.57	-	2.22×10^{-5}	-	-	-	-
C30	0	15.57	16.12	-	2.54×10^{-5}	-	-	-	-
C30	1	16.12	16.67	-	4.01×10^{-5}	-	-	-	-
C30	1.5	16.67	22.22	-	1.06×10^{-4}	-	-	-	-
C30	1.5	22.22	22.66	-	2.85×10^{-4}	-	-	-	-
C29	104	22.191	10.03	0.452	6.83×10^{-6}	3.894	0.1377	0.1939	0.71
C29	-	10.03	13.53	-	2.21×10^{-5}	-	-	-	-
C29	5	13.53	15.09	-	2.18×10^{-5}	-	-	-	-
C29	5	15.09	19.34	-	6.3×10^{-5}	-	-	-	-
C31	73	20.84	11.21	0.538	7.7×10^{-6}	2.455	0.1488	0.171	0.87
C31	0	11.21	15.97	-	2.54×10^{-5}	-	-	-	-
C31	7	15.97	13.64	-	1.36×10^{-5}	0.371	0.131	0.10	1.31
C31	0	13.64	21.78	-	5.25×10^{-5}	-	-	-	-
C32	86	22.76	11.88	0.522	1.05×10^{-5}	2.67	0.201	0.2049	0.981
C32	5	11.88	13.2	-	1.49×10^{-5}	-	-	-	-
C32	2	13.2	19.39	-	5.75×10^{-5}	-	-	-	-
C32	0	19.39	20.22	-	6×10^{-5}	-	-	-	-
C33	0	22.42	22.11	0.986	1.74×10^{-4}	0.028	-	0.1988	-
D31	368	22.44	7.76	0.346	3.64×10^{-7}	7.353	0.114	0.1483	0.575
D31	0	7.76	8.3	-	1.2×10^{-6}	-	-	-	-
D31	0	8.3	8.47	-	1.85×10^{-6}	-	-	-	-
D31	4	8.47	18.92	-	5.6×10^{-5}	-	-	-	-
D31	0	18.92	19.25	-	5.3×10^{-5}	-	-	-	-
D31	0	19.25	21.34	-	6.1×10^{-5}	-	-	-	-
D31	1	21.34	22	-	9×10^{-5}	-	-	-	-
D31	1	22	22.5	-	1.2×10^{-4}	-	-	-	-
D28	317	21.34	8.42	0.395	1.97×10^{-6}	5.423	0.171	0.1793	0.954
D28	2	8.42	9.3	-	3.05×10^{-6}	-	-	-	-
D28	5	9.3	17.93	-	5.6×10^{-5}	-	-	-	-
D28	5	17.93	15.84	-	4.25×10^{-5}	0.281	0.098	0.1266	0.774

TABLE 10 (cont.)

Spec. No.	t_i h	K_r $MN/m^{3/2}$	K_s $MN/m^{3/2}$	K_s/K_c	da/dt mm/s	ψ	a_i mm	r_r mm	a_i/r_r
D28	3	15.84	20.3	-	5.05×10^{-5}	-	-	-	-
D28	98	20.3	10	-	5.2×10^{-6}	3.121	0.152	0.1623	0.937
C62	37	22	14.69	0.668	2.1×10^{-5}	1.243	0.177	0.1906	0.929
C62	4	14.69	16.5	-	4.42×10^{-5}	-	-	-	-
C62	2	16.5	17.33	-	6.1×10^{-5}	-	-	-	-
C62	34	17.33	11.7	-	1.04×10^{-5}	1.194	0.103	0.1183	0.871
C78	23	22.42	17.25	0.769	6.12×10^{-5}	0.689	0.162	0.198	0.8183
C78	2	17.25	20.9	-	6.4×10^{-5}	-	-	-	-
C78	2.6	20.9	19.36	-	6.4×10^{-5}	0.166	0.143	0.172	0.8312
C78	3	19.36	20.56	-	6.4×10^{-5}	-	-	-	-
C78	92	20.56	9.9	-	3.82×10^{-6}	3.313	0.131	0.166	0.787
C82	145	22.94	10	0.434	3.86×10^{-6}	4.309	0.136	0.2073	0.6561
C82	15	10	14.3	-	2.47×10^{-5}	-	-	-	-
C82	9	14.3	16.5	-	4.44×10^{-5}	-	-	-	-
C82	8	16.5	18.2	-	5.7×10^{-5}	-	-	-	-
C82	33	18.2	10.58	-	-	1.959	0.104	0.1305	0.7972
C80	54	23.6	13.26	0.562	1.51×10^{-5}	2.053	0.128	0.2194	0.5835
C80	2	13.26	15.4	-	2.25×10^{-5}	-	-	-	-
C80	4	15.4	19.8	-	6.3×10^{-5}	-	-	-	-
C80	45	19.8	13.26	-	1.51×10^{-5}	1.229	0.164	0.1544	1.062
C80	5	13.26	20.32	-	6.2×10^{-5}	-	-	-	-
C80	143	20.32	8.36	-	1.22×10^{-6}	4.908	0.124	0.1626	0.7625
C84	237	23.21	8.66	0.373	2.02×10^{-6}	0.174	0.174	0.2222	0.7211
C85	280	23.75	8.64	0.364	2.08×10^{-6}	0.181	0.181	0.224	0.7832

TABLE 11

Stress Corrosion Data for RR58 (Vertical Specimen Orientation)

Spec. No.	t_i h	K_r $MN/m^{3/2}$	K_s $MN/m^{3/2}$	K_s/K_c	da/dt mm/s	ψ	a_i mm	r_r mm	a_i/r_r
C69	0	20.8	19.8	0.952	1.15×10^{-4}	0.1033	-	0.1704	-
C69	2	19.8	18.0	-	1.1×10^{-4}	0.21	-	-	-
C69	1.2	18.0	16.75	-	8.4×10^{-5}	0.1585	0.088	0.1276	0.6896
C69	3	16.75	17.0	-	1.23×10^{-4}	-	-	-	-
C69	1	17.0	17.5	-	1.28×10^{-4}	-	-	-	-
C69	2	17.5	21.43	-	1.31×10^{-4}	-	-	-	-
C69	8.7	21.43	15.2	-	5.42×10^{-5}	0.99	0.139	0.1809	0.7685
C51	28	23.82	12.76	0.536	3.14×10^{-5}	2.496	0.224	0.22347	1.002
C51	2	12.76	15.34	-	6.87×10^{-5}	-	-	-	-
C51	17.8	15.34	9.68	-	1.02×10^{-5}	1.518	0.0827	0.0927	0.892
C51	2	9.68	13.8	-	2.88×10^{-5}	-	-	-	-
C51	1.5	13.8	14.1	-	4.33×10^{-5}	-	-	-	-
C51	2.5	14.1	15.66	-	6.17×10^{-5}	-	-	-	-
C51	3	15.66	16.5	-	7.97×10^{-5}	-	-	-	-
C66	42	22.72	11.13	0.489	1.68×10^{-5}	3.162	0.153	0.2033	0.7525
C66	0	11.13	11.6	-	1.88×10^{-5}	-	-	-	-
C66	0	11.6	12	-	2.28×10^{-5}	-	-	-	-
C66	9.5	12	8.45	-	5.49×10^{-6}	1.0166	0.0513	0.0567	0.9048
C66	0	8.45	8.7	-	7.97×10^{-6}	-	-	-	-
C66	2.5	8.7	10.15	-	1.29×10^{-5}	-	-	-	-
C66	3	10.15	12.3	-	2.38×10^{-5}	-	-	-	-
C66	4	12.3	13.25	-	2.91×10^{-5}	-	-	-	-
C67	83	22.10	9.29	0.42	9.82×10^{-6}	4.641	0.148	0.1924	0.7694
C67	4.5	9.29	12.76	-	2.28×10^{-5}	-	-	-	-
C67	2.5	12.76	13.25	-	2.86×10^{-5}	-	-	-	-
C67	6	13.25	14.5	-	4.07×10^{-5}	-	-	-	-
C67	31	14.5	7.6	-	3.31×10^{-6}	2.639	0.0796	0.0828	0.9614
C81	0	23.75	23.1	0.973	2.28×10^{-4}	0.057	-	0.2222	-
C81	0.75	23.1	22.1	-	1.48×10^{-4}	0.093	0.228	0.210	1.086
C81	154	22.1	6.64	-	1.32×10^{-6}	10	0.162	0.1924	0.8421
C81	4	6.64	22.1	-	1.52×10^{-4}	-	-	-	-
C81	274	22.1	5.72	-	2.57×10^{-7}	13.86	0.190	0.1924	0.9877
C81	2	5.72	6.1	-	6.97×10^{-7}	-	-	-	-
C81	6	6.1	7	-	1.82×10^{-6}	-	-	-	-

TABLE 12

Stress Corrosion Data for LM30

Spec No.	t_i (h)	K_r $MN/m^{3/2}$	K_s $MN/m^{3/2}$	K_s/K_c	da/dt mm/s	ψ	a_i (mm)	r_r (mm)	a_i/r_r
F12	90	21.52	7.91	0.368	1.94×10^{-6}	6.39	1.116	1.092	1.022
F12	7	7.91	9.5	-	5.16×10^{-5}	-	-	-	-
F12	15	9.5	8.5	-	5.23×10^{-6}	0.249	0.203	0.213	0.953
F12	3	8.5	11	-	7.44×10^{-5}	-	-	-	-
F12	2	11	12.34	-	5.96×10^{-5}	-	-	-	-
F12	1.5	12.34	18.35	-	5.98×10^{-5}	-	-	-	-
F12	130	18.35	5.9	-	7.22×10^{-7}	8.673	0.695	0.794	0.875
F12	-	5.9	5	-	No growth	0.392	-	0.082	-
F13	16.5	21.36	19	0.889	1.25×10^{-4}	0.264	0.833	1.084	0.768
F13	38	19	15.82	-	7.78×10^{-5}	0.442	0.596	0.851	0.7
F13	13	15.82	14.24	-	7.93×10^{-5}	0.234	0.527	0.59	0.893
F13	60	14.24	7.2	-	5.82×10^{-6}	2.912	0.398	0.478	0.833
F13	-	7.2	4	-	No growth	2.24	-	0.112	-
F14	7.5	20.9	20	0.957	2.29×10^{-4}	0.092	0.923	1.03	0.896
F14	26.5	20	15.76	-	4.3×10^{-5}	0.61	0.795	0.943	0.879
F14	53	15.76	8.5	-	3.31×10^{-5}	2.44	0.515	0.586	0.879
F14	3.5	8.5	18.5	-	4.89×10^{-5}	-	-	-	-
F14	9.5	18.5	17.0	-	5.2×10^{-5}	0.118	0.639	0.805	0.794
F14	42	17.0	10.5	-	1.61×10^{-5}	1.621	0.614	0.681	0.902

TABLE 13

Theoretical and Experimental Deflection Values

(DCB Specimen - BS15)

Monotonic Loading P = 5.5kN

(All values in mm)

a	δ^M_{el}	δ^M_{pl}	δ_M	δ^S_{el}	δ^S_{pl}	δ^R	δ_t	δ_{exp}
70	1.94	5.37	7.31	0.06	0.09	0.41	7.87	7.924
80	2.65	5.15	7.80	0.08	0.09	0.47	8.44	-
90	2.98	4.3	7.28	0.09	0.10	0.51	7.98	-
100	3.87	3.43	7.30	0.09	0.11	0.53	8.03	8.145
110	4.23	2.30	6.53	0.10	0.11	0.54	7.30	-
120	4.96	1.35	6.31	0.11	0.12	0.56	7.10	-
130	5.34	0.99	6.33	0.11	0.13	0.59	7.16	-
140	6.13	0.69	6.82	0.12	0.15	0.61	7.70	-
150	6.91	0.34	7.25	0.14	0.16	0.63	8.18	-
160	7.96	0.0	7.96	0.15	0.17	0.66	8.94	8.83

TABLE 14

Theoretical and Experimental Data for Load Cycling - DCB Specimen BS15

a mm	N	da/dN mm/cycle	$(\Delta\delta_N)_t$ mm	$(\Delta\delta_N)_{exp}$ mm	ΔU Nmm	$(\Delta J)_t$ N/mm	$(\Delta J)_{exp}$ N/mm
$\Delta P = 4.5$ kN Spec. MS14							
70	1	1.62×10^{-2}	3.282	3.36	1080	128.86	140.35
70.625	50	1.52×10^{-2}	3.427	3.55	1959	118.35	121.5
71.25	100	1.3×10^{-2}	3.5	-	-	96.94	-
73.375	250	1.15×10^{-2}	3.702	-	-	94.28	-
76.75	500	1.09×10^{-2}	4.03	4.29	4770	82.96	88.5
79.75	750	9.5×10^{-3}	4.288	-	-	80.46	-
82.75	1000	9.04×10^{-3}	4.54	4.79	6335	75.22	79.1
87.875	1500	7.9×10^{-3}	4.915	-	-	64.58	-
92.125	2000	7.7×10^{-3}	5.222	5.44	8315	69	64.62
96.125	2500	6.2×10^{-3}	5.448	-	-	45.08	-
99.375	3000	5.5×10^{-3}	5.629	5.88	9575	39.06	45.55
102.5	3500	5.1×10^{-3}	5.788	-	-	33.46	-
105.5	4000	4.58×10^{-3}	5.904	6.28	10813	24.54	29.76
107.25	4500	4.58×10^{-3}	6.001	-	-	24.54	-
109.5	5000	4.58×10^{-3}	6.084	6.41	11382	24.54	27.52
114	6000	4.28×10^{-3}	6.276	-	-	24.54	-
118.5	7000	4.58×10^{-3}	6.452	6.76	11892	24.54	27.52
123.125	8000	4.58×10^{-3}	6.55	-	-	24.54	-
127.625	9000	4.58×10^{-3}	6.798	7.1	12657	24.54	27.52
132.125	10000	4.58×10^{-3}	6.985	7.29	13085	24.54	27.52
136.75	11000	$4.58xx.10^{-3}$	7.149	7.46	13467	24.54	27.52
141.25	12000	4.58×10^{-3}	7.336	7.61	13805	25.54	27.52
145.75	13000	4.58×10^{-3}	7.508	7.8	14232	24.54	27.52
150.25	14000	4.58×10^{-3}	7.686	7.96	14592	24.54	27.52
155	15000	4.58×10^{-3}	7.874	8.14	14997	24.54	27.52
$\Delta P = 5.0$ kN Spec. MS15							
70	1	4.98×10^{-2}	4.522	4.618	6108	339.81	352.62
70.375	10	4.57×10^{-2}	4.308	4.59	6922	331.38	343.6
73.125	100	3.31×10^{-2}	5.016	5.41	9942	261.49	290.4
75.875	200	3.08×10^{-2}	5.61	5.92	13650	258.68	267.42
81.25	400	2.54×10^{-2}	6.882	7.22	19652	212.32	228.63

TABLE 14 (cont.)

a mm	N	da/dN mm/cycle	$(\Delta\delta_N)_t$ mm	$(\Delta\delta_N)_{exp}$ mm	ΔU Nmm	$(\Delta J)_t$ N/mm	$(\Delta J)_{exp}$ N/mm
86	600	2.1×10^{-2}	7.718	8.09	-	185.16	204.12
90.5	800	2.02×10^{-2}	8.421	8.91	25794	173.63	195.18
94.625	1000	1.7×10^{-2}	9.032	-	-	129.5	-
98.75	1200	1.56×10^{-2}	9.502	10.13	32813	118.53	142.62
102.375	1400	1.4×10^{-2}	9.814	-	-	115.02	-
105.625	1600	1.24×10^{-2}	10.157	10.71	32573	111.73	125.03
108.25	1800	1.08×10^{-2}	10.428	-	-	88.83	-
110.625	2000	8.8×10^{-3}	10.581	11.18	33688	69.12	81.77
112.375	2200	7.1×10^{-3}	10.72	-	-	48.99	-
113.75	2400	6.8×10^{-3}	10.744	11.32	34487	44.68	48.68
115.125	2600	6.8×10^{-3}	10.823	-	-	33.5	-
116.375	2800	6.8×10^{-3}	10.891	11.44	34816	29.21	32.48
117.75	3000	6.8×10^{-3}	10.901	-	-	29.21	-
124.25	4000	6.8×10^{-3}	11.158	11.86	36093	29.21	32.48
130.75	5000	6.8×10^{-3}	11.501	-	-	29.21	-
137.25	6000	6.8×10^{-3}	11.817	12.48	38225	29.21	32.48
143.75	7000	6.8×10^{-3}	11.992	-	-	29.21	-
150.25	8000	6.8×10^{-3}	12.24	13.15	40543	29.21	32.48
156.75	9000	6.8×10^{-3}	12.523	-	-	29.21	-

TABLE 15

Theoretical and Experimental Data for Load Cycling

DCB Specimen BS15

a mm	N	da/dN mm/cycle	$(\Delta\delta_N)_t$ mm	$(\Delta\delta_N)_{exp.}$ mm	$\Delta\delta^R$ mm	ΔU Nmm	$(\Delta J)_t$ N/mm	$(\Delta J)_{exp.}$ N/mm
ΔP = 5.5kN Spec. MS17								
70	1	7.5×10^{-2}	7.92	7.98	1.278	19686	515.9	536.84
70.625	10	7.02×10^{-2}	8.142	8.33	1.270	20454	459.72	469.63
72.250	50	5.75×10^{-2}	8.682	8.98	1.261	22788	391.24	414.56
74.5	100	5.28×10^{-2}	9.304	9.59	1.249	25863	373.6	397.85
80.75	250	4.68×10^{-2}	10.951	11.27	1.208	34002	335.8	370.75
88.75	500	3.66×10^{-2}	12.954	13.20	1.145	41063	301.74	316.03
95.875	750	3.25×10^{-2}	14.563	14.81	1.084	51607	278.32	269.32
102	1000	2.77×10^{-2}	16.225	16.21	1.027	59824	239.47	233.77
107.25	1250	2.5×10^{-2}	16.822	17.05	0.977	62341	223.32	216.26
112.125	1500	2.23×10^{-2}	17.752	17.96	0.930	66729	210.81	206.98
116.125	1750	1.98×10^{-2}	18.302	18.50	0.980	69157	172.44	198.07
119.875	2000	1.83×10^{-2}	18.762	18.93	0.853	71128	157.38	153.69
126.5	2500	1.55×10^{-2}	19.221	19.44	0.788	72600	119.86	119.22
131.875	3000	1.25×10^{-2}	19.882	20.03	0.735	75500	111.87	113.93
136.25	3500	1.1×10^{-2}	20.365	20.36	0.692	77488	90.88	101.49
140.25	4000	9×10^{-3}	20.551	20.71	0.653	77936	77.36	87.13
143.875	4500	8.2×10^{-3}	20.792	20.80	0.618	78770	68.12	63.45
147.375	5000	7.3×10^{-3}	20.954	21.18	0.584	79428	60.35	59.31
150.75	5500	6.65×10^{-3}	21.201	21.41	0.552	79946	51.89	52.33
154.125	6000	5.9×10^{-3}	21.383	21.60	0.520	80432	43.75	44.42
157.5	6500	4.8×10^{-3}	21.503	21.72	0.382	80904	35.8	35.72
160.875	7000	4.8×10^{-3}	21.614	21.80	0.376	81325	35.8	35.72
ΔP = 6.0 kN Spec. MS18								
70	1	1.3×10^{-1}	12.204	12.48	1.389	33650	710.04	726.84
71	10	9.75×10^{-2}	12.563	12.83	1.383	35449	638.35	653.98
74.25	50	7.75×10^{-2}	13.712	14.09	1.364	42161	520.04	531.76
77.875	100	6.9×10^{-2}	15.134	15.40	1.339	49502	456.37	468.41

TABLE 15 (cont.)

a mm	N	da/dN mm/cycle	$(\Delta\delta_N)_t$ mm	$(\Delta\delta_N)_{exp}$ mm	$\Delta\delta^R$ mm	ΔU Nmm	$(\Delta J)_t$ N/mm	$(\Delta J)_{exp}$ N/mm
8 45	200	5.75×10^{-2}	17.101	17.41	1.287	60544	492.96	451.26
94.125	400	4×10^{-2}	19.732	20.12	1.199	74542	368.8	379.65
101.5	600	3.2×10^{-2}	21.383	21.68	1.125	82948	325.08	335.14
107.625	800	2.9×10^{-2}	22.904	23.13	1.062	90694	280.14	290.08
112.75	1000	2.6×10^{-2}	23.897	24.27	1.007	95866	260.22	261.93
117.75	1200	2.4×10^{-2}	24.782	25.11	0.954	100046	237.51	251.51
122.375	1400	2.15×10^{-2}	25.509	25.91	0.904	104460	209.86	211.36
126.5	1600	2.0×10^{-2}	26.098	26.42	0.859	106700	178.74	187.43
130,25	1800	1.8×10^{-2}	26.686	27.02	0.819	108940	160.0	163.84
133,625	2000	1.6×10^{-2}	27.198	27.53	0.783	112140	143.62	145.29
136.625	2200	1.4×10^{-2}	27.523	27.81	0.751	113160	132.18	133.09
139.375	2400	1.33×10^{-2}	27.802	28.08	0.721	115050	128.23	127.37
142	2600	$1,24 \times 10^{-2}$	28.089	28.37	0.694	115770	117.79	118.04
144.25	2800	1.21×10^{-2}	28.287	28.49	0.67	116550	112.39	110.0
146.375	3000	1.19×10^{-2}	28.572	28.58	0648	117650	107.62	107.75
148.375	3200	1.1×10^{-2}	28.781	28.79	0.627	118360	100.21	98.2
150.125	3400	9.75×10^{-3}	28.904	29.04	0.609	119060	91.48	92.61
151.875	3600	9.5×10^{-3}	29.037	29.18	0.591	120300	77.65	88.08
$\Delta P = 6.5$ kN Spec. MS19								
70	1	1.85×10^{-1}	17.314	17.61	1.495	74453	1100.26	1120.84
71,875	10	1.6×10^{-1}	18.208	18.69	1.471	81079	944.19	962.47
77.375	50	1.26×10^{-1}	20.885	21.33	1.382	97081	788.26	805.11
82.5	100	8.7×10^{-2}	23.006	23.5	1.324	110100	584.36	600.35
90.5	200	7.3×10^{-2}	25.844	26.19	1.277	125910	482.31	501.27
97.125	300	6.8×10^{-2}	27 .771	28.18	1.196	137456	450.08	455.98
102.75	400	5.9×10^{-2}	28.860	29.28	1.145	143415	410.16	417.70
108.125	500	5.2×10^{-2}	30.004	30.08	1.066	147486	383.12	385.33

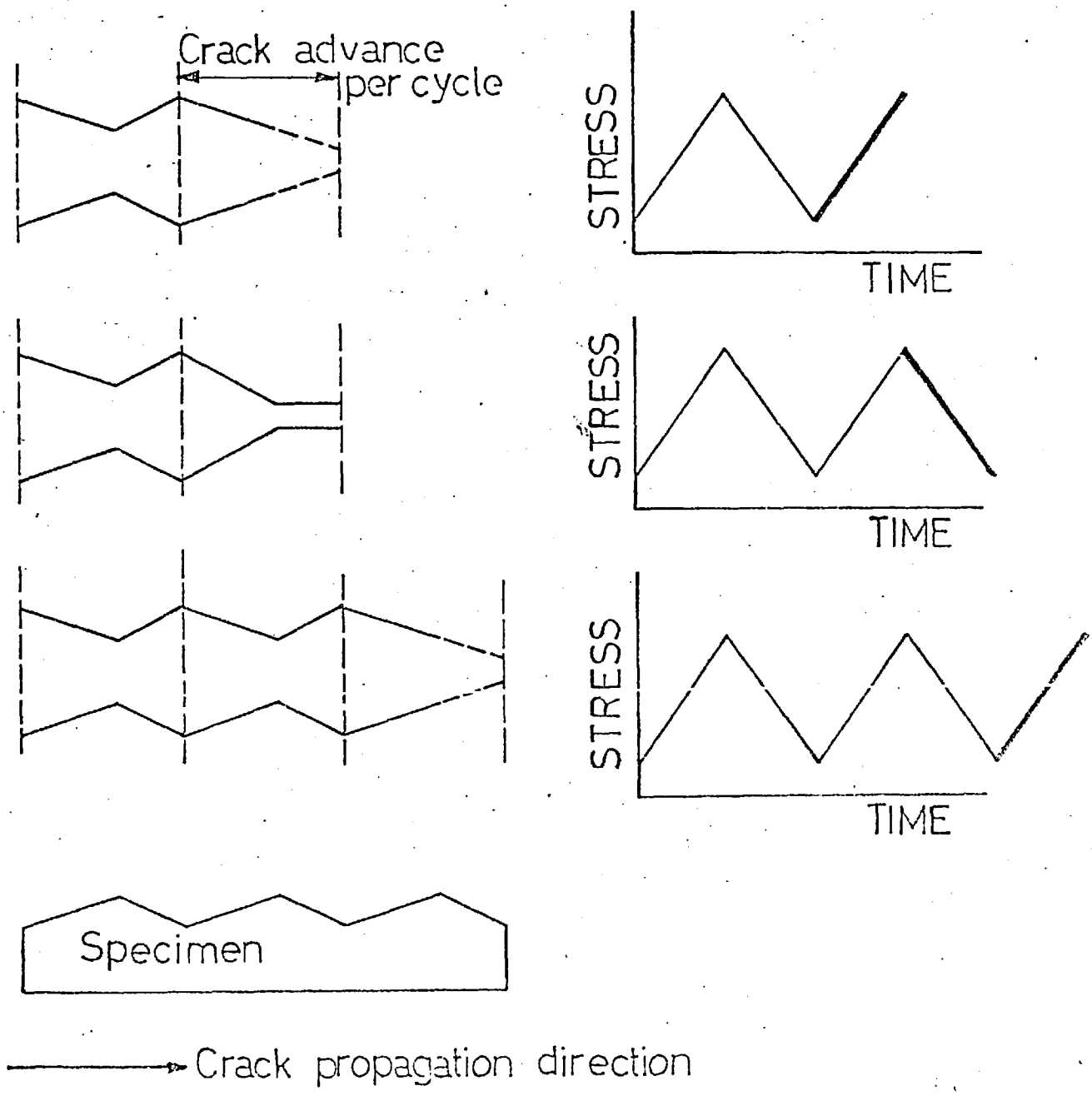


FIG. 1 Sketch Showing the Formation of a Fatigue Striation

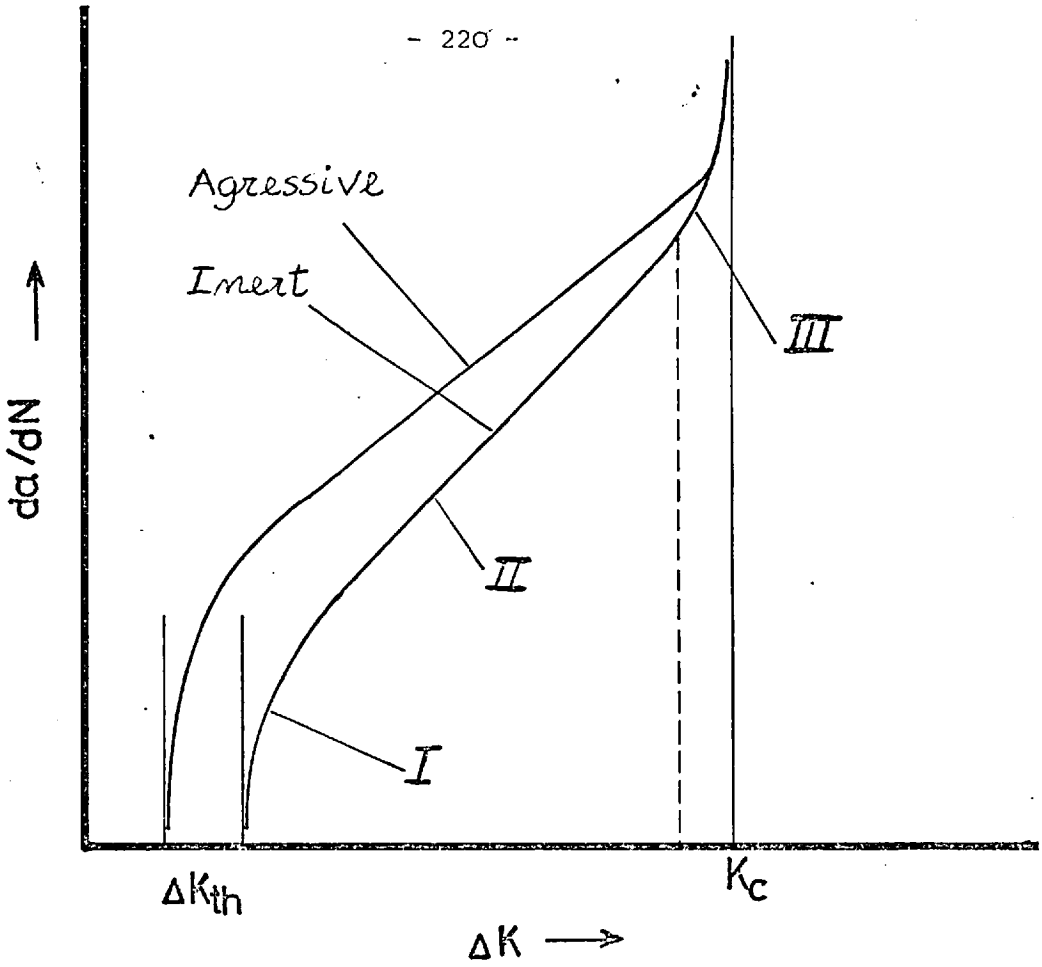


FIG. 2 A Typical Fatigue Crack Propagation Curve Showing the Environmental Effect

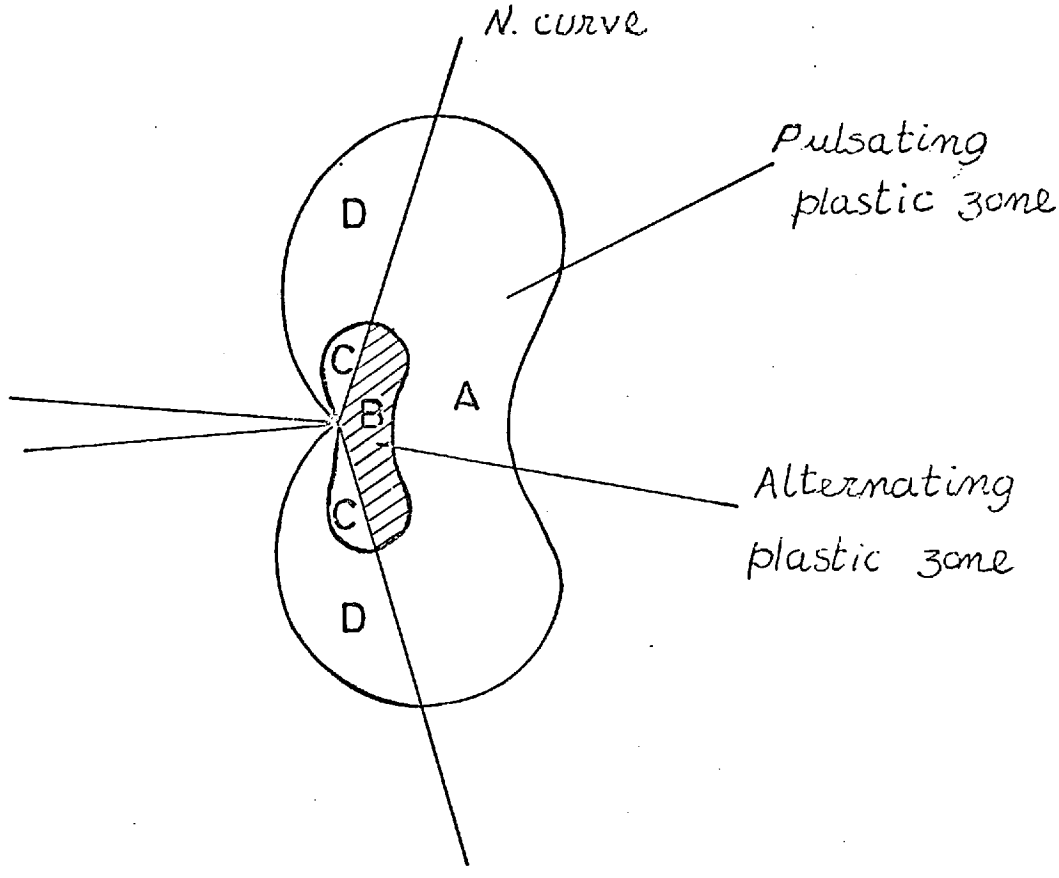


FIG. 3 The Alternating and Pulsating Plastic Zones Considered by Raju(105)

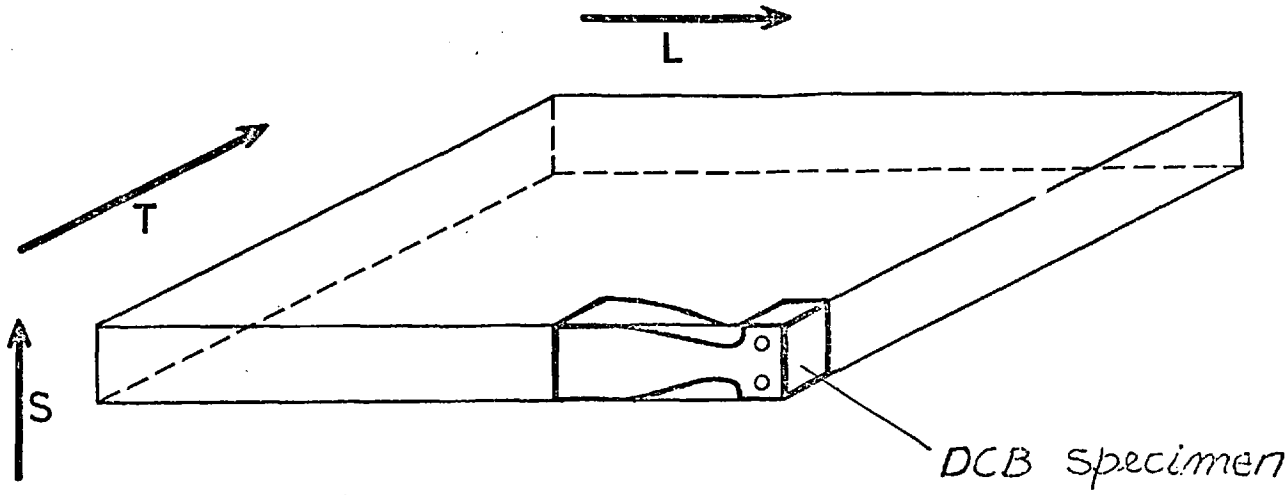


FIG. 4 The Directions in a Plate Material of a High Strength Aluminium Alloy

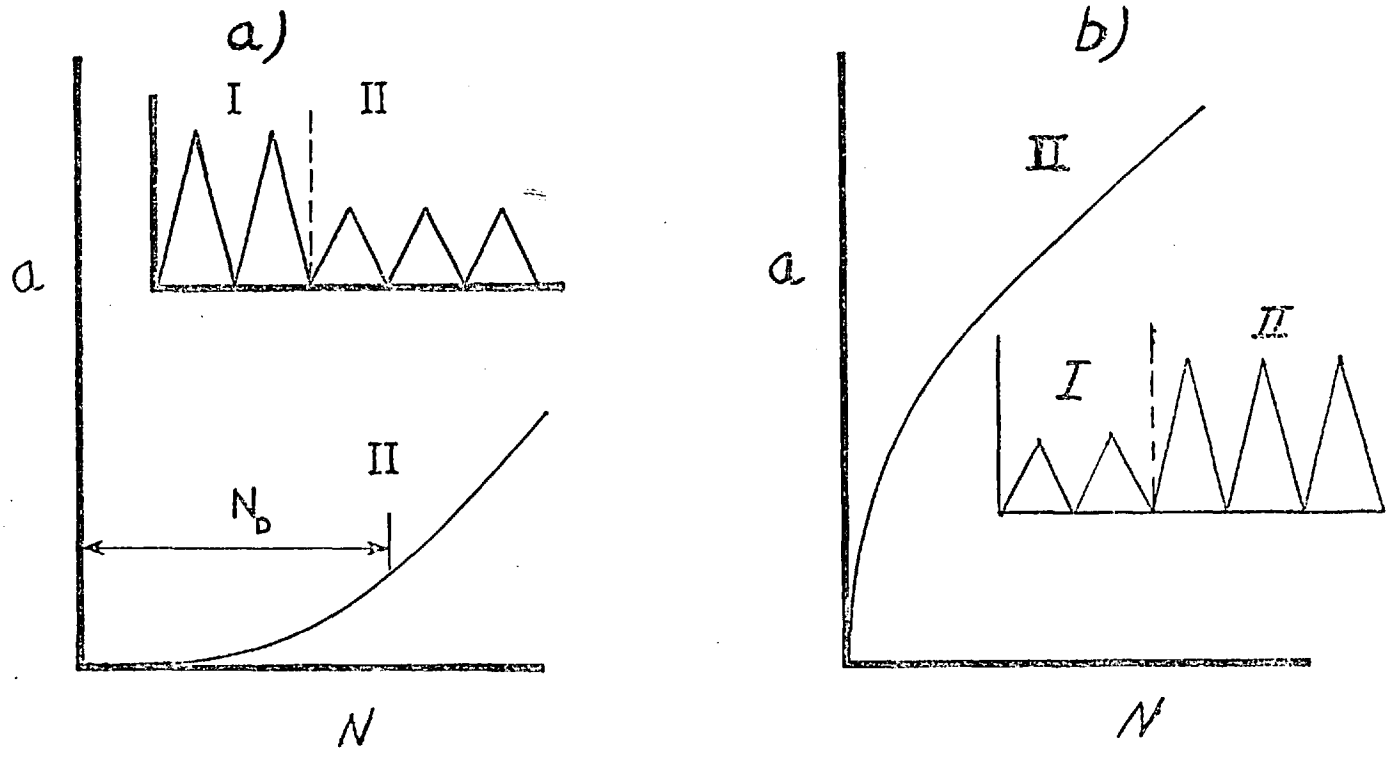


FIG. 5 The Delay and Transient Acceleration Phenomena

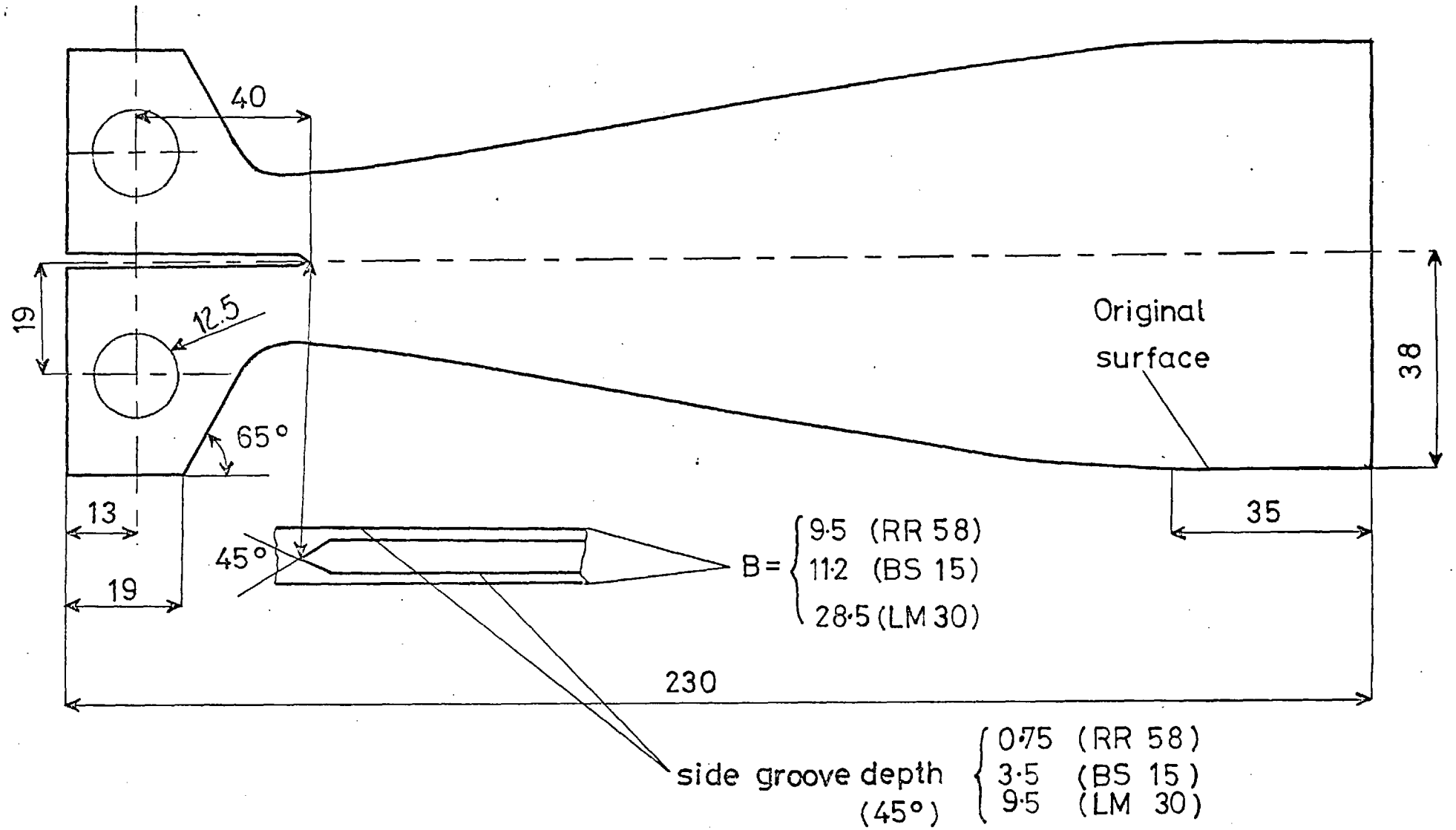


FIG. 6 The Contoured DCB Specimen Used in the Experimental Programme

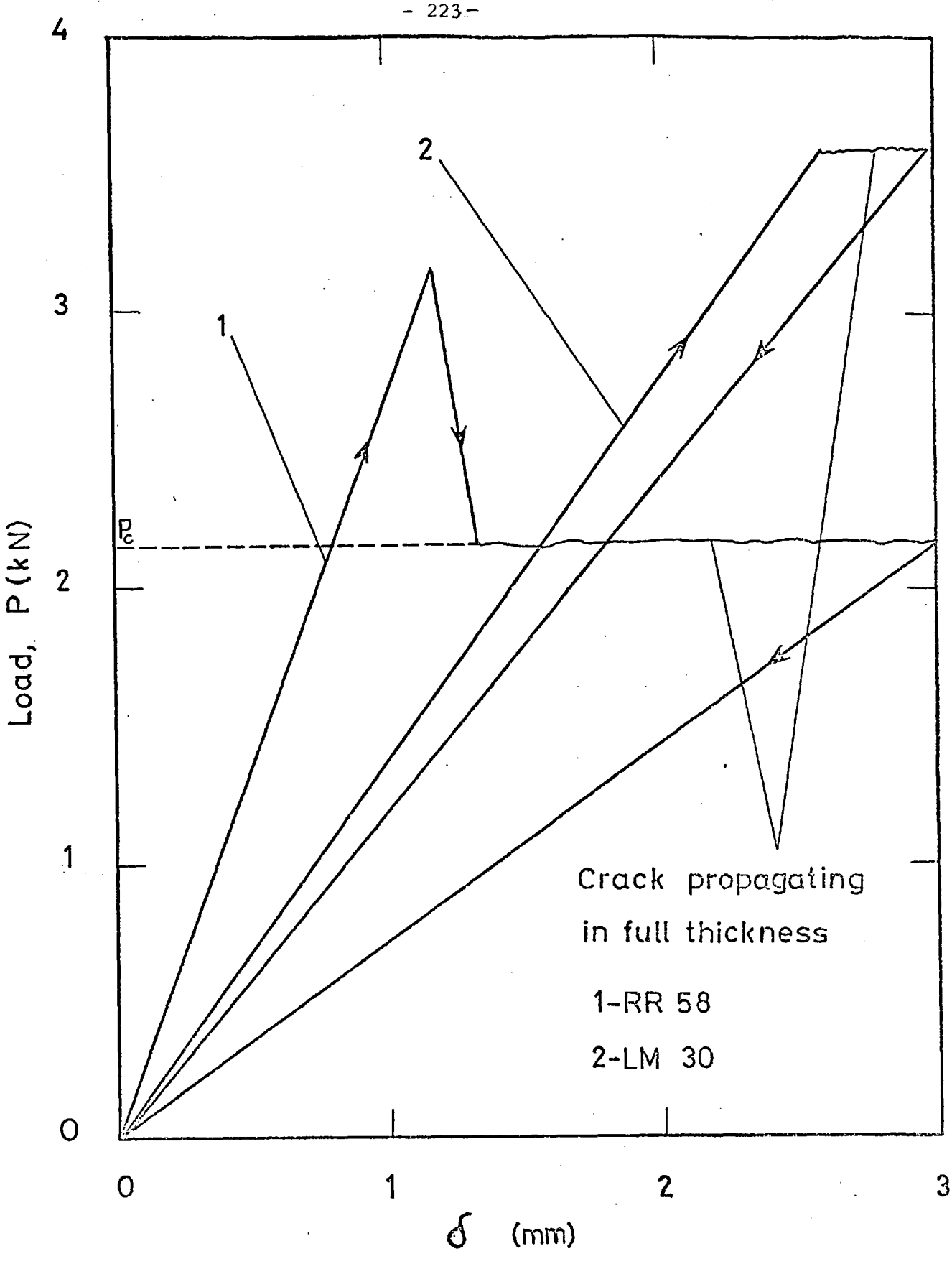


FIG. 7 Typical Load vs. Deflection at the Loading Points Record. RR58 and LM30 Laboratory air

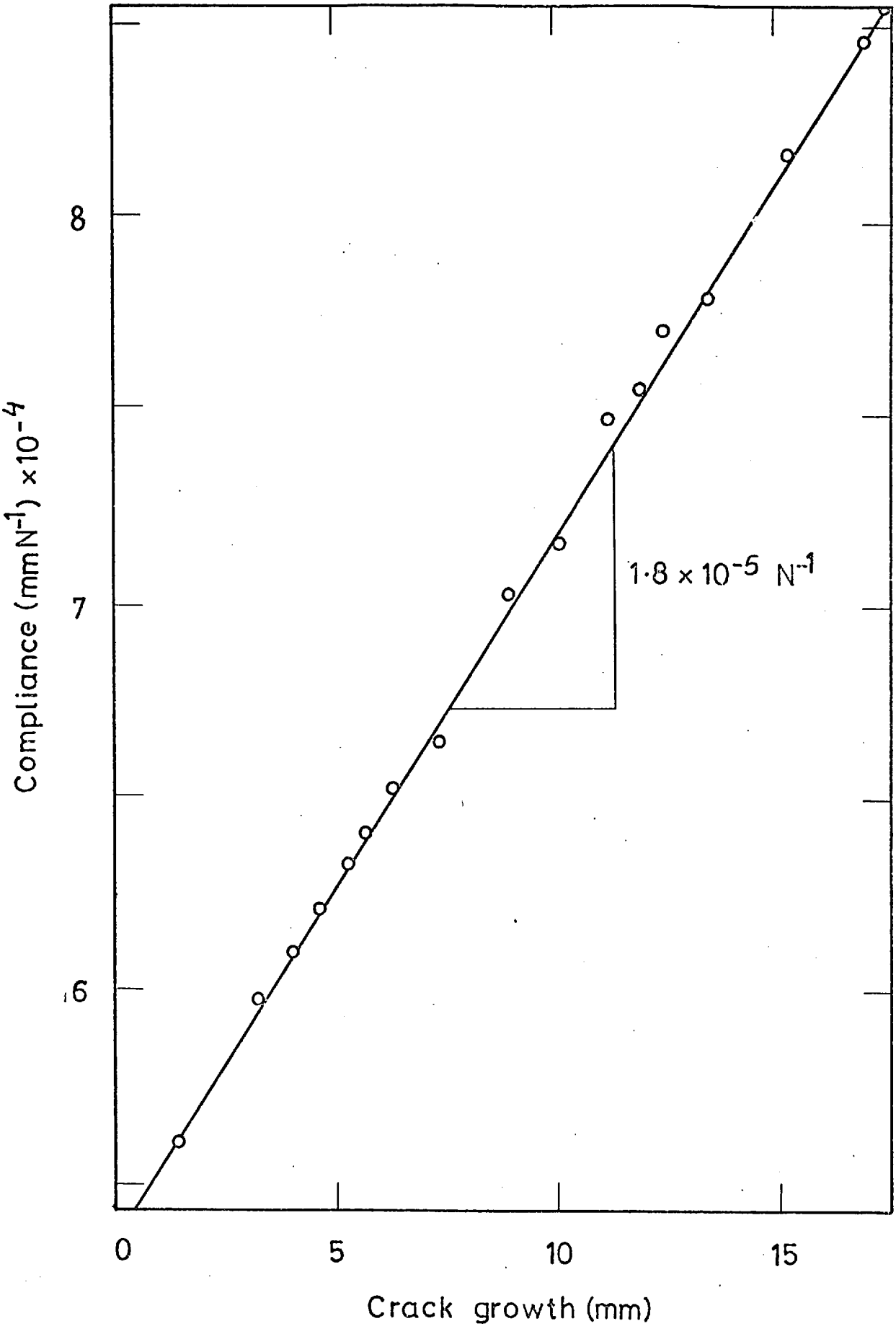


FIG. 8 Typical Compliance vs. Crack Growth Curve. RR58. Laboratory air

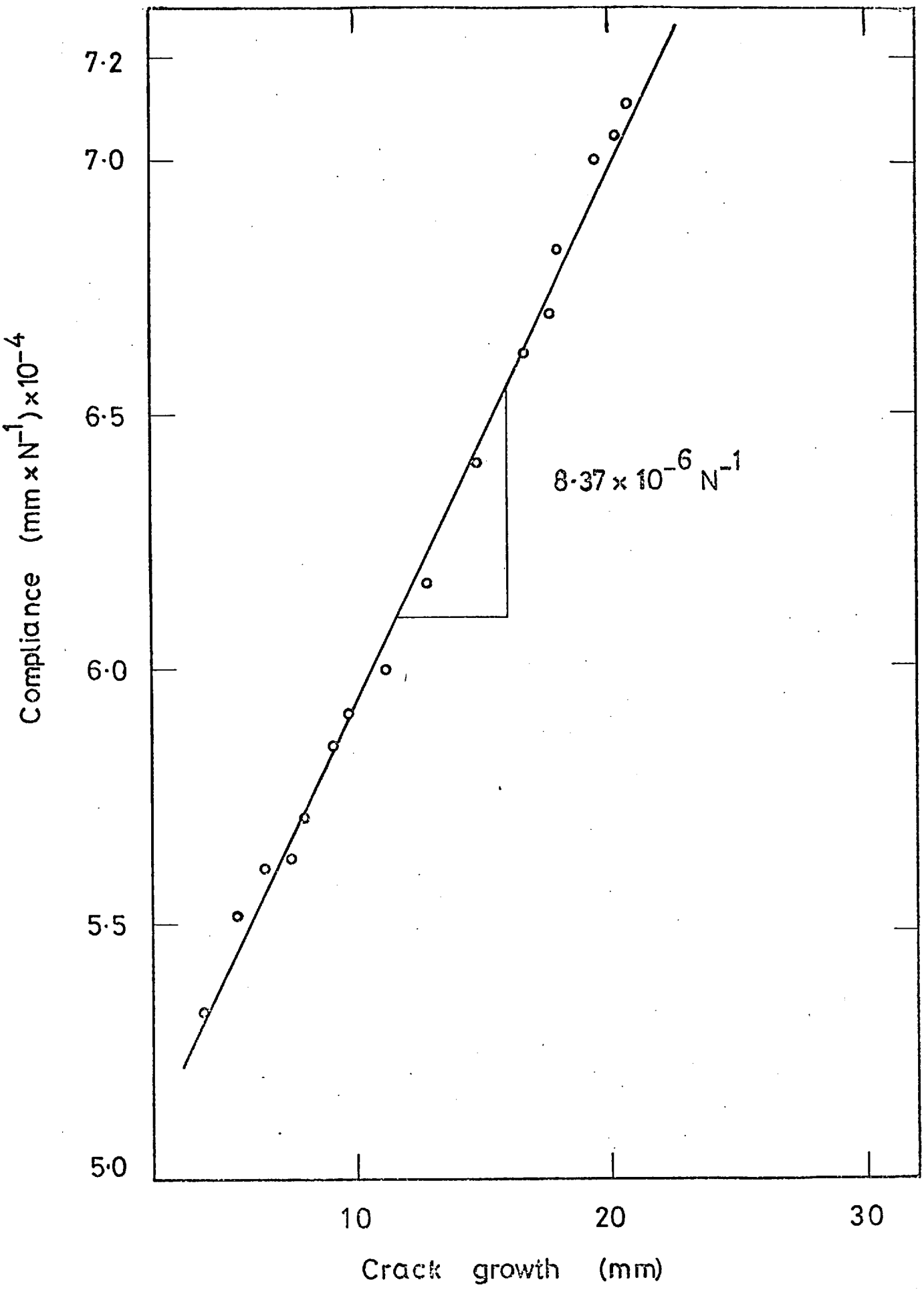


FIG. 9 Typical Compliance vs. Crack Growth Curve. LM30. Laboratory air

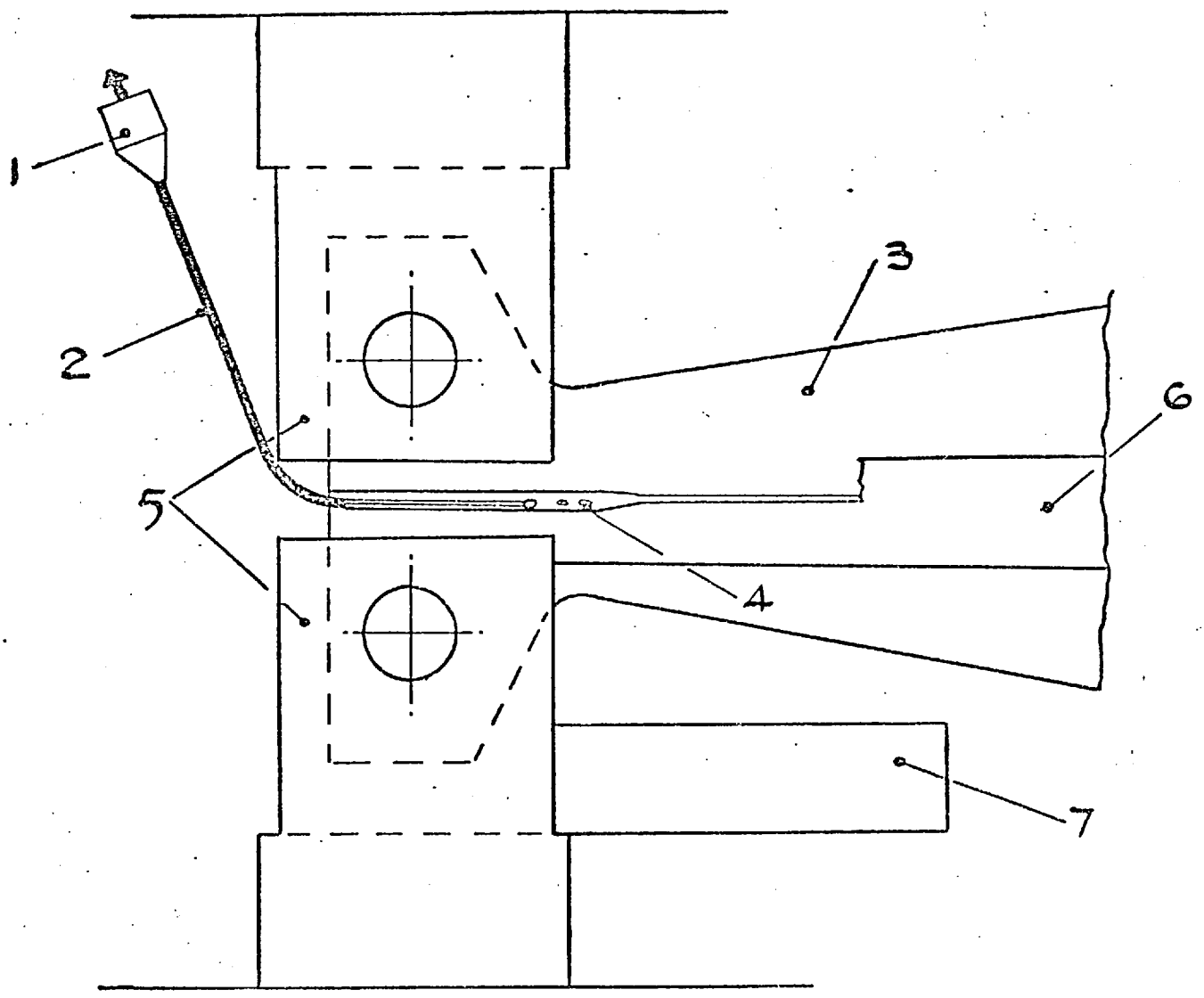


FIG. 10 Loading and Drip Feed Arrangement.

1 - Adaptor to aspirator bottle
2 - Plastic tube
3 - Specimen
4 - Corrodent
5 - Shackles
6 - Plastic tape
7 - Drip tray

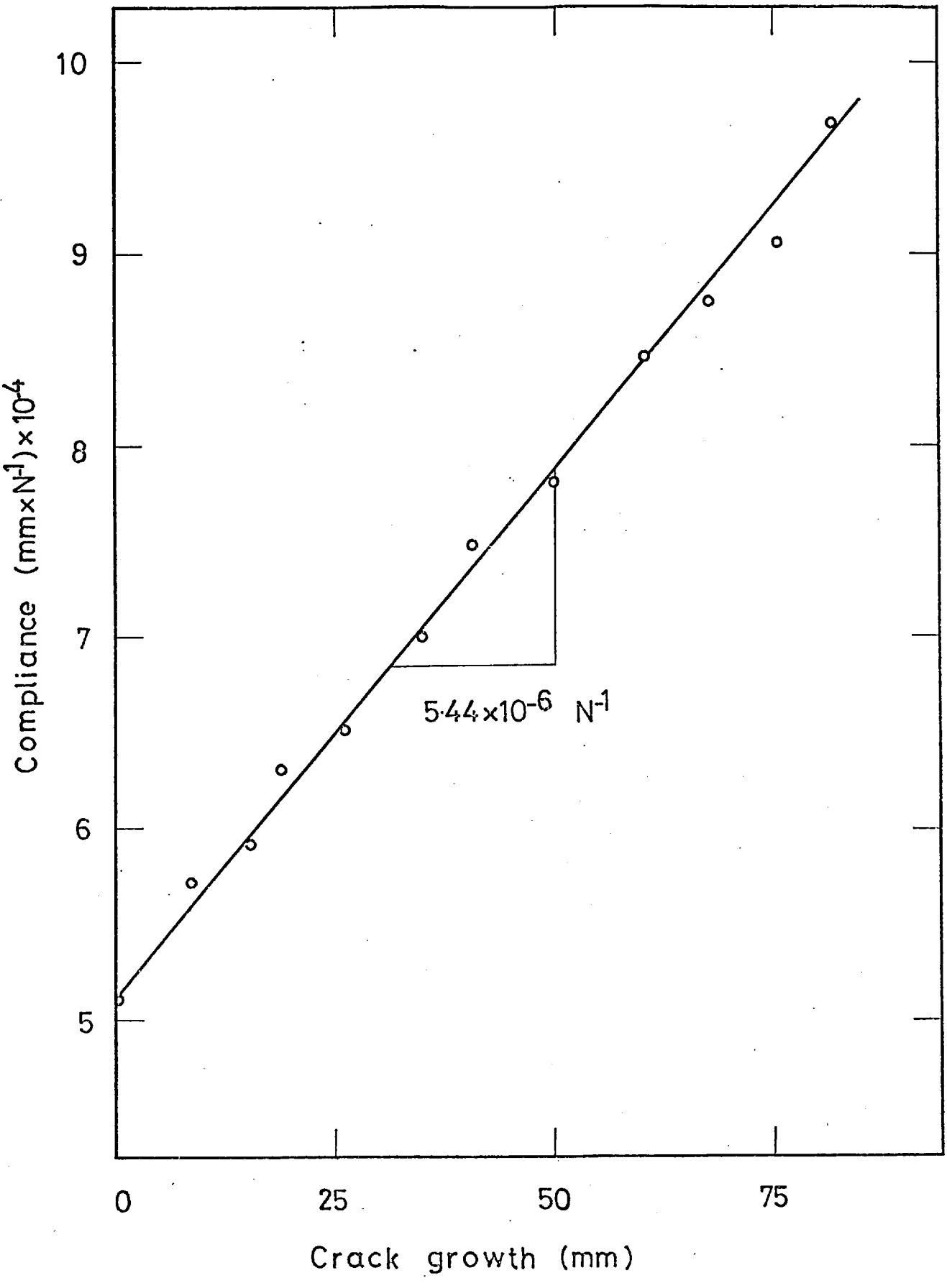


FIG. 11 Typical Compliance vs. Crack Growth Curve. BS15. Laboratory air

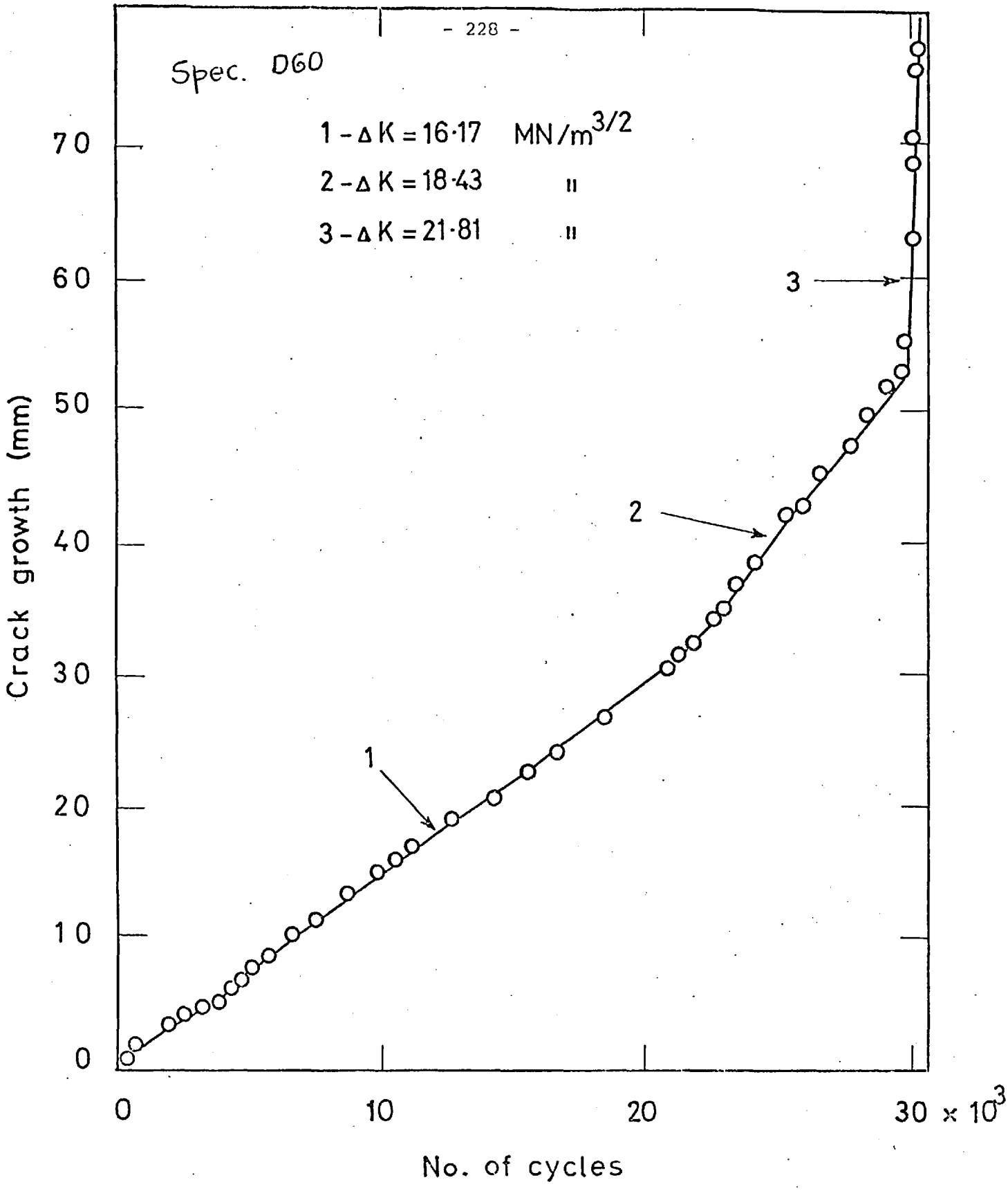


FIG. 12 Crack Growth Pattern at Different Values of ΔK for R = 0. RR58. Laboratory air. 0.15 Hz

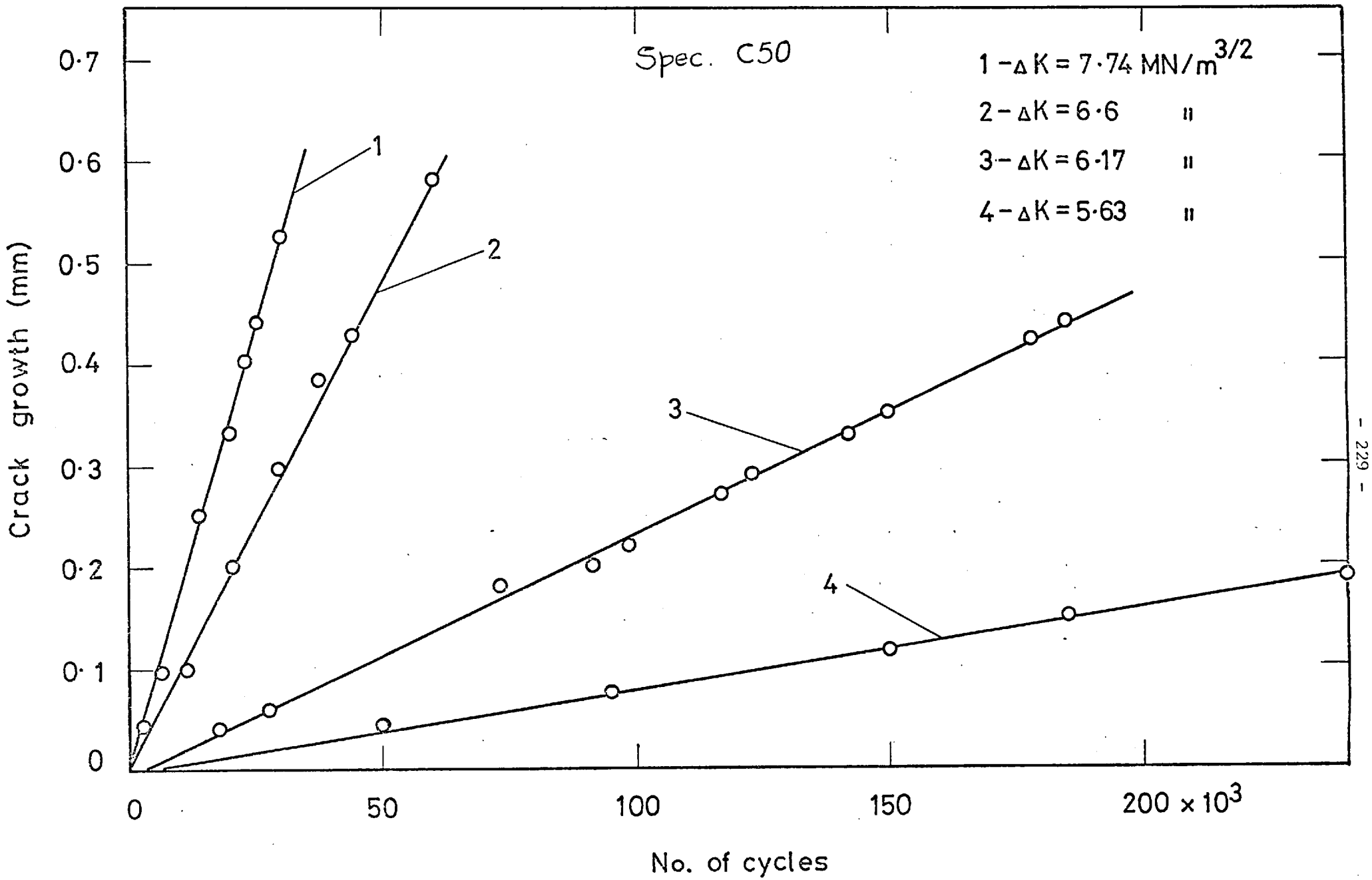


FIG. 13 Crack Growth Pattern at Different low ΔK values for R = 0. RR58. Laboratory air. 0.15 Hz

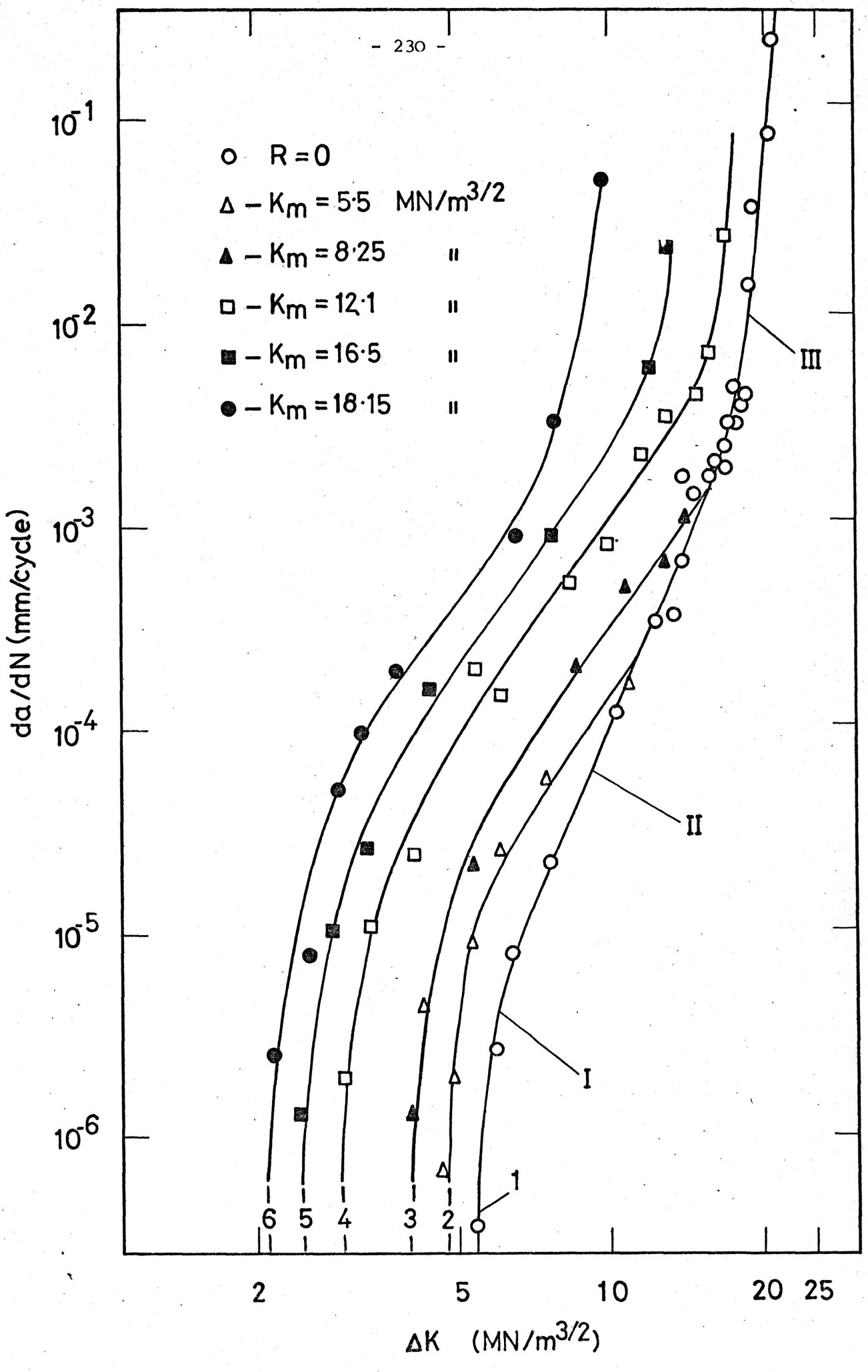


FIG. 14 Crack Growth Rate vs. ΔK. RR58. Laboratory air. 0.15 Hz

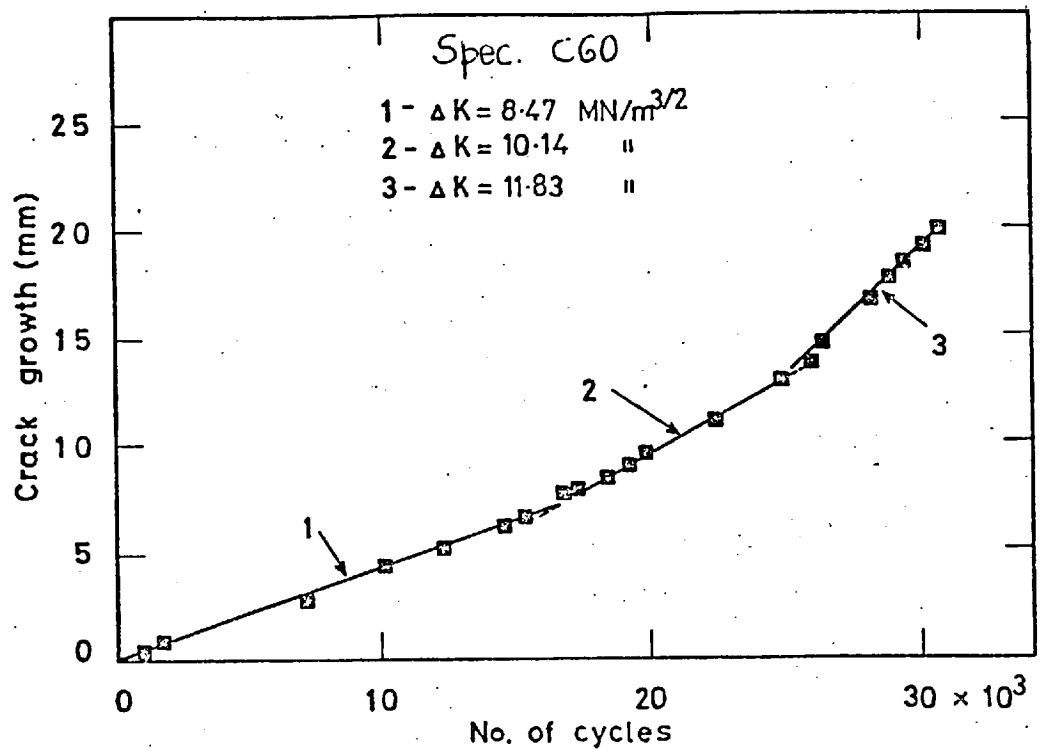


FIG. 15 Crack Growth Pattern at a Constant Value of K_m=12.1 MN/$m^{3/2}$.

RR58.Laboratory air. 0.15 Hz

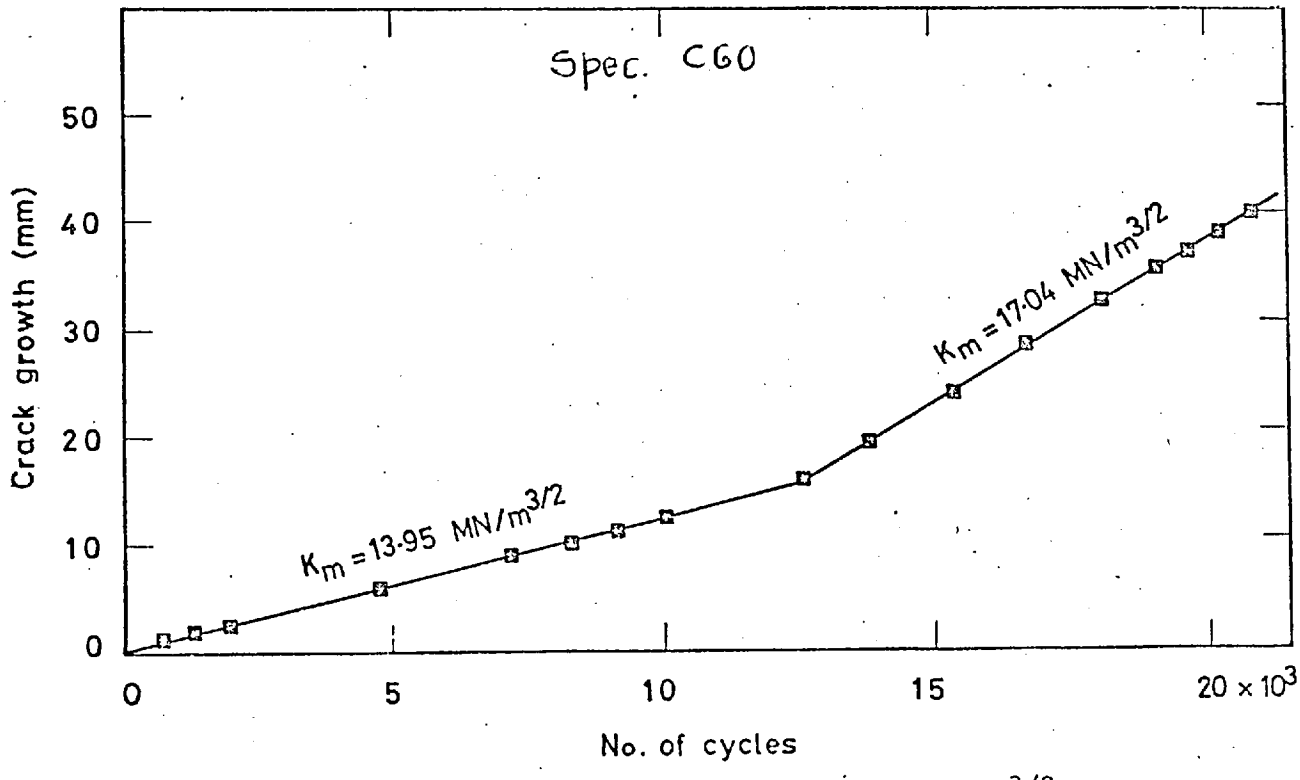


FIG. 16 Crack Growth Pattern at a Constant Value of ΔK=8MN/$m^{3/2}$.

RR58. Laboratory air. 0.15 Hz

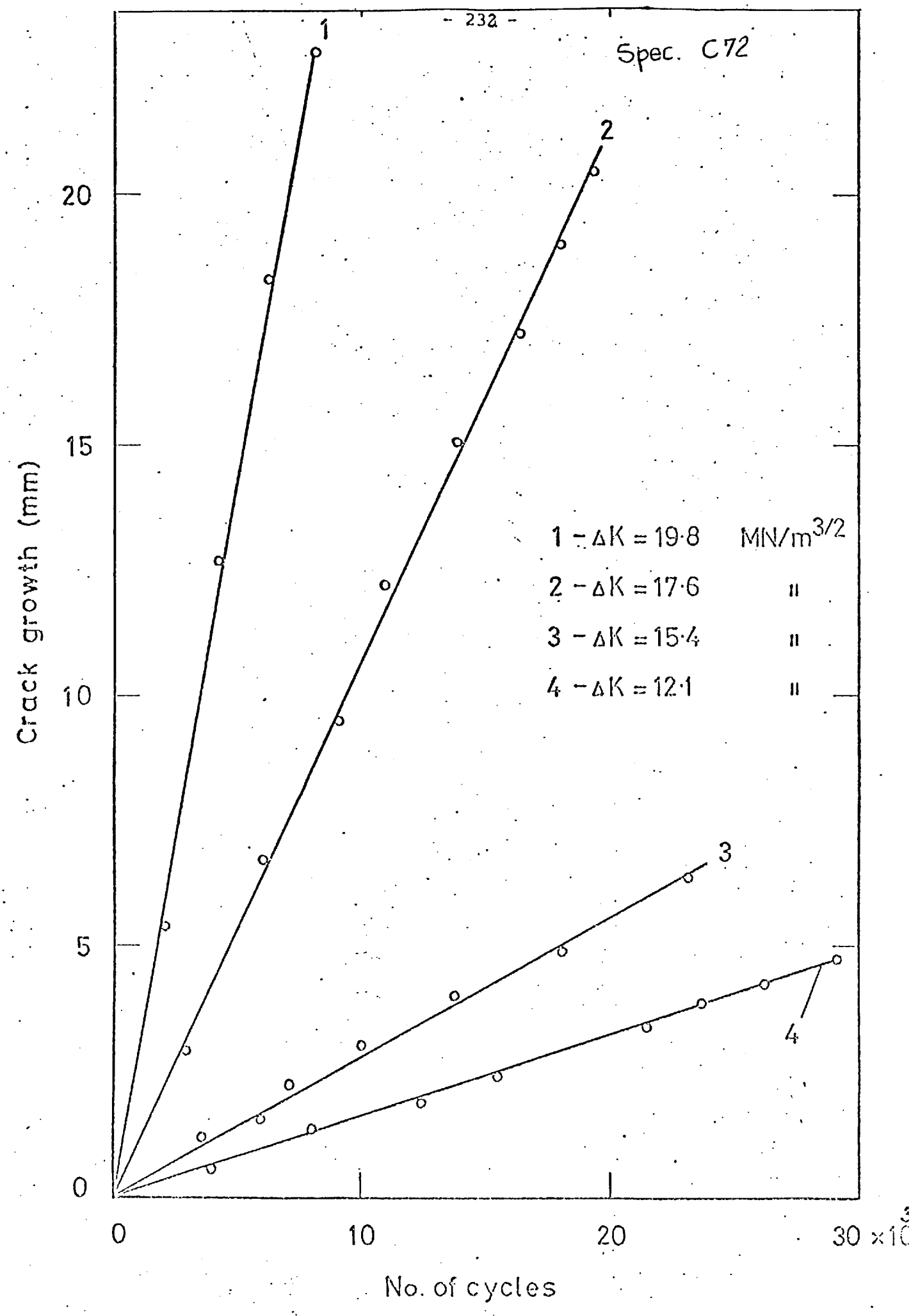


FIG. 17 Crack Growth Pattern at a Constant Value of K_m = 12.1 MN/m$^{3/2}$. RR58.

Laboratory air. 35 Hz

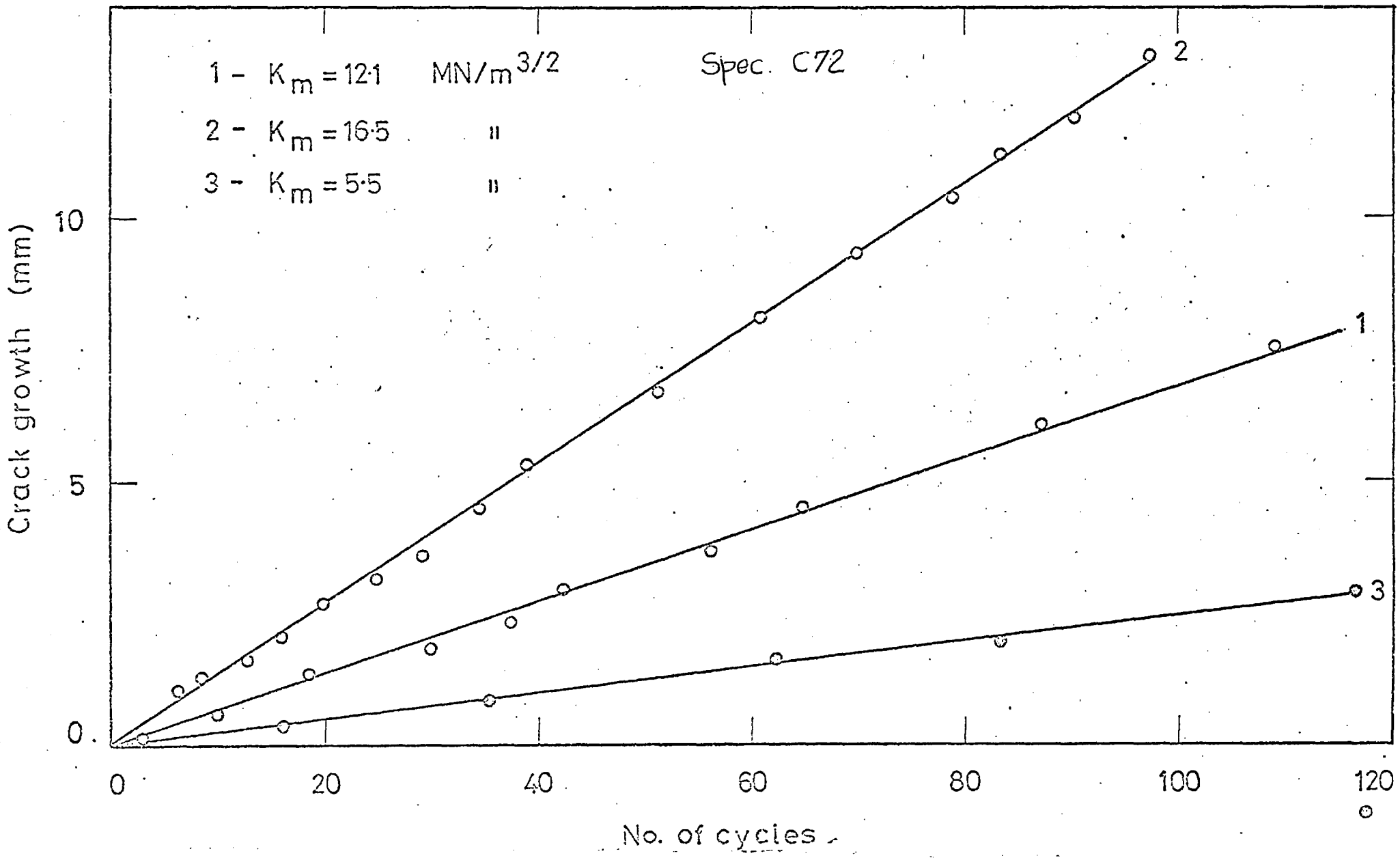


FIG. 18 Crack Growth Pattern at a Constant Value of ΔK = 6.6 MN/m$^{3/2}$.

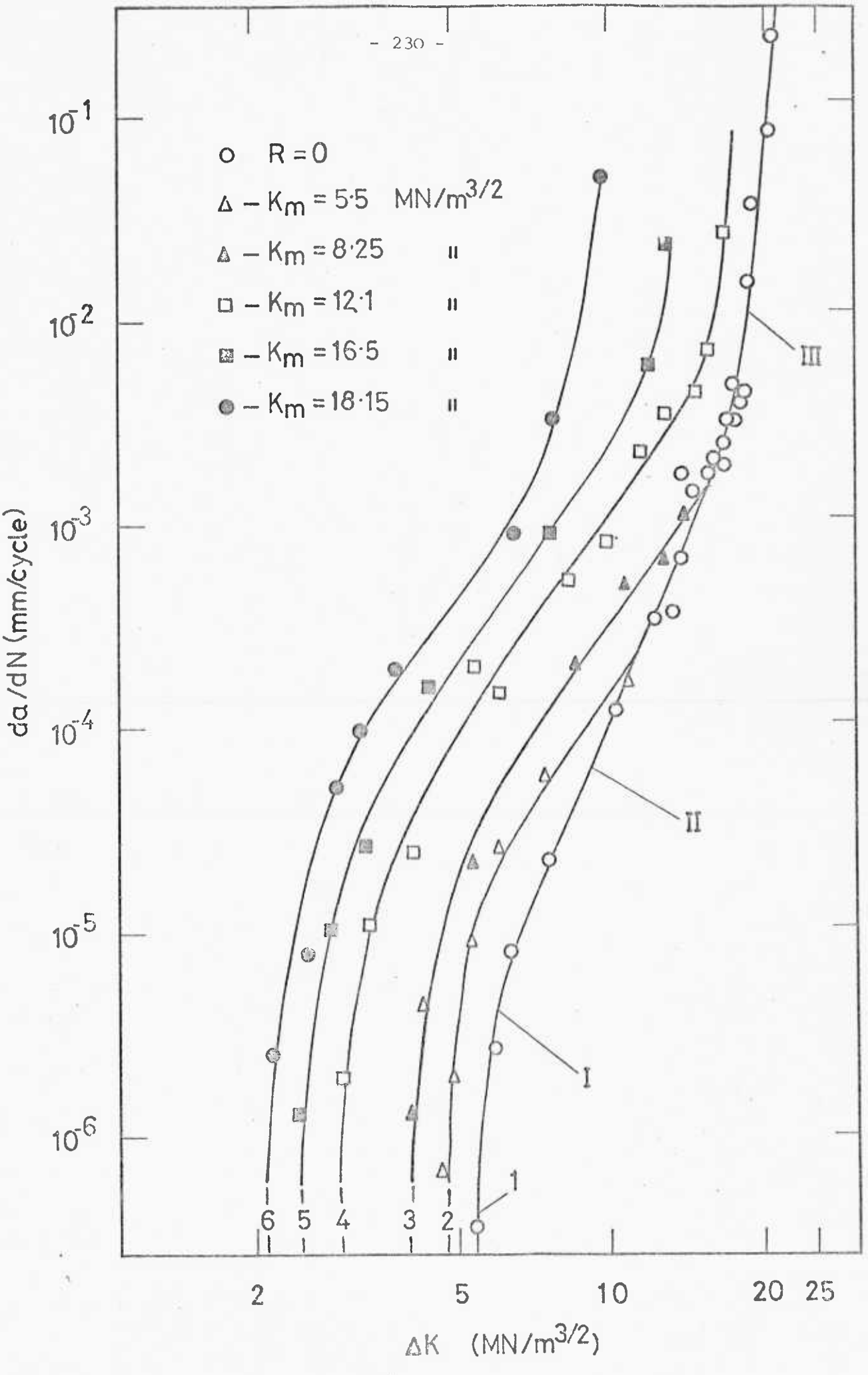


FIG. 14 Crack Growth Rate vs. ΔK. RR58. Laboratory air. 0.15 Hz

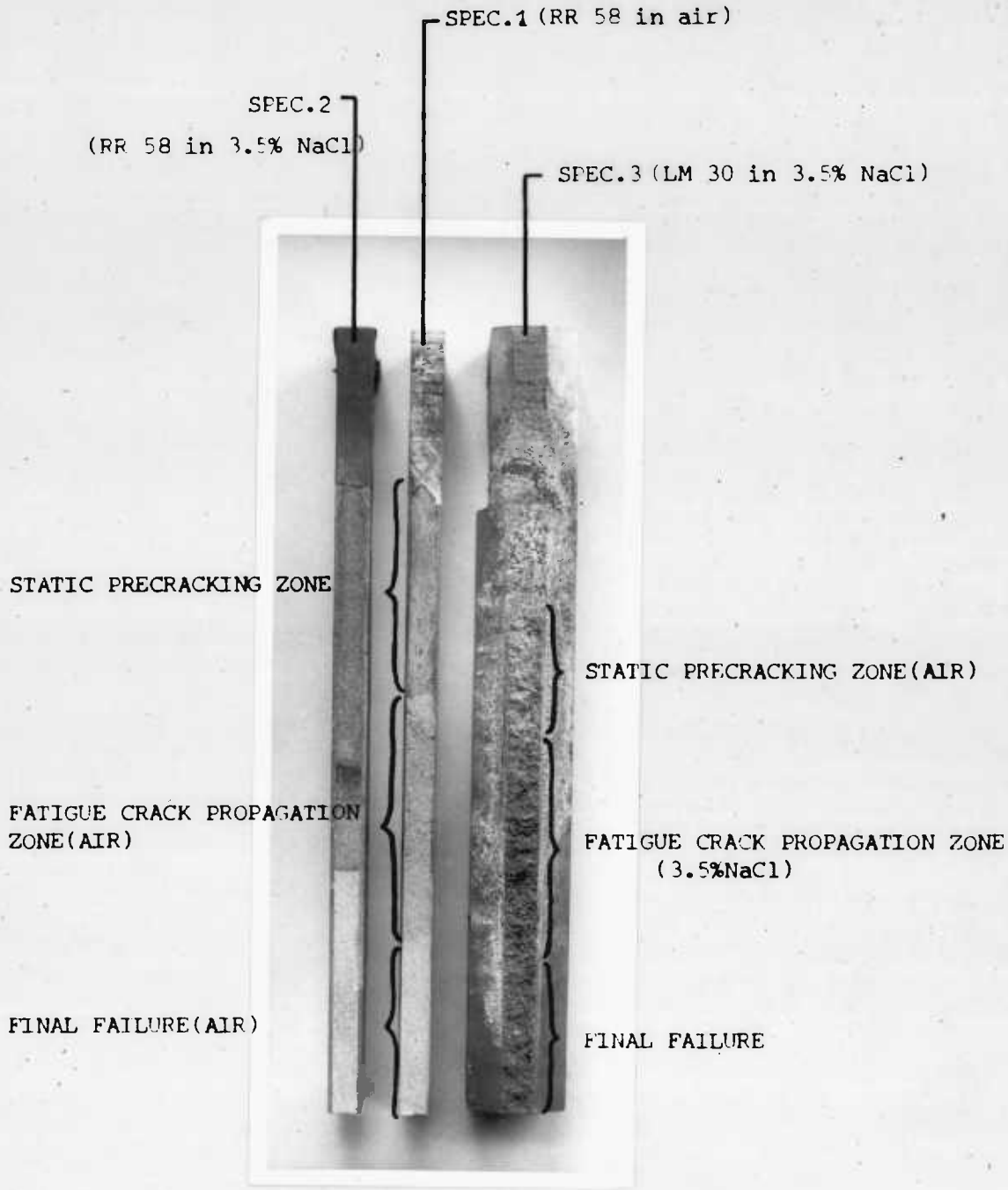


FIG. 20 Macroscopic Fracture Surface Appearance of the DCB Specimens



FIG. 20 Macroscopic Fracture Surface Appearance of the DCB Specimens

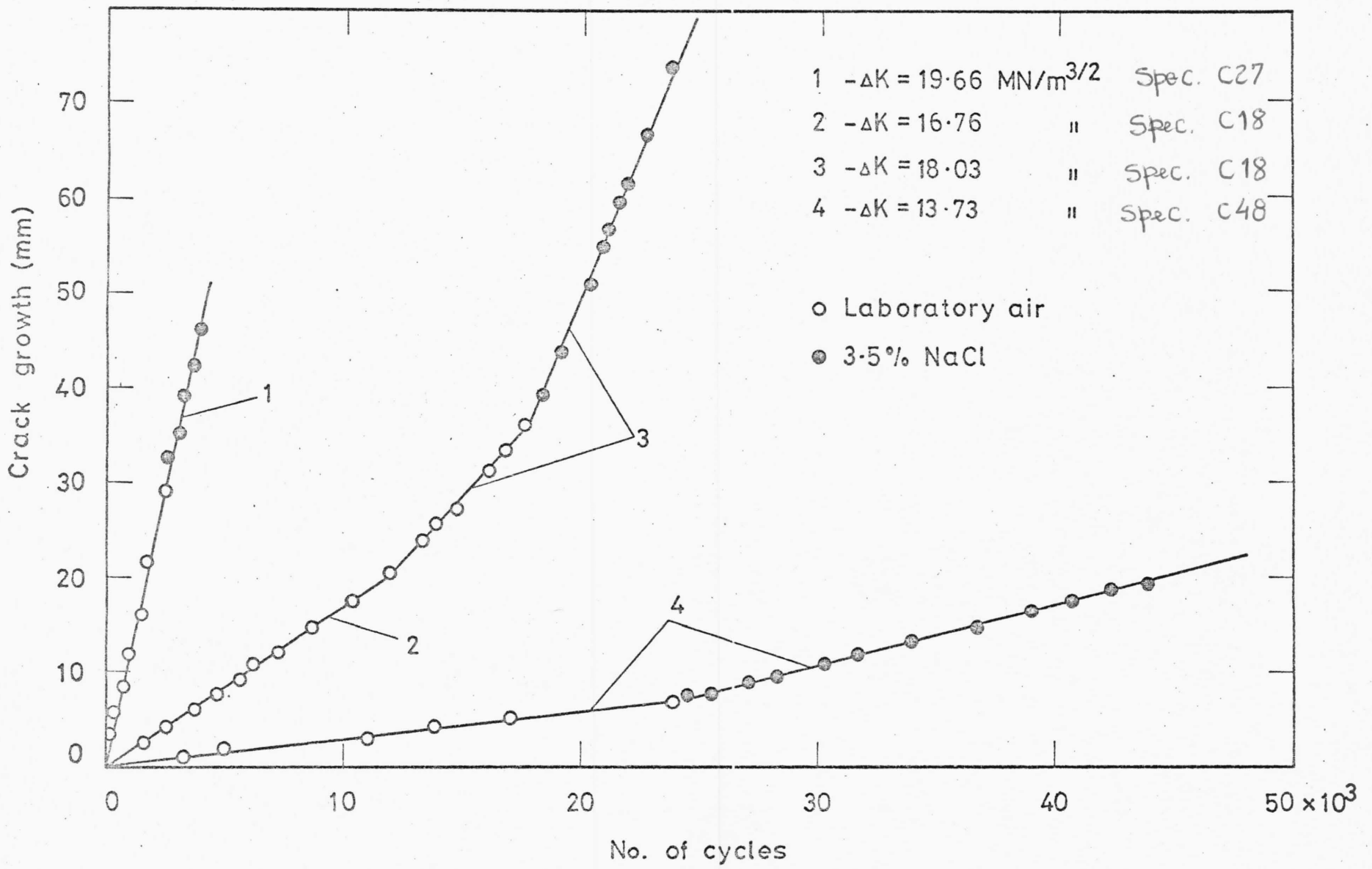


FIG. 21 Crack Growth Pattern at Different Values of ΔK for R = 0. RR58. Laboratory air and 3.5% NaCl. 0.15 Hz

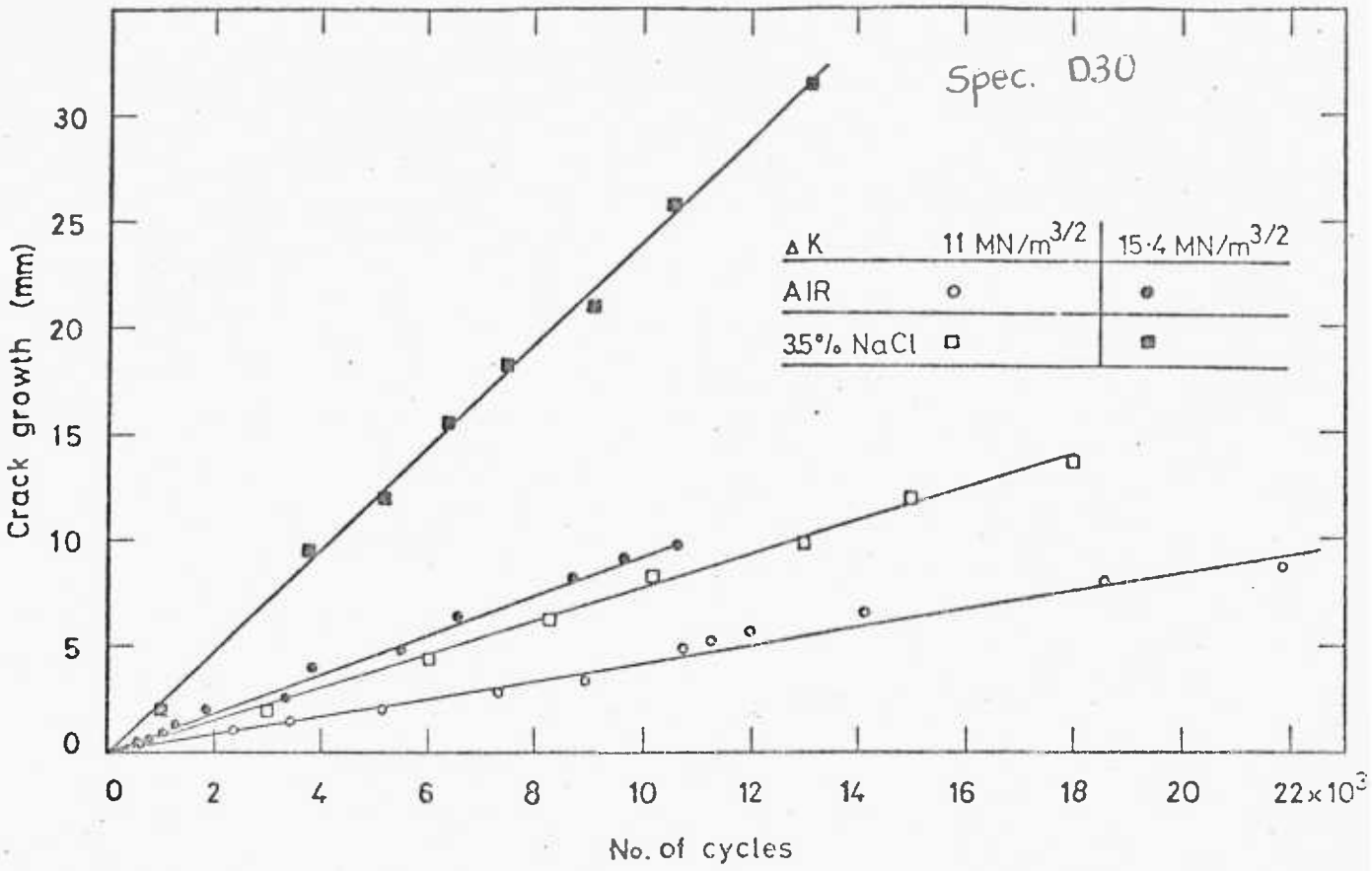


FIG. 22 Crack Growth Pattern at a Constant Value of K_m = 8.25 MN/$m^{3/2}$. RR58. Laboratory air and 3.5% NaCl. 0.15 Hz

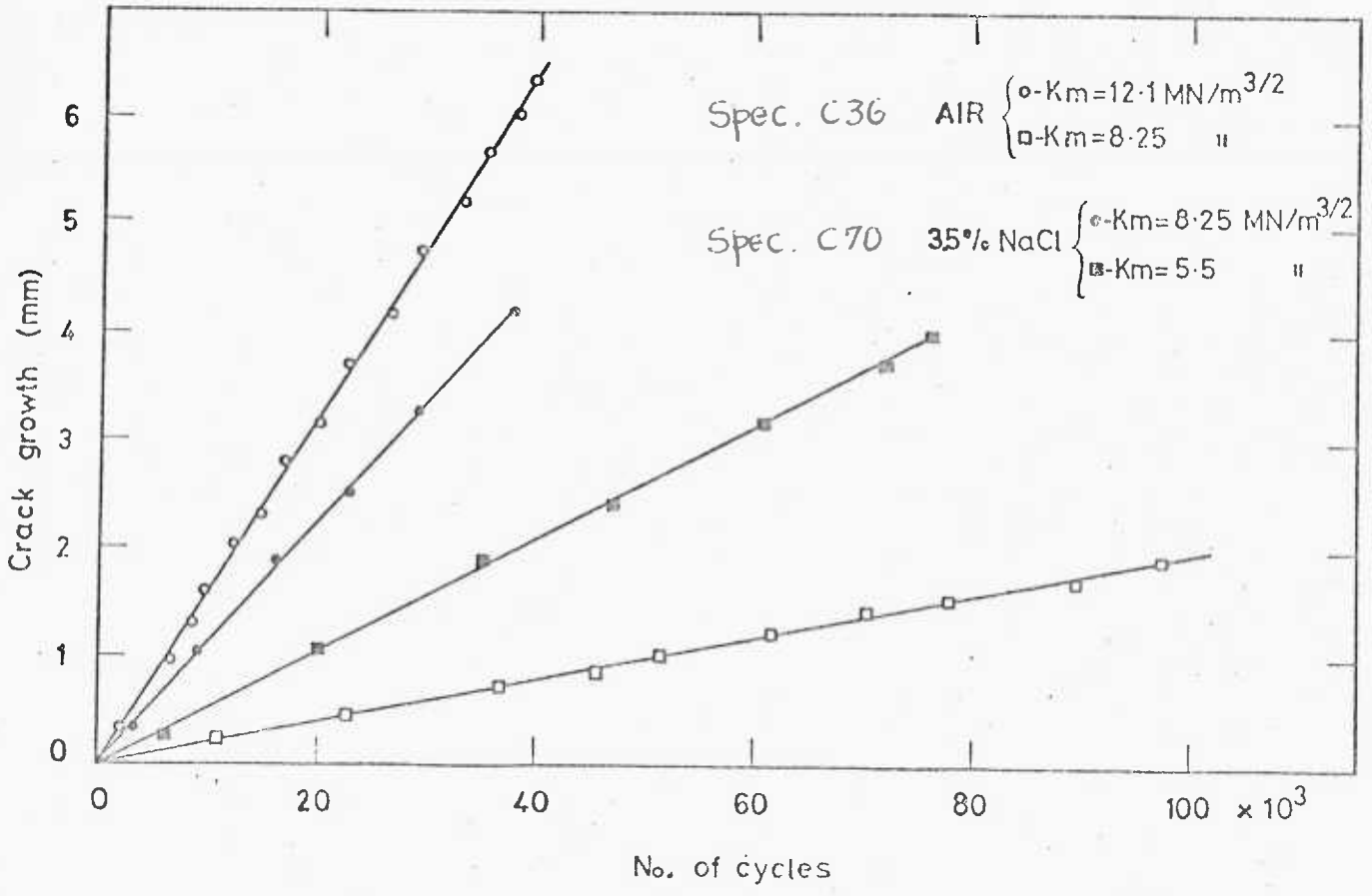


FIG. 23 Crack Growth Pattern at a Constant Value of ΔK = 5.5 MN/$m^{3/2}$. RR58. Laboratory air and 3.5% NaCl. 0.15 Hz

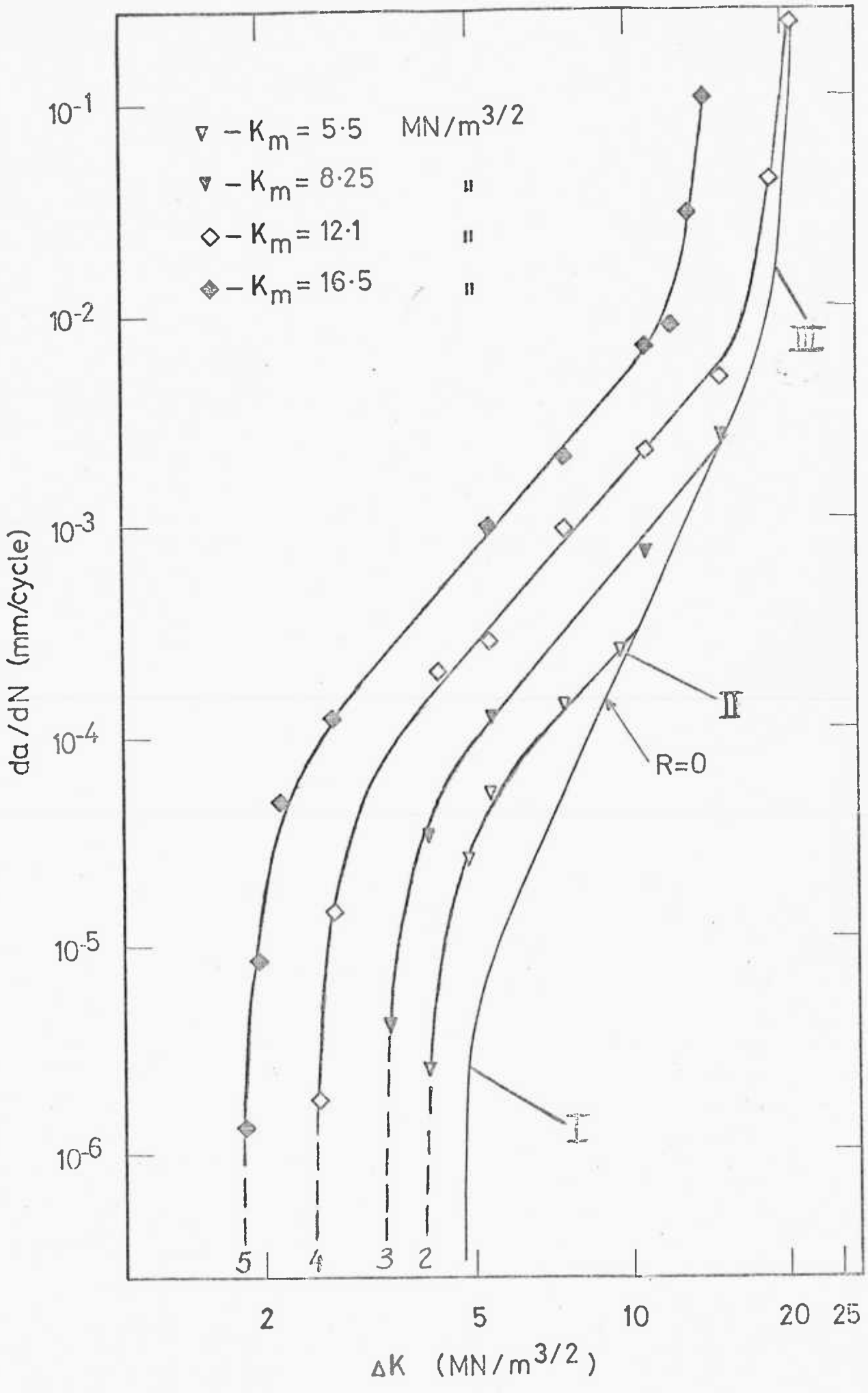


FIG. 24 Crack Growth Rate vs. ΔK. RR58, 3.5% NaCl. 0.15 Hz

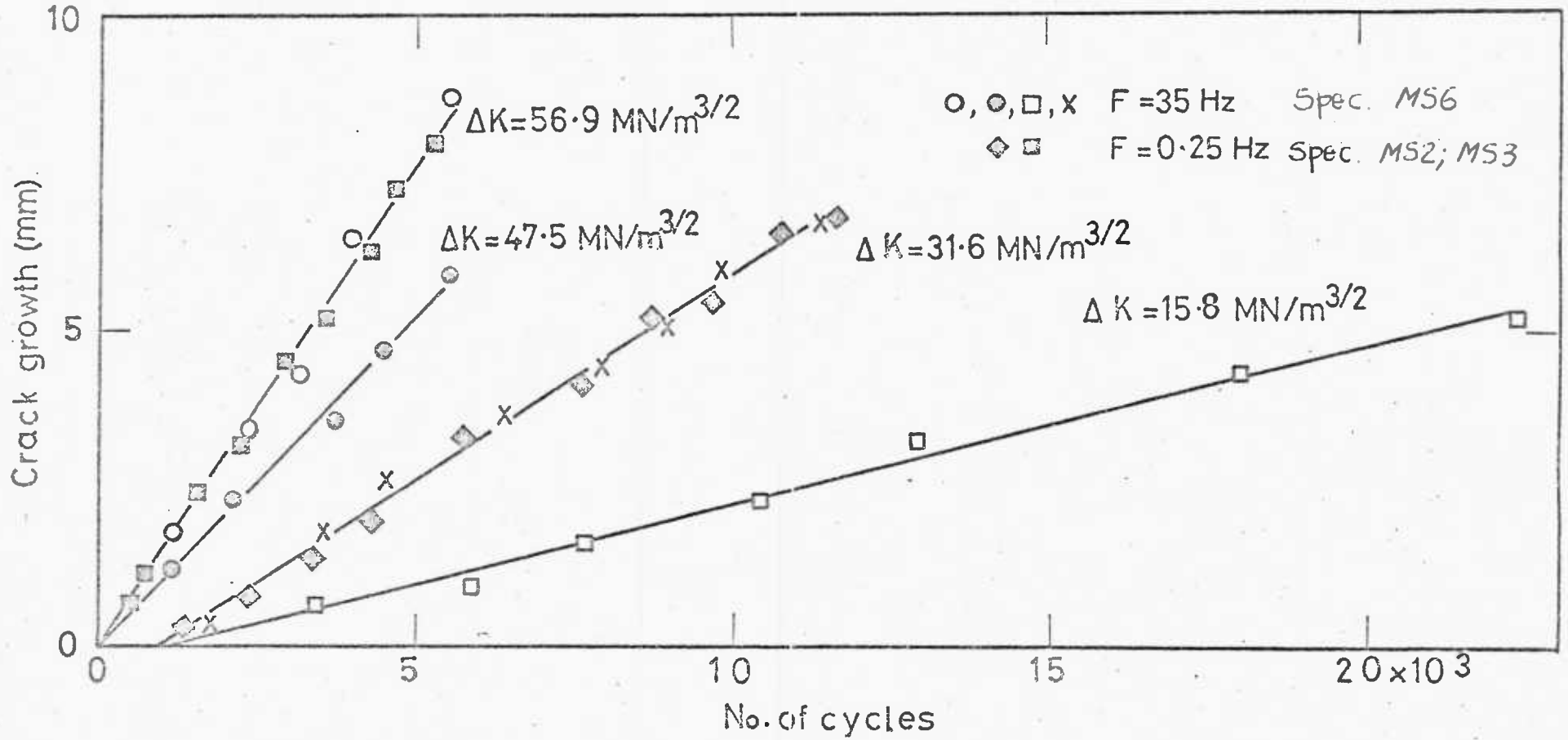


FIG. 25 Crack Growth Pattern at a Constant Value of K_m=31.6 MN/m$^{3/2}$. BS15. Laboratory air. 0.25 and 35 Hz

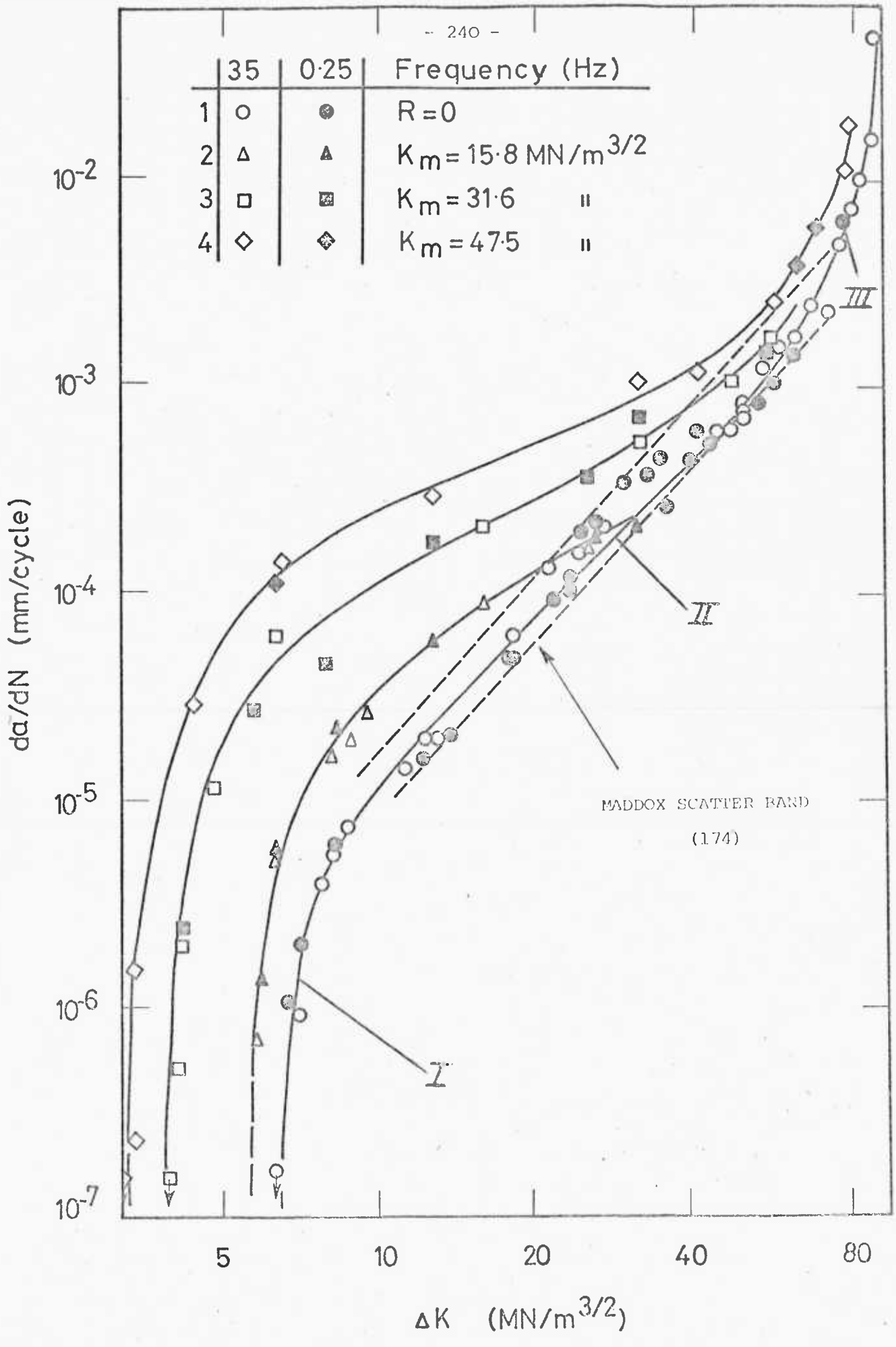


FIG. 26 Crack Growth Rate vs. ΔK. BS15. Laboratory air. 0.25 and 35 Hz

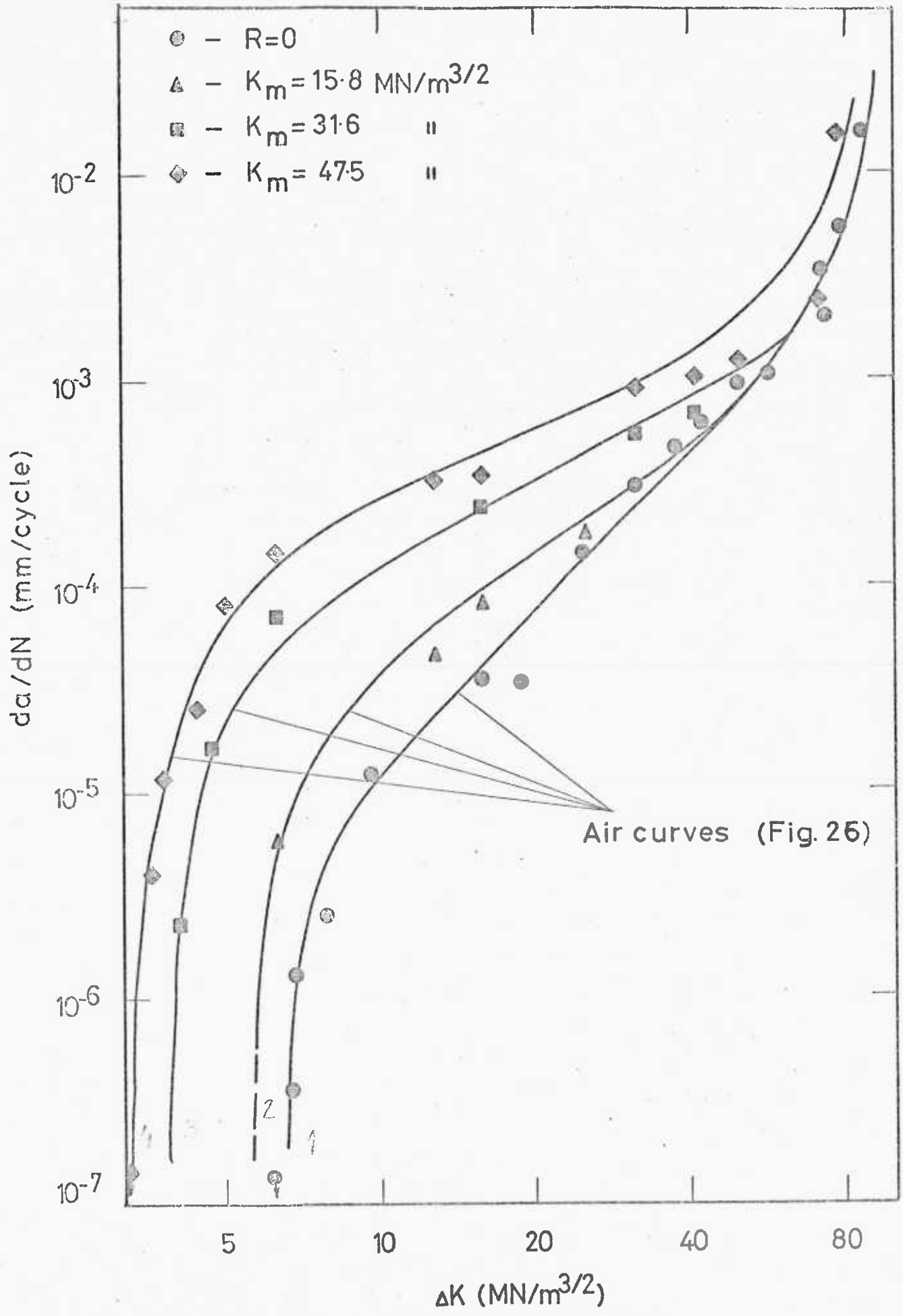


FIG. 27 Crack Growth Rate vs. ΔK. BS15. 3.5% NaCl. 35 Hz

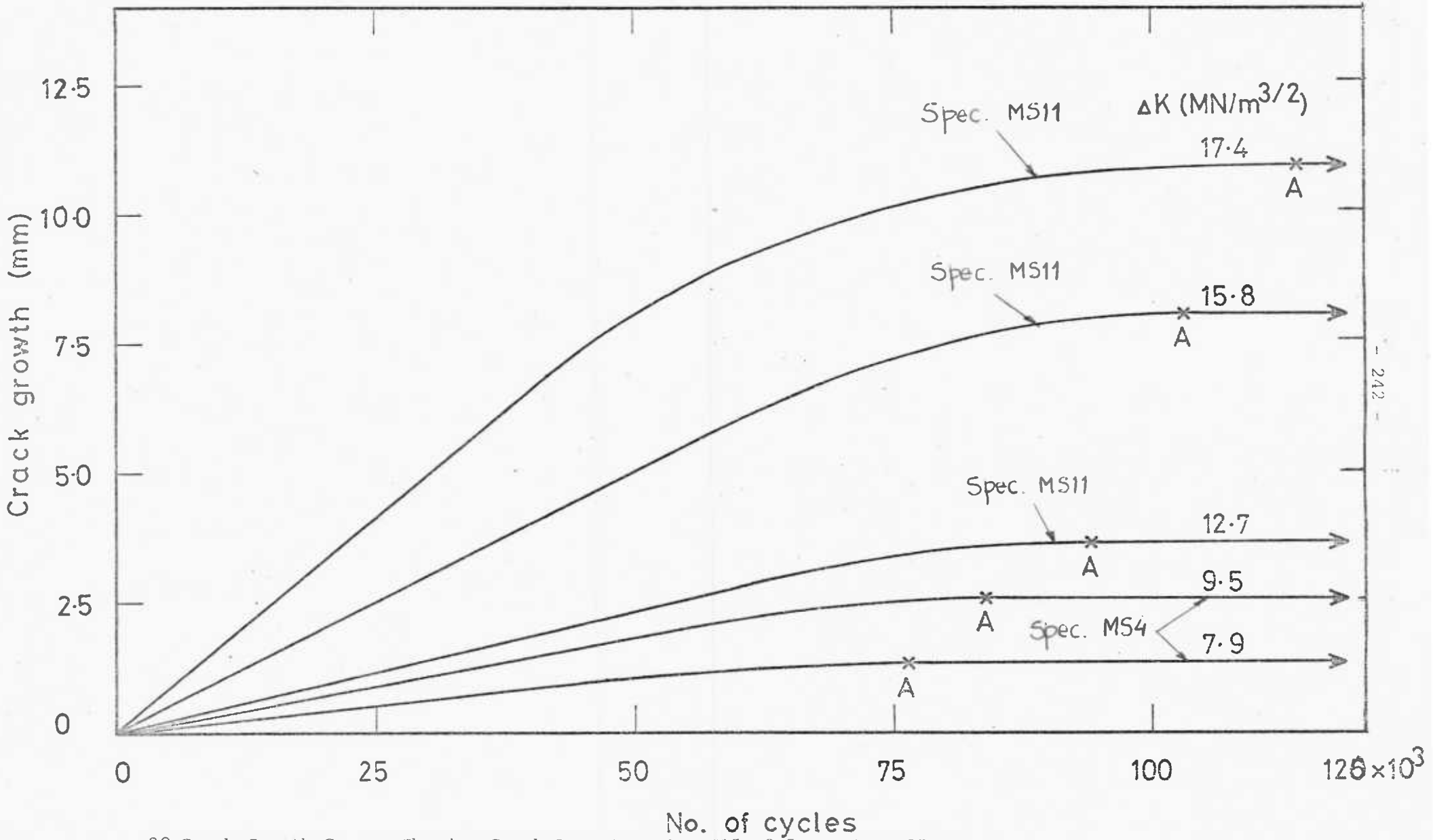


FIG. 28 Crack Growth Curves Showing Crack Arrest. R=O. BS15. 3.5% NaCl. 0.25 Hz

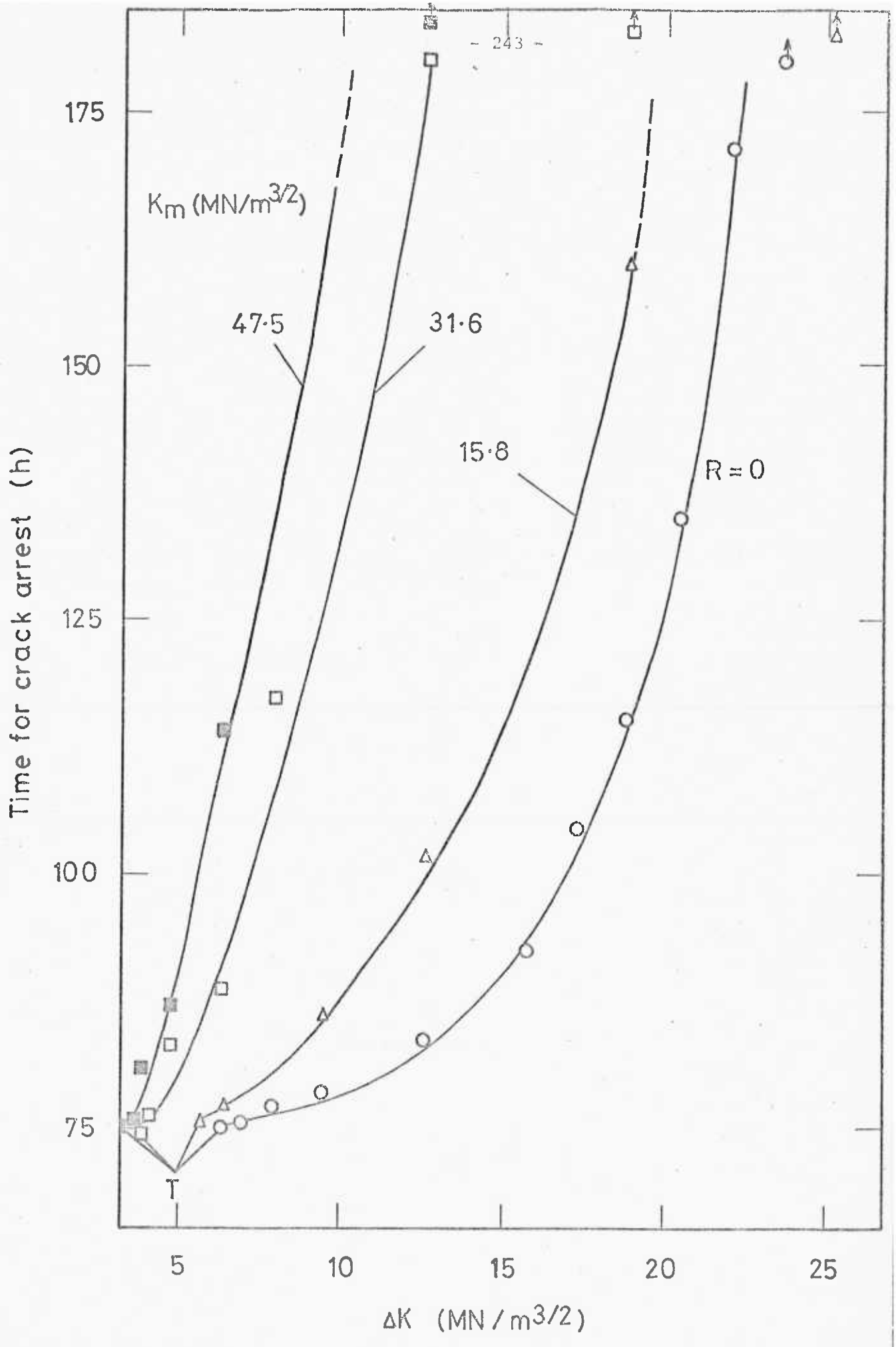


FIG. 29 Time for Crack Arrest vs. ΔK. BS15. 3.5% NaCl. 0.25 Hz

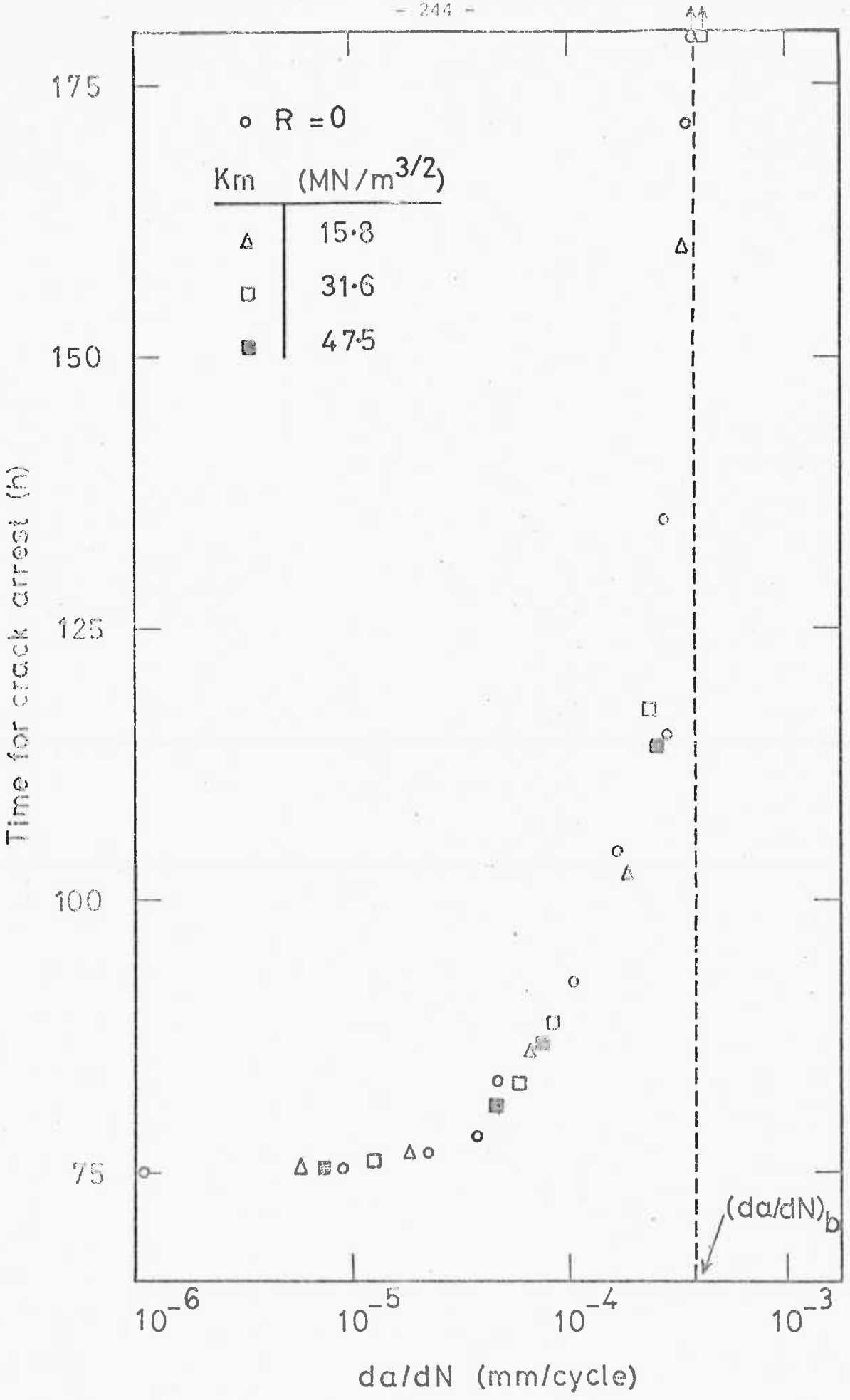


FIG. 30 Time for Crack Arrest vs. Crack Growth Rate for an Initially Sharp Crack. BS15. 3.5% NaCl. 0.25 Hz

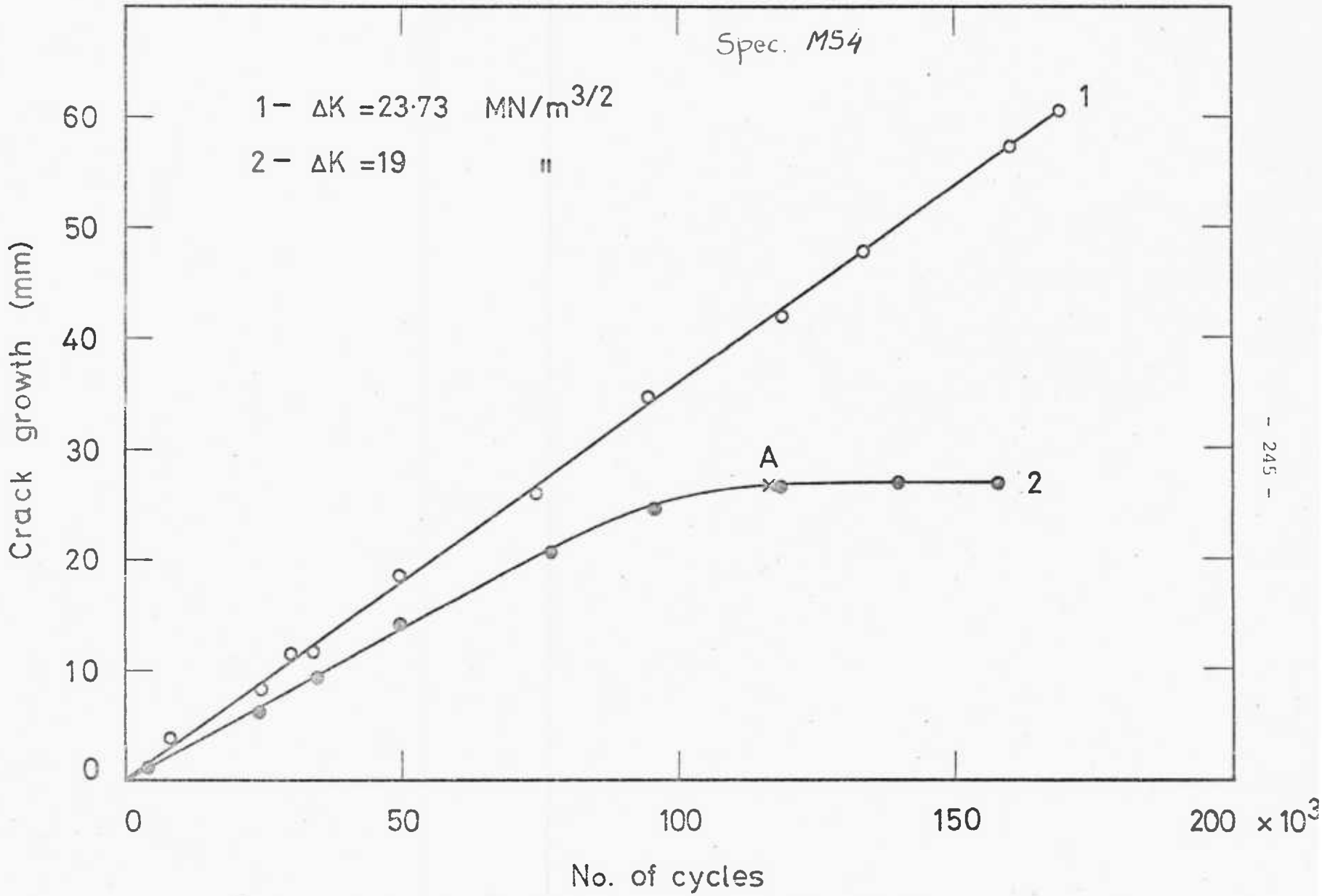


FIG. 31 Crack Growth Curves Showing Crack Arrest and Continous Propagation. BS15. 3.5% NaCl. 0.25 Hz

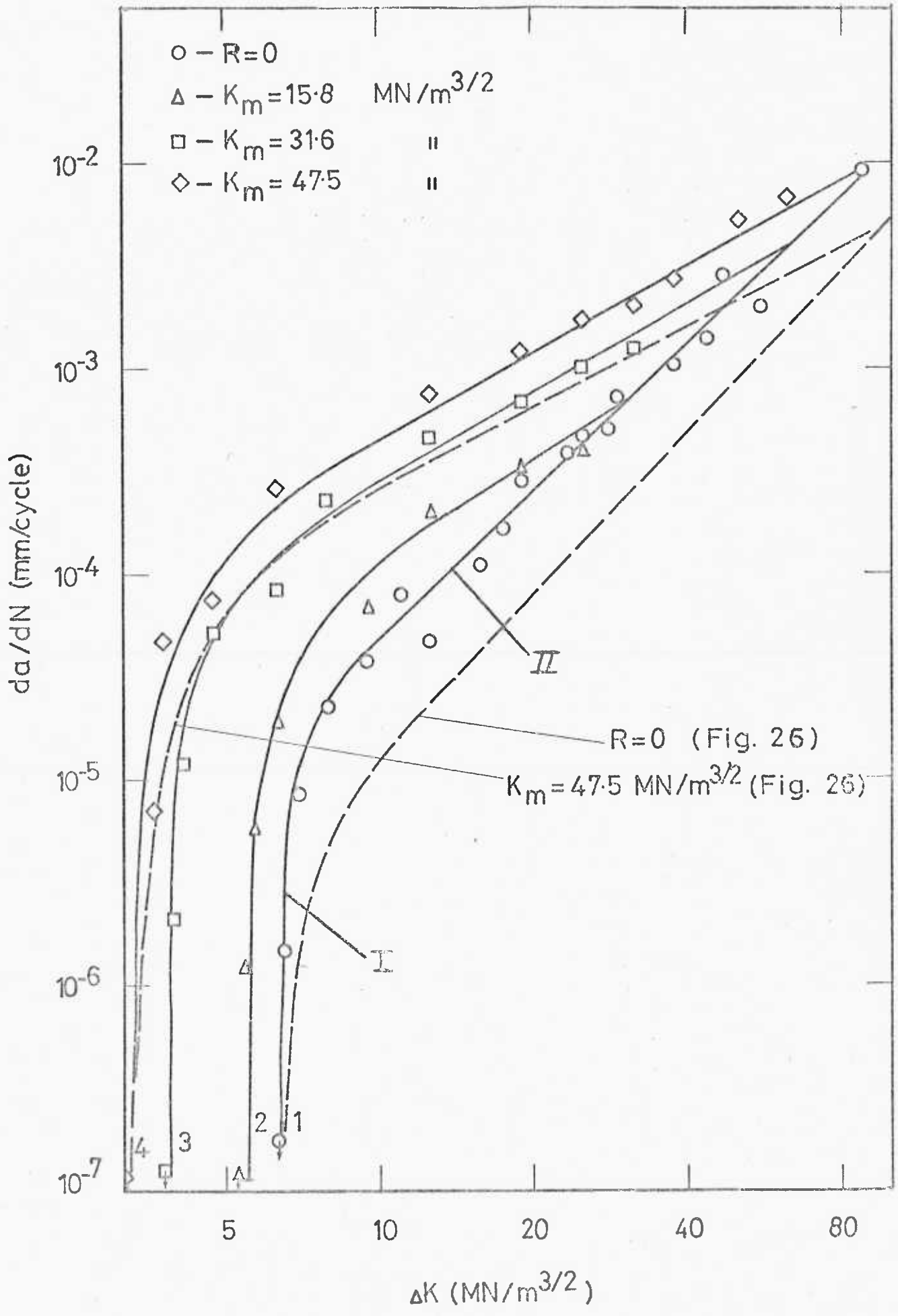


FIG. 32 Crack Growth Rate vs. ΔK. BS15. Laboratory air and 3.5% NaCl. 0.25 Hz

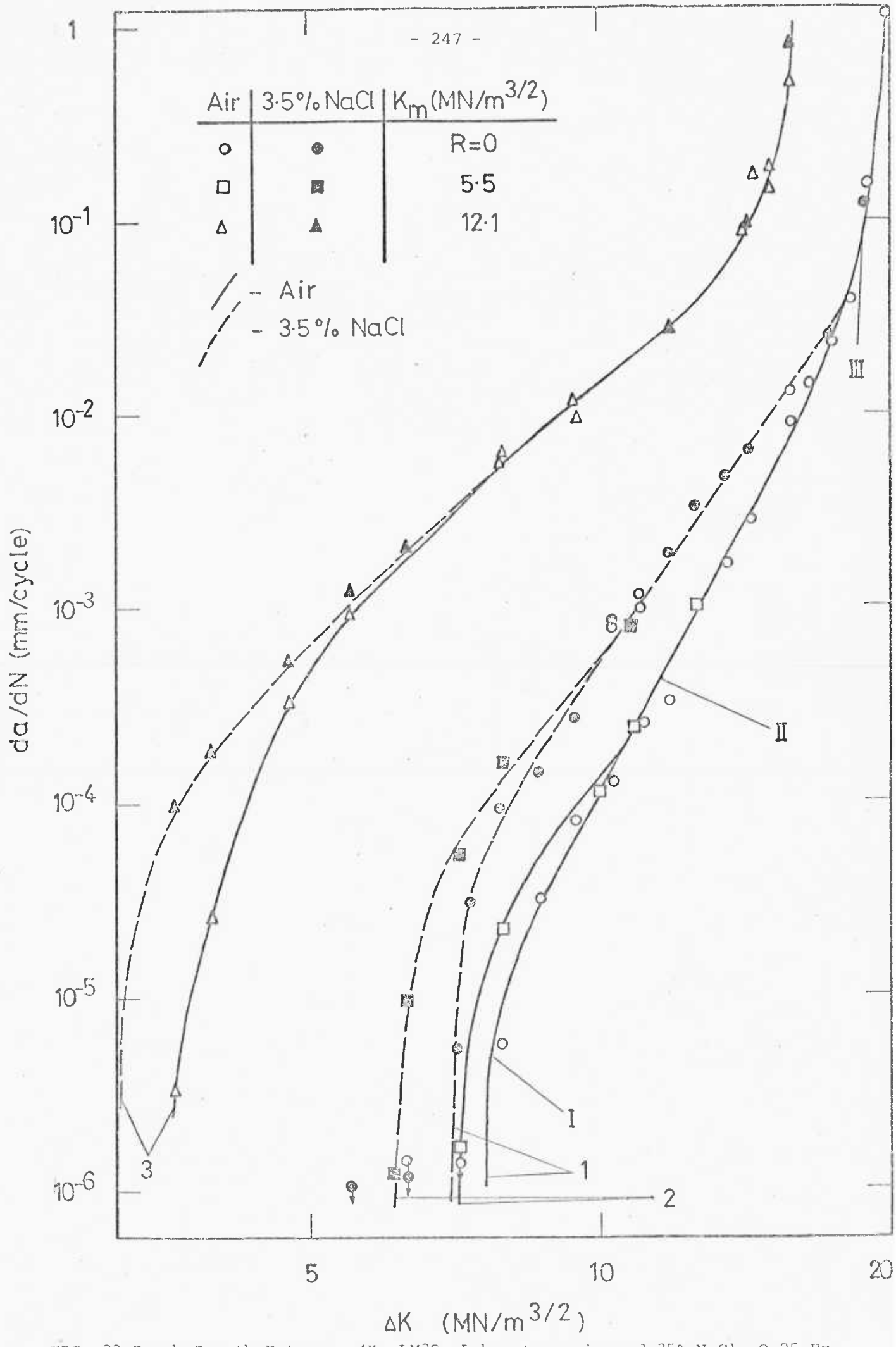


FIG. 33 Crack Growth Rate vs. ΔK. LM30. Laboratory air and 35% NaCl. 0.25 Hz

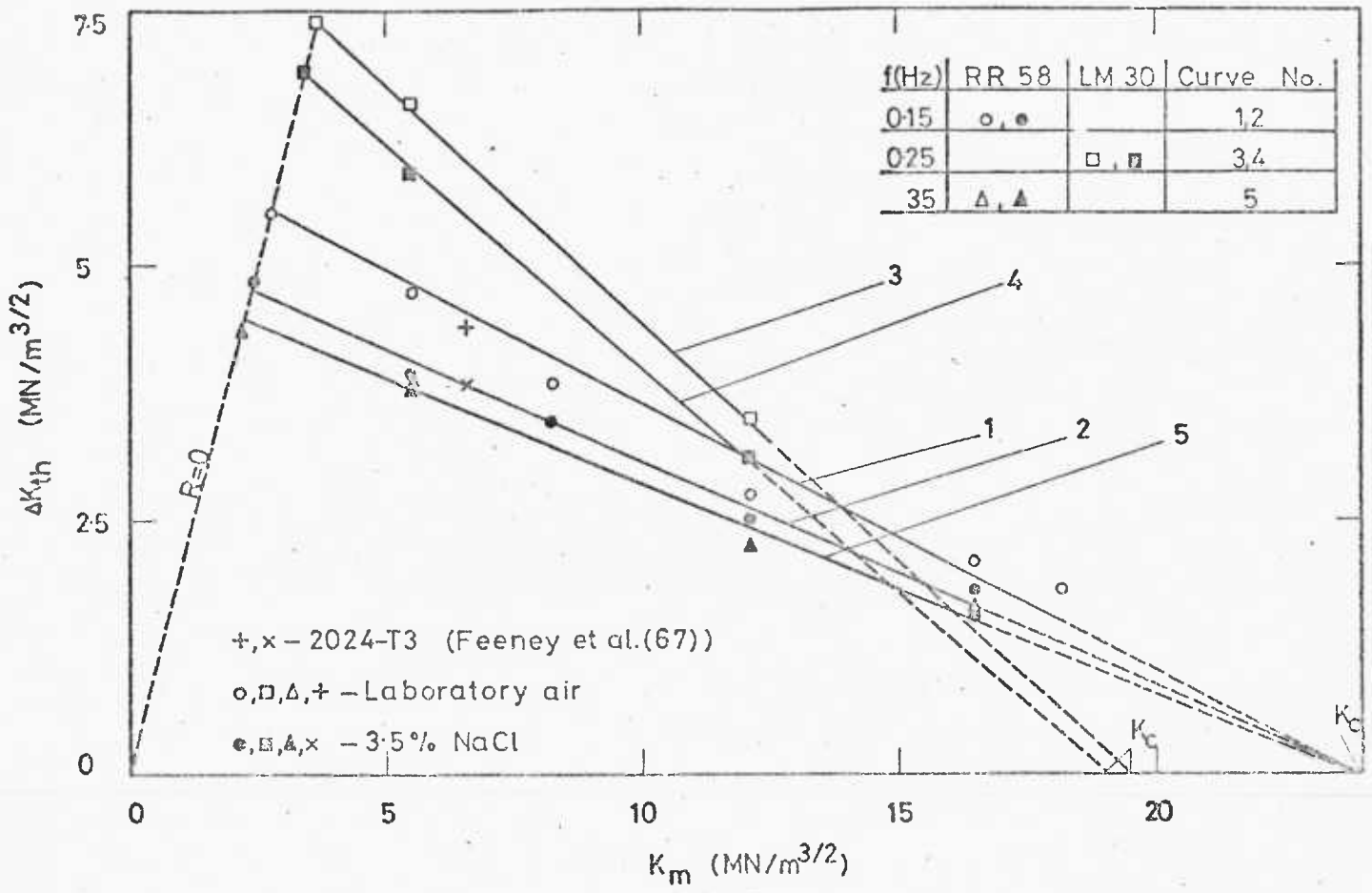


FIG. 34 Threshold Value of ΔK vs. K_m. RR58 and LM30. Laboratory air and 3.5% NaCl. 0.15, 0.25 and 35 Hz

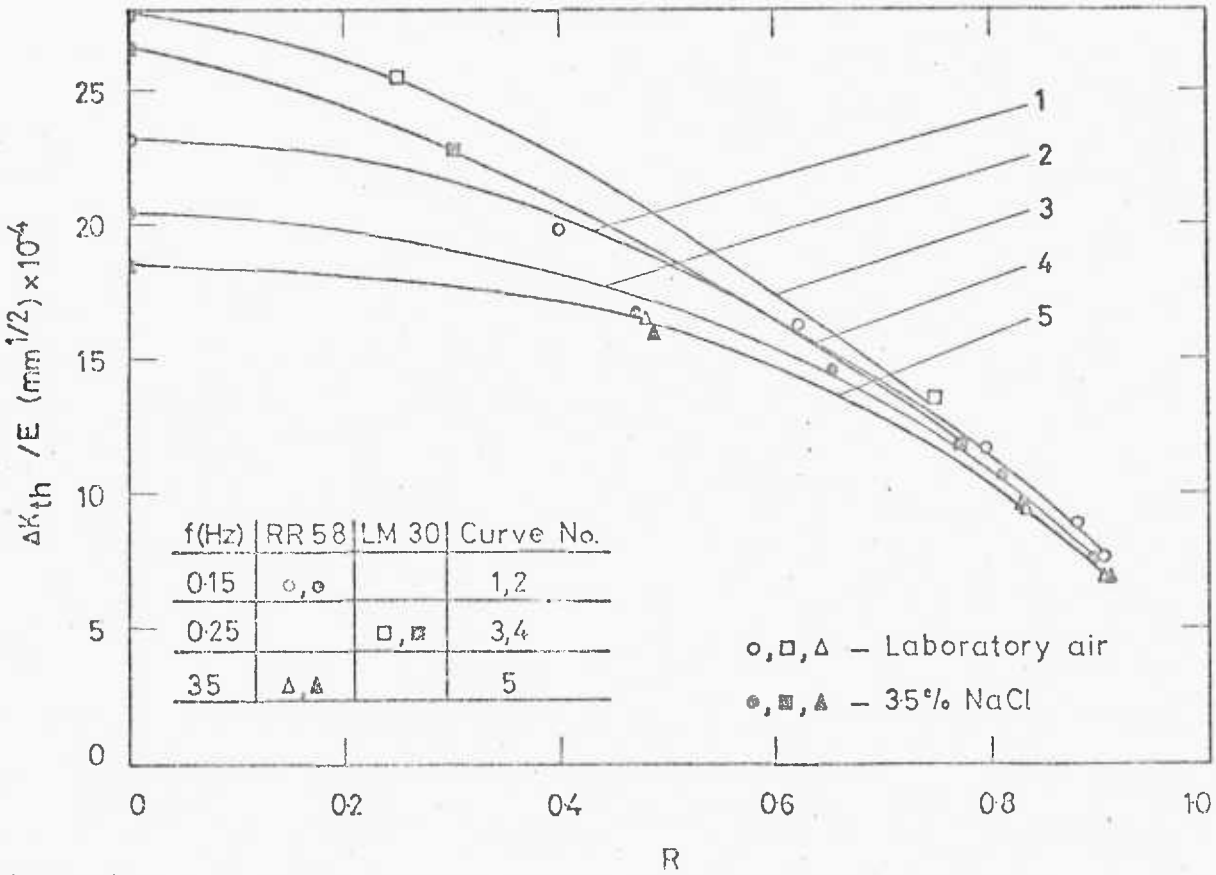


FIG. 35 $\Delta K_{th}/E$ vs. R. RR58 and LM30. Laboratory air and 3.5% NaCl. 0.15, 0.25 and 35 Hz

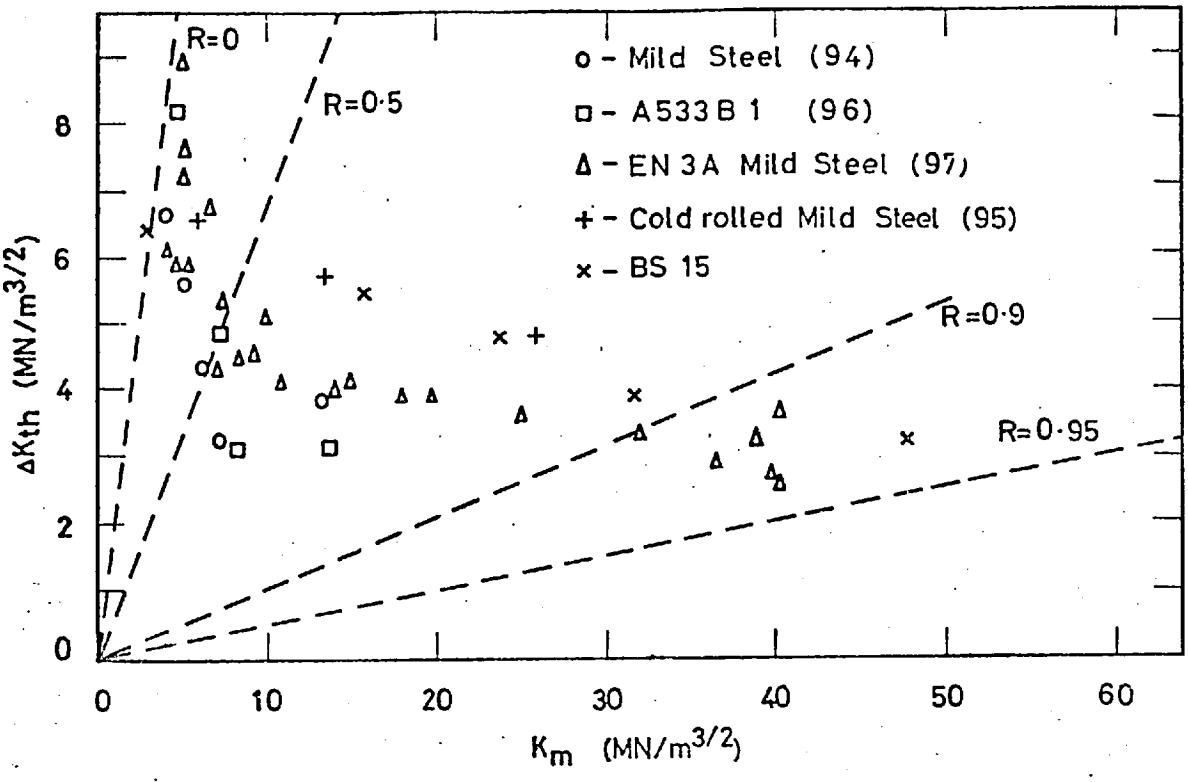


FIG. 36 Threshold Value of ΔK vs. K_m. BS15 and Other Steels. Laboratory air.

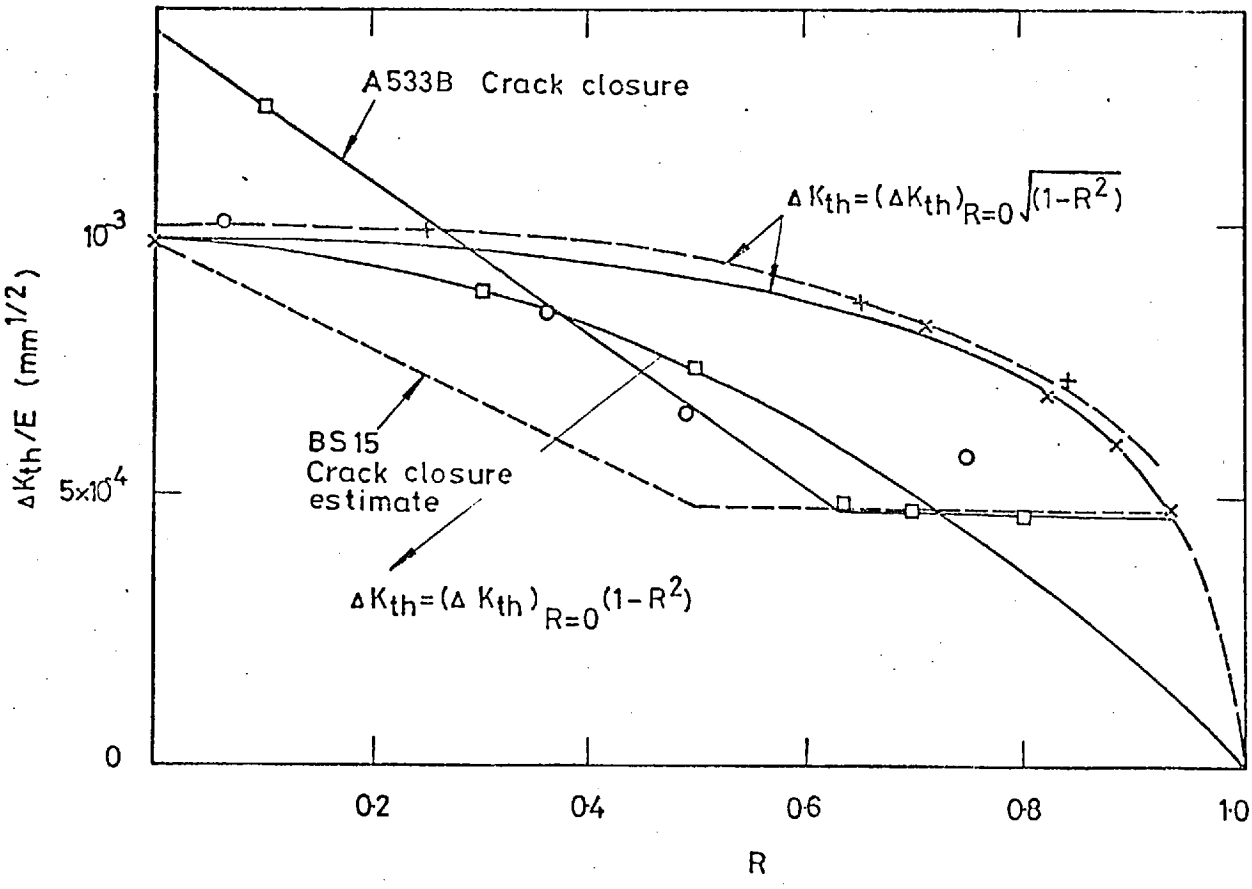


FIG. 37 $\Delta K_{th}/E$ vs. R. BS15 and Other Steels. Laboratory air

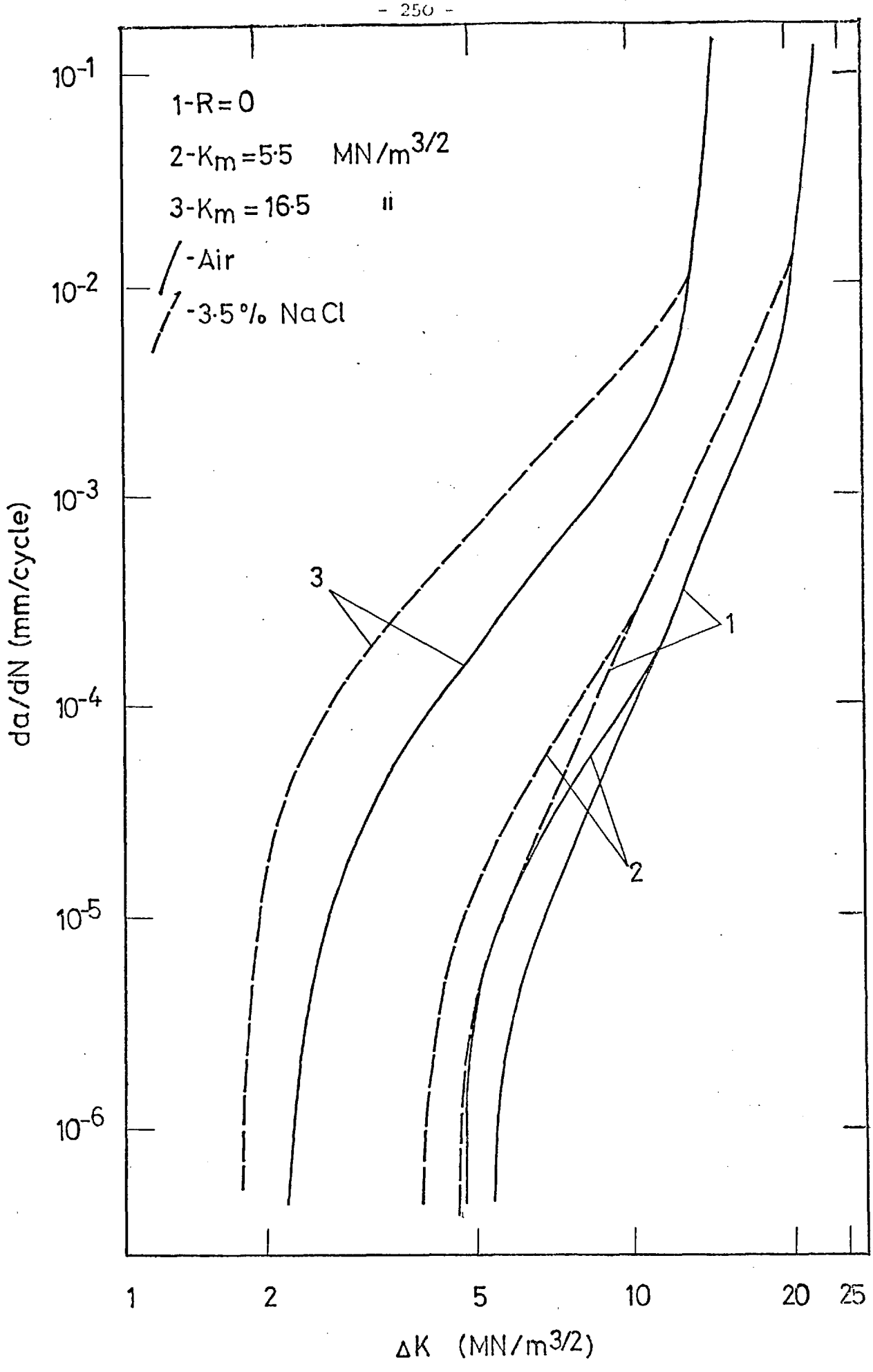


FIG. 38 Crack Growth Rate vs. ΔK Curves. RR58. Laboratory air and 3.5% NaCl 0.25 Hz

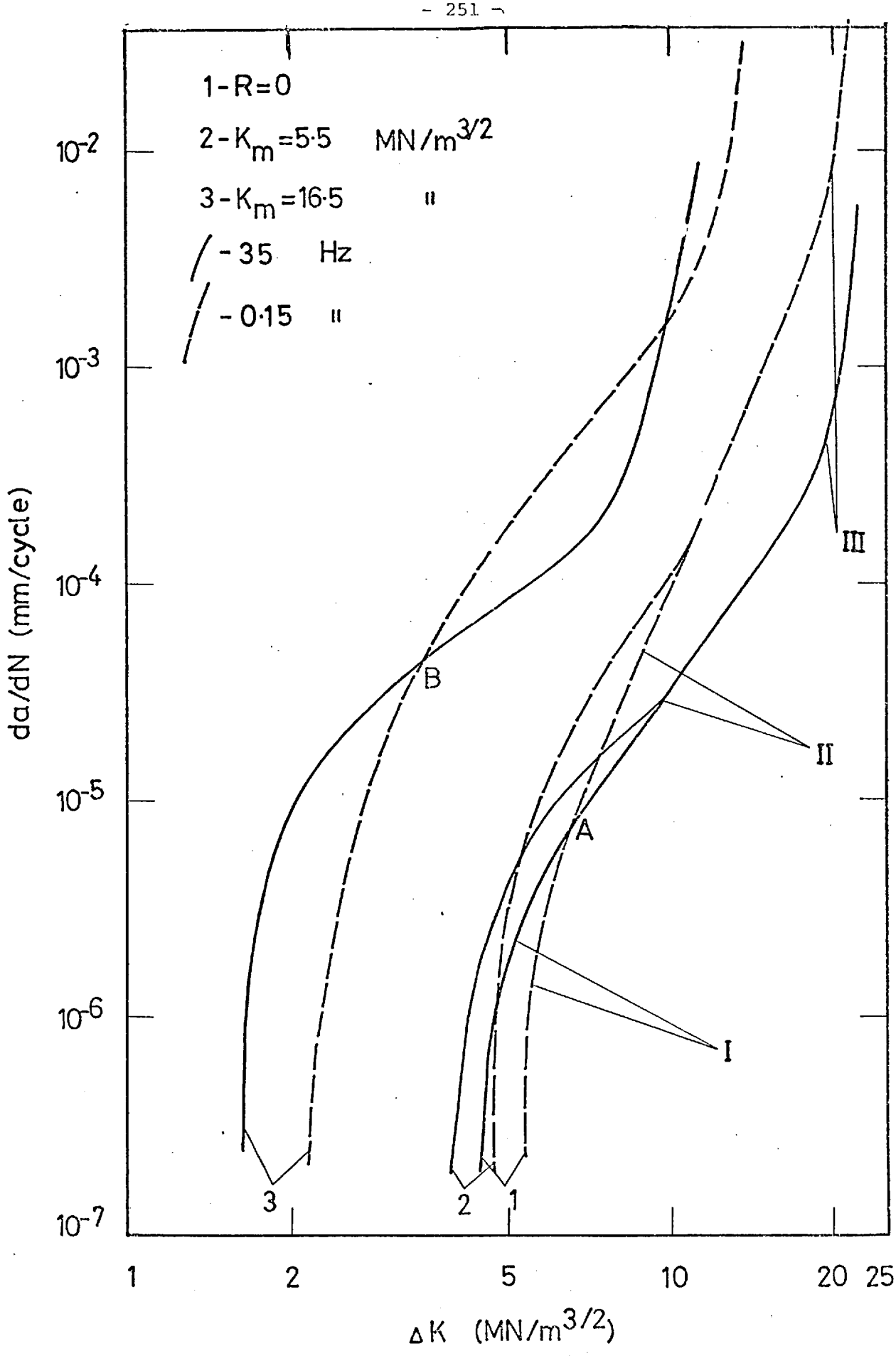


FIG. 39 Crack Growth Rate vs. ΔK Curves. RR58, Laboratory air. 0.25 and 35 Hz

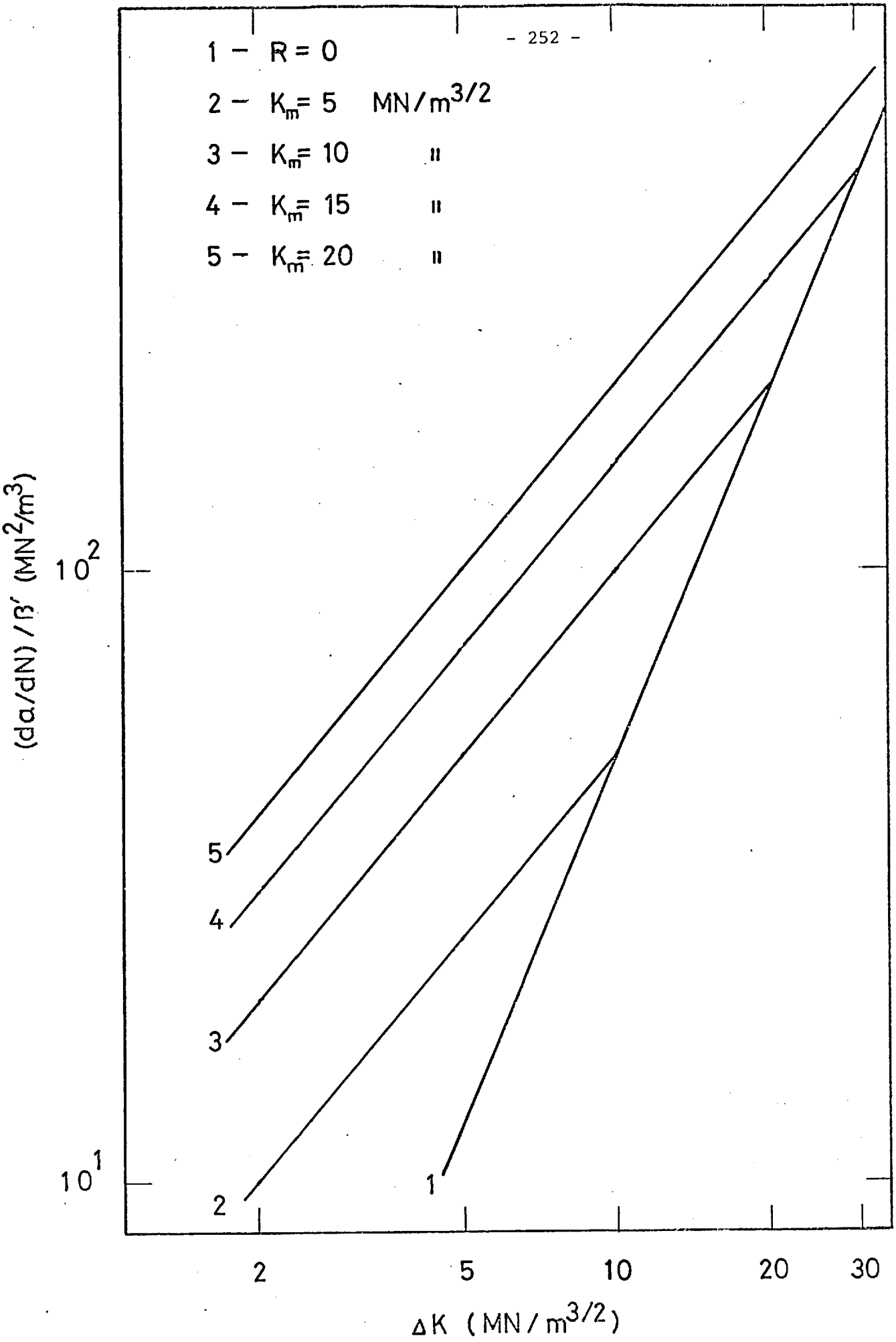


FIG. 40 Theoretical LInes of (da/dN)/β' vs. ΔK for a value of η_T=1

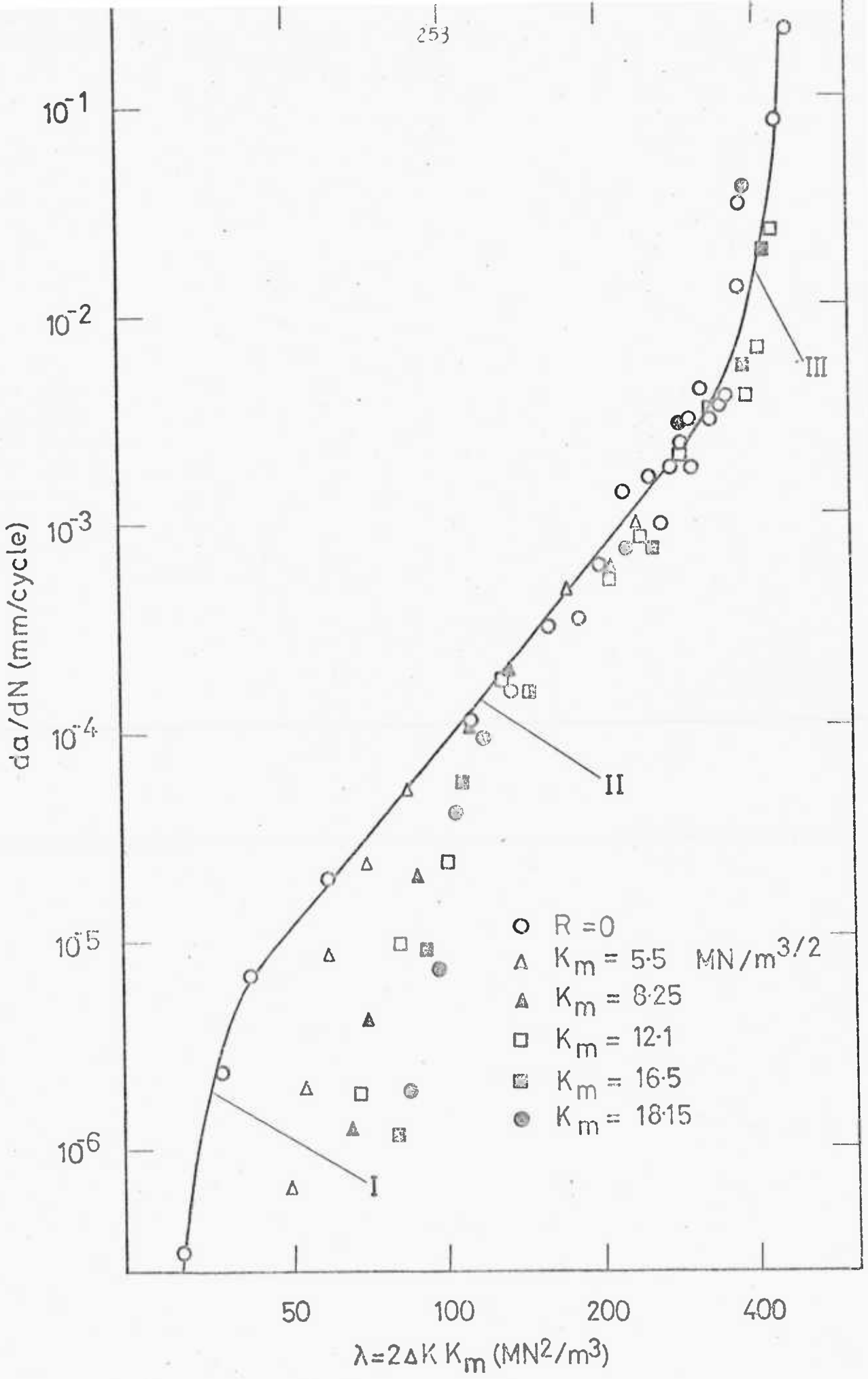


FIG. 41 Crack Growth Rate vs. $\lambda = 2\Delta K K_m$•RR58. Laboratory air. 0.15 Hz

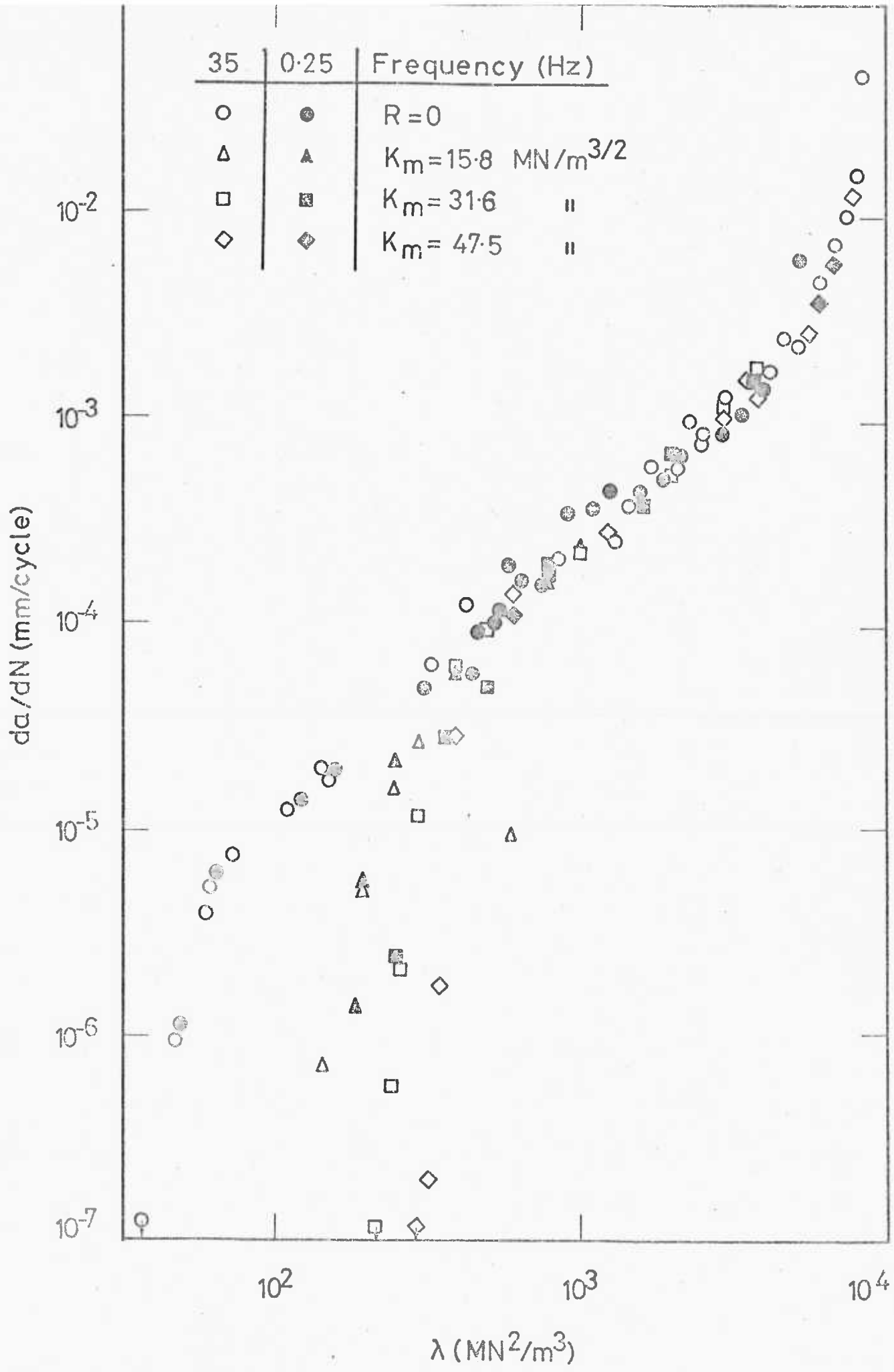


FIG. 42 Crack Growth Rate vs. $\lambda = 2\Delta K K_m$. BS15. Laboratory air. 0.25 and 35Hz

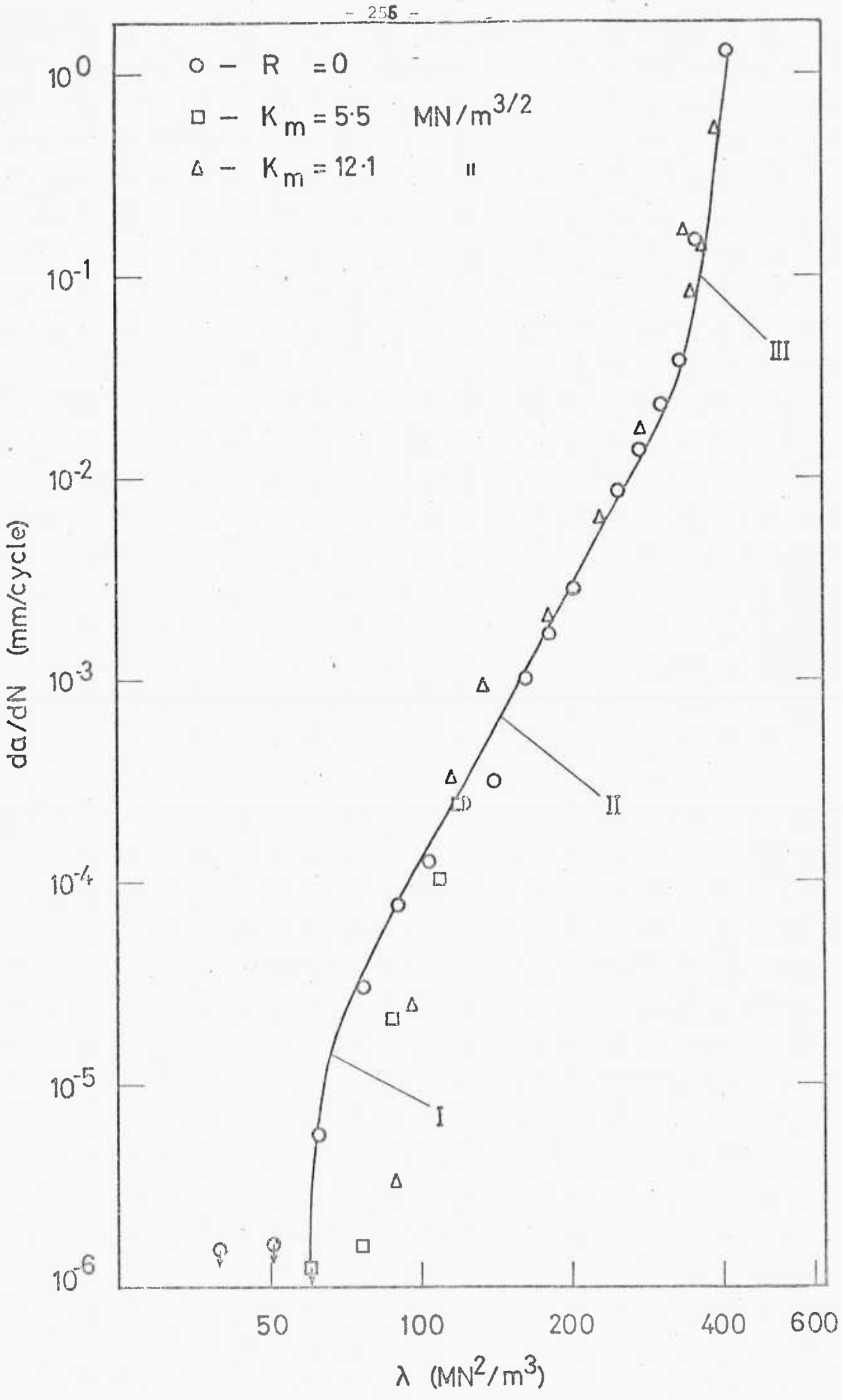


FIG. 43 Crack Growth Rate vs. $\lambda = 2\Delta K K_m$. LM30. Laboratory air. 0.25 Hz

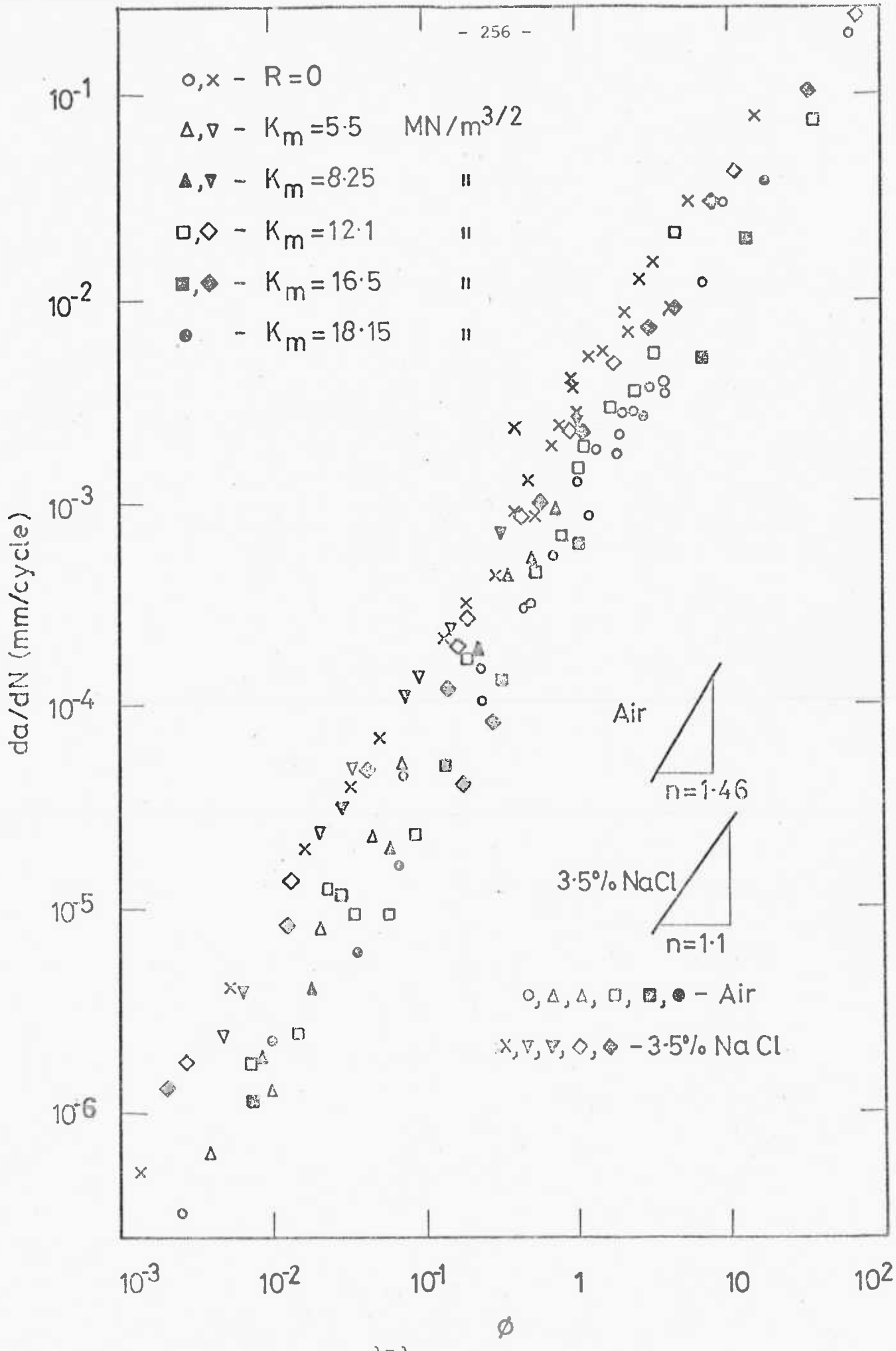


FIG. 44 Crack Growth Rate vs. $\Phi = \frac{\lambda - \lambda_{th}}{K_c^2 - K_{max}^2}$ • RR58. Laboratory air. and 3.5%NaCl. 0.15 Hz

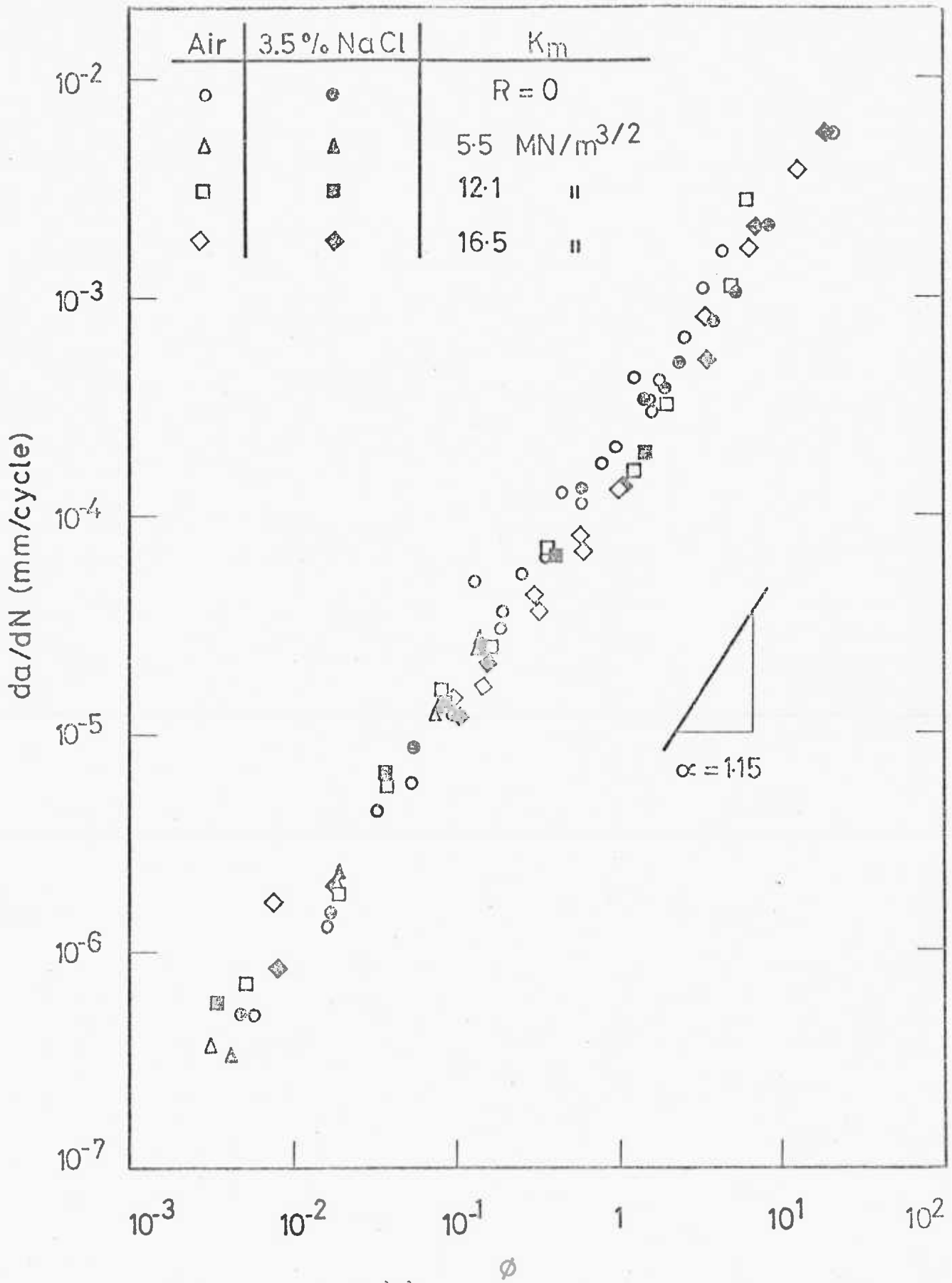


FIG. 45 Crack Growth Rate vs. $\Phi = \frac{\lambda - \lambda_{th}}{K_c^2 - K_{max}^2}$. RR58. Laboratory air and 3.5%NaCL. 35 Hz

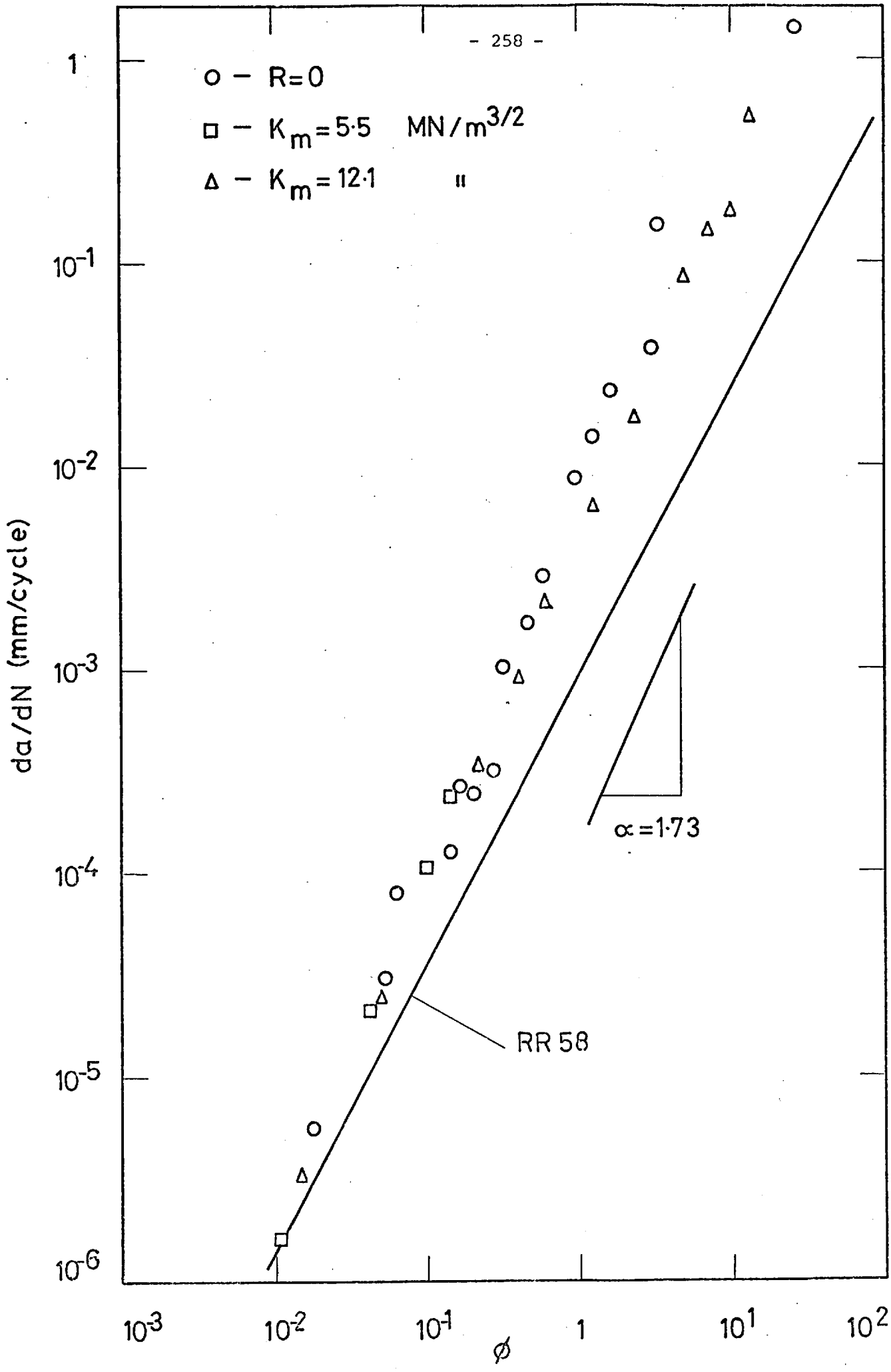


FIG. 46 Crack Growth Rate vs. $\Phi = \frac{\lambda-\lambda_{th}}{K_c^2-K_{max}^2}$. LM30. Laboratory air. 0.25 Hz

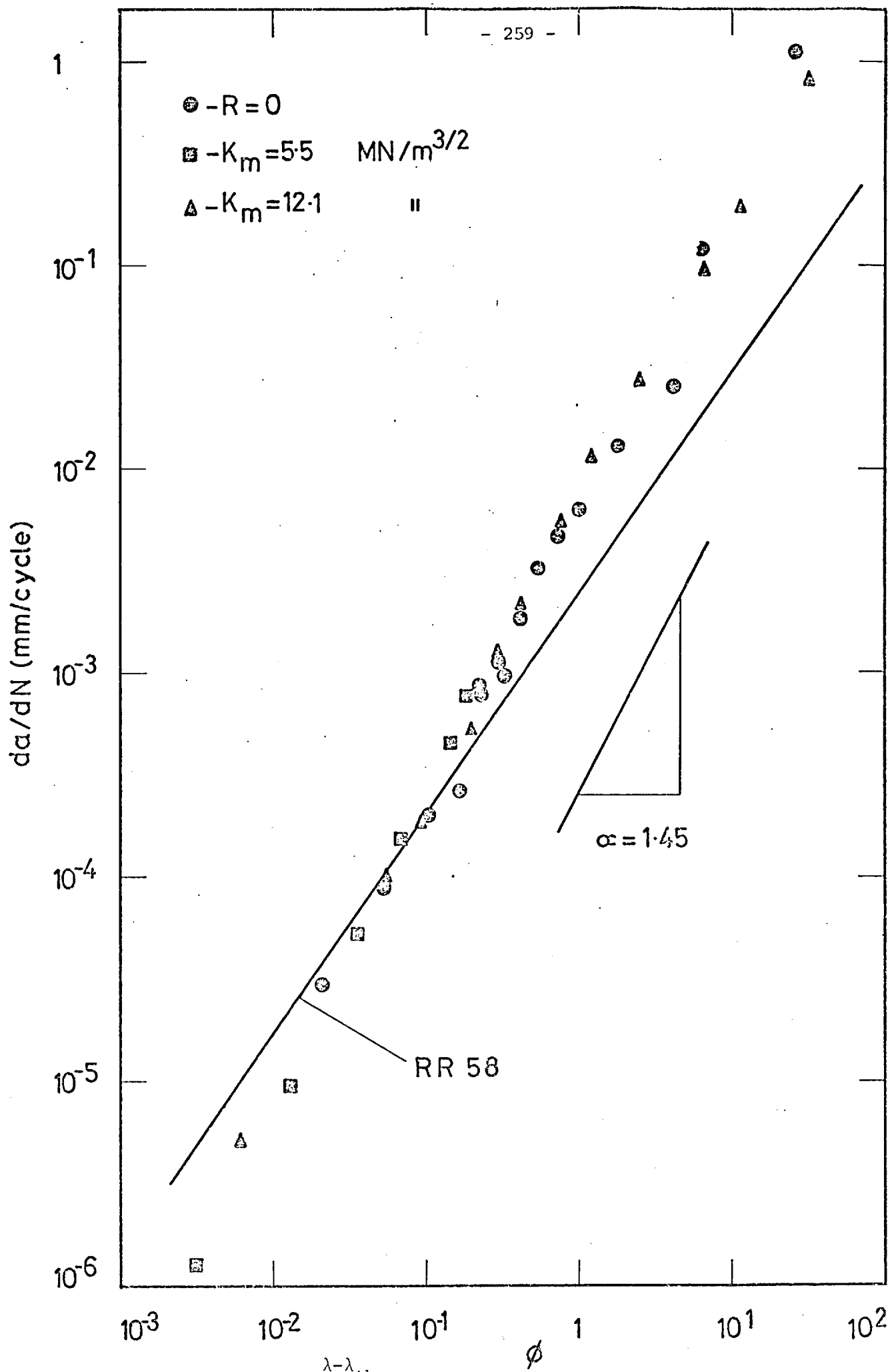


FIG. 47 Crack Growth Rate vs. $\phi = \frac{\lambda-\lambda_{th}}{K_c^2-K_{max}^2}$ • LM30. 3.5% NaCl. 0.25 Hz

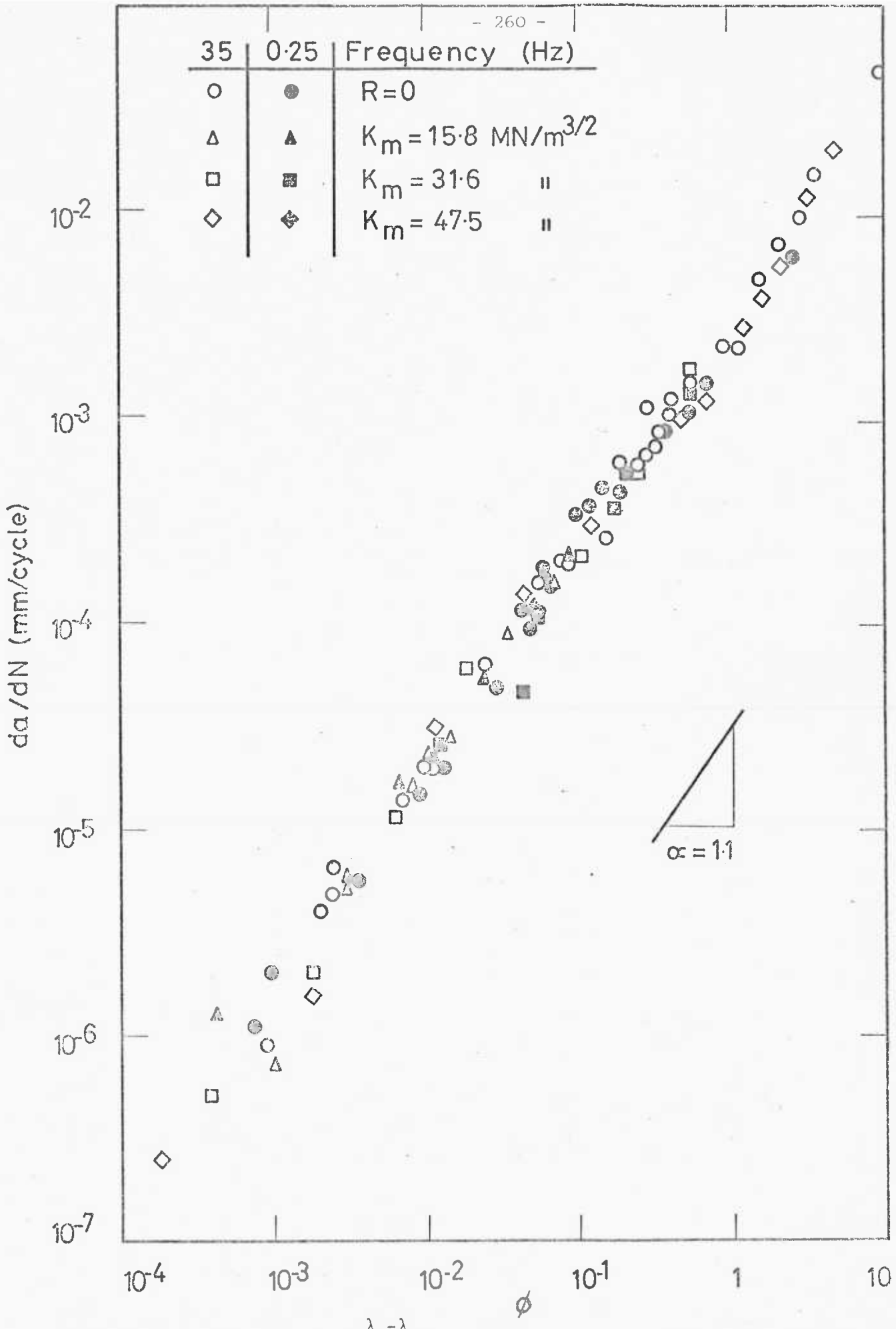


FIG. 48 Crack Growth Rate vs. $\Phi = \frac{\lambda - \lambda_{th}}{K_c^2 - K_{max}^2}$ • BS15. Laboratory air. 0.25 and 35 Hz

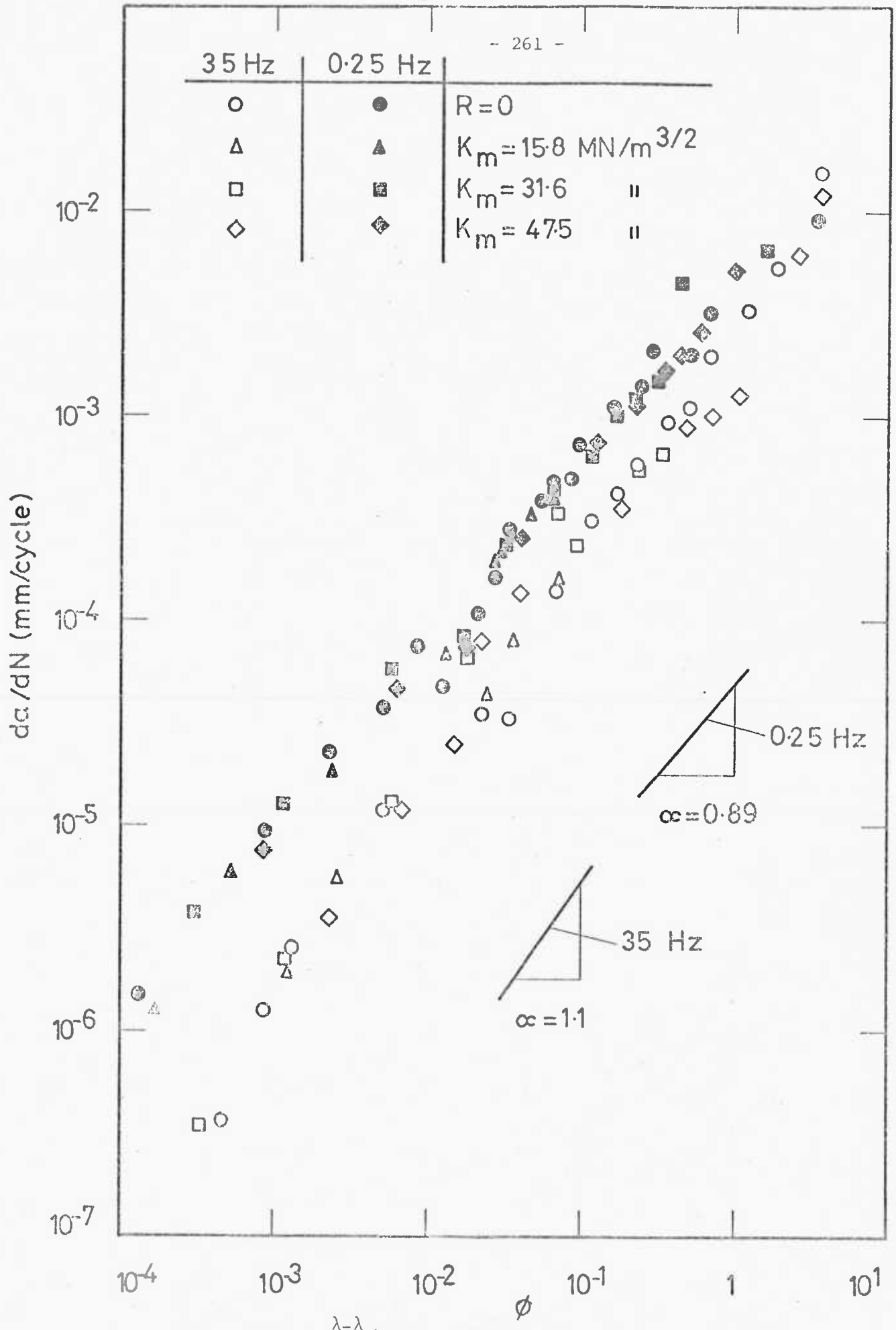


FIG. 49 Crack Growth Rate vs. $\Phi = \frac{\lambda - \lambda_{th}}{K_c^2 - K_{max}^2}$ •BS15. 3.5% NaCl. 0.25 and 35 Hz

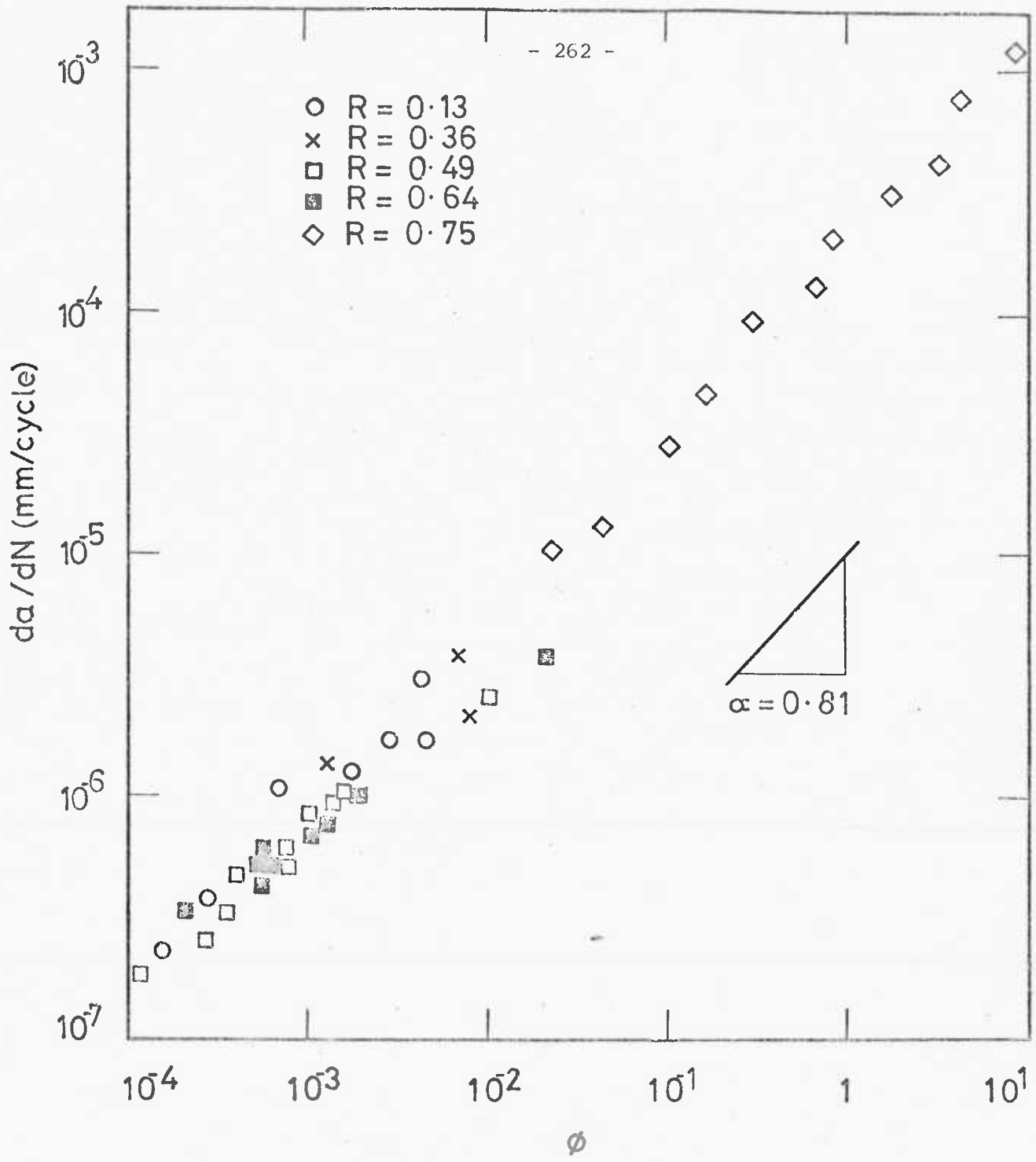


FIG. 50 Crack Growth Rate vs. $\Phi = \frac{\lambda-\lambda_{th}}{K_c^2-K_{max}^2}$ • Mild Steel (94). Laboratory air

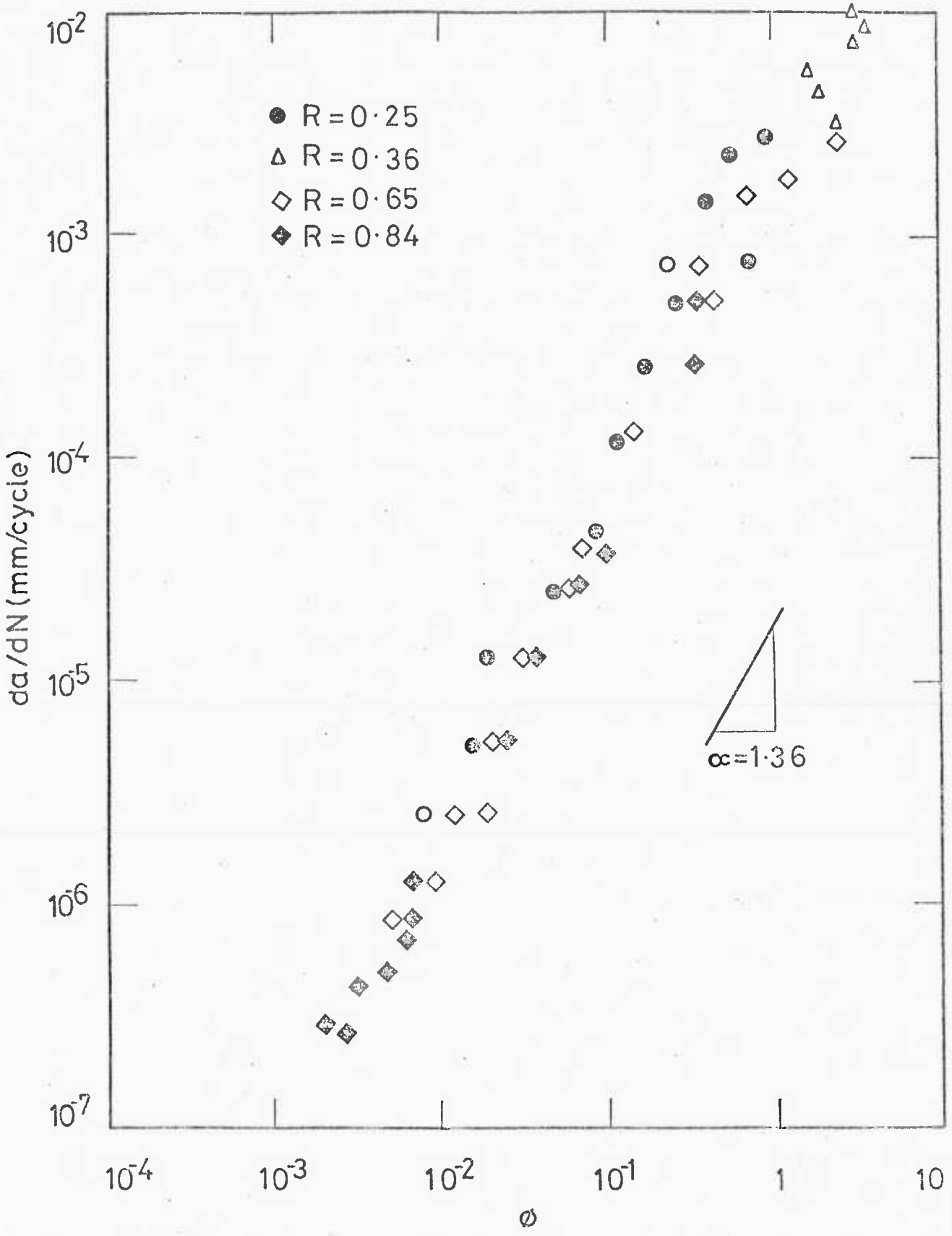


FIG. 51 Crack Growth Rate vs. $\Phi = \frac{\lambda-\lambda_{th}}{K_c^2-K_{max}^2}$ · Cold Rolled Mild Steel (95). Laboratory air

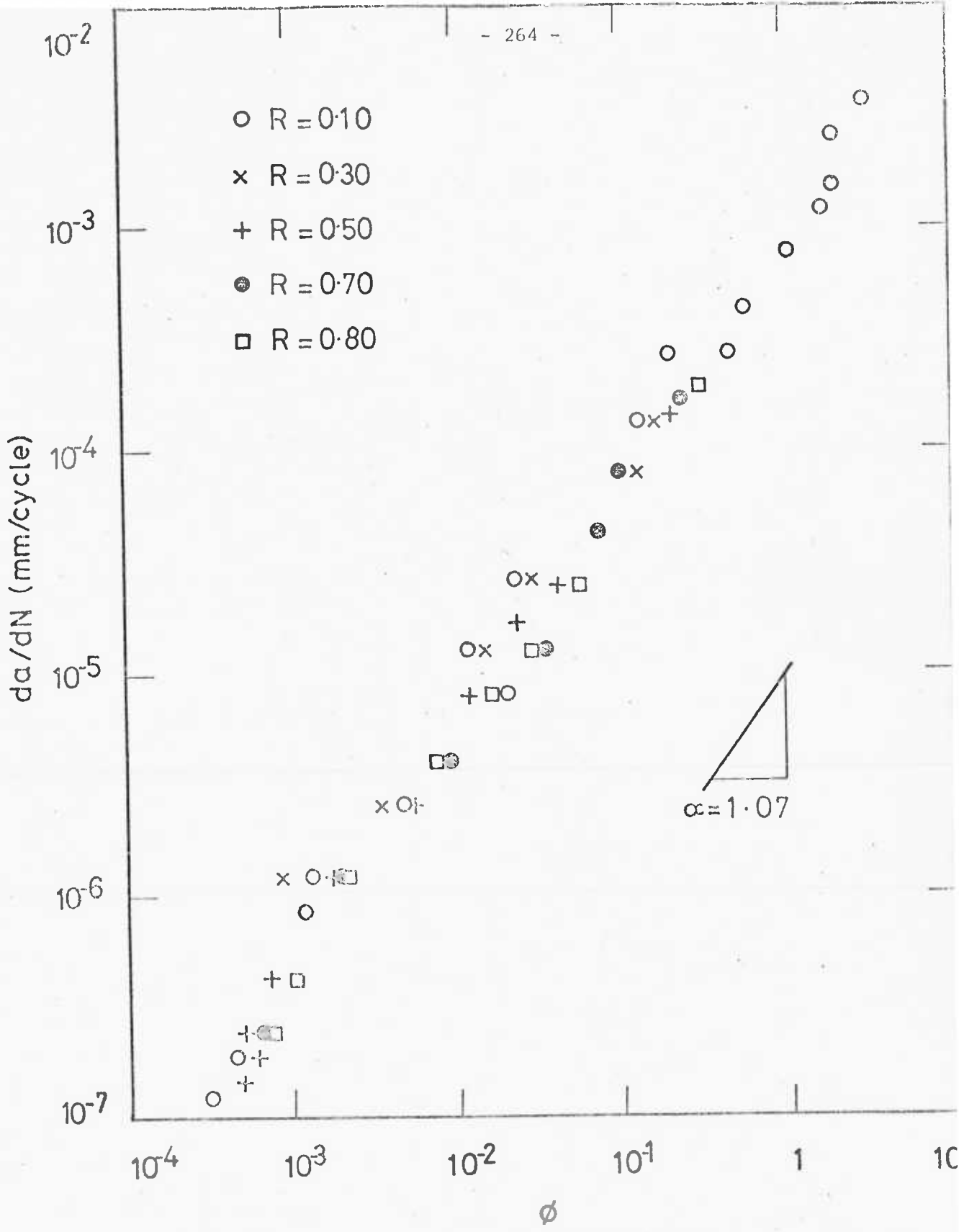


FIG. 52 Crack Growth Rate vs. $\Phi = \frac{\lambda-\lambda_{th}}{K_c^2-K_{max}^2}$. • ASTM A533 B-1 Steel (96). Laboratory air

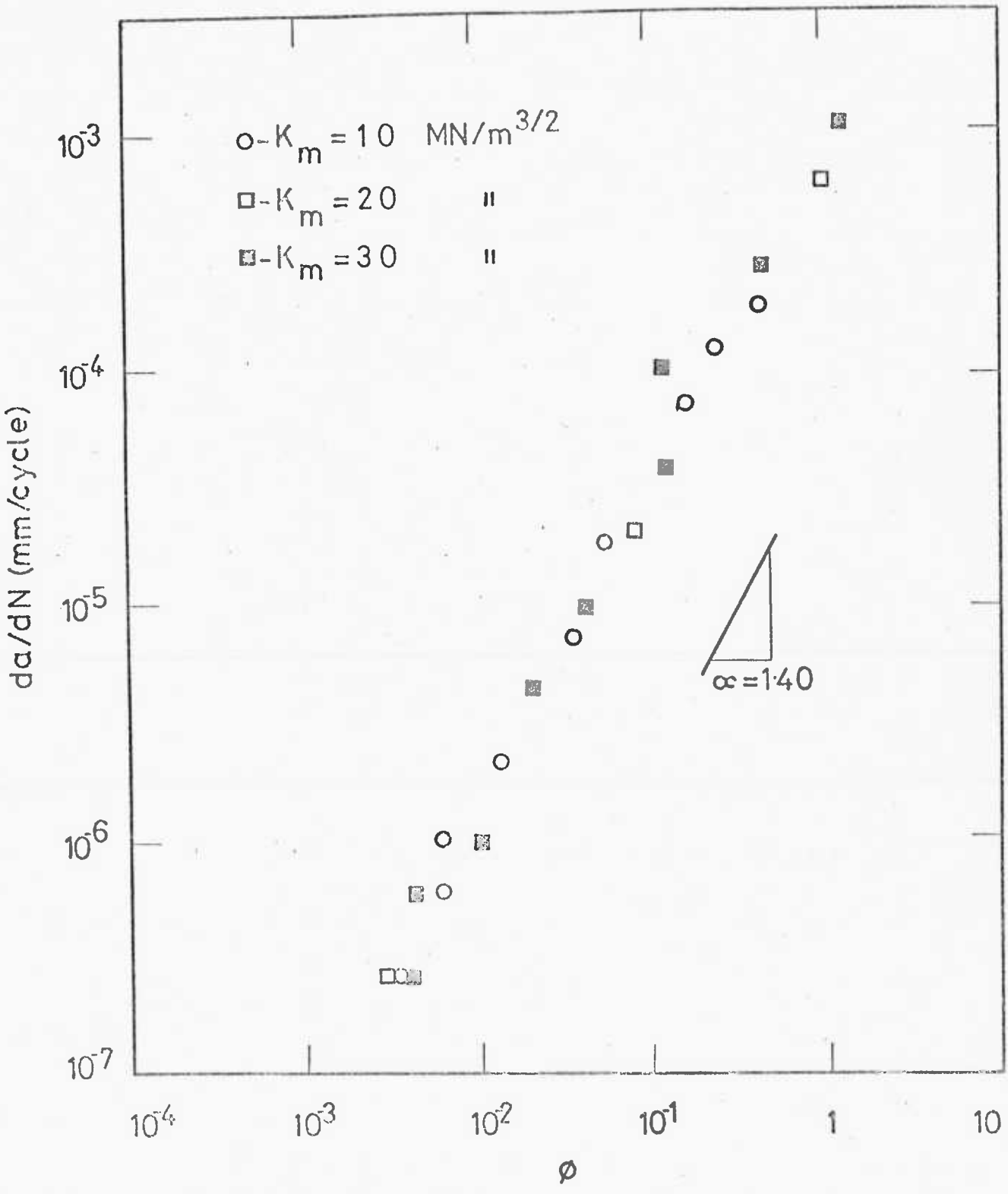


FIG. 53 Crack Growth Rate vs. $\Phi = \frac{\lambda - \lambda_{th}}{K_c^2 - K_{max}^2}$. EN3A Mild Steel (97). Laboratory air

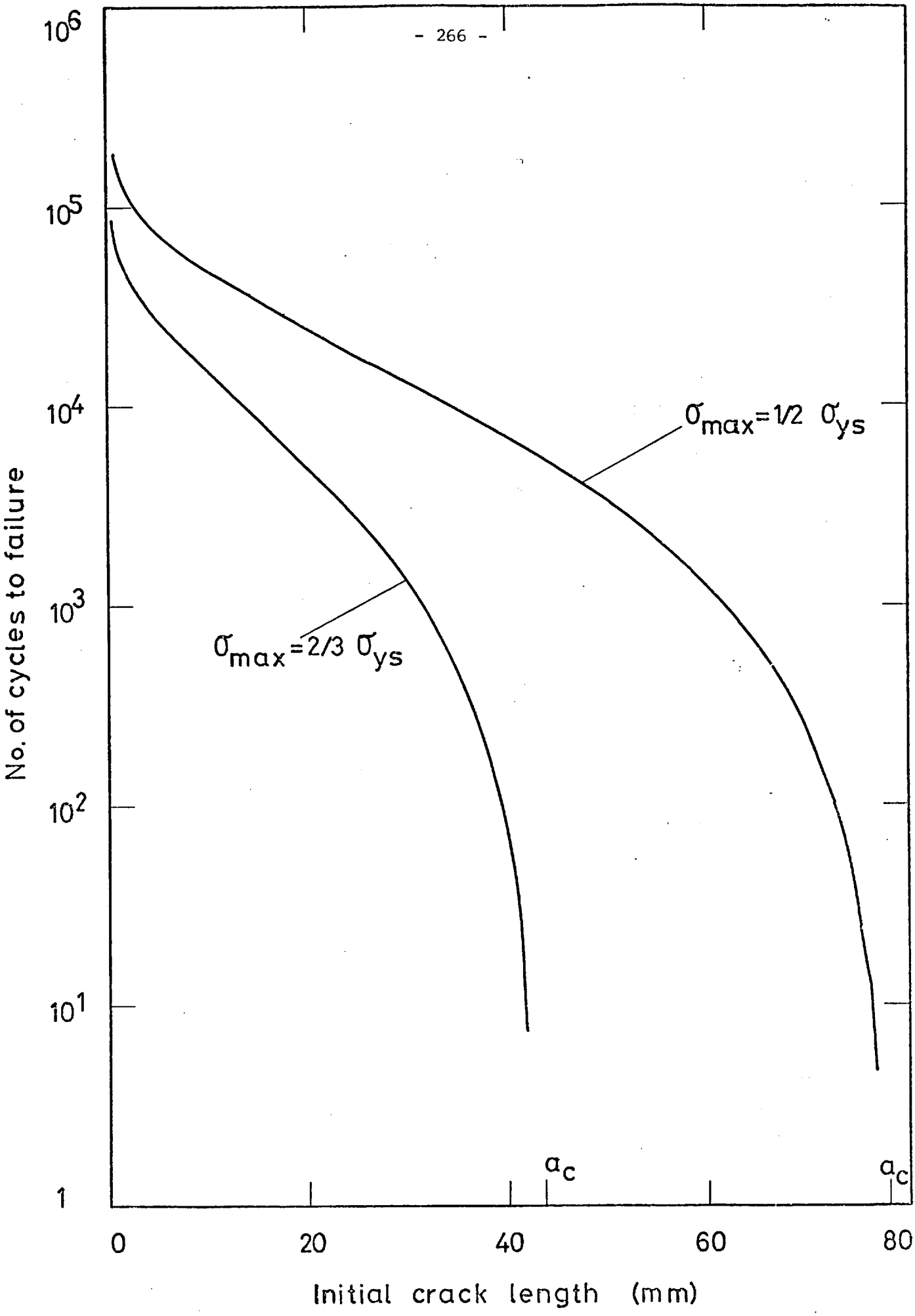


FIG. 54 Number of cycles to failure vs. Initial Crack Length. R = O. BS15. Laboratory air. O.25 and 35 Hz

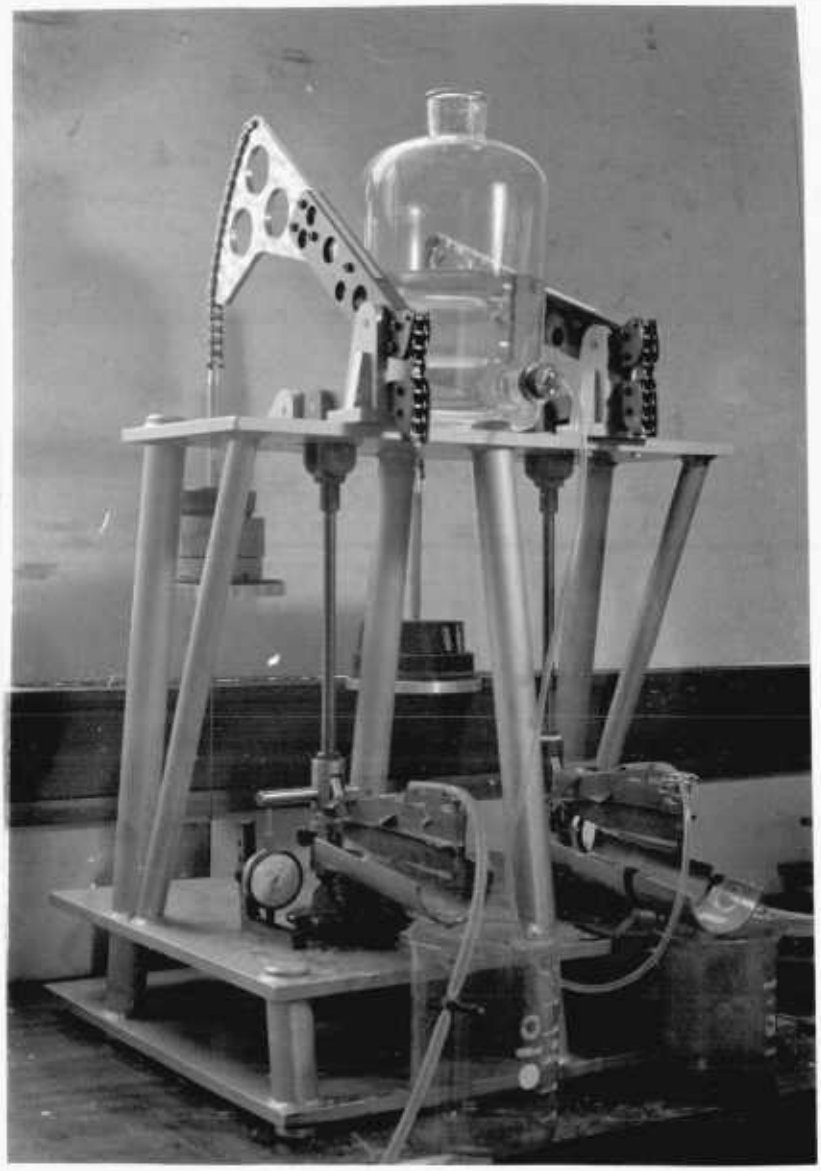


FIG. 55 Two of the Stress Corrosion Rigs Used in the Experimental Programme

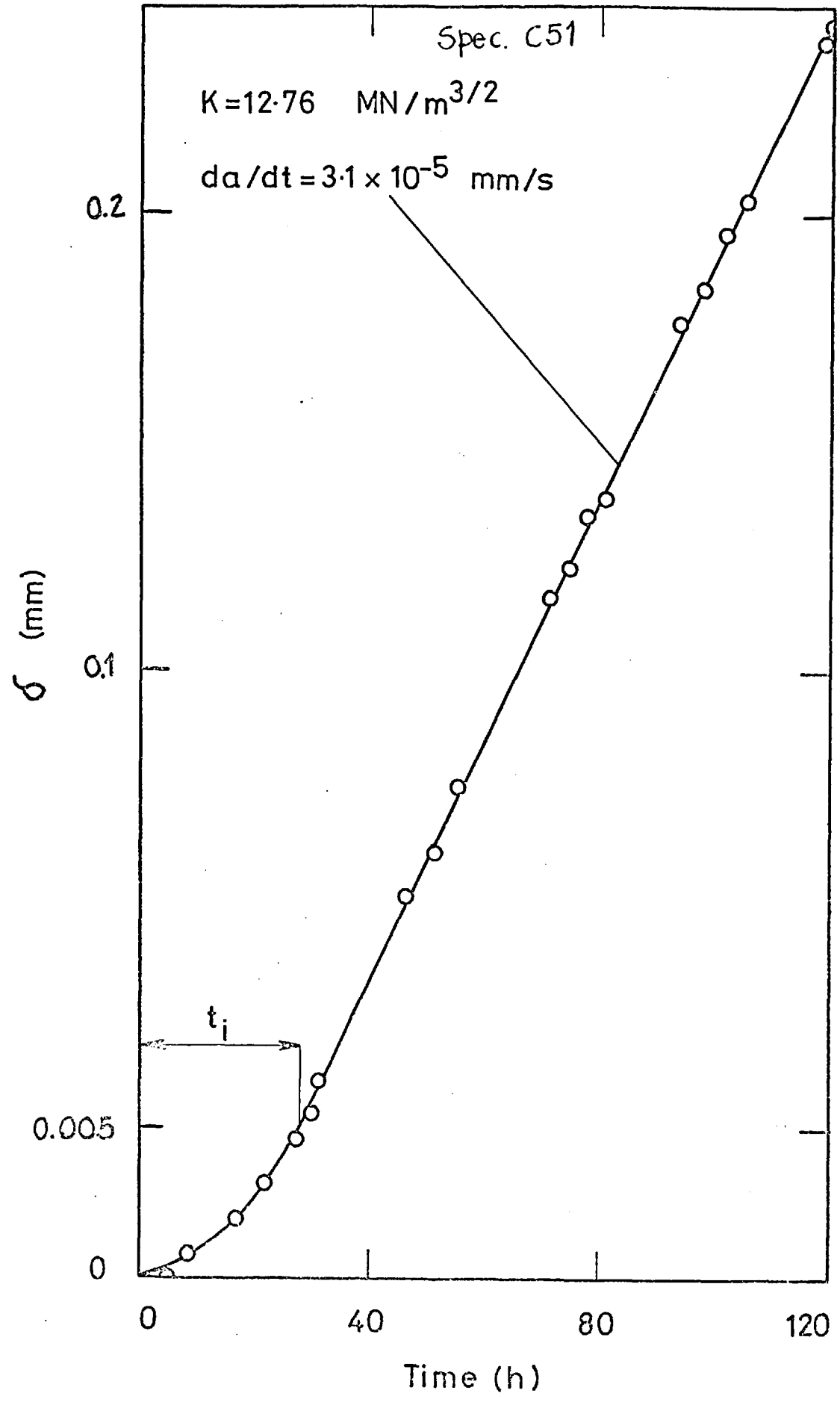


FIG. 56 A Typical Deflection at the Loading Point vs. Time Curve. RR58. 3.5% NaCl

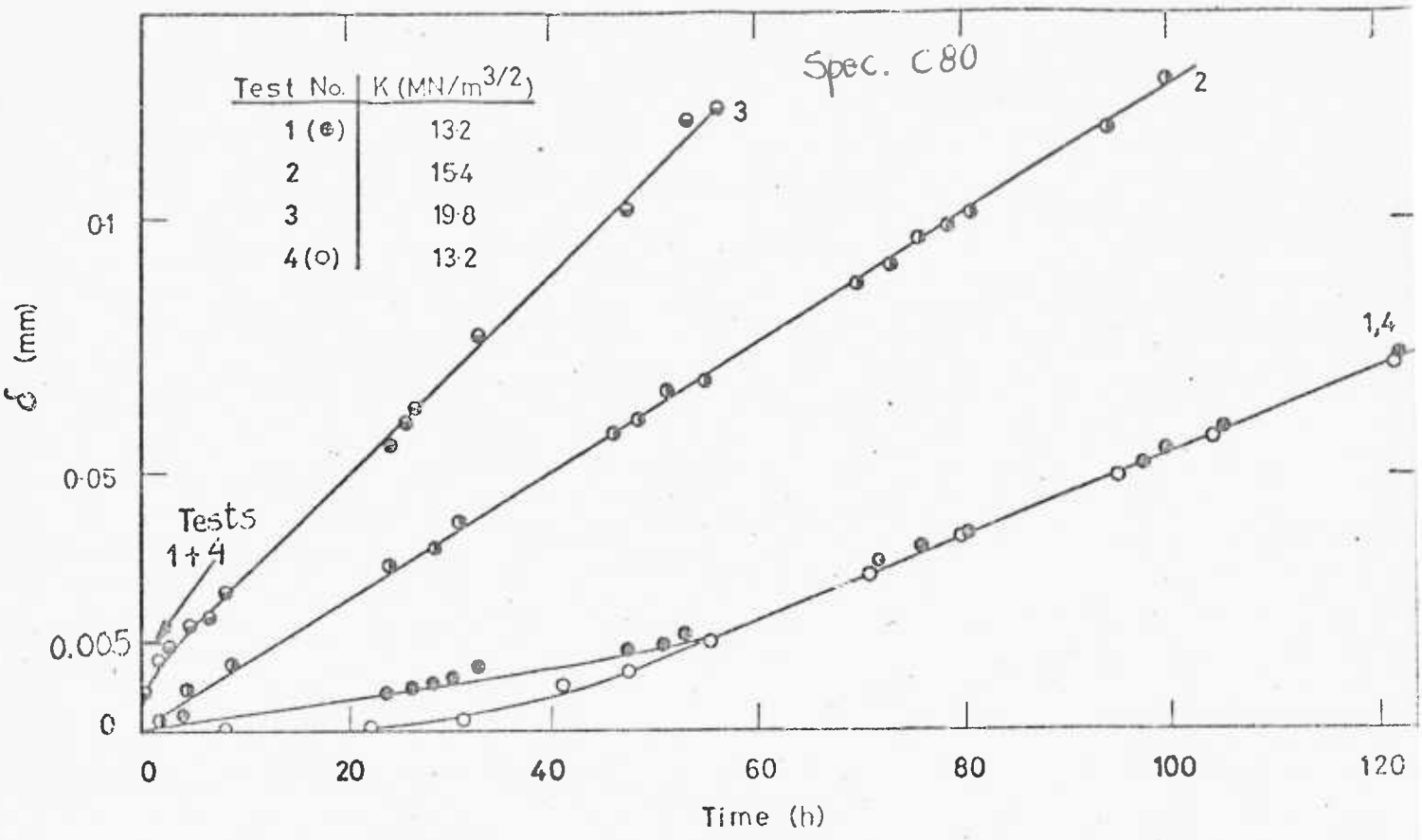


FIG. 57 Deflection at the Loading Points vs. Time Curves Showing the Effect of Loading History. RR58, 3.5% NaCl

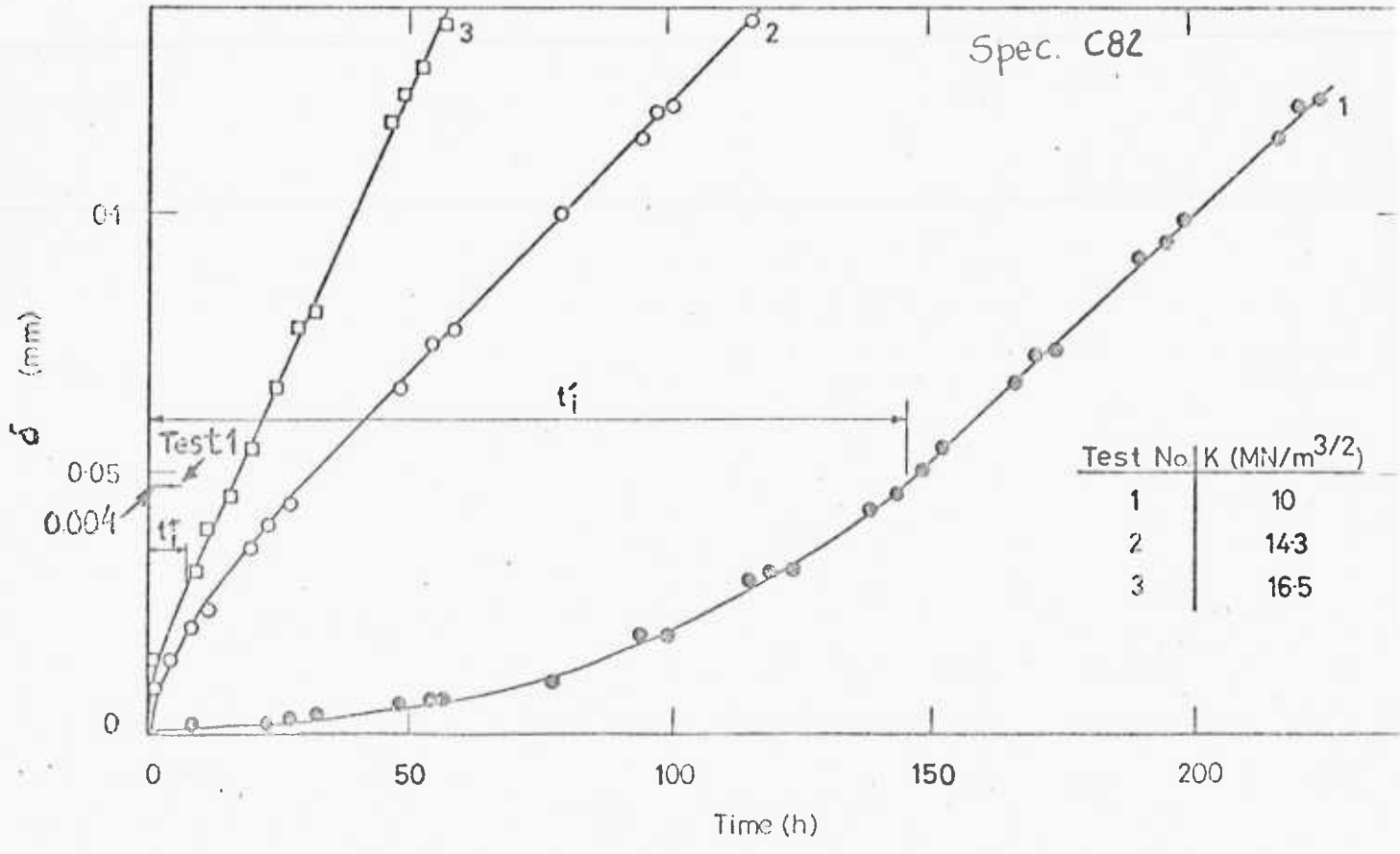


FIG. 58 Deflection at the Loading Points vs. Time Curves for Increasing Values of K. RR58. 3.5% NaCl

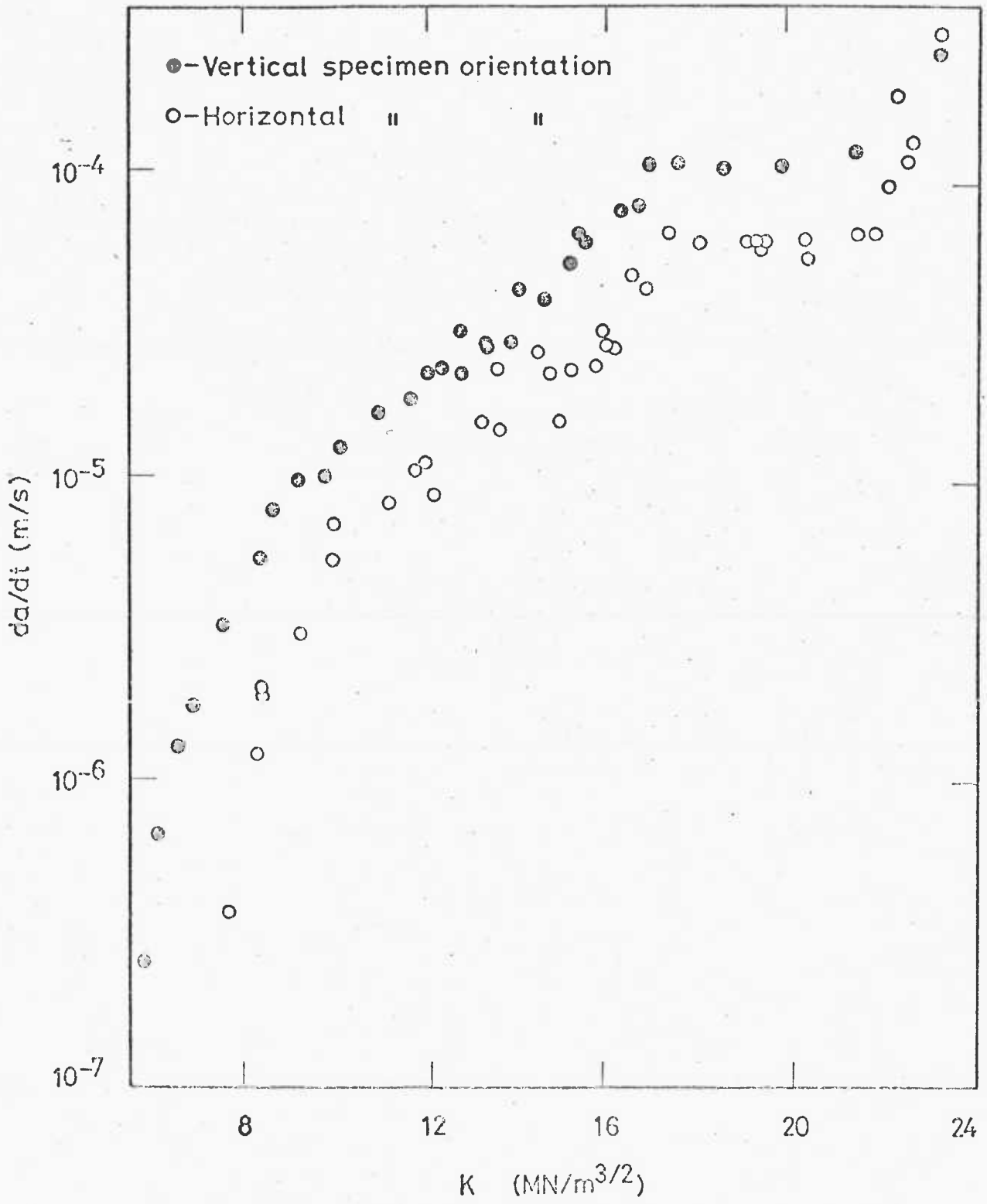


FIG. 59 Crack Growth Rte vs. K. for the Horizontal and Vertical Specimen Orientation. RR58. 3.5% NaCl

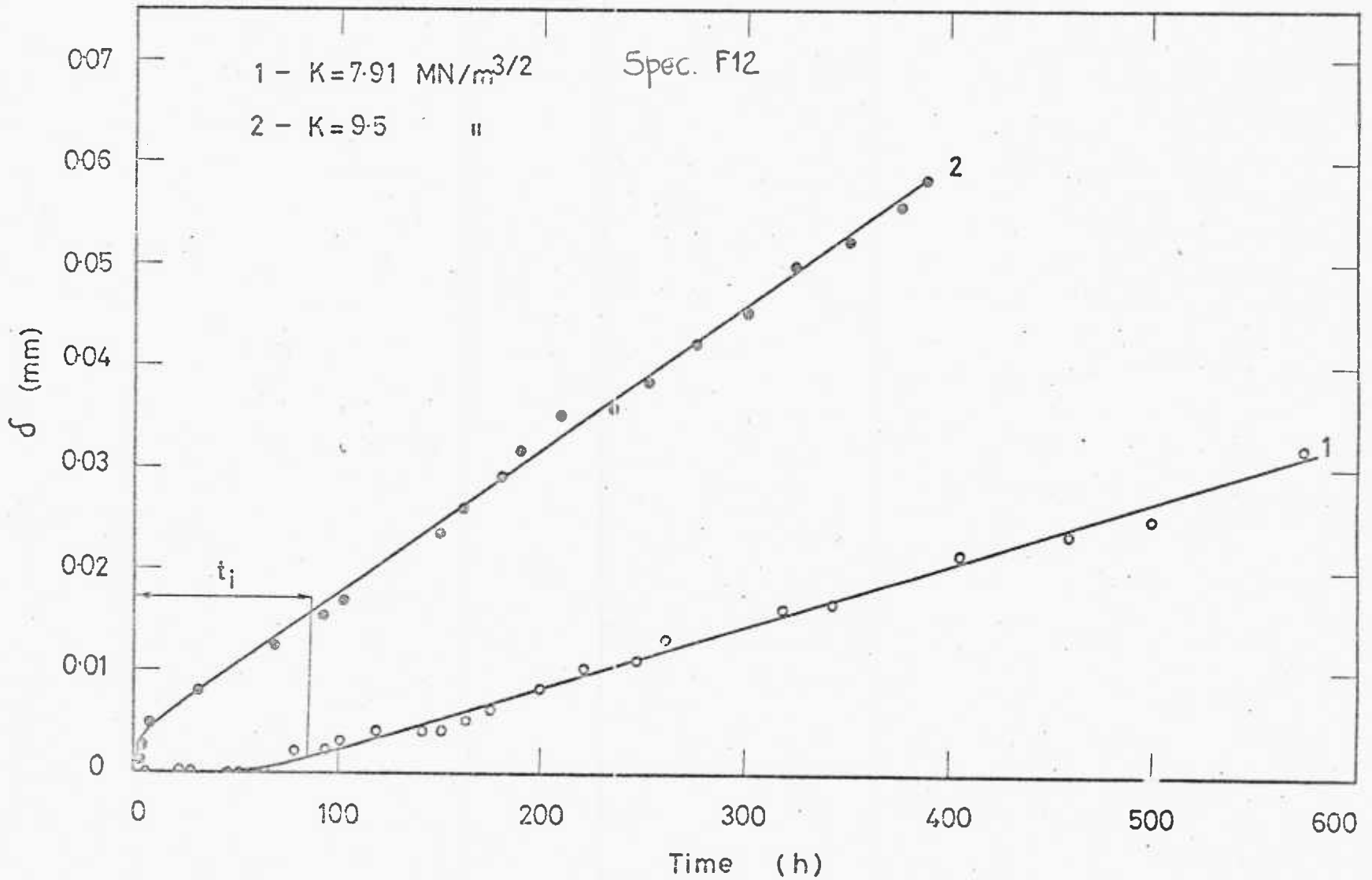


FIG. 60 - Deflection at the Loading Points vs. Time Curves for Increasing K Values. LM30. 3.5% NaCl

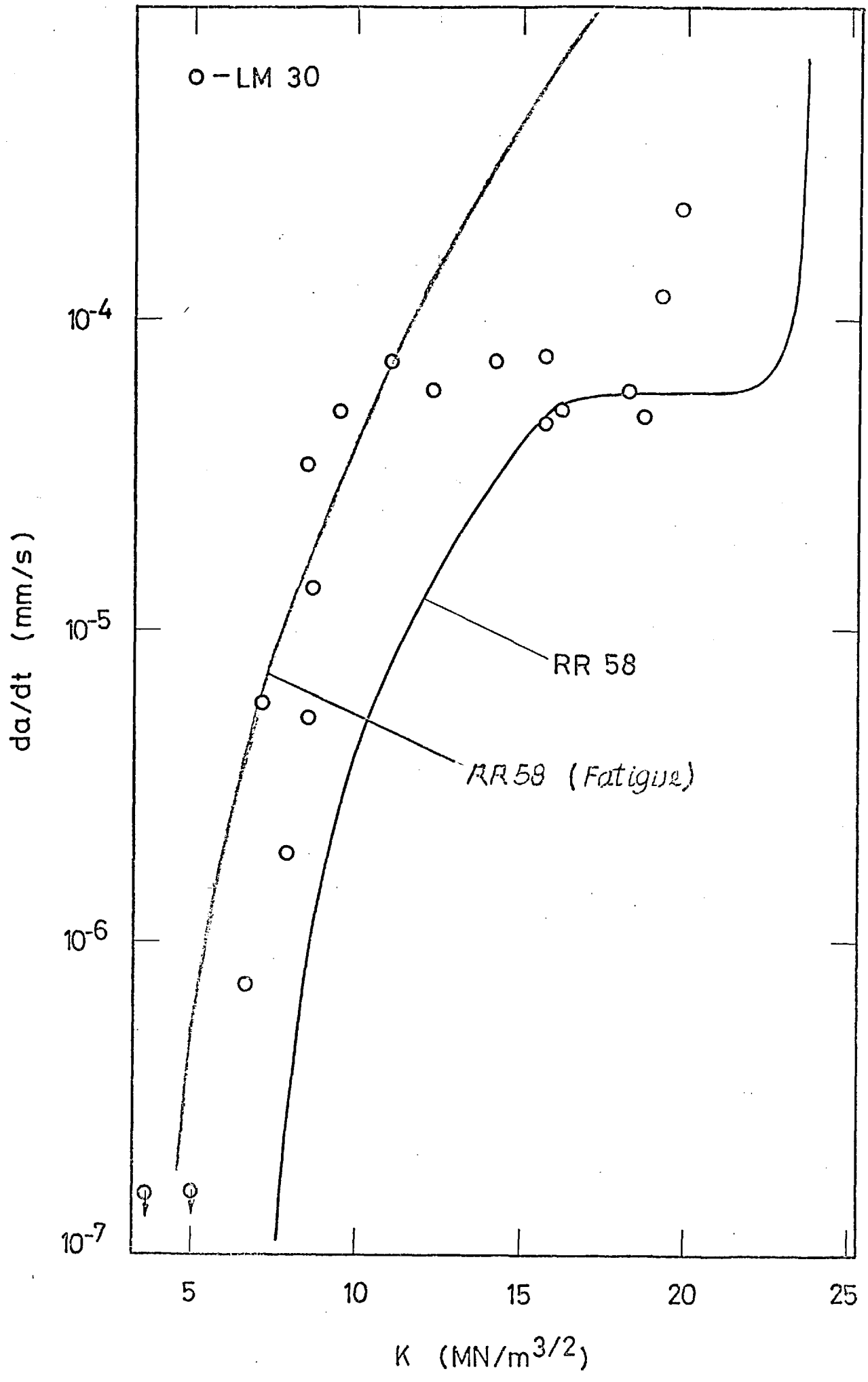


FIG. 61 Crack Growth Rate vs. K. LM30.3.5% NaCl

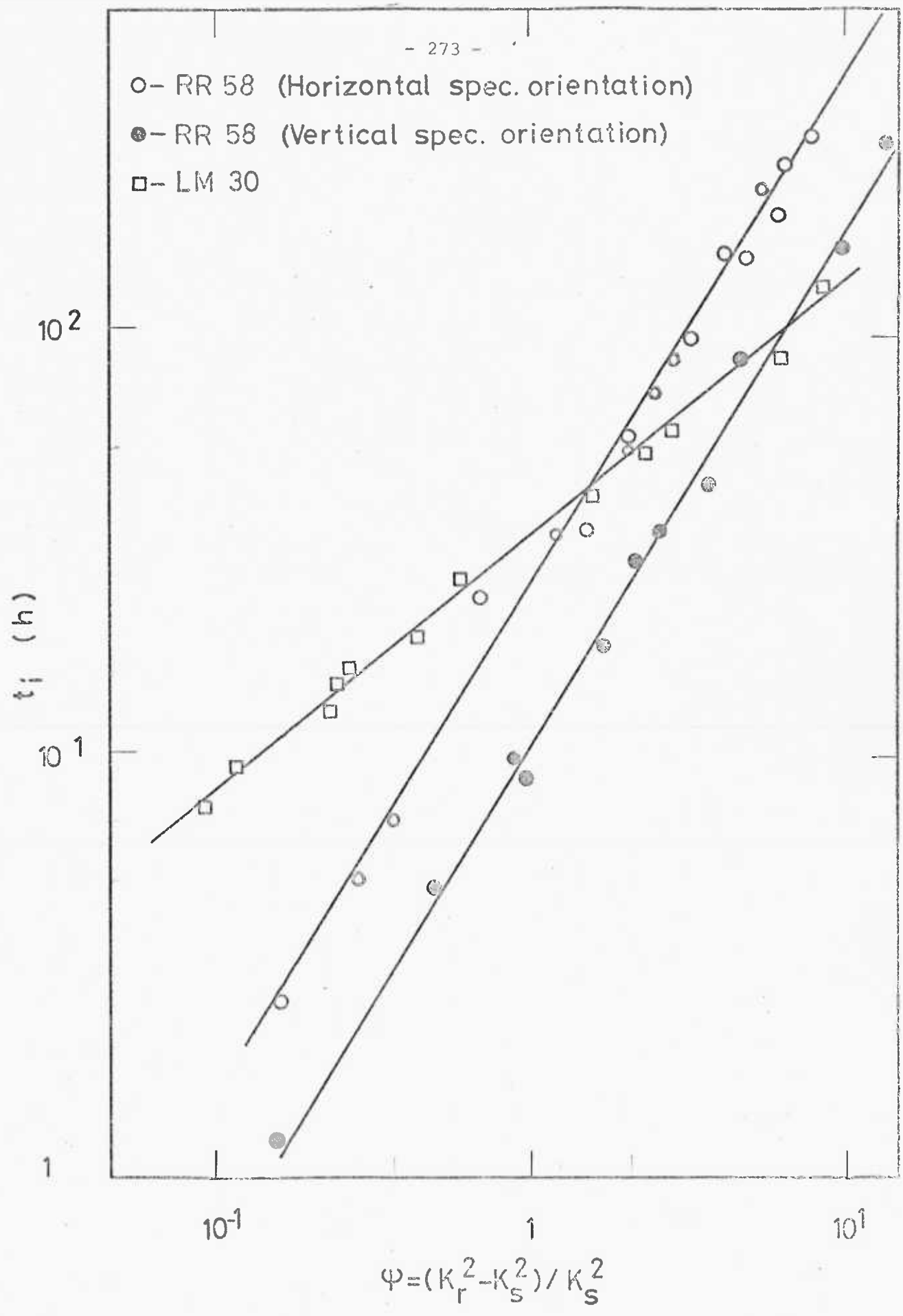


FIG. 62 Incubation Time vs. ψ , RR58 and LM30. 3.5% NaCl

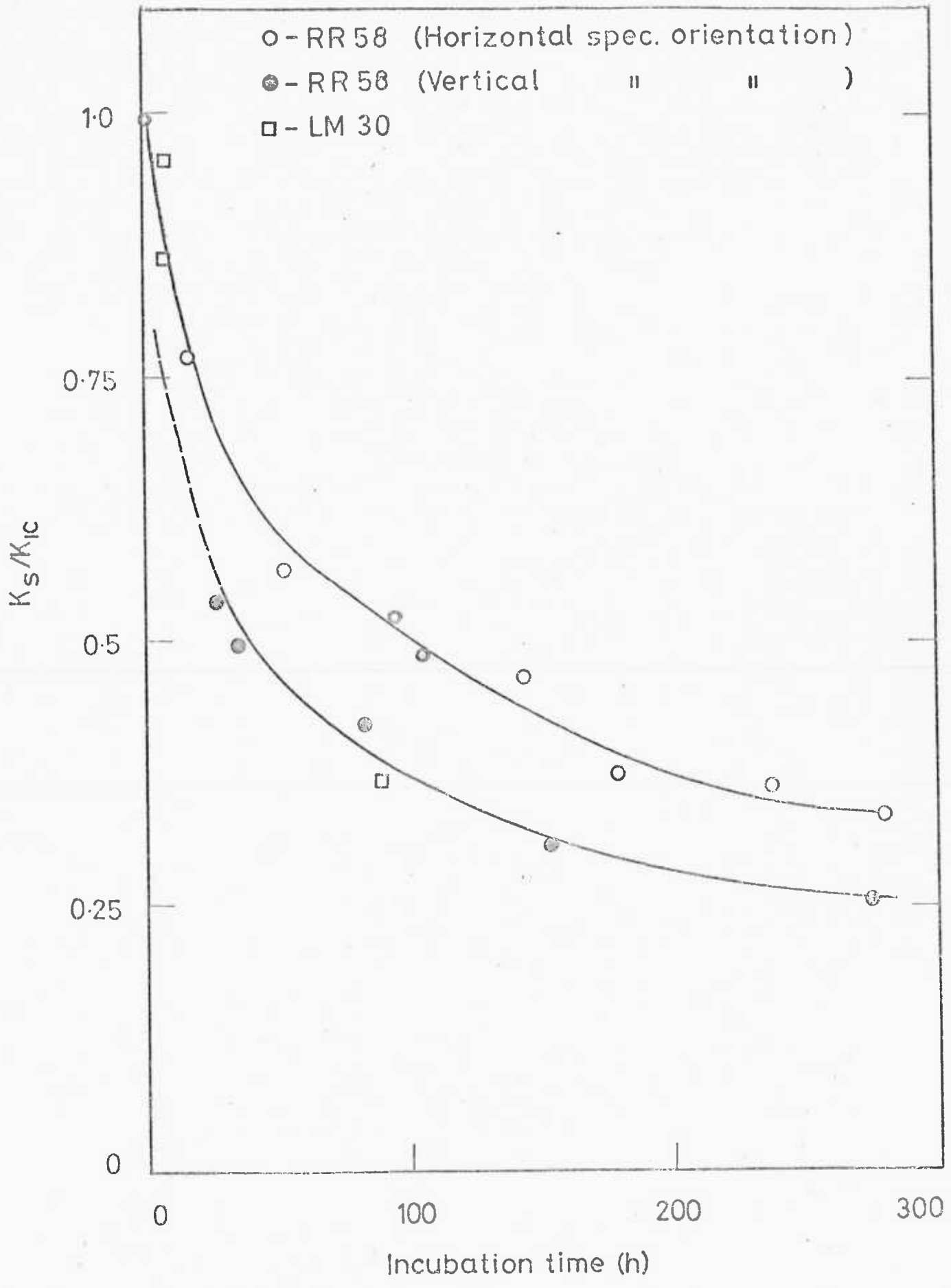


FIG. 63 Ratio K_s/K_c vs. the Incubation Time. RR58 and LM30. 3.5% NaCl

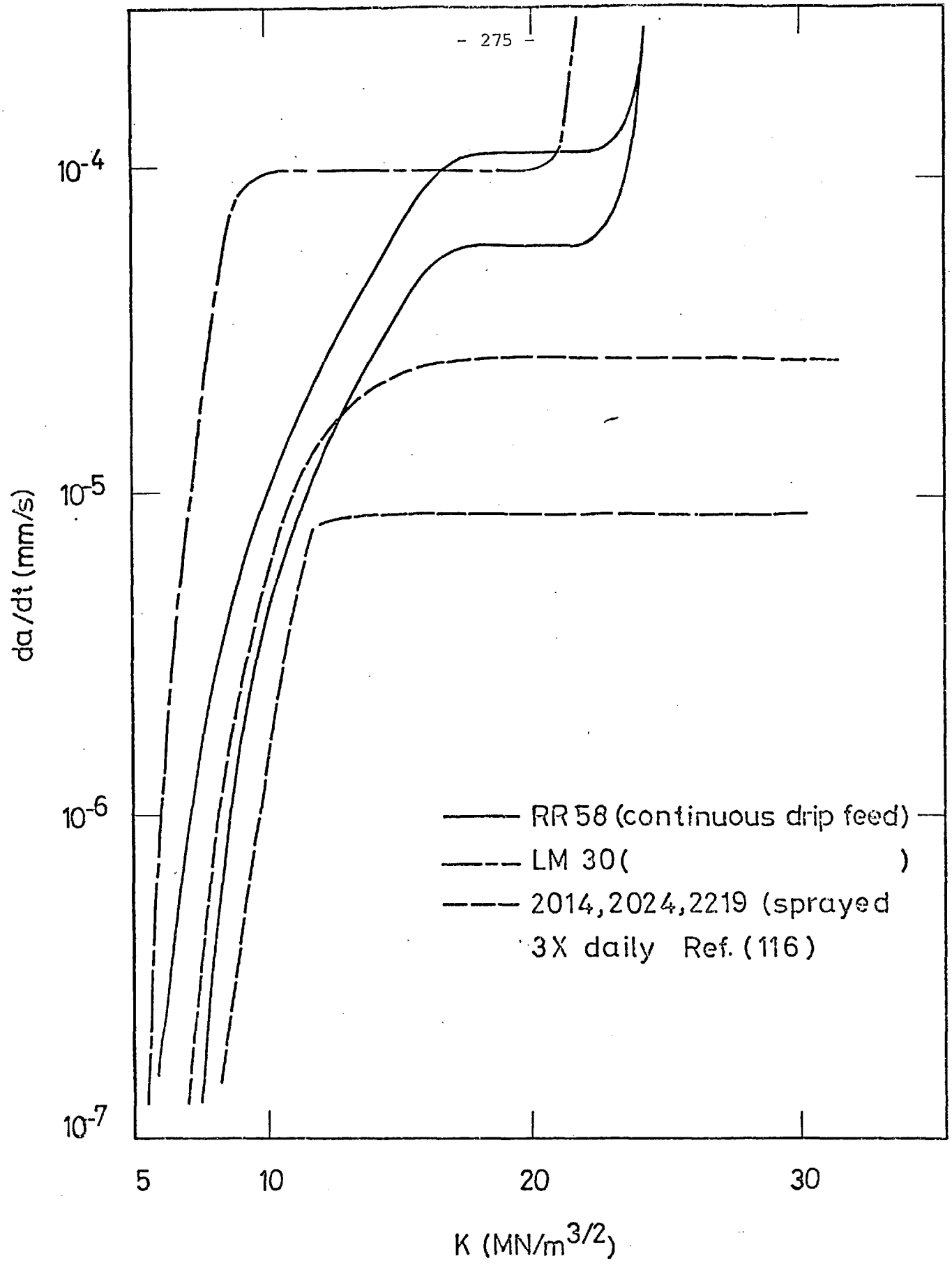


FIG. 64: Crack Growth Rate vs. K. RR58, LM30 and other 2000Series Aluminium Alloys. 3.5% NaCl

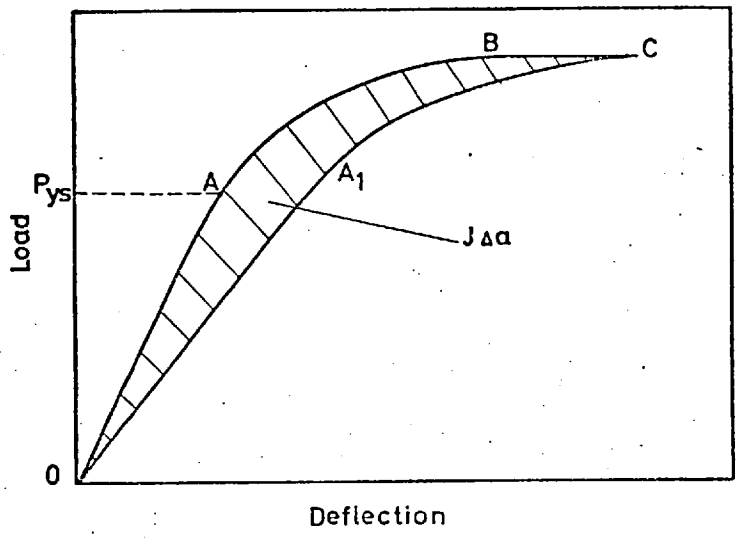


FIG. 65 The Energy Definition of the J Contour Integral for Monotonic Loading

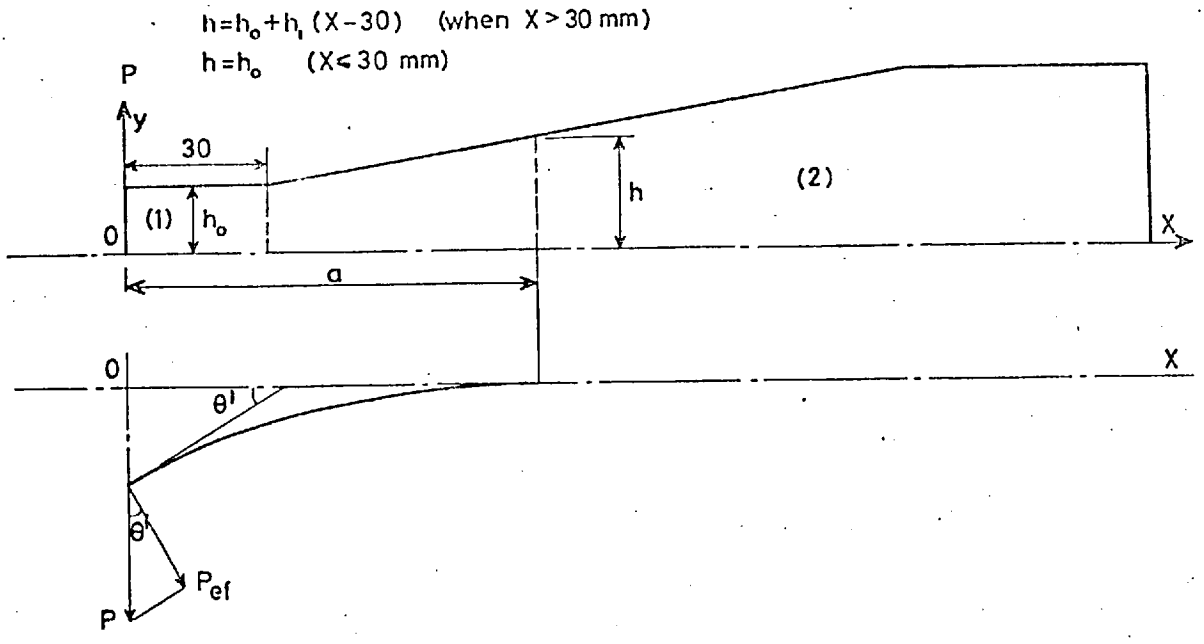


FIG. 66 Specimen Geometry Used in the Theoretical Analysis

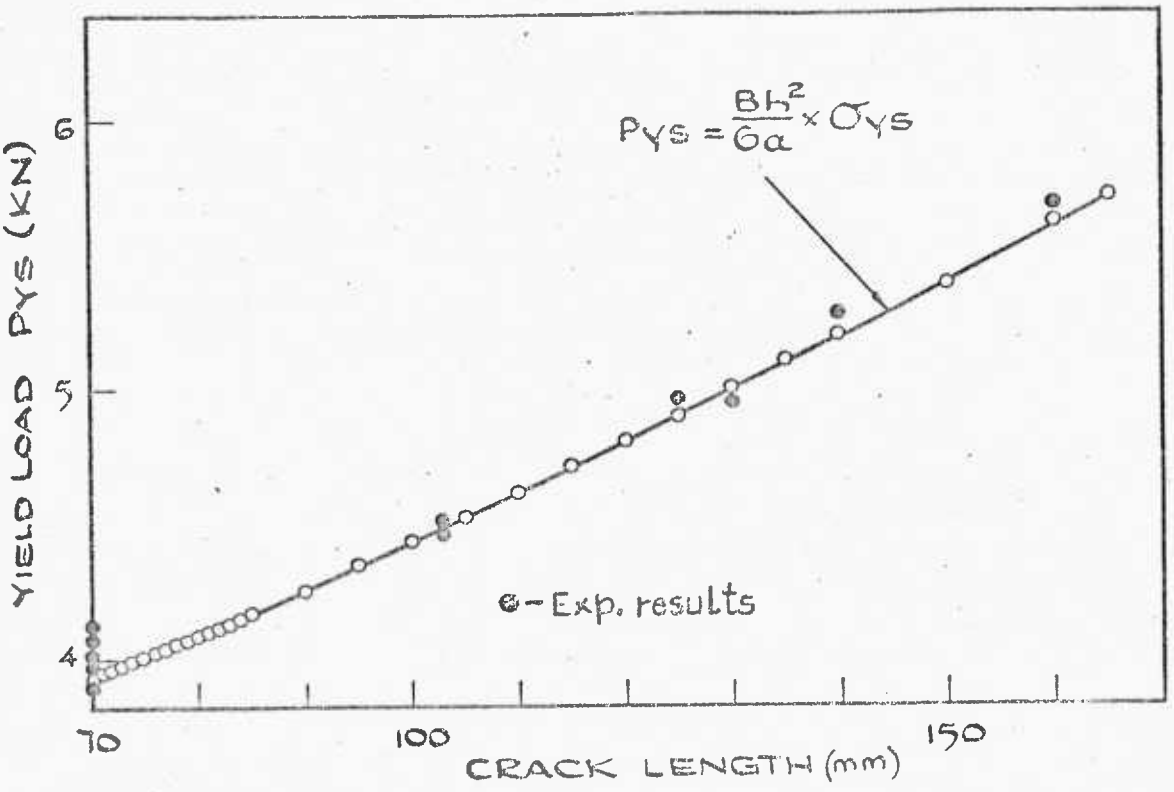


FIG. 67 Variation of the Yield Load with Crack Length. BS15. DCB Specimen

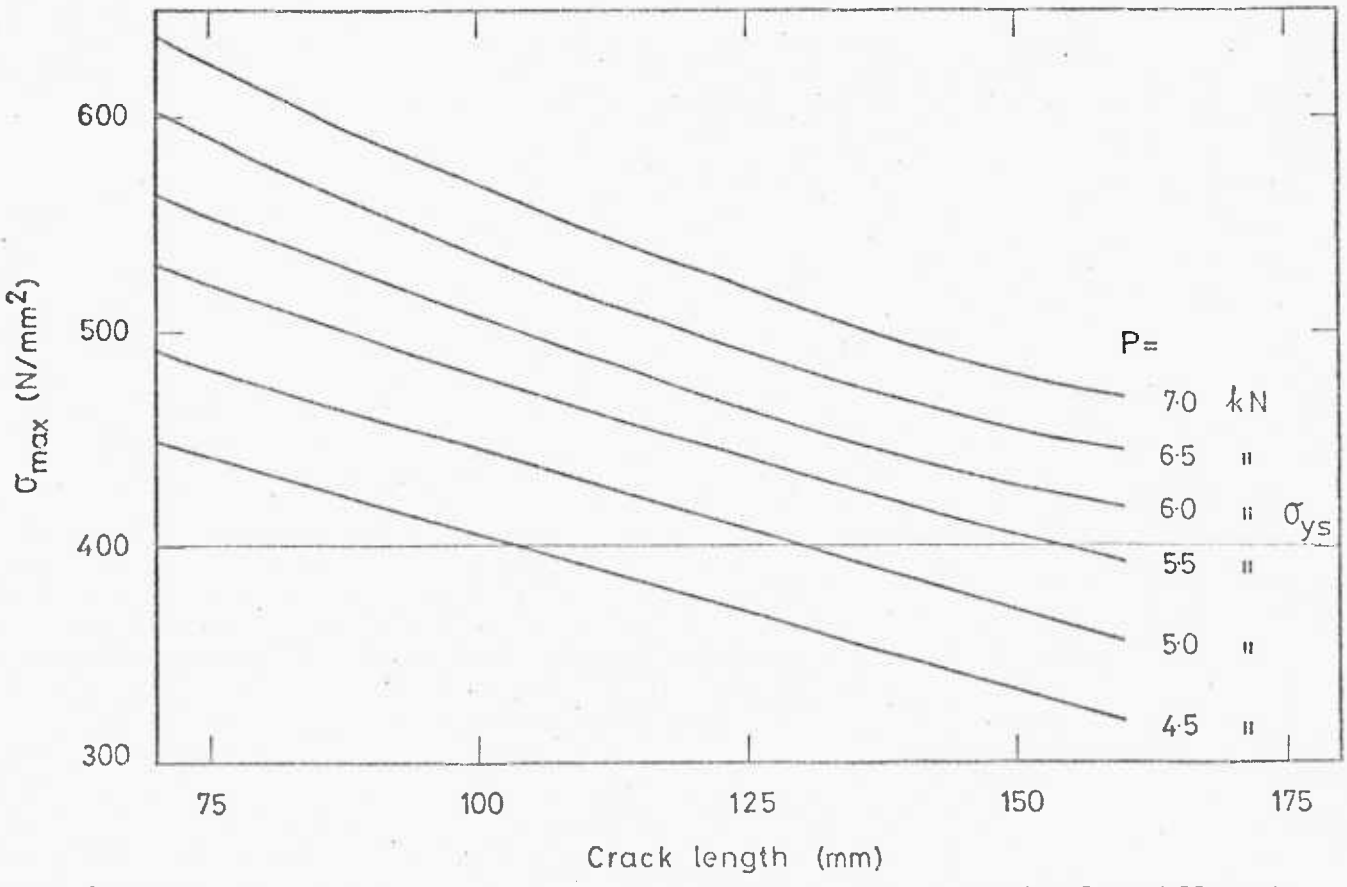


FIG. 68 Variation of the Maximum Bending Stress with Crack Length for Different Load Values. BS15. DCB Specimen

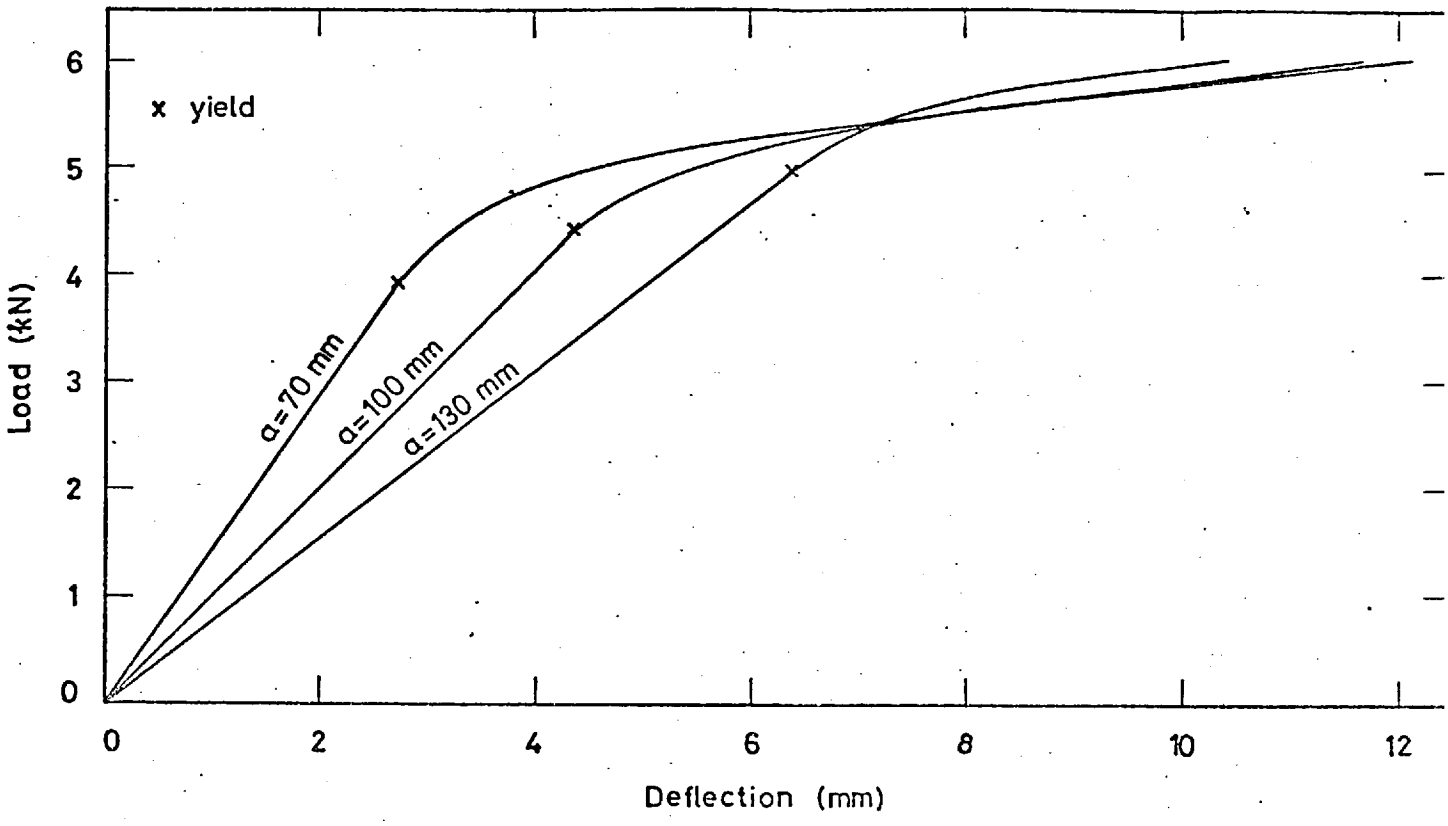


FIG. 69 Theoretical Load-Total Deflection Curves for Monotonic Loading at P = 6kN BS15. DCB Specimen

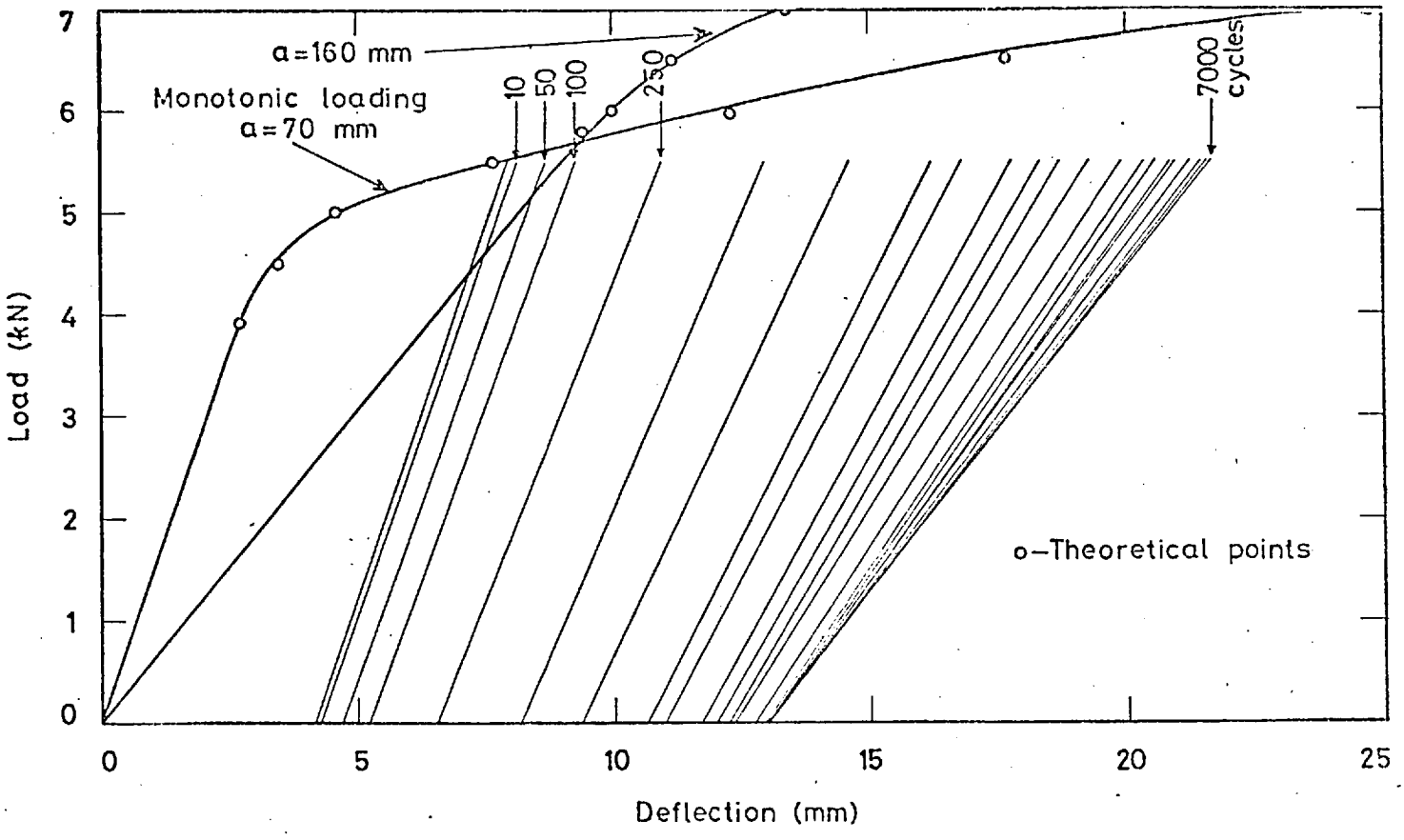


FIG. 70 Theoretical Load-Total Deflection Curves for Monotonic Loading at P=7.0kN and Experimental Load Deflection Loops at ΔP=5.5kN. BS15 DCB Specimen

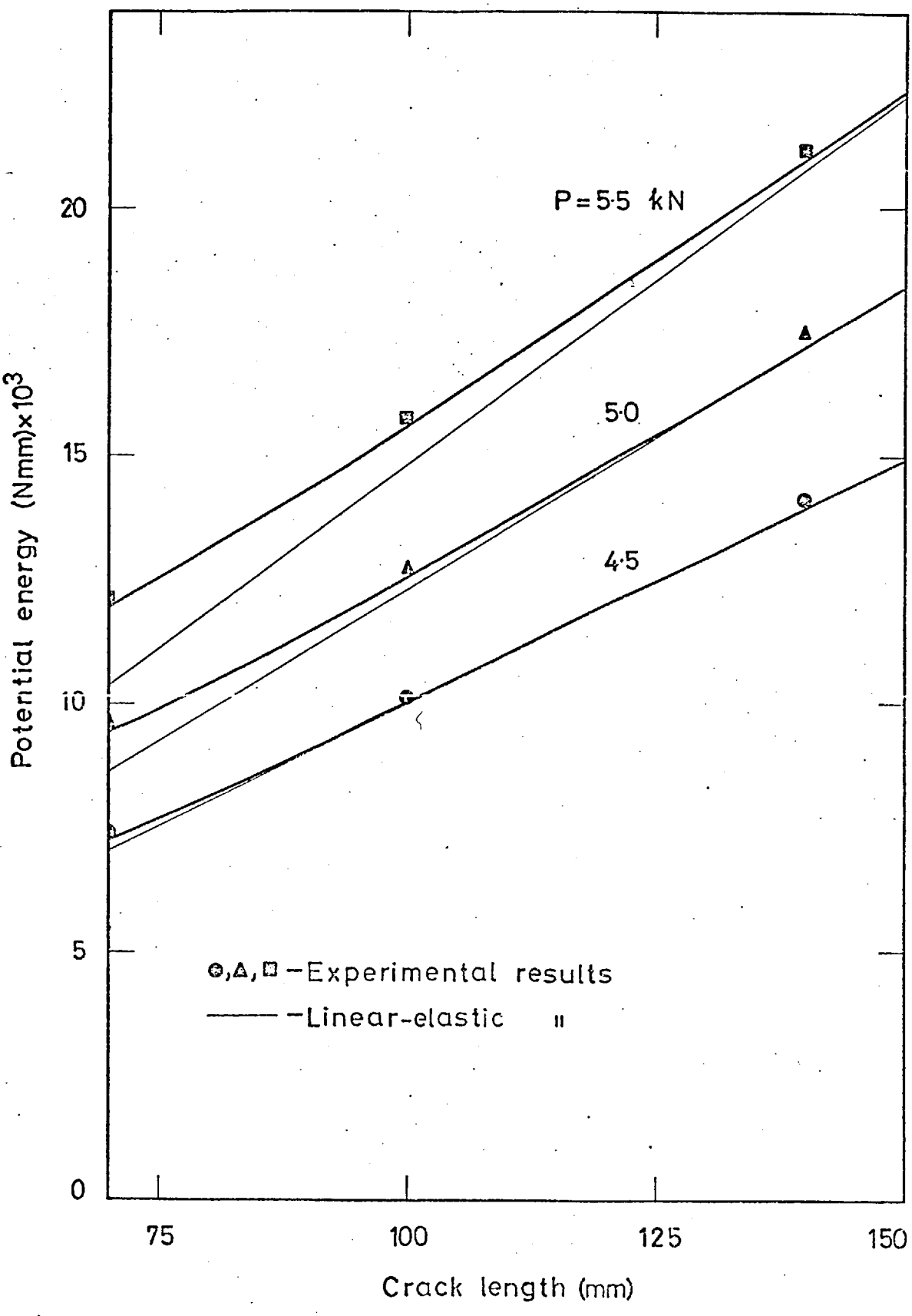


FIG. 71a Potential Energy vs. Crack Length, P = 4.5, 5.0 and 5.5 kN. BS15. DCB Specimen

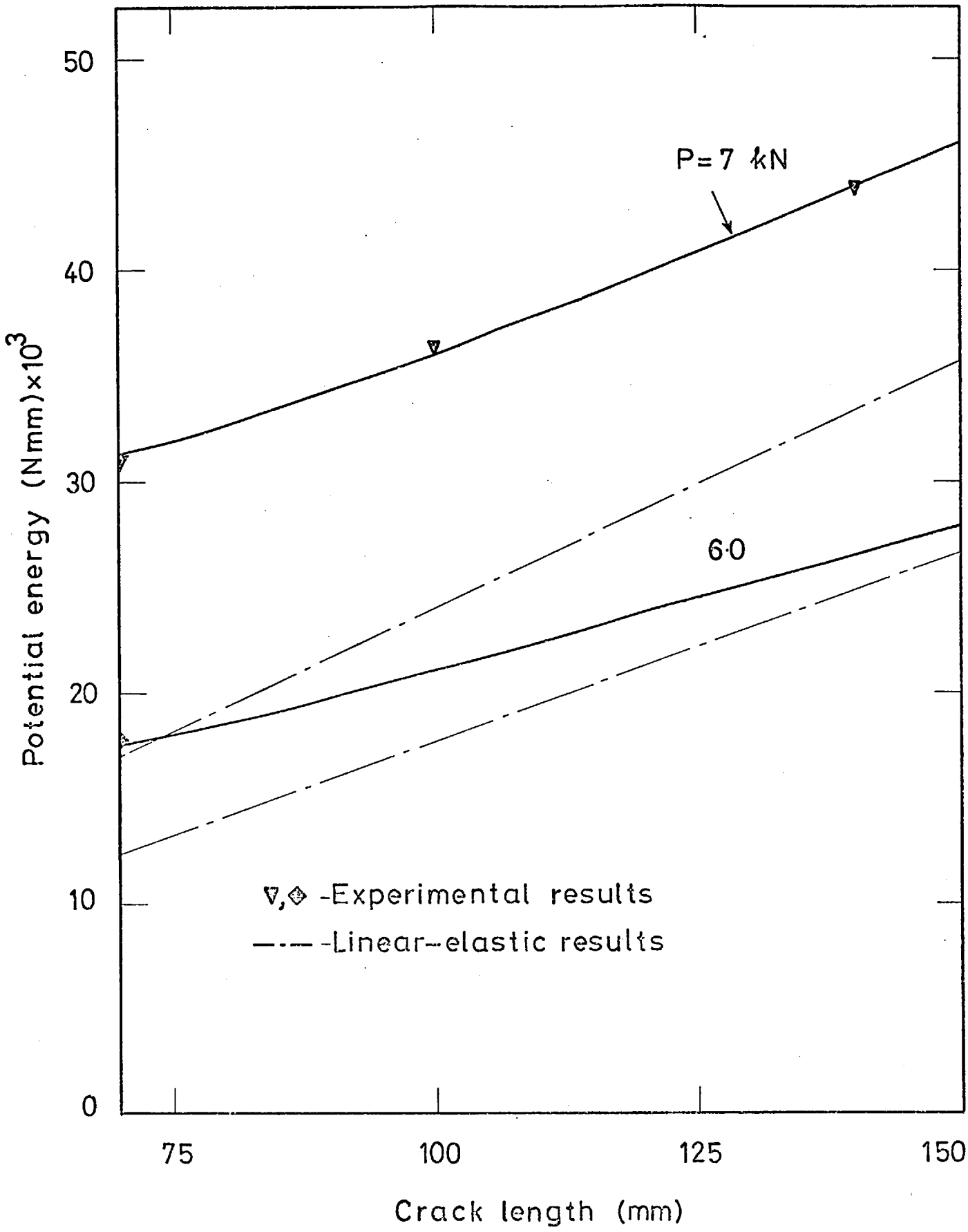


FIG. 71b Potential Energy vs. Crack Length P = 6.0 and 7.0 kN. BS15. DCB Specimen

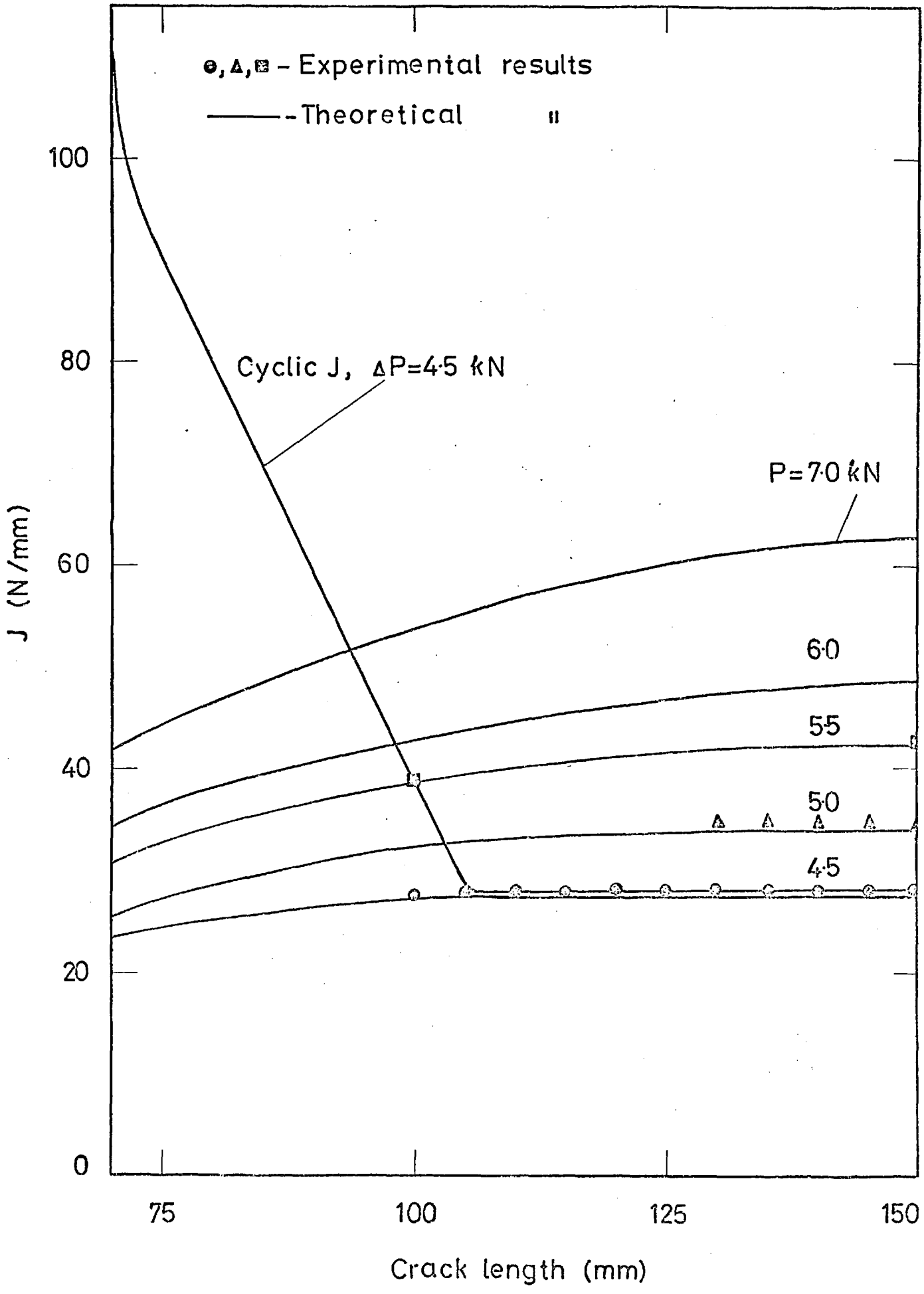


FIG. 72 J vs. Crack Length. BS15. DCB Specimen

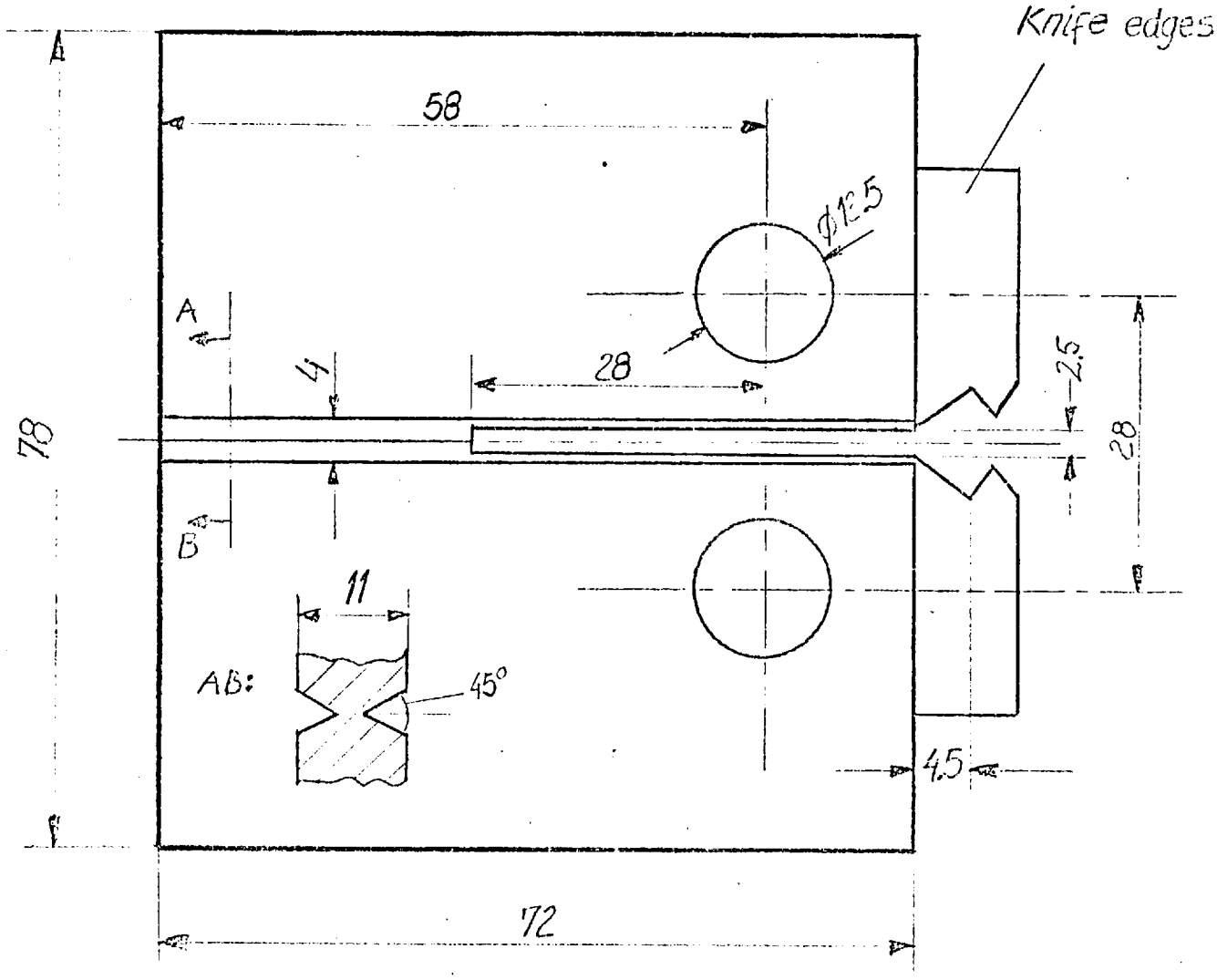


FIG. 73 The Compact Tension Specimen Used in the Experimental Programme. BS15.

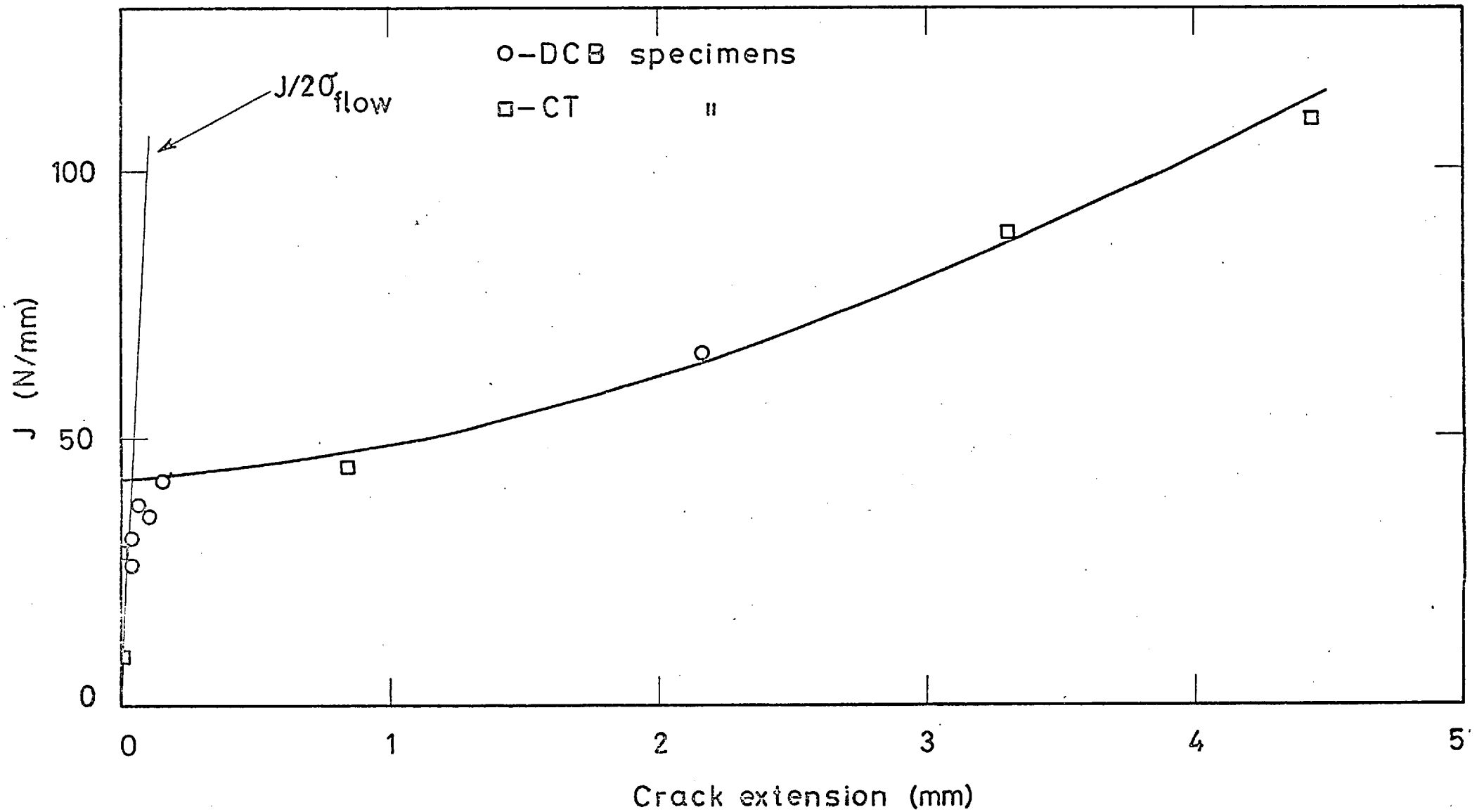


FIG. 74 J vs. Crack Extension Curve (R-Curve). BS15

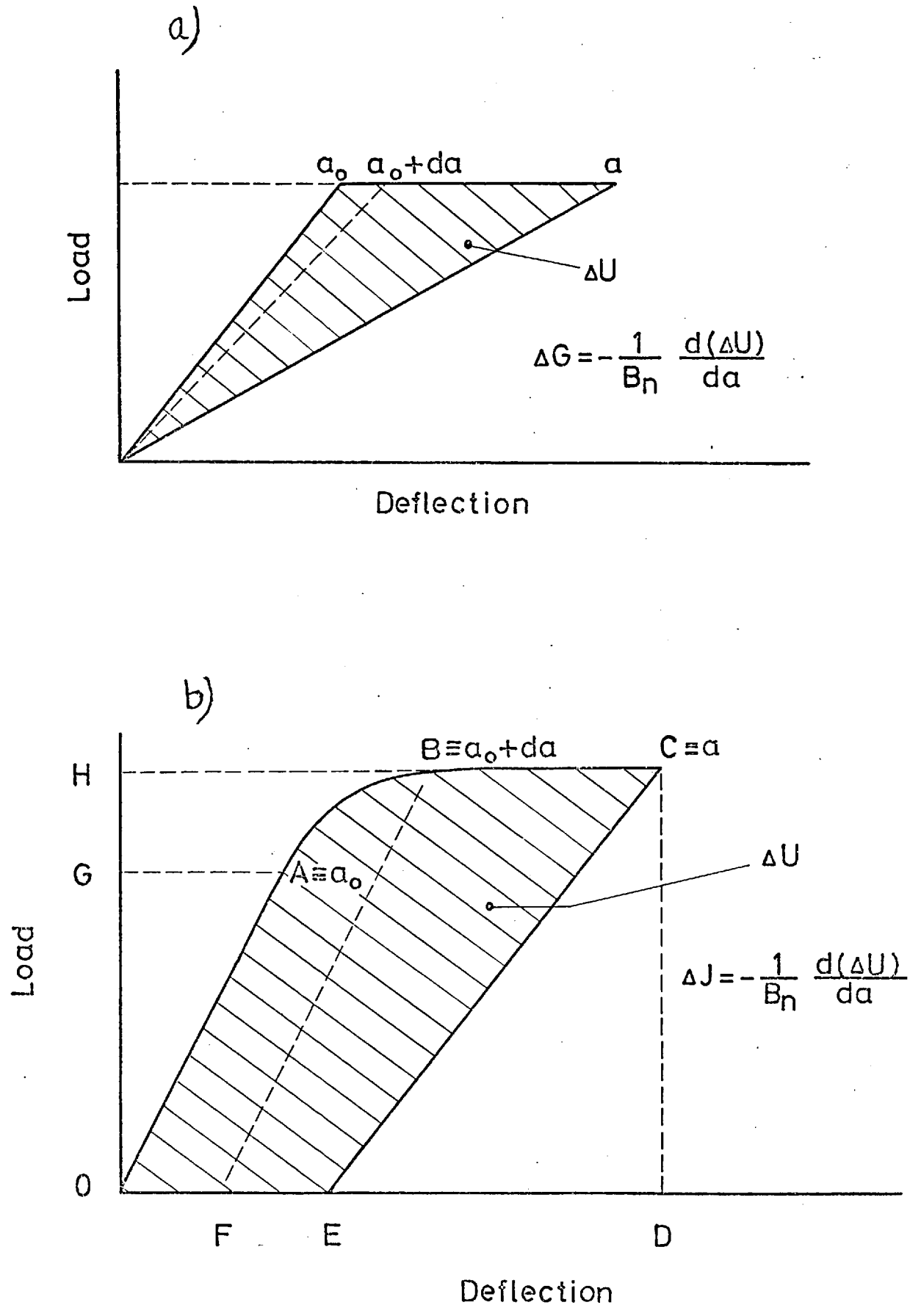


FIG. 75 Operational Definitions of Cyclic ΔG and ΔJ after N Loading Cycles

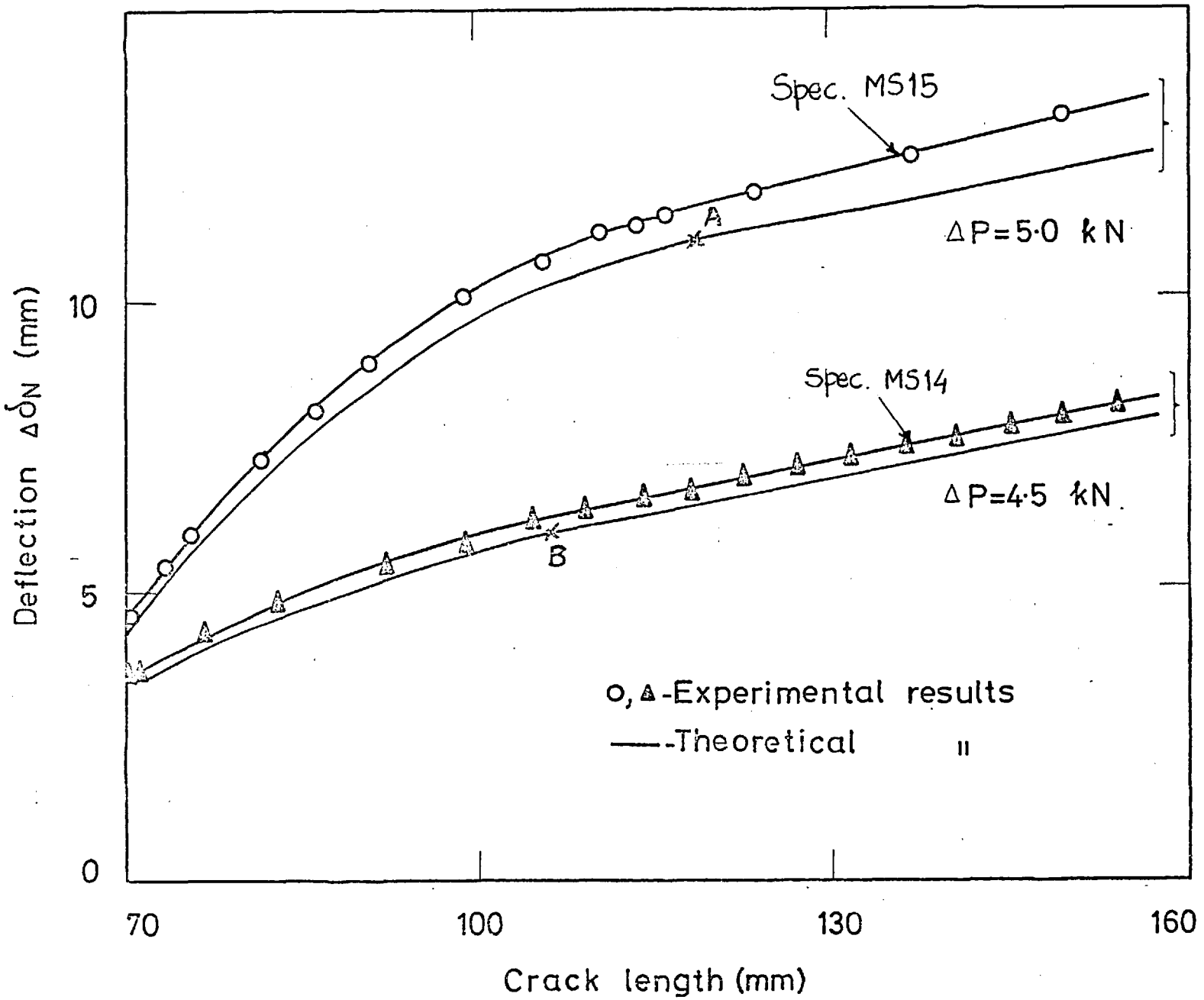


FIG. 76 Total Deflection vs. Crack Length. ΔP = 4.5 and 5.0 kN. BS15. DCB Specimen

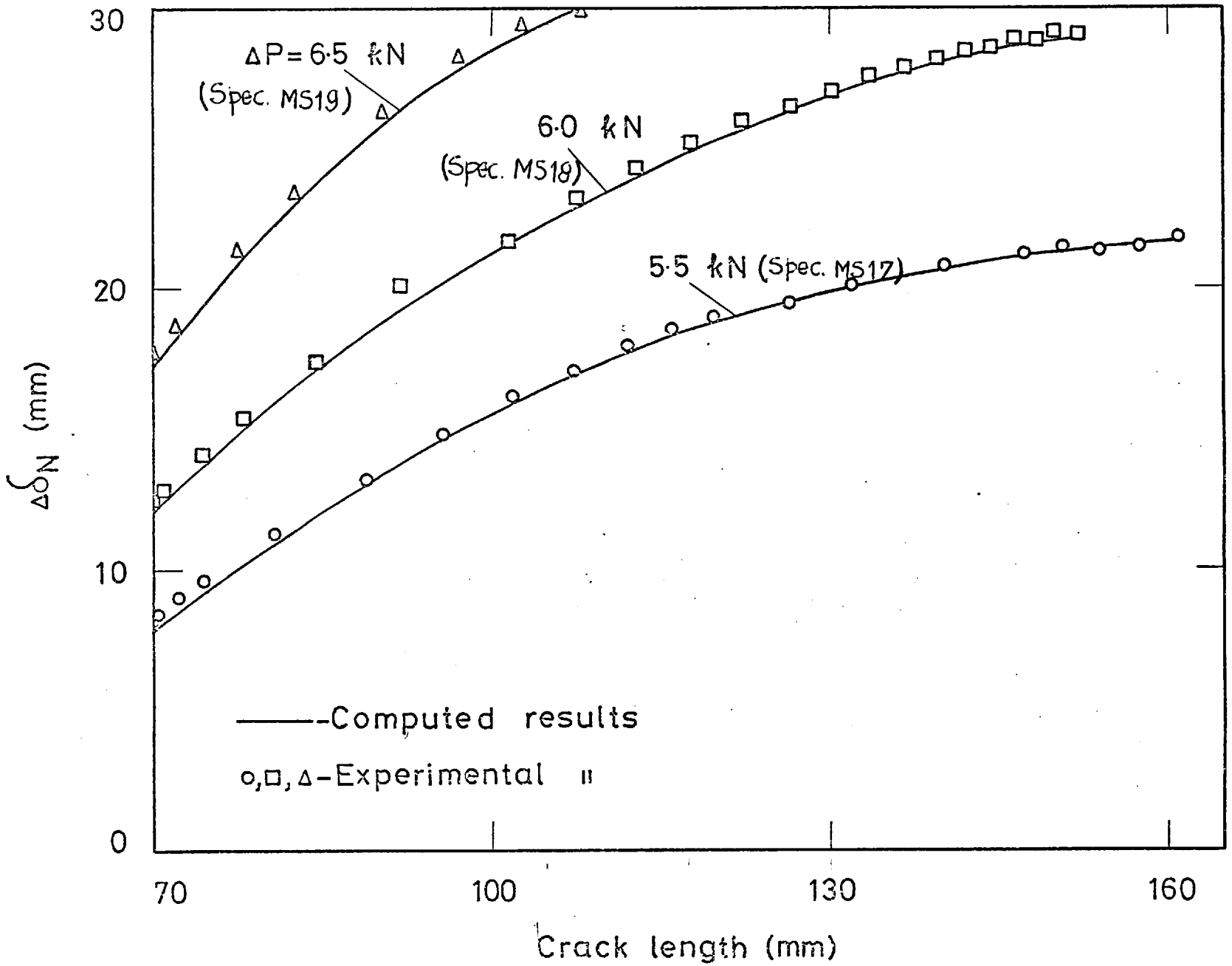


FIG. 77 Total Deflection vs. Crack Length. ΔP = 5.5, 6.0 and 6.5 kN. BS15. DCB Specimen

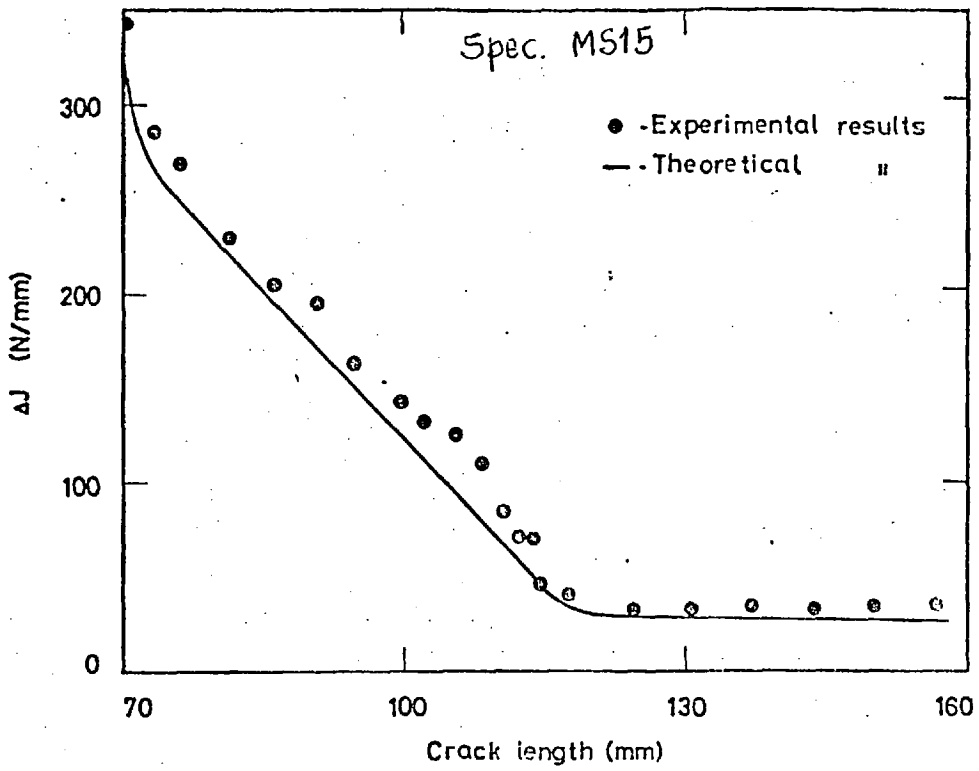


FIG. 78 ΔJ vs. Crack Length. ΔP = 5.8 kN. BS15. DCB Specimen

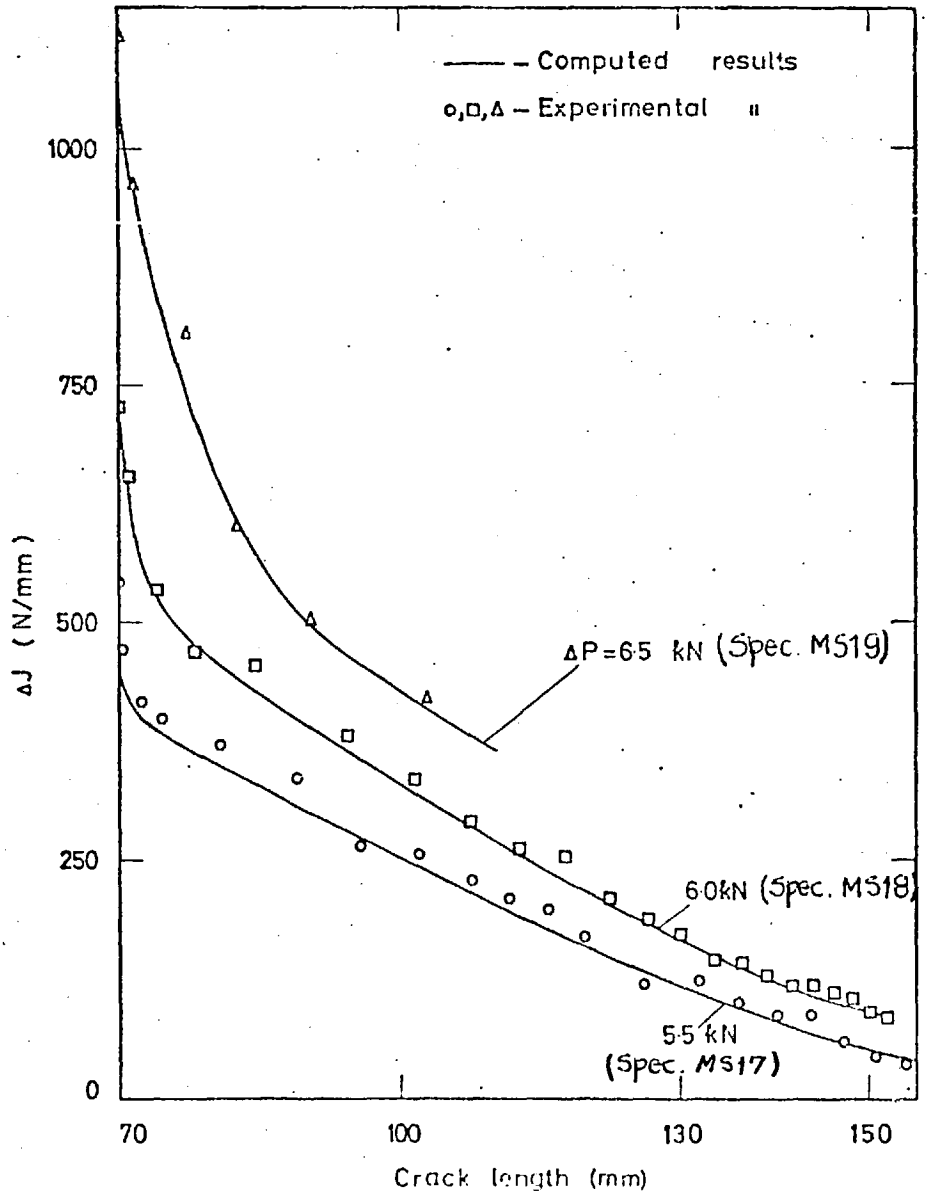


FIG. 79 ΔJ vs. Crack Length. ΔP = 5.5, 6.0 and 6.5 kN. BS15 DCB Specimen

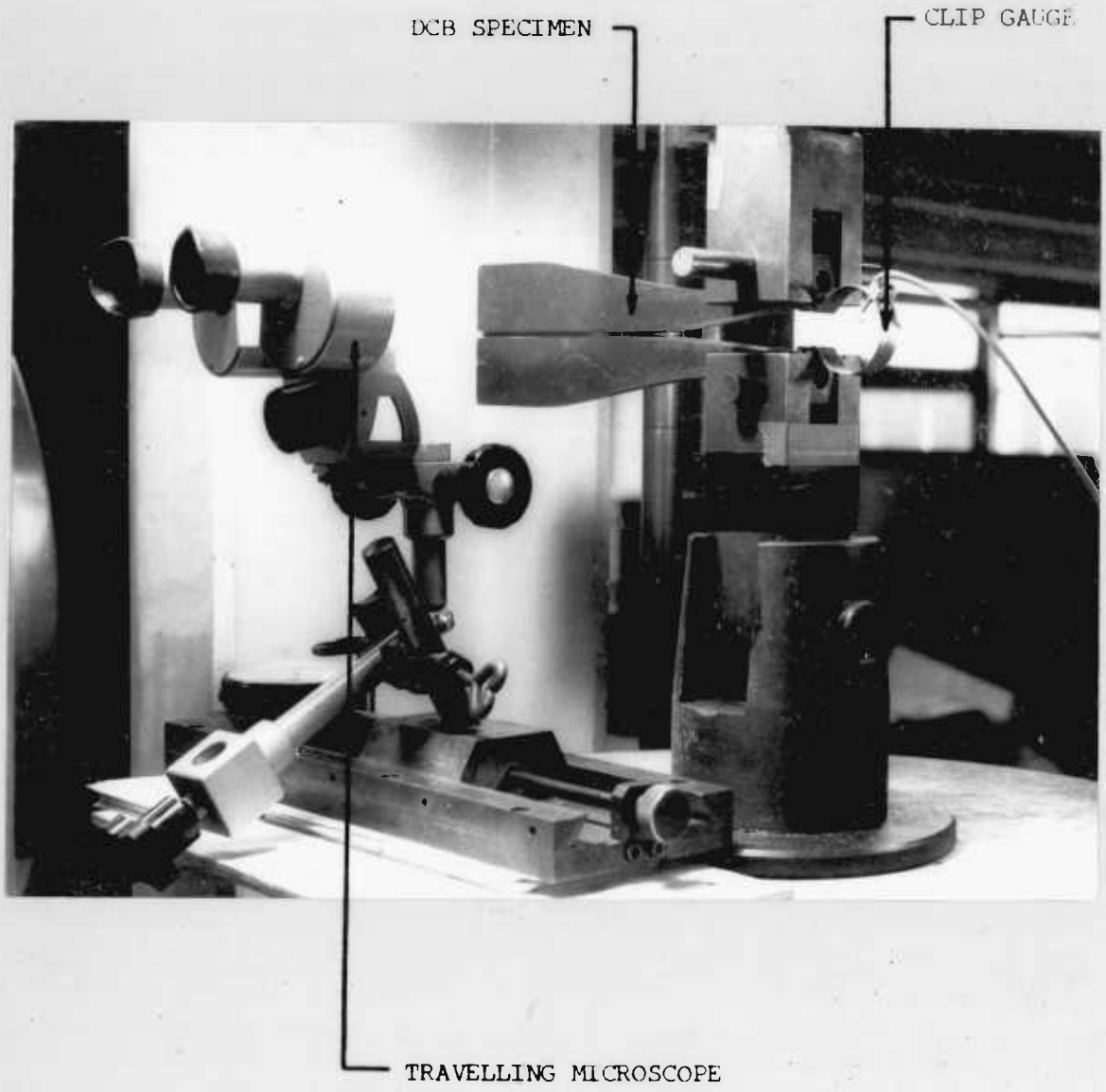


FIG. 80 View of one of the Specimens in a Load Cycling Test

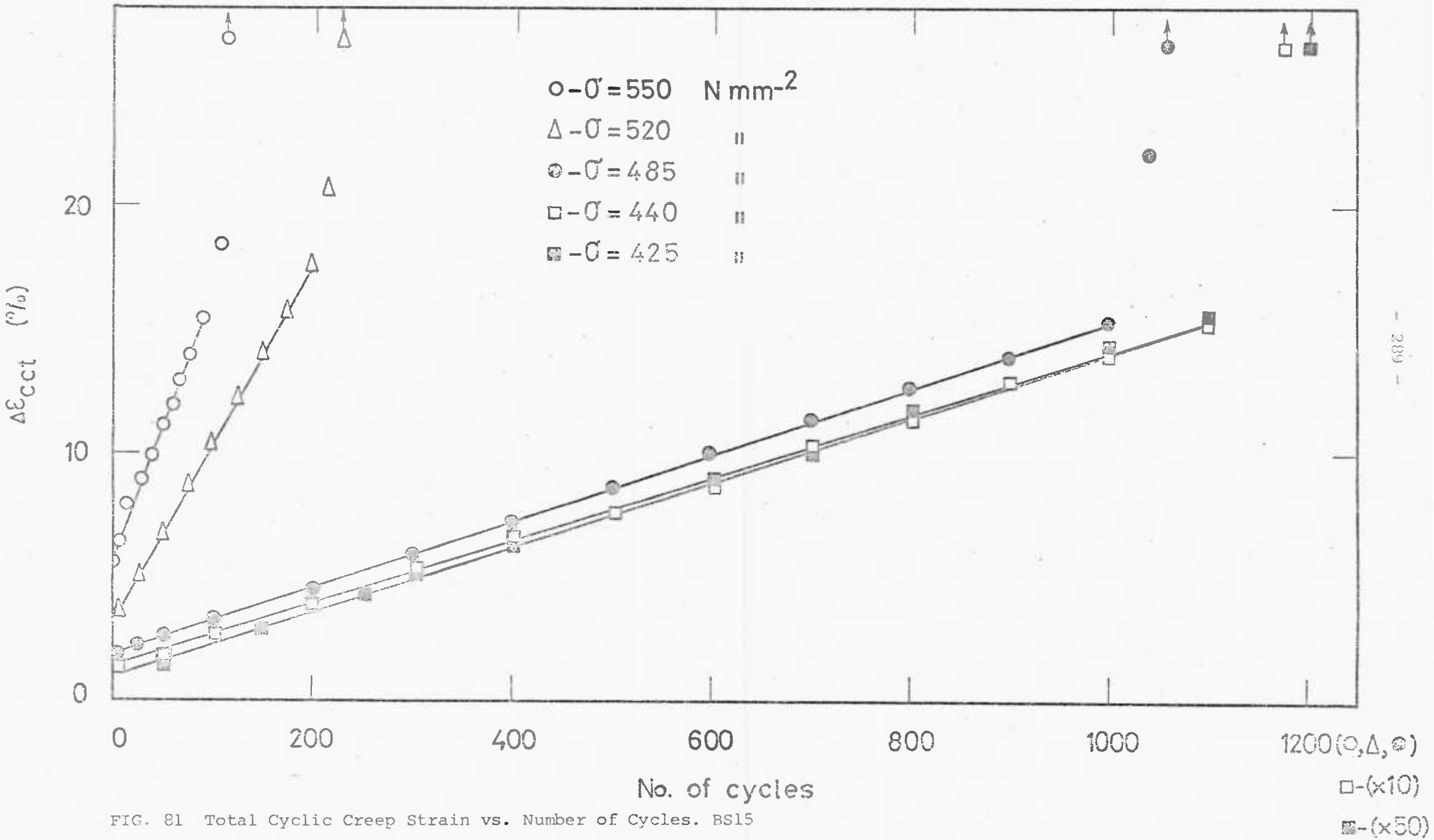
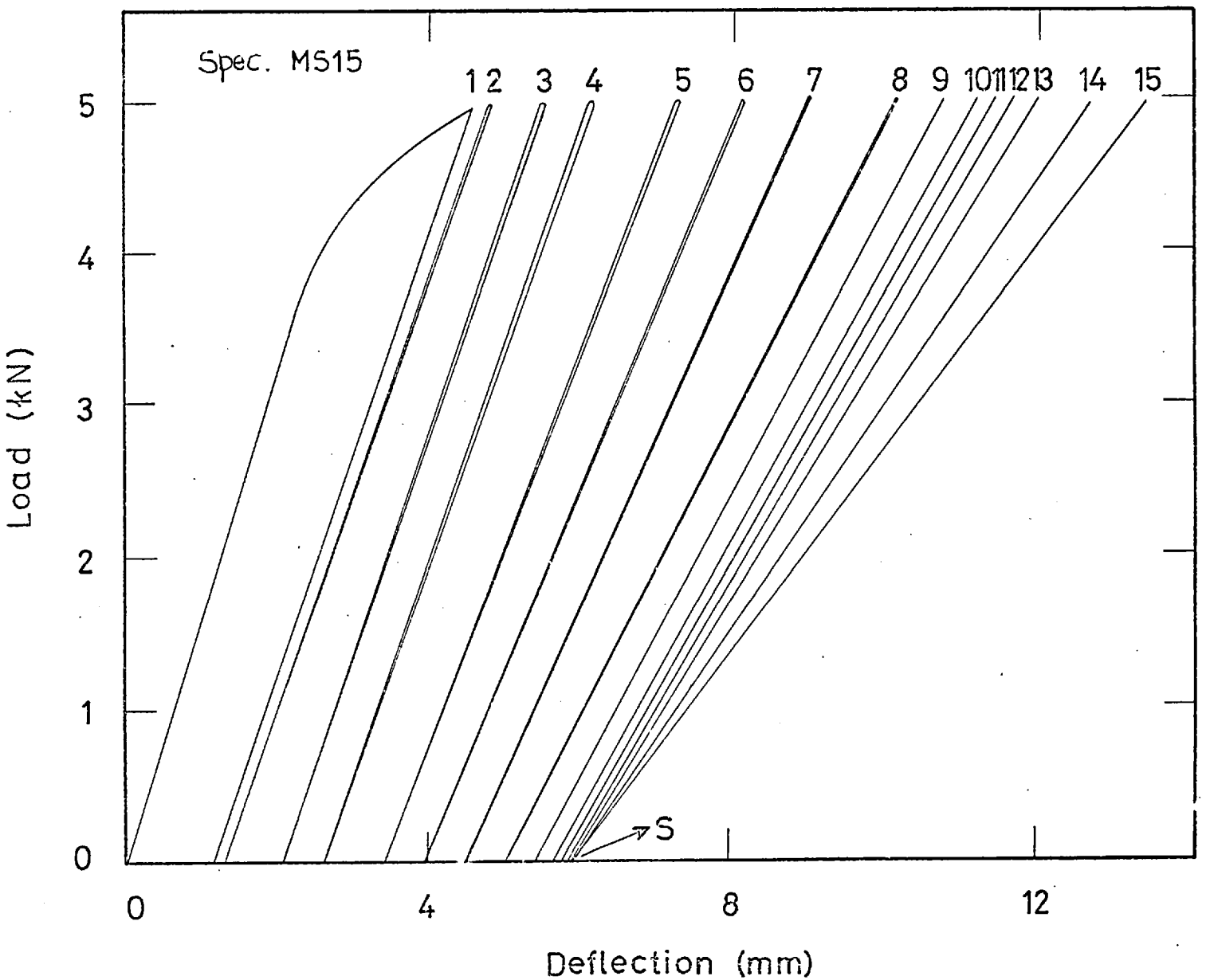


FIG. 81 Total Cyclic Creep Strain vs. Number of Cycles. BS15



Loop No.	Cycle No.
1	1
2	10
3	100
4	200
5	400
6	600
7	800
8	1200
9	1600
10	2000
11	2400
12	2800
13	4000
14	6000
15	8000

FIG. 82 Experimental Load-Deflection Loops. ΔP = 5.0 kN. BS15. DCB Specimen

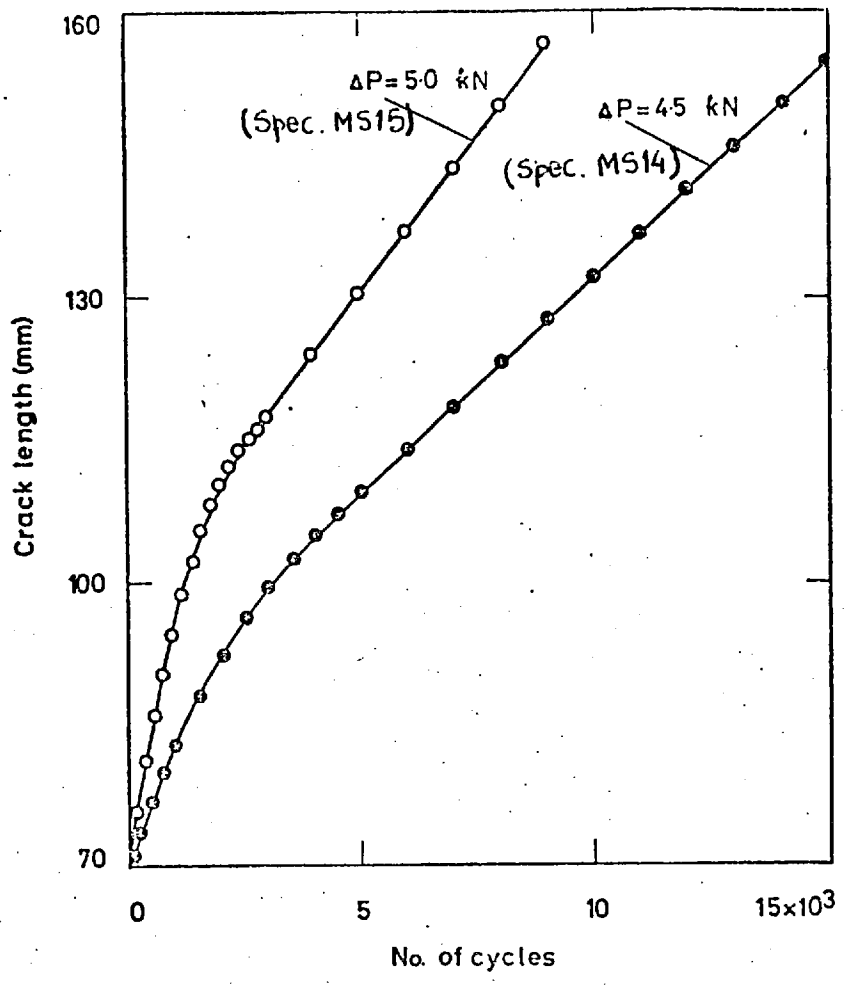


FIG. 83 Crack Growth Pattern for Load Cycling. BS15

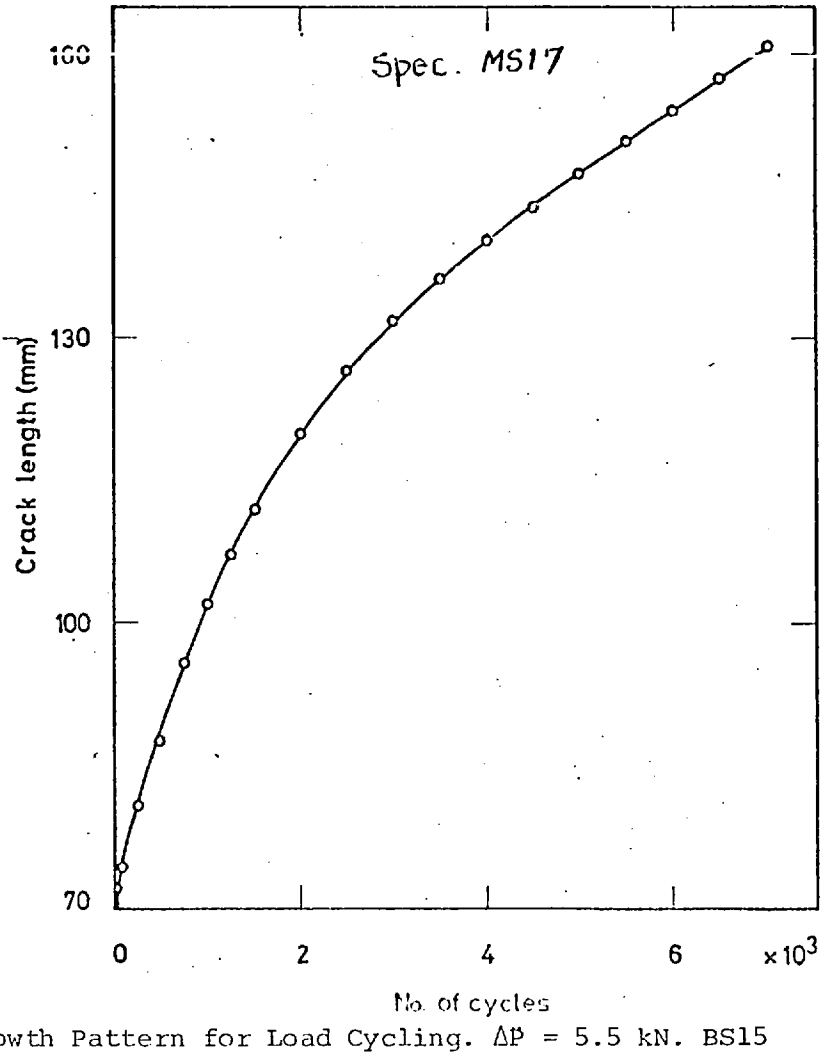


FIG. 84 Crack Growth Pattern for Load Cycling. ΔP = 5.5 kN. BS15

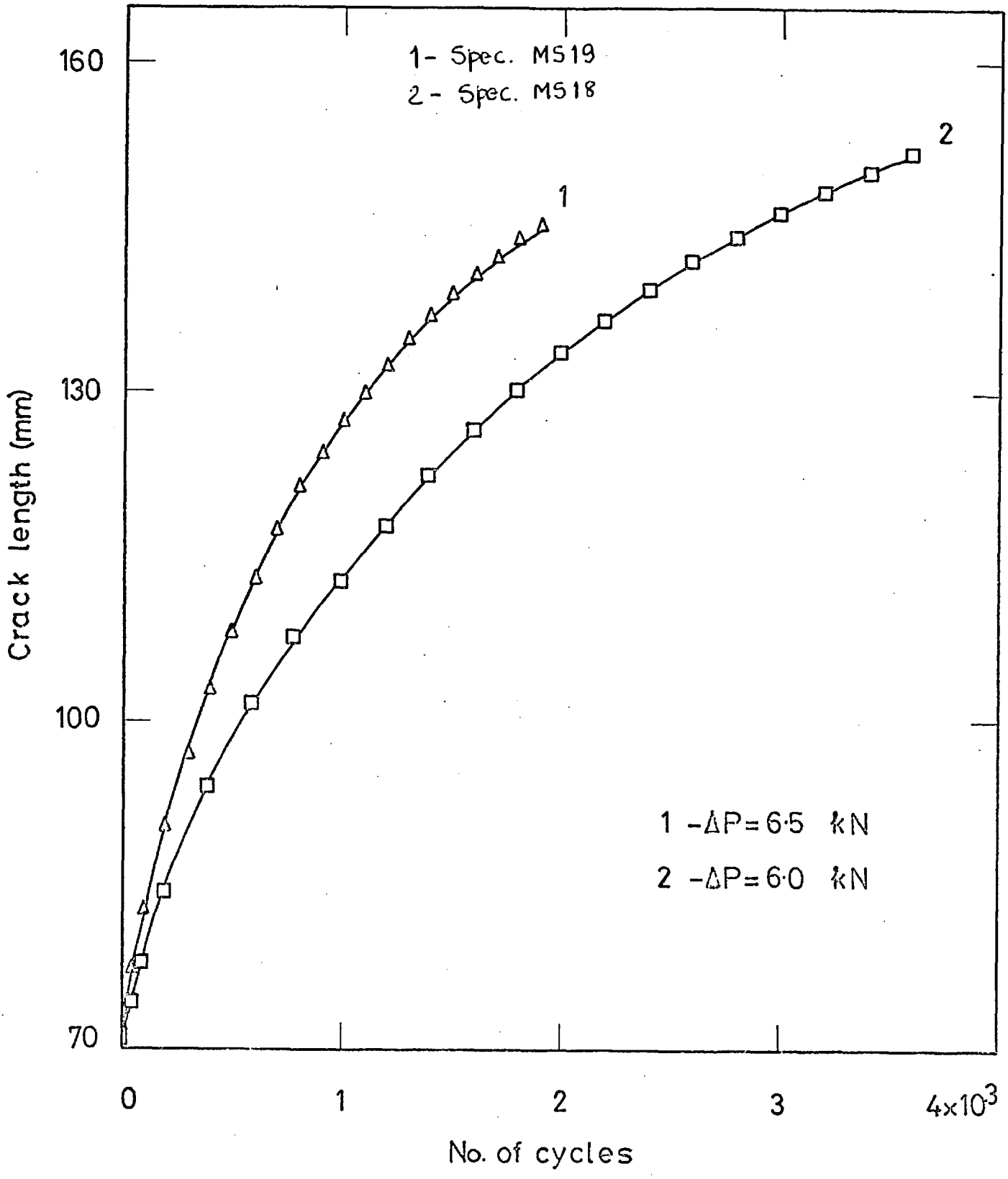


FIG. 85 Crack Growth Pattern for Load Cycling. BS15

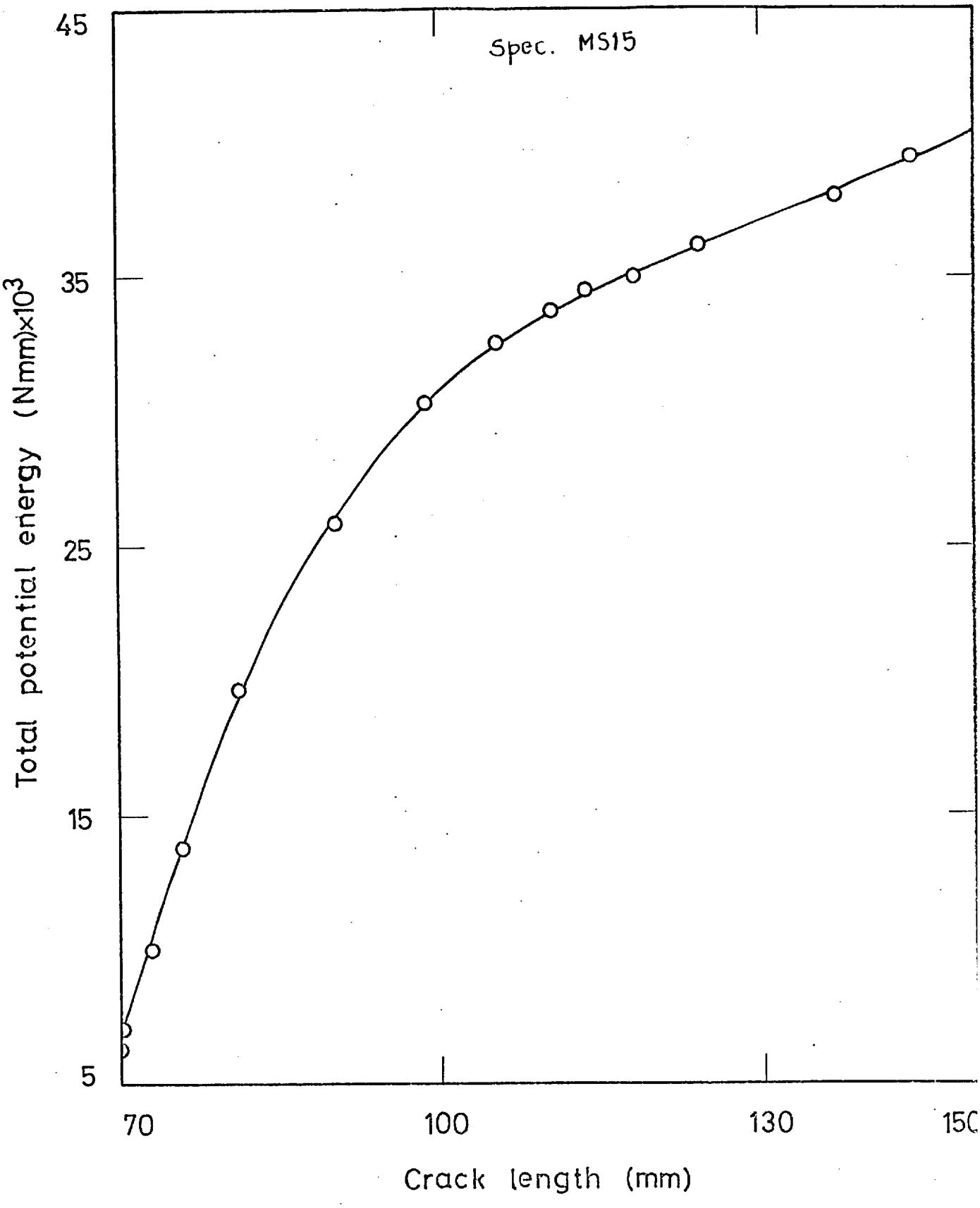


FIG. 86 Total Potential Energy vs. Crack Length. ΔP = 5.0 kN. BS15

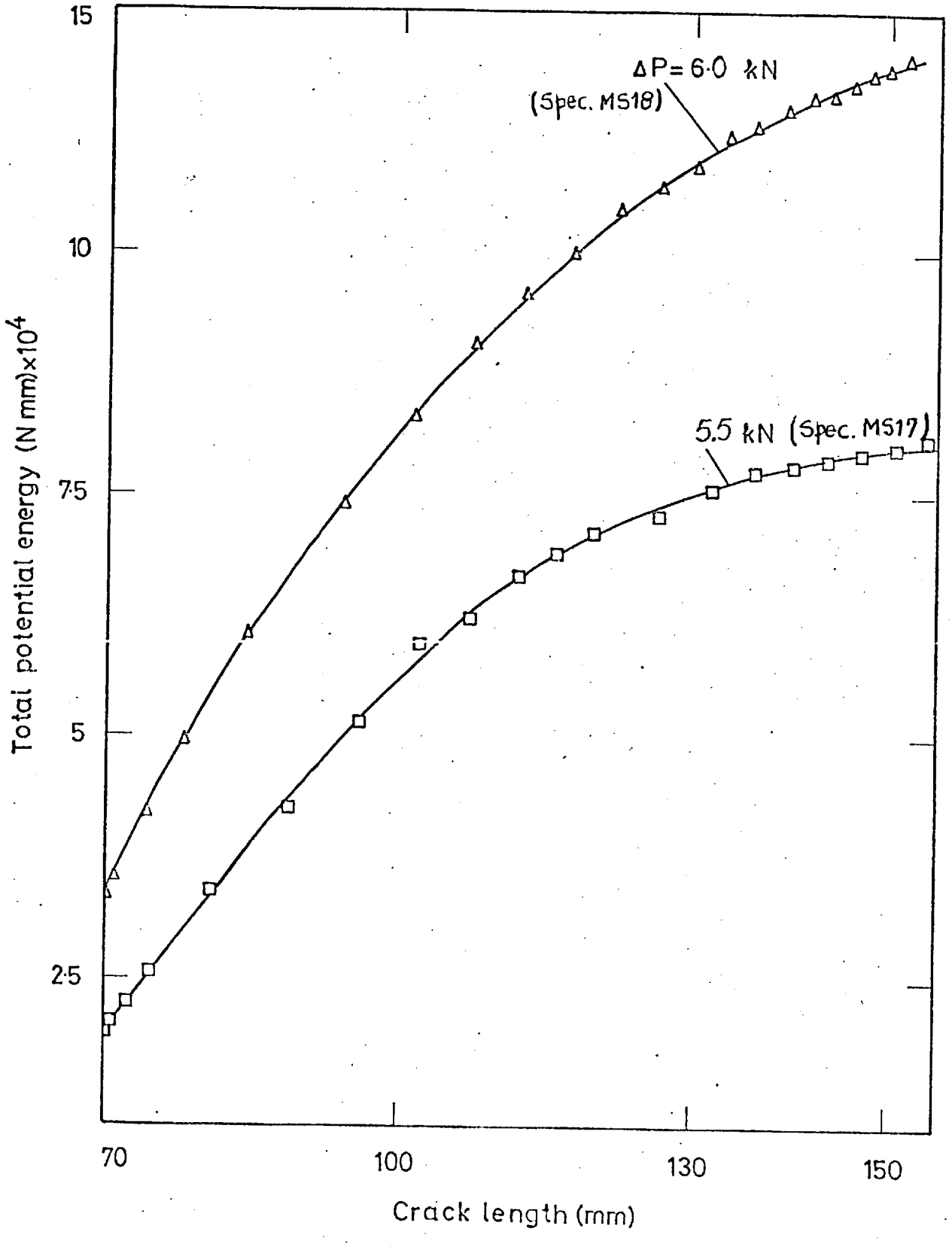


FIG. 87 Total Potential Energy vs. Crack Length. BS15

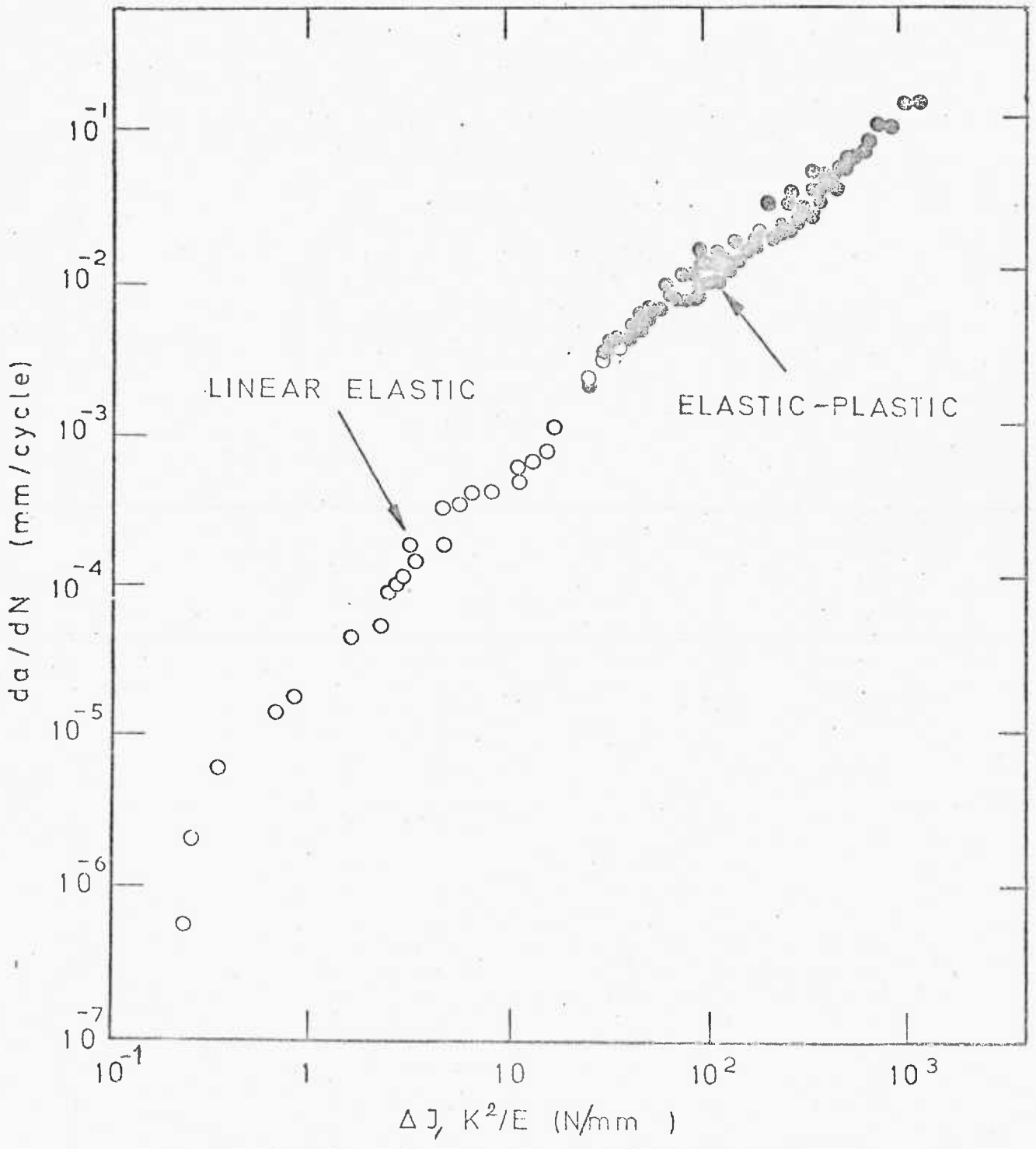


FIG.88 Crack Growth Rate vs. $\Delta J, K^2/E$. BS15. Laboratory air

LIST OF PUBLICATIONS

"Influence of Mean Stress Intensity on Fatigue Crack Growth in an Aluminium Alloy"
Journal of Mechanical Engineering Science, Vol. 17, No. 4, p. 199, (1975) (enclosed)

"An Analysis of the Influence of Mean Stress Intensity and Environment on Fatigue Crack Growth in a New High Strength Aluminium Alloy" ASTM's Journal of Testing and Evaluation, Vol. 3, No. 6, p. 407 (1975) (enclosed)

"Growth of Fatigue Cracks in Steels"
Metal Science, Vol. 10, No. 5, p. 149 (1976) (enclosed)

"Influence of Specimen Orientation and Loading History on SCC in an Aluminium Alloy"
Accepted for publication in Corrosion Science (February 1976)

"Fatigue Crack Growth under Gross Plasticity Cycling"
Accepted for presentation at the 2nd International Conference on the Mechanical Behaviour of Materials, Boston, August 1976.

"Crack Blunting and Arrest in Corrosion Fatigue of Mild Steel"
Accepted for publication as a Technical Note in the International Journal of Fracture (March 1976)

"Elastic-Plastic Fatigue Crack Growth under Load Cycling"
Submitted for publication in the Journal of Strain Analysis for Engineering Design, May 1976

"Cyclic and Monotonic J_{1c} values for Mild Steel"
Accepted for presentation at the ASTM's 10th National Symposium on Fracture Mechanics, Philadelphia, Pa. (August 1976)

INFLUENCE OF MEAN STRESS INTENSITY ON FATIGUE CRACK GROWTH IN AN ALUMINIUM ALLOY

C. M. Branco* J. C. Radon† L. E. Culver‡

The effects of the mean stress-intensity factor, K_m, and the range of the stress intensity, ΔK, on crack propagation phenomena in the Al-alloy RR58 have been studied using contoured double-cantilever beam specimens providing a constant stress-intensity factor for all crack lengths.

Based on the experimental data available, a relationship of the following form, between the cyclic crack growth rate, da/dN, and the tensile loading levels, has been proposed:

$$\frac{da}{dN} = A\left[\frac{2K_m(\Delta K - \Delta K_{th})}{K_{1C}^2 - K_{max}^2}\right]^{\alpha}$$

where $\Delta K = (K_{max} - K_{min})$; K_{max}, K_{min} and K_m are the maximum, minimum and mean values of the stress-intensity factor; ΔK_{th} is the threshold value of ΔK for crack propagation; K_{1C} is the critical fracture toughness in plane strain conditions; A and α are constants. In tests at room temperature (21 °C) in laboratory air and at a loading frequency of 0.15 Hz, it was found that ΔK_{th} decreased with increasing values of K_m, α was equal to 1.36 and A equalled 3.16 $\times 10^{-5}$ (in/cycle).

1 INTRODUCTION

Increasing use of higher strength materials confronts the structural engineer with formidable problems in the field of fatigue, in particular those connected with crack growth rates. The study of crack propagation caused by the application of cyclic loading aims to provide data of engineering materials in a form suitable for use in stress analysis and design. A great deal of fatigue research is now being directed towards a detailed investigation of subcritical crack growth from the initiation period up to the critical crack size. The development of Linear Elastic Fracture Mechanics (LEFM) concepts gave a promising approach to the investigations of crack growth in statically-loaded engineering structures; stress-intensity factors, K, are now known for a wide range of cracked configurations. Subsequent application of LEFM methods in cyclically-loaded situations offered yet further possibilities for reliable evaluations of engineering materials. Recent work (1)(2)§ provided some evidence that the LEFM approach may be conveniently used to describe the propagation of cracks under fatigue conditions in aluminium alloys. Because of the increasing volume of these alloys used in advanced engineering structures, more detailed information concerning their behaviour is needed. One of the recently developed Cu–Al alloys, RR58, used in the aeronautical industry was chosen for the present study.

In the last ten years, a number of fatigue crack growth 'laws' have been proposed and are fully described in (3). While some of the laws suggest that the critical parameter may be a function of stress or of strain, the majority are based on LEFM concepts. The basic and probably most widely known crack propagation equation, due to Paris, has been successfully applied to analyse cyclic crack growth in many materials:

$$\frac{da}{dN} = C_1(\Delta K)^m \quad . \quad . \quad . \quad . \quad . \quad . \quad . \quad . \quad . \quad . \quad (1)$$

where a is the crack length, N is the number of cycles and C_1 and m are constants dependent on the material tested, the environment and the conditions of cyclic loading.

In an investigation of fatigue crack growth in RR58, Pearson (4) applied the equation

$$\frac{da}{dN} = C_2\frac{(\Delta K)^{m_1}}{[(1-R)K_C - \Delta K]^{\frac{1}{2}}} \quad . \quad . \quad . \quad . \quad . \quad (2)$$

where R is the stress ratio ($K_C = K_{min}/K_{max}$), C_2 and m_1 are constants, and K_C is the critical fracture toughness. Good agreement was found in the limited range between 10^{-6} and 10^{-4} in/cycle but at high values of ΔK some discrepancies were observed.

Recent results of a comprehensive programme of work on a range of materials (5) provided detailed information on the effects of frequency and of the mean level, K_m, and the amplitude, ΔK, of the stress-intensity factor. They led to a crack propagation model of the form

$$\frac{da}{dN} = \beta(2\Delta K\, K_m)^n = \beta(K_{max}^2 - K_{min}^2)^n \quad . \quad . \quad . \quad (3)$$

where β and n are constants dependent upon the test conditions. Because of the encouraging correlation of the above results analysed by equation (3) it was decided to apply the method to the present alloy RR58. Preliminary tests on this material indicated that the criterion could probably find a wider application although the tests had been restricted to a comparatively narrow range of ΔK; in particular, the effect of cycling at very low values of K—usually described as Region I and associ-

The MS. of this paper was received at the Institution on 19th June 1974 and accepted for publication on 29th April 1975.

* *Department of Mechanical Engineering, Imperial College of Science and Technology, London.*

† *Department of Mechanical Engineering, Imperial College of Science and Technology, London. Fellow of the Institution.*

‡ *Senior Lecturer, Department of Mechanical Engineering, Imperial College of Science and Technology, London. Fellow of the Institution.*

§ *References are given in the Appendix.*

ated with a limiting threshold value, ΔK_{th}—was not investigated.

The forms of equations (1), (2) and (3) indicate that crack growth will take place at any value of ΔK—even very small values. However, it has been shown recently (6) that there exists a critical range of stress intensity below which crack propagation occurs either extremely slowly or not at all. The threshold value, ΔK_{th}, seems to be dependent on the basic material properties and could be expressed as

$$\Delta K_{th} = \eta E \quad . \quad . \quad . \quad . \quad . \quad . \quad . \quad . \quad . \quad . \quad . \quad (4)$$

where E is Young's modulus and η is a constant dependent on the material tested, environment and loading rate (7). Information on threshold values for structural materials, such as higher strength Al-alloys or low-alloy steels, is needed.

Early cyclic fatigue investigations performed on metals, in particular on steels, indicated that the mean stress was of only minor importance in the process of crack propagation. However, other more recent work (8) has shown that in certain materials the mean stress effect may not be negligible. Some evidence that Al-alloys belong to this class of materials is now available (9) but information on the effects of variations in the mean stress intensity in the full subcritical range and threshold data for low frequencies are at present scarce.

This paper reports on a study of the effect of the mean value of the stress-intensity factor, K_m, on the crack propagation rate in 2.6 per cent Cu–Al alloy RR58 under repeated tension fatigue conditions at 21 °C and at low cyclic speeds. Also, the variation in the value of the threshold stress intensity, ΔK_{th}, is discussed in terms of K_m.

2 EXPERIMENTAL

The composition and principal mechanical properties of RR58 are presented in Table 1. The material was supplied

Table 1. *RR58. Chemical composition and principal mechanical properties*

Composition (per cent by weight)	Cu 2.64	Mg 1.65	Mn 0.03	Si 0.23	Fe 1.15	Ti 0.06	Zn 0.06	Ni 1.15
Properties (at 21 °C and 10^{-3} strain rate)	Young's modulus, E				10.84×10^6 lbf/in^2 (75.0×10^3 MN/m^2)			
	Poisson's ratio, ν				0.33			
	Ultimate tensile stress, σ				65×10^3 lbf/in^2 (450 MN/m^2)			
	0.1 per cent proof stress, σ_Y				53×10^3 lbf/in^2 (367 MN/m^2)			
	Minimum elongation				6 per cent on 1 in gauge length			

in plates 36 × 36 × 3 in (910 × 910 × 76 mm) and the DCB specimens (Fig. 1) were cut in such a way that the crack propagated along the rolling direction whilst the load was applied in the short transverse direction. The maximum height of the specimens corresponded to the full thickness of the plate (3 in), thus the lowest toughness values could be investigated.

Stress-intensity factors for plane strain conditions can be calculated from the well-known relationship

$$K_1 = P\left[\frac{E}{2B(1-\nu^2)}\frac{dC}{da}\right]^{\frac{1}{2}} \quad . \quad . \quad . \quad . \quad . \quad . \quad . \quad . \quad (5)$$

where P is the applied load, ν is Poisson's ratio, B is the net fracture width and C is the compliance. For a suitably shaped DCB testpiece, K_1 will remain constant with crack length.

The design of the 'contoured' double-cantilever beam specimen (Fig. 1) was described in detail in (10). Basically, in order to comply with the condition of dC/da = constant, a contoured shape was chosen having the form

$$\frac{3a^2}{h^3} + \frac{1}{h} = 38 \quad . \quad . \quad . \quad . \quad . \quad . \quad . \quad . \quad . \quad . \quad (6)$$

where h is the specimen height at crack length a. Tests performed with specimens of this geometry (10) showed only a minimal (±2 per cent) variation of K. Deep side grooves were provided in the mid-plane of symmetry on both sides of the specimen to enhance plane strain conditions and to help direct crack propagation. The finished specimens were given a heat treatment consisting of ageing at 190 °C for 30 hours in a salt bath; the resulting hardness values varied within the range 145–150 VPN (20 kg). The crack starter was a saw cut, extended to a chevron notch, and sharpened with a razor blade.

In order to establish static values of K_{1C} at room temperature, all specimens were pre-cracked and tested in an Instron tensile testing machine, type TT-C, 10 000 lbf capacity, at a cross-head speed of 0.002 in/min (0.05 m/min). The crack propagated smoothly and without deviations from the crack plane, and the crack length was monitored with a travelling microscope for about 1 in (25 mm). A linear variation of compliance with crack length was obtained. The total load variation along the test-length of the specimen (6 in approximately) was within ±2 per cent, which was found to be satisfactory in the subsequent fatigue tests. Values of K_{1C} for all specimens tested varied between 20 400 and 21 850 lbf/in^2 × in$^{\frac{1}{2}}$ (22.44 and 24.03 MN/m$^{\frac{3}{2}}$), thus agreeing with previously established values (10). It should be noted that all fracture toughness results quoted in this paper were obtained from specimens $\frac{3}{8}$ in (9.5 mm) thick. It should be mentioned that the static K_{1C} value quoted by Pearson (4) for the same alloy $\frac{1}{2}$ in (12 mm) thick, albeit tested in a different orientation, was 21 000 lbf/in^2 × in$^{\frac{1}{2}}$ (23.1 MN/m$^{\frac{3}{2}}$).

The fatigue tests were carried out in a Denison T42C2 hydraulic testing machine specially fitted with a cycling mechanism; basically, this consisted of two limit microswitches to regulate the load. Tests were conducted in laboratory air, 50 per cent r.h. at 21 °C, and at a cycling frequency of 0.15 Hz with a tensile sinusoidal load wave. Two test series were completed: in the first, cycling was under constant K_m conditions whilst ΔK was varied; in the second, cycling was under constant ΔK conditions, K_m being the variable. The crack propagation was monitored with a travelling microscope of 50× magnification with an accuracy better than 0.0001 in (0.0025 mm).

The plastic zone side, r_p, at the crack tip was calculated

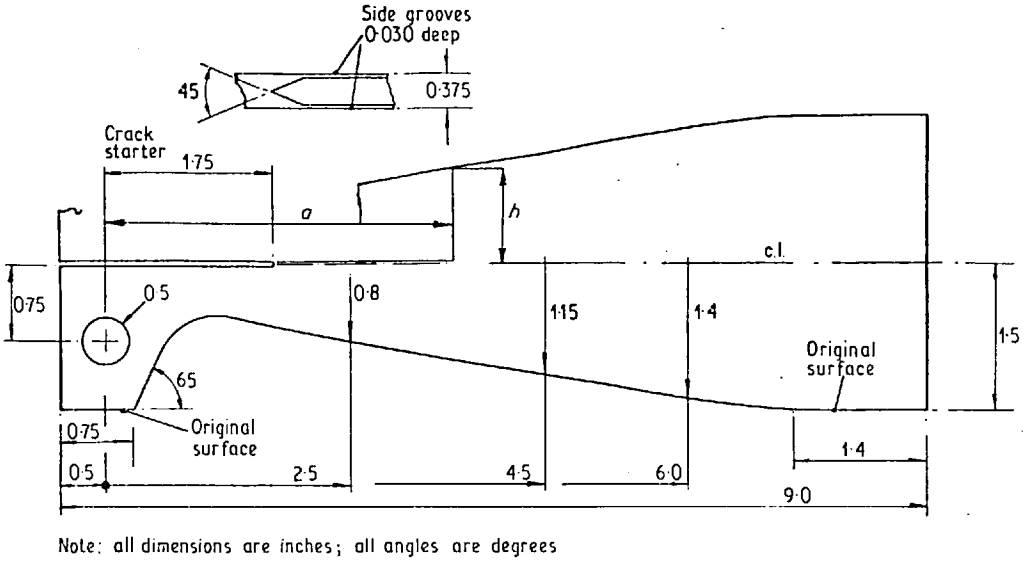


Fig. 1. *Contoured double-cantilever beam specimen*

for plane strain conditions (11) from

$$r_p = \frac{1}{6\pi}\frac{K_1^2}{\sigma_Y^2} \quad . \quad . \quad . \quad . \quad . \quad . \quad . \quad . \quad . \quad . \quad . \quad (7)$$

where σ_Y is the yield stress measured at the appropriate test conditions. For the highest value of K_{max} (= 19 380 lbf/in^2 × in$^{\frac{1}{2}}$), r_p was 1.03×10^{-2} in (0.26 mm). This value was considered small when compared with the specimen net thickness of 0.315 in (8 mm).

3 RESULTS AND DISCUSSION

The dependence of crack growth on ΔK was investigated in previous work (12) using tensile cyclic tests at $R = 0$. A typical linear relationship between crack length and the number of cycles is shown in Fig. 2. Crack speed, da/dN, increased with increasing values of applied ΔK.

It should be remembered that the results of the tests in which ΔK is varied at $R = 0$ inevitably include the influence of the mean value of stress intensity as well since K_m increases proportionately with increasing ΔK. Thus, the results of tests in which $R = 0$ and K_m (and hence ΔK) is varied (curve 1, Fig. 3), may be described (in the linear region) by a crack propagation law such as equation (1), but they cannot indicate the separate effects of ΔK and K_m.

In order to separate the individual effects, two further series of tests were conducted. In the first series, K_m was maintained at a constant value whilst ΔK was varied. Thus, for a specific value of K_m equal to 11 000 lbf/in^2 × in$^{\frac{1}{2}}$ (12.1 MN/m$^{\frac{3}{2}}$) and ΔK varying between 2600 and 15 700 lbf/in^2 × in$^{\frac{1}{2}}$ (2.86 and 17.27 MN/m$^{\frac{3}{2}}$), the results (Fig. 4) show a linear dependence of crack growth on the number of load cycles. Similar results were obtained from further tests with K_m constant and equal to 5000, 7500, 11 000, 15 000 and 16 500 lbf/in^2 × in$^{\frac{1}{2}}$ (5.5, 8.25, 12.1, 16.5 and 18.15 MN/m$^{\frac{3}{2}}$).

Crack growth rates were calculated for each test and superimposed on Fig. 3 to form a family of curves (2–6), for given K_m values at $R \neq 0$, which may be compared with curve 1 obtained from the R = 0, variable K_m,

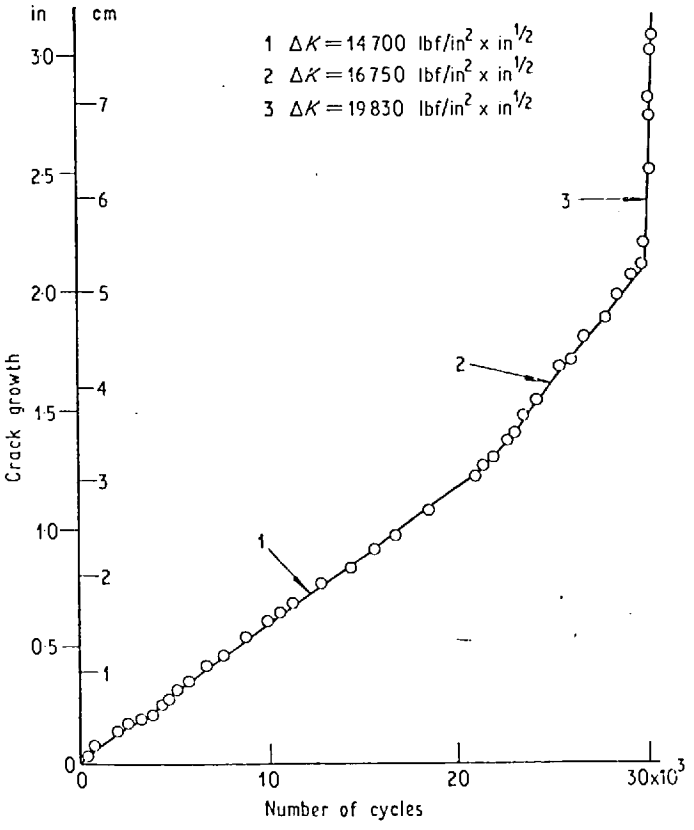


Fig. 2. *Crack growth at different values of* ΔK ($R = 0$)

tests. Numerical results appertaining to these tests are included in Table 2. The slopes of the crack growth curves in Fig. 3 tend to decrease with increasing values of mean stress intensity, K_m. In tests performed at constant values of ΔK and varying mean stress intensity, K_m, the crack growth rate may be expected to vary within wide limits, and this was the case. In the tests at ΔK = 5000 lbf/in^2 × in$^{\frac{1}{2}}$ (5.5 MN/m$^{\frac{3}{2}}$), increasing K_m (from 2500 to 16 500 lbf/in$^{\frac{3}{2}}$) increased the crack growth rate by

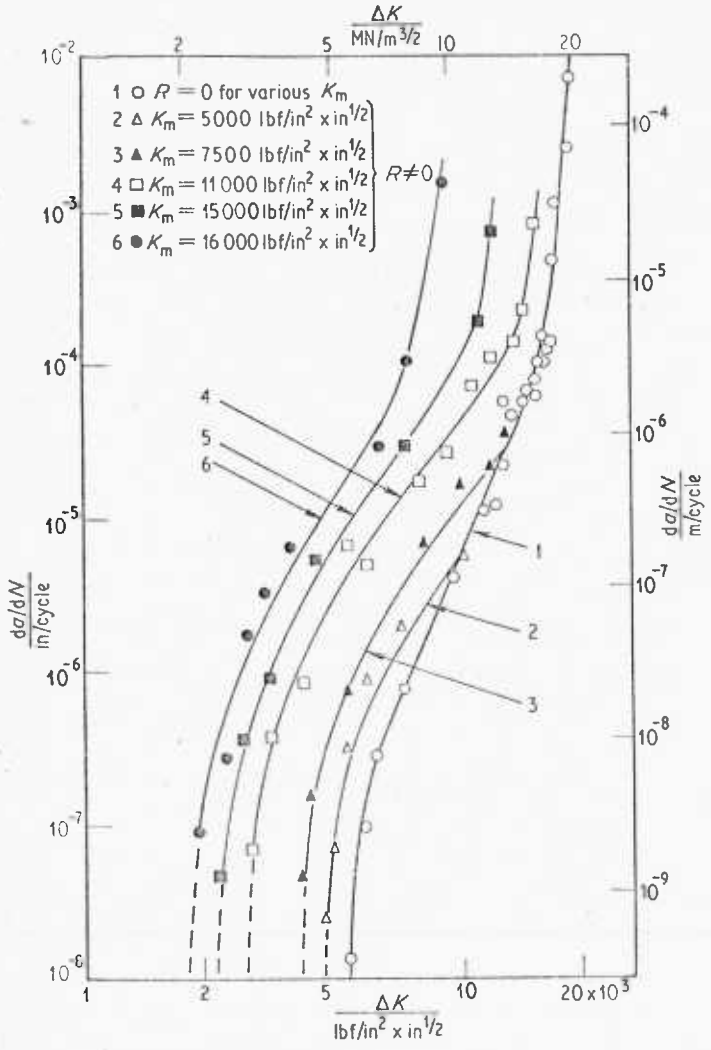


Fig. 3. *Crack growth rate versus ΔK at 0.15 Hz, in air at 21 °C*

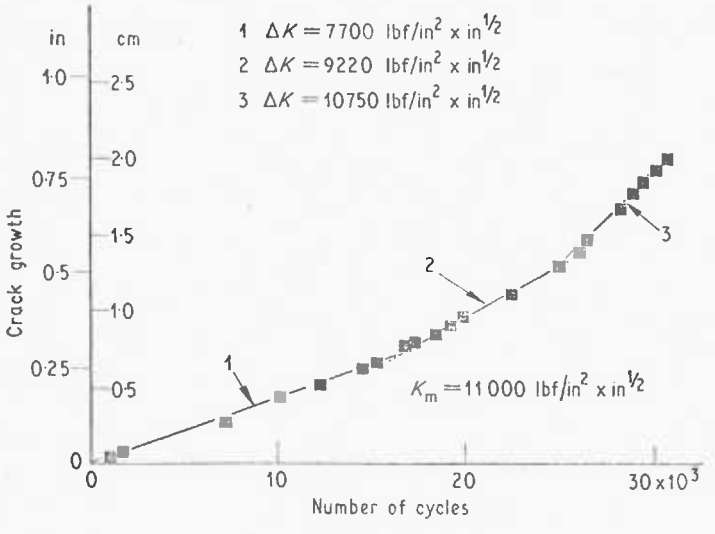


Fig. 4. *Crack growth at constant K_m*

three orders of magnitude (from 10^{-8} to 10^{-5} in/cycle). However, this rate of increase did not remain constant but decreased with increasing ΔK.

In the second series of tests (Fig. 5), ΔK was maintained constant whilst K_m was varied. Again, a linear relationship between the crack growth rate and the number of load cycles was obtained, but the rate of increase of the crack growth was not proportional to K_m. These two series of tests indicate that both K_m and ΔK exert a distinct influence on the crack g.owth rates in alloy RR58.

A fatigue crack growth curve (e.g. curve 1, Fig. 3) may be divided into three parts. Region I represents a fatigue threshold below which cracks do not propagate; in this region, at very low crack growth rates, ΔK reaches a threshold value, ΔK_{th}. The higher crack growth rate in Region II can be described by basic equations such as equation (1). An even faster rate is observed in Region III, culminating in a $\frac{1}{2}$ cycle loading when K_{max} will reach its critical value, K_{1C}.

The steep downward trend in Region I obtained in the present tests (Fig. 3) suggests that the threshold values, ΔK_{th}, can be confidently established at crack speeds around 10^{-8} in/cycle (2.5×10^{-7} mm/cycle). Data obtained in the present programme for values of ΔK at $R = 0$ form the typical sigmoidal curve 1 in Fig. 3, having a threshold value of 5000 lbf/in$^{\frac{3}{2}}$ (5.5 MN/m$^{\frac{3}{2}}$) which may be read directly from the figure. Values of ΔK_{th} for curves 2–6 may be similarly taken from Fig. 3, the curves being extrapolated to 10^{-8} in/cycle as indicated. Other tests conducted at values of ΔK below the quoted ΔK_{th} failed to produce any growth from the statically precracked testpieces and were discontinued. It is clear from the figure that the value of ΔK_{th} is dependent upon K_m, ΔK_{th} decreasing as K_m increases.

Some data available (13) suggest that ΔK_{th} could be considered as independent of cyclic conditions but these disagree with the present results on RR58. Similar discrepancies have previously been noted in steels (14), but in other recent work (15) using Al-alloy 2024–T3 it was found that ΔK_{th} decreased as K_m increased and as frequency increased above 300 Hz. The above trends were explained in terms of crack closure and crack-tip heating respectively, but further experimental evidence, particularly for the high-frequency regime, is needed.

The magnitude of 5000 lbf/in^2 × in$^{\frac{1}{2}}$ obtained for ΔK_{th} in the present $R = 0$ tests is high compared with 1500 lbf/in^2 × in$^{\frac{1}{2}}$ (1.75 MN/m$^{\frac{3}{2}}$) for pure aluminium and 1900 lbf/in^2 × in$^{\frac{1}{2}}$ (2.09 MN/m$^{\frac{3}{2}}$) for a 4.5 per cent Cu–Al alloy (BSL65) quoted in (6), both materials having been tested at frequencies between 25 and 30 Hz (16). It is, however, comparable with the value of 6000 lbf/in^2 × in$^{\frac{1}{2}}$ (6.6 MN/m$^{\frac{3}{2}}$) quoted by Pearson (4) for $\frac{1}{2}$ in thick RR58 at 25 Hz and at a growth rate of 10^{-6} in/cycle(2.5×10^{-8} m/cycle). At a testing frequency of 20 Hz, Hudson (17) obtained a threshold value of 2500 lbf/in^2 × in$^{\frac{1}{2}}$ (2.75 MN/m$^{\frac{3}{2}}$) for 2024–T3 Al-alloy, but data presented in (13) give 5000 lbf/in^2 × in$^{\frac{1}{2}}$ for the same alloy and testing frequency. It should be pointed out that all the data for 2024–T3 were obtained on specimens of about 0.1 in (2.5 mm) thickness while Frost's work (16) was on $\frac{1}{4}$ in (6.25 mm) thick specimens, although all the tests were under $R = 0$ conditions. It seems that, in addition to the effect of K_m quoted above,

Table 2. *RR58. Crack growth rate and ϕ values [equation (10)] for a range of K_m and ΔK at 0.15 Hz and 210 °C in air*

K_m (lbf/in^2 × in$^{\frac{1}{2}}$)	ΔK (lbf/in^2 × in$^{\frac{1}{2}}$)	K_{1C} (lbf/in^2 × in$^{\frac{1}{2}}$)	$2\Delta K\,K_m$ (lbf/in^2 × in)	da/dN (in/cycle)	ϕ
5000	4300	21550	4.3 × 10^7	2.5 × 10^{-8}	0.00364
5000	4500	21550	4.5 × 10^7	7.2 × 10^{-8}	0.0085
5000	5000	21550	5.0 × 10^7	3.1 × 10^{-7}	0.0208
5000	6000	21550	6.0 × 10^7	8.95 × 10^{-7}	0.0462
5000	7000	21550	7.0 × 10^7	1.98 × 10^{-6}	0.0728
7500	3750	21550	5.625 × 10^7	4.85 × 10^{-8}	0.010
7500	4000	20400	6.0 × 10^7	1.58 × 10^{-7}	0.0184
7500	5000	21550	7.5 × 10^7	7.7 × 10^{-7}	0.0612
7500	8000	20400	12.0 × 10^7	7.1 × 10^{-6}	0.232
7500	10000	20400	15.0 × 10^7	1.715 × 10^{-5}	0.368
7500	12000	20400	18.0 × 10^7	2.24 × 10^{-5}	0.540
7500	14000	20400	21.0 × 10^7	3.68 × 10^{-5}	0.756
11000	2600	21550	5.72 × 10^7	6.9 × 10^{-8}	0.00705
11000	3000	21550	6.6 × 10^7	3.55 × 10^{-7}	0.0357
11000	3800	21550	8.36 × 10^7	8.6 × 10^{-7}	0.089
11000	5000	21550	11.0 × 10^7	6.3 × 10^{-6}	0.190
11000	5600	21500	12.32 × 10^7	4.75 × 10^{-6}	0.246
11000	7700	20500	16.95 × 10^7	1.73 × 10^{-5}	0.565
11000	9220	20500	20.3 × 10^7	2.64 × 10^{-5}	0.835
11000	10570	20500	23.25 × 10^7	7.18 × 10^{-5}	1.140
11000	12250	20500	26.9 × 10^7	1.08 × 10^{-4}	1.690
11000	13820	20500	30.4 × 10^7	1.36 × 10^{-4}	2.480
11000	14905	20500	32.8 × 10^7	2.21 × 10^{-4}	3.40
11000	15700	20500	34.5 × 10^7	7.88 × 10^{-4}	4.43
15000	2250	21550	6.75 × 10^7	4.45 × 10^{-8}	0.0074
15000	2600	21550	7.8 × 10^7	3.45 × 10^{-7}	0.061
15000	3100	21550	9.3 × 10^7	1.88 × 10^{-6}	0.143
15000	4100	21550	12.3 × 10^7	507 × 10^{-6}	0.330
15000	7100	21500	21.3 × 10^7	2.4 × 10^{-5}	1.075
15000	11000	21500	33.0 × 10^7	1.9 × 10^{-4}	6.80
15000	12000	21500	36.0 × 10^7	7.4 × 10^{-4}	13.65
16500	2000	21850	6.6 × 10^7	8.9 × 10^{-8}	0.0021
16500	2400	21850	7.92 × 10^7	2.4 × 10^{-7}	0.038
16500	2700	21850	8.9 × 10^7	1.58 × 10^{-6}	0.188
16500	3000	21600	9.9 × 10^7	3.16 × 10^{-6}	0.3
16500	3500	21600	11.55 × 10^7	6.1 × 10^{-6}	0.447
16500	6000	21600	19.8 × 10^7	2.88 × 10^{-5}	1.64
16500	7200	21600	23.75 × 10^7	1.0 × 10^{-4}	2.90
16500	9500	21600	31.4 × 10^7	1.47 × 10^{-3}	18.2

1000 lbf/in^2 × in$^{\frac{1}{2}}$ = 1.0998 MN/m$^{3/2}$, 1 in = 25.4 mm.

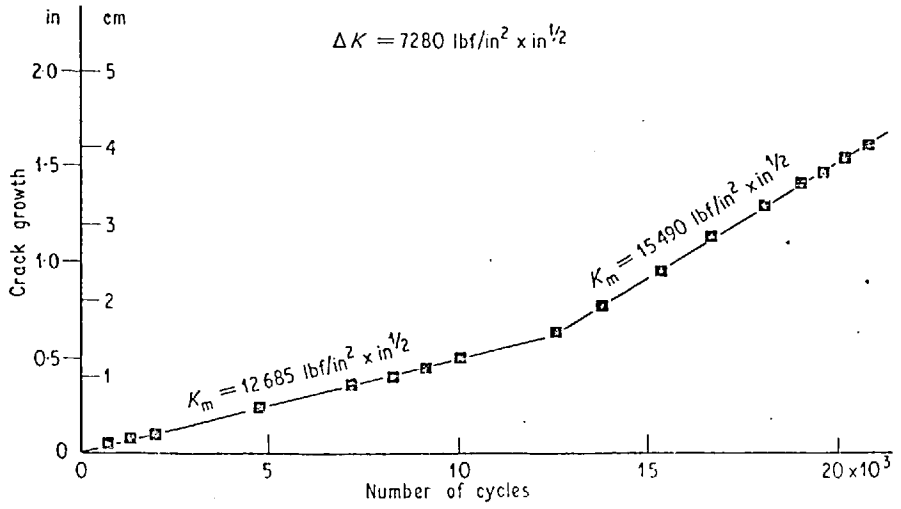


Fig. 5. *Crack growth at constant ΔK*

other significant factors that may affect the value of ΔK_{th} are specimen thickness, frequency and the method of pre-cracking. In view of the discrepancies mentioned, additional work is being conducted to further clarify these points.

Specific threshold data, ΔK_{th}, evaluated from Fig. 3 are plotted as a function of K_m in Fig. 6, together with results from Frost (6) for alloy L65 and Feeney *et al.* (18) for 2024–T3. The present results show that the magnitude of the threshold level, ΔK_{th}, decreases linearly with increasing values of K_m, for K_m values greater than 2500 lbf/in^2 × in$^{\frac{1}{2}}$ ($R \geqslant 0$). For steels (14)(19), ΔK_{th} was also found to decrease with increasing K_m but no linear relationship was found.

$$(2\Delta K\, K_m - 2\Delta K_{th} K_m) \to 0 \qquad \text{when } da/dN \to 0$$

and

$$(K_{1C} - K_{max}) \to 0 \qquad \text{when } da/dN \to \infty \quad (8)$$

Inserting these two conditions into equation (3), a generalized equation is obtained, viz:

$$\frac{da}{dN} = A\phi^{\alpha} \quad . \quad . \quad . \quad . \quad . \quad . \quad . \quad . \quad . \quad . \quad . \quad . \quad (9)$$

where A is a constant and

$$\phi = \frac{2K_m(\Delta K - \Delta K_{th})}{K_{1C}^2 - K_{max}^2} \quad . \quad . \quad . \quad . \quad . \quad . \quad . \quad . \quad (10)$$

The generalized equation is presented in Fig. 8 and shows

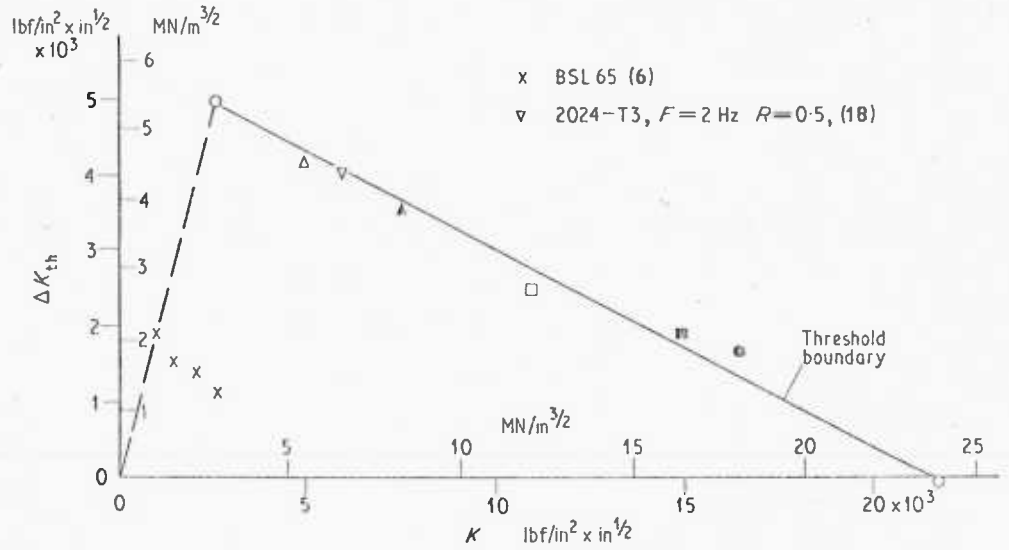


Fig. 6. ΔK_{th} *versus* K_m *at 0.15 Hz, in air at 21 °C*

As shown in Fig. 6, Feeney's data, which were obtained using a stress ratio of 0.5, a testing frequency of 2 Hz and with the crack growing along the rolling direction, agree well with the present results. However, no such agreement exists in relation to Frost's data for a testing frequency of 25–30 Hz. At low frequencies, no threshold data for Al-alloys are available in the literature, but the above results again seem to indicate a frequency dependence of the threshold for crack propagation in these alloys.

In a study of cyclic crack growth in various materials, at constant K_m and at constant ΔK (5), the authors found it possible to express the results in the form given in equation (3). As the results of the present tests on RR58 were obtained under comparable testing conditions (temperature, strain rates, etc.), the use of equation (3) may again be appropriate. The respective values of the factor $2\Delta K\, K_m (= K_{max}^2 - K_{min}^2)$ in the equation are included in Table 2 and a logarithmic plot of the results, including those from tests in which $R = 0$ (Fig. 7), indicates a family of fatigue crack growth curves converging into a single line at higher values of $2\Delta K\, K_m$.

The threshold value, $2\Delta K_{th} K_m$, will influence crack growth in Region I, which is highly dependent on K_m, whereas K_{1C} is the critical parameter at the instability point. These two values provide the limiting conditions a single linear relationship with $\alpha = 1.36$ and $A = 3.16 \times 10^{-5}$ in/cycle (8.03×10^{-7} m/cycle), which confirms that for RR58 this parameter correlates the crack growth process well.

4 CONCLUSIONS

A study of the propagation of fatigue cracks in contoured double-cantilever beam specimens of Al-alloy RR58 under cyclic tension conditions at 0.15 Hz and 21 °C has been presented.

Fatigue crack growth rate is dependent upon the range of the stress-intensity factor, ΔK, and its mean value, K_m.

Fatigue crack growth rate in RR58 can be described as $da/dN = A\phi^{\alpha}$, where

$$\phi = \frac{2K_m(\Delta K - \Delta K_{th})}{K_{1C}^2 - K_{max}^2}$$

K_{1C} is the static fracture toughness and A and α are constants.

The threshold stress-intensity factor, ΔK_{th}, decreases linearly with increasing K_m (Fig. 6).

The absolute value of ΔK_{th} appears to depend on cyclic frequency. A more detailed study of the frequency effect is necessary for a full understanding.

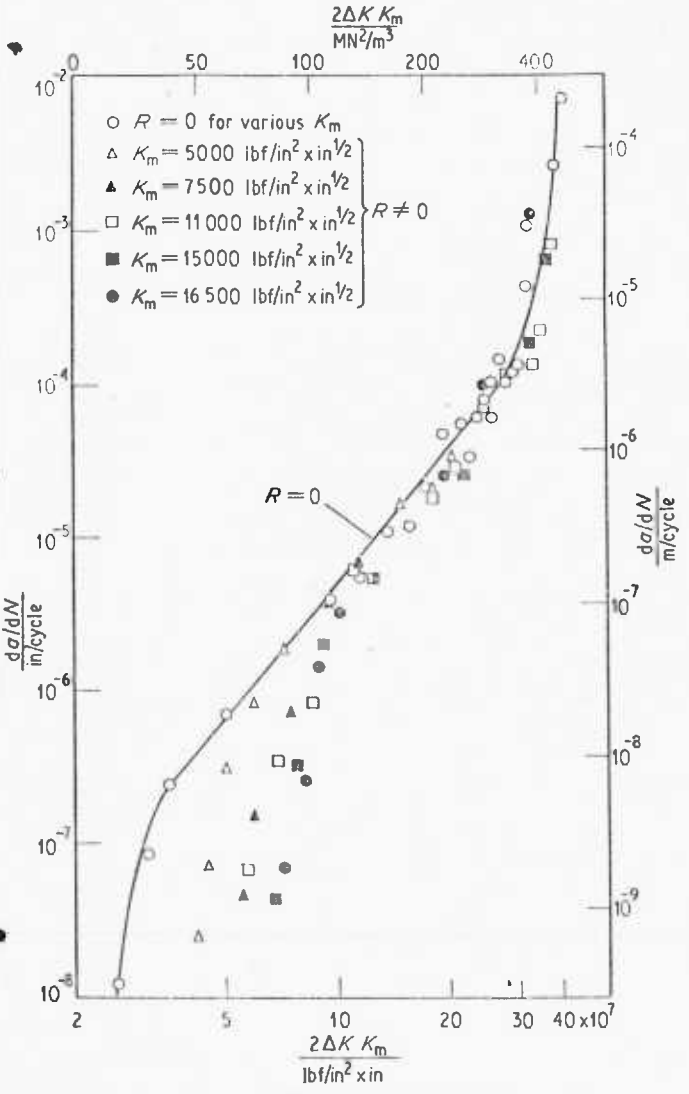


Fig. 7. *Crack growth rate versus* $2\Delta K K_m$ *at 0.15 Hz, in air at 21 °C*

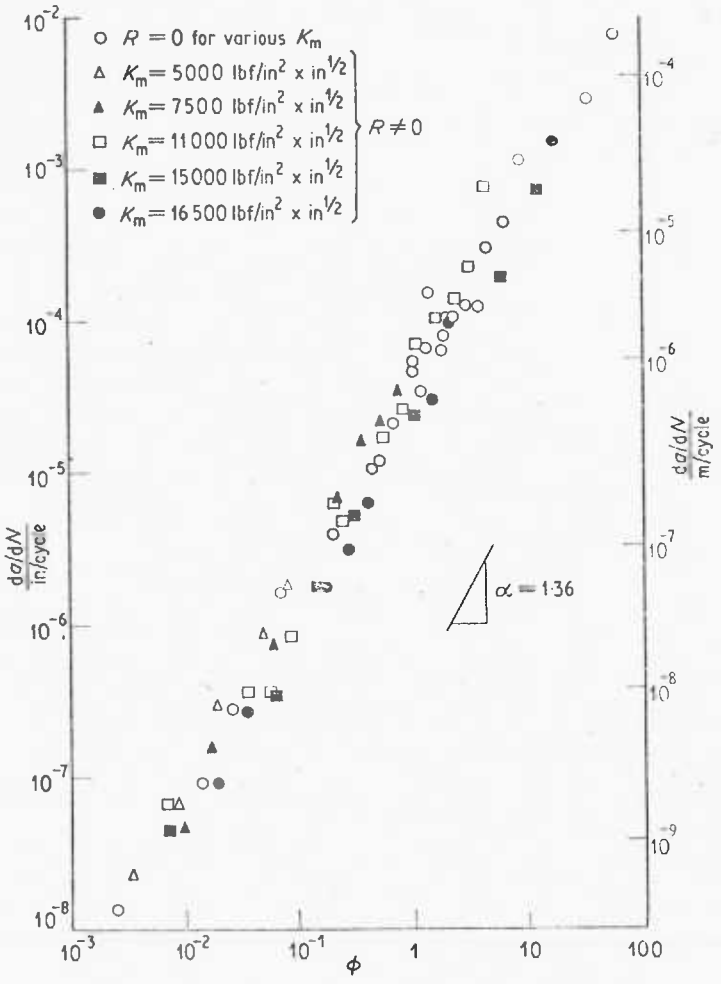


Fig. 8. *Crack growth rate versus* ϕ *at 0.15 Hz, in air at 21 °C*

APPENDIX

REFERENCES

(1) WALKER, E. K. 'The effect of stress ratio during crack propagation and fatigue life for 2024-T3 and 7075–T6 Al-alloys', *Effects of environment and complex load history on fatigue life* 1970, 1 (ASTM STP 462).

(2) KRUPP, W. E., HOEPPNER, D. W. and WALKER, E. K. 'Crack propagation of Al-alloys in corrosive environments', *International conference on corrosion fatigue* 1972, 468 (University of Connecticut).

(3) HOEPPNER, D. W. and KRUPP, W. E. 'Prediction of component life by application of fatigue crack growth knowledge', *Engng Fract. Mech.* 1974 **6** (No. 1). 47.

(4) PEARSON, S. 'The influence of mean stress on fatigue crack growth in 1/2 in thick specimens of Al-alloys of high and low fracture toughness', *Engng Fract. Mech.* 1972 **4** (No. 1), 9.

(5) ARAD, S., RADON, J. C. and CULVER, L. E. 'Growth of fatigue cracks in metals and polymers', *Engng Fract. Mech.* 1974 **6** (No. 1), 195.

(6) FROST, N. E., POOK, L. P. and DENTON, K. 'A fracture mechanics analysis of fatigue crack growth data for various materials', *Engng Fract. Mech.* 1971 **3** (No. 1). 109.

(7) SPEIDEL, M. O., BLACKBURN, M. J., BECK, T. R. and FEENEY, J. A. 'Corrosion fatigue and stress corrosion crack growth in high strength Al-alloys, Mg-alloys and Ti-alloys exposed to aqueous solutions', *International conference on corrosion fatigue* 1972, 324 (University of Connecticut).

(8) ARAD, S., RADON, J. C. and CULVER, L. E. 'Fatigue crack propagation in polymethylmethacrylate: the effect of the mean value of stress intensity factor', *J. mech. Engng Sci.* 1971 **13** (No. 2), 75–81.

(9) CHU, H. P. 'Effect of mean stress intensity on fatigue crack growth in a 5456-H117 Al-alloy', *ASTM 7th NSFM* 1973 (University of Maryland).

(10) JOHNSON, F. A. and RADON, J. C. 'Mechanical and metallurgical aspects of fracture behaviour of an Al-alloy', *Int. J. Fract. Mech.* 1972 **8**, 21–36.

(11) BROWN, W. F. and SRAWLEY, J. E. *Plane strain fracture toughness of high strength metallic materials* 1966 (ASTM STP 410).

(12) BRANCO, C. M., RADON, J. C. and CULVER, L. E. 'Corrosion fatigue of Al-alloy RR58 – a fracture mechanics approach', *Symposium on mechanical behaviour of materials* 1974, Paper C3 (Kyoto, Japan).

(13) DONAHUE, R. J., ATANMO, P., KUMBLE, R. and McEVILY, A. J. 'Crack opening displacement and the rate of fatigue crack growth', *Int. J. Fract. Mech.* 1972 **8**, 209.

(14) KLESNIL, M. and LUKAS, P. 'Effect of cyclic stress asymmetry on fatigue crack growth', *Mater. Sci. Engng* 1972 **9**, 231.

(15) SCHMIDT, R. A. and PARIS, P. C. 'Threshold for fatigue crack propagation and the effects of load ratio and frequency', *ASTM STP 536* 1973, 79–95.

(16) FROST, N. E. Private communication, 1974.

(17) HUDSON, C. M. 'Effect of stress ratio on fatigue crack growth in 7075-T6 and 2024–T3 aluminium-alloy specimens', *NASA TN D-5390* 1969.

(18) FEENEY, J. A., McMILLAN, J. C. and WEI, R. P. 'Environmental fatigue crack propagation of Al-alloys at low stress intensity levels', *Met. Trans.* 1970 **1** (June), 1741.

(19) JERRAM, K. and PRIDDLE, E. K. 'System for determining the critical range of stress-intensity factor necessary for fatigue-crack propagation', *J. mech. Engng Sci.* 1973 **15** (No. 4), 271–273.

C. M. Branco,[1] *J. C. Radon,*[1] *and L. E. Culver*[1]

An Analysis of the Influence of Mean Stress Intensity and Environment on Fatigue Crack Growth in a New High Strength Aluminum Alloy

REFERENCE: Branco, C. M., Radon, J. C., and Culver, L. E., "An Analysis of the Influence of Mean Stress Intensity and Environment on Fatigue Crack Growth in a New High Strength Aluminum Alloy," *Journal of Testing and Evaluation*, JTEVA, Vol. 3, No. 6, Nov. 1975, pp. 407–413.

ABSTRACT: The effects of the mean stress intensity factor K_m and the range of the stress intensity ΔK on fatigue crack propagation during wholly tensile loading cycles in the aluminum (Al) alloy RR58 in laboratory air and in a 3.5% NaCl solution have been studied using contoured double-cantilever beam specimens. In general the fatigue crack growth rate in NaCl solution was greater than in air under similar conditions except for tests in which high values of the maximum stress intensity factor were used when no significant difference was observed.

Based on the experimental data a relation between the cyclic crack growth rate da/dN and the tensile loading levels has been proposed. The threshold value of ΔK, ΔK_{th}, is approximately 12% higher in air than in the 3.5% NaCl solution, and its value decreases linearly with increasing values of K_m.

KEY WORDS: fracture properties, aluminum alloys, corrosion fatigue, stresses, crack propagation

Failure of structural parts is frequently caused by the initiation of cracks and their subsequent subcritical propagation to a critical size. Aggressive environments and cyclic stresses may adversely influence the speed of a propagating crack. The fatigue process is normally divided into three stages: crack initiation, crack propagation to a critical size, and unstable fast fracture.

If cycling takes place at higher stresses most of the life of the component is spent on crack propagation. Therefore, data to determine crack growth rates in structural materials are urgently needed.

The design approach used in the aircraft industry and for other advanced engineering structures requires a precise knowledge of crack propagation rates in structural materials. Aluminum alloys are in increasing use in those structures, and one of the recently developed copper-aluminum (Cu-Al) alloys, RR 58, being used in aeronautical designs (such as Concorde), was considered relevant for the present study.

In the last ten years a large number of fatigue crack growth "laws" has been proposed, an extensive review of which may be found in Ref *1*. While some of the early laws suggest that the crack growth rate da/dN may be a function of the applied stress or of the crack length, most are based on linear elastic fracture mechanics (LEFM) concepts. Such equations are of the following type:

$$da/dN = C_1 f(K) \tag{1}$$

[1] Graduate student, research fellow, and senior lecturer, respectively, Imperial College of Science and Technology, Department of Mechanical Engineering, Exhibition Road, London, England.

where C_1 is a constant depending on the material, environment, frequency, etc., and K is the stress intensity factor that describes the intensity of the local stresses at the crack tip. For a limited crack propagation range (frequently described as Region II) and in the absence of environmental effects the well-known Paris [*2*] equation had some success in fitting crack growth data.

$$da/dN = C_2(\Delta K)^n \tag{2}$$

where ΔK is the range of the stress intensity factor $= K_{max} - K_{min}$, and C_2 and n are constants depending on the material, environment, and other cyclic conditions. The implication of the above relation is that the mean level of the stress intensity K_m should be treated as of secondary importance compared to ΔK. This line of approach has been further developed, and the influence of K_m, the importance of which has now been fully realized, and the stress ratio $R = K_{min}/K_{max}$ investigated in detail. Thus a relation proposed by Forman et al [*3*] is an example of a modified Paris law in the following form:

$$\frac{da}{dN} = C_3 \frac{\Delta K^m}{(1 - R)\,K_c - \Delta K} \tag{3}$$

Equation 3 has found applications in some Al alloys with reasonable success [*4*]. However, as pointed out later [*5*], it should be noted that it does not take into account the threshold value for crack propagation ΔK_{th}. A simple but effective way to incorporate the influence of the threshold stress intensity in the Paris Eq 2 was suggested by Liu [*6*]:

$$da/dN = C_4(\Delta K - \Delta K_{th})^n \tag{4}$$

and later by Donahue et al [*7*] in a more elaborate form:

$$\frac{da}{dN} = \frac{4C_5}{\pi\sigma_{ys}E}(\Delta K^2 - \Delta K_{th}^2) \tag{5}$$

where C_5 is a material constant, σ_{ys} is the yield stress, and E is Young's modulus. More recently other relations were developed not only to describe precisely the stress ratio effect but also to predict the fatigue crack growth rates for the entire range of loading spectrum, from ΔK_{th} to K_c. An interesting example may be provided by the relation of Chu [*8*]:

$$\frac{da}{dN} = \frac{C_6(\Delta K^{n_1} - \Delta K_{th}^{n_2})}{[(1 - R)\,K_c - \Delta K]^m} \tag{6}$$

Unfortunately, sufficient experimental evidence of the general validity of any of the above equations is not yet available.

Thus, further work on particular aspects, such as on the effect of the shape of loading cycles, environment, and other factors, for a range of materials is needed. Although it is known that, for example, ΔK_{th} decreases with K_m (that is, with the stress ratio R) for several structural steels [9] and Al alloys [10], their exact relation has not been successfully assessed. Similarly, frequency and specimen thickness are two variables that will undoubtedly influence ΔK_{th}, but their effects are again not adequately clear. These and a variety of other factors connected with testing methods, crack growth relationships, etc., are at present the subjects of detailed studies by specific task groups organized by the Subcommittee 4 on Subcritical Crack Growth of ASTM Committee E-24 on Fracture Testing of Metals. They are mentioned here as a particularly important source of up-to-date information.

Recent results of a comprehensive fatigue program in this department on a range of polymers in low speed tensile cycling [11] led to the development of a simplified crack propagation model of the form

$$da/dN = \beta\lambda^n \qquad (7)$$

where $\lambda = K_{max}^2 - K_{min}^2 = 2\Delta K K_m$ and β and n are constants depending on the test conditions. Subsequent analysis of the fatigue data obtained in tests on other viscoelastic materials [5,12] confirmed the suitability of the proposed model in a wide subcritical region where other laws showed serious deviations from experimental results. Also, application of Eq 7 to metals met considerable success for Al alloys 2024-T3 and 7075–T6, using data obtained from Ref 4 at different stress ratios over a range of crack growth rates between 10^{-6} and 10^{-3} in./cycle (10^{-5} and 10^{-2} mm/cycle). Good agreement was also obtained with medium carbon steel [13] and cold rolled mild steel [14]; a detailed analysis of these results may be found in Ref 12.

It is well known that corrosive environments such as sodium chloride (NaCl) solutions accelerate fatigue crack growth rates in Al alloys [15–19]. The environment exerts its greatest effects at low frequencies and low ΔK levels, where time dependent corrosion phenomena have more time to develop. The rate of fatigue crack growth is also affected by R in corrosive environments, but so far no single expression has been found to fit the experimental data in a satisfactory way.

One recent approach to the corrosion fatigue problem is the superposition model [20,21]. The fatigue crack growth rate in an aggressive environment is computed by the sum of the cyclic fatigue crack growth rate in an inert environment plus a term obtained from a static stress corrosion crack growth rate test in the same aggressive environment. The validity of these superposition models in Al alloys is under discussion [21] particularly because they imply the same rupture mechanism for different deformation processe. .

Under variable amplitude loading a high tensile load followed by lower tensile load might cause a delay in crack propagation before the crack growth rate assumes a steady state value for the low load. On the other hand, a transient acceleration might occur when a low-high sequence is applied [23]. These interaction effects seem to be dependent on environment and frequency, differ from material to material [23], and have been explained in terms of residual stresses, crack tip closure, or crack tip geometry [22]. The above phenomena are not discussed now although they were previously noted in stress corrosion studies [24].

The purpose of this paper is to report a study of the effect of the mean value K_m and the range ΔK of the stress intensity factor on the crack propagation rate in Al alloy RR 58 under repeated tension fatigue conditions at 21°C in laboratory air at 50% relative humidity and in a 3.5% NaCl solution at low cyclic speeds of 0.15 Hz. Also, the change in the value of the threshold stress intensity ΔK_{th} is discussed in terms of K_m for both environments.

Experimental

The composition and principal mechanical properties of the Al alloy RR 58 are presented in Tables 1 and 2. The material was supplied in plates 36 × 36 × 3 in. (914 × 914 × 76 mm) from which crack-line-loaded double-cantilever beam (DCB) specimens ⅜ in. (9.525 mm) thick (Fig. 1) were prepared. With this geometry the stress intensity factor is kept constant over a wide range of crack lengths. Additionally, lateral side grooves [0.03 in. (0.76 mm) deep] were introduced to enhance plane strain conditions.

Specimens were heat-treated by aging at 190°C for 30 h and after aging the surface of the specimen was wire brushed and the side grooves polished. Hardness values taken at 1-in. (25.4-mm) intervals on both sides along the side grooves varied between 145–150 VHN (20 kg). The crack was opened with a saw cut extended to a 45-deg chevron notch and sharpened with a razor blade. The maximum height of the specimen corresponded to the full plate thickness, and the crack grew along the rolling

TABLE 1—*Chemical composition of Al alloy RR 58.*

Element	Weight, %
Copper (Cu)	2.64
Magnesium (Mg)	1.65
Manganese (Mn)	0.03
Silicon (Si)	0.23
Iron (Fe)	1.15
Titanium (Ti)	0.06
Zinc (Zn)	0.06
Nickel (Ni)	1.15

TABLE 2—*Principal mechanical properties of Al alloy RR 58 at 21°C and 10^{-3} strain rate.*

Young's Modulus (E), psi (kPa)	10.84×10^6	(75.0×10^6)
Poisson's Ratio (ν)	0.33	
Ultimate Tensile Strength (σ), ksi (MPa)	65	(450)
0.1% Yield Strength (σ_{y_s}), ksi (MPa)	53	(367)
Minimum Elongation (ϵ_r), %	6	

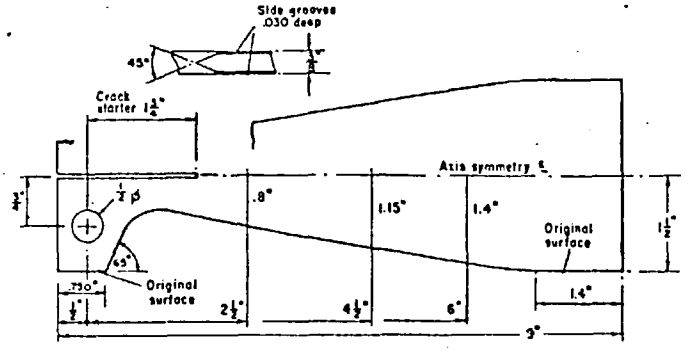


FIG. 1—*Crack-line-loaded double-cantilever beam contoured specimen.*

direction while the specimen was loaded in the short transverse direction (S–L orientation). In this orientation fracture toughness is lowest and the effects of stress corrosion and corrosion fatigue are considerable.

Stress intensity factors may be calculated from the well-known relation

$$K_I = P\left(\frac{E}{2B(1-\nu^2)}\frac{dc}{da}\right)^{1/2} \quad (8)$$

where

P = applied load,
B = the net fracture width,
C = the compliance, and
ν = Poisson's ratio.

For a suitably shaped DCB test piece K_I will remain constant (within 4% for the geometry used here) along the crack length of approximately 5 in. (127 mm). The design of the "contoured" DCB specimen (Fig. 1) was described in detail in Ref *25*.

To establish static values of K_{Ic} at room temperature all the specimens were precracked and then pulled in an Instron tensile testing machine, Type TT-C, 10 000-lbf capacity at a crosshead speed of 0.002 in. (0.05 mm)/min. The crack propagated smoothly and without deviations from the cracking plane, the crack length being monitored with a travelling microscope. A linear variation of compliance with crack length was obtained and the total load variation was within ±2%, which was found satisfactory in the subsequent fatigue tests. Critical values of the plane strain static fracture toughness K_Q varied between 20 400 and 21 800 psi × in.$^{1/2}$, thus agreeing with previously established values [*25*].

As reported in Ref *25*, it is to be expected that these K_Q values would decrease substantially with increasing thickness of specimen. To compare the present results on RR 58 with other Al alloys, fracture toughness tests on compact tension specimens ⅜ in. (9.525 mm) and 1 in. (25.4 mm) thick complying with the ASTM Test for Plane-Strain Fracture Toughness of Metallic Materials (E 399-74) are in progress.

The fatigue tests were carried out on specimens having their crack planes in the horizontal position in a Denison T42C2 hydraulic universal testing machine specially fitted with a cycling mechanism. Basically, this consisted of two limit microswitches to regulate the load range. Tests were carried out in laboratory air, 50% relative humidity at 21°C and also in a 3.5% NaCl solution that was drip fed onto the crack surfaces through a hypodermic needle attached to an aspirator bottle provided with a flow regulator, maintaining a flow of about 6 drops per minute (0.5 litre per day).

Cyclic tests were carried out under constant K_m and ΔK conditions. The cycling frequency used was 0.15 Hz with a tensile sinusoidal load wave. The crack length was monitored with a ×50 magnification travelling microscope at an accuracy better than 0.0001 in. (0.00254 mm). When observation of the crack tip became difficult due to corrosive attack the side grooves were cleaned and polished.

The plastic zone size at the crack tip r_p was calculated (assuming a nearly plane strain situation) [*26*] from

$$r_p = \frac{1}{6\pi}\frac{K_I^2}{\sigma_{ys}^2} \quad (9)$$

where σ_{ys} is the yield stress under the appropriate testing conditions. The maximum value of r_p did not exceed 10^{-2} in. (0.254 mm), which was considered small compared to the specimen net thickness of 0.375 in. (9.525 mm).

Results and Discussion

The dependence of crack growth on ΔK was investigated in a previous work [*19*] using wholly tensile cyclic tests at $R = 0$.

Data obtained in laboratory air for values of ΔK at $R = 0$ are plotted in Fig. 2: they can be represented by a sigmoidal curve with an apparent threshold value of 5000 psi × in.$^{1/2}$ (5.5 MN/m$^{3/2}$) obtained by extrapolation of the lower rate data. Testing in the region $10^{-8} \leqslant da/dN \leqslant 10^{-9}$ in./cycle ($10^{-10} \leqslant da/dN \leqslant 10^{-11}$ m/cycle) at low frequencies is very time consuming, however. Although comparable threshold data for a range of frequencies and R ratios for RR 58 are not available, the present results are considered to be high even when compared with the value of 3650 psi × in.$^{1/2}$ (4.0 MN/m$^{3/2}$) reported by Schmidt and Paris [*9*] for 2024-T3 Al alloy (the same series as RR 58) at a very high frequency of 300 Hz. The threshold determination might be sensitive to the test method used, as discussed by Bucci [*27*]. However, careful precautions, such as adequate precracking or avoidance of overloading and of residual stresses, have been carried out in the present tests. All threshold data were obtained on cracks approximately 0.04 in. (1.016 mm) long and the tests repeated. Moreover, work now in progress on the same material (unpublished data) at a substantially higher loading frequency of 50 Hz indicates only a slight decrease of ΔK_{th} with increasing testing frequency at crack growth rates in the range of 10^{-8} to 10^{-9} in./cycle (10^{-10} to 10^{-11} m/cycle). It thus seems possible that the high threshold value reported here might be genuine for this alloy in ⅜ in. (9.525 mm) thickness.

As mentioned earlier, the basic Eq 2 described the results for $R = 0$ reasonably well, although it does not account for the

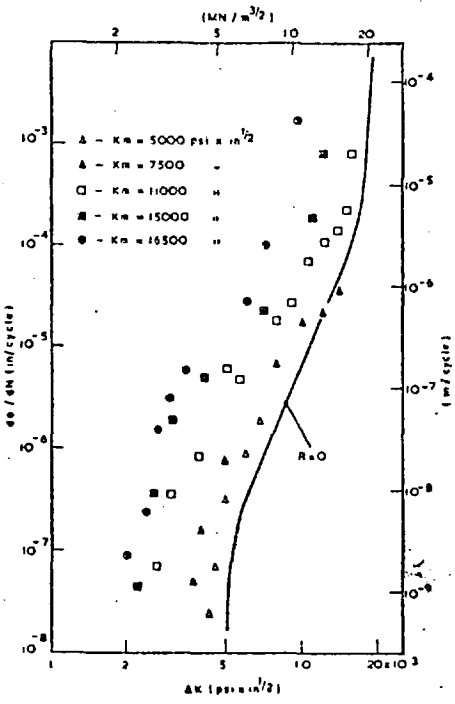


FIG. 2—*RR58 crack growth rate versus ΔK 0.15 Hz in air at 21°C.*

effect of the mean stress intensity K_m, which increases proportionately with increasing ΔK. However, the influence of both factors is incorporated in the modified relation in Eq 7. To separate the effects of the range of the stress intensity factor ΔK from those of K_m, two series of tests were conducted, first at constant values of K_m and then at constant ΔK values. Typical results from K_m = constant tests are shown in Fig. 3 for tests performed in laboratory air and in the 3.5% NaCl solution at 21°C. The figure indicates a linear dependence of crack growth with number of cycles, the crack growth rate accelerating in the 3.5% NaCl solution when compared to tests in air at the same K_m and ΔK values. Similar results were obtained from a further group of tests with K_m constant and equal to 5000, 7500, 11 000, 15 000, and 16 500 psi × in.$^{1/2}$ (5.5, 8.25, 12.1, 16.5, and 18.1 MN/m$^{3/2}$), respectively (see Tables 3 and 4).

Figure 4 shows a comparison between tests performed at constant ΔK values of 5000 psi × in.$^{1/2}$ (5.5 MN/m$^{3/2}$) while K_m was varied. Again a linear relation between crack growth rate and number of load cycles was obtained, but the rate of increase of crack growth rate was not proportional to K_m. These results indicate that Eq 2 does not entirely explain the crack propagation phenomena in this material, and both K_m and ΔK have a distinct influence on the crack growth rates.

The variations of the crack growth rate da/dN with ΔK (Figs. 2 and 5) show that both in laboratory air and in 3.5% NaCl solution da/dN increases with K_m for a given value of ΔK. The slopes of the crack growth curves in Figs. 2 and 5 decrease with increasing values of K_m. Consequently, in the tests performed at constant values of ΔK and varying mean stress intensity K_m the crack growth rate would also be expected to vary within wide limits. This is the case in the tests at ΔK = 5000 psi × in.$^{1/2}$ (5.5 MN/m$^{3/2}$). Increasing K_m from 2500 to 16 500 psi × in.$^{1/2}$ (2.75 to 18.1 MN/m$^{3/2}$) has increased the crack growth rate by more than three orders of magnitude. However, this range of crack growth rates does not remain constant but decreases with increasing ΔK. Two K_m = constant curves were taken from Figs. 2 and 5 and a comparison between them is made in Fig. 6, together with the R = 0 curves, to assess the effect of the 3.5% NaCl solution on the crack growth rate. In comparison to laboratory air the 3.5% NaCl solution lowers the threshold value for crack propagation ΔK_{th} and causes an increase in the fatigue crack growth rates. However, at higher K_{max} values, for example 19 000 psi × in.$^{1/2}$ (20.9 MN/m$^{3/2}$), no significant difference between the crack growth rates was observed. Acceleration of crack growth rates in a 3.5% NaCl solution is usual for Al alloys, but corrosion fatigue is a time-dependent phenomenon. Environmental sensitivity is reduced at high values of K_{max}, where the time available for water-metal reaction is shorter and the crack growth process consists mainly of mechanical deformation.

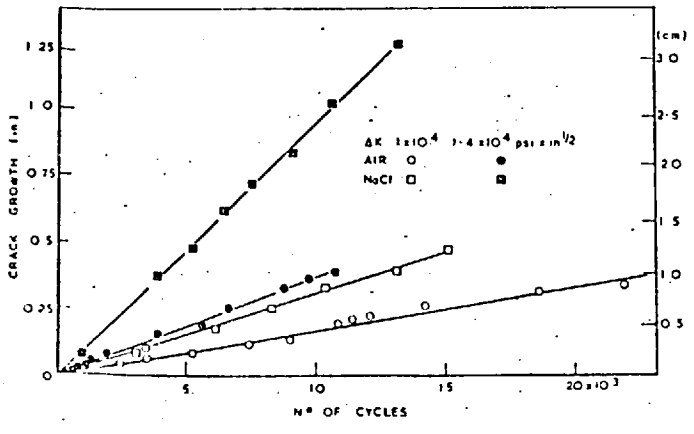


FIG. 3—*RR58 crack growth for* K_m = 7500 psi × in.$^{1/2}$ *in air and in 3.5% NaCl solution at 21°C, 0.15 Hz.*

TABLE 3—*Test data in air.*

K_m, psi × in.$^{1/2}$	ΔK, psi × in.$^{1/2}$	K_Q, psi × in.$^{1/2}$	λ, psi^2 × in.	da/dN in./cycle	ϕ
5 000	4 300	21 550	4.3 × 10^7	2.5 × 10^{-4}	0.00364
5 000	4 500	21 550	4.5 × 10^7	7.2 × 10^{-4}	0.0085
5 000	5 000	21 550	5.0 × 10^7	3.1 × 10^{-7}	0.0208
5 000	6 000	21 550	6.0 × 10^7	8.95 × 10^{-7}	0.0462
5 000	7 000	21 550	7.0 × 10^7	1.98 × 10^{-6}	0.0728
7 500	3 750	21 550	5.625 × 10^7	4.85 × 10^{-4}	0.010
7 500	4 000	20 400	6.0 × 10^7	1.58 × 10^{-7}	0.0184
7 500	5 000	21 550	7.5 × 10^7	7.7 × 10^{-7}	0.0612
7 500	8 000	20 400	12.0 × 10^7	7.1 × 10^{-6}	0.232
7 500	10 000	20 400	15.0 × 10^7	1.715 × 10^{-5}	0.368
7 500	12 000	20 400	18.0 × 10^7	2.24 × 10^{-5}	0.540
7 500	14 000	20 400	21.0 × 10^7	3.68 × 10^{-5}	0.756
11 000	2 600	21 550	5.72 × 10^7	6.9 × 10^{-5}	0.00705
11 000	3 000	21 550	6.6 × 10^7	3.55 × 10^{-7}	0.0357
11 000	3 800	21 550	8.36 × 10^7	8.6 × 10^{-7}	0.089
11 000	5 000	21 550	11.0 × 10^7	6.3 × 10^{-6}	0.190
11 000	5 600	21 500	12.32 × 10^7	4.75 × 10^{-6}	0.246
11 000	7 700	20 500	16.95 × 10^7	1.73 × 10^{-5}	0.565
11 000	9 220	20 500	20.3 × 10^7	2.64 × 10^{-5}	0.835
11 000	10 570	20 500	23.24 × 10^7	7.18 × 10^{-5}	1.140
11 000	12 250	20 500	26.9 × 10^7	1.08 × 10^{-4}	1.690
11 000	13 820	20 500	30.4 × 10^7	1.36 × 10^{-4}	2.480
11 000	14 905	20 500	32.8 × 10^7	2.21 × 10^{-4}	3.40
11 000	15 700	20 500	34.5 × 10^7	7.88 × 10^{-4}	4.43
15 000	2 250	21 550	6.75 × 10^7	4.45 × 10^{-9}	0.0074
15 000	2 600	21 550	7.8 × 10^7	3.45 × 10^{-7}	0.061
15 000	3 100	21 550	9.3 × 10^7	1.88 × 10^{-6}	0.143
15 000	4 100	21 550	12.3 × 10^7	3.07 × 10^{-6}	0.330
15 000	7 100	21 500	21.3 × 10^7	2.4 × 10^{-5}	1.075
15 000	11 000	21 500	33.0 × 10^7	1.9 × 10^{-4}	6.80
15 000	12 000	21 500	36.0 × 10^7	7.4 × 10^{-4}	13.65
16 500	2 000	21 850	6.6 × 10^7	8.9 × 10^{-8}	0.0021
16 500	2 400	21 850	7.92 × 10^7	2.4 × 10^{-7}	0.038
16 500	2 700	21 850	8.9 × 10^7	1.58 × 10^{-6}	0.188
16 600	3 000	21 600	9.9 × 10^7	3.16 × 10^{-6}	0.3
16 500	3 500	21 600	11.55 × 10^7	6.1 × 10^{-6}	0.447
16 500	6 000	21 600	19.8 × 10^7	2.88 × 10^{-5}	1.64
16 500	7 200	21 600	23.75 × 10^7	1.0 × 10^{-4}	2.90
16 500	9 500	21 600	31.4 × 10^7	1.47 × 10^{-3}	18.2

1000 psi × in.$^{1/2}$ = 1.0998 MN/m$^{3/2}$
1 in. = 25.4 mm

The effect of the mean stress intensity factor K_m is similar for both environments when compared with the R = 0 curves (Fig. 6).

The lowering of ΔK_{th} values in a 3.5% NaCl solution has been reported by Feeney et al [*17*] in 2024-T3 Al alloy, but Speidel et al [*15*] found no such variation for alloy 7079 T-651. Both sets of data were obtained with the same crack orientation as in the present tests, and the testing frequencies were 2 and 4 Hz, respectively.

The values of ΔK_{th} shown in Fig. 6 are plotted against K_m in Fig. 7 and ΔK_{th} is seen to decrease linearly with K_m for both environments. Note that the data from Feeney et al [*17*] superimposed on the figure agree well with the present results. An alternative plot of $\Delta K_{th}/E$ against R is shown in Fig. 8, and the data confirm the validity of the Grandt and Gallagher expression [*28*] in the range $0 \leqslant R \leqslant 0.9$, namely:

$$\Delta K_{th} = (\Delta K_{th})_{R=0}(1 - R^2) \qquad (10)$$

TABLE 4—*Test data in 3.5% NaCl.*

K_m, psi × in.$^{1/2}$	ΔK, psi × in.$^{1/2}$	λ, psi^2 × in.	K_Q, psi × in.$^{1/2}$	da/dN, in./cycle	ϕ
5 000	3 800	3.8 × 10^7	21 600	9.5 × 10^{-6}	0.00378
5 000	4 500	4.5 × 10^7	21 600	1.88 × 10^{-6}	0.0337
5 000	5 000	5.0 × 10^7	20 700	9.3 × 10^{-7}	0.0238
5 000	7 000	7.0 × 10^7	20 700	5.3 × 10^{-6}	0.0955
5 000	9 000	9.0 × 10^7	21 600	9.0 × 10^{-6}	0.144
7 500	3 200	4.8 × 10^7	21 600	1.78 × 10^{-7}	0.00651
7 500	3 800	5.7 × 10^7	20 700	1.22 × 10^{-6}	0.0308
7 500	5 000	7.5 × 10^7	21 600	4.45 × 10^{-6}	0.0778
7 500	10 000	15.0 × 10^7	21 600	3.1 × 10^{-5}	0.334
7 500	14 000	21.0 × 10^7	21 600	9.5 × 10^{-5}	1.045
11 000	2 350	5.175 × 10^7	20 700	6.9 × 10^{-6}	0.0028
11 000	2 500	5.5 × 10^7	20 700	5.4 × 10^{-7}	0.0164
11 000	4 000	8.80 × 10^7	21 800	7.2 × 10^{-6}	0.132
11 000	5 000	11.0 × 10^7	21 600	1.0 × 10^{-5}	0.334
11 000	7 000	15.4 × 10^7	20 700	3.15 × 10^{-5}	0.470
11 000	10 000	21.0 × 10^7	20 700	8.4 × 10^{-5}	0.92
11 000	14 000	30.8 × 10^7	21 600	1.78 × 10^{-4}	1.81
11 000	18 000	39.6 × 10^7	20 700	1.58 × 10^{-3}	11.9
11 000	19 200	42.25 × 10^7	20 700	8.9 × 10^{-3}	74.5
15 000	1 700	5.1 × 10^7	20 700	5.15 × 10^{-6}	0.0021
15 000	1 800	5.4 × 10^7	21 800	2.6 × 10^{-7}	0.0134
15 000	2 000	6.0 × 10^7	20 700	1.78 × 10^{-6}	0.044
15 000	2 500	7.5 × 10^7	20 700	4.48 × 10^{-6}	0.152
15 000	5 000	15.0 × 10^7	21 600	3.55 × 10^{-5}	0.63
15 000	7 000	21.0 × 10^7	21 800	8.1 × 10^{-5}	1.29
15 000	10 000	30.0 × 10^7	21 800	2.69 × 10^{-4}	3.34
15 000	11 000	33.0 × 10^7	21 800	3.4 × 10^{-4}	5.10
15 000	12 000	36.0 × 10^7	21 800	1.2 × 10^{-3}	9.15
15 000	13 000	39.0 × 10^7	21 800	3.9 × 10^{-3}	25.3

1000 psi × in.$^{1/2}$ = 1.0998 MN/m$^{3/2}$
1 in. = 25.4 mm

successfully used in the evaluation of a large number of Al alloys and steels.

Tests at very high stress ratios (above 0.9) have not been completed, but results to date provide a good fit to a smooth curve (Fig. 8) for both environments. A sudden change in the shape of similar curves observed by Schmidt and Paris [*9*] on 2024–T3 aluminium and A533 steel, albeit at lower values of R than those investigated here, was explained by a crack closure originally discussed by Elber [*29*], but it is doubtful that such a change would occur in RR 58. It should be mentioned here that the analysis of the fatigue tests on RR 58 performed by Pearson [*30*] in the crack growth range of 10^{-6} to 10^{-4} in./cycle (10^{-8} to 10^{-6} m/cycle) led to unexpected discrepancies; thus the possibility of behavior different from that commonly observed in class

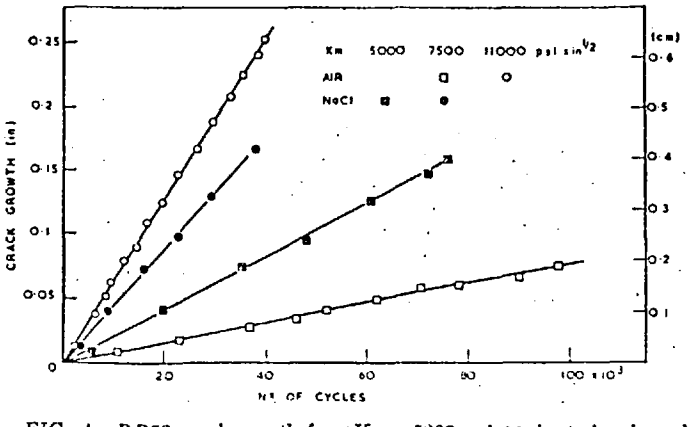


FIG. 4—*RR58 crack growth for* ΔK = *5000 psi* × *in.*$^{1/2}$ *in air and in 3.5% NaCl solution at 21°C, 0.15 Hz.*

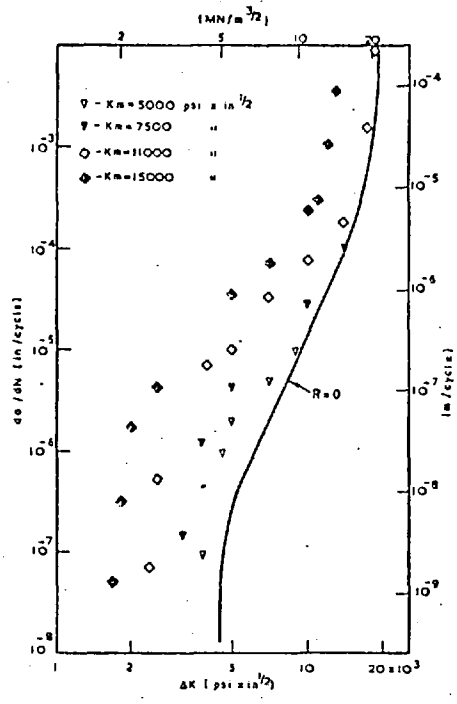


FIG. 5—*RR58 crack growth rate versus* ΔK *in 3.5% NaCl, 0.15 Hz.*

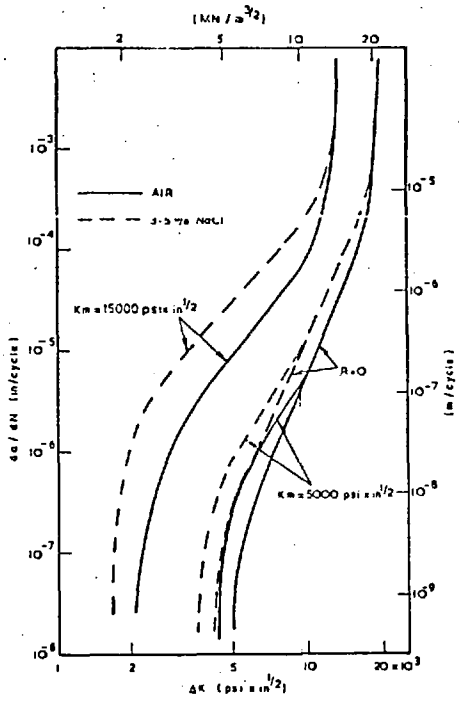


FIG. 6—*RR58 crack growth rate versus* ΔK *in air and in 3.5% NaCl at 21°C.*

2000 Al alloys should not be ruled out. The discrepancies mentioned above and the excellent data fit provided by Eq 7 for Al alloys support its application in further fatigue crack propagation studies.

A plot of crack growth rate against the parameter λ is presented in Fig. 9. As already observed in the study of Al alloys 2024–T3 and 7075–T6 [*12*], the agreement with λ is good between 10^{-5} and 10^{-3} in./cycle (10^{-8} to 10^{-5} m/cycle). Accelerated crack growth rates were noted in the 3.5% NaCl solution environment,

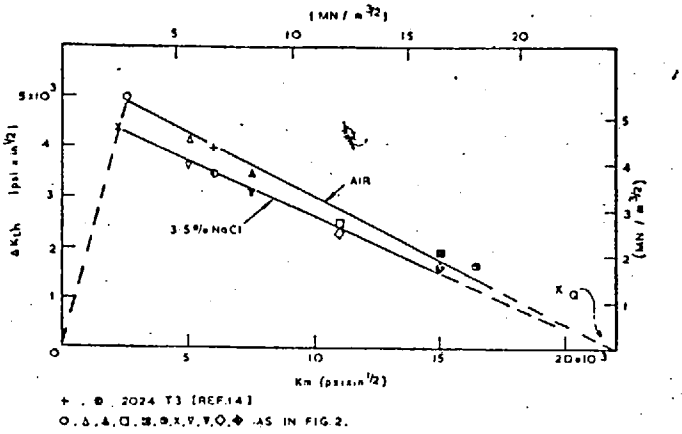


FIG. 7—*RR58* ΔK_{th} *versus* K_m *at 0.15 Hz in air in 3.5% NaCl at 21°C.*

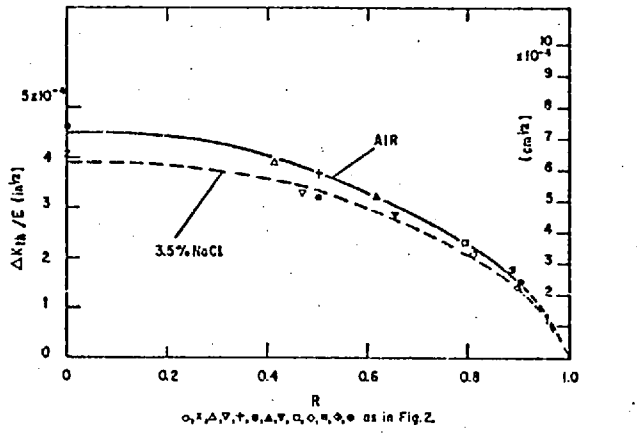


FIG. 8—*RR58* $\Delta K_{th}/E$ *versus* R *at 0.15 Hz in air and in 3.5% NaCl at 21°C.*

but for higher values of λ (Region III) the differences between the air and NaCl environment became small.

The situation may be described as follows: For lower crack growth rates (<10^{-6} in./cycle) (<10^{-8} m/cycle), λ is strongly dependent on K_m, and its threshold value influences crack growth in this region (Region I). A sharp increase in growth rate occurs for higher values of K_{max} approaching the critical value K_Q (Region III). These two values provide the limiting conditions

$$\lim_{\lambda \to \lambda_{th}} \quad da/dN = 0 \tag{11a}$$

and

$$\lim_{K_{max} \to K_Q} \quad da/dN = \infty \tag{11b}$$

A generalized equation

$$\frac{da}{dN} = A\phi^{\alpha} \tag{12}$$

where

$$\phi = \frac{\lambda - \lambda_{th}}{K_Q^2 - K_{max}^2} \tag{13}$$

and A and α are constants is presented in Fig. 10. A linear relation of a slope $\alpha = 1.46$ and $A = 1.0 \times 10^{-4}$ in./cycle (2.5×10^{-6} m/cycle) for laboratory air and $\alpha = 1.10$ and $A = 6.11 \times 10^{-3}$ in./cycle (1.55×10^{-5} m/cycle) for the 3.5% NaCl solution

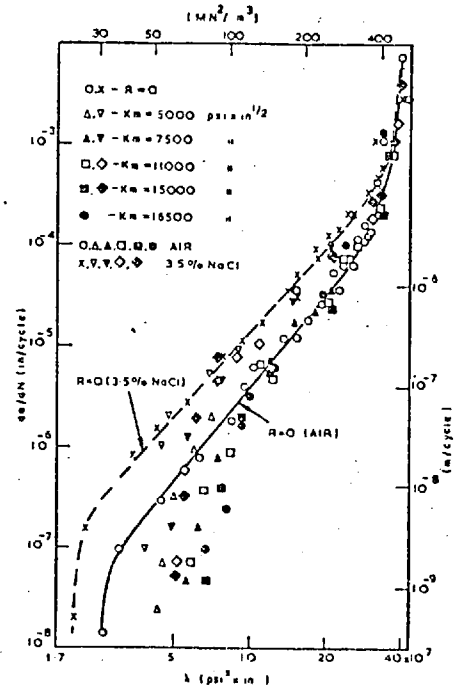


FIG. 9—*RR58 crack growth rate versus* λ *at 0.15 Hz, at 21°C.*

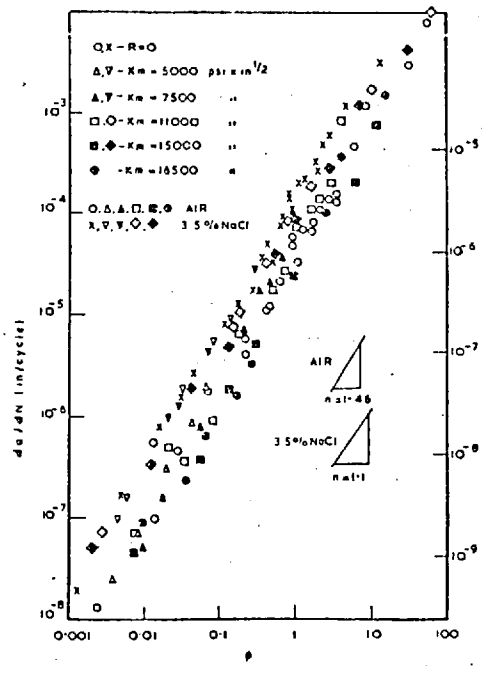


FIG. 10—*RR58 crack growth rate versus* φ *in air and in 3.5% NaCl at 0.15 Hz, 21°C.*

is produced. It may be concluded that for RR 58 and in the two investigated environments the parameter φ describes the crack growth process well. However, thickness and frequency effects require further investigation. Equation 12 offers the designer a simple expression covering the full subcritical range, normalizing the stress ratio effect and threshold behavior as well as the approach to fast fracture not fully accounted for by other expressions mentioned earlier. The good agreement found for Al alloys, mild steels, and polymers suggests that futher investigations of other materials might be rewarding.

Conclusions

1. A study of the propagation of fatigue cracks in contoured double cantilever beam specimens of Al alloy RR 58 under cyclic tension at 0.15 Hz and 21°C in laboratory air and in a 3.5% NaCl solution was presented.

2. Fatigue crack growth rate was found to be greater in the 3.5% NaCl solution in comparison with an air environment, but for higher values of the maximum value of the stress intensity factor K_{max} no measurable difference between the crack growth rates in the two environments was observed.

3. Fatigue crack growth rate was found to be dependent on the range of the stress intensity factor ΔK and its mean value K_m for both environments.

4. Fatigue crack growth rate can be described as $da/dN = A\phi^{\alpha}$ where $\phi = (\lambda - \lambda_{th})/(K_Q^2 - K_{max}^2)$, $\lambda = K_{max}^2 - K_{min}^2$, λ_{th} is the threshold value of λ, K_Q is the critical fracture toughness, and A and α are constants.

5. The threshold stress intensity factor K_{th} is only 12% lower in the 3.5% NaCl solution than in air and decreases linearly with increasing K_m. The threshold data fitted well the Grandt and Gallagher [28] expression $\Delta K_{th} = (\Delta K_{th})_{R=0}(1 - R^2)$, but the threshold behavior could not be satisfactorily explained in terms of crack closure.

Acknowledgment

The financial support of the Instituto de Alta Cultura, Ministry of Education, Culture, and Scientific Research, Lisbon, Portugal to one of the authors (CMB) is gratefully acknowledged.

References

[1] Hoeppner, D. W. and Krupp, W. E., "Prediction of Component Life by Application of Fatigue Crack Growth Knowledge," *Engineering Fracture Mechanics*, Vol. 6, No. 1, 1947, p. 47.

[2] Paris, P. C. and Erdogan, F., "Critical Analysis of Crack Propagation Laws," *Journal of Basic Engineering, Series D, Transactions*, American Society of Mechanical Engineers, Vol. 85, No. 4, 1963, p. 528.

[3] Forman, R. G., Kearney, V. E., and Engle, R. H., "Numerical Analysis of Crack Propagation in Cyclic Load Structures," *Journal of Basic Engineering, Series D, Transactions*, American Society of Mechanical Engineers, Vol. 89, No. 3, 1967, pp. 459–464.

[4] Hudson, C. M., "Effect of Stress Ratio on 2024-T3 and 7075-TG Al-Alloy Specimens," Report TN 5390, National Aeronautics and Space Administration, Washington, D.C., 1969.

[5] Arad, S., Radon, J. C., and Culver, L. E., "Growth of Fatigue Cracks in Metals and Polymers," *Engineering Fracture Mechanics*, Vol. 6, No. 1, 1974, p. 195.

[6] Liu, H. W., *Proceedings*, 10th Sagamore Army Materials Research Conference, Syracuse University Press, New York, 1964, p. 127.

[7] Donahue, R. J., Antanmo, P., Kumble, R., and McEvily, A. J., "Crack Opening Displacement and the Rate of Fatigue Crack Growth," *International Journal of Fracture Mechanics*, Vol. 4, No. 3, 1972, p. 511.

[8] Chu, H. P., "Effect of Mean Stress Intensity on Fatigue Crack Growth in a 5456-H117 Al-Alloy" in *Fracture Toughness and Slow-Stable Cracking, ASTM STP 559*, American Society for Testing and Materials, Philadelphia, 1974, pp. 245–261.

[9] Paris, P. C., Bucci, R. J., Wessel, E. T., Clark, W. G., and Mayer, T. R., "Extensive Study of Low Fatigue Crack Growth Rates in A 533 and A 508 Steel" in *Stress Analysis and Growth of Cracks, ASTM STP 513*, American Society for Testing and Materials, Philadelphia, 1972, p. 141.

[10] Schmidt, R. A. and Paris, P. C., "Threshold for Fatigue Crack Propagation and the Efferts of Load Ratio and Frequency" in *Progress in Flaw Growth and Fracture Toughness Testing, ASTM STP 536*, American Society for Testing and Materials, Philadelphia, 1973, 79.

[11] Arad, S., Radon, J. C., and Culver, L. E., "Design Against Fatigue Failure in Thermoplastics," *Engineering Fracture Mechanics*, Vol. 4, No. 3, 1972, p. 511.

[12] Sutton, S. A., "Fatigue Crack Propagation in an Epoxy Polymer," *Engineering Fracture Mechanics*, Vol. 6, No. 3, 1974, p. 587.

[13] Crooker, T. W. and Lange, E. A., *NRL Research Reports, No. 6805 and 7036*, Naval Research Laboratory, Washington, D.C., 1968 and 1970.

[14] Frost, N. E., Pook, L. P., and Denton, K., "A Fracture Mechanics Analysis of Fatigue Crack Growth Data for Various Materials," *Engineering Fracture Mechanics*, Vol. 3, No. 2, 1971, p. 109.

[15] Speidel, M. O., Blackburn, M. J., Beck, T. R., and Feeney, J. A., "Corrosion Fatigue and Stress Corrosion Crack Growth in High-Strength Al-Alloys, M_g-Alloys, and Ti-Alloys Exposed to Aqueous Solutions" in *International Conference on Corrosion Fatigue*, University of Connecticut, 1972, p. 324.

[16] Krupp, W. E., Hoeppnel, D. W., and Walker, E. K., "Crack Propagation of Al-Alloys in Corrosive Environments" in *International Conference on Corrosion Fatigue*, University of Connecticut, 1972, p. 468.

[17] Feeney, J. A., McMillan, J. C., and Wei, R. P., "Environmental Fatigue Crack Propagation of Al-Alloys at Low Stress Intensity Levels," *Metallurgical Transactions*, Vol. 1, No. 6, 1970, p. 1741.

[18] Hartman, A. and Schijve, J., "The Effects of Environment and Load Frequency on the Crack Propagation Law for Marco Fatigue Crack Growth in Al-Alloys," *Engineering Fracture Mechanics*, Vol. 1, No. 4, 1970, p. 615.

[19] Branco, C. M., Radon, J. C., and Culver, L. E., "Corrosion Fatigue of Al-Alloy RR 58—A Fracture Mechanics Approach," Paper No. C(3)b, presented at the 1974 Symposium on Mechanical Behavior of Materials, Kyoto, Japan, 1974.

[20] Wei, R. P. and Landes, J. D., "Correlation Between Sustained Load and Fatigue Growth in High-Strength Steels," *Materials Research and Standards*, MTRSA, Vol. 9, No. 7, 1969, p. 25.

[21] Gerberich, W. W., Birat, J. P., and Zackay, V. F., "On the Superposition Model for Environmentally Assisted Fatigue Crack Propagation" in *International Conference on Corrosion Fatigue*, University of Connecticut, 1972, p. 396.

[22] Euw, E. F. J., Hertzberg, R. W., and Roberts, R., "Delay Effects in Fatigue Crack Propagation" in *Stress Analysis and Growth of Cracks, ASTM STP 513*, American Society for Testing and Materials, Philadelphia, 1972, p. 230.

[23] Shih, T. T. and Wei, R. P., "Load and Environment Interactions in Fatigue Crack Growth," presented at the Conference of the Prospects of Advanced Fracture Mechanics, Delft, The Netherlands, 1974.

[24] Randon, J. C. and Culver, L. E., "Intergranular Stress Corrosion," Paper No. C(3)A, presented at the 1974 Symposium on Mechanical Behavior of Materials, Kyoto, Japan, 1974.

[25] Johnson, F. A. and Radon, J. C., "Mechanical and Metallurgical Aspects of Fracture Behavior of an Al-Alloy," *International Journal of Fracture Mechanics*, Vol. 8, No. 1, 1972, p. 21.

[26] Liu, H. W., "Fracture Criteria of Cracked Metalhe Plates," *International Journal of Fracture Mechanics*, Vol. 2, No. 2, 1966, p. 393.

[27] Bucci, R. J., Discussion to H. P. Chu (see Ref *8*) in *Fracture Toughness and Slow-Stable Cracking, ASTM STP 559*, American Society for Testing and Materials, Philadelphia, 1974.

[28] Grandt, A. F. and Gallagher, J. P., "Proposed Fracture Mechanics Criteria to Select Mechanical Fasteners for Long Service Lifes" in *Fracture Toughness and Slow-Stable Cracking, ASTM STP 559*, American Society for Testing and Materials, Philadelphia, 1974, p. 283.

[29] Elber, W., "The Significance of Fatigue Crack Closure" in *Damage Tolerance in Aircraft Structures, ASTM STP 486*, American Society for Testing and Materials, Philadelphia, 1971, p. 230.

[30] Pearson, S., "The Effect of Mean Stress on Fatigue Crack Propagation in Half Inch Thick Specimens of Al-Alloys of High and Low Fracture Toughness," Technical Note RAE TR 68297, Royal Aircraft Establishment, Farnborough, England, 1968.

Growth of fatigue cracks in steels

C. M. Branco, J. C. Radon, and L. E. Culver

An extensive study of fatigue-crack growth in BS15 mild steel has been made, in laboratory air at 21°C and at two cycling frequencies, namely 0·25 and 35 Hz. A wide range of cyclic growth rates, starting from the region associated with fatigue thresholds (10^{-7} mm/cycle) up to the region of rapid fracture, was investigated using contoured DCB specimens which provided constant stress-intensity factors over the crack lengths of ~150 mm. It was found that for BS15 a relationship between cyclic growth rate da/dN and the tensile loading levels of the form $da/dN = A\phi^{\alpha}$ was applicable. A and α are constants and ϕ a parameter dependent upon the loading conditions and material properties. The proposed equation is shown to be dependent upon the range of crack-opening displacement, the plastic zone size, and the J-contour integral. The relation has also been successfully applied in analysing published crack growth rate data obtained from four different steels as well as some Al alloys. Threshold values of stress intensity, varying with its mean, have been established, but they do not correlate with crack closure. Instead an explanation based upon the inclusion of the threshold term in the above equation is proposed.

Paper No. MS 507. Manuscript received 31 July 1975; in final form 9 December 1975. C. M. Branco, MSc, J. C. Radon, PhD, and L. E. Culver, PhD, are in the Department of Mechanical Engineering at Imperial College of Science and Technology, London.

The fatigue-failure process of engineering materials is not completely understood and a general criterion for the analysis of fatigue failures does not yet exist. However, with the development of linear elastic fracture mechanics (LEFM) a considerable number of problems associated with the assessment of service life of components, particularly in the crack-propagation stage, has been solved.

The original concept of applying a stress-intensity factor for characterization of the fatigue-crack behaviour of engineering materials was first used by Paris.[1] This relationship related the cyclic crack growth rate, da/dN, to the range, ΔK, of the stress-intensity factor, K:

$$\frac{da}{dN} = C_1 (\Delta K)^m \quad \ldots\ldots\ldots\ldots\ldots\ldots (1)$$

where C_1 and m are constants dependent upon the material and testing conditions. C_1 and m need to be determined experimentally.

Later it was proposed by Liu[2] that a certain threshold level of ΔK, ΔK_{th}, must be exceeded for crack growth to occur and the Paris equation was modified to

$$\frac{da}{dN} = C_2 (\Delta K - \Delta K_{th})^{m_1} \quad \ldots\ldots\ldots\ldots\ldots\ldots (2)$$

where C_2 and m_1 are constants. More recently[3] another equation based on crack opening displacement considerations and including the threshold term ΔK_{th} was suggested:

$$\frac{da}{dN} = \frac{C_3}{\pi \sigma_{ys} E} (\Delta K^2 - \Delta K_{th}^2) \quad \ldots\ldots\ldots\ldots\ldots\ldots (3)$$

where σ_{ys} is the yield stress, E is Young's modulus and C_3 is a constant.

It is now accepted that, in general and for metals in particular, the curve showing crack-growth rate as a function of ΔK presents three distinct regions. Region I is the threshold zone, Region II is the intermediate linear crack propagation region, and in Region III a sharp increase in crack-growth rate occurs when the maximum value of the stress-intensity factor in the loading cycle, K_{max}, approaches the critical value, K_C. An equation developed recently for the Al alloy 5456-H117 and valid in the three regions of crack propagation[4] is:

$$\frac{da}{dN} = C_4 \frac{(\Delta K^{n_1} - \Delta K_{th}^{n_2})}{(1-R)K_C - \Delta K^{m_2}} \quad \ldots\ldots\ldots\ldots\ldots\ldots (4)$$

where C_4, n_1, n_2, and m_2 are constants and R is the stress ratio ($=K_{min}/K_{max}$). It has been shown[5–7] that the threshold, ΔK_{th}, decreases with increasing values of the stress ratio, R, in a wide variety of Al alloys and steels. Also, the trend of the ΔK_{th} vs. R curve was explained in terms of crack closure by Schmidt and Paris.[5] The crack-closure concept as originally explained by Elber[8] implies that a certain value of the stress-intensity factor, K_{cl}, is necessary to open the crack and furthermore that crack growth would occur only when a certain stress-intensity range, ΔK_0, above K_{cl}, is exceeded. ΔK_0 was assumed to be constant for any value of stress ratio, hence, in the ΔK_{th} vs. R curve a 'plateau' exists starting from the point R_{cl} where $K_{min} = K_{cl}$.[5]

A wide variety of threshold data was analysed by Grandt and Gallagher[9] and a different expression to fit the experimental data suggested:

$$\Delta K_{th} = (\Delta K_{th})_{R=0} (1 - R^2) \quad \ldots\ldots\ldots\ldots\ldots\ldots (5)$$

This equation and also the present authors' results do not support the crack-closure approach for the materials investigated.

In the particular cases of mild steel and other low-alloy steels, data obtained by Frost *et al.*,[10] Pook,[11] Paris *et al.*,[12] and Priddle[13] suggested a considerable mean stress effect, but expressions capable of describing the full subcritical range on these materials are scarce. In particular, Cooke and

List of symbols

a	crack length
A	constant in eqns. (7) and (17)
B	net fracture width
C	compliance
C_1, C_2, C_3, C_4	constants in eqns. (1)–(4)
E	Young's modulus
K_1	stress-intensity factor in Mode 1 loading
K_{max}, K_m and K_{min}	Maximum, mean and minimum values of K in the loading cycle
$\Delta K = (K_{max} - K_{min})$	range of the stress-intensity factor in the loading cycle
K_{mth}, K_{maxth}, ΔK_{th}	mean, maximum, and range of the threshold value of K
K_C	critical value of K
m, m_1, m_2	exponents in eqns. (1), (2), and (4)
n, n_1, n_2	exponents in eqns. (4) and (6)
N	number of load cycles
P	applied load
R	stress ratio ($=K_{min}/K_{max}$)
R_{th}	threshold value of R
α	exponent in eqns. (7) and (17)
β	constant in eqn. (6)
δ	crack-opening displacement
δ_{max}, δ_{min}	maximum and minimum values of δ in the loading cycle
$\Delta\delta = (\delta_{max} - \delta_{min})$	range of crack-opening displacement in the loading cycle
$(\delta_{max})_{th}$, $(\delta_{min})_{th}$, $(\Delta\delta)_{th}$	maximum, minimum, and range of the threshold value of δ
$\lambda = (K_{max}^2 - K_{min}^2) = 2\Delta K K_m$	parameter in eqns. (6) and (14)
λ_{th}	threshold value of λ
ν	Poisson's ratio
σ_{ys}	0·2% yield stress
σ_{UTS}	ultimate tensile strength
$\phi = \dfrac{\lambda - \lambda_{th}}{K_C^2 - K_{max}^2}$	parameter in eqns. (7), (8), and (14)
K_{cl}	value of K necessary to close or open crack
ΔK_o	value of ΔK necessary for crack propagation

Beevers[14] observed a marked dependence of the threshold on the stress ratio R. They noted that the threshold value increased with increasing yield stress and this was shown for all five medium-carbon steels investigated. A wide range of steels was also tested by Nicholson and Priest[15(a)] who considered the influence of specimen geometries, thickness as well as crack-growth directions, and were able to express fatigue crack growth rates in a general form not dissimilar to the Paris law. However, a subsequent study[15(b)] of a high-strength steel has led to the development of another and more general relationship which takes into account not only the ultimate K_C value, but also the influence of the threshold. Maddox[16] published limited crack growth data on BS15 at $R=0$. Agreement with the Paris equation was obtained but no tests were performed at other stress ratios nor at low crack-growth rates (Region I), and Region III was not studied in detail.

Previous work[17(a)] on a range of metals and polymers suggested a crack-propagation model, to include mean stress effects, of the following form:

$$\frac{da}{dN} = \beta \lambda^n \quad \ldots\ldots\ldots\ldots\ldots\ldots\ldots\ldots (6)$$

where $\lambda = K_{max}^2 - K_{min}^2 = 2\Delta K K_m$, and β and n are constants. In Region II of crack propagation the above equation has been applied with considerable success in the analysis of a range of published data on high-strength Al alloys and steels.[17(a)] One of the particular materials being studied was cold-rolled mild steel[10] where agreement with λ was obtained in the range of crack-growth rates from $2{\cdot}5 \times 10^{-5}$ to $2{\cdot}5 \times 10^{-3}$ mm/cycle. A modification of eqn. (6) was subsequently made[17(b)] to correlate crack-growth rates in all three regions:

$$\frac{da}{dN} = A\phi^\alpha \quad \ldots\ldots\ldots\ldots\ldots\ldots\ldots\ldots (7)$$

where

$$\phi = \frac{\lambda - \lambda_{th}}{K_C^2 - K_{max}^2} \quad \ldots\ldots\ldots\ldots\ldots\ldots (8)$$

λ_{th} is the threshold value of λ and A and α are constants. Good correlation was obtained in the Al alloy RR58 over the full subcritical range.

The aim of the work now reported was to investigate fatigue crack propagation phenomena in BS15 mild steel in laboratory air, 50% R.H. at 21°C, and at two different cycling frequencies, 0·25 and 35 Hz, covering the full subcritical range. The applicability of the model described by eqn. (7) is also checked not only to BS15 but also to other steel data available in the literature. Finally the relationship provided by eqn. (7) to other fracture mechanics parameters is discussed.

EXPERIMENTAL

The composition and mechanical properties of the mild steel BS15 are: C 0·19–Mn 0·59–Si 0·028–P 0·021–Ni 0·02–Cr 0·01–Mo 0·02–Nb 0·005%; $\sigma_{ys} = 401$ MN/m², $\sigma_{UTS} = 585$ MN/m², $E = 207$ GN/m², and $\nu = 0{\cdot}3$.

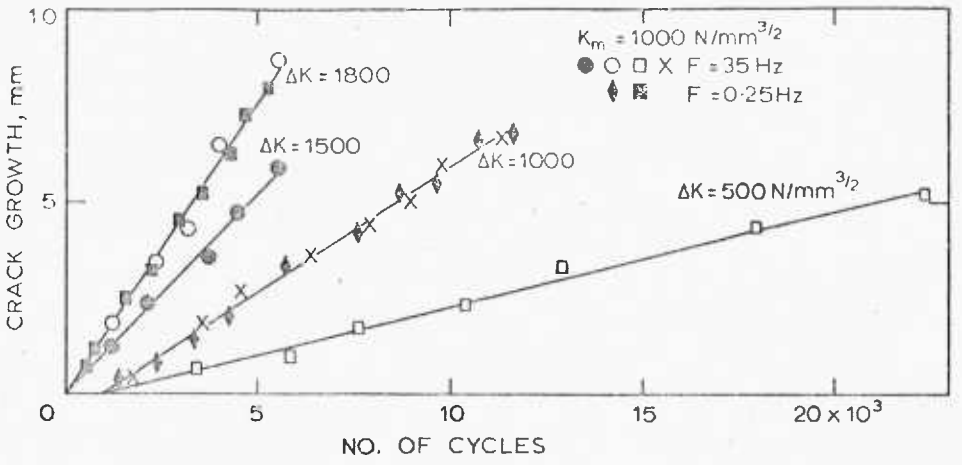
Crack-line-loaded contoured double cantilever beam (DCB) specimens, 12 mm thick, were manufactured from plate material and were orientated to ensure that the subsequent crack grew along the rolling direction. The design of these specimens is described in detail in Ref. 17(c), overall dimensions being 22·5 mm length and 75 mm maximum height. Side grooves, 4 mm deep, were used to enhance plane-strain conditions and the crack was opened with a saw cut extended to a 45° chevron notch and sharpened with a razor blade. The side grooves were polished for ease of observation of the crack tip.

Stress-intensity factors were calculated from the relationship

$$K_1 = P\left(\frac{E}{2B(1-\nu^2)}\frac{dC}{da}\right)^{1/2} \quad \ldots\ldots\ldots\ldots\ldots (9)$$

where P is the applied load, B is the net fracture width, C is the compliance, and a is the crack length. For a suitably shaped DCB testpiece the power term in eqn. (9), and consequently K_1, will remain constant along the crack length of ~150 mm.

Low-frequency fatigue tests were carried out in laboratory air, 50% R.H. at 21°C and 0·25 Hz in a 250 kN Avery



1 BS15: crack growth for K_m=const. and at various ΔK. Frequencies 0·25 and 35 Hz.

hydraulic universal testing machine fitted with a cycling mechanism consisting of two limit microswitches to regulate the load. Cyclic tension tests at a frequency of 35 Hz were performed in a Dowty electrohydraulic fatigue testing machine,[18] also at 21°C and in laboratory air 50% R.H. The possibility of differences in the results arising purely from the use of two different testing machines (due to the stiffnesses of the testing assemblies) was checked and found to be negligible; the repeatability of the results obtained in both machines was within 5%.

At each frequency, tensile fatigue crack propagation tests were conducted in turn at $R=0$, various K_m conditions, at constant ΔK, and at constant K_m conditions. Crack propagation was monitored with a travelling microscope, 50× magnification, with an accuracy better than 0·01 mm. Crack-growth rates were calculated and threshold data established under both progressively increasing and decreasing ΔK levels in long-term tests of $\sim 10^7$ cycles.

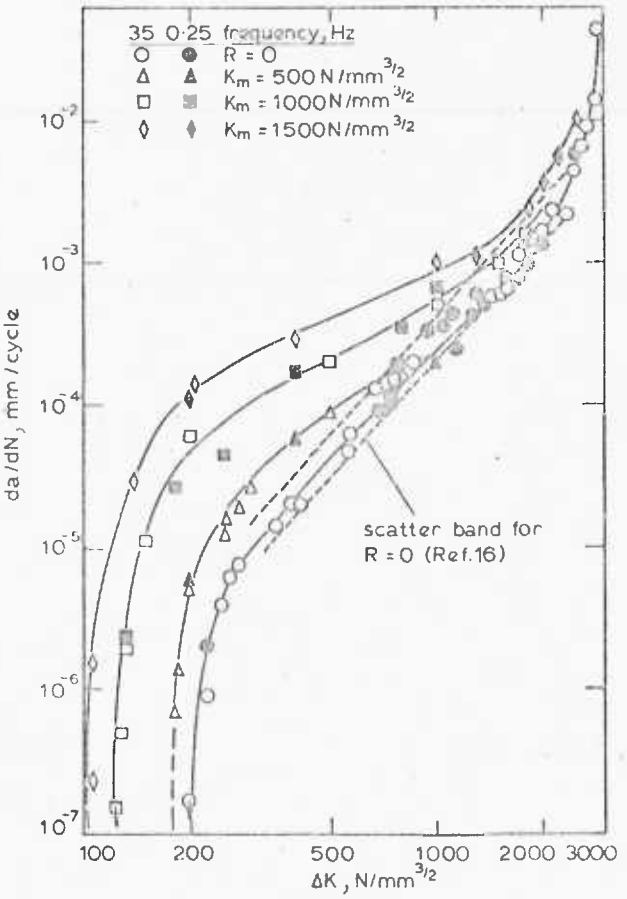
On completion of each fatigue test appropriate dC/da values were obtained, by pulling in an Instron tensile testing machine type TT-C, 44 kN capacity. A linear relationship between compliance and crack length was obtained.

RESULTS AND DISCUSSION

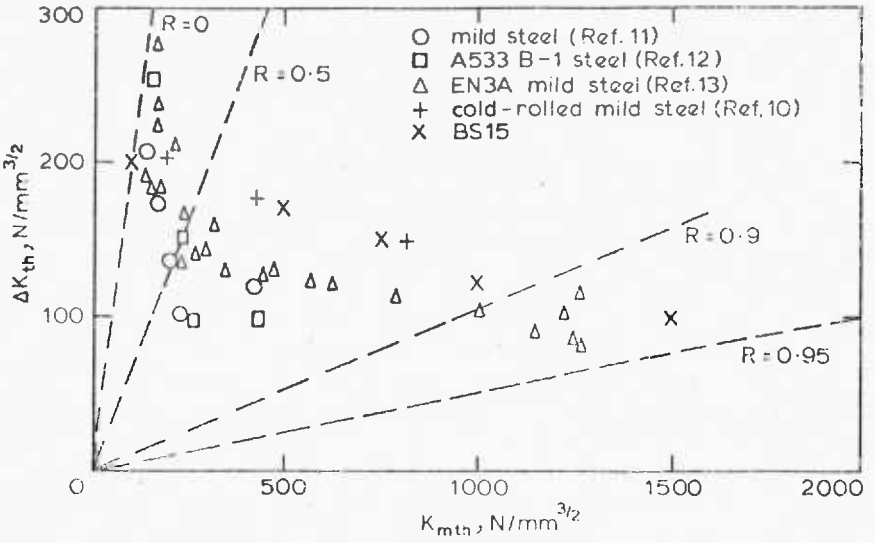
The crack-growth curves obtained from the tests at 35 Hz in which K_m was maintained constant at 1000 N/mm$^{3/2}$ and ΔK was fixed at specific levels between 500 and 1800 N/mm$^{3/2}$ are shown in Fig. 1. There is a typical linear relationship in each case and the growth rate increases with ΔK. The tests at ΔK equal to 1800 and 1000 N/mm$^{3/2}$ were repeated at a frequency of 0·25 Hz and the results are superimposed on Fig. 1. Clearly there is no frequency effect under these conditions.

Crack growth rate data for both frequencies are plotted as a function of ΔK in Fig. 2 and a family of K_m=constant curves drawn, corresponding to K_m=500, 1000 and 1500 N/mm$^{3/2}$, together with the curve corresponding to $R=0$, and various K_m conditions. Data for K_m =750 N/mm$^{3/2}$ at 0·25 Hz were also obtained, but omitted for clarity in Fig. 2. The present results for $R=0$ agree well with the Maddox data,[16] Fig. 2, obtained in what is usually described as Region II of crack propagation. It is also seen from the figure that in general the effect of frequency is negligible and for a given ΔK value crack-growth rate increases with K_m, although as ΔK increases the relative differences in crack-growth rates become smaller. Hence the early Paris law does not explain the large variations in crack-growth rates in tests at constant but different ΔK levels. Evidently both ΔK and K_m are significant factors in the crack growth rate process in this material.

Threshold data in the form of ΔK_{th} have been obtained from each curve in Fig. 2 plus the K_m = 750 N/mm$^{3/2}$ threshold value extrapolated to 10^{-7} mm/cycle and they are plotted against the mean value of the stress intensity at threshold K_{mth} in Fig. 3. Other threshold data included in Fig. 3 were obtained from four different steels[10–13] whose crack growth rate characteristics will be analysed in more



2 BS15: relation between crack-growth rate and ΔK. Frequencies 0·25 and 35 Hz.



3 ΔK_{th} **vs.** K_{mth} **for five steels tested in air at 21°C.**

detail later. The threshold data vary between stress ratios from 0 to ~0·95 as evidenced by the four constant R lines drawn in the figure. The BS15 threshold results agree well with Frost's cold-rolled mild steel. At stress ratios near 0, A533 B-1 and EN3A mild steels have better threshold behaviour than the other steels. But when $0{\cdot}5 < R < 0{\cdot}95$ the best results belong to cold-rolled mild steel and BS15. An alternative way of presenting the threshold data is given in Fig. 4 where the factor $\Delta K_{th}/E$ is shown as a function of the threshold stress ratio R_{th}. The same relation exists between R and R_{th} as between K_m and K_{mth}. This curve is significant since it has been suggested that for a given stress ratio the factor $\Delta K_{th}/E$ may be material-independent.[19] When plotted on this basis it is seen that for the Al alloy RR58 and the present steels data do not fall on one single line. Hence at least for these materials the ratio $\Delta K_{th}/E$ is not material-independent.

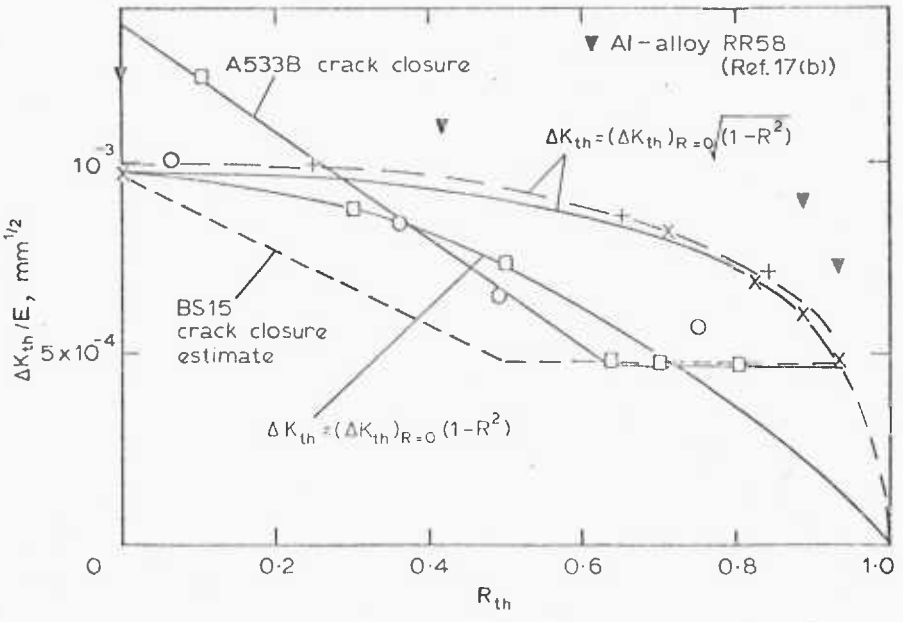
For cold-rolled mild steel and BS15 the following proposed equation fits the threshold data well:

$$\Delta K_{th} = (\Delta K_{th})_{R=0}\sqrt{1-R^2} \quad \ldots\ldots\ldots\ldots (10)$$

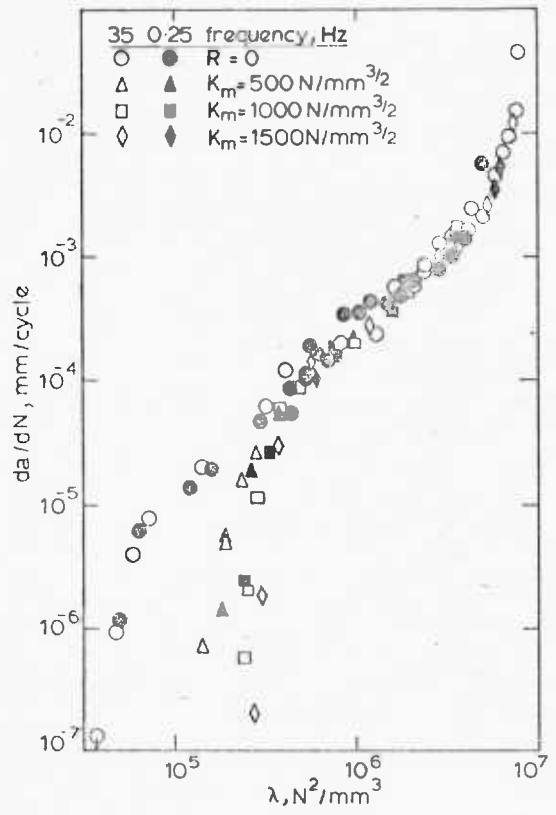
This equation gives a better correlation with these results than the Grandt and Gallagher expression, eqn. (5), shown superimposed on Fig. 4.

A crack-closure approach shows a reasonable correlation with data obtained for A533 B-1 steel[12] as indicated in Fig. 4, but no such agreement was obtained for BS15, the crack-closure estimate for which is also shown in the figure. This curve may be established since crack growth does not occur for cycling conditions in which $K_{min} \leqslant K_{cl}$ when

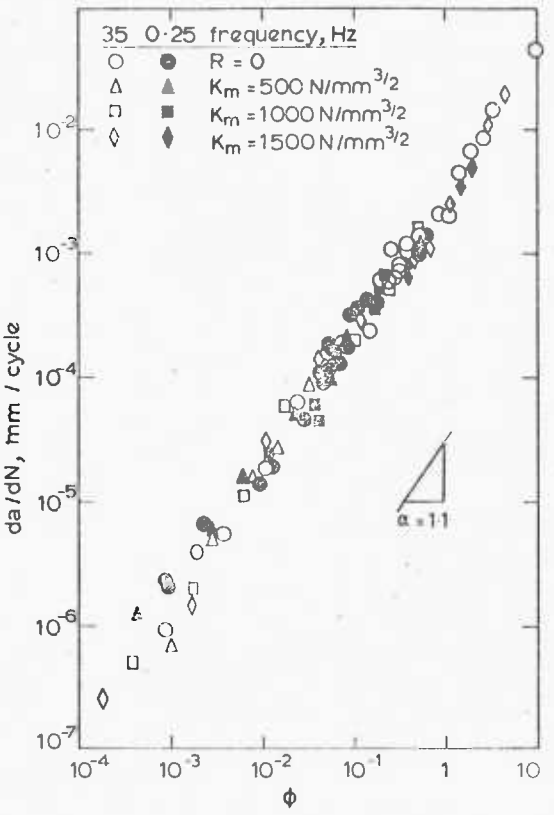
$$K_{max} = K_{cl} + \Delta K_o = \text{constant} \quad \ldots\ldots\ldots\ldots (11)$$



4 ΔK_{th} **vs.** R_{th} **for different steels (symbols as Fig. 3).**



5 **BS15**: crack-growth rate vs. λ. Frequencies 0·25 and 35 Hz, air 21°C.



6 **BS15**: crack-growth rate vs. ϕ. Frequencies 0·25 and 35 Hz, air 21°C.

Hence

$$\Delta K_{th} = (K_{max} - K_{min}) = (K_{cl} + \Delta K_o)(1 - R) \quad . \quad . \quad . \quad (12)$$

Also for $K_{min} \geqslant K_{cl}$ crack growth does not occur when $\Delta K_{th} = \Delta K_o =$ constant. Thus, when $R = 0$

$$(\Delta K_{th})_{R=0} = K_{cl} + \Delta K_o \quad . \quad . \quad . \quad . \quad . \quad . \quad . \quad . \quad . \quad . \quad . \quad . \quad . \quad (13)$$

and when $K_{min} \geqslant K_{cl}$

$$\Delta K_{th} = (\Delta K_{th})_{min}$$

This condition is met when $R_{th} = 0{\cdot}5$, enabling the two straight lines forming the curve for BS15 to be drawn. The inference then is that for all values of $R_{th} > 0{\cdot}5$ $\Delta K_{th}/E$ should remain constant. That this is not the case is clearly indicated by the data in Figs. 2–4. The crack-closure approach is not appropriate for cold-rolled mild steel or BS15 and any attempt to use it will lead to a very conservative estimate of ΔK_{th}.

The relationship between crack-growth rate and the parameter λ as defined in eqn. (6) is illustrated in Fig. 5. Use of this parameter has the effect of bringing all the experimental data into a single curve in Regions II and III although in Region I λ is dependent on K_m. This latter region is approaching threshold conditions and Region II represents an area of linear growth leading to a rapid increase in growth rate at higher values of λ in Region III. Similar behaviour has recently been reported in cold-rolled mild steel[17(a)] and in the Al alloy RR58.[17(b)] The divergence in Region I led to the suggestion of eqn. (7) as an improved model for crack propagation and it should be noted that the parameter ϕ may be expressed as

$$\phi = \frac{\lambda - \lambda_{th}}{K_C^2 - K_{max}^2} = \frac{2K_m(\Delta K - \Delta K_{th})}{K_C^2 - K_{max}^2} \quad . \quad . \quad . \quad . \quad . \quad . \quad (14)$$

This model satisfies the limiting conditions

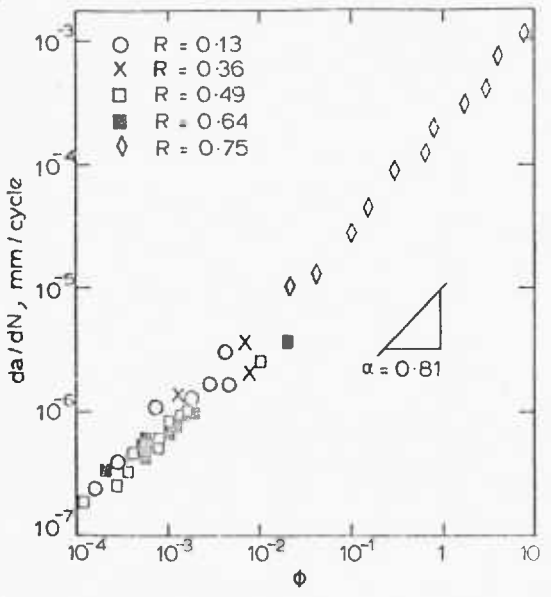
$$\text{Lim}\ \frac{da}{dN} \to 0 \quad \text{and} \quad \text{Lim}\ \frac{da}{dN} \to \infty \quad . \quad . \quad . \quad . \quad (15)$$
$$\lambda \to \lambda_{th} \qquad K_{max} \to K_C$$

In calculating ϕ appropriate values of K_C were taken from the literature. For BS15 K_C was taken as 3130 N/mm$^{3/2}$ (Ref. 20) and this was assumed to be the same for the other materials considered except for A533 B-1 where a value of 3800 N/mm$^{3/2}$ had been established.[21]

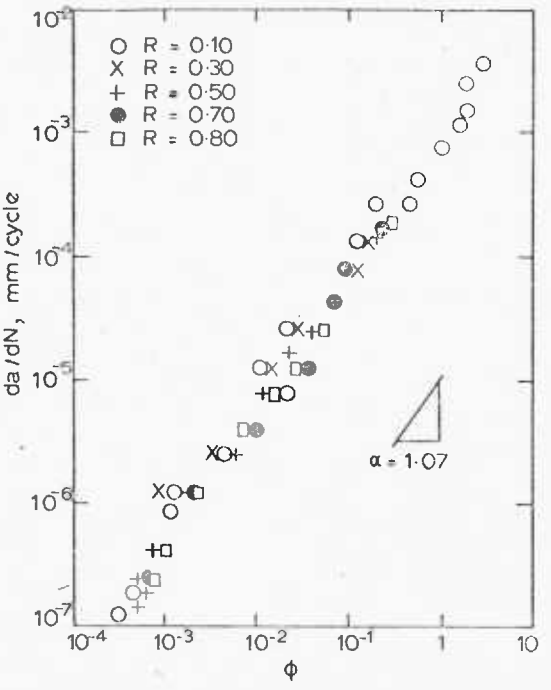
Crack-growth rate in BS15 as a function of ϕ is shown in Fig. 6 where it is seen that the test data from all tests have a linear correlation over the complete range from threshold to rapid fracture conditions. The model suggested as eqn. (7) is clearly very satisfactory for correlating crack-propagation phenomena in BS15 over the wide range considered. For the material the values of the constants are

$A = 2{\cdot}10 \times 10^{-3}$ mm/cycle
$\alpha = 1{\cdot}10$

In appropriate cases where the literature[10–13] gave sufficient data over a wide range of crack-growth rates the model has been applied to other materials. Relevant threshold data have been indicated in Figs. 3 and 4 and the variations of crack-growth rates with ϕ are shown in Figs 7–9 for tests in which the stress ratio R was constant. In



7 Crack-growth rate vs. ϕ. Mild steel, air 21°C (Ref. 11).



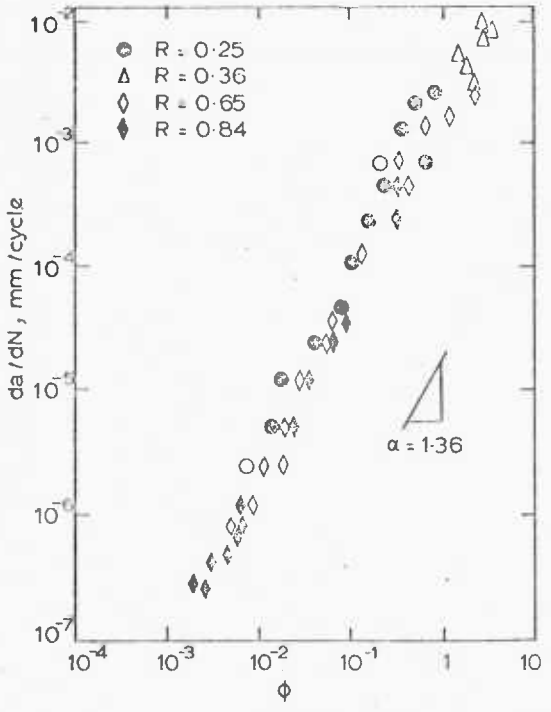
9 Crack-growth rate vs. ϕ. A533 B-1 steel, air 21°C (Ref. 12).

these cases the parameter ϕ could be calculated as

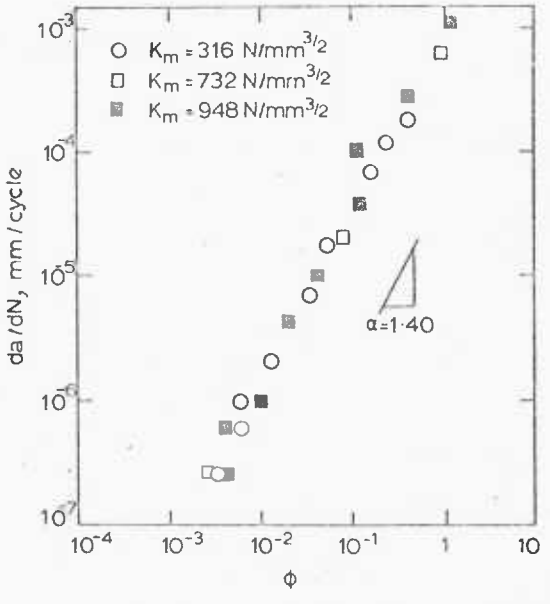
$$\phi = \frac{(1 - R_{th}^2)(K_{max}^2 - K^2_{maxth})}{K_C^2 - K_{max}^2} \quad \ldots\ldots\ldots (16)$$

where K_{maxth} is the threshold value of K_{max} in the particular stress-ratio curve being considered.

ϕ may be considered a valid crack-growth parameter for each of the materials over the range tested, e.g. for mild steel,[11] Fig. 7, a range of crack-growth rates of 10^{-7}–10^{-3} mm/cycle; for cold-rolled mild steel,[10] Fig. 8, 10^{-7}–10^{-2} mm/cycle; and for A533 B-1 steel[12] Fig. 9, 10^{-7}–10^{-2} mm/cycle approximately. In each of these cases the parameter may be considered valid over the full subcritical range. In the case of EN3A mild steel,[13] Fig. 10, the parameter appears equally valid although in this case the maximum crack growth rate had been restricted to 10^{-3} mm/cycle and the full range of Region III may not therefore have been explored. It should be noted that in Figs. 7 and 10 the authors' actual data points are indicated, but in Figs. 8 and 9 it was necessary to indicate the mid-points of



8 Crack-growth rate vs. ϕ. Cold-rolled mild steel, air 21°C (Ref. 10).



10 Crack-growth rate vs. ϕ. EN3A mild steel, air 21°C (Ref. 13).

scatter bands at randomly chosen da/dN values since only scatter bands were available.

The above results clearly demonstrated that for mild steels the parameter ϕ is able to place in one single line data obtained at any values of ΔK, R, or K_m. Similar checks on high-strength Al alloys and steels will be made before the relationship is generally considered as a good predictor of crack-growth rates in metals.

In LEFM the stress-intensity factor is related to the crack-opening displacement,[22] the plastic zone size r_p,[23] and the J-contour integral.[24] Hence eqn. (7) may be rewritten, when expressed in terms of the crack-opening displacement, as

$$\frac{da}{dN} = A\left(\frac{\Delta\delta - \Delta\delta_{th}}{\delta_C - \delta_{max}}\right)^{\alpha} \quad \ldots\ldots\ldots\ldots\ldots (17)$$

where $\Delta\delta = \delta_{max} - \delta_{min}$, δ_{max} and δ_{min} are the maximum and minimum values of δ in the loading cycle, $\Delta\delta_{th} = (\delta_{max})_{th} - (\delta_{min})_{th}$ at the threshold, and δ_C is the critical value of δ for unstable fracture. The above relation implies that the crack-growth rate is proportional to the crack-opening displacement and crack growth will occur when a certain level of $\Delta\delta > \Delta\delta_{th}$ is attained. Also when $\delta_{max} \to \delta_C$ unstable fracture occurs. Eqn. (17) may also be similarly expressed in terms of the plastic zone size or the J-contour integral through the direct relationship between these quantities. However, the validity of this equation expressed in terms of the J-contour integral needs to be checked in situations where general yielding occurs and its application is now being investigated.

CONCLUSIONS

A study has been made of the growth of fatigue cracks in BS15 mild steel in laboratory air at 0·25 and 35 Hz. Tests were conducted in cyclic tension under conditions of $R = 0$, ΔK = constant, or K_m = constant.

1. Both ΔK and K_m are significant factors in the crack-growth process in this material.

2. Threshold values of ΔK may be established at a crack-growth rate of $\sim 10^{-7}$ mm/cycle.

3. The fatigue threshold in BS15 and other materials is not satisfactorily established by the Schmidt and Paris crack-closure approach.

4. The frequency effect is negligible over the range considered.

5. A model to correlate crack-propagation data in mild steel BS15 over the full subcritical range has been proposed as

$$\frac{da}{dN} = A\phi^{\alpha} \qquad \text{where} \qquad \phi = \frac{\lambda - \lambda_{th}}{K_C^2 - K_{max}^2}$$

6. An analysis of data published by other authors has shown this model to be equally satisfactory for a range of other mild steels.

7. The above equation could be expressed alternatively in terms of the crack-opening displacement, the plastic zone size, or the J-contour integral.

REFERENCES

1. P. C. PARIS and F. ERDOGAN: *J. Bas. Eng. Trans. ASME*, 1963, **85**, 528.
2. H. W. LIU: Proc. 10th Sagamore Army Mat. Res. Conf., New York, 1964, p. 127.
3. R. J. DONAHUE, P. ATANMO, R. KUMBLE, and A. J. McEVILY: *Int. J. Fracture Mech.*, 1972, **4**, (3), 511.
4. H. P. CHU: 'Effect of Mean Stress Intensity on Fatigue-Crack Growth in 5456-H117 Al Alloy', Fracture Toughness and Slow-Stable Cracking, ASTM STP 559, 1974, p. 245.
5. R. A. SCHMIDT and P. C. PARIS: 'Threshold for Fatigue-Crack Propagation and Effects of Load Ratio and Frequency', Progress in Flaw Growth and Fracture-Toughness Testing, ASTM STP 536, 1973, p. 79.
6. K. JERRAM and E. K. PRIDDLE: *J. Mech. Eng. Sci.*, 1973, **15**, (4), 271.
7. M. KLESNIL and P. LUKAS: *Mater. Sci. Eng.*, 1972, **9**, 231.
8. W. ELBER: in 'Damage Tolerance of Aircraft Structures', ASTM STP 486, 1971, p. 230.
9. A. F. GRANDT and J. P. GALLAGHER: 'Proposed Fracture-Mechanics Criteria to Select Mechanical Fasteners for Long Service Life', Fracture Toughness and Slow-Stable Cracking, ASTM STP 559, 1974, p. 283.
10. N. E. FROST, L. P. POOK, and K. DENTON: *Eng. Fracture Mech.*, 1971, **3**, 109.
11. L. P. POOK: 'Fatigue Crack Growth Data for Various Materials Deduced from Fatigue Lives of Precracked Plates', Stress Analysis and Growth of Cracks, ASTM STP 513, 1972, p. 106.
12. P. C. PARIS, R. J. BUCCI, E. T. WESSEL, W. G. CLARK, and T. R. MAGER: 'Extensive Study of Low Fatigue-Crack Growth Rates in A 533 and A 508 Steels', Stress Analysis and Growth of Cracks, ASTM STP 513, 1972, p. 141.
13. E. K. PRIDDLE: 'Some Equations Describing Constant Amplitude Fatigue Crack Propagation Characteristics of Mild Steel', CEGB Berkeley Nuclear Laboratories, UK, CEGB Report RD/B/N2390.
14. R. J. COOKE and C. J. BEEVERS: *Eng. Fracture Mech.*, 1973, **5**, (4), 1061.
15(*a*). C. E. NICHOLSON and A. H. PRIEST: 'Fatigue-Crack Propagation in Steels', BSC Corporate Lab. Rep. MG/70/71.
15(*b*). C. E. NICHOLSON: 'Influence of Mean Stress and Environment on Crack Growth', Proc. Conf. Mechanics and Mechanisms of Crack Growth, Cambridge, April, 1973, p. 226.
16. S. MADDOX: 'Fatigue Strength of Welded Joints', PhD Thesis, Univ. London, 1972.
17(*a*). S. ARAD, J. C. RADON, and L. E. CULVER: *Eng. Fracture Mech.*, 1974, **6**, (1), 195.
17(*b*). C. M. BRANCO, J. C. RADON, and L. E. CULVER: 'Analysis of Mean Stress Intensity and Environment on a New High-Strength Al Alloy', submitted to ASTM J. of Materials Testing and Evaluation.
17(*c*). F. A. JOHNSON and J. C. RADON: *Int. J. Fracture Mech.*, 1972, **8**, (1), 21.
18. S. ARAD, J. C. RADON, and L. E. CULVER: *J. Mech. Eng. Sci.*, 1971, **13**, (2), 75.
19. M. O. SPEIDEL, M. J. BLACKBURN, T. R. BECK, and J. A. FEENEY: 'Corrosion Fatigue and Stress Corrosion Crack Growth in High-Strength Al, Ti, and Mg Alloys Exposed to Aqueous Solutions', Int. Conf. Corrosion Fatigue, Univ. Connecticut, 1972, p. 324.
20. N. BELLORIN: 'J_{IC} Tests in Mild Steel', MSc Thesis, Univ. London, Imperial College, 1974.
21. J. A. BEGLEY and J. D. LANDES: '*J* Integral as Fracture Criterion', Stress Analysis and Growth of Cracks, Part II, ASTM STP 514, 1972, p. 1.
22. F. M. BURDEKIN and D. E. W. STONE: *J. Strain Analysis*, 1966, **1**, 145.
23. W. F. BROWN and J. E. SRAWLEY: Plane Strain Crack Toughness Testing of High-Strength Materials, ASTM STP 410, 1966.
24. J. R. RICE: *J. Appl. Mech.*, 1968, **35**, 379.

© THE METALS SOCIETY 1976